Journal of Networks

ISSN 1796-2056

Volume 9, Number 1, January 2014

Contents

DAIM: a Mechanism to Distribute Control Functions within OpenFlow Switches

Ameen Banjar[a], Pakawat Pupatwibuli[b] and Robin Braun[c]
Centre for Real Time Information Networks, School of Computing and Communications, University of Technology, Sydney, Australia
[a]Ameen.r.Banjar@student.uts.edu.au, [b]Pakawat.Pupatwibul@student.uts.edu.au, [c]Robin.Braun@uts.edu.au

***Abstract*—Telecommunication networks need to support a wide range of services and functionalities with capability of autonomy, scalability and adaptability for managing applications to meet business needs. Networking devices are increasing in complexity among various services and platforms, from different vendors. The network complexity is required experts' operators. This paper explores an introduction to networks programmability, by distributing independent computing environment, which would be demonstrated through a structured system named DAIM model (Distributed Active information Model). In addition it seeks to enhance current SDN (Software-Defined Networking) approach which has some scalability issues. The DAIM model can provide richness of nature-inspired adaptation algorithms on a complex distributed computing environment. The DAIM model uses a group of standard switches, databases, and corresponding between them by using DAIM agents. These agents are imposed by a set of network applications, which is integrated with a DAIM model databases. DAIM model also considers challenges of autonomic functionalities, where each network's device can make its own decisions on the basis of collected information by the DAIM agents. The DAIM model is expected to satisfy the requirement of autonomic functionalities. Moreover, this paper discussed the processing of packets forwarding within DAIM model as well as the risk scenarios of the DAIM model.**

***Index Terms*—Distributed Networks, Information Model, Software-Defined Networking (SDN), DAIM, Self-X properties, Artificial Intelligence.**

I. Introduction

IN the last few years network technologies have been increasing significantly in performance, complexity, functionality, driven by the needs of the modern world. However, existing network infrastructure lacks adaptability, and demands device centric centralized management paradigms. Networks have become massive and intractable due to complexity, leading to challenges of scalability.

New network management paradigms may take several years to develop, and much longer to become widely spread. In addition, there is a gap between market requirements and network capabilities from vendor's side, where network operators need to design the network according to the requirements of users, which limits their abilities. Moreover, vendors lack standards and open interfaces [1].

Hence, there is a need for open and flexible architectures to implement autonomic management functionality [2], which has been considered as a solution to ameliorate the complexity of network management. This has given rise to a new network paradigm called Software-Defined Networking (SDN). It is aimed at reducing the complexity of management (see Fig. 1) [1]. The main idea of SDN is to separate the functionality of data path from control path. The data path remains in a switch whereas the high-level routing decisions are separated into a device called a controller, basically a routing server. The first industry developed standard for SDN is OpenFlow-based [1]. OpenFlow has a protocol, which is used between the switches and the controller to communicate and exchange messages such as get-stats, packets-receive, and packets-sent-out [3]. So, companies get the network programming ability to control the network with high scalability and flexibility, which can adapt easily according to ever changing circumstances. According to Fig. 1, the SDN structure has layers including an application layer, control layer, and infrastructure layer. In more detail the control layer has APIs (Application Programming Interfaces) ability, so it is possible to implement autonomic functionality such as self-protection and self-optimization [4].

One of the means to implement autonomic functionality within SDN is a new nature inspired active information model. It allows local decision-making in each network device which creates a complex distributed network environment. This paper proposes that a new information model called the Distributed Active Information Model (DAIM) can be implemented in OpenFlow-based SDN to meet the requirements of the autonomic components of the distributed network, such as self-management [5]. The benefits of implementing the proposed approach, include control devices and the rapid configuration of the entire network autonomically, without reconfiguring each individual device. In addition, the DAIM model can manage complex systems in any distributed network, which makes it possible to be autonomous, adaptable, and scalable.

DAIM is a sustainable information model, which collects, maintains, updates and synchronizes all the related information. Moreover, the decision making ability within each device locally, on the basis of collected information,

This work was supported by the Centre for Real-Time Information Networks (CRIN) in the Faculty of Engineering and IT at the University of Technology, Sydney (UTS). Corresponding author: Ameen Banjar, Ameen.r.Banjar@student.uts.edu.au

doi:10.4304/jnw.9.1.1-9

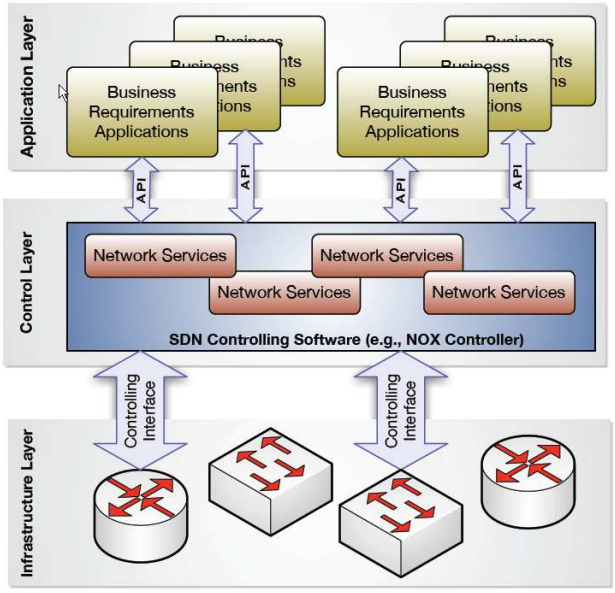

Figure 1: Software-Defined Networking Architecture

allows it to autonomically adapt according to the ever-changing circumstances [6]. The DAIM model structure is proposed with the hope that it addresses the limitation of previous network protocols such as Simple Network Management Protocol (SNMP) [7], Common Information Model (CIM) [8] and Policy-Based Network Management.

Ultimately, the proposed DAIM model will address the limitations of current approaches and future distributed network systems, creating an autonomic computing management strategy. The DAIM model approach will also satisfy the requirements of autonomic functionality for distributed network components like self-learning, self-adaptation and self-CHOP (configuration, healing, optimization and security). Each component can be adaptable according to any changed conditions of the dynamic environment without human intervention.

The remainder of the paper is organized as follows. In Section II we explain the limitations of current OpenFlow networks. Section III has details of related works to address those limitations. Our proposed new information model, which supports autonomic management for distributed systems is introduced in Section IV. Followed by Section V, which is the processing of the packets within the DAIM model. Section VI presents risk scenarios of DAIM model. Finally, we conclude the paper by summarizing the main contribution and future work in Section VII.

II. OpenFlow-Based SDN scalability issues

There are number of tests to prove that the current OpenFlow is lacking in scalability because of using a centralized controller. This part presents scalability issues of the current SDN approach. Also it covers related works that are relevant for addressing the SDN scalability issue.

One of the major limitations of a centralized OpenFlow controller is lack of scalability. The fundamental feature of the NOX controller is that it is responsible for establishing every forwarding rule in the network. As the size of production networks deploying OpenFlow increases, so will the number of flows that need to be processed [9]. If the NOX does not have the capacity to handle all these flow setups, it can present a scalability bottleneck. For example, an enterprise data center's networks may have 100 edge switches. The NOX controller could expect to see around 10 million flow requests per second [10], [11]. This could create significant challenges for deploying centralized OpenFlow controllers in large-scale data centers [10]. Another drawback of the NOX is that each flow request is processed individually, and all packets created accordingly are forward individually. In addition, sending out messages individually takes about 80% of the flow request processing time. This can cause an overhead of multiple socket write operations to forward each packet to the same destination individually instead of a single batched process. Moreover, the NOX does not provide sufficient flexibility to achieve scalability for application developers, nor adequately address reliability as the control platform must handle equipment and other failures gracefully [12].

Reference [13] explains that relying heavily on only one centralized controller for the whole network may not be feasible for a number of reasons. Firstly, the amount of control traffic destined for the controller increases according to number of switches. Secondly, despite where the controller is placed, if the networks have large diameter, some switches will face long flow setup latencies. Thirdly, since the network is bounded by the processing capacity of the controller, flow setup times can grow rapidly as demand grows in terms of network size and complexity [13]. Therefore, improving the performance of the NOX controller to keep up with the rising demand becomes a significant challenge. On the other hand, [14] highlight the difficulties of writing programs for the OpenFlow-based NOX platform as follows:

• Interactions between concurrent modules – Networks often process multiple tasks such as routing, monitoring, and access control. These functions cannot be processed independently unless they perform on non-overlapping portions of the traffic, since a rule (un)installed by one module could undermine the proper functioning of other modules

• Low level interface to switch hardware – OpenFlow maintains a low-level interface to the switches. Applications must establish rules that match on bits in the packet header. Because rules can have wild cards, a packet may match different overlapping rules with multiple priorities. This may translate high-level policy into multiple low-level rules.

• Two-tiered programming model – Controllers only receives packets that switches do not know how to process. This can limit the controller's visibility into the underlying traffic. Essentially, the execution of application is

split between the controller and the switches. Applications must avoid installing rules that hide vital information from the controller.

Software Defined Networking (SDN) is simple to manage and it is flexible. That depends on abstracting control and management functions as network applications. In addition, the controller has a wide view of the entire network [15]. Moreover, the SDN architecture has that control layer and forwarding layer, this architecture relies on central point, which control the forwarding layer. So, either interface has scalability bottleneck in the controller and in the switches [16]. For example bottleneck within switch can be in forwarding table memory. Thus, the current architecture lacks scalability when facing extended networks which include all the networks used in data transfer and information from distant places and in a wide geographical area (several kilometers to thousands of kilometers). Any such links between computer devices in places far away from each other, and which can connect branches of the institution within or outside the country with each other and allows users to exchange information and e-mail.

Scalability means that the network can increase the number of nodes and the length of links very widely, with the performance of the network is not affected. So, ensure network scalability necessary to use additional communications equipment and specially structured network. For example, good scalability has multi-segment networks, built using switches and routers and has a hierarchical structure of relationships. Such a network may include several thousand computers while providing each user the right network service quality. Thus, this research notes that by using the DAIM model, the scalability of the system could be solved by using a distributed environment as the control platform.

III. Related Works

Related work shows that, three approaches to scale central controller as following:

A. Using optimization techniques

• **Maestro** is a control system for centralized network, which has been developed to solve the limitations of OpenFlow control plane. Maestro has a central controller for a flow-based routing network, with an increasing of flow processing; it requires being extremely scalable, Maestro can achieve that and can coordinate between centralized controls and distributed routing protocols. Maestro approach works as hybrid control plane, which is robust than the centralized control plane. It uses parallelism technique to alleviate packet processing and solve the bottleneck on the controller of OpenFlow structure by using applications, such as “routing” or “learning switch” [10].

Maestro has programmable environment with a high-level language, which can deal with distribution and concurrency without involving the developer [17]. Maestro has a user interface to control hardware and also includes an analysis tools. It can auto-detects the attached hardware. Moreover, Maestro can make local decisions without involving master, and synchronize certain actions by using the master [18]. Developer is not involved which Maestro insert locks. As a result Maestro accepts as input high-level program actions, for protected structure [10]. However, Maestro still relies on only a single controller and send batching messages to the switches not in run time configuration. These challenges can significantly affect the packet forwarding process.

B. Devolving some control functions back to the switches

• **DevoFlow** (Devolved OpenFlow) modifies the Open Flow model to redistribute as many decisions as possible to the switches, in ways to enable simple and cost-effective hardware implementations [19]. DevoFlow can solve the bottleneck of the OpenFlow switch within high-performance networks. Where an unknown packet is usually forwarded to the controller. Assuming there are several thousand flows being forwarded per-second. DevoFlow proposes to tackle the problem by addressing short-lived (mice) and long-lived (elephant) flows separately. Switches only inform the controller about specific flows, which required more security or any other policies [20].

DevoFlow is forcing to use wild-carded rules of OpenFlow, so it can reduce interactions between switch-controller. DevoFlow mechanisms, allows the switches to make local decisions for routing when these do not actually require per-flow checking by the controller [19]. DevoFlow involves the OpenFlow controller, but puts too much load on the control plane so forcing wild-cards flow-match is reducing that load, however the controller disable to check some events [20].

• **DIFANE** is a distributed flow-based architecture built on OpenFlow switches. It aims to resolve the centralized issue by distributing the functionalities across “authority switches” and calculating matching rules at the switches themselves. The division of labor is changed by DIFANE between the centralized management system and the switches, by pulling some rule processing functions back to the switches, to achieve better scalability. DIFANE can solve the bottleneck of the current OpenFlow centralized controller by distributed some of the controller functionalities across authority switches. This authority can handle unknown packet received from other switches instead of sending packet to the controller [21].

DIFANE downgrades simpler tasks from the controller by translating high-level policies to low-level rules, and distributed the rules and processing all the packets in the switches. DIFANE reduces the memory usage for rules at the switches. So, DIFANE builds a distributed rule directory service among the switches by partitioning the rules between switches. DIFANE can be easily implemented with small software medications to commercial OpenFlow switches [22].

DIFANE architecture composed of a controller and authorized switches. The controller provides rules and

Wild card Rules	Description
Cache rules	Within the switches, the data traffic stays in the cache, where ingress switches are responsible for processing. Authority switches install the cache rules in the network.
Authority rules	The controller can update and install the authority rules in authority switches which is able to store authority rules.
Partition rules	Partition rules are installed in each switch by the controller, so packet could match one rule overall and stay in the forwarding plane.

Table I: DIFANE wild card rules

install them in the authority switches. The authority switches are receiving the packet and forward it according to the rules or encapsulate it and send it to other authority switches [23].

Ref. [21] indicate that DIFANE has three sets of wild-card rules, which can keep packet processing within forwarding plane instead to send to the controller. Wild-card rules include cache rules, authority rules, and partition rules as the following table I:

However, devolving control functions back to the switches is not easy to deploy a set of relatively rules and configurations installed in OpenFlow switches in terms of security perspectives.

C. Designing a distributed control platform

• **HyperFlow**

HyperFlow aims to have multiple controllers to manage the entire network each controller is respectable of its portion of the network [13]. HyperFlow is an application implemented on top of the NOX controller, where the implementation is changed operations, and allows reuse of existing NOX applications with minor modifications [24].

In addition, each switch makes a local decision (relies on its flow table and its controller) using the HyperFlow to passively synchronize state upon whole network of OpenFlow controllers. This can provide a local serve by controller to all packets flows, and thus significantly reduces the response time of control plane for data plane requests. Each controller in HyperFlow network has the ability to control the whole network because it has a coherent wide view of the network. If any controller fails, all affected switches have to reconfigure by themselves to join other nearest controller [13]. Thus, HyperFlow works as a centralized paradigm with centralized benefits, however it is scalable physically distributed network [25].

• **Onix**

Onix approach is to have reliability by distributed controller [12]. It provides programming API to build the network applications. Onix contents are distributed to the applications to ease distributed coordination. Onix deal with register per-packet instead of dealing with per-packet events for less frequent. Onix has been made for scalability purposes where controller can not forward packets faster than switch. Onix provides a Network Information Base (NIB), which gives access to several state synchronization frameworks with different consistency and availability requirements.

Onix has programming ability to access the network by providing control logic. In addition, Onix instance communicating with other instances via cluster, which is responsible for distributing the network state. Thus, Onix can scale large networks and provide flexibility for production deployments.

However, distributing the control platform in HyperFlow and Onix are not reliable in large data centres as they are not fully distributed.

IV. Distributed Active Information Model Theory

This section will introduce the designed architecture of the candidate system (the DAIM model). The objectives and uniqueness of the proposed DAIM model will also be discussed. It starts by describing the design goals for the DAIM model, the architectural overview of the DAIM model including databases using augmented OpenFlow protocol (DAIM protocol), within the DAIM model, and DAIM agents which is an important component of DAIM model.

A. Objectives of designing DAIM

The goals of designing DAIM is to address the research challenges such as managing the complexity of distributed electronic environment, and construct a reactive interpreter network with self-X autonomic functionalities for business needs. So, the design requirements to build the DAIM model according to [6], [26], [2] will be as following:

• Compatibility: Considering the complexity and the future grows of the networks, where there are varieties of network devices and business needs. So, DAIM will use OpenFlow-Based SDN environment as a programmable network to meet different varieties of needs. DAIM can abstract the network management model and services as network applications.

• Model simplicity: DAIM allows switches to make decisions locally. That ability is called autonomic network management. This means that the distributed self-adaptation strategies can maintain the system in the face of changing requirements and unexpected threats to provide for the defined requirement. So, Operators and programmers are no long required to handle any changes of the requirement either actively or re-actively. Network management model and services will be abstracted as network applications.

• End hosts modification: The DAIM model does not require software or hardware changing of the end hosts, where DAIM mainly focuses in forwarding packets.

• Security: DAIM is supporting security by using network security protocols. For example, the messages between System Requirement Database and OpenFlow switches, are encrypted by using Transport Layer Security (TLS).

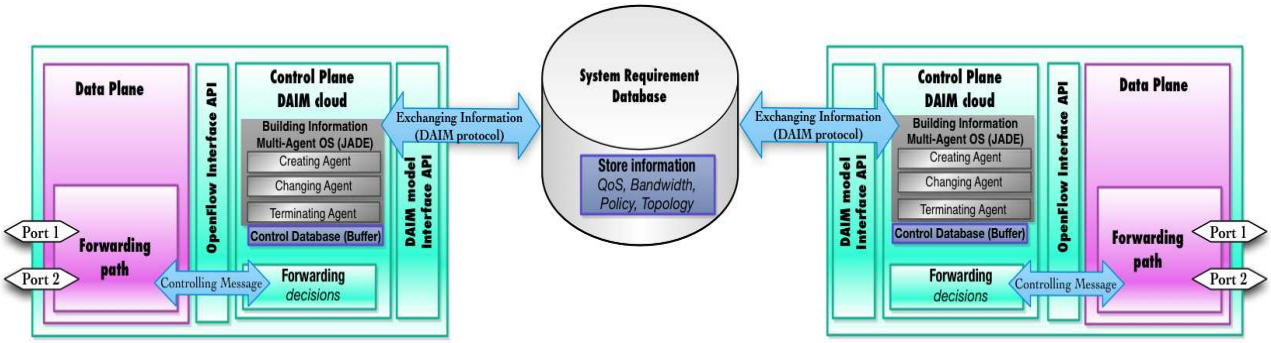

Figure 2: DAIM model architecture as an intelligent computational environment

B. Uniqueness of DAIM model

The DAIM model derives its design principles from all previous approaches. That is, dividing the control functions, and implementing them on data forwarding layer, as a distributed control plane so the switches will have more control functions. Furthermore, the DAIM model tries to solve the current issues of a centralized network control plane and difficulties to manage the network by having autonomic behaviors for network management based on DAIM agents [6], [26], [27].

There are five unique aspects of the DAIM model. Firstly, the DAIM model is a programming framework for creating a distributed control functions within the SDN environment. The DAIM model can be applied in a flow-based routing network such as OpenFlow. Secondly, DAIM model provides clear and direct control over interactions with the system requirement database, and over network state synchronization by using DAIM agents to gather information and set instruction. Thirdly, the DAIM model could solve the scalability issue of the centralization, by distributed control functions within OpenFlow switches. Fourthly, using the DAIM model in distributed network environment can solve the robustness and responsiveness issues of the current centralized paradigm. The adaptation algorithms can adapt the distributed nodes by synchronizing the state from the system requirement database. Finally, the DAIM model is not similar to the cloud computing model, where cloud computing generally has many separated computing entities, presented as a one computational infrastructure. While, the DAIM model has many of network entities, which are distributed and working independently, where each represented as independent computing environment.

C. DAIM model architecture

The DAIM model architecture is composed of a logically centralized System Requirement Database, Discover Routes Database, distributed Control Database, and DAIM agents residing in each switch as an independent computational environment. These components use augmented OpenFlow protocol called DAIM protocol for corresponding messages between them. Intelligent DAIM agents are implemented in a Java Virtual Machine environment (JVM). They interact with the databases, neighbouring switches, and exchange information with other agents to compute their own local decisions according to the business needs defined in those databases as shown in Fig. 2.

The DAIM model is implemented within each OpenFlow switch using a Multi-agent operating system, which is supported by DAIM agents as a field of distributed active artificial intelligent (AI) to enable the self-management. The basic information unit of the DAIM model is the DAIM agents and each of them include [6]:

- **Attributes:** specific variables that represent characteristics of the flow entries such as header fields, counters and actions.
- **Method behaviors:** actions that provide the autonomic functionalities such as self-awareness instantly (temperature, humidity), and self-configuration (switch down).
- **Algorithms:** algorithms for fulfillment a network task, can be embedded into DAIM agents, such as informing DAIM model if any circumstances change within the network and synchronize information between databases.
- **Messaging:** messages that can be created by DAIM model as a response of requests to get information (track host location, track topology changing and shortest route).

The Control Databases are connected together and use DAIM protocol for corresponding. At the same time each switch is connected to a System Requirement Database (SRD) and Discovered Route Database for optimizing the performance of the network.

To meet our approach of managing distributed environment autonomically, we need to analyze network operating system components. These components are supporting the DAIM agents to make local decisions in terms of forwarding, maintaining, and adapting to the unexpected changes. Components could be distributed within OpenFlow switches and databases.

The DAIM database schema holds the network information such as host identifier, business requirements, topology discovery, QoS, bandwidth, users, and global view of the entire network. The network business requirements are stored in the System Requirement and Discover Route Databases' tables, which must have well defined requirements. Records in other tables are significant only when they can be reached directly or indirectly from

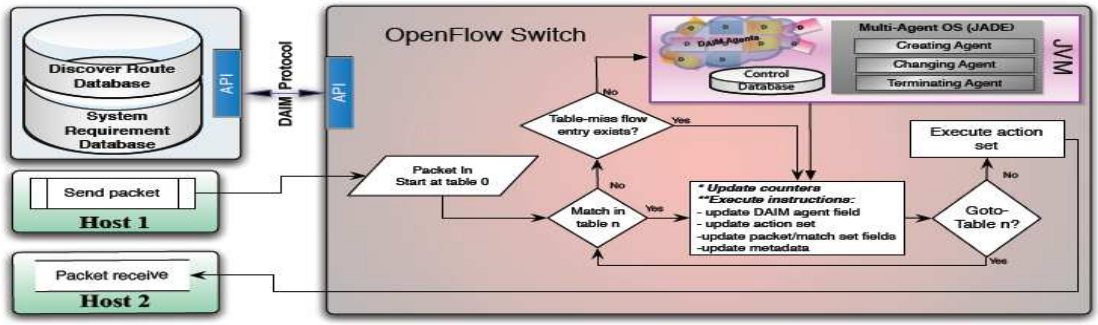

Figure 3: Flow chart detailing Packet processing within DAIM model

the System Requirement and Discover Route Databases' tables. Records that are not reachable from the root tables are automatically deleted from the databases; except for records in a few distinguish root tables.

In addition, the DAIM model uses this information to make management and local decisions. The observation includes changing of network links, network topology, changing of host location, so that would facilitate the calculation and install shortest route. The Control database resides within each switch, which synchronizes all information with other databases. Moreover, the Control database can also enhance agents to make management decisions locally and maintain the system in case uncertain changes such as failure of the main databases. There are three Databases of the DAIM model include: (1). System Requirement Database; (2). Discovered Rout Database; (3). Control Database.

We are proposing that by creating a DAIM model on the networks we could give effect to what we are calling a Reactive Interpreter Network. So it would be a truly distributed computing environment, where these DAIM agents reside in the network elements, which would be OpenFlow switches. The actual values in the OpenFlow tables, reside in the OpenFlow switches, and would then be the properties of DAIM agents. These agents would then have to do the work of modifying or adapting their values so as to implement the requirements of the network. So the whole DAIM model stretches across all these network elements and then could be thought of as reactive distributed interpreter that is interpreting the system requirements to enable the infrastructure to provide for the business needs.

V. Packet processing within DAIM model

Packet sending in this structure, using the OpenFlow environment, include DAIM, would typically depended on other structural components such as databases to obtain all network information needed, and to achieve autonomic functionalities as well as obtaining information of the entire network. Moreover, each database actively synchronizes with others according to the events registered. The DAIM cloud can publish events to databases and actively synchronize, so that other switches can reconstruct the whole information about the network. Individual switch can serve any coming packets locally or from other switches. As a benefit of databases, they give ability of self-configuration if any local change happens within individual switches, to adapt other switches. Thus, the distributed system structure has the feasibility to deploy the DAIM cloud, which has the ability to synchronize information of the entire network. As a result, it is possible to achieve that self-management when enabling all autonomic functions.

When the packet hits the OpenFlow switch, it performs the operations shown in Fig. 3. Packet headers are used for table look-ups depending on the packet type, and typically include various packet match fields, such as Source IP, Destination IP, and MAC destination address. The switch begins with performing a table look-up in the first flow table, and may perform table look-ups in other flow tables [28]. For example, the flow tables are sequentially numbered, so the packet is matched against flow entries of flow table 0. Other flow tables may be used depending on the outcome of the match in the table 0. If a flow entry is matched, the instruction set included in that flow entry is executed and the counters associated with the selected flow entry must be updated. Those instructions may direct the packet to another flow table, where the same process is repeated again. On the other hand, the instructions could forward the packet if not matched to Table-miss flow entry or the DAIM cloud.

If there is no matching rule in the flow table for that particular packet, it sends it to a Table-miss entry. The behaviour on a table-miss depends on the table configuration and using wild-carding rules. The table-miss flow entry in the flow table may specify how to process unmatched packets by other flow entries in the flow tables. This may include sending to the DAIM cloud or direct packets to a subsequent table. Moreover, the table-miss flow entry behaves similarly to any other flow entry. Where it does not exist by default in a flow table, the DAIM cloud may add it or remove it at any time, and it may expire. However, if the table-miss flow entry does not exist, by default packets unmatched by flow entries are sent to DAIM cloud.

The DAIM cloud has a multi-agent operating system such as JADE (Java Agent DEvelopment Framework) that can create, change, and terminate the intelligent

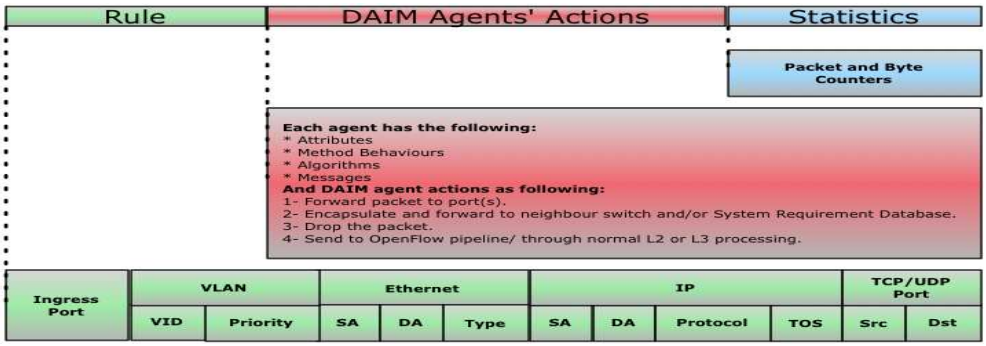

Figure 4: DAIM agent owns flow entries in the flow table

DAIM agents [29]. Essentially, the DAIM agents have the responsibility to maintain their own values, and they can adapt and modify their own value. According to the collected information DAIM agents can make their own local decisions based on the system requirements. In addition, DAIM agents will be bounded to a particular variable such as flow entry variables and have some level of self-adaptation strategy to manage the variables for forwarding according to the business needs. The properties or values are familiarity notions of object-oriented programming. Therefore the DAIM agents have the ingredients to implement autonomic behaviours. For example, when the DAIM cloud receives an unmatched packet, it creates DAIM agents which can access and control network elements such as the databases, and other switches to determine the forwarding rules. The DAIM agents should be able to check this flow against system requirements and other policies to see whether it should be allowed, and if allowed the DAIM agent needs to compute a path for this flow, and install flow entries on every switch along the chosen path. Finally, the packet itself will be forwarded (see Fig. 4)

The DAIM agents provide a distributed environment where the network information is the property (values) of software agents residing in virtual machines that are distributed throughout the network elements.

VI. Risk Scenarios of DAIM model

DAIM's current implementation comprises with central databases, which are System Requirement Database and Discover Route Database master. However, the DAIM model being distributed by synchronizes between the central databases and Control Database, which reside on each switch. So, the switch is responsible to fully serve all packets within its site, unless failure happens. If a failure happened then hosts that connected to the failure switch should be reconfigured to the nearest switch instead of that failed switch. The new switches can actively synchronize among all databases to know all the information and the requirements to serve connected hosts using adaptation strategies.

The SDN architecture relies heavily on a centralized paradigm, whereas the DAIM model is distributed. The failure consequences of the System Requirement Database and Discovered Route Database are the following:

Firstly, if the unknown flow arrives, it will not be able to forward and calculate a path to the destination. Furthermore, the switch will converts flow to be handled by Ethernet switching operation. However, the system will not perform optimally because autonomic functions will be disabled. For example, traditional Layer 2 switching capabilities, VLAN isolation, and QoS processing.

Secondly, the self-X autonomic functionalities are not able to store accumulated information in those databases, to perform some autonomic actions such as self-adaptation, self-configuration and self-protection [30].

However, the above issues can be avoided by the design and functions of Control Database (Buffer) and DAIM cloud, to maintain network state in case of any failure. Initially, DAIM model can be actively synchronized with the rest of the system components upon starting by using DAIM agents. The network information collected by these DAIM agents is served as a heartbeat of the proposed model. DAIM agents also exchange information generated by any switch and immediately synchronise them within all databases. Thus, collaboration of network elements can provide autonomic services such as self-adaptation and self-learning.

VII. Conclusions

Our approach was a combination of previous work approaches to gain a distributed active environment. This paper described the limitations of current OpenFlow-based SDN. In addition, it introduced programmability into the distributed network environment, illustrated in the SDN concept, with some level of distributed functionalities. SDN has a flow-based forwarding and separation of the control plan from the data plane, and provides new flexibility in network innovation. However, the new system requires some changes in the SDN approach. In this regard, implementation of the DAIM model through the compiled interpreted reactive paradigm within SDN environment have been proposed. Moreover, this paper introduced the concepts of autonomic communications and suggested how to implement them using the DAIM model. The new system can enable the development of different network services as network applications embedded with autonomic agents. This new paradigm

can be applied to other infrastructures or distributed environments that provide global services such as the National Broadband Network (NBN). The future work will be experimenting and evaluating the DAIM model using Omnet++ simulation, focusing specially on Open VSwitch capabilities.

ACKNOWLEDGMENT

This work is sponsored by the Centre for Real-Time Information Networks (CRIN) in the Faculty of Engineering & Information Technology at the University of Technology, Sydney (UTS).

REFERENCES

[1] ONF, 2012, "Open network foundation white paper, market education committee, software-defined networking: The new norm for networks, viewed 11-07-2012 www.opennetworking.org/images/stories/downloads/white-papers/wp-sdn-newnorm.pdf."

[2] L. Suresh, J. Schulz-Zander, R. Merz, A. Feldmann, and T. Vazao, "Towards programmable enterprise wlans with odin," in *Proceedings of the first workshop on Hot topics in software defined networks*. ACM, 2012, pp. 115–120.

[3] L. R. Bays and D. S. Marcon, "Flow based load balancing: Optimizing web servers resource utilization," *Journal of Applied Computing Research*, vol. 1, no. 2, pp. 76–83, 2011.

[4] F. Chiang and V. Mahadevan, "Towards the distributed autonomy in complex environments," in *Information and Multimedia Technology, 2009. ICIMT'09. International Conference on*. IEEE, 2009, pp. 169–172.

[5] F. Chiang, "Self-adaptability, resilience and vulnerability on autonomic communications with biology-inspired strategies," *PhD thesis University of Technology Sydney, Australia*, 2008.

[6] R. Braun and F. Chiang, "A distributed active information model enabling distributed autonomics in complex electronic enviornments," in *Broadband Communications, Information Technology & Biomedical Applications, 2008 Third International Conference on*. IEEE, 2008, pp. 473–479.

[7] J. Case, M. Fedor, M. Schoffstall, and C. Davin, *A simple network management protocol (SNMP)*. Network Information Center, SRI International, 1989.

[8] J. Strassner, S. van der Meer, and J. Hong, "The applicability of self-awareness for network management operations," *Modelling Autonomic Communications Environments*, pp. 15–28, 2009.

[9] N. McKeown, T. Anderson, H. Balakrishnan, G. Parulkar, L. Peterson, J. Rexford, S. Shenker, and J. Turner, "Openflow: enabling innovation in campus networks," *ACM SIGCOMM Computer Communication Review*, vol. 38, no. 2, pp. 69–74, 2008.

[10] Z. Cai, A. L. Cox, and T. E. N. Maestro, "Maestro: A system for scalable openflow control," Technical Report TR10-08, Rice University, Tech. Rep., 2010.

[11] J. Werner, "Description of network research enablers on the example of openflow," *New Network Architectures*, pp. 167–177, 2010.

[12] T. Koponen, M. Casado, N. Gude, J. Stribling, L. Poutievski, M. Zhu, R. Ramanathan, Y. Iwata, H. Inoue, T. Hama, *et al.*, "Onix: A distributed control platform for large-scale production networks," *OSDI, Oct*, 2010.

[13] A. Tootoonchian and Y. Ganjali, "Hyperflow: A distributed control plane for openflow," in *Proceedings of the 2010 internet network management conference on Research on enterprise networking*. USENIX Association, 2010, pp. 3–3.

[14] N. Foster, M. J. Freedman, R. Harrison, J. Rexford, M. L. Meola, and D. Walker, "Frenetic: a high-level language for openflow networks," in *Proceedings of the Workshop on Programmable Routers for Extensible Services of Tomorrow*. ACM, 2010, p. 6.

[15] M. Al-Fares, S. Radhakrishnan, B. Raghavan, N. Huang, and A. Vahdat, "Hedera: Dynamic flow scheduling for data center networks," in *Proceedings of the 7th USENIX conference on Networked systems design and implementation*, 2010, pp. 19–19.

[16] M. Jarschel, S. Oechsner, D. Schlosser, R. Pries, S. Goll, and P. Tran-Gia, "Modeling and performance evaluation of an openflow architecture," in *Proceedings of the 23rd International Teletraffic Congress*. ITCP, 2011, pp. 1–7.

[17] S. Kandula, S. Sengupta, A. Greenberg, P. Patel, and R. Chaiken, "The nature of data center traffic: measurements & analysis," in *Proceedings of the 9th ACM SIGCOMM conference on Internet measurement conference*. ACM, 2009, pp. 202–208.

[18] A. Greenberg, J. R. Hamilton, N. Jain, S. Kandula, C. Kim, P. Lahiri, D. A. Maltz, P. Patel, and S. Sengupta, "Vl2: a scalable and flexible data center network," in *ACM SIGCOMM Computer Communication Review*, vol. 39, no. 4. ACM, 2009, pp. 51–62.

[19] W. Kim, P. Sharma, J. Lee, S. Banerjee, J. Tourrilhes, S.-J. Lee, and P. Yalagandula, "Automated and scalable qos control for network convergence," *Proc. INM/WREN*, vol. 10, 2010.

[20] A. R. Curtis, J. C. Mogul, J. Tourrilhes, P. Yalagandula, P. Sharma, and S. Banerjee, "Devoflow: scaling flow management for high-performance networks," *SIGCOMM-Computer Communication Review*, vol. 41, no. 4, p. 254, 2011.

[21] M. Yu, J. Rexford, M. J. Freedman, and J. Wang, "Scalable flow-based networking with difane," in *ACM SIGCOMM Computer Communication Review*, vol. 41, no. 4. ACM, 2010, pp. 351–362.

[22] N. Mohan and M. Sachdev, "Low-leakage storage cells for ternary content addressable memories," *Very Large Scale Integration (VLSI) Systems, IEEE Transactions on*, vol. 17, no. 5, pp. 604–612, 2009.

[23] T. Mori, M. Uchida, R. Kawahara, J. Pan, and S. Goto, "Identifying elephant flows through periodically sampled packets," in *Internet Measurement Conference: Proceedings of the 4 th ACM SIGCOMM conference on Internet measurement*, vol. 25, no. 27, 2004, pp. 115–120.

[24] N. Gude, T. Koponen, J. Pettit, B. Pfaff, M. Casado, N. McKeown, and S. Shenker, "Nox: towards an operating system for networks," *ACM SIGCOMM Computer Communication Review*, vol. 38, no. 3, pp. 105–110, 2008.

[25] J. Naous, D. Erickson, G. A. Covington, G. Appenzeller, and N. McKeown, "Implementing an openflow switch on the netfpga platform," in *Proceedings of the 4th ACM/IEEE Symposium on Architectures for Networking and Communications Systems*. ACM, 2008, pp. 1–9.

[26] P. Pupatwibul, B. Jozi, and R. Braun, "Investigating o: Mib-based distributed active information model (daim) for autonomics," pp. 7–12, 2011.

[27] T. Feng, J. Bi, H. Hu, and H. Cao, "Networking as a service: a cloud-based network architecture," *Journal of Networks*, vol. 6, no. 7, pp. 1084–1090, 2011.

[28] ONF, 2012, "Open network foundation, openflow switch specification version 1.3.0 (wire protocol 0x04) viewed 20-08-2012 www.opennetworking.org/images/stories/downloads/specification /openflow-spec-v1.3.0.pdf."

[29] V. R. Komma, P. K. Jain, and N. K. Mehta, "An approach for agent modeling in manufacturing on jadeŹ reactive architecture," *The International Journal of Advanced Manufacturing Technology*, vol. 52, no. 9, pp. 1079–1090, 2011.

[30] F. Chiang and R. Braun, "Self-adaptability and vulnerability assessment of secure autonomic communication networks," *Managing Next Generation Networks and Services*, pp. 112–122, 2007.

Ameen Banjar received his B.Sc from Taibah University (Saudi Arabia) and M.I.T advanced from University of Wollongong (Australia). He is currently working towards Ph.D. degree in Computing and Communications, at University of Technology Sydney UTS, Faculty of Engineering and Information Technology. He began his working career as a database designer and programmer at Taibah University, Information Technology Centre (ITC) in Saudi Arabia, for two years. He has a research interest in network management, especially in the area of intelligent agent-based network management systems.

Pakawat Pupatwibul is currently working towards the Ph.D. degree in Information Systems, faculty of Engineering and IT from University of Technology Sydney, Australia, having graduated from Naresuan University with a B.Sc. in Computer Science, and Master's of Information Technology from UTS. He has worked attentively as a network administrator for Suan Dusit Rajabhat University, a government sponsored university in Thailand, for 7 years. His research interests include next generation networks, data center network, QoS and network management, especially in the area of intelligent agent-based network management systems.

Robin Braun received his B.Sc (Hons) from Brighton University (UK), and his M.Sc and Ph.D from the University of Cape Town. He holds the Chair of Telecommunications Engineering in the Faculty of Engineering and Information Technology of the University of Technology, Sydney, Australia. He is an executive member of the Centre for Real Time Information Networks (CRIN) at the University of Technology, Sydney (UTS). Prof. Braun was a member of staff of the Department of Electrical Engineering of the University of Cape Town from 1986 to 1998. He was the founder, and Director of the Digital Radio Research Group at the University of Cape Town, which supervised over 50 research degree candidates in the years that he was attached to it. Prof. Braun is currently a Senior Member of the Institute of Electrical and Electronic Engineers of the United States (IEEE).

An Evolutionary Game-Based Mechanism for Routing P2P Network Flow among Selfish Peers

Fang Zuo
Department of Computer Networks, Software School, Henan University, Kaifeng 475001, China
Email: zuofang@henu.edu.cn

Wei Zhang
Department of Computer Science and Technology, East China Normal University, Shanghai 200241, China
Email: wzhang@cs.ecnu.edu.cn

***Abstract*—Aimed to improving the efficiency of self-interested P2P node's routing traffic through a congested network and overcoming confusion condition caused by selfish routing in P2P networks, we introduce an evolution game-based routing model to study the selfish routing behaviors of nodes in P2P networks. In the paper, we model the routing behaviors of nodes as a noncooperative routing game, in which self-interested player's route traffic through a congestion-sensitive network. We extend the model of selfish routing to study the dynamical behaviors of nodes, by adopting a generalized approach of imitative dynamics. We not only analyze the model's stability and convergence, but reveal that the efficiency of P2P node's routing can be improved when the model reach an equilibrium state. Finally we also give an algorithm and experiments on how to improve P2P traffic efficiency based on our evolutionary game model.**

***Index Terms*—Selfish Routing; P2P Networks; Routing Efficiency; Evolution Game**

I. INTRODUCTION

The emergence of peer-to-peer(P2P) is a popular and powerful networking paradigm, which permits sharing of unlimited files and computational resources in a distributed, fault-tolerant, scalable, and manner, in many Internet applications, such as on line games, file sharing, live video streaming, etc. The basic idea of P2P is to organize a virtual overlay network on top of the physical network so that nodes in the overlay can be customized to cooperate in a flexible pair-matching manner without modifying native routers. Peer matching and cooperation among self-interested nodes in many P2P applications rely basically on routing in the networks. For example, each node in P2P file-sharing systems is responsible for selecting a full path of links to his interested destination and the node always want to seek paths of minimum cost without considering other nodes routing policy and the whole network's traffic condition. However, such egomaniacally routing will lead to over loading or long delays on one path and oscillations and chaos in traffic

How to solve these traffic and routing problems aroused by nodes selfish routing behaviors in P2P applications? Assuming that each node is responsible for selecting a full path of links to his interested destination and nodes seek paths of minimum cost, nodes in such networks correspond to the players of a selfish routing game, and how to find a mechanism to reach such an equilibrium that all paths in use by an equilibrium flow f have minimum-possible cost (given their source, sink, and the congestion caused by f) is the key factor to solve those problems mentioned above [1] [14]. In this context, we introduce a P2P network evolutionary game model as the P2P network efficient traffic optimization mechanism.

In our mechanism, we adopt a P2P network evolutionary model as a sample and intuitive way to model routing process of nodes and the traffic generated by nodes. We will use replicate dynamics mechanism to analyze the evolutionary trend of strategies among nodes and show the computational complexity of evolutionarily stable strategy and existence of the Nash equilibrium or approximate equilibrium under reasonable assumptions on the traffic latency function for a P2P network. The contribution of this work is (1) to propose a P2P overlay traffic routing model with evolutionary game-theoretic analysis to help overcome selfish routing and (2) to route traffic such that the overall average latency is minimized by using node evolutionary game mechanism, namely counteracting and imitating the other node's routing strategies; and (3) to steer the whole network system towards a stable state (also can be called equilibrium state, namely both peer optimal and network system optimal), where at such equilibrium no network user has an incentive to switch paths or route and this occurs when all traffic flow travels on the same minimum-latency paths.

The structure of the paper is as followings. In Section II, we summarize some existed researches on how to eliminate selfish routing in P2P networks. In Section III, we establish the evolution game model for P2P routing under appropriate conditions. We then focus, in Section IV, on the computation of the equilibrium, stability and convergence analysis for the model. In section V, a traffic routing optimization scheme for a P2P network will be proposed and implemented by simulation within the established model. Finally, the paper ends with the concluding remarks of Section VI.

doi:10.4304/jnw.9.1.10-17

II. RELATED WORKS

The game theoretical aspects of network routing have been of growing interest to the computer science community and some highlight researches [2] [3] [4] [5] [6] get useful results on analyzing disadvantages of selfish routing and how to eliminate it. In P2P systems, there are some interesting works on how to solve selfish behaviors under the framework of game theory. In reference [7], authors assume that users choose their routes completely without regard to the delay that their choice may cause for other users in the system. In order to discourage this selfishness in P2P system, they proposed four different self-optimization protocols are presented. The selfish protocols allow peers to modify their routing tables to suit their individual needs, and are easy to implement, but the improvements are limited. Compared to this, the altruistic protocols that allow peers to adjust the routing tables based on the needs of other processes, promise a better performance. Since selfish peers may not comply, a penalty mechanism is proposed to discourage selfishness. In this paper, authors formulated the flow f(i,j) to denote the number of packets from i to j delivered per unit time, and d(i,j) to be the latency (as measured by the number of hops) for one such communication after each peer added its strategy edges; then according to such definition, they give cost functions of each peer. Specific formulated analysis of protocols showed that altruistic approach is much better than selfish ones, however, concrete simulations was not given in the paper.

Fabrikant [8] presented a game theoretic view of network creation by selfish agents, and studied the existence of Nash equilibria under various cost models. Subsequently, many researchers (for example [9]) extended this to P2P systems. Moscibroda et al [9] studied the effects on the topology of a P2P network if peers selfishly select the peers to connect to. For the perspective of price of anarchy, authors showed that P2P topologies formed by selfish peers under Fabrikant's cost model may not stabilize, even if there is no churn. Extreme selfishness in neighbor selection can be detrimental, since it can cause network partition.

In reference [10], authors give another game theory schema for selfish routing in Internet, especially in overlay networks (such as P2P systems or Detour). In this paper, authors firstly analyze how selfish overlay routing results in poor performance in Internet-like environments (i.e., under realistic overlay network topologies and various traffic demands) and how such selfish traffic affects the remaining traffic routed using the traditional routing protocols. Then they use game model to formulate selfish routing in overlays and structure a complete simulation to reveal that in contrast to theoretical worst cases, selfish routing achieves close to optimal average latency in such environments by using metrics such as average latency, max link utilization, etc. However, such performance benefits come at the expense of significantly increased congestion on certain links. Moreover, the adaptive nature of selfish overlays can significantly reduce the effectiveness of traffic engineering by making network traffic less predictable.

In [11], authors model P2P networks as competition game for bandwidths and design a selfish-proof overlay network and routing mechanisms to permit efficient bandwidth allocation and gives incentive for nodes to share information and provide services. In this work, nodes is to enable service differentiation in bandwidth based on the amount of services each node has provided to its community, thereby encouraging all network nodes to share resources and make the allocation of network bandwidth fairness.

Koloniari and Pitoura [12] have modeled peers in a clustered overlay as players that dynamically change the set of clusters they belong to according to an individual cost function, which is based on a cluster membership cost and the recall for their local query workload. Authors compared the strategies based on different motives behind the peers behavior (selfish or altruistic) and showed how by following them, the peers can change the clustered overlay to reflect the current system conditions thus, maintain its quality under updates. Their experimental results showed that altruistic strategies are able to cope well with the changes and gradually improve system performance by reducing the query latency and routing time.

Besides game theory based approaches for selfish routing and selfishness of peers, there are some works to study how to eliminate the selfish routing in P2P systems by using non-game theoretic methods. Self-optimization protocols [13] were proposed in structured p2p networks (DHT) for restricting the selfish routing selection in the clusters, and reducing the deployment of inactive nodes for further reduction of the routing latency via request profiling and identifying interest-based clusters.

III. P2P TRAFFIC ROUTING MODEL WITH EVOLUTION DYNAMIC

Routing, one of the most basic tasks in P2P network, has been view as a large multi-valued optimization problem. So the selection of the path on the various routes greatly impacts the overall P2P application performance. As part of the optimization process, the goal of different individual peers is contrasted with the selfish desire and aim to achieve a high utilization of the network resources. The strategy space of peers is also far richer than the binary choice of share/not-share, corporation/non-corporation etc. Peers make strategic decisions concerning the revelation of private information and non-observables hidden actions, such as local resource availability, workload, contribution cost, or willingness-to-pay. Peers may adjust their routes within the network through strategy churning.

Therefore, in order to limit P2P nodes' disordered routing behavior and make P2P network robust, we model nodes' strategies accurately firstly and deduce a P2P evolving mechanism to standardize peers' strategic behaviors and encourage peers' traffic flow to achieve a Nash flow.

A. Preliminary

In P2P network, since the interactions of nodes are happened randomly, each node is lack of global network information and other peers' strategy information. This characteristic of nodes can be regarded as bounded rationality in the incomplete information peer game. Regarding to the different strategies, the adjustment period of a node selecting its dominant strategy is a gradual process, which can be model by imitative dynamics of evolution game to simulate nodes' learning and strategic adjustment process in network. In the following context, we will give some important definitions and preliminaries about our research.

Considering an initial population of peers in P2P network, each node is assigned a pure strategy. At some point of time, each node pairs another node chosen uniformly at random and observes its own and its opponent payoff and decides whether to imitate its opponent or not by adopting its strategy with probability proportional to the payoff difference. Nodes interaction is regarded as evolutionary game with a payoff function F. Let A denote the set of actions available to both players, and let $\Delta(A)$ denote the set of probability distributions or mixed strategies over A, then $F:\Delta(A)\times\Delta(A)=\Re$. Suppose that there is a $(1-\varepsilon)$ fraction nodes who play strategy s, and call these nodes-incumbents, and suppose that there is a ε fraction who play t, and call these nodes-mutants. The strategy s is an ESS if the expected payoff of a node playing s is higher than that of a node playing t. Since an incumbent will meet another incumbent with probability (1- ε) and it will meet a mutant with probability ε, we can calculate the expected payoff of an incumbent, which is simply $(1-\varepsilon)F(s\mid s)+\varepsilon F(s\mid t)$. Similarly, the expected payoff of a mutant is $(1-\varepsilon)F(t\mid s)+\varepsilon F(t\mid t)$. Thus we come to the formal definition of the P2P-ESS according to reference [14, 17].

Definition 1: If nodes interact, a strategy s is a P2P evolutionarily stable strategy (P2P-ESS) for the P2P evolutionary game given by payoff function F, if for every strategy t ≠ s, there exists a ε_t such that for all $0<\varepsilon<\varepsilon_t$,

$$(1-\varepsilon)F(s\mid s)+\varepsilon F(s\mid t)>(1-\varepsilon)F(t\mid s)+\varepsilon F(t\mid t)$$

Definition 2: Evolution game imitative dynamics in P2P. Let x_i denote the fraction of nodes playing strategy i, node population vector $\vec{x}$ and payoff function *f*.

$$\begin{aligned}\dot{x}_i &= \lambda(\vec{x})x_i[Ef(x_i)_{payoff}-\overline{E}f_{payoff}]\\ &= \lambda(\vec{x})x_i((\vec{A})_i-\vec{x}A\vec{x})\end{aligned}\quad(1)$$

where, $A = (a_{ij})$ is the payoff of strategy i. The function $\lambda(x)$ accounts for the growth rate of node's population. As a fact, one can join or leave a P2P network freely and the growth rate of the node's population does not depend on the network's latency; so that we choose $\lambda(x) = 1$ or any other constant to replace $\lambda(x)$ in following context.

Let $G = (V, E)$ be a P2P overlay network with latency function $L(\cdot)$ and with vertex set V, edge set E, and k source-destination vertex pairs $\{ s_1, t_1\},\ldots, \{ s_k, t_k \}$. We also assume that from source vertex s to destination vertex t denote the set of s-t paths by P. Each edge $e\in E$ is given a load-dependent latency function that we denote by $l_e(\cdot)$. We assume that l_e is nonnegative, continuous, and non-decreasing. The latency of a path *p* with respect to a P2P traffic flow f is then the sum of the latencies of the edges in the path, denoted by $l_p(f)=\sum_{e\in p}l_e(f_e)$. We call the triple (G,t,l) a P2P network traffic model. With respect to a finite and positive traffic rate t, where $\sum_{p\in P}f_p=t$. We define the payoff $C(f)$ of a flow f incurred by a node in G choosing path *p*, $C(f)=\sum_{p\in P}l_p(f)f_p=\sum_{e\in E}l_e(f_e)f_e$.

Definition 3: Flows at Nash Equilibrium. A flow f feasible for (G,t,l) is said to be at Nash equilibrium (or is a Nash flow) if for every two s-t paths *p1*, *p2* ∈ P with $f_{p1} > 0$, $l_{p1}(f) \le l_{p2}(f)$. Nash flow means the latency of unused paths is equal or even greater than the latency of used paths. In particular, all latencies of used paths belonging to the same node group or the same node type are equal.

Definition 4: Equivalence of equilibrium and optimal flows. Optimal Flows means every flow that minimizes total latency. As we can see, the optimal flow is the P2P traffic system optimal solution; the situation in such optimal solution is often an ideal state, where most optimization methods can not achieve such a best situation.

Assuming mild extra conditions on the latency functions of an instance, there is a well-known characterization of optimal flows that mirrors the definition of Nash flows. Let (G,t,l) have the property that, for each edge e, the function $x\cdot l_e(x)$ is convex and continuously differentiable. We define the marginal cost function $C(e)=x\cdot l_e(x)$. Then, a flow f' for (G,t,l) is optimal if and only if it is at equilibrium flow for (G,t,f').

B. P2P Routing Model with Imitative Dynamics

We use replicate dynamics mechanism to analyze the evolutionary trend of strategies among nodes. Peers adopt replication or imitation method for choosing and updating their strategies.

We are given a P2P network and a rate of traffic between a source peer node and a destination peer node, and seek an assignment of traffic to source-destination paths. We assume that each peer node controls a negligible fraction of the overall traffic, so that feasible assignments of traffic to paths in the network can be modeled as end to end flows in the triple (G,t,l). We also assume that the time needed to traverse a single link of the network is load-dependent, that is, the common latency by all traffic on the link increases as the link becomes more congested. In the absence of network regulation, peer nodes often act in a selfish manner.

Under this assumption, our aim is to expect network traffic to converge to Nash flow.

Generally speaking, the latency functions are strictly increasing, and then Nash flows are ESS, the proof referred to [14-16]. Consider an initial population of peer nodes in which each node is assigned an arbitrary pure strategy (original arbitrary route from itself to its target node). At each point of time, each node plays against an opponent chosen uniformly at random from its neighborhood network domain. The node observes its own and its opponents latency as payoff and decides to imitate its opponent by adopting its strategy. One could argue that how often it is not possible to observe the opponent's latency. In this case, consider a random aspiration level for each node. Whenever a node falls short of this level, it adopts a regular observed strategy. We use evolution dynamics formulation to express the above scenario, the evolution dynamics process can be defined as:

$$\frac{dx}{dt} = \lambda(\vec{x})x[l(\vec{x}) - \bar{l}(\vec{x})] \tag{2}$$

To analyze the dynamics to either a Nash flow, it is necessary to compute the rate of change of the amount of flow over each path. We will use the notation x' to denote the derivative with respect to time of the variable x, that is, $x' = dx/dt$.

Let x_p the amount of P2P flow routed over path *p*, $x_e = \sum_{e \in P} x_p$ is the total load of edge e. And p can also be seen as the fraction population of nodes choosing route *p* at some given point of time, that is, x_p is a probability of nodes selecting route *p*.

We combine the individual values x_p into a vector X. The vector $X = (x_1, x_2, \ldots, x_p)$, which is indexed by the paths in number P, will describe number of the flows over G at a given point in time. A flow *x* is feasible if it routes 1 unit of flow from s to t. Let The total latency of an edge is denoted $l_e(x_e)$ and the total latency of a path is the sum of the latencies of the edges in the path, $l_p(X) = \sum_{e \in p} l_e(x_e)$ and the average latency of the entire network is $\bar{l}(\mathrm{X}) = \sum_{p \in P} x_p l_p(X) \big/ t$.

We use $l_p(X)$, $\bar{l}(X)$ and x_p replace those variables in equation(2), and will get:

$$x_p{}' = \frac{dx_p}{dt} = x_p[l(X) - \bar{l}(X)] \tag{3}$$

Intuitively, Equation 3 shows that paths with below average latency will have more agents switching to them than from them; paths with above average latency will have more agents switching from them than to them. Since the equation (3) contains cubic term $x_p{}^3$, according to reference [16, 17], we can deduce that there is no general method for solving this differential equation. But it can be found that under some reasonable conditions stable points of this dynamics will meet with Nash equilibria.

In next section, we bound the time it takes for the system to converge to an approximate equilibrium, meanwhile we would like to give the stability analysis about our P2P imitative dynamics model.

IV. Stability and Convergence Analysis

In this section, we exploit the stability and convergence characterizations of Nash flow and of P2P ESS in our model.

A. Existence of Flows at Nash Equilibrium

Theorem 1. A P2P instance (G,t,l) evolution game dynamics process $x_p' = x_p[l(X) - \bar{l}(X)]$ with continuous nondecreasing latency function, (a) There is at least one feasible Nash flow in (G,t,l), namely there exits at least one solution $x^*(t)$ in equation (3) and (b) if t x_e, $\tilde{x}_e$ are also Nash flow for (G,t,l), then $l_e(x_e) = l_e(\tilde{x}_e)$ for every edge e. Property (b) of theorem 1 means that a flow f is at Nash equilibrium then all s-t edges have equal latency in the P2P routings.

Proof. We assume that $x(t)$ is a solution of equation (3). Let x^* be in equation (3).

$$\begin{aligned}
\sum_{p \in P} x'_{p|x=x^*} &= \sum_{p \in P} x_p[l(X) - \bar{l}(X)] \\
&= \sum x^* l(X) - \sum x^* \bar{l}(X) \\
&= \sum x^* \cdot \sum x^{*-1} \sum x^* l(X) - \sum x^* \bar{l}(X) \\
&= x^* \cdot \sum \bar{l}(X) - \bar{l}(X) \sum x^* \\
&= \sum x^* \bar{l}(X) - \sum x^* \bar{l}(X) \\
&= 0
\end{aligned}$$

$\sum_{p \in P} x'_{p|x=x^*} = 0$, therefore $\sum x_p$ is a constant at Nash equilibrium. Since $x_e = \sum_{e \in P} x_p$, then $l_e(x_e)$ is also a constant for every edge.

B. Stability Analysis

Theorem 2. The triple (G,t,l) with nonnegative, continuous, and non-decreasing latency function $l(\cdot)$ in evolution game, if flow *x* is at a Nash equilibrium, then $xl(y) < yl(y)$ for all *y*, and hence *x* is evolutionary stable.

Proof. According to Definition 1, we will give formalized proof about the proof.Let *x* be a Nash equilibrium. Since *x* is in a Nash equilibrium, all latencies of used paths belonging to the same commodity are equal and he latency of unused paths is equal or even greater than the latency of used paths. Therefore $xl(y) < yl(y)$ for all population *y*.

C. Conergence Analysis

It has been shown that as time goes to infinity, any initial traffic flows that has support overall paths will eventually converge to a Nash flow. It seems lack of techniques for figuring out how to yield a bound on the

time to convergence of Nash flow [14]. So we do not go into specific details of the Nash flow convergence analysis in our model. Since this subsection is focused on convergence properties of our dynamics model, we shall instead give more attention to another result, which bounds the time of convergence to an approximate equilibrium.

To analyze the convergence of the dynamic of P2P imitative model to an approximate equilibrium, we will give some definition and theorem about approximate equilibrium.

Definition5 ε-approximate equilibrium: Let P_ε be the set of paths that have latency at least $(1+\varepsilon)\overline{l}$, that is $P_\varepsilon = \{p \in P \,|\, l_p() \geq (1+\varepsilon)l\}$, and let $x_\varepsilon = \sum_{p \in P_\varepsilon} x_p$ be the number of agents using these paths. A population $\vec{x}$ is said to be at a ε-approximate equilibrium if and only if $x_\varepsilon \leq \varepsilon$.

This definition ensures at such equilibrium that only a small fraction of agents experience latency significantly worse than the minimal latency. In contrast, the definition of a Nash flow requires that all agents experience the same minimal latency.

Theorem 3. The imitative dynamics converge to a ε-approximate equilibrium within time $O(\varepsilon^{-3} \ln(l_{\max} / \hat{l}))$, where $l_{\max}$ mean the maximum latency; $\hat{l}$ means the minimum latency of the traffic flow.

This theorem reveals the upper bound on the time it takes for reach an approximate equilibrium for imitative dynamics model; and also reveals that algorithm based on imitative dynamics model can be achieved within polynomial time. More details about proving the convergence of imitative dynamic to such approximate equilibrium can be referred to works [14] [15].

V. Case Study and Simulation

The preceding section gives theoretical foundation about our schema. In this section, we carry on a concrete example and algorithm specification to illustrate our aims by simulations.

A. Evolution Game Routing Algorithm for P2P(EGRAP)

Our P2P imitative dynamics model can be deduced to form an optimal algorithm for how to converge to a Nash flow in P2P application and how to reduce bottleneck caused by routing oscillations and selfish routing. Intuitively, we expect each unit of such a flow to travel along the minimum-latency path available to it, where latency is measured with respect to the rest of the flow. Otherwise, this flow would reroute itself on a path with smaller latency.

Recalling that the problem of finding the cost of a flow f is expressed $l_p(X) = \sum_{e \in p} l_e(x_e)$, note that the problem of finding the minimum latency feasible flow in a P2P network will follow the optimal program:

Min $\sum_{e \in p} C_e(f_e)$

Subject to:

$$\sum f_p = t_i \qquad \forall i \in \{1, \cdots, k\}$$

$$f_e = \sum_{e \in p} f_p \qquad \forall e \in E$$

$$f_p \geq 0 \qquad \forall p \in P$$

$$C_e(f_e) = l_e(f_e) f_e$$

According to those above optimal program description, the pseudo-code of the original EGRAP algorithm shown in Figure 1, where rNum is the number of running round.

Evolution Game Routing Algorithm for P2P (EGRAP)
1. initializing connection using Bit Torrent protocol
2. **for** i =1 to rNum **do**
3. {for node i gets itself $l_i^{\min}$ and its opponent's $\hat{l}_j$
4. solve the $x' = x[l_i^{\min}(x) - \hat{l}_j(x)]$ and get x
5. compare payoff of node i and node j value x_i and x_j
6. **If** $x_i - x_j > 0$,
7. node i will change strategy to the path of $\hat{l}_j$
8. **Else** keep the same path
}

Figure 1. Evolution game routing algorithm for P2P application

First, when a node i wants to start an application session in P2P network, it determines one route randomly. The node tests the latency of edges by query packet and then marks this edge with minimum latency $l_i^{\min}$ as connection path to send data packets.

Second, nodes will choose their best routing path according to their payoff of routing strategies by computing $\delta = x_i - x_j$. If $\delta>0$, the path of $l_i^{\min}$ will be replaced by the path of $\hat{l}_j$; if $\delta<0$, the path of $l_i^{\min}$ will still be a routing path in the network.

Third, with the evolution game process in the peer routing, all nodes will gradually achieve a Nash flow statement, where large populations of nodes may converge towards routing equilibrium. If the latency of one node's path is less than the latency of the other agent's path, the agent experiencing higher latency switches to the lower latency path with probability proportional to the difference in latencies. So that flow reroutes itself on a path with smaller latency and the total cost $\sum_{e \in p} C_e(f_e)$ of the paths in P2P network is also in the lowest values.

B. Simulation and Evaluation

Network: Each peer in homogeneous environment has a set of neighbors with which it communicates by message passing. Links are directed. Traffic can however flow in both directions on the links. We consider a P2P network made of total 1024 nodes and each node has 2 Mbps capacity in both directions.

Application: Our implementations for BitTorrent-based application are carried on the java-based simulator "peersim", where peers are organized in an overlay network. We follow the simulation methodology and implement in the selfish routing of BitTorrent protocol, and we implement additional type of BitTorrent:

evolution game routing algorithm for BitTorrent, in which a peers use imitative mechanism to choose Nash flow paths. Both in selfish BitTorrent and the EGRAP for BitTorrent, trackers choose peers randomly and peers compare their strategies randomly. When a peer completes the download, it reports the event to the tracker. In addition, peers regularly report information such as the total amount of data downloaded so far, the number of bytes that still need to be downloaded, downloaded traffic rate, etc. The tracker keeps all the information in the log files. Hence, we can analyze the tracker log files and retrieve useful information.

Content: In the simulations, 50 unique files of 256 MB are introduced into the system. Each file has been stored at different locations chosen at random. For each experiment, we run the simulation multiple times and the variance in results from multiple rounds is just low, always <10%.

1) Complete Time:

We take completion time as a metric. It measures the downloading performance of selfish BitTorrent and Evolution Game Algorithm for P2P (EGRAP) and it is also a metric for evaluate the whole system efficiency. It is defined as the total time for a swarm of peers to finish downloading files.

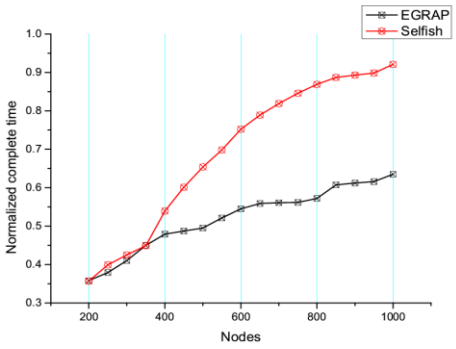

(a)

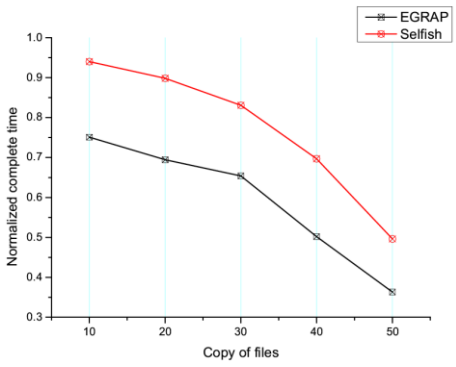

(b)

Figure 2. Complete time

In first scenario, we begin the experiment with 200 nodes and 50 files as seeds in the network at first stage then join nodes into the simulation gradually and the number of nodes will be 1024 at final. Fig.2 (a) plots the curve of complete time for two applications. At first time, the difference of complete time between selfish BitTorrent and evolution game routing algorithm seems very small. However, with the incensement of the number of nodes, EGRAP's result performs much better than selfish BitTorrent. In EGRAP, peers reach a approximate Nash equilibrium after a period time, so that they are routing efficiently in the equilibrium state and their complete time do not increase sharply than selfish BT. Clearly, the reason that EGRAP can perform better is due to the evolving process in peers routing, which makes peers select their route by comparing and learning others' strategy in order to find lower latency path and makes peers more interested in achieve Nash flow.

In the second scenario, we begin the experiment with 1024 nodes and 10 files as seeds in the network firstly. Fig. 2 (b) plots the results of this scenario. As shown in the figure, EGRAP' downloading complete time is always shorter than selfish one with respective of incensement of the number of file copies. In both two scenarios, the EGRAP's complete time is dominant to selfish manner.

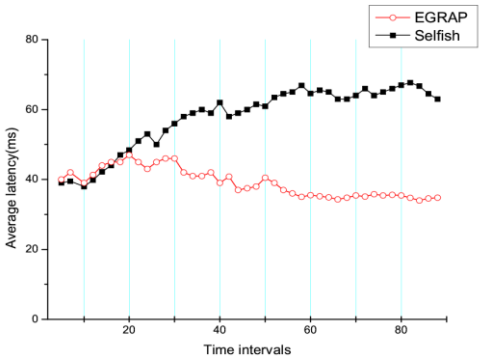

Figure 3. Latency comparison

2) Latency Comparing:

During every 5-minute time interval, we plots the curve of average latency under different routing paths by computing the traffic equilibria based on the current topology and traffic demands using the approach in EGRAP and in selfish BT in the network with 1024 nodes and 50 copies of file. Given a rate of traffic between each pair of nodes, and a latency function for each edge specifying the time needed to traverse the edge given its congestion. In our experiment we define the ratio of the sum of nodes' FIFO buffering time and the number of nodes as average latency time. Average latency time reflects the downloading performance of applications. As shown in Fig.3, improved BT performs better than selfish manner after a long run time. Considering the average latency time in relation to system expense such as the CPU load and memory cost the nodes have available, it can be seen that the more average latency time nodes have, the more system expense needed to complete downloading tasks. Meanwhile since there is more time needed to empty the queue of packets in selfish BT and routing requests that make into it will always be added at the end, it takes

considerably longer time to process the amount of queries and the time the packet spends waiting to be handled is increased.

That is because the EGRAP algorithm would converge to an approximate Nash flow with minimum average latency after nodes evolution game process in routing, while the selfish algorithm would still in routing chaos situation. In selfish BT performance such a selfishly motivated routing assignment of traffic to paths will not minimize the average latency; hence, it carries the cost of decreased network downloading performance.

3) Link Occupation:

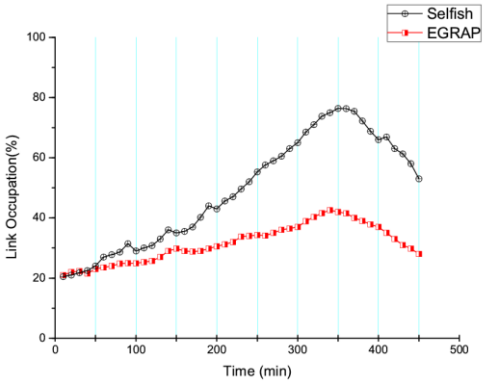

Figure 4. Link occupation

Fig. 4 plots the link occupation of two applications. We collected the log files of the BitTorrent tracker for a time period of 400 minutes in the network with 1024 nodes and 50 copies of file. For concreteness, the case of traditional ISP traffic engineering for link occupation can be shown as $(b_e + \sum t_{peer\,i\,j}) / c_e$, where b_e is the amount of background traffic on edge e (i.e. http traffic) and c_e is the capacity of edge e, and $t_{peer\,i\,j}$ indicates traffic of edge e on the route from node i to j of application session in the P2P network [18]. In this scenario, we take link occupation as metric and simplify the format of link occupation. Here, link occupation means the ratio of between the sum of packets sampled of BT application and the whole link capacity. The higher link occupation is, the more congest the nodes shares. Fig.4 shows that the line of EGRAP has less half link occupation than selfish in peak situation. This is because evolution game based algorithm for BT will get efficiency use of links by achieving a Nash flow statement. The both curves of two methods' results is not be plotted completely in Fig.4, the remaining curves will be foresighted as such situation that the red line will firstly reaches zero point and the dark line will reaches zero point more later than red line, which means EGRAP algorithm always shares a smaller link occupation than selfish.

4) Bottleneck Comparing:

In this scenario, we define bottlenecks typically are at the links of over 10000 packets. Fig.5 and Fig.6 show the bottleneck comparison between selfish BT and improve BT in the network with 500 nodes and 50 copies of file.

Fig. 5 plots the normalized result of bottleneck paths as a function of time during every 5-minute time interval. The normalized result of bottlenecks can be expressed by percentile format of $\sum path_{bottlenecks} / \sum path_{observed}$. $\sum path_{bottlenecks}$ is the numbers of bottleneck path on the snapshot of sampled time and $\sum path_{observed}$ reflects the numbers of paths used on the point of sampled time. This normalized result shows the ratio of bottleneck paths and used paths on the sampled time. As shown in the plot, the selfish BT application suffered an explicit higher bottleneck than improved one, especially began from the time intervals at 30. Reasons of this phenomenon can be concluded that larger amount of bottleneck traffic caused by disordered search in selfish BT routing behaviors. Whereas, improved BT can perform a well-ordered routing strategy with small latency first from a global view, so the numbers of bottlenecks can be reduced and the efficiency of the whole network will also be better than the selfish.

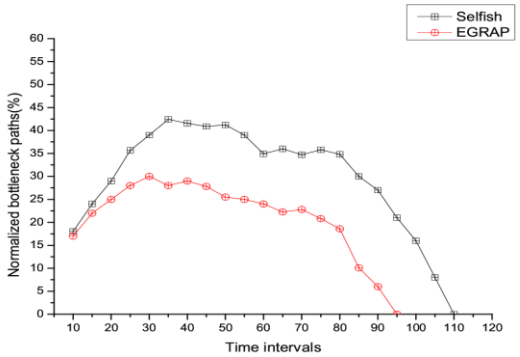

Figure 5. Normalized bottlenecks

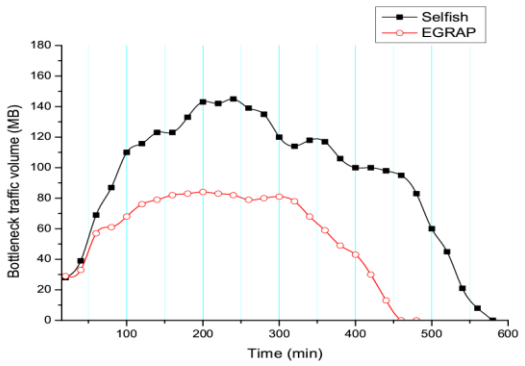

Figure 6. Traffic volume on bottleneck links

Fig. 6 plots the total traffic volume of both selfish BT and improved BT on bottleneck paths. The bottleneck traffic volume means the total traffic volume on bottleneck paths (bottleneck path threshold >10000 packets) of both selfish BT and improved BT, namely $\sum_{threshold>10000} traffic_{bottlenecks}$.

In Fig. 6, as we can see that the total traffic volume of selfish BT on bottleneck paths is larger than those of EGRAP in the whole experiment period. Specifically,

selfish Bit Torrent results in more than 40% higher traffic volume on the bottleneck links at peak minutes. Bottleneck traffic volume curve of selfish BT increases sharply than that of EGRAP at the beginning stage and goes down undulatingly after reaching peak point. That is because selfish and out of order routing in selfish BT will make all send packets jammed on paths instead of arriving destination unobstructed. Compared against selfish BitTorrent, EGRAP significantly reduces P2P bottleneck traffic, also achieving objective of minimizing whole system's traffic volume.

VI. CONCLUSION

In this paper, we presented an evolution game based model for how to eliminate selfish routing behaviors and improve routing efficiency in P2P applications. Specifically, we proved that a proximate Nash equilibrium exists; under which each peer travels along the minimum-latency path available to it. On the other hand, nodes are motivated to use the algorithm because it guarantees Nash equilibrium. We also implemented some empirical evaluations for the complete time, the average latency, link occupation and bottleneck traffic etc, which explicitly give us insight on how the network performance is improved by using evolution game algorithm for P2P application.

REFERENCE

[1] L. Qiu, Y. R. Yang, Y. Zhang, and S. Shenker, "Selfish routing in Internet-like environments," *In Proc of SIGCOMM, Karlsruhe, Germany*, 2003.

[2] T. Roughgarden, *Selfish Routing and the Price of Anarchy*, MIT Press, 2005.

[3] T. Roughgarden. "Selfish routing with atomic players," In Proc. 16th Symp. *Discrete Algorithms*, pp. 1184–1185, 2005.

[4] T. Roughgarden. "On the severity of Braess's Paradox: Designing networks for selfish users is hard," *J. Computer System Sci*., 72(5) pp. 922–953, 2006.

[5] G. Christodoulou and E. Koutsoupias, "The price of anarchy of finite congestion games," *In Proc. 37th Symp. on Theory of Computing*, pp. 67–73, 2005.

[6] R. Cominetti, J. R. Correa, and N. E. S. Moses, "Network games with atomic players," *In Proc. 33rd Intl. Colloq. in Automata, Languages, and Programming*, LNCS 4051:525–536, 2006.

[7] Bhattacharya, A. and Ghosh, S., "Self-optimizing Peer-to-Peer Networks with Selfish Processes," *SASO '07. First International Conference on*, vol. 9, no. 11, pp. 340-343, 2007.

[8] Fabrikant A, Luthra A, Maneva E, Papadimitriou C. H., and Shenker, S, "On a Network Creation Game," *ACM PODC*, pp. 347-351, 2003.

[9] Moscibroda T, Schmid S, Wattenhofer, R, "On the Topology formed by Selfish Peers," *ACM PODC* 2006.

[10] Lili Qiu, Yang Richard Yang, Yin Zhang, Scott Shenker, "On selfish routing in internet-like environments". *IEEE/ACM Transaction on Network* vol. 1063-6692. 14 No. 4, pp. 725-738, 2006.

[11] Richard T. B. Ma, Sam C. M. Lee, "Incentive and service differentiation in P2P networks: a game theoretic approach," *IEEE/ACM Transactions on Networking*, Volume 14 Issue 5, 2006.

[12] Georgios Smaragdakis, Nikolaos Laoutaris, Azer Bestavros and John W. Byers, "Selfish Overlay Network Creation and Maintenance," *IEEE/ACM Transactions On Networking*, Vol. 19, No. 1, Apr 2011.

[13] Alina Bejan and Sukumar Ghosh, "Self-optimizing DHTs Using Request Profiling", *Lecture Notes in Computer Science*, 2005. Springer Berlin.

[14] Noam Nisan, Tim Roughgarden, *Algorithmic Game Theory. Cambridge University Press*, New York. 2007.

[15] K. Etessami and A. Lochbihler, "The computational complexity of evolutionarily stable strategies," *Technical Report TR04-055, Electronic Colloquium on Computational Complexity*, 2004.

[16] N. Nisan, "A note on the computational hardness of evolutionary stable strategies," *Technical Report TR06-076, Electronic Colloquium on Computational Complexity*, 2006.

[17] Jorgen W. Weibull, Evolutionary Game Theory, *MIT press*, 1995.

[18] Haiyong Xie, Y. Richard Yang, "P4P: Provider Portal for Applications," *Proceedings of SIGCOMM'08*, 17–22, 2008.

Fang Zuo received the B.Sc. degree in computer science in 2005 and the M.Sc. degree in applied mathematics in 2008, both from the Henan University. He got his Ph.D. degree at East China Normal University, in 2013. He is now an assistant-professor in Henan University. His research interests are in P2P networks, distributed multimedia systems, algorithmic game theory and mathematical optimization theory.

Wei Zhang is now a professor of department of Computer Science & Technology in East China Normal University. His research interests are wireless sensor network, computer networks and communication technology, network applications and management, multicast technology, network protocol conformance testing.

IDDTL: A Novel Identified Internet Data Transport Layer Mechanism

Yangyang Gao, Fei Song, and Yajuan Qin
Next Generation Internet and Interconnection Devices Laboratory, Beijing Jiaotong University, Beijing, China
Email: 09111032@bjtu.edu.cn, {fsong, yjqin}@bjtu.edu.cn

***Abstract*—This paper proposes an identified data transport layer (IDDTL) mechanism, which is implemented based on our present concepts of connection identifier (CID) and CID additional information (CID-info). Since the fast evolved Internet scale and largely emerging various applications, especially with the new Internet architectures developed such as information centric network (ICN), the traditional end-to-end transport model has been exposed many defects in sorts of aspects, such as network management, flexibility and security. The novelty of the mechanism consists of two points: 1) it always conceals part of the communication information during the specific data transport process; 2) it splits the whole end-to-end communication process into two segments and forms a three-party and two-segment communication process model. Performance analysis shows that the mechanism could easily mitigate the problems such as distributed denial of service (D/DOS) attacks and greatly improve the network management, flexibility and mobility. Furthermore, our simulation and test results demonstrate that IDDTL can be implemented with unique identifiers within an acceptable extra time cost of about 3.6 useconds compared with the traditional end-to-end model.**

***Index Terms*—Connection Identifier; Three-Party and Two-Segment Communication Process; Security; Mobility; Management; Cost Evaluation**

I. INTRODUCTION

In the early days of the Internet TCP/IP suite design, it does not anticipate the later rapid development and new requirements. There are three key points leading to the drawbacks of the traditional Internet: 1) data packets are just delivered with best-effort model; 2) the Internet protocol (IP) addresses are semantic overloaded by the identity and the network locators; 3) the data delivery process directly exposes the IP addresses and their port numbers to all network nodes. The three points are the root of the problems of security, scalability, multi-homing support, mobility, flexibility and management. They are just the directions for improving the Internet at the same time.

Many research communities have dedicated in designing a new Internet architecture and naming mechanism intending to solve the problems. A successful Internet architecture modification is the Locator/Identifier Separation Protocol (LISP) [1]. It separates the IP addresses into two semantic identifiers. The host identity protocol (HIP) [2] proposes the mechanism of host identifiers to substitute IP addresses. The Internet indirection infrastructure (I3) [3] offers a new architecture for indirect communication and uses the identifiers to forward the data packets. Recently, the information centric network (ICN) gained the attention of research community. It revolutionizes the IP-based Internet concept by proposing the in-network caching and communication based on the interest packets. [24]. All the above solutions could be classified into two types: 1) they substitute IP address with new IDs to cope with its semantic overload; 2) they change the traditional end-to-end data transport process within the new Internet architectures.

This paper focuses on the data transport process to solve the drawbacks of the traditional Internet, which has not been well studied. As in the previous research, we analyzed the performance of reliable transmission on multiple paths and single path [25]. As shown, in general, both multiple paths and single path transmissions are just typical patterns of transmission connections.

In this work, we propose a connection identifier (CID)-based overlay transport system that embeds the service obtainment process-related information in its internal structure (CID-info). Starting from the definition of CID and CID-info, we present the overall system architecture based on CID managing nodes and CID mapping nodes. Based on the proposed structure, we can separate the host identity identifiers and port numbers from the packet header in order to protect them from being exposed to malicious hosts. Further, we can split the original end-to-end communication process into two segments. This architecture could facilitate the above two kinds of separations in the Internet and thereby improve the network performances greatly.

The rest of this paper is organized as follows. Section II states why we need IDDTL. The overview of IDDTL is illustrated in section III. What the IDDTL is made up of is shown in section IV. The deployment of IDDTL over existing networks is described in Section V. Section VI discusses the solutions to the Internet traditional problems of IDDTL from various perspectives. Section VII evaluates the performance of the IDDTL mechanism. Finally, we conclude this paper in Section VIII.

II. WHY WE NEED IDDTL

In the first place, let us consider the traditional Internet behavior without CID. The original Internet provides very limited management capability of the data delivery

doi:10.4304/jnw.9.1.18-27

connections. Although some people may insist that the lack of management can be one advantage of the Internet, however with the emergence of Internet commerce, there is an urgent requirement of management. Without CID, the Internet leaks some important connection-related information to the Internet including malicious attackers definitely. Further, the Internet endures the D/DoS attacks and port attacks without efficient solutions because of the original design. Without CID, the communication process can hardly be changed or flexibly migrated seamlessly; besides, it is hard to be aware of the traffic pattern of the data flowing in the Internet and it is nearly impossible to supervise the data traffic state in the Internet.

In the second place, the CID structure is made up of CID and CID-info. They are used to substitute some crucial information in the data packets. The change of the mapping information between CID and CID-info can lead to the change of direct end-to-end data packet communication process. Therefore, the established communication can flexibly migrate among the end points only by changing the CID mapping information. Besides, we should classify the mapping entries of CID to CID-info into specific patterns according to the type of the corresponding IP address pairs in order to adapt to various kinds of applications.

In addition, another important problem with this proposed CID-based Internet architecture is the scalability problem. As for this case, we assume each terminate can only establish 30 times of service obtainment process at the same time. This assumption is reasonable since the current maximum limitation of connections is also 30 times as the default value for windows users. The terminal should also maintain some part of CID mapping information to complete the data communication process. This method can provide both security and scalability of the Internet.

Different from the previous id-related research (i3), which introduces an overlay into the Internet to achieve indirect communication, we employ the mapping system into the proposed Internet architecture to protect some important information related to the communication process, such as the source and destination IP addresses. We can also utilize the CID to detect the connection state information. Further, we can know the traffic pattern according to the CID characteristics in the Internet as long as the CID-info can record the traffic characteristics through some statistics results. In general, the CID-based Internet architecture can bring about many advantages and achieve better performances of the Internet.

III. OVERVIEW

This IDDTL architecture is based on the concepts of CID and CID-info and their related network nodes. Using identifiers to substitute the IP addresses in the Internet can bring about the advantages of enhanced flexibility and management in the data packet delivery process. Besides, the identifiers can conceal the IP addresses and port numbers in the data delivery process, which can further enhance the security performances of the Internet.

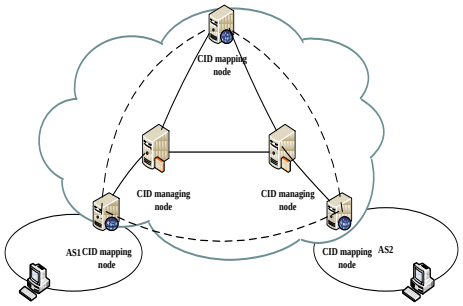

Figure 1. Components of CID-related Nodes.

As shown in figure 1, there are two kinds of CID-related nodes in IDDTL, which are the CID managing nodes and the CID mapping nodes respectively. The CID managing nodes located in the core network are responsible for generating and distributing CIDs. The CID mapping nodes located in the access network take the responsibility of substituting and forwarding data packets with the mapping information.

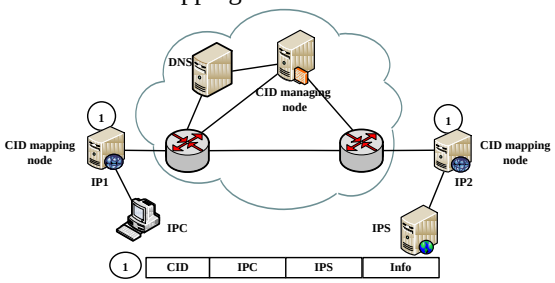

Figure 2. One sample of the CID-based Internet architecture.

In the managing nodes, they create CID with the necessary information sent from DNS and the data sender. In the CID mapping nodes, they keep the information about the CID and the related CID-info. Within IDDTL, we can separate the original communication process into two segments and split the identity identifier and the port number. The main contribution of IDDTL architecture is the three-party and two-segment communication process.

The CID-based Internet topology can be sketched one sample as shown in figure 2. It is composed of one client, one server, one CID managing node, two CID mapping nodes and two routers for forwarding the data packets. The IPC refers to the IP address of the client, while IPS indicates the IP address of the server. In the part of end points, they maintain the IP and port number information and conserve them for substituting the data packets according to the carried CIDs.

The sample of IDDTL works with the beginning of IPC accessing one web page, there are several steps before actually finishing the service obtainment process as follows.

1) The IPC accesses one web page, it will send DNS request to the DNS server, and the DNS server will reply the IPS to the CID managing node instead of the IPC, which is different from the original Internet. Besides the IPS, the CID managing node will also learn the IPC information.

2) When the CID managing node receives the IPS and the IPC information, it will hash the two elements to

create a random hash value. Then the hash value together with the random number and the time stamp would make up one unique 160-bit string of characters as the CID value. The CID and CID-info will be distributed to the related CID mapping nodes.

3) When the CID mapping nodes receive the CID and CID-info mapping entries, it will store it according to the CID-info classification. At the same time, the CID mapping node will inform the IPC of the CID value.

4) After the IPC knows the CID value, it will encapsulate the CID value into the data packets before sending them.

5) When the data packets sent from the IPC arrive at the CID mapping node, the CID mapping node will check whether the IPC is authenticated and its credit record. If it is allowed to be handled, the CID mapping node would look up the CID-info according to the CID value. The data packet source IP address and the destination addresses will be substituted and forwarded to the destination host.

6) In the reverse communication process, the CID encapsulation, the host authentication and looking up, the CID forwarding process is exactly the same.

The three-party and two-segment communication process can be implemented through the above six steps.

IV. WHAT MAKE UP IDDTL

In this section, we illustrate the detail of CID generation and its mapping with CID-info, which are the core components of the IDDTL architecture.

A. Connection Identifier

The CID stands for the connection identifier, indicating one service obtainment process. In other words, CID identifies the resources distributed to the specific communication process between the corresponding end points.

CID is a 160-bit identifier, which is a hash value of some source information about the service obtainment process. As for the creation of CID, we describe the detail of generation process in figure 3.

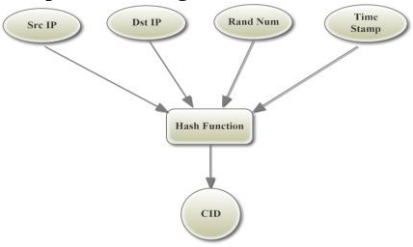

Figure 3. Generation of CID.

The fundamental objects of CID generation include the source IP address, the destination IP address, the random number and the time stamp in millisecond. We select the SHA-1 hash algorithm to generate the CID value in the managing node. As shown in equation (1), IPs and IPd are the resource and destination IP address respectively; TS states the timestamp; Random dedicates the random number.

$$CID = SHA1(IPs, IPd, TS, Random) \quad (1)$$

There is a key problem concerning about creating a CID, which is the collision avoidance and collision handling. However, the introduction of timestamp and the random number associated to each identifier can greatly mitigate this problem. When the newly generated CID is the same as one has been distributed to the CID mapping nodes and taken by one service obtainment process, the newly generated CID will be substituted with another value to avoid the CID collision easily. The evaluation of CID collision would be shown in the section VIII.

B. Mapping between CID and CID-info

The integrated mapping entry contains CID and its additional information known as CID-info [22]. The mapping between CID and CID-info can provide many advantages such as enhanced security, more flexibility and strong management. Here, we illustrate the detail of the CID to CID-info mapping.

The CID to CID-info mapping is used for managing the logical connection resources and information in the service obtainment processes. The data transport process can be abstracted as the mapping between CID and CID-info in IDDTL. The mapping between CID and CID-info are shown in figure 4.

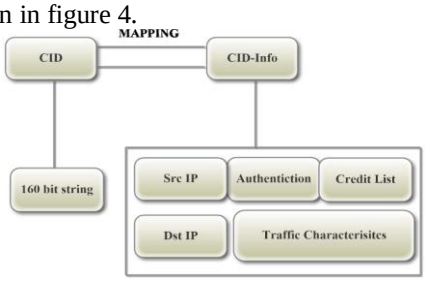

Figure 4. Components of the CID mapping entry.

The CID-info covers the source IP address, destination IP address, the source Port number and the destination Port number, the authentication information and the host credit record list etc.

Since we employ the mapping information into the IDDTL, in order to improve the efficiency of the mapping system, we use a distributed mapping cache to rapidly record and look up the mapping information between CID and CID-info. The sender can obtain the mapping information with a short delay from the nearby CID mapping node and its related caches. This design can sharply reduce the packet delivery delay in the Internet.

Apart from the distributed cache related to the mapping node, there are still some aspects about the mapping system worth consideration. The most urgent one is security, especially with the development of the security-based Internet applications. Since there are problems like updating and looking up CID to CID-info mapping, it is necessary to devise the authentication mechanism, secure update and efficient look up in IDDTL. Additionally, this mechanism based on the mapping system should be scaled easily with the Internet scale growth.

Just because there are still some problems, we propose some mechanisms accordingly. There is a limitation of the maximum number of connections can be established

for one end point to avoid the D/DOS attacks; some of the logical connections do not abort when the data packets are finished, and this can be resumed to transmit other application data packets by only updating the CID to CID-info mapping entries in the CID mapping nodes and such mechanisms can improve the connection utilization efficiency. These situations can be detected and identified through the lookup frequency of the specific mapping entry. A threshold time period can be used to identify the intermittent communication where the connection resources can be reused. Due to one CID can only be kept by the corresponding end points and the CID-related nodes. Even if the other spoofing end point intercepts the CID, it is hard to attack the mapping system since the CID mapping is only exposed to the specific hosts and its authentication mechanism. Therefore, both CID to CID-Info mapping entries and the structure of the CID managing nodes and CID mapping nodes contribute to guarantee its security and efficiency.

V. DEPLOYMENT OVER EXISTING NETWORK

The original Internet is based on the end-to-end model between fixed end points. The LISP network is based on the split of identity identifier and locator. How to deploy IDDTL in the Internet and LISP network is one common problem for any newly born architecture.

As for the IDDTL deployment over the Internet, it includes two parts: user endpoints and network nodes. The modifications of endpoint for IDDTL is shown in figure 5. The host adds one CID-related processing in the data encapsulation and de-capsulation process. As for the network nodes, we add the CID mapping into the access switch routers to work as the CID mapping nodes. The data packets are generally handled with steps in figure 6.

For the application of broadcast [7, 8], the IDDTL will create one CID for the service obtainment process. The characteristics of the broadcast application CID have only one source IP address and it can map with many destination IP addresses. When the broadcast application is initiated, there will be an established CID distributed to the CID-related mapping nodes. The data packets will be encapsulated with CID and forwarded to the broadcast destination IP addresses according to the mapping entry.

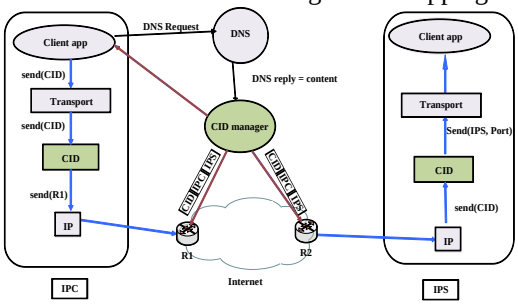

Figure 5. The end-point modification of CID-based communication.

For the application of multicast [9-11, 26], there will also be only one CID in the same multicast application obtainment process. The multicast CID maps to one source IP address and a group of destination IP addresses. If we change the CID-info, the multicast application will be changed accordingly. When the multicast source begins to send data packets, they will be duplicated and forwarded to the group of IP addresses according to the mapping entry. This process is just like the broadcast application, except that the multicast has to establish the multicast group of destination IP addresses.

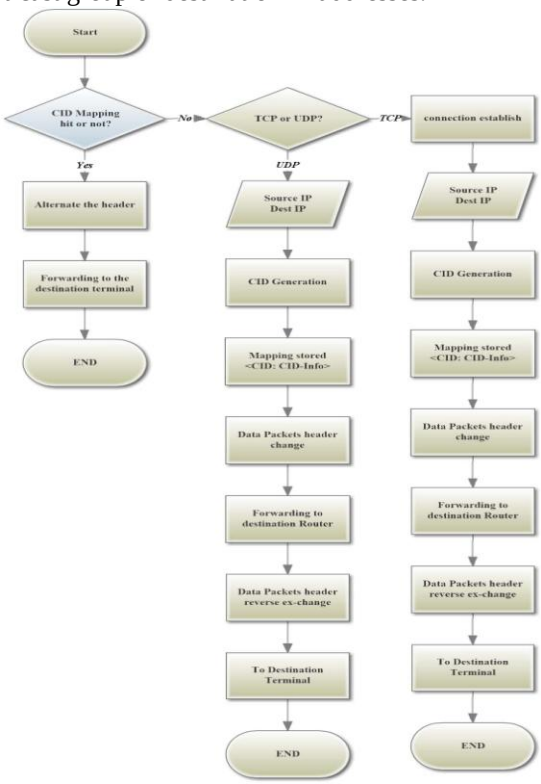

Figure 6. Flow chart of IDDTL deployed in traditional Internet

For the application of peer-to-peer application [12-14, 36], the CID will dynamically change as the peer information changes. In P2P applications, there will be a process of detecting whether the peers are active to provide the specific P2P services. With the active peers, we can obtain the P2P services. In addition, the initiator of P2P application can also be added to the source IP list. In the IDDTL, the CID mapping nodes are responsible for detecting the active peers.

Further, we consider the compatibility of the IDDTL architecture to the LISP networks, which also employs the mapping system between the identifiers and network locators. As for IDDTL applied in the context of LISP network, we take the transport layer into consideration and propose the mapping system-based mechanism to solve the problems including security, avoidance of D/DOS attacks in both terms of port and host identifiers. IDDTL in LISP would bring about the advantages such as more efficient connection utilization and more flexible connection management.

From the perspective of the above applications of IDDTL, it is suggested that one service obtainment process has only one CID and all the connections of the same one service obtainment process would map to the same CID. All the applications are employing the same principle of CID to CID-info mapping, but the CID could have different mapping patterns. They could facilitate IDDTL to adapt to various application requirements.

VI. IDDTL Solutions to Traditional Problems

The IDDTL architecture can bring about advantages from many perspectives. One among the advantages is that we can easily identify and classify the data traffic [23, 33, 34]. Contained in the CID-info, the data traffic characteristics can be helpful for traffic classification. The statistics results of the Internet service obtainment process can be reflected into the CID and CID-info, thereby they can also help to identify the data traffic.

In addition, the security threats of the IP address-based and the port-based attacks can also be avoided within IDDTL. The data migration can also be implemented securely and flexibly. The other advantage aspects of robustness, management and scalability will also be considered in this section.

A. Security

In IDDTL architecture, during the three-party and two-segment communication process, since the data packets would not carry the sender IP address and the receiver IP address in synchronism, the malicious terminals can never know the communication-related information easily by capturing the data packets. Attributed to the CID mapping node would check the authentication before substituting and forwarding data packets, the malicious terminals can rarely trace the same data packet throughout all the Internet entities.

The IP addresses and port numbers can be concealed in the terminal and the CID-related nodes to avoid the information leak in the IDDTL architecture. Without the disclosure of the private information concerning about the complete communication process, the malicious terminals can hardly pinpoint the object they want to attack. The IP address anonymity [15] can guarantee the whole Internet security. The shadowing of IP addresses in each segment of communication process can guarantee the unfeasibility of D/DOS attacks in the Internet. As for the port number, they are distributed to the communication between two end points and have much to do with the information interaction between the application layer and the transport layer. Thus the concealing of the port number can further improve the security and avoid the attacks based on the port number.

If the malicious terminals attack hosts randomly, the malicious terminals will compromise their credit report, so they would hardly be served by the IDDTL. In this case, we can gradually reduce the malicious terminals attacks. Besides, this mechanism of credit list can also prevent the normal users from switching to malicious users. In addition, the CID mapping nodes could have the function of encryption and decryption to further enhance network security.

In general, introducing CID to the Internet architecture could provide enhanced security guarantee. The private information concealing and the three-party and two-segment communication process all contribute to network security.

B. Management

The management of the service obtainment process is based on the stored CID and CID-info mapping entries in the CID-mapping nodes. Thanks to the record of CID to CID-info mapping, the data traffic characteristics and the logical connection states can both be managed by the CID-related nodes. As for the Internet management, there are two perspectives of customers and Internet service providers (ISPs).

For customers, if we enhance the management over the Internet, the Internet can detect abnormal data flows and attacks. Thus, the legal customers will not be easily attacked by malicious terminals. Within the data delivery process, we can detect the Internet logical connections and store them as CID-info in the CID mapping nodes. In some sense, we could know the network connections by looking up the CID-info stored in the CID mapping nodes. Hence, we can easily control the network service obtainment connections. If there is some abnormal information, we can also detect the situation and adopt some operations to handle easily.

From the perspective of the Internet service providers, the data traffic and the characteristics of the Internet connections can also be reflected into the CID-info. This will help for identifying the real-time data traffic classification. Through the traffic pattern identification based on the CID-info, we could learn more about the traffic characteristics. In this sense, we could know more about the data characteristics and avoid the specific pattern of data flows. If the ISPs want to forbid some types of data traffic in the Internet, such as P2P application flows, the proposed identified Internet architecture can easily achieve it because the CID-info can be employed to inform the ISPs of the data traffic characteristics. If we use this mechanism together with the port number-based identification and classification, the data traffic can be identified more precisely. Thus, the IDDTL architecture can help the ISPs to identify and classify the real-time data traffic.

C. Robustness

Apart from the management, the IDDTL can guarantee the robustness of the Internet as well [16].

In our IDDTL architecture, there would not only be one CID mapping node and one managing node. Since the CID managing nodes and mapping nodes could interact with one another, if one of them breaks down, the CID and CID-info in the node will be reestablished in one of the neighboring CID mapping nodes by requesting CID managing nodes. All the hosts previously connected to the broken CID mapping node will redirect their data packets to the newly selected CID mapping node. Thus, the IDDTL will contribute to the robustness of the hardware devices.

In the second place, the robustness of the IDDTL architecture also depends on the process of updating CID mapping entries and their interactions with the CID managing nodes. The CID managing nodes distribute CID mapping entries into the CID mapping nodes and the CID mapping nodes update the CID to CID-info mapping information for the CID managing node. They are all implemented based on the secure transmission mechanism. This can greatly enhance the security and correctness of the updating data.

In conclusion, the structure of the CID managing nodes and the CID mapping nodes can contribute to robustness of the CID-based Internet architecture. The reestablishment of CID to CID-info mapping information and the redirection of the delivered data packets can also enhance the robustness of the proposed architecture. Therefore, the IDDTL can offer the guarantee of the robustness for the Internet.

D. Flexibility

Based on the fact that the CID to the CID-info mapping entries could guide the data packets delivery process, the flexible migration of one service obtainment process can be implemented based on changing the CID to CID-info mapping information. The flexibility of the Internet contains many aspects including flexible migration among the various terminals [17]. Based on the end point who initiates the migration, we can classify the migration into two kinds, one of which is the server migration and the other is the client migration.

The server migration can be described as follows. If the service that the client wants to obtain is moved to another server during the communication process, we would change the previous CID to CID-info mapping entry with the new server IP address. In order to achieve seamless migration between the two servers, we have to inform the CID mapping node of the changed CID to CID-info mapping information before the actual server migration happens.

The client migration works as follows. When there are two users playing on-line games, if one of them wants to switch to another platform like the mobile phone and this is one client migration example. The migration process can be the same as the server migration. As long as we change the CID to CID-info mapping information before the client migration actually happens, we could achieve seamless migration.

With the updating of CID to CID-info mapping entries, the mapping entries can meet the requirements of the communication migration. Since the changes of CID to CID-info mapping information can directly change the data delivery process, the CID-based Internet migration can be flexibly implemented based on updating the CID to CID-info mapping entries. Hence, the CID to CID-info mapping information provides the basis for flexibly migrating communication between the corresponding end points seamlessly.

E. Mobility

In the traditional Internet, the mobility [18, 31, 33] can result in various kinds of problems in the original Internet, such as the triangle routing problem. To the simplest, there are two kinds of mobility in the Internet including the host mobility and the server mobility. Based on the IDDTL architecture of the CID managing nodes and the CID mapping nodes, we can easily implement mobility by moving or fetching the CID to CID-info mapping entries for the moved hosts or servers.

There are two kinds of mobility, one is the mobility of host/server does not change the CID mapping node and the other one is the mobility of host/server changes the directly connected CID mapping node. If the mobility is the first kind, we do not have to do anything about this mobility since we can deliver the data packets as the mobility did not happen. If the mobility leads to the change of CID mapping node, we have to move or fetch the related CID to CID-info mapping entry for the newly connected CID mapping node. Thus, the host mobility can be easily implemented by distributing the related CID mapping entries to the newly connected CID mapping nodes.

Drawn from the mobility support of the IDDTL architecture, we can see that it mainly concerns about adding the CID to CID-info mapping entries of the moved host/server into the newly connected CID mapping node. If the host and the host-related CID to CID-info mapping entries can move to another place accordingly, the mobility of the host mobility can be implemented easily.

We should pay attention to the problem of the triangle routing problem [20, 21]. This problem will become much fierce with the host mobility. Introducing the CID mapping nodes to the CID-based Internet architecture, we use the CID-info to indicate whether the route is applicable for data delivery. If so, we will directly use the appropriate routing. If not, we will forward the data packets to the previous mapping node and then deliver the data packets using the previous feasible route. This only increases one hop for the previous appropriate route. In this sense, with the CID mapping nodes, we can avoid the problem of triangle routing, thereby, we can improve the efficiency of the data delivery.

To sum up, when the host moves to the other mapping node area, the original related CID mapping entries will be restored in the new CID mapping nodes. If we change the source IP address or destination IP address, the connection can guide the data packets to the changed communication process. Therefore, in the IDDTL, we can easily fulfill the host and service mobility in the Internet. Further, based on the CID-info, we can solve the triangle routing problem to some extent. Therefore, in the aspect of mobility, the IDDTL architecture could offer better solutions.

F. Multi-homing

The multi-homing means one host has multiple interfaces. The service obtainment process for the multi-homing hosts can include more communication modes than the single interface host [25, 27-30, 32, 35]. Due to the various modes of communication for the multi-homing host, our IDDTL could fulfill the requirements by employing different CID mapping patterns.

As for the multi-homing hosts, there are four kinds of communication modes. Assume there are two hosts with two interfaces respectively, namely eth0 and eth1 with host1, eth2 and eth3 with host2. One communication mode for the multi-homing hosts can be the eth0 to eth2 or eth1 to eth3. The second mode is to use eth0 to eth2 and eth1 to eth3 at the same time. Another mode is the eth0 to eth2 and eth3 or the eth1 to eth2 and eth3. The fourth communication mode is to use both the eth0 to eth2 and eth3 and the eth1 to eth2 and eth3. The four

modes can be abstracted as one-to-one, one-to-multiple, multiple-to-one and multiple-to-multiple.

As is obvious about the multi-homing host, one host with more than one interface can use multi-path to obtain one service. The characteristics of multi-path can be realized easily based on the CID to CID-info mapping information. The CID and its mapping CID-info can be used for multi-path transmitting by adapting the mapping pattern.

We present the communication mode information of the multi-homing host in the CID-info. When the data packets for the multi-homing communication are received, they will be substituted according to the mapping entries. After that, they will be forwarded to the specific destination IP addresses listed in the CID mapping entries. With these mapping entries, we can easily realize the multi-path for IDDTL. So we can use the CID to CID-info mapping information to identify the characteristics of the multi-homing transmitting process definitely.

VII. EVALUATION

After all the detail illustration of IDDTL, we could conclude that the significant factor impacting the IDDTL's performance is the identifier introduced in the architecture. Therefore, to evaluate the IDDTL performance, we must investigate the metric of the identifier-CID in the communication process.

A. Identifier Uniqueness

In the previous sections, we illustrate the detail of generating the identifier-CID. As it has been discussed, the identifier uniqueness guarantees the normal communication and enhanced performance. Here, we analyze the uniqueness of the CID generation.

This simulation is done with a C program written on purpose, running under the Linux operating system. We input several different orders of magnitude of service requesting for generating CID in different time slot and different end hosts. The data set of identifier is collected among different end hosts. The results of the identifier collision distribution and statistical collision probability are shown in figure 7. In figure 7.a and 7.b, the X-axis stands for the order of magnitude of service requests number as shown in equation (2), while the Y-axis presents the percentage of e as the base index of the identifier collision percentage, as shown in equation (3). The total size of the data sets is about 1TB.

$$x = \lg(Service\ Request\ Num) \quad (2)$$

$$y = \lg(e^{collision\ percentage} / Service\ Request\ Num) \quad (3)$$

$$y = collision\ num / service\ request\ num \quad (4)$$

In figure 7.c, it proves that the probability of collision stays well as zero under very strict circumstances, the parameter of Num in the figure means the number of rerunning count of the service requests. The X-axis stands for the order of magnitude of service requests number as shown in equation (2), and the Y-axis presents the CID collision percentage, as shown in equation (4). And the last two figures have the same rerunning count to verify the collision percentage is still zero with the same two end-points.

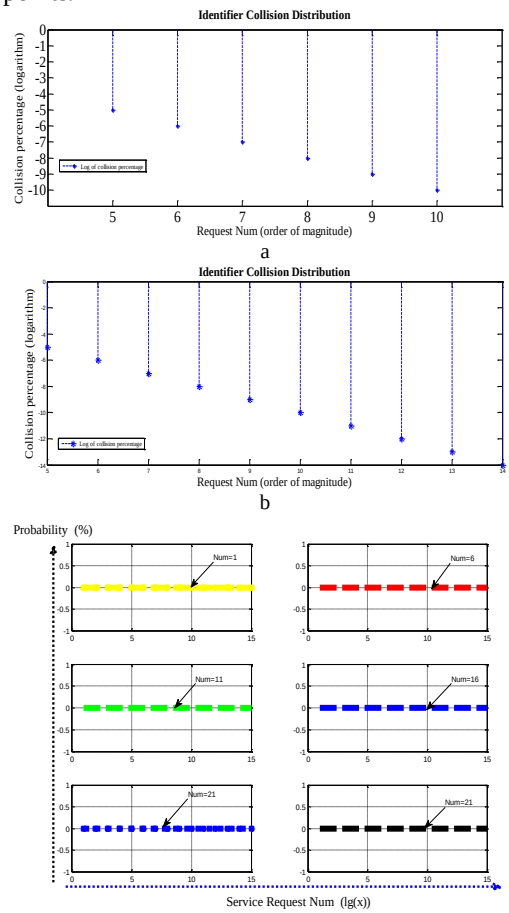

a. Request Number = 10^{10}, b. Request Number = 10^{14} c. Statistical Collision Probability

Figure 7. Identifier uniqueness vs. various request number

From the evaluation results of figure 7, we could conclude that with the increase of the total identifier number, the percentage of the collision is negligible, even to the extent of zero collision. With the identifier uniqueness, we could guarantee the basis of flexible host mobility, security and other improvement.

B. Cost

Although IDDTL has its advantages analyzed in the previous sections, when implementing IDDTL we should consider whether the time cost and network traffic load inducted in the communication process is acceptable. The cost items must also be the metrics to make evaluation complete.

The average time overhead in end-point stays far below 8 useconds in the endpoints, as shown in figure 8. Here, we do not consider the transport time along the network path, which depends on the network condition in the specific time period. The endpoint time cost includes CID generation, packet encapsulate and CID mapping information capture time. By use of the implementation of IDDTL in the prototype of our lab, we can conclude

that the average time cost is not big enough to compromise the network performance compared with TCP. In theory, the TCP connection establish time is three times of the ping time. While the IDDTL is about two times of ping time added with the CID generation time. Thus, at the stage of connection establishment, the IDDTL is quicker than the end-to-end TCP.

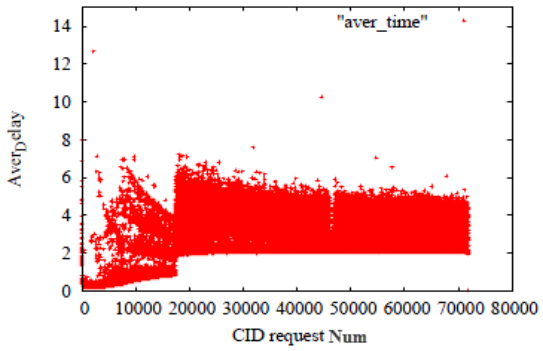

Figure 8. Average delay vs. CID request Number

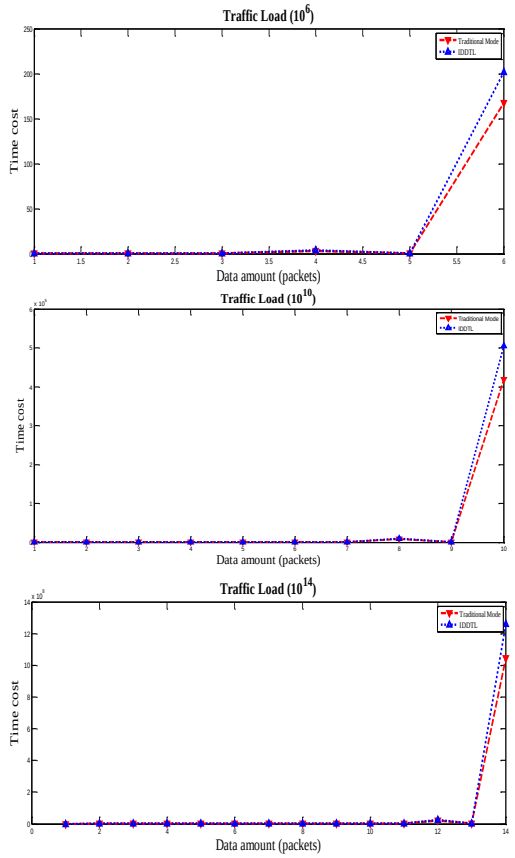

Figure 9. Time cost comparison of various traffic load

We analyze three groups of various data amount to compare the time cost of the IDDTL and the end-to-end transport model in the traditional Internet. In each comparison scenario, we set the transmitted data packet size as 1500 Byte per packet. Besides, the network condition for transmission is assumed unchanged with the same topology.

In figure 9, we could conclude that with the traffic amount increasing, the time cost for transmitting the same size of content IDDTL would be about 10% larger than the TCP end-to-end model. It is easy to note that the majority of the extra time is spent on interacting with the CID mapping nodes. Although the extra time cost increases with the traffic amount, however, the average extra time cost remains the same. Due to the evaluation is just based on a single path communication model and the CID mapping pattern is one-to-one, its advantage could not be shown as clear as possible. But we must admit that the IDDTL overcomes the drawbacks of the Internet by bringing extra time cost.

In order to prove that the IDDTL is capable of achieving its advantages within an acceptable extra time. We deploy a test to further investigate the average transmission time of IDDTL compared with the end-to-end model. In this test, we deploy ten group of data transmission with the same data size. As shown in figure 10, we could conclude that the average extra packet transmission delay is about 3.6 useconds compared with the traditional Internet. In other words, when we download 1.5GB content, the extra delay of IDDTL will be about 3.6 seconds. Considering its advantages, the time cost of IDDTL is acceptable.

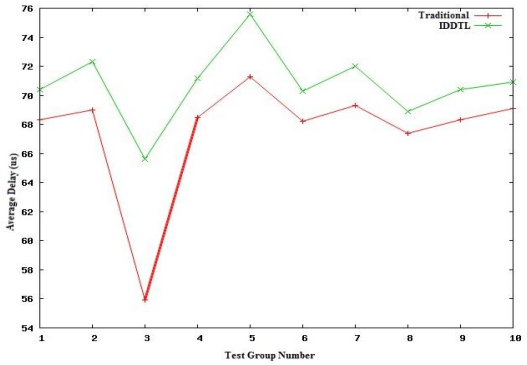

Figure 10. Average Delay vs. Ten test group

VIII. CONCLUSION

In this work, we present the identifier data transport layer mechanism (IDDTL) based on the definition of CID and CID-info. How the mechanism works and its advantages have been illustrated as well. To give a better understanding of the mechanism, we performed a simulation analysis comparing the IDDTL with the traditional end-to-end transport model. Drawn from the simulation results, we proved that the IDDTL is feasible with unique identifier and the time cost brought about by IDDTL is acceptable for network customers. Furthermore, in future research, we would use more mapping patterns to verify its additional advantages one by one. On the other hand, we could also combine IDDTL and the wireless access network and other mobile applications to further improve management, security and flexibility of the current Internet.

ACKNOWLEDGMENT

This paper is supported in part by the National Natural Science Foundation of China (NSFC) under Grant No.61271201 and No.61271202, in part by the SRFDP

under Grant No.20120009120005, in part by the MIIT of China under Grant No. 2012ZX03005003-04 and the Fundamental Research Funds for the Central Universities No.2012YJS018.

REFERENCES

[1] D. Meyer, The Locator/Identifier Separation Protocol (LISP), http://www. 1-4-5. net/~dmm/lisp/.

[2] R. Moskowitz, P. Nikander, Host identity protocol, RFC-4423, May 2006.

[3] I. Stoica, D. Adkins, S. Zhuang, S. Shenker, and S. Surana, "Internet Indirection Infrastructure", *Proc. of the 2002 conference on Applications, technologies, architectures, and protocols for computer communications*, vol. 32, issue 4, October 2002.

[4] H. Balakrishnan, K. Lakshminarayanan, S. Ratnasamy, S. Shenker, I. Stoica, M. Walfish, "A layered naming architecture for the internet", *Proc. ACM SIGCOMM'04*, 2004, pp. 343-352.

[5] P. Francis, R. Gummadi, "IPNL: A NAT extended internet architecture", *Proc. Of ACM SIGCOMM'01 2001*, pp. 69–80.

[6] W. Adjie-Winoto, E. Schwartz, H. Balakrishnan, and J. Lilley, "The design and implementation of an intentional naming system", *Proc. ACM Symposium on Operating Systems Principles*, 1999, pp. 186–201.

[7] D. Katabi, J. W. Wski, "A framework for scalable global IP-anycast (gia)", *Proc. of SIGCOMM 2000, August* 2000, pp. 3–15.

[8] C. Partridge, T. Mendez, W. Milliken, Host anycasting service, RFC-1546, November 1993.

[9] Y. Chu, S. G. Rao, H. Zhang, "A case for end system multicast", *Proc. of ACM SIGMETRICS'00*, June 2000, pp. 1–12.

[10] K. Lakshminarayanan, A. Rap, I. Stoica, S. Shenker, Flexible and robust large scale multicast using i3. Tech. Rep. *CS-02-1187, University of California -Berkeley*, 2002.

[11] I. Stoica, T. NG, H. Zhang, "REUNITE: A recursive unicast approach to multicast", *Proc. Of INFOCOM'00, March 2000*, pp. 1644–1653.

[12] P2P, http://en. wikipedia. org/wiki/Peer-to-peer.

[13] A. Rowstron, P. Druschel, "Pastry: Scalable, distributed object location and routing for large-scale peer-to-peer systems", *Proc. of the 18th IFIP/ACM International Conference on Distributed Systems Platforms, November* 2001, pp. 329–350.

[14] I. Stoica, R. Morris, D. Karger, M. F. Kaashoek, and H. Balakrishnan, "Chord: A scalable peer-to-peer lookup service for internet applications", *Proc. Of ACM SIGCOMM'01*, 2001, pp. 149–160.

[15] C. Yarvin, R. Bukowski, and T. Anderson, "Anonymous rpc: Low-latency protection in a 64-bit address space", *Proc. of USENIX, June* 1993, pp. 175–186.

[16] S. D. Gribble, M. Welsh, J. R. V. Behern, E. A. Brewer, D. E. Culler, N. Borisov, S. E. Czerwinski, R. Gummadi, J. R. Hill, A. D. Joseph, R. H. Katz, Z. M. Mao, S. Ross, and B. Y. Zhao, "The ninja architecture for robust internet-scale systems and services. *Computer Networks*", vol. 35, issue 4, 2001, pp. 473–497.

[17] A. Vahdat, M. Dahlin, and T. Erson, "A. Aggarwal, Active names: Flexible location and transport", *Proc. of USENIX Symposium on Internet Technologies & Systems, October* 1999.

[18] A. C. Snoeren, H. Balakrishnan, "An end-to-end approach to host mobility", *Proc. of ACM/IEEE MOBICOM'99*, August 1999.

[19] S. Zhuang, K. Lai, I. Stoica, R. Katz, and S. Shenker, Host mobility using an internet indirection architecture. Tech. Rep. *UCB/CSD-02-1186, Computer Science Division, U. C. Berkeley*, June 2002.

[20] A. Whitaker, D. Wetherall, "Forwarding without loops in Icarus", *Proc. of OPENARCH* 2002, June 2002.

[21] T. S. E. Ng, H. Zhang, "Predicting internet network distance with coordinates-based approaches", *Proc. of INFOCOM'*02, 2002.

[22] Y. Y. Gao, K. Wang, and Y. J. Qin, "An Identified Transport Layer Mechanism In The Locator/Identifier Separation Context", *Proc. of the 2011 International Conference on Advanced Intelligence and Awareness Internet, October* 2011 pp. 12-15.

[23] Y. Y. Gao, F. Song, and Y. J. Qin, "A Novel Real-time Traffic Identification Mechanism", *Proc. of the 2011 International Conference on Advanced Intelligence and Awareness Internet, October* 2011, pp. 72-75.

[24] K. Katsaros, G. Xylomenos, and G. C. Polyzos, "MultiCache: An overlay architecture for information-centric networking", *Computer Networks*, vol. 55, issue 4, Mar. 2011, pp. 936 – 947.

[25] F. Song, H. C. Zhou, S. D. Zhang, H. K. Zhang, and I. You, "Performance Analysis of Reliable Transmission on Multiple Paths and Single Path", *Sixth International Conference on Innovative Mobile and Internet Services in Ubiquitous Computing (IMIS)*, 2012, pp. 185-190.

[26] S. G. Li, K. Xu, Y. Liu, and J. P. Wu, "Edge overlay multicast to support comparable multi-class services", *Journal of High Speed Networks*, vol. 17, 2008, pp. 13-36.

[27] R. S. Cheng, H. T. Lin, "Modified TCP startup procedure for large bandwidth-delay networks", *Journal of High Speed Networks*, vol. 17, 2008, pp. 37-50.

[28] F. H. V. Teles, G. R. Bianchi, and L. L. Lee, "A network traffic prediction approach based on multifractal modeling, *Journal of High Speed Networks*", vol. 17, 2010, pp. 83-96.

[29] L. Shi, W. J. Li, and B. Liu, "Flow-based packet-mode load-balancing for parallel packet switches", *Journal of High Speed Networks*, vol. 17, 2010, pp. 97-128.

[30] H. Byun, "An explicit window adaptation algorithm over TCP networks using supervisory control", *Journal of High Speed Networks*, vol. 17, 2010, pp. 207-218.

[31] T. H. Yang, C. Y. Ku, D. C. Yen, and Y. C. Lin, "Utilizing the interactive techniques to achieve automated service composition for Web Services", *Journal of High Speed Networks*, vol. 17, 2010, pp. 219-236.

[32] L. Fàbrega, T. Jové, P. Vilà, and J. L. Marzo, "A network scheme for TCP elastic traffic with admission control using edge-to-edge per-aggregate measurements in class-based networks", *Journal of High Speed Networks*, vol. 17, 2010, pp. 15-32.

[33] P. Chitra, R. Rajaram, and P. Venkatesh, "Load balanced reliable task scheduling algorithm for heterogeneous systems", *Journal of High Speed Networks*, vol. 17, 2010, pp. 33-45.

[34] S. F. El-Zoghdy, Y. M. Asem, "Secure group re-keying using key inverses", *Journal of High Speed Networks*, vol. 17, 2010, pp. 47-68.

[35] A. M. Sukhov, D. I. Sidelnikov, A. P. Platonov, M. V. Strizhov, and A. A. Galtsev, "Active flows in diagnostic of troubleshooting on backbone links", *Journal of High Speed Networks*, vol. 17, 2010, pp. 69-81.

[36] M. S. Sendil, N. Nagarajan, "Improving the performance of P2P networks using SPIS with Query Filtering, *Journal of High Speed Networks*", vol. 17, 2010, pp. 131-140.

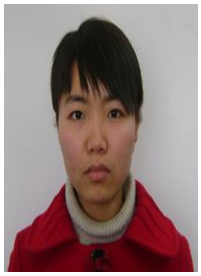

Yangyang Gao received her B.S. degree in communication engineering from Beijing Jiaotong University in 2009. She is a directly Ph.D. candidate in Beijing Jiaotong University since 2009. Now she is studying in the national engineering lab of next generation Internet and Interconnection Devices. Her major is communication and information system. She is interested in researching the future Internet data transport control, traffic control and resource distribution.

Fei Song received his Ph.D. degree from Beijing Jiaotong University. He is now a Lecturer in National Engineering Laboratory for Next Generation Internet Interconnection Devices, School of Electronic and Information Engineering, Beijing Jiaotong University. His current research interests are Protocols Optimization, Wireless Communications and Cloud Computing.

Yajuan Qin received her B.S. and M.S. degrees in Radio Technology from the University of Electronic Science and Technology of China (formerly known as Chengdu Institute of Radio Engineering) in 1985 and 1988, respectively, and Ph.D. degree in communication engineering from Beijing University of Posts and Telecommunications in 2003. She joined Beijing Jiaotong University (formerly known as Northern Jiaotong University) in 2004, where she is now a professor. Her research interests are in the areas of computer networks and wireless communications.

The Improvement of RFID Authentication Protocols Based on R-RAPSE

QingLing Cai and YiJu Zhan
School of Engineering, Sun Yat-sen University, Guangzhou, China
Email: caiqingl@mail.sysu.edu.cn, zhanyiju@mail.sysu.edu.cn

Jian Yang
Faculty of Automation, Guangdong University of Technology, Guangzhou, China
Email: jimmyyoungyj@163.com

***Abstract*—Numerous RFID authentication protocols proposed often have some security vulnerabilities, since they lack systematic theory support. We had proposed a series of rules called R-RAPSE (RFID Authentication Protocol Security Enhanced Rules) for RFID authentication protocol design and verification. By three examples, this paper justifies why the protocols do not offer sufficient security and privacy protection, and thereafter, proposes relevant solutions to fix the security holes based on R-RAPSE, which demonstrates how R-RAPSE can be used to verify and improve RFID authentication protocols.**

***Index Terms*—RFID; Authentication; Indistinguishability; Vulnerability; Privacy**

I. Introduction

Radio frequency identification (RFID), as one of the most important component of the Internet of Things (IoT) sensing layer, has been widely deployed in various applications [1]. In particular, RFID systems with the low-cost RFID tag are more extensively applied. However, the embedded nature of the technology and a lack of awareness of its potential social and personal consequences make a special issue dedicated to security and privacy [2-12]. Although there are recent investigations of low cost RFID security protocols [2-10], it is challenging to deploy higher quality safety technology to low-cost RFID tags.

To resolve the security and privacy issues of RFID systems [2-5], numerous security protocols for RFID systems have been proposed [2-12]. However these protocols often have more or less vulnerabilities since they lack systematic theory support. Even RFID protocols are proposed by some senior experts, these RFID protocols may often have some weaknesses without regard to the comprehensive security issues and special requirements for RFID systems, As a result, a protocol was proposed; its security vulnerabilities were soon discovered. Such as HY Chien proposed an ultralightweight RFID authentication protocol [6], however, there are two de-synchronization attacks to break the protocol, as pointed out by Sun et al. [7]. H. Y. Chien et al. proposed another lightweight RFID protocol in the literature [8]; the algorithm did not take the distinguishability issues into consideration, and would allow the location of the tag owner to be exposed. That is, the tag can be tracked. Meanwhile, the weaknesses of the schemes [9-12] have been reported. Thus, it is imperative to propose principled rules to provide systematic theory support for RFID authentication protocols. Therefore, we had proposed a series of RFID authentication protocol security enhanced rules (R-RAPSE, Rules — RFID Authentication Protocol Security Enhanced) (see Appendix R-RAPSE), designed to provide systematic theory support for RFID authentication protocol design and verification.

In this paper, our aims are to present R-RAPSE applications. Based on R-RAPSE, we verify and improve E. J. Yoon's scheme [2], J. S. Cho's scheme [3] and S. I. Ahamed's scheme [5]. In a more general sense, we show that these algorithms are insecure, which demonstrates how R-RAPSE is used to verify and improve RFID authentication protocols.

The contribution of the paper lies in the following aspects: This paper provides R-RAPSE applications. We demonstrate how R-RAPSE is used to verify and improve RFID authentication protocols. By three examples, we verified and improved RFID authentication protocols based on R-RAPSE. We justified why the protocols do not offer sufficient security and privacy protection, and thereafter, proposed relevant stronger protocols to fix the security holes.

The remaining parts of this paper are organized as follows: Section 2, by three examples, we identified some vulnerabilities of previous protocols and demonstrate how R-RAPSE is disobeyed by these protocols, and then propose relevant solutions to mend those security holes based on R-RAPSE. Our conclusions are presented in section 3. We discuss the security issues, security requirements, R-RAPSE in Appendix R-RAPSE.

II. Security Analysis and Improvement of RFID Authentication Protocols Based on R-RAPSE

In this section, this paper verifies and improves three RFID authentication protocols [2, 3, 5] based on R-RAPSE. Firstly, we illustrate that the protocols have some vulnerabilities and analyze why the protocols do

doi:10.4304/jnw.9.1.28-35

not offer sufficient security and privacy protection, and then suggest relevant solutions to mend the security vulnerabilities.

For each protocol considered in this section, due to space considerations, the paper only provides a rough description of the complicated steps necessary. The interested readers are referred to the original publications for the detailed descriptions of these protocols. Let us quickly revisit the protocol.

The universal notations used in this paper are given as follows:

$H(.)$ an irreversible one way hash function.

$P(.)$ a pseudo-random number generator.

$\|$ concatenation operation.

=? determine whether both sides are equal.

DATA the corresponding information of the tag kept in the server.

$\oplus$ XOR operation.

A. The J. S. Cho et al. Protocol

J. S. Cho's paper [2] presents a hash-based mutual authentication protocol. The J. S. Cho et al. protocol is designed to send a random number generated by a tag to the server without leakage. Moreover, it uses secret values instead of random numbers as response information, which is able to produce distinct response information in every session without interference from intentional or accidental requests generated by an adversary, and the secret value is not directly transmitted.

However, according to R-RAPSE, J. S. Cho's protocol, as opposed to their claims, does not follow Data Integrity Rule, and the protocol may give rise to de-synchronization issues between the server and the tag. This can be accomplished as follows:

1. Prior conditions and assumptions

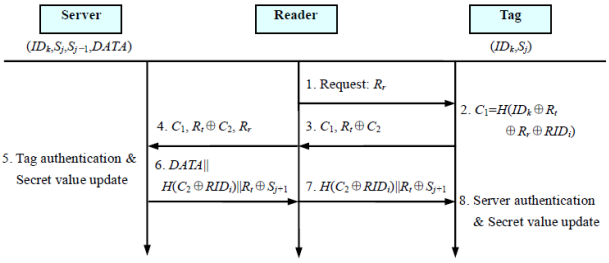

Figure 1. The J. S. Cho et al. protocol.

The communication between the reader and the server is secure, while the communication between tags and readers is insecure.

The notations used in J. S. Cho's paper are given as follows:

R_r random number generated by reader (96-bit).

R_t random number generated by tag (96-bit).

RID_i group *ID* of random number (96-bit).

ID_k the ID of the Tag k.

S_j secret value (96-bit) mutually shared by the server and the tag, and used in the jth session.

C_1 information generated by tag for authentication.

C_2 blind factor.

In initialization phase, the information shared by the server and each tag is kept within respective devices:

Tag: (ID_k, S_j)

Server: (ID_k, S_j, S_{j-1}, *DATA*)

2. Protocol description

J. S. Cho's protocol authenticates an RFID tag with a secret value. This is represented by Fig. 1. Step 2, 5 and 8 of protocol are described as follows:

Step 2: Generating response information

The tag generates some values by the following steps:

Generates: random number R_t.

Generates:

$RID_i=(R_t-R_t \bmod S_j+1)(0:47)\|(R_t+S_j-R_t \bmod S_j)(48:95)$, where RID_i of group involve R_t.

Computes: $C_1=H(ID_k \oplus R_t \oplus R_r \oplus RID_i)$.

Computes: $C_2=S_j(0:47)\|ID_k(48:95)$; Executes: $R_t \oplus C_2$.

Step 5: Tag authentication

The server authenticates the tag, and updates the secret value.

The server performs the following steps, based on the saved information of each tag.

Retrieves ID_k and S_j of a tag in the table of the server.

Generates C_2 with the retrieved ID_k and S_j.

Retrieves R_t from $R_t \oplus C_2$ with the generated C_2.

Compute group RID_i^* with the retrieved S_j and R_t.

Generates C_1^* with R_r obtained from reader, and computed RID_i^*, retrieved R_t and ID_k.

Repeats steps (a) ~ (e) until C_1^* is the same as C_1.

If the same C_1^* is found, the server will send the relevant tag data to the reader and update the secret value of the tag. It performs the following steps.

Updates the secret value S_j of the tag with S_{j+1} ($S_j \leftarrow S_{j+1}$), where S_{j+1} is generated at the discretion of the server.

Modifies the table of the relevant tag. S_{j+1}, S_j are saved into row S_j, Sj_{-1} respectively.

Generates: $DATA\|H(C_2 \oplus RID_i)\|R_t \oplus S_{j+1}$.

Data to be transmitted the reader.

$H(C_2 \oplus RID_i)$ to authenticate the server for the tag.

$R_t \oplus S_{j+1}$ to update the secret value of the tag.

If the same C_1^* is not found, retrieves S_{j_1} from row S_{j_1} instead of S_j and repeats phase Step 5(1).

It is the case that a synchronization issue has occurred in the previous session.

If the process also fails, the protocol will be stopped at that time, and the transmitted information cannot be trusted.

Step 8: Server authentication

The tag authenticates the server, and updates the secret value.

The tag authenticates the server by $H(C_2 \oplus RID_i)$.

The tag retrieves the new secret value S_{j+1} from $R_t \oplus S_{j+1}$ with R_t.

Updates the secret value S_j with S_{j+1}, after the server passes through authentication.

3. Vulnerability analysis and improvement

Analysis:

The protocol does not follow Data Integrity Rule (see R-RAPSE). The adversary can desynchronize information in the server and the tag. This can be accomplished as follows:

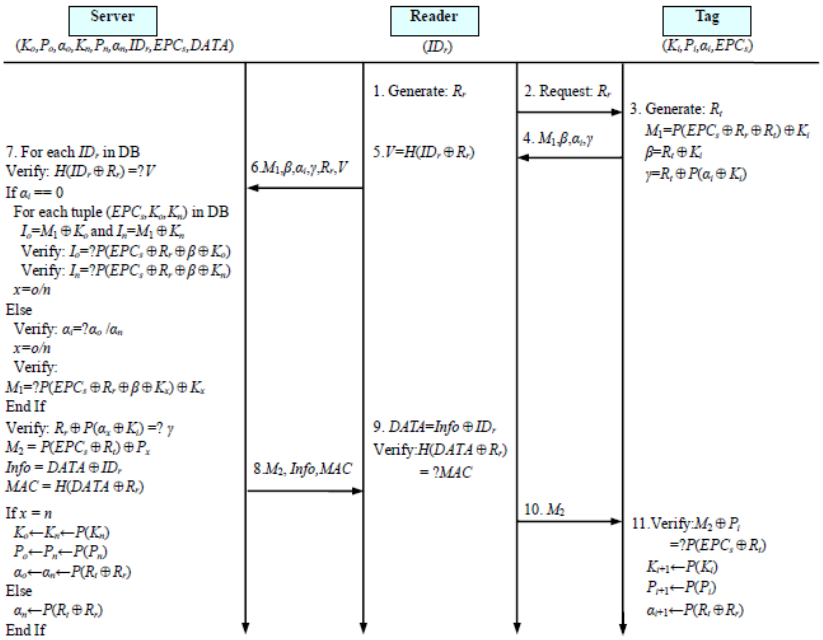

Figure 2. The protocol of E. J. Yoon.

Step 7 The adversary may send $H(C_2 \oplus RID_i)||R_t \oplus S_{j+1}^*$ instead of $H(C_2 \oplus RID_i)||R_t \oplus S_{j+1}$.

To do the following:

The adversary can acquire $H(C_2 \oplus RID_i)||R_t \oplus S_{j+1}$ via eavesdropping.

At the same time, blocks $H(C_2 \oplus RID_i)||R_t \oplus S_{j+1}$ to the tag.

Then sends $H(C_2 \oplus RID_i)||R_t \oplus S_{j+1}^*$ to the tag, where $R_t \oplus S_{j+1}^*=(R_t \oplus S_{j+1}) \oplus \Lambda$ (Λ may be any number 96-bit).

Step 8

Now the tag receives $H(C_2 \oplus RID_i)||R_t \oplus S_{j+1}^*$, but not $H(C_2 \oplus RID_i)||R_t \oplus S_{j+1}$.

The tag retrieves the new secret value S_{j+1}^* from $R_t \oplus S_{j+1}^*$ with R_t.

Updates the secret value S_j with S_{j+1}^* (but not S_{j+1}).

At the moment, the de-synchronization attack will be successful.

Improvement:

According to Data Integrity Rule (see R-RAPSE), the hash function can be used to protect data integrity, by doing the following:

Step 7 Replaces $H(C_2 \oplus RID_i)||R_t \oplus S_{j+1}$ with $H(C_2 \oplus RID_i)||R_t \oplus S_{j+1}$, $R_t \oplus H(S_{j+1})$, and transmits to the tag, where the hash function $H(.)$ can ensure S_{j+1} data integrity.

$H(C_2 \oplus RID_i)$ to authenticate the server for the tag.

$R_t \oplus S_{j+1}$ to update the secret value of the tag.

$R_t \oplus H(S_{j+1})$ to verify S_{j+1} data integrity for the tag.

B. The E. J. Yoon Protocol

Firstly, E. J. Yoon's paper [3] demonstrates that Yeh et al.'s protocol [4] has two serious security issues such as data integrity problems and forward secrecy problems. Then E. J. Yoon's paper proposes an improved protocol and claims that it can prevent these security issues and adapt to the low-cost RFID environments which require a high level of security.

However, according to R-RAPSE, E. J. Yoon's protocol may give rise to distinguishability issues, exposing the location of the tag owner. This might result in the privacy of the tag owner being violated and the traffic of the tag owner to be analyzed. The analysis is described as follows:

1. Prior conditions and assumptions

The communication of between the server and the readers is insecure, and the communication between readers and tags is also insecure.

The notations used in E. J. Yoon's paper are defined as follows:

EPC_s the 96-bit of EPC code are divided into six 16-bit blocks, and then the six blocks perform XOR into EPC_s.

K_i the authenticate key kept in the tag to authenticate the tag by the server at the (i+1)th authentication session.

P_i the access key kept in the tag to authenticate the server by the tag at the (i+1)th authentication session.

K_o the old authentication key kept in the server.

K_n the new authentication key kept in the server.

P_o the old access key kept in the server.

P_n the new access key kept in the server.

α_i the server index kept in the tag to find the corresponding information of the tag in the server.

α_o the old server index kept in the server.

α_n the new server index kept in the server.

ID_r the reader identification number.

In initialization, the manufacturer generates some random values for the server, reader and tag, the information is stored in respective devices:

Tag: (K_i, P_i, α_i, EPC_s)

Reader: ID_r

Server: (K_o, P_o, α_o, K_n, P_n, α_n, ID_r, EPC_s, DATA)

2. Protocol description

The E. J. Yoon protocol proposes an improvement of Yeh et al.'s protocol. The information kept within respective devices is same as Yeh et al.'s protocol. Moreover, the initialization phase is same as in Yeh et al.'s protocol. The improved (i+1)th authentication session is depicted in Fig. 2. Step 7 and 11 of the protocol are described as follows:

Step 7: Reader and tag authentication

The server authenticates the reader and the tag, and updates the secret values.

After receiving (M_1, β, α_i, γ, R_r, V), the server performs the following operations:

Extracts each stored ID_r sequentially to compute $H(ID_r \oplus R_r)$ with R_r, and matchs the received V to identify the correct tuple and authenticate the reader.

Checks the value of α_i in the tag to decide which of the two following procedures is preceded.

When α_i = 0, represents the first access. The server picks up an tuple (K_o, P_o, α_o, K_n, P_n, α_n, ID_r, EPC_s, $DATA$) stored in itself. Computes the values: $I_o=M_1 \oplus K_o$ and $I_n=M_1 \oplus K_n$, and examines whether I_o or I_n matches $P(EPC_s \oplus R_r \oplus \beta \oplus K_o)$ or $P(EPC_s \oplus R_r \oplus \beta \oplus K_n)$ computed by the server itself, where $\beta \oplus K_o$ or $\beta \oplus K_n$ needs to obtain R_t, which is repeated for each tuple until a match is found. Once the matching tuple is found, set $x=n$ or $x=o$ according to which authentication key (K_n or K_o) in the tuple found matched with the one in the tag.

When $\alpha_i \neq 0$, using α_i as an index to find the corresponding tuple in the server. If the tuple is found by matching up by its field α_o, set $x=o$; otherwise set $x=n$ if α_n matches up. Then verify M_1, received from the reader, if it is equal to $P(EPC_s \oplus R_r \oplus \beta \oplus K_x) \oplus K_x$ computed by the server itself.

Retrieves K_x from the matched tuple and verifies whether the received γ matches $R_r \oplus P(\alpha_x \oplus K_i)$ computed by the server itself. If the two values do not match, then the protocol stops.

Computes (M_2, $Info$, MAC) as follows:

$M_2=P(EPC_s \oplus R_t) \oplus P_x$

$Inf_o=D_ATA \oplus ID_r$

$MAC=H(DATA \oplus R_r)$

Finally forwards them to the reader.

If $x=n$, then updates the tuple by replacing K_o with K_n, P_o with P_n and α_o with α_n, resets $K_n=P(K_n)$, $P_n=P(P_n)$ and $\alpha_n=P(R_t \oplus R_r)$ respectively. If $x=o$, then resets $\alpha_n=P(R_t \oplus R_r)$.

Step 11: Server authentication

The tag authenticates the server, and updates the secret value.

The tag extracts P_i kept in to compute XOR with the received M_2. If the product matches $P(EPC_s \oplus R_t)$ computed by the tag itself, the authentication to the server is completed.

The content kept in tag is update as $K_{i+1}=P(K_i)$, $P_{i+1}=P(P_i)$ and $\alpha_{i+1}=P(R_t \oplus R_r)$ for next session.

3. Vulnerability analysis and improvement

Analysis:

The protocol does not follow Indistinguishability Rule I, III (see R-RAPSE). In Step 7, Step 11 of this protocol, the server and the tag update K_x, P_x, α_x respectively. However in Step 10, if an adversary blocks M_2 and transmits a meaningless value M_2^* to the tag, the authentication will fail, the value K_i, P_i, α_i in the tag will not be updated. In new session Step 4, the tag response information (M_1, β, α_i, γ), while α_i remains constant. This way, the adversary may continuously send requests to the tag, which may give rise to a distinguishability issue (α_i remains constant in each new session). The location of the tag owner can be exposed, and the privacy of the tag owner can be violated and the traffic of the tag owner can be analyzed.

Improvement:

According to Indistinguishability Rule III (see R-RAPSE), the transmitted information should be ensured randomization after the authentication failed to pass, and the tag key cannot be updated. In the new session Step 4, the tag response information is (M_1, β, α_i, γ), while α_i remains constant. Thus, α_i should be changed into a "random" number.

According to Indistinguishability Rule I (see R-RAPSE), we can introduce random numbers into the static information (constant) by some operations (such as XOR) to ensure indistinguishability of the tag. Modifying as follows: In Step 4, α_i may be replaced with $\alpha_i \oplus R_t$.

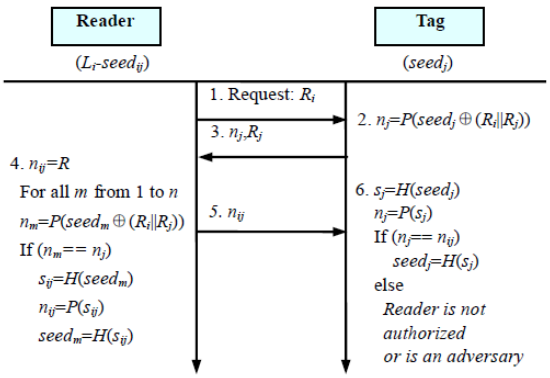

Figure 3. The protocol of S. I. Ahamed et al.

C. The S. I. Ahamed et al. Protocol

S. I. Ahamed et al.'s paper presents an authentication protocol [5] that described as serverless, lightweight, forward secured and untraceable authentication protocol for RFID tags, and claims that the protocol ensures security against almost all major attacks without the intervention of server, and is very critical to guarantee intractability and scalability simultaneously.

However, according to R-RAPSE, S. I. Ahamed's protocol may give rise to distinguishability issues. There is a possibility of exposing the location of the tag owner, violating the privacy of the tag owner can and analyzing the traffic of the tag owner. The analysis is described as follows:

1. Prior conditions and assumptions

The communication between the reader and the tag is insecure, without the intervention of the server.

The notations used in S. I. Ahamed's paper are given as follows:

R_{ij} random number generated by Reader *i*, and the related Tag *j*.

R_j random number generated by Tag *j*.

$seed_{ij}$ the seed of Reader *i*, and shared with Tag *j*.

$seed_j$ the seed of Tag *j*, and shared with Reader *i*

In initialization phase, the information shared by the reader and each tag is kept within respective devices:

Tag: (id_j, $seed_j$)

Reader: (L_i-$seed_j$)

where $L_i = \begin{Bmatrix} seed_1 & : & id_1 \\ \cdots & : & \cdots \\ seed_n & : & id_n \end{Bmatrix}$

In RFID system, every reader R_i has a L_i. For any tag T_j and 1≤j≤n, $seed_j$ is a seed used by R_i to communicate with T_j and id_j is the identifier of T_j, where $seed_j = f(r_i, t_j)=H(r_i||t_j)$. The initial $seed_j$ is computed by TC and stored in R_i.

2. Protocol description

S. I. Ahamed's protocol authenticates an RFID tag by a secret value $seed_x$. This is represented by Fig. 3. Step 4 and 6 of the protocol are described as follows:

Step 4: Tag authentication

The reader authenticates the tag, and updates the secret value.

Generates: random number *R*, and set $n_{ij}=R$.

For all *m* from 1 to *n* by running through list L_i, to computes: $n_m=P(seed_m \oplus (R_i||R_j))$. If the product n_m matches n_j, the tag passes through authentication by the reader.

The content kept in the reader is updated as $s_{ij}=H(seed_m)$, $n_{ij}=P(s_{ij})$ and $seed_m=H(s_{ij})$ for next session.

Step 6: Reader authentication

The tag authenticates the reader, and updates the secret value.

The tag extracts $seed_j$ kept inside to compute $s_j=H(seed_j)$, $n_j=P(s_j)$. If the product n_j matches n_{ij}, the reader passes through authentication by the tag.

The content kept inside tag is updated as $seed_j=H(s_j)$ for next session.

3. Vulnerability analysis and improvement

De-synchronization Issue

Analysis:

The protocol does not follow Key Synchronization Rule I, II (see R-RAPSE). In Step 4, Step 6 of this protocol, the reader and the tag update $seed_{ij}$, $seed_j$ respectively. However in Step 5, if an adversary blocks n_{ij} and transmits a meaningless value n_{ij}^* to the tag, the authentication will fail and the tag $seed_j$ will not be updated. This way, the key of the reader and tag will become desynchronized.

Improvement:

According to Key Synchronization Rule II (see R-RAPSE), Step 4 and Step 6 adopt the Double Key Update method. Like this, the desynchronized issue can be prevented to a large extent.

Distinguishability Issue

Analysis:

The protocol does not follow Mutual Authentication Rule II and Indistinguishability Rule I, II, III (see R-RAPSE). As stated above (see II. C. 3 (1)), in Step 6, after the reader authentication fails, and the shared key between the reader and the tag become desynchronized, resulting in the fact that the tag $seed_j$ is not updated. The value $seed_j$ thus becomes a constant. At this time, the adversary may launch a new session with a request: R_i (where R_i=0). In Step 3 the adversary receives (n_j, R_j), where $n_j= P(seed_j \oplus (0||R_j))$. As $seed_j$ is a constant, the MSB ($seed_j \oplus (0||R_j)$) is a constant and the LSB ($seed_j \oplus (0||R_j)$) only is of 8-bit (PRNG is 16-bit), and R_j can be intercepted by the adversary. Based on attributes PRNG i, ii, iii, (see Appendix R-RAPSE. B), it is easy to obtain $seed_j$, which may give rise to distinguishability issues. The location of the tag owner can be exposed, the privacy of the tag owner can be violated and the traffic of the tag owner can be analyzed.

Improvement:

According to Indistinguishability Rule II (see R-RAPSE), we can choose the random number R_i, R_j with high entropy and without 0/1.

According to Indistinguishability Rule III (see R-RAPSE), the transmitted information should be ensured randomization after the authentication failed to pass, and the tag key cannot be updated. In the new session Step 3, the tag response information is n_j, R_j, while n_j remains constant. Thus, n_j should be changed into a "random" number.

According to Indistinguishability Rule I (see R-RAPSE), we can introduce random numbers into the static information (constant) by some operations (such as XOR) to ensure indistinguishability of the tag. Modifying as follows: In Step 2, $seed_j$ may be replaced with $seed_j \oplus (R_j \, ||R_j^*)$, where R_j, R_j^* are two random numbers generated by the tag.

According to Mutual Authentication Rule II (see R-RAPSE), a single RN16 by itself cannot effectively protect the transmitted information to secure the information based on attributes PRNG i, ii, iii. Thus, a single RN16 by itself is not suitable for the encryption and authentication tools of RFID systems.

III. CONCLUSIONS

Design and verification of RFID authentication protocol should be supported by theoretical guarantees, rather than depending on intuition and experience. We had summed up a series of rules called R-RAPSE (see Appendix R-RAPSE). This paper's aims are to present R-RAPSE applications. Based on R-RAPSE, we verify and improve E. J. Yoon's scheme [2], J. S. Cho's scheme [3] and S. I. Ahamed's scheme [5]. In a general sense, we show that these algorithms are insecure, and demonstrate how R-RAPSE is used to verify and improve RFID authentication protocols. The results of the study suggest that R-RAPSE will be significant for design and validation of RFID authentication protocols.

IV. APPENDIX R-RAPSE

Security Issues and Requirements: The security issues of RFID systems mainly includes eavesdropping, unauthorized access, tampering, key leakage, key update

issue, privacy leakage, traffic analysis, location tracks replay attacks, impersonation attacks, DoS attacks, de-synchronization attacks, and cloning attacks. Thereinto, privacy leakage, traffic analysis, location tracks and cloning attacks are the special security issues for RFID systems. Thereinto, privacy leakage, traffic analysis, location tracks and cloning attacks are the special security issues for RFID systems.

We had summarized the following security requirements based on the essence of the security issues within RFID systems. The security requirements mainly include: indistinguishability, confidentiality, data integrity, forward security, impersonation resistance and de-synchronization resistance. Thereinto, indistinguishability is the special security requirements for RFID systems.

RFID Authentication Protocol Security Enhanced Rules (R-RAPSE): Design and verification of RFID authentication protocol should be supported by theoretical guarantees, rather than depending on intuition and experience. Based on the specific security issues and security requirements of RFID systems, we had summed up a series of rules called R-RAPSE, designed to provide systematic theory support for RFID authentication protocol design and verification. R-RAPSE is described as follows:

A. Lightweight Rule (LR): RFID authentication protocols should be lightweight. Restrained by cost and resources, the low-cost RFID tag is only able to support HASH, PRNG, XOR, and CRC.

B. Mutual Authentication Rule (MAR): MAR is necessary and critical. One of the parties (readers and tags) involved in a transaction needs to verify the identity of the other in RFID systems. Without the mutual authentication rule, it is possible for either or both of the parties to engage in illegitimate operations.

In RFID systems, algorithms that can usually be used to establish authentication protocols primarily include HASH, PRNG and CRC; their performances are analyzed as follows:

HASH

The hash function usually possesses three additional attributes when it is employed in cryptography [13, 14]:

Authorization verification.

Signature verification.

File verification.

Based on attributes HASH i, ii, the hash function is suitable for RFID authentication protocols that implement mutual authentication between the reader and the tag.

Based on the attribute HASH iii, the hash function can be use to protect the transmitted information between the readers and the tags from tampering, thus ensuring data integrity.

PRNG

Being consistent with EPC Gen2, this paper defines the low-cost RFID tag as having a 16-bit pseudo-random number generator. The attributes are as follows [10, 14]:

Probability of a single RN16: $0.8/2^{16}<Prob(RN16=RN)<1.25/2^{16}$.

Collisions: $Prob<0.1\%$, for a tag population of 10.000.

Predicting a RN16: Prob<0.025%, if the prior draws are known.

Based on attributes PRNG i, ii, iii, a single RN16 by itself cannot effectively ensure the transmitted information security. Thus, a single RN16 by itself is not suitable for the encryption and authentication tools of RFID systems.

CRC

A 16-bit CRC can be generated as follows:

CRC possesses three attributes:

$$CRC(A \oplus B) = CRC(A) \oplus CRC(B) \quad (1)$$

$$CRC(A \cdot x^{n\cdot(k-1)}) = CRC(CRC(\cdots CRC(A))) \rightarrow CRC^k(A) \quad (2)$$

If P, Q are 16-bit numbers, then

$$CRC(P(x)+Q(x)) = CRC(P(x)) + CRC(Q(x)) + CRC(0) \quad (3)$$

Based on CRC generation algorithms and CRC attributes, the CRC by itself cannot effectively protect against the intentional (malicious) alteration of data [10]. Therefore, CRC by itself is not suitable for the encryption and authentication tools of RFID systems.

C. Key Update Rule (KUR): To ensure forward security, keys or secret values should be updated after each successful authentication. It guarantees forward security by disconnecting the relation between the previous key and secret values.

D. Key Synchronization Rule (KSR): Key synchronization mostly depends on the key update methods. Based on the number of keys, existing key update methods can be categorized as follows:

Single Key Update: the server and tag only preserve the single latest key. Based on the mode, it is generally difficult to maintain key synchronization. If one party (such as the server) has updated its key successfully and the other party (such as the tag) cannot update its key, the key shared between the server and the tag will become desynchronized.

TABLE I. THE RELATIONSHIP OF SECURITY ISSUES, SECURITY REQUIREMENTS AND SECURITY RULES.

R-RAPSE	Security Issues	Security Requirements
Confidentiality Rule Mutual Authentication Rule	Eavesdropping Unauthorized access	Confidentiality
Data integrity Rule	Tampering	Data integrity
Indistinguishability Rule	Privacy leakage Traffic analysis Location track	Indistinguishability
Confidentiality Rule Indistinguishability Rule Mutual Authentication Rule	Replay attack Cloning attack	Impersonation resistance
Key Update Rule	Key leakage	Forward security
Key Synchronization Rule	Key update issue DoS attack De-synchronization attack	De-synchronization resistance

Double Key Update: The server and the tag preserve the double latest keys. Based on the mode, it is possible to maintain key synchronization. If the authentication

fails, and one party (such as the server) has updated its key successfully and the other party

(such as the tag) cannot update its key, the updated party can still take advantage of the previous key (the backup key) instead of the present key (the updated key), thus the desynchronized issue can be prevented to a large extent.

E. Scalability Rule (SR): There is a need for efficient communication protocols that allow the scalable deployment of RFID systems with a large number of tags [16, 17].

F. Confidentiality Rule (CR): To ensure confidentiality of the tag, the reader and the tag should be complied with the following.

RFID tags should only be allowed access by authorized readers.

RFID tags should not leak any secret information to unauthorized readers.

Minimizing the information exposure as possible (even random numbers) [9].

G. Indistinguishability Rule (IR): To ensure indistinguishability of the tag, the transmitted information should be randomized. The reader and the tag should be complied with the following.

Ensuring indistinguishability of the tag by introducing random numbers into the static information (remains constant) by some operations (such as XOR).

Ensuring transmission information security when the random numbers are all 0s or all 1s.

Ensuring randomization of the transmitted information after the authentication failed to pass, and the tag key cannot be updated.

H. Data Integrity Rule (DIR): To protect the important information (such as keys or secret values) from being tampered, and to ensure validity of the information, DIR should be followed. Based on the attribute HASH iii, the hash function can be used to protect the data integrity.

V. CONCLUSIONS

The general principles of RFID authentication protocols should comply with Rules A-E

The transmitted information of RFID authentication protocols should comply with Rules F-H

The relationship of security issues, security requirements and security rules is given in Table I

ACKNOWLEDGEMENTS

This work is sponsored by Project 61071038 supported by NSFC (National Natural Science Foundation of China), Project 61102034 supported by NSFC, Project 61172156 supported by NSFC, and the Combination Project of Industry and Research by the Ministry of Education of Guangdong Province 2011A090200128.

REFERENCES

[1] W. Zhou, S. Piramuthu, "Framework, strategy, and evaluation of healthcare processes with RFID," *Decision Support Systems*, vol. 50, pp. 222–233, January 2010.

[2] J. Cho, S. Yeo, S. S, & S. K. Kim, "Securing against brute-force attack: A hash-based RFID mutual authentication protocol using a secret value," *Computer Communications*, vol. 34, pp. 391–397, March 2011.

[3] E. J. Yoon, "Improvement of the securing RFID system conforming to EPC Class 1 Generation2 standard," *Expert Systems with Applications*, vol. 39, pp. 1589–1594, January 2012.

[4] T. C. Yeh, Y. J. Wang, T. C. Kuo, & S. S. Wang, "Securing RFID systems conforming to EPC Class 1 Generation 2 standard," *Expert Systems with Applications*, vol. 37, pp. 7678–7683, December 2010

[5] S. I. Ahamed, MD. E. Hoque, F. Rahman, F. Kawsar, and T. Nakajima, "Ya-Srap: Yet Another Serverless Rfid Authentication Protocol," *IE08*, pp. 1–8, July 2008, [In The 4th IET international conference on intelligent environment].

[6] H. Y. Chien, "SASI: A new ultralightweight rfid authentication protocol providing strong authentication and strong integrity," *IEEE Transactions on Dependable and Secure Computing*, vol. 4, pp. 337-340, April 2007.

[7] H. M. Sun, W. C. Ting, and K. H. Wang, "On the Security of Chien's Ultralightweight RFID Authentication Protocol," *IEEE Transactions On Dependable And Secure Computing*, vol. 8, pp. 315-317, February 2011.

[8] H. Y. Chien, & C. W. Huang, "A Lightweight Authentication Protocol for Low-Cost RFID," *J Sign Process Syst*, vol. 59, pp. 95–102, January 2010.

[9] C. L. Chen, & Y. Y. Deng, "Conformation of EPC class 1 and generation 2 standards RFID system with mutual authentication and privacy protection," *Engineering Applications of Artificial Intelligence*, vol. 22, pp. 1284–1291, August 2009.

[10] M. Burmester, B. D. Medeiros, J. Munilla, and A. Peinado, "Secure EPC Gen2 Compliant Radio Frequency Identification," *ADHOC-NOW*, pp. 227–240, 2009.

[11] S. Piramuthu, "RFID mutual authentication protocols," *Decision Support Systems*. vol. 50, pp. 387–393, 2011.

[12] J. S. Cho, S. S. Yeo, and S. K. Kim, "An analysis of RFID tag authentication protocols using secret value," *FGCN2007*, vol. 1, pp. 481–486, December 2007, [In: 2007 International Conference on Future Generation Communication and Networking].

[13] W. B. Mao, *Modern Cryptography: Theory and Practice*, Prentice Hall PTR, New Jersey, USA, 2003.

[14] A. Menezes, P. C. V. Oorschot, and S. A. Vanstone, *Handbook of Applied Cryptography*, CRC Press, FL, USA, 1996.

[15] S. Agusti, D. F. Josep, M. B. Antoni, & D. Vanesa, "A distributed architecture for scalable private RFID tag identification," *Computer Networks*, vol. 51, pp. 2268–2279, September 2007.

[16] S. Boyeon, & J. M. Chris, "Scalable RFID security protocols supporting tag ownership transfer," *Computer Communications*, vol. 34, pp. 556–566, April 2011.

[17] T. R. Rolando, & S. Agusti, "Efficient probabilistic communication protocol for the private identification of RFID tags by means of collaborative readers," *Computer Networks*, vol. 55, pp. 3211–3223, October 2011.

QingLing Cai has received her B. S. degree and M. S. degree in microcomputer research institute from Hefei University of Technology, P. R. China, and Ph. D. degree in Communication and Information System from Sun Yat-sen University, P. R. China, in 2009. Currently, she is associate

professor in School of Engineering, Sun Yat-sen University. Her research interests include information security, communication security and wireless networks.

YiJu Zhan has received his B. S. degree in Electrical Engineering, Hefei University of Technology, P. R. China, 1982, M. S. degree in Electrical Engineering, Hefei University of Technology, P. R. China, 1986, and Ph. D. degree in Electrical Engineering, the University of Hong Kong, in 1998. Currently, he is a professor in School of Engineering, Sun Yat-sen University. His research interests include automation control, intelligent information, automation distinguishing technology and wireless networks.

Jian Yang received the B. S. degree and M. S. degree in Biology Engineering from Northeastern University, Ph. D. degree in Communication and Information System from Sun Yat-sen University, China, in 2003, 2006 and 2009, respectively. His areas of specialized research interest include cognitive network, RFID MAC protocol and intelligent signals processing. Now he is a lecturer of faculty of automation, Guangdong University of Technology.

An Upper Bound on the Coding Capacity of Matroidal Network Associated with R_8

Hang ZHOU [1, 2]
1. State Key Laboratory of Integrated Services Networks (ISN), Xidian University, Xian, 710071, China
2. Engineering University of the Chinese People's Armed Police Force, Xian, 710086, China
Email: zhouhang2010@163.com

***Abstract*—In this paper, according to Dougherty et al.'s method, we construct a matroidal network associated with vector matroid R_8. Then we use Ingleton inequality and Zhang-Yeung non-Shannon-type information inequality respectively to compute upper bounds on coding capacity of the constructed matroidal network. Finally, We prove that the coding capacity of the matroidal network associated with R_8 is at most $7/4$.**

***Index Terms*—Network Coding; Information Inequality; Matroid; Upper Bound; Capacity**

I. INTRODUCTION

Traditionally, network messages are treated as physical commodities, which are routed throughout the network without replication or alteration. However, the network coding approach introduced by Ahlswede et al. [1], generalizes the routing approach by allowing the intermediate nodes to combine data received from their incoming edges. This technique has several important benefits, such as an increase in throughput and an improvement in the reliability and robustness of the network.

Matroids are a mathematical structure that generalize and unify several diverse topics including linear algebra, graph theory, and geometry. Matroid theory was widely used in combinatorial optimization, integer programming and network flowing in the past. The heart of matroid theory is the abstraction of "independence relation". It has been found have some close connections with the information-theoretic notion of entropy and some new applications in the field of network coding. Dougherty et al. defined matroidal networks and proposed a method for constructing matroidal networks from matroids in Ref. [2]. Such constructions allow interesting properties of matroids to be transferred to networks. Using this method, several well-known examples of matroids have been turned into networks that exhibit similar properties.

One fundamental problem in network coding is to understand the capacity region and the classes of codes that achieve the capacity. In the single session multicast scenario, the problem is well understood. In 2000, Ahlswede et al. [1] showed that the capacity of a multicast network is equal to the minimum of the max flows from the source to the destinations. Soon afterwards, Li, Yeung, and Cai [3] proved that linear network coding is sufficient for multicast networks to achieve the maximal throughput. Nonetheless, significant complications arise in more general scenarios, involving more than one session. Dougherty et al. used matroidal networks to show the insufficiency of linear network coding and the inachievability of network coding capacity in Ref. [4]. This has increased our knowledge about the limitations of network coding.

In this paper, we specifically construct a matroidal network from matroid R_8 according to Dougherty et al.'s method. The upper bounds on coding capacity of the matroidal network associated with R_8 are deduced from Ingleton inequality [5] and Zhang-Yeung non-Shannon-type information inequality [6] respectively. The rest of the paper is organized as follows. In Section II, we review basic definitions and relevant results of network coding, information inequality and matroid theory. Our main results are presented in section III. Conclusion appears in section IV.

II. PRELIMINARIES

A. Network Fundamentals

A point-to-point communication network is usually represented by a directed acyclic graph $\mathtt{G}=(\mathtt{V},\mathtt{E})$, where the set of nodes $\mathtt{V}$ and the set of directed edges $\mathtt{E}$ respectively model the set of communication nodes and error free, point-to-point directed links. A directed edge $e=(i,j)\in\mathtt{E}$ stands for a channel leading from node i to node j. Node i is called the tail of e and j is called the head of e. We write this as $i=tail(e)$ and $j=head(e)$. Correspondingly, the channel e is called an outgoing channel of i and an incoming channel of j. For a node i, we define $Out(i)=\{e\in\mathtt{E}: tail(e)=i\}$ and $In(i)=\{e\in\mathtt{E}: head(e)=i\}$. There are two disjoint subsets of special nodes $\mathtt{S}$, $\mathtt{T}\subseteq\mathtt{V}$. The nodes in $\mathtt{S}$ are called sources and have in-degree zero. The nodes in $\mathtt{T}$ are called sinks and have out-degree zero. All other nodes in $\mathtt{V}$ are called intermediate nodes. The goal of the problem is to transmit a collection of messages from the sources to the sinks. Each message is a symbol drawn from a specified alphabet $\mathtt{A}$ with an algebraic structure (such as a group or field). Each source s_i has a set of

doi:10.4304/jnw.9.1.36-41

available messages and each sink t_i demands a set of messages. One symbol from $\mathtt{A}$ can been transmitted over each edge in the directed graph $\mathtt{G}=(\mathtt{V},\mathtt{E})$.

A network code is an assignment of an edge function for each edge and a decoding function for each terminal. One way of modeling multiple uses of a network is to view each network edge as carrying a vector of alphabet symbols. Given an alphabet $\mathtt{A}$, a (k,n) code for a network is an assignment of edge functions

$$f_e:\mathtt{A}^k\to\mathtt{A}^n,\ \text{if } tail(e)\in S \tag{1}$$

$$f_e:\mathtt{A}^{n|In(v)|}\to\mathtt{A}^n,\ \text{if } tail(e)\notin S \tag{2}$$

for every edge $e\in\mathtt{E}$ and decoding functions

$$g_v:\mathtt{A}^{n|In(v)|}\to\mathtt{A}^k \tag{3}$$

for every receiver v. All message vectors are assumed to have the same dimension k and all edge vectors are assumed to have the same dimension n. For general k and n, a code that allows the sink nodes to deduce their demands is called a (k,n) fractional coding solution. A fractional coding solution is said to be linear if all edge functions and demand functions are linear combinations of their vector inputs.

When a (k,n) solution exists over an alphabet $\mathtt{A}$, the number k/n is said to be an achievable rate of the network, with respect to $\mathtt{A}$. An important goal in network coding is to find an achievable coding rate which is as large as possible for a network.

Definition 1: The coding capacity of a network over an alphabet $\mathtt{A}$ and a class of network codes C is

$$\sup\{k/n:\exists\ (k,n)\text{ coding solution in }\mathtt{C}\text{ over }\mathtt{A}\}.$$

If C consists of all network codes, then we simply refer to the above quantity as the coding capacity of the network with respect to $\mathtt{A}$. If we restrict attention to routing solutions or linear solutions, then the coding capacity is referred to as the routing capacity or linear coding capacity, respectively. The coding capacity of a given network is said to be achievable if there is some (k,n) solution for the network for which k/n equals the capacity.

The routing capacity of an arbitrary network can in principle be determined using a linear programming approach [7]. However, there are presently no known techniques for computing the coding capacity or the linear coding capacity of an arbitrary network.

B. Entropy and Information Inequalities

The characterization of the coding rate regions, the capacity achievable in different scenarios and, more generally, the solvability of a network coding problem reached the actual solutions mostly due to the information-theoretic results presented in this subsection.

Let $H(X)$ denote Shannon's entropy of a discrete random variable X over $\mathtt{A}$. When evaluating a network, we often consider the messages to be independent random variables. This allows us to consider the entropy for any collection of messages and packets, and thus keep track of the information as it flows through the network. The basic requirements of a network coding solution are summarized by the following lemma.

Lemma 1 ([3], Lemma III.1): If a network has a (k,n) coding solution over an alphabet $\mathtt{A}$, and the message components are independent random variables uniformly distributed over $\mathtt{A}$, then

(N1) (source rates) $H(X)=k|X|$ for any message set X.

(N2) (edge capacities) $H(x)\le n$ for any edge $x\in\mathtt{E}$.

(N3) (node input/output functional dependencies) $H(In(x))=H(In(x)\bigcup Out(x))$,

for any node $x\in\mathtt{V}$.

Let A, B and C be collections of discrete random variables over $\mathtt{A}$. The conditional entropy of A given B by

$$H(A|B)=H(A,B)-H(B), \tag{4}$$

the mutual information between A and B by

$$I(A;B)=H(A)-H(A|B), \tag{5}$$

and the conditional mutual information between A and B given C by

$$I(A;B|C)=H(A|C)-H(A|B,C). \tag{6}$$

The following information theoretic facts will be used in the remainder of this paper.

$$H(A)\ge H(A|B)\ge 0 \tag{7}$$

$$I(A;B)\ge 0, \tag{8}$$

$$H(A,B|C)\le H(A|C)+H(B|C) \tag{9}$$

$$H(A|B,C)\le H(A|B)\le H(A,C|B) \tag{10}$$

Definition 2: Let q be a positive integer, and let $S_1,\cdots,S_k$ be subsets of $\{1,\cdots,q\}$. Let $\alpha_i\in R$ for $1\le i\le k$. A linear inequality of the form

$$\alpha_1 H(\{A_i:i\in S_1\})+\cdots+\alpha_k H(\{A_i:i\in S_k\})\ge 0 \tag{11}$$

Is called an information in equality if it holds for all jointly distributed random variables $A_1,\cdots,A_q$.

Definition 3: A Shannon-type information inequality is any information inequality that is a finite sum of the form

$$\sum_i \alpha_i I(A_i;B_i|C_i)\ge 0, \tag{12}$$

where each α_i is a nonnegative real number. Any information inequality that cannot be expressed in the form (12) will be called a non-Shannon-type information inequality.

In 1998, Zhang and Yeung gave the first example of an information inequality on four variables in Ref. [6], which is a non-Shannon-type information inequality. It usually be written in the following form:

$$2I(C;D) \le I(A;B)+I(A;C,D) +3I(C;D|A)+I(C;D|B) \quad (13)$$

Unlike the preceding inequalities, the Ingleton inequality

$$I(A;B) \le I(A;B|C)+I(A;B|D)+I(C;D) \quad (14)$$

is not an information inequality — there exist jointly distributed random variables that violate the Ingleton inequality. However, the Ingleton inequality does hold for the special case of random variables that vary uniformly and independently over specified subspaces of a given finite vector space.

C. Matroid Fundamentals

We review here various definitions and results in matroid theory, as they are useful in the remainder of the paper. For more details, the reader is referred to [8].

Definition 4: A matroid $\mathtt{M}$ is an ordered pair $(E,\mathtt{I})$, where E is a finite set and $\mathcal{I}$ is a set of subsets of E satisfying the following three conditions:

(I1) $\varnothing \in \mathtt{I}$.

(I2) If $I \in \mathtt{I}$ and $J \subseteq I$, then $J \in \mathtt{I}$.

(I3) If $I, J \in \mathtt{I}$ and $|J| < |I|$, then there exists an element $x \in I \setminus J$ such that $J \bigcup x \in \mathtt{I}$.

The set E is called the ground set of the matroid. The matroid $\mathtt{M}=(E,\mathtt{I})$ is called a matroid on E. The members of $\mathcal{I}$ are called independent sets and any subset of E not in $\mathcal{I}$ is called a dependent set. A maximal independent set of E is called a base of $\mathtt{M}$. A minimal dependent set of E is called a circuit.

Definition 5: The rank function is a function r from subsets of E to integers satisfying the following three conditions:

(R1) If $X \subseteq E$, then $0 \le r(X) \le |X|$.

(R2) If $X \subseteq Y \subseteq E$, then $r(X) \le r(Y)$.

(R3) If $X \subseteq Y \subseteq E$, then

$r(X \bigcup Y)+r(X \bigcap Y) \le r(X)+r(Y)$.

Definition 6 (Matroid Isomorphism)**:** Two matroids $\mathcal{M}_1=(E_1,\mathcal{I}_1)$ and $\mathcal{M}_2=(E_2,\mathcal{I}_2)$ are isomorphic if there is a bijection map $\varphi: E_1 \to E_2$, such that for all $I \in \mathtt{I}_1$ if and only if $\varphi(I) \in \mathtt{I}_2$.

The primary example of a matroid comes from graph theory.

Definition 7 (Graphic Matroid) Let $\mathtt{G}$ be an undirected graph with the set of edges E. Let

$\mathtt{I}=\{X \subseteq E : X$ does not contain a cycle$\}$.

We define the graphic matroid associated with $\mathtt{G}$ as $\mathcal{M}(\mathtt{G})=(E,\mathtt{I})$

Another important example of a matroid is obtained from linear algebra.

Definition 8 (Vector Matroid): Let A is an $m \times n$ matrix over field $\mathtt{F}$. If $E=\{1,2,\cdots,n\}$ is the set of column indices of A and $\mathtt{I}$ is the set of all $X \subseteq E$ such that the multiset of columns of A indexed by the elements of X is linearly independent, then $(E,\mathtt{I})$ forms a matroid, called the vector matroid of A, denoted by $\mathtt{M}[A]$.

If a matroid $\mathtt{M}$ is isomorphic to the vector matroid $\mathtt{M}[A]$ over $\mathtt{F}$, then $\mathtt{M}$ is called $\mathtt{F}$-representable, and A is called an $\mathtt{F}$-representation of $\mathtt{M}$.

Let

$$\begin{array}{cccccccc} a & b & c & d & e & f & g & h \end{array}$$

$$A=\begin{bmatrix} 1 & 0 & 0 & 0 & -1 & 1 & 1 & 1 \\ 0 & 1 & 0 & 0 & 1 & -1 & 1 & 1 \\ 0 & 0 & 1 & 0 & 1 & 1 & -1 & 1 \\ 0 & 0 & 0 & 1 & 1 & 1 & 1 & -1 \end{bmatrix}_{GF(3)} \quad (15)$$

be a matrix over the finite field $GF(3)$ and the columns of A are indexed by a,b,c,d,e,f,g,h, as labeled above the matrix. Particularly, this vector matroid $\mathtt{M}[A]$ is denoted by R_8 in matroid theory and matrix A is a $GF(3)$-representation of R_8.

D. Matroidal Networks

In this subsection, we describe the method for building networks from matroids which was introduced by Dougherty et al. Such constructions allow interesting properties of matroids to be transferred to networks.

Definition 9([3], Definition V.1): Let $\mathcal{N}$ be a network with message set μ, node set $\mathtt{V}$ and edge set $\mathtt{E}$, let $\mathtt{M}=(E,\mathtt{I})$ be a matroid with rank function r. The network $\mathcal{N}$ is a matroidal network associated with $\mathtt{M}$ if there exists a function $f: \mu \bigcup \mathtt{E} \to E$, call the network-matroid mapping, such that the following conditions are satisfied:

(M1) f is one to one on μ.

(M2) $f(\mu) \in \mathtt{I}$.

(M3) $r(f(In(x))) = r(f(In(x) \bigcup Out(x)))$ for every $x \in \mathtt{V}$.

Let $\mathtt{M}=(E,\mathtt{I})$ be a matroid with rank function r. Let $\mathcal{N}$ denote the network to be constructed, with message set μ, node set $\mathtt{V}$. The construction will simultaneously construct the network $\mathcal{N}$, the network-matroid mapping $f: \mu \bigcup \mathtt{E} \to E$, and an auxiliary function $g: E \to \mathtt{V}$, where for each $x \in E$, $g(x)$ is either

(1) a source node with message m and $f(m)=x$, or

(2) a node with in-degree 1 and whose in-edge e satisfies $f(e)=x$.

The construction is carried out in four steps and each step can be completed in potentially many different ways.

Step 1: Create network source nodes $n_1, n_2, ..., n_{r(E)}$ and corresponding messages $m_1, m_2, ..., m_{r(E)}$. Choose any base $B = \{b_1, b_2, ..., b_{r(E)}\}$ for M and let $f(m_i) = b_i$, $g(b_i) = n_i$.

Step 2: (to be repeated until it is no longer possible) Find a circuit $\{x_0, x_1, ..., x_j\}$ in M, such that $g(x_1), ..., g(x_j)$ have been already defined, but $g(x_0)$ has not yet been defined. Add a new node y and edges $e_1, ..., e_j$ such that e_i connects $g(x_i)$ to y, and we define $f(e_i) = x_i$. Then add another new node n_0 with a single in-edge e_0 that connects y to n_0. Let $f(e_0) = x_0$ and $g(x_0) = n_0$.

Step 3: (to be repeated as many times as desired) If $\{x_0, x_1, ..., x_j\}$ is a circuit in M and $g(x_0)$ is a source node with message m_0, then add to the network a new receiver node y, which demands the message m_0 and which has in-edges $e_1, ..., e_j$ where e_i connects $g(x_i)$ to y. Let $f(e_i) = x_i$.

Step 4: (to be repeated as many times as desired) Choose a base $B = \{x_1, ..., x_{r(E)}\}$ of M and create a receiver node y that demands all of the network messages, and such that y has in-edges $e_1, ..., e_{r(s)}$, where e_i connects $g(x_i)$ to y. Let $f(e_i) = x_i$.

III. Main Results

A. The Matroidal Network Constructed from R_8

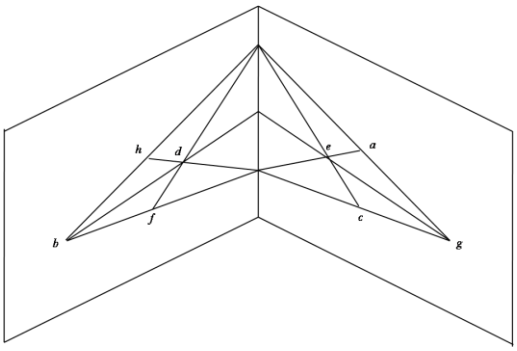

Figure 1. Geometric depiction of the matroid R_8.

R_8 is an eight-element matroid with rank four. The matrix A in (15) is the $GF(3)$-representation of R_8. Fig. 1 is a geometric depiction of R_8 whose dependent sets are the four-element sets which are coplanar in the three-dimensional drawing.

The network $\mathcal{N}$ illustrated in Fig.2 is a matroidal network associated with R_8 and we do not go into more depth regarding this construction. If additional explanation of each step are required, see subsection II-D. The network-matroid mapping is partially shown over $\mathcal{N}$ where the mapping on the unlabeled edges is given by the usual convention.

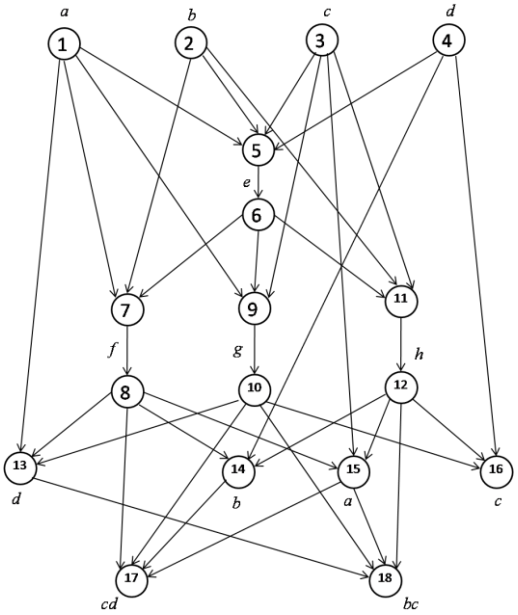

Figure 2. A matroidal network $\mathcal{N}$ associated with R_8.

Table I lists the dependencies in vector matroid R_8, which are directly reflected in the matroidal network $\mathcal{N}$.

TABLE I. Dependencies in vector matroid R_8 that are reflected in the matroidal network $\mathcal{N}$

Step	Variables	Node	Type
1	{a, b, c, d}	n_1, n_2, n_3, n_4	Message
2	{a, b, c, d, e}	n_5, n_6	Circuit
2	{a, b, e, f}	n_7, n_8	Circuit
2	{a, c, e, g}	n_9, n_{10}	Circuit
2	{b, c, e, h}	n_{11}, n_{12}	Circuit
3	{a, d, f, g}	n_{13}	Circuit
3	{b, d, f, h}	n_{14}	Circuit
3	{a, c, f, h}	n_{15}	Circuit
3	{c, d, g, h}	n_{16}	Circuit
4	{a, b, f, g}	n_{17}	Independent set
4	{a, d, g, h}	n_{18}	Independent set

B. Upper Bounds on the Coding Capacity of Matroidal Network $\mathcal{N}$ Associated with R_8

In this subsection, we deduce the upper bound on the coding capacity of matroidal network $\mathcal{N}$ as shown in Fig. 2.

Theorem: The coding capacity of the matriodal network $\mathcal{N}$ associated with R_8 is at most $7/4$.

Proof: Consider the (k, n) solution to the matriodal network $\mathcal{N}$ in Fig. 2**.** Assume that the network messages a, b, c, d are independent k-dimensional random vectors with uniformly distributed components and assume each edge in the network has capacity n. Let e, f, g, h denote the random variables carried by edges $e_{5,6}, e_{7,8}, e_{9,10}, e_{11,12}$, respectively. By condition (N3) of lemma 1, we can obtain

$$H(e|a,b,c,d)=0\ [\text{at } n_5] \quad (16)$$

$$H(f|a,b,e)=0\ [\text{at } n_7] \quad (17)$$

$$H(g|a,c,e)=0\ [\text{at } n_9] \quad (18)$$

$$H(h|b,c,e)=0\ [\text{at } n_{11}] \quad (19)$$

$$H(d|a,f,g)=0\ [\text{at } n_{13}] \quad (20)$$

$$H(b|d,f,h)=0\ [\text{at } n_{14}] \quad (21)$$

$$H(a|c,f,h)=0\ [\text{at } n_{15}] \quad (22)$$

$$H(c|d,g,h)=0\ [\text{at } n_{16}] \quad (23)$$

$$H(c,d|a,b,f,g)=0\ [\text{at } n_{17}] \quad (24)$$

$$H(b,c|a,d,g,h)=0\ [\text{at } n_{18}] \quad (25)$$

Let $A=(a,g)$, $B=(d,f)$, $C=(b,e)$, $D=(c,h)$. Then we obtain

$I(A;B)=I(a,g;d,f)$
$=H(a,g)+H(d,f)-H(a,d,g,f)$
$=H(a,g)+H(d,f)-H(a,g,f)$ [from (20)]
$=H(d,f)-H(f\,|\,a,g)$ [from (4)]
$\geq H(d,f)-n$ [from (7), (N2)]

$I(A;B|C)=I(a,g;d,f|b,e)$
$=H(a,b,e,g)+H(b,d,e,f)-H(b,e)$
$-H(a,b,d,e,g,f)$
$=H(a,b,e,g)+H(b,d,e,f)-H(b,e)$
$-H(a,b,c,d,e,g,f)$ [from (24)]
$=H(a,b,e,g)+H(b,d,e,f)-H(b,e)-H(a,b,c,d)$
$\leq H(a,b)+H(e,g)+H(d,f)+H(b,e)$
$-H(b,e)-4k$ [from (9), (N2)]
$\leq 2k+2n+H(d,f)-4k$ [from (N1), (N2)]
$=H(d,f)-2k+2n$

$I(A;B|D)=I(a,g;d,f|c,h)$
$=H(a,c,g,h)+H(c,d,f,h)-H(c,h)$
$-H(a,c,d,f,g,h)$
$=H(a,c,g,h)+H(c,d,f,h)-H(c,h)$
$-H(a,b,c,d,f,g,h)$ [from (21)]
$=H(a,c,g,h)+H(c,d,f,h)-H(c,h)-H(a,b,c,d)$
$=H(a,c,g,h)+H(d,f)+H(c,h)$
$-H(c,h)-4k$ [from (9), (N1)]
$\leq H(a,c)+H(g,h)+H(d)+H(f)-4k$
$\leq 3n-k$ [from (N1), (N2)]

$I(C;D)=I(b,e;c,h)$
$=H(b,e)+H(c,h)-H(b,c,e,h)$
$=H(b,e)+H(c,h)-H(b,c,e)$ [from (19)]
$=H(c,h)-H(c\,|\,b,e)$ [from (4)]
$\leq H(c,h)$ [from (7)]
$\leq H(c)+H(h)$ [from (9)]
$\leq k+n$ [from (N1), (N2)]

From Ingleton inequality (Equation (14)), we get

$H(d,f)-n\leq I(A;B)$
$\leq H(d,f)-2k+2n+3n-k+k+n$
$=H(d,f)-2k+6n$.

Then, we obtain

$$\frac{k}{n}\leq\frac{7}{2}. \quad (26)$$

Similarly, let $A'=(a,g)$, $B'=(b,f)$, $C'=(c,e)$, $D'=(d,h)$. Then

$I(C';D')=I(c,e;d,h)$
$=H(c,e)+H(d,h)-H(c,d,e,h)$

$I(A';B')=I(a,g;b,f)$
$=H(a,g)+H(b,f)-H(a,b,g,f)$
$=H(a,g)+H(b,f)-H(a,b,c,d,g,f)$ [from (24)]
$=H(a,g)+H(b,f)-H(a,b,c,d)$
$=H(a,g)+H(b,f)-4k$ [from (N1)]

$I(A';C',D')$
$=I(a,g;c,e,d,h)$
$=H(a,g)+H(c,e,d,h)-H(a,c,\mathrm{d},\mathrm{e},\mathrm{g},h)$
$=H(a,g)+H(c,e,d,h)-H(a,b,c,\mathrm{d},\mathrm{e},\mathrm{g},h)$ [from (25)]
$=H(a,g)+H(c,e,d,h)-H(a,b,c,\mathrm{d})$
$=H(a,g)+H(c,e,d,h)-4k$ [from (N1)]

$I(C';D'|A')$
$=I(c,e;d,h|a,g)$
$=H(a,c,e,g)+H(a,d,g,h)-H(a,g)$
$-H(a,c,\mathrm{d},\mathrm{e},\mathrm{g},h)$
$=H(a,c,e,g)+H(a,d,g,h)-H(a,g)$
$-H(a,b,c,\mathrm{d},e,g,h)$ [from (25)]
$=H(a,c,e,g)+H(a,d,g,h)-H(a,g)$
$-H(a,b,c,\mathrm{d})$

$= H(a,c,e)+H(a,d,g,h)-H(a,g)-4k$ [from (18), (N1)]

$I(C';D'|B')$

$= I(c,e;d,h|b,f)$

$= H(c,e,b,f)+H(b,d,f,h)-H(b,f)$

$-H(b,c,d,e,f,h)$

$= H(b,c,e,f)+H(d,f,h)-H(b,f)$

$-H(a,b,c,d,e,f,h)$ [from (21), (22)]

$= H(b,c,e,f)+H(d,f,h)-H(b,f)-H(a,b,c,d)$

$= H(b,c,e,f)+H(d,f,h)-H(b,f)-4k$

From Zhang-Yeung non-Shannon-type information inequality:

$2I(C';D') \le I(A';B')+I(A';C',D')$

$+3I(C';D'|A')+I(C';D'|B')$,

we obtain

$2H(c,e)+2H(d,h)-2H(c,d,e,h)$

$\le H(a,g)+H(b,f)-4k$

$+H(a,g)+H(c,d,e,h)-4k$

$+3H(a,c,e)+3H(a,d,g,h)-3H(a,g)-12k$

$+H(b,c,e,f)+H(d,f,h)-H(b,f)-4k$.

Then , we have

$24k \le -2H(c,e)-2H(d,h)+3H(c,d,e,h)$

$-H(a,g)+3H(a,c,e)+3H(a,d,g,h)$

$+H(b,c,e,f)+H(d,f,h)$

$= 2H(c,d,e,h)-2H(c,e)+H(c,d,e,h)$

$-H(d,h)+H(a,d,g,h)-H(d,h)$

$+H(a,d,g,h)-H(a,g)+3H(a,c,e)$

$+H(a,d,g,h)+H(b,c,e,f)+H(d,f,h)$

$= 2H(d,h|c,e)+H(c,e|d,h)+H(a,g|d,h)$

$+H(d,h|a,g)+3H(a,c,e)+H(a,d,g,h)$

$+H(b,c,e,f)+H(d,f,h)$

$\le 2H(d)+2H(h)+H(c)+H(e)+H(a)$

$+H(g)+H(d)+H(h)+3H(a)+3H(c)$

$+3H(e)+H(a)+H(d)+H(g)+H(h)$

$+H(b)+H(c)+H(e)+H(f)$

$+H(d)+H(h)+H(f)$ [from (9)]

$\le 16k+14n$ [from (N1), (N2)]

Therefore

$$\frac{k}{n} \le \frac{7}{4}. \qquad (27)$$

From (26), (27), we know that the upper bound on coding capacity of the matroidal network $\mathcal{N}$ associated with R_8 is at most $7/4$.

IV. Conclusion

In this paper, a matroidal network associated with R_8 is constructed using the method proposed by Dougherty et al. A tighter upper bound on the capacity of the matroidal network associated with R_8 is deduced from Zhang-Yeung non-Shannon-type information inequality.

Acknowledgment

The author would like to thanks Prof. Ning CAI, my supervisor, for his patient guidance and helpful discussions. This work is funded by the National Natural Science Foundation of China under grants No.61271174 and No.61272492.

References

[1] R. Ahlswede, N. Cai, R. Li S.-Y, and R. W. Yeung, "Network information flow," *IEEE Trans. Inf. Theory*, vol. 46, no. 4, pp. 1204-1216, Jul. 2000.

[2] R. Li S.-Y, R. W. Yeung, and N. Cai, "Linear network coding," *IEEE Trans. Inf. Theory*, vol. 49, no. 2, pp. 371-381, Feb. 2003.

[3] R. Dougherty, C. Freiling, and K. Zeger, "Networks, matroids, and non-Shannon information inequalities," *IEEE Trans. Inf. Theory*, vol. 53, no. 6, pp. 1949-1969, Jun. 2007.

[4] R. Dougherty, C. Freiling, and K. Zeger, "Insufficiency of linear coding in network information flow," *IEEE Trans. Inf. Theory*, vol. 51, no. 8, pp. 2745-2759, Aug. 2005.

[5] A. W. Ingleton, Representation of Matroids in Combinatorial Mathematics and Its Applications , *D. J. A. Welsh, Ed. London, U.K.: Academic*, 1971, pp. 149-167.

[6] Z. Zhang and R. W. Yeung, "On characterization of entropy function via information inequalities," *IEEE Trans. Inf. Theory* , vol. 44, no. 4, pp. 1440-1452, Jul. 1998

[7] J. Cannons, R. Dougherty, C. Freiling, and K. Zeger, " Network routing capacity," *IEEE Trans. Inf. Theory*, vol. 52, no. 3, pp. 777-788, Mar. 2006

[8] J. G. Oxley, Matroid Theory, *Oxford University Press, New York*, 1992.

Hang ZHOU was born in 1975. He received the B.S. degree in pure mathematics from Yunnan University, Yunnan, China in 1998, and received the M.S. degree in pure mathematics from Northwestern Polytechnical University, Xi'an, China in 2005. Now he is a Ph.D. candidate at school of telecommunications engineering, Xidian University.

He is currently an associated professor in Engineering University of the Chinese people's Armed Police Force, Xi'an, China. His research includes network coding and matroid.

Case Study for a GPON Deployment in the Enterprise Environment

Stanislav Milanovic
Highest Institute of Education, Science and Technology, Athens, Greece
Email: stanislav.milanovic@ieee.org

***Abstract*—Enterprise networks are facing disruptive change caused by the use of Internet versus enterprise based applications, increasing video content, integration of voice services onto the LAN, and the transition from wired to wireless LANs. This paper explores this opportunity to adopt Passive Optical LANs (POLs), based on Gigabit Passive Optical Network technology (GPON), rather than continuing with use of traditional two- or three-tier switched Ethernet solution.**

***Index Terms*—GPON based POLs; Single Mode Fibre; Cloud Computing; WLAN; IP and RF Video; Surveillance; VoIP; Security; QoS**

I. Introduction

The rapid growth of bandwidth requirements and the changing role of enterprise networking are causing disruptive change in the enterprise LANs. Accommodating increased bandwidth, though it is the primary agent causing disruptive change, is not the only one [1]. Other change agents include the need to:

- accommodate wired and wireless connectivity
- support voice, video, and data services
- migrate from perimeter to role-based security
- reduce labor- intensive network operations tasks
- deploy environmentally friendly solutions

While facing disruptive change to either an existing enterprise site or a new enterprise site, a global organization had the opportunity to dramatically reduce Total Cost of Ownership (TCO) by moving to a Passive Optical LAN (POL), based on GPON technology (Gigabit Passive Optical Network), rather than continuing with use of traditional two- or three-tier switched Ethernet solution. GPON technology is used to establish a passive infrastructure that does not require any electrical power at the intermediate nodes between the aggregation and the user nodes.

Passive Optical LAN is being adopted at a fast pace by large government and enterprise LAN customers attracted to the benefits of significant cost savings. Migrating to a high-performance local area network does not have to mean paying more in equipment costs or energy consumption [2]. A new generation of Passive Optical LAN technology actually reduces long-term costs, while delivering all the performance benefits expected of optical networks.

II. Requirements and Goals

When deploying LANs, a global enterprise juggled three, often conflicting, requirements. Budgetary constraints dictated the need to control both initial and long-term networking costs. Yet enterprise business also wanted to install the latest technology — in terms of network speed, functionality and security — in a way that enables the cost-effective evolution of networks in step with inevitable advances in technology. Finally, as an environmentally conscientious enterprise, a global organization seeked the greenest-possible route to achieving the other two objectives, namely by deploying LANs that would reduce the organizations' energy consumption.

Fortunately it now has been possible to achieve all three goals at the same time by deploying advanced optical LANs solution, based on GPON technology.

III. What is Passive Optical LAN and How does the GPON Work?

Passive Optical LAN is alternative to the traditional layer-2 copper based LAN infrastructure. It is covered by ITU-T G984.x industry standard (Full Service Access Network), which is based upon the GPON technology, using a Generic Encapsulation Method (GEM) that supports Ethernet, ATM, and TDM data transport. POL enables the delivery of highly-secure unified networks providing IP voice, data, and any type of video over a single fiber [3].

Gigabit-speed Passive Optical Networks use single-mode fiber, connecting the headend-optical line terminal (OLT) through one or more passive optical splitters, to multiple endpoints called optical network terminals (ONTs). GPON delivers 2.5 Gbps of bandwidth to each ONT. ONT converts optical signals to the signals used in building wiring, such as Ethernet and wired analogue plain old telephone service [4]. Each PON can incorporate from 1:1 up to 1:128 splits and is dependent upon the committed and peak information rates. In practice most PONs are deployed with a split ratio of 1:32 or 1:64 (Figure 1).

Distances of up to 20 km with a 32-way split can be supported. The technology is considered "passive" because transmission is powered directly from the OLT to the ONT and there is no switching or routing in between.

doi:10.4304/jnw.9.1.42-47

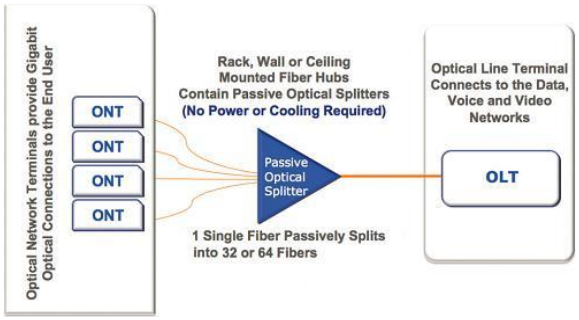

Figure 1. GPON connectivity

IV. Architecture Comparison

Throughout enterprises, Category 3/5/6 copper cables typically connect 3 layers of routers and switches in a traditional active Ethernet LAN [5]. A router in the top-most layer (CoreLayer) links to the campus or building aggregation switches (Distribution Layer) below. These switches, in turn, connect down to the access layer switches in the communications closets. Copper cables extend from the communications closets to the users (Figure 2).

An optical LAN, on the other hand, simplifies the network and eliminates aggregation levels [6]. This solution retains the router at the top-most layer and the Optical Line Terminal (OLT) serves the same purpose as the campus aggregation switches, which effectively eliminates the campus- and building-aggregation switches, as well as the communications closets. Instead, a single-mode fiber, typically equipped with a 1x32 optical splitter, runs between the router and OLT to the Optical Network Terminals (ONTs) serving end-users [7]. An optical splitter is a passive device so there are no power requirements. (Figure 3).

Both solutions provide data access via 1000Base-T Ethernet connections to the user. Therefore, no client or PC reconfiguration is required when upgrading from active Ethernet to a GPON infrastructure.

V. Closer Look at the GPON

GPON is a Layer 2 non-fragmented multiservice network architecture that complements the Layer 3 services offered by a core switch through native or tagged VLANs, native SIP support and bit, port, and segment visibility, control and management [8]. It takes advantage of wavelength division multiplexing (WDM), using one wavelength (1490nm) for 2.5G downstream traffic and another (1310nm) for 1.2G upstream traffic on a single fiber. The 1550 nm wavelength is reserved for optional overlay services, typically RF (analog) video.

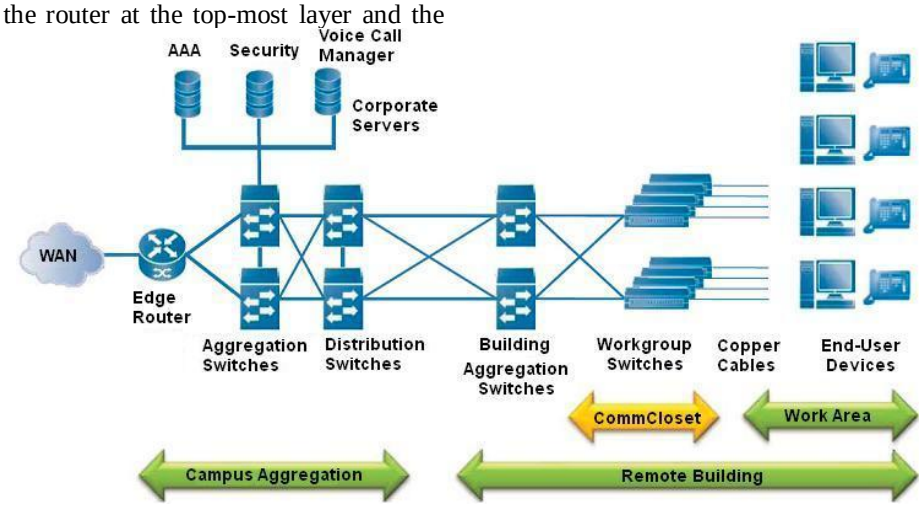

Figure 2. Traditional active Ethernet LAN

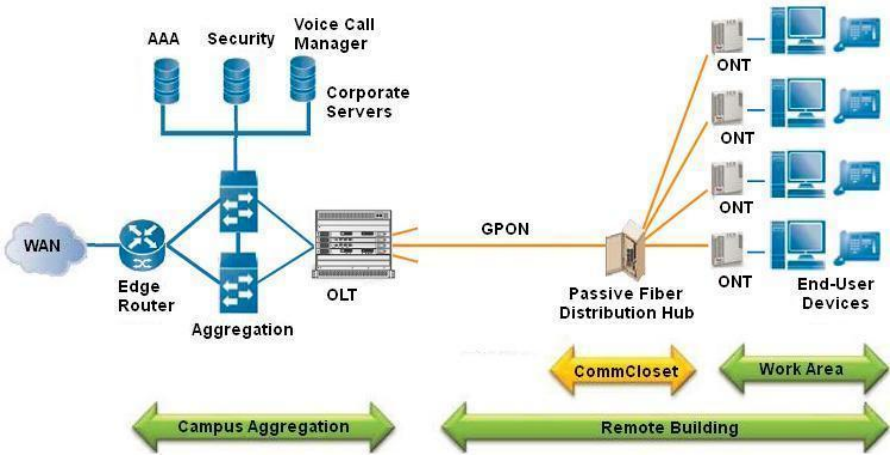

Figure 3. Passive optical LAN

GPON is a point to multi-point aggregation core network architecture that offers port and bit segmentation for guaranteed Quality of Service (QoS). GPON does not broadcast and instead, it distributes all downstream signals through secure, virtual point-to-point connections, which utilize AES-128 encryption between the OLT and ONT [9]. Upstream signals are combined using a multiple access protocol, usually time division multiple access (TDMA) or a dynamic bandwidth-allocation scheme, which prevents different users' data frames from interfering with each other.

A GPON Ethernet port that connects to a VoIP phone operates in the same fashion as a traditional switched network. If the ONT is configured in support of QoS for the VoIP connection, it will support that bit rate [10]. If additional port capacity is needed, it is a simple matter of configuring the port capacity for the required services.

GPON traffic flows in symmetric fashion within assigned segments and VLANs. Up to 4000 VLANs are supported per OLT. ONTs configured for one VLAN can not be swapped for another VLAN or segment at any time [11]. This improves security, manageability and network performance. When the GPON is properly designed for Peak and Committed Information Rate (PIR/CIR), segmented by VLAN and service for QoS, and established according to the input capacity to include the core switch, performance will be exceptional largely from the elimination of switch fragmentation.

GPON bit rates are configured according to QoS requirements for given services. A fully integrated GPON network actually reduces the number of disjointed network management systems and bandwidth requirements within a data center or wiring closet [12]. GPON provides convergence of voice, data, IP and RF Video, POTS, security, surveillance, alarms, environmental systems and access control systems over a single network utilizing the advanced security features of QoS, class of service and VLAN mechanisms.

GPON chassis (OLT) is accompanied by a management workstation (Element Management System) that presents a Graphical User Interface (GUI) and Command Line Interface (CLI) for configuration purposes [13]. The ability to manage bit, port, and power levels across the system, in VLANs and groups, and down to individual ports provides performance assurance that is just not available in legacy switched network configurations.

GPON ONTs are available with Power over Ethernet (PoE), both in low power IEEE 802.3af and high power IEEE 802.3at standard configurations. The GPON configuration can also provide guaranteed power management or elimination of PoE [14]. Broadcast storms from loopback cables are also eliminated via a 5ms default port shutdown and non-conductive fiber.

VI. Passive Optical LAN vs. Traditional LAN

Figure 4 depicts differences between the POL and traditional active Ethernet LAN infrastructure.

Traditional LAN	Passive Optical LAN
High Initial and Recurring Expense	Lower Cost to Implement in building and throughout a campus
Recurring switch and cable forklift upgrades	Collapse overlapping network services – eliminates forklift upgrades
High Operating Cost	Significant reduction in budgetary consumption
Voice and Data capable with limited QoS capability	Voice, Video, Data, Sensors any configuration. Port and Bit level control maximizes QoS
Migration to Edge Routing and Layer 3 "intelligence" calling for AC in telco closets	No power consumed in passive middle.Chassis doesn not require an Air Conditioned room
Fragmented data and voice network that was never designed for video	Non-fragmented point to multi-point fiber network, designed first for video
Fragmentation limits security capability and adds cost	Port and Bit level control, non-fragmented, no added cost
Voice and Data with up to 8 ovelapping communication oriented networks	Capability to collapse network services to a common Operational Services Network platform
Point to Point Distributed Edge Services	Point to multi-point distributed core

Figure 4. Differences between active Ethernet LAN and passive optical LAN

VII. Shift to Cloud Computing

Although virtualization and consolidation are driving very high capacity needs in the corporate data center, the trend for applications and data to be increasingly located at a different physical site from most users changes some of the fundamental design requirements for enterprise premises LANs [15]. The emergence of cloud computing models compounds this effect (Figure 5). In "traditional" premises LAN designs supporting local servers, LAN (especially backbone) capacity was more important than WAN capacity [16]. But with remote servers and resources in centralized data centers or "in the cloud", WAN and premises LAN/backbone capacity requirements converge.

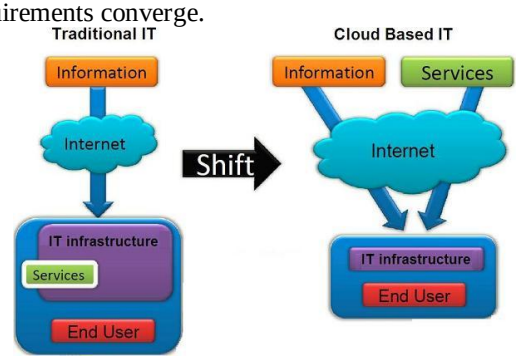

Figure 5. Trend towards the cloud computing model

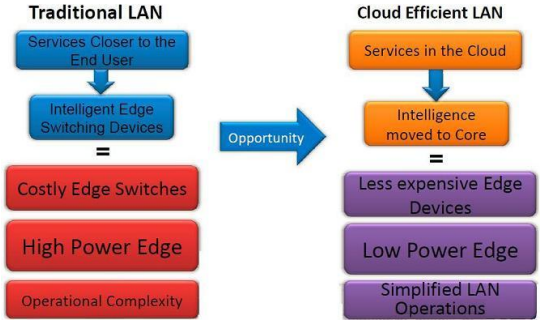

Figure 6. Opportunity to rethink the enterprise LAN

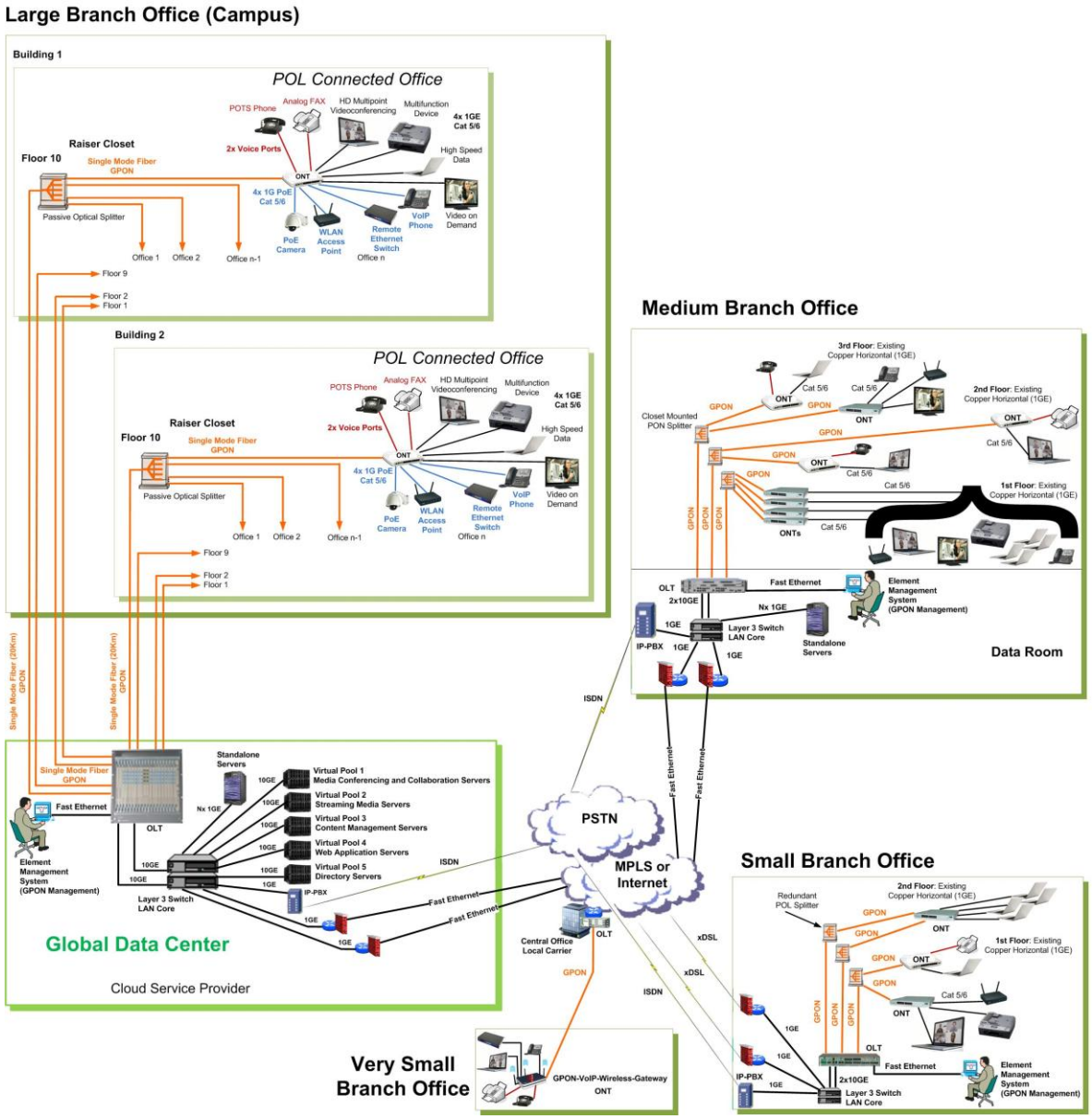

Figure 7. GPON based POLs in the enterprise environment of a global organization

In addition, the enterprise networks are increasingly using wireless for user access, and Wi-Fi is becoming the default wireless choice. Because the floor area supported by a typical Wi-Fi access point is less than that supported by a typical wired Ethernet switch, the physical reach of the backbone needs to increase. Fiber-optic cabling meets these needs, and the fiber backbone/wireless access model has already been dubbed "Fi-Wi“ [17]. GPON is a good match for these needs and also enables lower-cost campus networks, as it is more cost-effective at long distances than switched Ethernet.

This opens up opportunity for GPON's simpler and less expensive, but shared bandwidth model for enterprise premises LAN (Figure 6).

VIII. GPON Deployment in the Enterprise Environment

Applied optical LAN solution architecture uses GPON technology to provide connectivity between the OLT and the ONT. The transmission is powered directly from the OLT to the ONT and there is no switching or routing in between. The Figure 7 describes the high-level architecture of deployed optical LAN solution. It depicts Passive Optical LANs deployment for a global organization, based on GPON technology, including the LAN use cases for a large office, medium office, small office, and a very small office, as well as a global data center operating in a hybrid cloud model.

ONT converts fiber optic “light signals” to copper’s “electric signals” for delivery of advanced services like IPTV, VoD (Video on Demand), VoIP and other packet-based video and voice services directly to the end user equipment. At the end user desktop, an ONT provides a managed demarcation point for network services. The ONT itself has no user controls and is managed via the OLT’s Element Management System. A key security feature provided by optical LAN solution ensures that the ONT cannot function unless provisioned by the OLT.

OLT enables symmetrical broadband service delivery to the end-user device, which is the ONT, and end user equipment like IPTV box, surveillance camera, VoIP phone and laptop computers. It also supports quality of service (QoS) and flexible dynamic bandwidth allocation. OLT sends a single stream of downstream traffic that is seen by all ONTs. Each ONT only reads the content of those packets that are addressed to it. Encryption is used to prevent eavesdropping on downstream traffic. The data stream between the OLT and the ONT is encrypted using AES encryption standard with AES-128 block cipher.

Applied GPON based POLs in the enterprise environment enabled the convergence of voice, data and video onto a single strand of single mode fiber, which reduced the network infrastructure hardware to a fraction of what is required in terms of cabling and electronics in the conventional Ethernet approach. The solution not only enabled easier maintenance, but also improved efficiency with regard to end user-related, adds, moves and changes.

Since there are no active electronic components between the data center and the end user, particularly in the riser closets, there are significant power savings as cooling is not required in the riser closets. Implemented fiber optical LANs are more energy-efficient and environmentally friendly and they take up less floor, rack and closet space than traditional active Ethernet LANs. Applied solution also requires no signal regeneration for up to 20 kilometers between the data center and the end user. Those features and capabilities enable a faster return on investment and significantly reduce total cost of ownership, both in terms of capital and operating expenditures during the life of the infrastructure (Figure 8).

Expense	250 Users	500 Users	1000 Users	Campus 5000 Users
TCO	32%	46%	57%	68%
CapEx	31%	41%	48%	55%
OpEx	40%	50%	65%	70%
Power	48%	61%	68%	75%
Cooling	48%	61%	68%	75%

Figure 8. POL savings compared to active Ethernet LAN

Single-mode fiber is expected to support advances in GPON technology for years to come. Passive Optical LANs can be upgraded without new cable infrastructure deployment. Expanding a GPON based POL is simply a matter of adding new OLT connectivity. As 10GPON (or XGPON) emerges, a global enterprise can upgrade its Optical LANs simply by upgrading the terminal electronics. Unlike traditional Ethernet LANs where the cabling infrastructure must be replaced each time the Ethernet switches increase link speed, Optical LANs will not require fiber infrastructure upgrades or any work environment changes.

Thus by replacing its legacy LANs with optical solution based on GPON technology, a global organization could readily achieve its overriding LAN objectives. Applied GPON based POLs delivered the necessary speeds, capacity and functionalities in the enterprise environment. The Enterprise controls now both near- and long-term CapEx and OpEx. Equally important, by deploying GPON based POLs, a global organization has got a network that's designed to satisfy its unique requirements for years to come.

IX. Conclusion

The centralization of data centers and emergence of cloud computing, combined with the increasing shift from wired to wireless at the edge of the enterprise network, are subtly changing the requirements for enterprise LANs [18]. These trends are shifting the needs for high-performance and advanced features into data center networks, with a resulting opportunity for simpler premises LANs.

Deployed GPON based POLs in the enterprise environment extended service to any stationary Ethernet end point. It enabled the delivery of reliable and highly-secure unified network providing IP voice, data, and any type of video over a single fiber. It also increased the size of the network building block which greatly simplified enterprise network deployment, operation, and management. The solution supported energy conservation, since the optical LAN infrastructure utilized passive components like optical distribution hubs and fiber plant that required no power or cooling, resulting in significant energy savings. Implemented POLs provided immediate return on investment and a low total cost of ownership compared to copper-based LANs.

Communications Service Providers (CSPs) that are already operating GPON as part of their FTTH services will be in an interesting position to operate passive optical LAN infrastructure for enterprises that are interested in outsourcing their LANs. As such, passive optical LAN could become an integral part of CSPs' cloud strategies.

References

[1] "Deploying a Passive Optical Network in a Standards-Based Enterprise Environment", *Craig Kegerise, BICSI News Magazine*, 2013

[2] "Next Generation LAN Solutions from Verizon Business", *Verizon* 2012.

[3] "GPON - The new enterprise cable infrastructure standard", *Armored Shield Cable Manufacturing Business*, 2012.

[4] "Next-Generation PON Evolution", *Huawei Technologies Co., Ltd.* 2012.

[5] Rodney Casteel, "Passive Optical LAN", *CommScope, Inc.*, 2012.

[6] Xianbin Yu, Ying Zhao, Lei Deng, Xiaodan Pang, Monroy, I. T., "Existing PON infrastructure supported hybrid fiber-wireless sensor networks", *IEEE Optical Fiber Communication Conference and Exposition (OFC/NFOEC), and the National Fiber Optic Engineers Conference*, 2012.

[7] Haotian Wang, Yongjun Zhang, Wei Wang, Lei Yan, Zheng Ma, Wanyi Gu, Zhiyun Chen, "Study on Application of GPON-Based Transmission Hierarchy in

Mesh Network", *IEEE Symposium on Photonics and Optoelectronics (SOPO)*, 2012.
[8] Benyuan Zhu, Au, D., Farooq Khan, Yaowen Li, "Coexistence of 10G-PON and GPON reach extension to 50-km with entirely passive fiber plant", *37th IEE European Conference and Exhibition on Optical Communication (ECOC)*, 2011.
[9] Jain, S., Effenberger, F., Szabo, A., Zhishan Feng, Forcucci, A., Wei Guo, Yuanqiu Luo, Mapes, R., Yixin Zhang, O'Byrne, V., "*World's First XG-PON Field Trial*", *Journal of Lightwave Technology*, 2011.
[10] Weis, E., Breuer, D., Lange, C., "Technologies for next generation optical access", *14th IEEE International Conference on Transparent Optical Networks (ICTON)*, 2-5 July 2012.
[11] Matavulj, P. S., Blanusa, M. S., "Techno-economic analysis of GPON and FTTC/VDSL access networks", *19th Telecommunications Forum (TELFOR)*, 2011.
[12] Gebizlioglu, O. S. ; Kuwahara, H. ; Jain, V. ; Spencer, J., " Passive optical networks (PONs): toward next-generation PONs ", *IEEE Communications Magazine*, 2011
[13] Yixin Wang, Wu Kuang, Weifeng Rong, "Some considerations on the design of passive optical networks", *10th IEEE International Conference on Optical Communications and Networks (ICOCN 2011)*.
[14] Zhaoqing, Wang, "Research on the Application of GPON Technologies", *International IEEE Conference on Multimedia and Signal Processing (CMSP)*, 2011.
[15] Parra, O. J. S., Pantoja, G. N., Rubio, G. L., "Strategies for a Solution Convergence Networks", *7th IEEE International Conference on Wireless Communications, Networking and Mobile Computing (WiCOM)*, 2011.
[16] S. S. Riaz Ahamed, "A novel view on Passive Optical Network strategies in the computer communication", *International Journal of Engineering Science and Technology*, 2010.
[17] Aurzada, F., Scheutzow, M., Reisslein, M., Ghazisaidi, N., Maier, M., "Capacity and Delay Analysis of Next-Generation Passive Optical Networks (NG-PONs) ", *IEEE Transactions on Communications*, 2011.
[18] Stanislav Milanovic, "Case Study for Unified Backhaul Performance Optimization", *Journal Of Computers*, Volume 2, Issue 10, pp. 38-44, ISSN 1796-203X, Academy Publisher, Finland, Dec. 2007.

Stanislav Milanovic received in 2003 his Ph.D. in Computer Science and Engineering from Highest Institute of Education, Science and Technology, Athens, Greece. Dr. Milanovic also attained his M.Sc. and B.Sc (Honors 1st Class) in 2001 and 1992 respectively, both in Electrical Engineering, at University of Belgrade, Department of Electrical Engineering.

He is associate at Highest Institute of Education, Science and Technology in Athens, Greece. He has been a Senior Network Architect with IBM Global Services in Germany. His major responsibility included support in information technology services to IBM's portfolio of global customers. Prior to IBM, he was working as a Network Engineer with Serco Group plc and KPMG Consulting Group. His assignments included support to the networking services departments at European Space Agency, Italian Ministry of Defence, Hutchison 3G, Telecom Italia Mobile (TIM), Wind, Ericsson, Telecom Italia and Agip Petroli.

Dr. Milanovic is WSEAS Honorary Member and IEEE Member. He has served as a member of international scientific committee at various WSEAS and IEEE conferences. Dr. Milanovic is a GLG Leader (Top3% of GLG Council Members) at Gerson Lehrman Group Inc, delivering expertise and decision-making assistance to business, government and investment leaders from around the world.

Artificial Intelligence based Profit-Sharing Algorithm in Multi-Agent Systems

Jianjun Lang [1, 2] and Qigang Jiang [1*]
1. JiLin University, ChangChun, China
2. ChangChun University of Technology, ChangChun, China
*Corresponding author, Email: jiangqigang11@jlu.edu.cn

***Abstract*—In a dynamic environment, it is quite reasonable to implement functions as a set of rules into an agent to react to unexpected situations, because it is very difficult to have a correct model of the environment. This paper describes a reinforcement studying method to acquire the rules, each of which consists of state and action pair, for coordinating execution of the multiple cranes in a coil-yard of steel manufacture. The cranes are operated asynchronously, based on the decision of each crane's operator who only knows locally available information in this domain where it is natural to use a decentralized multi-agent model. However, decentralization causes other serious problems, such as conflicts among the agents. It is very difficult to design rules to resolve conflicts by means of mathematical analysis, because information is scattered, missions are generated stochastically and it is very hard to execute missions on schedule. In this paper, we, here, give a kind of Profit-sharing strategy, which is based on artificial intelligence. Profit-sharing strategy solves the issue that when conscious aliasing and concurrent studying occur. In a true multi-agent environment, a fact is that movement actions means more under certain circumstance, if you consider the surroundings as MDPs. Since Profit-sharing is an exploitation intensive method, it reinforces meaningful actions remarkably to resolve the conflicts.**

***Index Terms*—Artificial Intelligence; Crane; Decentralized Multi-Agent Model; Profit-Sharing Algorithm; Conscious Aliasing; Concurrent Studying**

I. INTRODUCTION

This paper describes a reinforcement studying method to acquire the rules, each of which consists of state and action pair, for coordinating execution of the multiple cranes in a coil-yard of steel manufacture. The cranes are operated asynchronously, based on the decision of each crane's operator who only knows locally available information in this domain where it is natural to use a decentralized multi-agent model. However, decentralization causes other serious problems, such as conflicts among the agents. It is very difficult to design rules to resolve conflicts by means of mathematical analysis, because information is scattered, missions are generated stochastically and it is very hard to execute missions on schedule.

For a stochastic domain, a reinforcement studying approach is notable and attractive to acquire the rules to react without any model. But, in fact, difficulties exist all the time, such as applying the reinforcement studying methods to different areas where full of multiple agents. In this paper, we present Profit-Sharing (PS) [1]-[3] algorithm. Under such circumstances, different agents have the ability to study all the time, including competitive counterparts which may share the same resource. It is guaranteed to converge to the rational policy even in the non-Markov Decision Processes (MDPs), if a credit is assigned by the certain reinforcement function which satisfies "Rationality Theorem".

We corroborated that PS is the better reinforcement studying algorithm than QL for Pursuit Game. A typical multi-agent environment through some experimental results [4]-[6] show. But in Pursuit Game, agents pursue a common goal without conflict over the resource. The conflicts would cause non-determinism in state transitions of the environment where the DP-based algorithms could not guarantee the convergence. Such as Q-studying (QL) [7]-[9] and Temporal Difference Studying (TD) [10]. Also, it is still unknown whether PS, which is not based on DP, is available or not to share the same resources among counterparts. Thus, the problem arises. Cranes is appropriate to evaluate the performance of PS toward the competitive domain, because there exist ugly conflicts. Multiple agents may share the same limited resources among cranes.

There are two purposes of this paper; one is to clarify the problems reinforcement studying among multiple agents. The other purpose, however, is to show the advantages of PS approach in the domain where agents have close relations and act competitively through some experiments.

In Sect. 2, we give the meaning of Cranes Control. In Sect. 3, we briefly introduce the principles of PS and its advantage over QL in the Crane Control Problem we treat here. In Sect. 4, we demonstrate that the performance of cranes executing by PS agents is better than that of QL ones through several experiments. It introduces the QL. In addition, we show that the performance of our model using reinforced cooperative rules is superior to the one using a reactive planning framework in the dynamic coil-yard environment. Finally, we take the actual environment into account. Our PS strategy's applicability is considered and in the end, we give the future point of view.

doi:10.4304/jnw.9.1.48-55

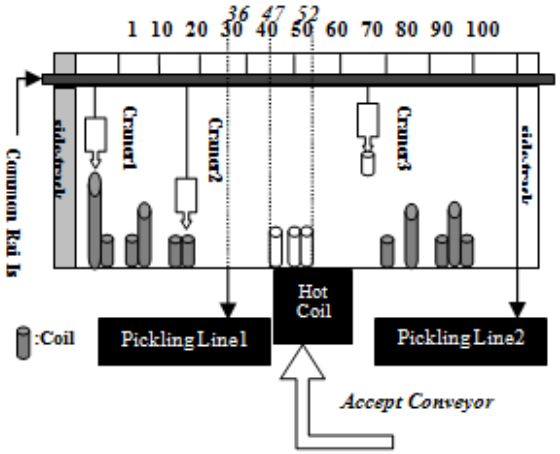

Figure 1. Coil-yard model and types of missions

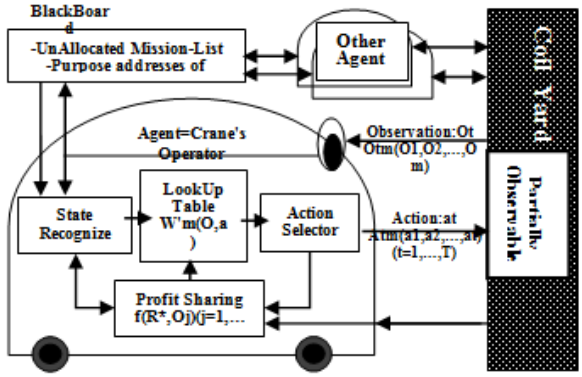

Figure 2. Cranes operating field

II. PROBLEM DOMAIN

A. Crane Control Problem

We consider the coil-yard manufacture as the primary field. If you do the such industrial process, a lot of problems arise. For example, many tons of coils, are in the process of turning cold and hot. Different cranes do individual missions. Although processes are asynchronously, they should share some special resources, thus leading to coordination. So they must cooperate with counterparts agent, which, however, could not be predicted ahead of time. Because cranes are running through the common rails and it is very hard to transact missions on schedule, the operators need to react rationally to avoid collisions which cause very serious accident.

We treat this problem using two dimensional model where location in the coil-yard is identified by an address, as shown in Fig. 1(a). The coil-yard consists of 100 addresses. And at both ends (address1 and address100), there are the side-tracks to take refuge from a collision among cranes. Every mission is showed by two separated addresses which mean the initial location and destination of the agent, respectively. The missions can be classified into two types. One is the mission to carry a hot coil into the coil-yard, and the other is the one to carry a cool-downed coil out to be in a special mark. Such as Fig. 1, in which Mission2 and 4 are the former one, and Mission1, Mission3 and Mission5 belong the latter type of mission as shown in Fig. 1(b).

From the other point of view about the cranes, limited required time to get one mission over must be minimized, which is very hard to achieve using formalized strategy because the circumstance is extremely full of uncertainty. That is, you must use other ways to get agent knowledge board.

B. Multi-Agent Model

We modeled this problem as a multi-agent environment, and have embedded an agent into each crane's operator to manage assignment of mission and its execution.

Firstly, a set of missions is broadcasted by the process of higher level, then each operator recognizes missions generation and decides its assignment of mission by means of the blackboard, as shown in Fig. 2. The type of Mission1 is assigned to Crane1 and Mission5 is assigned to Crane3. The assignment of Mission2, Mission3, and Mission4 is based on (Start, End) of Mission and (CPi, InitPi) of Crane's. (CPi: current position of Cranei, InitPi: predefined territory of each Crane, Crane1=0, Crane2 = 50,Crane3 = 80) Each of these mission types is assigned to the Cranei which could minimize |Start - CPi| +|End - InitPi|.

Secondly, after getting the assignment, each crane moves from its current address to the Start of the coil's to take it. Then the crane grasps the coil and carries it to its destination (End), and finally puts it into there.

Looking at Fig. 2, there are four parts in the model, in which the most important is the Learner. Profit-sharing algorithm is included here. Firstly, a mark named ot is got by the agent, which means the usable state of the surrounding at time t. Then individual action is accordingly choosed (Roulette-Selection strategy, in which the main step is selected in proportion to its weight) from the required set at. It includes usable steps at t. After the step is choosey, the individual decides whether an outcome is gave out. Once no outcome is generated, corresponding strategy is stored. If you do the same way in cranes, seamless outcome would be also integrated in the Leaner. We define an episode as a period between a start time and a final time. When one individual get the outcome, R, the routines stored in the Learner would be reinforced by adding the heurstic table to the logic function. Thus is defined by the Rationality Theorem (see Sect. 3.2).

There are four states of each crane, that is,{To Start ,To End, Rolling, Vacant}. To start means that crane is getting from individual start mark to the stored mark of the coil. To End means that crane is moving to put the coil to the destination address.

And Vacant means that crane has no assigned mission. As for an action set of the crane, three kind of basic steps are included. Backward move is defined first, and then is forward move, which should include waiting status of course.

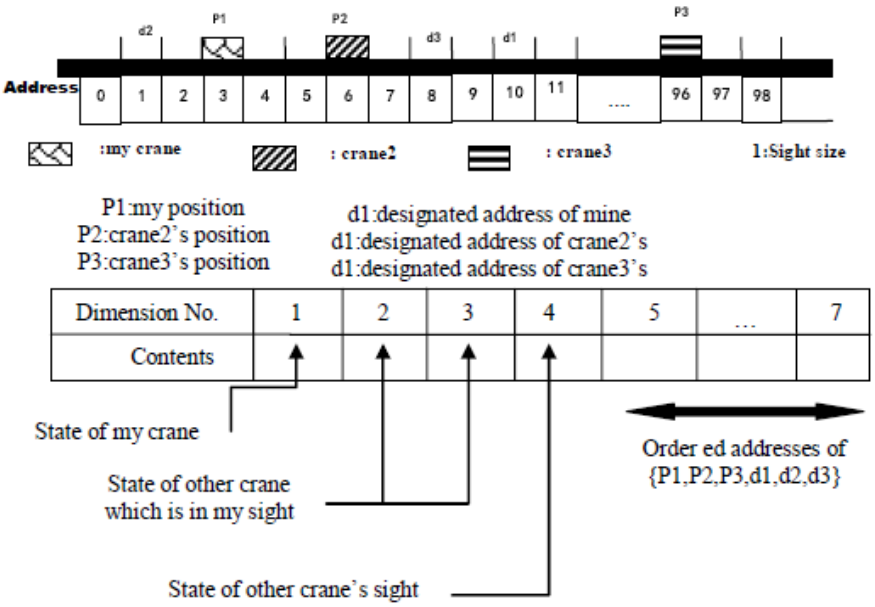

Contents of the Dimension : (*in case of cane*1)

$NO.5: x = P1 - d1$ if $x > 0_{then}1$, if $x < 0_{then} -1$, if $x = 0_{then}0$

$NO.6: y1 = P1 - d2$ if $y1 > 0_{then}1$, if $y1 < 0_{then} -1$, if $y1 = 0_{then}0$

$NO.7:$ if $x - y1 > 0_{then}1$, if $x - y1 < 0_{then} -1$, if $x - y1 = 0_{then}0$

$NO.8: z1 = P1 - P2$ if $x - z1 > 0_{then}1$, if $x - z1 < 0_{then} -1$, if $x - z1 = 0_{then}0$

$NO.9:$ if $y1 - z1 > 0_{then}1$, if $y1 - z1 < 0_{then} -1$, if $y1 - z1 = 0_{then}0$

$NO.10:$ if $z1 - x > y1_{then}1$, if $z1 - x < y1_{then} -1$, if $z1 - x = y1_{then}0$

$NO.11: y2 = P1 - d3$ if $y2 > 0_{then}1$, if $y2 < 0_{then} -1$, if $y2 = 0_{then}0$

$NO.12:$ x $- y2 > 0_{then}1$, if x $- y2 < 0_{then} -1$, if x $- y2 = 0_{then}0$

$NO.13: z2 = P1 - P3$ if x $- z2 > 0_{then}1$, if x $- z2 < 0_{then} -1$, if x $- z2 = 0_{then}0$

$NO.14:$ if $y2 - z2 > 0_{then}1$, if $y2 - z2 < 0_{then} -1$, if $y2 - z2 = 0_{then}0$

$NO.15:$ if $z2 -$ x $> y2_{then}1$, if $z2 -$ x $< y2_{then} -1$, if $z2 -$ x $= y2_{then}0$

$NO.16:$ if $y1 > y2_{then}1$, if $y1 < y2_{then} -1$, if $y1 = y2_{then}0$

$NO.17:$ if $z1 > z2_{then}1$, if $z1 < z2_{then} -1$, if $z1 = z2_{then}0$

Figure 3. Representation of state space

C. Representation of State Space

A representation of agent's state space is one of serious problems applying reinforcement studying to the true world. If a single agent manages those state spaces using absolute addresses of each crane, it must treat about (4 ·106)3 in the case of three cranes. On the other hand, if an agent managed one crane and has a limited sight l (Fig. 3), it treats about (4 ·106) ·(4 ·l ·104) 2. Even in the latter representation, it is very difficult to handle them.

Our representation of the agent's state space consists of 17 dimensions as shown in Fig. 3. Here, information of others is represented in terms of the relative locations of cranes' and their destinations, which are more important than the absolute ones. By means of this representation, we obtain an extremely conservative estimate of the state size is about 107.

We are concerned here with acquisition of rules to evade collision among the cranes of which states are To Start or To End. Because these situations are most difficult to design the knowledge. As for in the other situations, agent acts according to the rules as shown in Figs. 4(a), (b). For example, the case where one is in Rolling and the other is in To Start, the former crane gets priority. Figure 4(c) shows the rules which are embedded into RAP model which is used to compare with our model (see Sect. 4.2). The agent moves toward its purpose address (forward-move) when other cranes are out of its sight. When other crane(s) is(are) in its sight, the agent can recognize the information of other's state(s) and the purpose address(es). Then, agent learns rules to resolve conflicts using PS.

In section 3, the main idea is reinforcement studying and describe our approach concerning multiple agent environment.

(a) Evade Collision Rules of Crane1/3 against Crane2

State of other crane's		Other:Crane2					
State of other crane's		ToStart	ToEnd	Rolling	Wait	Back	Vacant
My:Crane1	ToStart	Reinforcement Target Area		Wait	Wait	Back	Forward
	ToEnd			Wait	Wait	Back	Forward
	Vacant	B/W	B/W	Wait	Wait	Back	Wait

(b) Evade Collision Rules of Crane2 against Crane1/3

State of other crane's		Other:Crane1/3			
State of other crane's		ToStart	ToEnd	Rolling	Vacant
My:Crane2	ToStart	Reinforcement Target Area		Wait	Forward
	ToEnd			Wait	Forward
	Vacant	B/W	B/W	Wait	Wait
	Wait for Crane3/1	Wait	Wait	Wait	Wait
	Back for Crane3/1	Back	Back	Wait	Back

(c) Hand-coded Heuristic Evade Collision Rules in RAP model in the Case of Target Area

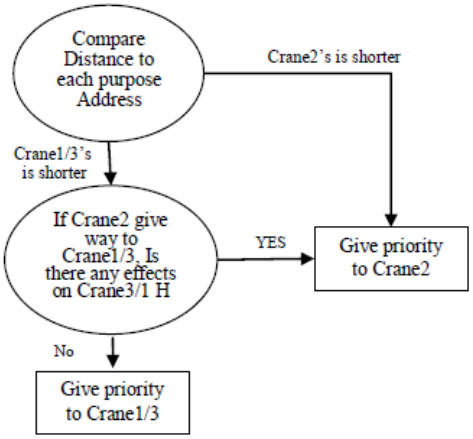

Figure 4. Reactive rules to evade collision.

III. Approach by Reinforcement Studying

A. Requirements of Multi-Agent World

Two major problems which cause non-determinism in state transitions are brought about with the same reason showing as crane control problem. The most important is treated as the limited sensing ability. In such case, one individual has to sensing more than two marks as a single mark. This issue is named conscious aliasing. Then corresponding problem comes. When one single action is needed by all separated states, conscious aliasing is showed out. Finally it leads to a makeable state space. Although different actions are needed by different agents, much confused status hence performs steps that are out of imagine. Moreover, second issue is contributed to concurrent studying. This is because the dynamics of the surroundings change unpredictably. When it need studying, each individual varies each own rules and actions asynchronously. Accordingly, an individual could not compute the structure of the transitional abilities for its surrounding. What mentioned above can lead to non-determinism when happens in state variations.

For these two problems, DP-based methods, such as QL and TD, would be weaker than the non-DPbased method, such as PS. Because the former methods assume that he environment has a MDPs'property; i.e. the DP-based methods use mark of special sequence (V (ot+1)) , in order to change the initial mark (V (ot)) as listed in Eq. (1), their weakness would be exposed in the environment where state transition probabilities could be varied. On the other hand, the latter does not need any MDPs' property, to acquire the effective rules. To relax the limiting effects that result with using MDPs' property, TD(λ), Q(λ) and Sarsa (λ) method are proposed. But they need a lot of extra memory to manage the delayed reward which is one of important issue to be considered in our domain. In this paper, we discuss the advantage of PS toward multiagent world through the comparison with QL which is a typical DP-based method and fully uses MDPs'property,

$$Q_{n+1}(o_t,a_t) \leftarrow Q_n(o_t,a_t)+\alpha\left(r+\gamma V_n(o_{t+1})-Q_n(o_t,a_t)\right)$$

With the mark changed, individual renews Qn(ot, at) by discounting future issues once again and counting them by positive studying mark α . In this paper γ (0.5 < γ < 1) is a computing mark in discounting, and V (ot+1) is showd then. When no immediate reward r exists, the agent uses r = 0 to update Qn(ot, at).

$$V_n(o_{t+1}) = \max_{b \in acttions} Q(o_{t+1},b)$$

B. Profit-Sharing Approach

Our approach is based on PS, in which rules in an episode are reinforced after agents getting a reward according to the certain logic function in the Rationality Theorem. Here, we would emphasis two special rules which are very important. One is that "Rationality Theorem" is treated as converging on a method. What is more, the other is that PS does not need MDPs' property, such as transitional probabilities from state to state.

$$W_{n+1}(o_t,a_t) \leftarrow W_n(o_t,a_t)+f(t,R,T)$$

Here, W and n indicate weight (value) of rule (ot, at) and the number of episodes, respectively.

Rationality Theorem (Ineffective rule suppression theorem): Any related strategy should be showed if

$$\forall t = 1,2,...,T,\ L\sum_{j=0}^{t} f(\mathrm{j},\mathrm{R},\mathrm{T}) < f(\mathrm{t},\mathrm{R},\mathrm{T})$$

A representation of agent's state space is one of serious problems applying reinforcement studying to the true world. If a single agent manages those state spaces using absolute addresses of each crane, it must treat about in the case of three cranes. On the other hand, if an agent managed one crane and has a limited sight l. Even in the latter representation, it is very difficult to handle them.

In PS algorithm, MDPs' property (mentioned in Sect. 3.1) is not necessary; all rules on an episode are reinforced by traditional marks, which are not any tables of issue estimation. On the other hand, the QL-agent must be deceived in state1. This is due to that individual estimation depend on separate movement related to lower valued priority. The effectiveness about PS toward a partially observable environment is discussed.

In the global point of view, the environment's subgoal is each agent's final achievement. We treat this problem using two dimensional models where location in the coil-yard is identified by an address. The coil-yard

consists of 100 addresses. And at both ends, there are the side-tracks to take refuge from a collision among cranes. Every mission is showed by two separated addresses which mean the initial location and destination of the agent, respectively. The missions can be classified into two types. One is the mission to carry a hot coil into the coil-yard, and the other is the one to carry a cool-downed coil out to be in a special mark. Such as PS, in which Mission2 and 4 are the former one, and Mission1, Mission3 and Mission5 belong the latter type of mission.

The designing reward has a key to resolve the conflicts among the agents. In the coil-yard, there would be happened a serious conflicts, for example. In this case, more than three changes can be imagined on designing the goals. First is the priority that needs the subgoal. It can be stopped at any time under any environment. The second one is the performance difference. Higher result would come out in better rules, that is, agent who finished the mission first learned the actions which he should do after his finishing mission. However, this exposes some drawbacks, especially when requiring bundles of time to study from the error issue, such as increasing number of missions and individuals. It would be given after a serious delay which makes the length of the episode become to be longer. In the latter case, we should design the rules to manage his (operator's) movement when the mission is achieved, for that every individual studies just matters related to critical movement before the final goal is achieved and he never care about after finishing his goal. If these rules, concerning after finishing his mission, are not given to the agents, the agent who finished his mission will stay at the goal, then another agent cannot reach his goal. Fortunately, in this case, such algorithm is easily generated. We set agent who finish his mission to give the priority to others.

IV. EXPERIMENT

This section describes the method of our experiments. There are two purposes in our experiments. The first is getting about the outcome of making the prizes about the individual' actions. The other is to know the performance of PS in the dynamic and competitive domain. Table 1 show the parameters of simulation.

A. Effects of Designing the Reward

Two issues on making the marks showed in Sect. 3.3 should be treated. In both cases, the reward is never shared among the agents.

Issue 1: The marks are showed to the entire group while the global goal is achieved.

Issue 2: The mark is showed to the individual whose goal is achieved. In such issue, the individual is decided to whose mission is finished, considering the priority to the counterpart whose mission is still in process.

In a PS structure, the individual chooses its behavior from the steps using Roulette selection (mentioned in Sect. 2.2) at each time step. The starting mark of each weight is 10 and the feedback is 100, and a geometrically decreasing function: f = 100 · (0.3)T− t (T: time when agent reached the goal, t: time step in the episode), which satisfies "Rationality Theorem" as a credit assignment function.

$$p(a_i|s)=\frac{e^{Q(o,a_i)}/T}{\sum_{k\in actions}e^{Q(o,a_i)}/T}(T=0.2)$$

by studying mark, starting grade of every point and the feedback.

1) Experimental Results and Discussion

TABLE I. PARAMETERS OF SIMULATION.

Parameter	Value
The processing time	10 ms
Data size	2 kBytes
Transmission time	2ms/hop

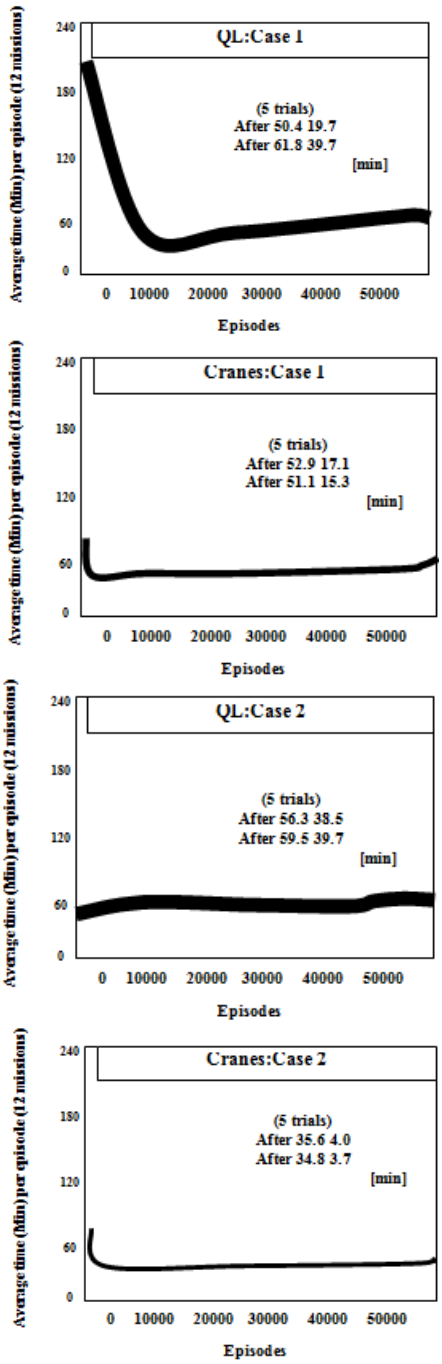

Figure 5. Performance in different design of rewards.

(a)Acquired Priority Rules between Crane1 and Crane2

State of Crane2			ToStart		ToEnd	
State of Crane1	Remained Distance	Sight of Crane2	Crane3 is out of Crane2's Sihgt	Crane3 is Insight of Crane2	Crane3 is out of Crane2's Sihgt	Crane3 is Insight of Crane2
To Start	R2>R1		Crane1	Crane2	Crane2	Crane1
	R2=R1		Crane1	Crane2	Crane2	Crane1
	R2<R1		Crane1	Crane2	Crane2	Crane1
To End	R2>R1		Crane2	Crane2	Crane2	Crane2
	R2=R1		Crane2	Crane2	Crane2	Crane2
	R2<R1		Crane2	Crane2	Crane2	Crane2

R1:Remained Distance of Crane1 R2:Remained Distance of Crane2

(b)Acquired Priority Rules between Crane3 and Crane2

State of Crane2			ToStart		ToEnd	
State of Crane3	Remained Distance	Sight of Crane2	Crane3 is out of Crane2's Sihgt	Crane3 is Insight of Crane2	Crane3 is out of Crane2's Sihgt	Crane3 is Insight of Crane2
ToStart	R2>R3		Crane3	Crane3	Crane3	Crane2
	R2=R3		Crane3	Crane3	Crane3	Crane2
	R2<R3		Crane3	Crane2	Crane2	Crane2
ToEnd	R2>R3		Crane3	Crane3	Crane3	Crane2
	R2=R3		Crane3	Crane3	Crane2	Crane2
	R2<R3		Crane3	Crane2	Crane2	Crane2

Acquired Priority is different from Heuristic Rules

Figure 6. Acquired rules to evade collision

TABLE II. COMPARISON OF THE PROPOSED SYSTEM UNDER DIFFERENT CASES.

Name	Case	Start State				End State				
		Commercial Sys.			Ours	Commercial start.			Middle	End
QL	1	S	S	S	S	F	P	D	S	S
QL	2	S	S	S	S	NULL	COM	F	S	NULL
Crane	2	S	S	S	S	F	F	F	NULL	S
Crane	1	S	S	S	S	COM	COM	COM	S	NULL

First, we come to talk about the difference between PS and QL. Pay attention to their cases of rewards design. We make twelve missions in all, and list two cranes for simplicity in Fig. 5, which is wholly a random process.

The performance of the PS agents is better than that of QL one in the both cases of rewards design. Here, we found that QL is not a better reward design when considering the issue 1. So do Profit Sharing strategy. In Issue 1, all group individuals share the same resources, and the influence each other dramatically. In Issue 2, the same thing happens that QL individual is caused to draw by other counterpart.

We also experimented on the environment including 3 individuals, in which the Q-values are in the still place, keeping oscillating all the time in the whole design process. When QL agents increase in the environment, the number gets bigger. And then the state transition problem turns more uncertainty. The oscillation of QL is caused by the change of individuals' rules. Sensing limitation is as the primary concentration. Thus, QL should not generate any usable polices to the whole in the issue of 3 cranes.

Moreover, table 2 shows the comparison of the proposed system under different cases. Start state and end state are tested. Either QL or Crane in case 1 or 2, share the same start state, as "S". However, different marks come out, with the process carrying, as expected. Table 3 infers the user distribution, which contribute to the result in what shows in table 2.

TABLE III. THE USER DISTRIBUTIONS.

Case1	Info. ratio	0.2	0.4	0.6	0.8	1.0
	users%	40	30	17	10	3
Case2	Info. ratio	0.3	0.6 0.8			1.0
	users%	50	30 15			5
Case1&Case2	Info. ratio	0.2	0.4	0.6	0.8	1.0
	users%	45	25	15	10	5

B. Performance of Profit-Sharing

In the second place, the performance of Profit-Sharing is concentrated in the coil-yard publication that includes 3 cranes. Table 4 gives the initial setting. And to confirm PS's learn-ability toward the dynamic environment, we set 10% noise to the agent's action, which means that

agent fails in doing his intended action in a ratio of one to ten actions. These kind of noise would be frequently occurred in this environment in the forms of execution delay. Then, we make a comparison between the rules acquired by PS and the reasonable hand-coded rules which we implemented in the RAP model's.

TABLE IV. INITIAL SETTING.

Parameter	Means	Value
λ0	arrival rate of QLs to request one service	110
λ11	arrival rate of QLs with joint request for CH(11, 21)	66
λ12	arrival rate of Cranes with joint request for CH(11, 12, 21, 22)	Dynamic
λ13	arrival rate of Cranes with joint request for all CHs	Dynamic
μ0	service rate of QLs with single request	40MA/s
μ1	service rate of QLs with joint request	20MA/s
μ2	service rate of Cranes for just getting the lacking CH	60MA/s

We compare our PS-multi-agent model with RAP model, a one of typical reactive planner, to know applicability of PS to the true problem. In the former model, the acquired rules by PS are embedded, and in the latter one, hand-coded rules are embedded into the agent. The average time to finish 12 missions of each model is 29.7 [min], and 41.2 [min], respectively. The difference of the rules between them is shown in Fig. 6. The reason why the rules acquired by PS show the better performance than the hand-coded ones is that profit sharing gives some precise surroundings which, however, must not be realized ahead of time.

V. CONCLUSION

This paper describes a reinforcement studying method to acquire the rules, each of which consists of state and action pair, for coordinating execution of the multiple cranes in a coil-yard of steel manufacture. The cranes are operated asynchronously, based on the decision of each crane's operator who only knows locally available information in this domain where it is natural to use a decentralized multi-agent model. On the other hand, decentralization causes other serious problems, such as conflicts among the agents. It is very difficult to design rules to resolve conflicts by means of mathematical analysis, because information is scattered, missions are generated stochastically and it is very hard to execute missions on schedule.

In this paper, we, here, give a kind of Profit-sharing strategy, which is based on artificial intelligence. Profit-sharing strategy solves the issue that when conscious aliasing and concurrent studying occur. In a true multi-agent environment, a fact is that movement actions mean more under certain circumstance, if you consider the surroundings as MDPs. Since Profit-sharing is an exploitation intensive method, it reinforces meaningful actions remarkably to resolve the conflicts.

The outcomes are the entrance to mark the designing grades which is the one of the most important problem to apply Profit-sharing to more complicated domain, because to design the reward is more difficult than to show agent knowledge box. Especially, in the real environment, we should consider the case in which it is not clear who contributes to achieve the goal, because this kind of case would be frequently occurred in this world. This problem, the reward-sharing among the agents, is much more difficult than the credit-assignment problem. Therefore, some theoretical aspects are required in multi-agent reinforcement studying. We have been pursuing reward-sharing method among the agents and shown a theoretical result. However, we have much still remains to be done.

REFERENCES

[1] Serrano, Emilio; Botia, Juan, "Validating ambient intelligence based ubiquitous computing systems by means of artificial societies" *Information Sciences*, pp. 111– 120, 2013.

[2] Bennett, Casey C., Hauser, Kris, "Artificial intelligence framework for simulating clinical decision-making: *A Markov decision process approach" Artificial Intelligence*, vol. 13, no. 4, pp. 609–618, 2013.

[3] J. J. Grefenstette, "Credit assignment in rule discovery systems, based on genetic algorithms," *Machine Studying* vol. 3, pp. 225–245, 1988.

[4] Li, Fu-Dong, Wu, Min, He, Yong, "Optimal control in microgrid using multi-agent reinforcement studying" *ISA TRANSACTIONS*, 2012.

[5] Wu Zhihai, Fang Huajing, She Yingying, "Weighted Average Prediction for Improving Consensus Performance of Second-Order Delayed Multi-Agent Systems" *Ieee Transactions On Systems Man And Cybernetics Part B-Cybernetics*, 2012.

[6] Y. Gal, S. Reddy, S. Shieber, A. Rubin and B. Grosz. Plan Recognition in Exploratory Domains. *Artificial Intelligence*. 176(1) pp. 2270--2290, 2012.

[7] Y. Gal, B. Grosz, S. Kraus, A. Pfeffer, S. Shieber. Agent Decision-Making in Open Mixed Networks. *Artificial Intelligence*, 174(18) pp. 1460--1480, 2010.

[8] E. Kamar, Y. Gal, and B. J. Grosz, Incorporating helpful behavior into collaborative planning. In Proc. of The 8th International Conference on Autonomous Agents and Multiagent Systems, Vol. 2. *IFAAMAS, Richland, SC* pp. 875-882, 2009.

[9] E. Kamar, Y. Gal, and B. J. Grosz. Modeling information exchange opportunities for effective human-computer teamwork. *Artificial Intelligence.* 195 pp. 528--550, 2013.

[10] D. Sarne and B. J. Grosz. Determining the Value of Information for Collaborative Multi-Agent Planning. *Autonomous Agents and Multi-Agent Systems*. 26(3) pp. 456-496, 2013.

[11] Georgios Chalkiadakis, Valentin Robu, Ramachandra Kota, Alex Rogers, Nicholas R. Jennings, Cooperatives of distributed energy resources for efficient virtual power plants, *The 10th International Conference on Autonomous Agents and Multiagent Systems*, May 02-06, 2011, Taipei, Taiwan

[12] Chowdhury, S., Chowdhury, S. and Crossley, P. Microgrids and Active Distribution Networks. *Institution of Engineering and Technology (IET)*, 2009.

[13] Matthias Deindl, Carsten Block, Rustam Vahidov, Dirk Neumann, Load Shifting Agents for Automated Demand Side Management in Micro Energy Grids, *Proceedings of the 2008 Second IEEE International Conference on Self-Adaptive and Self-Organizing Systems*, pp. 487-488, October 20-24, 2008

Lang JianJun, born in 1978-08-01 HunChun, JiLin province, China. He is currently a doctoral candidate in JiLin University. His research interests include Geographic Information System (GIS), Remote Sensing (RS), control theory and control engineering,Spatial information science and engineering and operating system security.

Jiang QiGang was born in 1964-03-01. Professor and Ph. D. in JiLin University. His research interests include Geographic Information System (GIS), Remote Sensing (RS), Automatic remote sensing image interpretation, Geographic system modeling and application, Analysis and application of remote sensing information model.

Modified Particle Swarm Optimization for Hybrid Wireless Sensor Networks Coverage

Bing Cheng
School of Mathematics and Computer Science, Yangtze Normal University, Chongqing, China
Email: powerodie@gmail.com

***Abstract*—Efficient network coverage and connectivity are the requisites for most Wireless Sensor Network deployments, particularly those concerned with area monitoring. The Coverage Control Technology is one of the basic technologies of wireless sensor network, and is mainly concerned about how to prolong the network lifetime on the basis of meeting users' perception demand. To optimize wireless sensor networks coverage, an algorithm which is based on particle swarm optimization with dynamic clonal selection is proposed. This algorithm controls the clonal quantity and variation range of particle which represents the locations of all mobile sensor nodes, by coverage rate and similarity among the swarm to avoiding being trapped in local optimum. By comparison of the simulation results with other algorithms, this optimization algorithm could improve the performance of network coverage more effectively.**

***Index Terms*—Particle Swarm Optimization; Dynamic Clonal Selection; Hybrid Wireless Sensor Networks; Coverage**

I. INTRODUCTION

A wireless sensor network (WSN) is a large collection of densely deployed, spatially distributed, autonomous devices or nodes that communicate via wireless and cooperatively monitor physical or environmental conditions [1, 2]. In such networks, sensor nodes are deployed over a geographic area by aerial scattering or other means. Each sensor node can only detect events within some very limited distance from itself, called the sensing range. In addition, sensor nodes normally have fairly limited transmission and reception capabilities so that sensing data have to be relayed via a multihop path to a distant base station, which is a data collection center with sufficiently powerful processing capabilities and resources. After being deployed, sensor nodes are usually left unattended for a very long period of time so that they may fail over time due to various reasons such as battery exhaustion and physical destructions by attackers. They may also be moved away from where they were deployed by animals, winds, or other environmental means [3].

The sensor deployment methods [4] of WSN are deterministic versus random. A deterministic sensor placement may be feasible in friendly and accessible environments. Random sensor distribution is generally considered in military applications and for remote or inhospitable areas. Due to random deployment is easy to form coverage blind spots and overlaps, the problem could be solved with a hybrid WSN in combination of static nodes and mobile nodes [5]. A hybrid WSN deployment strategy is to randomly deploy static nodes mixed with mobile nodes by certain proportion and then adjust location of the mobile nodes to enhance coverage.

There have been some achievements on the study of WSN coverage. Reference [6] proposes the heuristic algorithm for WSN key areas coverage nevertheless the region must be divided into key areas and normal areas in this algorithm to achieve effective coverage. To optimize the coverage, randomly scheduling subset to divide optimal solutions was adopted in reference [7]. The method uses the coverage redundancy among sensors to expand the lifetime of networks, but it couldn't enlarge the coverage areas. Two methods are proposed for the mobile nodes deployment [8,9], however, there is no full use of the pilot action of global information on locations while adjusting the locations of mobile nodes. Zou Lei etc proposed a deployment method for hybrid sensor networks based on virtual force. This method requires each node to send broadcast messages and response messages periodically to calculate the repulsive force, gravity, border binding between nodes which is easily led to networks congestion and decrease of the networks lifetime in the case of abundant nodes and widely distributed. Zeng Yinglan etc proposed a coverage strategy using differential evolution algorithm for WSN mixed nodes optimizing. But the algorithm performs slow convergence near the optimal solution and the real-time performance of nodes scheduling needs to be improved.

To overcome the deficiencies of existing technologies, a modified particle swarm algorithm (PSO) was adopted on the basis of synthesizing the above research findings. The modified PSO uses a particle to simulate all mobile node location. Take dynamic clonal selection and chaotic mutation to the results of each particle iteration and select the optimal results in the next evolution to improve the WSN coverage.

II. RELATED WORK

In this section, an overview of related work in WSN coverage and PSO is provided.

A. WSN Coverage

General Coverage Metrics: Coverage in sensor networks has been extensively studied, in terms of the coverage resulting from various deployment patterns created

doi:10.4304/jnw.9.1.56-62

by node placement [10, 11]. The worst and best-case coverage has been studied in Megerian et al. With the help of techniques from computational geome-try and graph theory, the authors study the maximal breach paths and maximal support paths for the coverage problem, where the maximal breach path is the path with the minimum distance to a sensor and the maximal support path is the path with the maximum distance to a sensor. In Veltri et al. [12], the authors study the minimal and maximal exposure paths corresponding to the worst and best-case coverage in WSNs. The authors propose a localized approximation algorithm for a WSN to determine its minimal exposure path. In Chin et al. [13, 14], the exposure metric has been further studied for col-laboration in WSNs of mobile nodes in the presence of noise and obstacles. Using the definition of exposure as the least probability of target detection, the authors propose low-computationally intensive algorithms to obtain the upper and lower bounds on exposure.

Directional Coverage. Directional coverage has been studied in [15, 16, 17]. The authors study the optimal patterns that provide connectivity in WSNs. The authors propose scheduling mechanisms to achieve higher connectivity and full coverage in WSNs with nodes equipped with directional antennas. In [18], the authors study optimal worst-case coverage with sensors equipped with video cameras, and directionality is studied in terms of the field-of-view of sensors. In [19], the authors propose the use of directional antennas for power-conservation and greater coverage in the WSN Coverage in Sensor Networks with Mobile Nodes. The coverage provided by mobile and static nodes has been studied in Liu et al., Xing et al., and Tan et al. The use of mobile nodes to provide improved coverage has been studied in Liu et al. and Wang et al.. In Xing et al., the authors study collaboration of mobile and static networks to meet stringent spatial and temporal application requirements of sensor networks deployed for surveillance applications. The authors propose a multi-sensor fusion and movement model to achieve three performance metrics: bounded detection delay, high detection probability and low false alarm rate. Collaboration and mobility in sensors has also been studied in [20].

In [21], the authors study the characteristics of mobility in a network of both mobile and static nodes. They study the scenarios under which the coverage provided by mobile sensors is higher than that provided by static sensors by analyzing the mobility framework of node velocity, mobility pattern, number of mobile sensors and dynamics of the phenomenon being sensed. The authors study this quality of coverage problem and propose motion planning algorithms to bound the probability of event loss in the network.

The use of mobile nodes to provide improved coverage has been studied in Liu et al. and Wang et al. [22]. The authors study collaboration of mobile and static networks to meet stringent spatial and temporal application requirements of sensor networks deployed for surveillance applications. The authors propose a multi-sensor fusion and movement model to achieve three performance metrics: bounded detection delay, high detection probability and low false alarm rate. The authors study the characteristics of mobility in a network of both mobile and static nodes.

B. PSO

The PSO which is originally introduced in terms of social and cognitive behavior by Kennedy and Eberhart in 1995, has come to be widely used as a problem-solving method in engineering and computer science. PSO was inspired from studies of various animal groups, and has since proven to be a powerful competitor to other evolutionary algorithms such as genetic algorithms. Several researchers have analyzed the performance of the PSO and its variants with different settings, like neighborhood settings, hybrid PSO with breeding and subpopulations. Work presented in describes the complex task of parameter selection in a PSO model. Comparisons between PSO and the standard genetic algorithm were done analytically and also with regards to performance in.

The PSO algorithm simulates social behavior among individuals (particles) "flying" through a multidimensional search space. Each particle represents a point at the inter-section of all search dimensions. The particles evaluate their locations relative to a goal (fitness) at every iteration, and particles in a local neighborhood share memories of their "best" locations; then use those memories to adjust their own velocities and locations. The original PSO formulae developed by Kennedy and Eberhart is modified by Shi and Eberhart with the introduction of an inertia parameter and that was shown empirically to improve the overall performance of PSO.

The PSO formulae defines each particle as a potential solution to a problem in a D -dimensional space, with the i -th particle represented as $X_i = \{X_i 1, X_i 2, \cdots, X_i D\}$. Each particle also maintains a memory (*lBest*) of its previous best location $L_i = \{L_i 1, L_i 2, \cdots, L_i D\}$ and velocity along each dimension represented as $V_i = \{V_i 1, V_i 2, \cdots, V_i D\}$. In each generation, the *lBest* vector of the particle with the best fitness in the local neighborhood, designated *gBest* , and the *lBest* vector of the current particle are combined to adjust the velocity along each dimension; the velocity is then used to compute a new location for the particle. The portion of the adjustment to the velocity influenced by the own location *lBest* of individual is considered as the cognition component and the portion influenced by *gBest* is the social component.

The basic PSO first initializes a bulk of particles location and velocity and then iterates for the optimal solution. Each particle updates its data for tracing better solutions of their location and velocity in iteration. One of the best solution for location that particle iterated is called individual peak location noted as *lBest* . Another is for the whole swarm location which is called global solution noted as *gBest* . When the two data are found, the velocity and location of particles in the next minutes will follow these equations bellow:

$$V_i(t+1) = \omega \cdot V_i(t) + c1 \cdot r1 \cdot (lBest_i(t) - X_i(t)) + c2 \cdot r2 \cdot (gBest(t) - X_i(t)) \quad (1)$$

$$V_i(t+1) = \omega(t) \cdot V_i(t) + c1 \cdot r1 \cdot (lBest_i(t) - X_i(t)) + H_i \cdot c2 \cdot r2 \cdot (gBest(t) - X_i(t)) \quad (2)$$

$$X_i(t+1) = X_i(t) + V_i(t+1) \quad (3)$$

In these equations ω is called inertia weight always taken between 0.4 and 0.95; $X_i(t)$ denotes the location of particle i and $V_i(t)$ denotes the velocity of particle i; $c1$ and $c2$ are accelerate index; $r1$ and $r2$ are random data in $[0,1]$; $lBest_i(t)$ is the peak location of particle i at time t and $gBest(t)$ is the peak location of particle swarm.

There are three parts in the right of (1). The first part is the particle's local velocity indicates the particles present status and will affect to the status later. The second is called individual cognitive part which stimulates particles move to the optima location they find. The last part is the particle swarm cognitive part where every particle corporate and share their information in order to get the global solution for all the particles. These three parts together shows both cooperate and competition for their balance and limits, so in this way can the performance of algorithm is determined.

C. Premature Convergences and Dimension Disaster Analysis

When Conventional algorithm of PSO is used in multimodal high-dimensional problems premature convergences and dimension disaster are always exists. It relevant to three main reasons below:

From the equation mentioned above, inertia weight is constant in the process of particle iteration. However, initial value of w lead to a dilemma. If w is too small, the particle's velocity in the next minute will affect too much and easy to trapped in local optima. In the contrary, the initial value set too big will lead to particle moving too fast to miss the global solution. Although some improved algorithms have proposed linear or nonlinear method to adjust inertia weight, it is hard to balance local and global search capacity of multimodal high-dimensional problems rely only on inertia weights.

Secondly, the third part (1) shows that all the particles in standard PSO iteration receive a swarm perceive ability from the *gBest* of particle swarm. Without reference to the distance away from *gBest*, each particle gets the same information. Thus, all the particles are quickly attracted by it and reduce the variety of swarm. In fact, in the situation of function search with multitude local optima and multimodal high-dimensional, *gBest* is probably happening to be one of the local optima [23].

At last, because (1) has no effect on *gBest* particles in search will only decided by their father swarm optima and recent optima they find. Problems will be more complex in the situations with multitude local optima. Without escaping mechanisms in use of *gBest* which is the most important memory cell will be hard to escape local optima when in trap.

III. COVERAGE MODEL

An important problem addressed in literature is the sensor coverage problem. This problem is centered around a fundamental question: How well do the sensors observe the physical space? As pointed out in, the coverage concept is a measure of the quality of service of the sensing function and is subject to a wide range of interpretations due to a large variety of sensors and applications. The goal is to have each location in the physical space of interest within the sensing range of at least one sensor.

Set the target area for two-dimensional rectangular plane A which is discretized into $L \times W$ grids, then randomly deploy a hybrid WSN with N static nodes and M mobile nodes in this region. Each grid is a monitoring point. Assumptions: a) all nodes have the same communication radius rc and sensing radius rs; b) all nodes are based on Boolean sensing and commuication model; c) a sensor can be in work or sleep states; d) locations of all sensors can be knowable.

If the distance between any one point k whose coordinates is (x, y) in region A and sensor s $d(k,s) < rs$, the probability k perceived by s $p(k,s) = 1$, otherwise , as in (4):

$$I((x,y), N+M) = 1 - \prod_{i=1}^{N+M} [1 - P(k, s_i)] \quad (4)$$

The hybrid WSN coverage area is the union of grids covered by sensor nodes and , denoted by , as in (5):

$$area(N+M) = \int_0^W \int_0^L I((x,y), N+M) d_x d_y \quad (5)$$

$$coverage(A) = \frac{area(N+M)}{L+W} \quad (6)$$

The maximum coverage problem is how to optimize the location of the mobile node, under the premise to ensure the network connectivity, to obtain which is the hybrid WSN coverage of the target area A as maximum as possible.

IV. THE MODIFIED PSO

The basic PSO is easily trapped into a local minimum and has some problems such as premature convergence or the curse of dimensionality. As proposed in [23], a nonlinear dynamic adaptive control inertia weight PSO improves to better balance global search ability and local development capability of the particle swarm, but converges slowly near the optimal solution and has poor stability, therefore we dynamically clone the particles and control the variation range according to the level of adaptation values after each iteration and amplitude of variation choose the particles of highest adaptive value in the next iteration. The algorithm flow is shown in Figure 1.

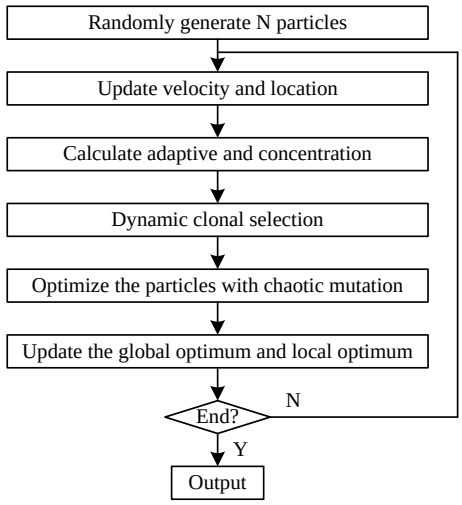

Figure 1. The modified PSO algorithm flow.

A. Dynamic Clonal Selection

To provide new particle location, the algorithm achieves expansion of the particle swarm on purpose by cloning. For different particle, calculate the quantity of clonal particles based on their adaptive values and concentration. The fundamental principle is that particles with high adaptive value have larger quantity of cloning while given consideration to the diversity of particles and introduced into particle concentration to inhibit excessive clone and avoid premature convergence. The quantity of clonal particles is calculated as in (7):

$$q_i = Int\left[M_c \times f(i) \times (1 - C_i)\right] \tag{7}$$

Equation (7) means to round up to an integer; represents the maximum number of cloning; is the result after normalization of adaptation value of particle ; represents the similarity degree and it is also as known as the concentration of the particles between other particles in the current particle swarm with particle i , which is defined as the ratio of the particles number of distance between particle i when it is less than the threshold δ to the total.

B. Adaptive Chaotic Mutation

The particle optimization with mutation operation is defined as random variation within the predetermined range for the respective components of the vector represented by the clonal particles, thereby effectively increasing local search of the particle current location. The m -th component Z_m^i of the particle i with adaptive chaotic mutation operation is defined as in (8):

$$Z_m^{i'} = \begin{cases} Z_m^i + \lambda \times \left(1 - \dfrac{t}{T}\right) \times e^{-f(i)} \\ \times L_i(k) \times (-1)^k, r_{im} \geq \dfrac{f(i)}{f(best)} \\ Z_m^i, else \end{cases} \tag{8}$$

In (8), the is the parameter which controls the amplitude of variation; is the -th value in the Logistic Mapping Sequence; represents the current number of iterations; is the maximum number of iterations; r_{im} is generated for the -th component of i -th particle value of a random number in . On the one hand from (8), the particle component variation occurs to some extent by the particle adaptation value. The greater the value of adaptation is, the fewer opportunities for variation will be and therefore fewer components would mutate. On the other hand, the size of the variation range is controlled by the adaptive value and the number of iterations, the greater the value of adaptation and the number of iterations is, the smaller the variation range would become.

From (7) we can see that, on the one hand, the number of variation components of particles is affected by the fitness value of particles, the greater the fitness value, the less chance of variation, so the variation components is less; on the other hand, the variation amplitude is controlled by the fitness value and the number of iterations, the larger the fitness value, the smaller the variation range; and with the increasing number of iterations, the variation amplitude is gradually reduced.

C. Pheromone Diffusion Function

In natural zoology system individuals diffuse pheromone to each other with a scope affected by pheromone intensity and distance. According to this phenomenon, the *gBest* in (1) has a different power to attract each particles will relevant to two kinds of factors. That is the distance of particle's location to *gBest* and the corresponding adaptive value between particle and *gBest* . When closer to *gBest* or higher *gBest* -to-present location adaptive value ratio means particles will quickly react to the attraction of *gBest* and change their direction and velocity to *gBest* . Reversely, particles will slow their activities to *gBest* or even escape its control.

The improvement can bring with two advantages. Firstly, the particles away from *gBest* won't quickly convergence to these locations. So the global search ability boosts up and degrades the risk of local optima. The second advantage is that the particles near *gBest* with little change of adaptive value lessened the velocity. It is no doubt to advance local search capabilities and improve the precision.

So pheromone diffusion function H is adopted in (9):

$$H_i = k \times \left(1 - \frac{d_i + \delta}{\max\limits_{1 \leq j \leq m} d_j + \delta}\right) \tag{9}$$

In this function above the value of k is decided as follow:

$$k = \begin{cases} \dfrac{s_i + \delta}{\max\limits_{1 \leq j \leq m} s_j + \delta} & if \ \dfrac{s_i + \delta}{\max\limits_{1 \leq j \leq m} s_j + \delta} > 0.6 \\ 0.6 & else \end{cases} \tag{10}$$

H_i denotes the power of *gBest* attract to particle i. The pheromone diffusion function conclude two parts. The first part is depending on value k determined by (9) to bridge the links between the movement of particle swarm to *gBest* and their corresponding adaptive value improvement.

In (10) s_i the value of particle i 's adaptive value subtract *gBest* 's adaptive value; m denotes the quantity of particles in particle swarm; s_j is the max value of s_i. By experiment and test k is suggest not to less than 0.6.

Equation (8) the second part link particle's move scale to the distance between particle and *gBest*. d_i denotes the Euclidean distance of particle i to *gBest*, d_j is the max value of d_i. Positive number δ is adopted in (9) and (10) with the purpose of avoiding numerator and denominator to be zero (in test it is adopted as 0.0001) and keep no effect on final result.

D. Diversity Feedback

PSO algorithm is easy to trap in local optima because of fast downsizing of particle swarm diversity and lacking escape mechanism when in trap. In this case, diversity feedback mechanism is adopted in this paper. For one thing, feedbacks can dynamic and adaptive to adjust inertia weight so as to limit the shade of swarm diversity. The next is providing a method at the moment of diversity fall to threshold. Some way similar to genetic algorithm is introduced to enlarge the swarm diversity by means of adjusting particles direction.

The diversity of Particle swarm is supposed to measure by (11):

$$diversity(t)=\frac{1}{m\times|L|}\times\sum_{i=1}^{m}\sqrt{\sum_{d=1}^{D}\left(x_{id}-\overline{x_d}\right)^2} \quad (11)$$

In the equation above, m represent the particle swarm scale; x_{id} means the d dimension component of particle i at t times; $\overline{x_d}$ is the average of x_{id}; D is the scale of dimensions, $|L|$ denotes the longest diagonal of search area.

Inertia weigh is adaptable followed by (12):

$$w(t)=w_{final}+e^{-diverdity(t)}\left(1-\frac{Iter}{Iter_{\max}}\right)\left(w_{initial}-w_{final}\right) \quad (12)$$

In (12), $Iter_{\max}$ represents the max interaction times and $Iter$ is the number of local iteration times; $w_{initial}$ is initial weights and w_{final} is the final weights (the typical value $w_{initial}=0.95$ and $w_{final}=0.4$ in test)

Equation (11) creates a link of inertia weight to swarm diversity and iteration times. In the former iteration, large lumber of diversity swarm iteration leads to high value of the inertia weight. This is helpful for particle's global search ability. Accompanied with the iteration, diversity is gradually fall down which prohibited inertia weight's fast degeneration. So particle swarms will receive local search ability with little cost of global search capability to decrease the risk of premature.

V. Hybrid WSN Coverage Optimization

For a hybrid WSN constituted by N static sensor nodes and M mobile nodes which is random deployed to the target area, the strategy for coverage optimization is by adjusting the location of the mobile nodes to cover a larger monitoring area as much as possible.

A. Coding Method

Each particle represents a deployment of M mobile nodes. Set the particle as , where for location of the -th mobile node.

B. Velocity and Location Update

Velocity and location update of i -th particle as (13) and (14).

(13)

$$X_i(t+1)=X_i(t)+V_i(t+1) \quad (14)$$

In (13), is the inertia weight for nonlinear dynamic adjustment in iteration, $V_i(t)$ and represent the velocity and location of i -th particles at time t; $c1$ and $c2$ stand for acceleration factors; $r1$ and $r2$ are the two random numbers within the range $[0,1]$; $lBest_i(t)$ is the location the best adaptive value of the particle corresponding to until the time and is the location the global optimum of the particle swarm corresponding to until the time .

C. Clonal Selection

Every particle clones themselves after each iteration according to the calculation results of (7) and with adaptive chaotic mutation operation according to (8), then calculate all the adaptive value of the particles after variations and compare the best adaptive value on condition of network connectivity with *lBest* and before cloning. The value would be The Algorithm Replaces the corresponding value if it is better, or else gives it up and starts to the next iteration until completion of the default number of iterations.

VI. Experiment and Analysis

A. Parameter Settings

In order to evaluate the performance of the algorithm in WSN coverage optimization, the target area has the same parameters as [24]. Randomly deploy 60 nodes on the area of including 20 mobile nodes. Sensing radius , the commuication radius , the moving velocity the mobile node is . Set the swarm size of 10 , the maximum clonal number of 10 , the maximum variation range as half of , parameters, $0.4\le\omega\le0.9$, the maximum number of iterations $T=50$.

B. Validation of the Algorithm

The simulation is carried out with MATLAB. Figure 2 (a) shows the initial locations of the nodes randomly

deployed on area A. Blue circles represent the static nodes, red ones for the mobile nodes. The coverage rate is 66.8% according to (1,2,3); Figure 2 (b) shows the WSN coverage after adjustment of mobile nodes on the same area. The coverage rate is 85.7% and 18.9% higher than the initial value. The algorithm has a significant effect on improving the network coverage.

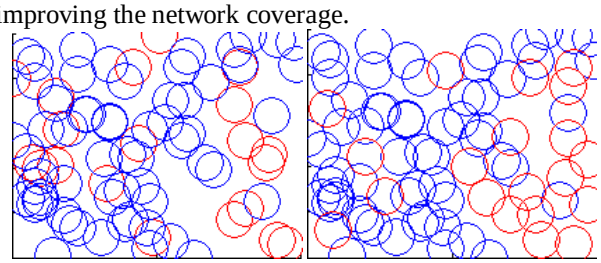

(a) Before Adjustment (b) After Adjustment

Figure 2. WSN coverage.

C. Stability of the Algorithm

In order to verify the stability of the proposed algorithm, the results of 10 runs of the algorithm is shown in Figure 2, which shows changes in the the algorithm run before and after. In the Figure, the dotted line indicates the pre-optimized random the initial coverage of the network deployment, the solid line represents the optimized coverage, the figure indicates the number of sleeping nodes after the optimization.

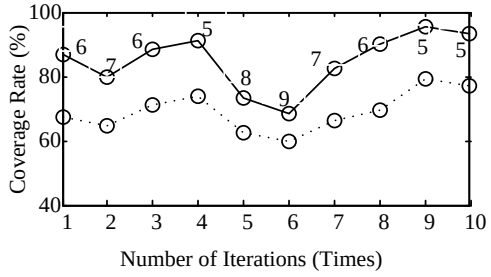

Figure 3. Comparison of the coverage rate for optimization.

D. Comparison with Other Algorithms

To further validate the performance of the algorithm, We comparison the proposed algorithm (denoted by MPSO) with PSO-based WSN coverage optimization (denoted by PSO). The same area to be monitoring, each algorithm independently run 10 times, statistics in the evolutionary process, the number of iterations and the corresponding average coverage, shown in Figure 4.

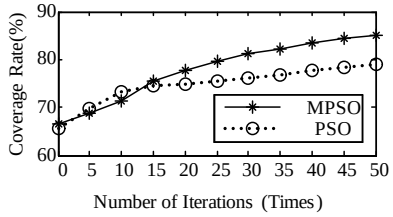

Figure 4. Comparison of the coverage rate for Modified PSO with PSO.

From the contrast curve in Figure 4, we see that the algorithm has slightly faster convergence velocity in initial than that of the algorithm in this paper, but after about 8 times iterations, the curve slope becomes very small and slow increase in coverage, then, gradually stabilize at near constant, and fall into the trap of premature. However, although the convergence velocity at the beginning is slightly slow in this algorithm, during the first 35 iterations, it jumps from the local trap constantly. At last, the greater network coverage is achieved, and the result is much better.

E. Experimental Results Analysis

In this paper, the PSO based on dynamic clone is adopted to enhance hybrid WSN coverage which is randomly deployed, and the better simulation results are achieved. This is due to the introduction of the dynamic clone variation operation in the elementary particle algorithm. Each particle clones itself according to its fitness value and mutate under the control of the adaptability and the similarity after finishing iteration.So, for the particles, on the one hand, the stronger the adaptability, the larger the clone number, and the amplitude of variation is smaller, so that the local precise search capability is enhanced efficiently. On the other hand, since the particles clone number is also restricted by the similarity between particles, thus ensure a certain variety of particle swarm to avoid falling into the trap of premature. Meanwhile, for the particles of poor adaptability, increasing the degree of variation of clone can increase the chance of finding a better location.

From the coverage curves in Figure 4 we can see that the clone variation selection operation is always after iteration each time in the algorithm, so the search concentrates on location where the relative adaptability is not very high initially, and so the convergence velocity is slow. However, during the whole iterative process, the algorithm will constantly find new and better location to avoid fall into the trap of premature easily.

VII. Conclusion

In this paper, a modified PSO algorithm for hybrid WSN coverage gets better simulation results. This is due to the introduction of dynamic clonal selection and chaotic mutation into basic PSO. Every particle clones themselves after each iteration according to its adaptability and with adaptive chaotic mutation operation. Therefore on the one hand, adaptable particles have more clonal number and lower variation, so as to enhance the local precise search capabilities; On the other hand, due to the clonal number of particles is also affected by the constraints of the similarity between the particles, thus ensuring particle swarm certain diversity and avoid premature convergence. Meanwhile, for the poor adaptability particles, increasing the degree of variation expands the opportunity to find better locations.

References

[1]. IF. Akyildiz, W. Su, Y. Sankarasubramaniam, and E. Cayirci, “Wireless sensor networks: a survey,” *Computer Networks*; vol. 38, issue 4, pp. 393–422, 2002. doi: 10.1016/S1389-1286(01)00302-4.

[2]. H. Karl and A. Willig, *Protocols and Architectures for Wireless Sensor Networks*. John Wiley Sons, Ltd., 2005.

[3]. Chi Zhang, Yanchao Zhang, and Yuguang Fang, "A Coverage Inference Protocol for Wireless Sensor Networks," *IEEE Transactions on Mobile Computing*, vol. 9, no. 6, pp. 850-864, June 2010, doi:10.1109/TMC.2010.29.

[4]. M. Cardei and J. Wu: Coverage in Wireless Sensor Networks, *Hand book of Sensor Networks*, CRC Press, 2004.

[5]. Lyudmila Mihaylova, Donka Angelova, David R. Bull, and Nishan Canagarajah, "Localization of Mobile Nodes in Wireless Networks with Correlated in Time Measurement Noise," *IEEE Transactions on Mobile Computing*, vol. 10, no. 1, pp. 44-53, Jan. 2011, doi:10.1109/TMC.2010.132.

[6]. J. Neyman and E. L. Scott: *Processes of clustering and applications. In: Stochastic Point Processes: Statistical Analysis, Theory, and Applications*. (P. A. W. Lewis, ed.), Wiley- Interscience, New York, pp. 646-681, 1972.

[7]. C. Onof, et al. Rainfall modelling using poisson-cluster processes: A review of developments. *Stochastic Environmental Research and Risk Assessment* 19, pp. 403-416, 2000. doi:10.1007/s00477-005-0011-8.

[8]. T. Shu, M. Krunz , and S. Vrudhula, Power balanced coverage-time optimization for clustered wireless sensor networks. In Proceedings of the *6th ACM International Symposium on Mobile Ad Hoc Networking and Computing.* ACM, New York, pp. 111–120, 2005.

[9]. R. Tan, G. Xing, J. Wang, and H. So, Collaborative target detection in wireless sensor networks with reactive mobility. In Proceedings of the *16th International Workshop on Quality of Service*, pp. 50–59, 2008.

[10]. J. Ai and A. Abouzeid, Coverage by directional sensors in randomly deployed wireless sensor networks. J. *Combinat.* Optimiz. 11, 21–41, 2006.

[11]. Fengjun Shang, "An Energy-Efficient Communication Protocol for Wireless Sensor Networks," *Journal of Networks*, Vol 6, No 7 (2011), 999-1008, Jul 2011, doi:10.4304/jnw.6.7.999-1008

[12]. S. Megerian, F. Koushanfar, M. Potkonjak, and M. B. Srivastava, Worst and best-case coverage in sensor networks. *IEEE Trans. Mobile Computing*. 4, pp. 84–92, 2005.

[13]. L. Lazos, R. Poovendran, and J. A. Ritcey. On the deployment of heterogeneous sensor networks for detection of mobile targets. In Proceedings of the *5th International Symposium on Modeling and Optimization in Mobile, Ad Hoc and Wireless (WiOpt'07)*. IEEE Computer Society Press, Los Alamitos, CA, pp. 1–10, 2007.

[14]. B. Liu, D. Towsley, and O. Dousse, Mobility improves coverage of sensor networks. In Proceedings of the *6th ACM International Symposium on Mobile Ad Hoc Networking and Computing (MobiHoc'05)*. ACM, New York, pp. 300–308, 2005.

[15]. Rongbo Zhu, Intelligent Collaborative Event Query Algorithm in Wireless Sensor Networks. International Journal of Distributed Sensor Networks, Volume 2012, Article ID 728521, 11 pages.

[16]. Rongbiao Zhang, Yongxian Song, Fuhuan Chu, and Biqi Sheng. Study of Wireless Sensor Networks Routing Metric for High Reliable Transmission. *Journal of Networks*, 2012, 7(12) pp. 2044-2050.

[17]. A. Chatterjee and P. Siarry. Nonlinear inertia weight variation for dynamic adaptation in particle swarm optimization. *Computers & Operations Research* (S0305-0548), 2006, 33(3) pp. 859-871.

[18]. Xiao-Min Hu, et, al. Hybrid Genetic Algorithm Using a Forward Encoding Scheme for Lifetime Maximization of Wireless Sensor Networks. *Ieee Transactions On Evolutionary Computation*, 14(5) pp. 766-780, 2010.

[19]. G. Xing, J. Wang, K. Shen, Q. Huang, X. Jia, and C. So, Mobility-assisted spatiotem-poral detection in wireless sensor networks. In Proceedings of the *28th International Conference on Distributed Computing Systems (ICDCS'08)*. IEEE Computer Society Press, Los Alamitos, CA, pp. 103–110, 2008.

[20]. J. Luo, D. Wang, and Q. Zhang, Double mobility: Coverage of the sea Surface with mobile sensor networks. In Proceedings of the *Annual Conference of the IEEE Communication Society (INFOCOM'09)*, IEEE Computer Society Press, Los Alamitos, CA, pp. 118–126, 2009.

[21]. G. Veltri, G. Qu, Q. Huang, and M. Potkonjak, Minimal and maximal exposure path algorithms for wireless embedded sensor networks. In Proceedings of the *ACM Conference on Embedded Networked Sensor Systems (SenSys'03)*. ACM, New York, pp. 40–50, 2003.

[22]. Z. Yu, J. Teng, X. Bai, D. Xuan, and W. Jia. Connected coverage in wireless sensor networks with directional antennas, submitted. In Proceedings of the *31st Annual Conference of the IEEE Communication Society*. IEEE Computer Society Press, Los Alamitos, CA, 2010.

[23]. T. Chin, P. Ramanathan, K. Saluja, and K. Wang, Exposure for collaborative detection using mobile sensor networks. In Proceedings of the *IEEE International Conference on Mobile Adhoc and Sensor Systems*. IEEE Computer Society Press, Los Alamitos, CA, pp. 743–750, 2005.

[24]. Muhammad Aljuaid and Halim Yanikomeroglu. Investigating the Gaussian Convergence of the Distribution of the Aggregate Interference Power in Large Wireless Networks, *Ieee Transactions On Vehicular Technology*, 2010, 59(9) pp. 4418-4424.

Infrastructure Communication Reliability for WSN on Cluster Topology and Tree Topology

Chunyu Miao
Zhejiang Normal University Xingzhi College, Jinhua Zhejiang, China
Email: netmcy@zjnu.cn

Lina Chen
Zhejiang Normal University, Mathematics, Physics and Information Engineering College, Jinhua Zhejiang, China
Email: chenlina@zjnu.cn

***Abstract*—We consider the problem of the infrastructure communication reliability (ICR) of wireless sensor networks (WSN) on sink-manycast and sink-anycast model. We formulate ICR metrics for WSN with hierarchical clustered topology and tree topology base on an reduced ordered binary decision diagrams (ROBDD) approach. Furthermore, we give the case study of the metrics application of WSN with hierarchical clustered topology and tree toplogy. Based on the reliability metrics, we will optimize the structure of WSN to achieve the optimal network reliability.**

***Index Terms*—Wireless Sensor Network; Infrastructure Communication Reliability; Cluster Topology; Tree Topology**

I. INTRODUCTION

Wireless sensor network (WSN) is the current domestic and international hot topic in the fields of sensor technology [1]. A WSN consists of a large number of sensor nodes and a base station. The sensor nodes are designed to collect data from the environment. The base station is an aggregation node for collecting data and it can also performs as an interface between the WSN and other networks or human operators. The communication within WSN can be conceptually classified into two categories: application communication and infrastructure communication [2, 3, 4]. Application communication relates to the transfer of sensed data collected from the physical environment. Infrastructure communication relates to the delivery of configuration and maintenance messages (e.g. network set-up, query, path discovery, processing tool, operating system, and policies). The reliable data delivery in both paradigms must be guaranteed. Refer [5] for studies on the reliability analysis of WSN under the application communication paradigm. This work only addresses the infrastructure communication reliability (ICR) of WSN.

Presently, star, tree, mesh, and hierarchical clustered topologies have emerged as the topology choices for WSN. Each topology has its own pros and cons in terms of communication efficiency, complexity in routing protocol design, and overhead to setup and maintain the topology with the presence of node failure and possible mobility [6]. Hierarchical clustered topologies is very porpular in WSN application, so in the section 3,we formulates ICR metrics for WSN with hierarchical clustered topology and tree topology. We also give the case study in the section 4.

II. PROBLEM STATEMENT

For the infrastructure communication for WSN with hierarchical clustered and tree architecture, three different data delivery models have been considered for the WSN reliability analysis in [7, 8]. They are: 1) sink unicast where the base station sends control messages to a single sensor; 2) sink multicast where the base station sends control messages to a group of sensors; 3) sink broadcast where the base station sends control messages to all sensors. In this work, we consider two new data delivery models for WSN, namely sink manycast and sink anycast. In the sink manycast model, the base station sends control messages to a subset of sensors out of a large group of qualified sensors. For example, when there are n qualified sensors, the control message is expected to be received by any m out of n sensors. As a special case of sink manycast, sink anycast requires the base station to send control messages to any one out of a group of qualified sensors (i.e., m = 1) [9, 10]. To the best of our knowledge, no work has been done to address the infrastructure communication reliability (ICR) of WSN under the sink manycast and anycast models. This section proposes new reliability metrics for the manycast and anycast ICR analysis in WSN with hierarchical clustered architecture.

In the hierarchical clustered topology, sensors are organized into clusters with cluster heads (CH), and low-level cluster heads form high-level clusters. Communications within a cluster and between cluster heads are based on multi-hop mesh routing [11]. Figure 1 illustrates a small example of WSN with hierarchical

doi:10.4304/jnw.9.1.63-70

clustered topology. Note that level 0 is the lowest level in the hierarchy.

In the tree topology, sensors are organized into clusters, where the sensor nodes are connected to a central node (parent node) via direct (or point-to-point) links. Additionally, lower-level parent nodes can be connected to higher-level parent nodes via direct links. The top-level parent node, also referred to as the root node, is connected to the sink node (or base station) directly.

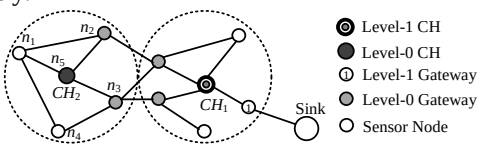

Figure 1. An example of WSN.

III. RELIABILITY MODEL

The binary decision diagrams are very popular in network reliability analysis [12]. The progressive reduction method proposed in [13] can greatly reduce the complexity of reliability analysis in WSN. A level-i graph can be reduced to a graph containing only the level-i CHs and level-i inter-cluster gateways. Here, inter-cluster gateways are the nodes that are connected to the nodes in the neighboring clusters within one hop. With this reduction, it is sufficient to analyze only the clusters/sub-networks for reliability, instead of the entire network.

The level-i graph is modeled by an undirected probabilistic graph G(i)(V, E), where V is the set of vertices (sensor nodes) and E is the set of edges (links). Let CH(k) denote the level-k cluster heads, and g(k) denote the gateway nodes connecting two neighboring level-k clusters. The progressive reduction scheme starts from G(0)(V, E); G(i)(V, E) is reduced to G(i+1)(V, E) which contains only CH(i) and g(j) where $j \geq i$ and the two-terminal reliabilities between CH(i) and g(i) are computed from G(i)(V, E) and assigned as reliability of the corresponding CH to gateway link at G(i+1)(V, E). This reduction scheme is iterated until the top level of the hierarchy is reached.

Reliability is generally defined as "the probability that the system will perform its intended function under stated conditions for a specified period of time" [14]. In particular, the infrastructure communication reliability (ICR) of WSN is the probability that there exists an operational path from the sink node to the required nodes.

A. Sink Anycast for Cluster Topology

The ICR in this scenario is the probability that there exists an operational path from the sink node to at least one sensor node out of a group of qualified nodes. For hierarchical clustered topology, the ICR is the probability that there exists an operational path from the sink node to top hierarchical level CH, then to the next hierarchical level CH and so on to the destination group's CH and finally to any sensor node in that group. Note that the qualified sensor nodes in the group may not belong to a single cluster. Let Q denote the set of qualified nodes, a denote any sensor node in Q, and hk denote the CH that is hierarchically above a at parent level k, $0 \leq k \leq t$. Then the ICR of WSN with hierarchical clustered topology for sink anycast can be formulated as equation 1.

$$ICR_{anycast} = \Pr\left\{ \bigcup_{\forall a \in Q} \begin{bmatrix} \mathrm{E}_2\left(\text{sink to}\mathrm{CH}^{(t)}h_t\right) \cap \\ \mathrm{E}_2\left(\mathrm{CH}^{(t)}h_t \text{ to } \mathrm{CH}^{(t-1)}h_{t-1}\right) \cap \cdots \cap \\ \mathrm{E}_2\left(\mathrm{CH}^{(1)}h_1 \text{ to } \mathrm{CH}^{(0)}h_0\right) \cap \mathrm{E}_2\left(\mathrm{CH}^{(0)}h_0 \text{ to } a\right) \end{bmatrix} \right\} \quad (1)$$

where E2 represents the event that there exists an operational communication path between a given pair of nodes. Thus, Pr(E2) can be evaluated as two-terminal reliability.

Consider the special case in which all the qualified sensor nodes belong to a single cluster r. The ICR of WSN for this special case can be formulated as equation 2.

$$ICR_{anycast-r} = \Pr\left\{ \begin{bmatrix} \mathrm{E}_2\left(\text{sink to}\mathrm{CH}^{(t)}h_t\right) \cap \mathrm{E}_2\left(\mathrm{CH}^{(t)}h_t \text{ to } \mathrm{CH}^{(t-1)}h_{t-1}\right) \cap \cdots \cap \\ \mathrm{E}_2\left(\mathrm{CH}^{(1)}h_1 \text{ to } \mathrm{CH}^{(0)}h_0\right) \cap \left[\cup_{\forall a \in Q} \mathrm{E}_2\left(\mathrm{CH}^{(0)}h_0 \text{ to } a\right)\right] \end{bmatrix} \right\} \quad (2)$$

B. Sink Manycast for Cluster Topology

The manycast-based ICR is the probability that there exists an operational path from the sink node to at least one subset of sensor nodes out of a larger group of qualified sensor nodes. For hierarchical clustered topology, the manycast-based ICR is the probability that there exists an operational path from the sink node to top hierarchical level CH, then to the next hierarchical level CH and so on to the destination group's CH and finally to all sensor nodes in any one subset. Note that the qualified sensor nodes in the group may not belong to a single cluster. Let Rx denote a subset of qualified nodes, a denote any sensor node in Rx, n denote the number of sensor nodes in the qualified group, m denote the required number of sensor nodes in each subset, H0,x denote the set of CH(0) for nodes in Rx, and Hl,x denote the set of CH that is hierarchically above Rx at parent level l, $0 \leq l \leq t$. Then the ICR of WSN with hierarchical clustered topology for sink manycast can be formulated as equation 3.

$$ICR_{manycast} = \Pr\left\{ \bigcup_{x=1}^{C_n^m} \begin{bmatrix} \left[\cap_{\forall i \in H_{t,x}} \mathrm{E}_2\left(\text{sink to}\mathrm{CH}^{(t)}_i\right)\right] \cap \left[\cap_{\substack{\forall i \in H_{t,x} \\ \forall j \in H_{t-1,x}}} \mathrm{E}_2\left(\mathrm{CH}^{(t)}_i \text{ to } \mathrm{CH}^{(t-1)}_j\right)\right] \\ \cap \cdots \cap \\ \left[\cap_{\substack{\forall i \in H_{1,x} \\ \forall j \in H_{0,x}}} \mathrm{E}_2\left(\mathrm{CH}^{(1)}_i \text{ to } \mathrm{CH}^{(0)}_j\right)\right] \cap \left[\cap_{\substack{\forall i \in H_{0,x} \\ \forall a \in R_x}} \mathrm{E}_2\left(\mathrm{CH}^{(0)}_i \text{ to } a\right)\right] \end{bmatrix} \right\} \quad (3)$$

Consider the special case in which all the qualified sensor nodes belong to a single cluster r. Let hl be the

parent CH of cluster r at the level l. The ICR of WSN for this special case can be formulated as equation 4.

$$ICR_{manycast-r} = \Pr\left\{\begin{array}{l} \mathrm{E}_2\left(\text{sink to CH}^{(t)}h_t\right)\cap \mathrm{E}_2\left(\text{CH}^{(t)}h_t \text{ to CH}^{(t-1)}h_{t-1}\right)\cap\cdots\cap \\ \mathrm{E}_2\left(\text{CH}^{(1)}h_1 \text{ to CH}^{(0)}h_0\right)\cap\left\{\bigcup_{x=1}^{C_n^m}\left[\bigcap_{\forall a\in R_x}\mathrm{E}_2\left(\text{CH}^{(0)}h_0 \text{ to } a\right)\right]\right\} \end{array}\right\} \quad (4)$$

Note that the ICR expressions (1), (2), (3), and (4) can be simplified to obtain tight approximations. For example, (4) can be tightly lower-bounded by (5). This is an efficient simplification because storing and manipulating symbolic expressions are very computationally intensive. This simplification is also realistic under the practical assumption that the clusters are non-overlapping, and nodes that participate in communication between CH(k) and CH(k+1) do not generally participate in communication between CH(k) and CH(k-1); and when they do participate, their contribution is insignificant. That is all the sub-events are disjoint provided that we account for each CH reliability only once along any operational path.

$$\begin{aligned} &ICR_{manycast-r} \\ &= \Pr_2\left(\text{sink to}\text{CH}^{(t)}h_t\right)\times \Pr_2\left(\text{CH}^{(t)}h_t \text{ to CH}^{(t-1)}h_{t-1}\right) \\ &\times\cdots\times \Pr_2\left(\text{CH}^{(1)}h_1 \text{ to CH}^{(0)}h_0\right)\times \Pr\left\{\bigcup_{x=1}^{C_n^m}\left[\bigcap_{\forall a\in R_x}\mathrm{E}_2\left(\text{CH}^{(0)}h_0 \text{ to } a\right)\right]\right\} \end{aligned} \quad (5)$$

Similar simplified lower bound expressions can also be obtained for (1), (2) and (3) which are not shown here due to the space limitation.

C. Sink Unicast for Tree Topology

The unicast-based ICR is the probability that there exists an operational path from the sink node to the destination sensor node. For WSN with tree topology, the ICR for the sink unicast model is the probability that there exists an operational path from the sink node to the top-level parent node (PN), then to the next level PN and so on to the destination sensor node's PN, and finally to the desired node. Let a represent the destination node, hk represent PN that is hierarchically above a at level-k, $0\le k\le t$. Then the ICR of WSN with tree topology under unicast data delivery model is

$$ICR_{unicast} = \Pr\left\{\begin{array}{l} \mathrm{E}_2\left(\text{sink to PN}^{(t)}h_t\right)\cap \mathrm{E}_2\left(\text{PN}^{(t)}h_t \text{ to PN}^{(t-1)}h_{t-1}\right)\cap\cdots\cap \\ \mathrm{E}_2\left(\text{PN}^{(1)}h_1 \text{ to PN}^{(0)}h_0\right)\cap \mathrm{E}_2\left(\text{PN}^{(0)}h_0 \text{ to } a\right) \end{array}\right\} \quad (6)$$

D. Sink Multicast for Tree Topology

The multicast-based ICR is the probability that there exists an operational path from the sink node to all the sensor nodes in a qualified group. For WSN with tree topology, the ICR for sink multicast model is the probability that there exists an operational path from the sink node to the top level parent node (PN), then to the next level PN and so on to the destination group's PN, and finally to all sensor nodes in the group. Note that the qualified sensor nodes in the group may not belong to a single cluster. Let Q denote the set of qualified nodes, a denote any sensor node in Q, H0 denote the set of PN(0) for nodes in Q, and Hl denote the set of PN that is hierarchically above nodes in Q at parent level-l, $0\le l\le t$. Then the ICR of WSN with tree topology under multicast data delivery model is

$$ICR_{multicast} = \Pr\left\{\begin{array}{l} \left[\bigcap_{\forall i\in H_t}\mathrm{E}_2\left(\text{sink to PN}^{(t)}i\right)\right]\cap\left[\bigcap_{\substack{\forall i\in H_t \\ \forall j\in H_{t-1}}}\mathrm{E}_2\left(\text{PN}^{(t)}i \text{ to PN}^{(t-1)}j\right)\right] \\ \cap\cdots\cap\left[\bigcap_{\substack{\forall i\in H_1 \\ \forall j\in H_0}}\mathrm{E}_2\left(\text{PN}^{(1)}i \text{ to PN}^{(0)}j\right)\right]\cap\left[\bigcap_{\forall a\in Q}\mathrm{E}_2\left(\text{PN}^{(0)}i \text{ to } a\right)\right] \end{array}\right\} \quad (7)$$

E. Sink broadcast for Tree Topology

The broadcast-based ICR is the probability that there exists an operational path from the sink node to all sensor nodes in the WSN. For WSN with tree topology, the ICR for sink broadcast model is the probability that there exists an operational path from the sink node to top level PN, then to all the next level PN and so on to all the lowest level PN and finally to all sensor nodes. Let a denote any node in the WSN. Then the ICR of WSN with tree topology under broadcast data delivery model is

$$ICR_{broadcast} = \Pr\left\{\begin{array}{l} \left[\bigcap_{\forall i}\mathrm{E}_2\left(\text{sink to PN}^{(t)}i\right)\right]\cap\left[\bigcap_{\forall i,\forall j}\mathrm{E}_2\left(\text{PN}^{(t)}i \text{ to PN}^{(t-1)}j\right)\right] \\ \cap\cdots\cap\left[\bigcap_{\forall i,\forall j}\mathrm{E}_2\left(\text{PN}^{(1)}i \text{ to PN}^{(0)}j\right)\right]\cap\left[\bigcap_{\forall i,\forall a}\mathrm{E}_2\left(\text{PN}^{(0)}i \text{ to } a\right)\right] \end{array}\right\} \quad (8)$$

Note that broadcast is a special case of multicast when all nodes in the WSN are in the qualified group.

F. Sink Anycast for Tree Topology

The anycast-based ICR is the probability that there exists an operational path from the sink node to any one sensor node out of a qualified group [13]. For WSN with tree topology, the ICR for sink anycast model is the probability that there exists an operational path from the sink node to the top level PN, then to the next level PN and so on to the destination group's PN and finally to any sensor node in the qualified group. Note that the qualified sensor nodes in the group may not belong to a single cluster. Let Q denote the set of qualified nodes, a denote any sensor node in Q, hk denote PN that is hierarchically above a at level-k, $0 \leqslant k \leqslant t$. Then ICR of WSN with tree topology under anycast data delivery model is

$$ICR_{anycast} = \Pr\left\{\bigcup_{\forall a\in Q}\left[\begin{array}{l} \mathrm{E}_2\left(\text{sink to PN}^{(t)}h_t\right)\cap \mathrm{E}_2\left(\text{PN}^{(t)}h_t \text{ to PN}^{(t-1)}h_{t-1}\right)\cap\cdots\cap \\ \mathrm{E}_2\left(\text{PN}^{(1)}h_1 \text{ to PN}^{(0)}h_0\right)\cap \mathrm{E}_2\left(\text{PN}^{(0)}h_0 \text{ to } a\right) \end{array}\right]\right\} \quad (9)$$

Note that unicast is a special case of anycast when there is only one node in the qualified group.

G. Sink Manycast for Tree Topology

The manycast-based ICR is the probability that there exists an operational path from the sink node to at least one subset of sensor nodes out of a qualified group [13]. The sensor nodes in the qualified group may not belong to a single cluster. For WSN with tree topology, the ICR for sink multicast model is the probability that there exists an operational path from the sink node to top level PN, then to the next level PN and so on to the destination group's PN and finally to all sensor nodes in any one subset. Let Rx denote a subset of qualified nodes, a denote any sensor node in Rx, n denote the number of sensor nodes in the qualified group, m denote the required number of sensor nodes in each subset, H0,x denote the set of PN(0) for nodes in Rx, and Hl,x denote the set of PN that is hierarchically above Rx at parent level l, 0≤l≤t. Then the ICR of WSN with tree topology under manycast data delivery model is

$$ICR_{manycast} = \Pr\left\{\bigcup_{x=1}^{C_n^m}\left\{\left[\left[\bigcap_{\forall i\in H_{t,x}} \mathrm{E}_2\left(\text{sink to PN}^{(t)}i\right)\right]\cap\left[\bigcap_{\substack{\forall i\in H_{t,x}\\ \forall j\in H_{t-1,x}}} \mathrm{E}_2\left(\text{PN}^{(t)}i \text{ to PN}^{(t-1)}j\right)\right]\right\}\right.$$
$$\left.\left\{\cap\cdots\cap\left[\bigcap_{\substack{\forall i\in H_{1,x}\\ \forall j\in H_{0,x}}} \mathrm{E}_2\left(\text{PN}^{(1)}i \text{ to PN}^{(0)}j\right)\right]\cap\left[\bigcap_{\substack{\forall i\in H_{0,x}\\ \forall a\in R_x}} \mathrm{E}_2\left(\text{PN}^{(0)}i \text{ to } a\right)\right]\right\}\right\} \quad (10)$$

Note that multicast is a special case of manycast when n = m.

IV. Case Study

A. Cluster Topology Case

The proposed metrics are illustrated via the analysis of the example WSN with two clusters in Figure 1, where CH1 and CH2 are CH(0) of cluster 1 and cluster 2 respectively, and CH1 is the CH(1) of the two clusters. In this example, links and nodes are assumed to fail s-independently. The fixed failure rates of 2e-6 hr-1, 5e-7 hr-1, and 1e-6 hr-1 are assigned to the links, base station (sink node), and sensor nodes (including both cluster heads and gateway nodes), respectively. Note that our analysis methodology has no limitation on the type of failure distributions. For simplification of illustration, we assume all qualified sensor nodes are in the same cluster 2. In other words, the set of all qualified sensor nodes Q belongs to {n1, n2, n3, n4, n5}. After applying progressive reduction scheme, G(0)(V, E) in Figure 1 is reduced to G(1)(V, E) containing only CH(0), g(0) and g(1) as shown in Figure 2(a). G(1)(V, E) is further reduced to obtain G(2)(V, E) composed of only CH(1) and g(1) between level 1 cluster and the sink as shown in Figure 2(b).

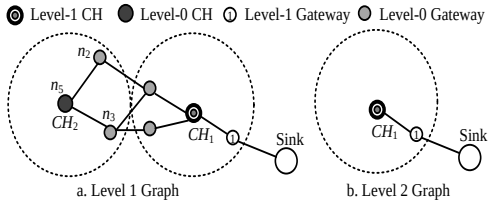

Figure 2. Graphs after reduction.

In this section, we study ICR of the example WSN for both anycast and manycast data delivery models.

1) Sink Anycast

Since all qualified nodes are in cluster 2, equation 2 is used to evaluate the anycast-based ICR of the example WSN. We consider four cases with different qualified sensor nodes groups: 1) Q1 = {n1} (unicast); 2) Q2 = {n1, n2}; 3) Q3 = {n1, n2, n3}; 4) Q4 = {n1, n2, n3, n4}.

As an example, for the case Q2 = {n1, n2}, equation 2 can be rewritten as equation 6.

$$ICR_{anycast-2} = \Pr\left\{\begin{matrix}\mathrm{E}_2(\text{sink to } CH_1)\cap\mathrm{E}_2(CH_1 \text{ to } CH_2)\\ \cap\left[\mathrm{E}_2(CH_2 \text{ to } n_1)\cup\mathrm{E}_2(CH_2 \text{ to } n_2)\right]\end{matrix}\right\} \quad (11)$$

The above reliability expression can be computed directly from the graphs in Figure 1 and Figure 2. In particular, the last two terms in equation 6 are obtained from Figure 1; Figure 2(a) is analyzed to obtain the second term E2(CH1 to CH2); Figure 2(b) is used to evaluate the first term E2(sink to CH1).

If a component's failure probability has been considered at a lower-level graph, it is considered zero in higher-level graphs. For example, since the failure probabilities of CH2 and the gateway node in cluster 2 g2(0) (n2) are already considered when evaluating the last term, failure probability of zero is assigned to CH2 and n2 in G(1)(V, E) to evaluate Pr2(CH1 to CH2). However, the inter cluster gateway-to-gateway link (g1(0), g2(0)) failure probability needs to be considered at G(1)(V, E).

Q1 is a special case of anycast where the data delivery model is actually sink unicast and the evaluation expression is equation 7.

$$ICR_{unicast} = \Pr\{\mathrm{E}_2(\text{sink to}CH_1)\cap\mathrm{E}_2(CH_1 \text{ to } CH_2)\cap\mathrm{E}_2(CH_2 \text{ to } n_1)\} \quad (12)$$

The reliability expressions for the other two cases Q3 and Q4 can be similarly derived from equation 2. The reliability results for the four cases are given in Figure 3.

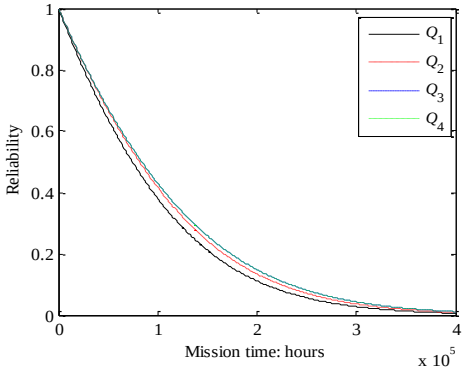

Figure 3. Reliability results for sink anycast-based WSN

Note that the results under cases Q3 and Q4 are exactly the same. The reason is that all the paths between CH2 and n4 have to pass through n1, n2, or n3. In other words, there is an operational path between CH2 and n4 only when there is an operational path between CH2 and

n1, between CH2 and n2, or between CH2 and n3. In this case, adding n4 to the group of qualified sensor nodes has no effect on the ICR of WSN. However, as shown in Figure 3 the reliability of WSN increases as the number of sensor nodes in the qualified group increases for other cases. In general, WSN using sink anycast data delivery model is more reliable than WSN using sink unicast because sink anycast provides more flexibility than sink unicast. For this example system at the mission time of 200,000 hours, the reliability of anycast under the case Q3 is 10.53% better than that of anycase under the case Q2, which is 20.17% better than that of unicast under the case Q1.

2) Sink Manycast

Since all qualified nodes are in cluster 2, Equation 4 is used to evaluate the ICR of WSN for manycast data delivery model.

Assume the required number of sensor nodes in each subset is 2, i.e., m = 2. We consider two cases for the qualified sensor nodes: Q1 = {n1, n2} and Q2 = {n1, n2, n3}. For the case Q2, n = 3. Thus, there are combinations: 1) R1 = {n1, n2}; 2) R2 = {n1, n3}; 3) R3 = {n2, n3}.

Simplification technique in Section 2 is used to obtain the lower-bound for the case Q2. Equation 5 can be rewritten as equation 8.

$$ICR_{manycast-2} = \Pr_2(\text{sink to } CH_1) \times \Pr_2(CH_1 \text{ to } CH_2) \times \Pr\left\{\begin{array}{l}\left[\mathrm{E}_2(CH_2 \text{ to } n_1) \cap \mathrm{E}_2(CH_2 \text{ to } n_2)\right] \\ \cup\left[\mathrm{E}_2(CH_2 \text{ to } n_1) \cap \mathrm{E}_2(CH_2 \text{ to } n_3)\right] \\ \cup\left[\mathrm{E}_2(CH_2 \text{ to } n_2) \cap \mathrm{E}_2(CH_2 \text{ to } n_3)\right]\end{array}\right\} \quad (13)$$

Q1 is a special case of manycast where there are only two sensor nodes, n1 and n2. In this scenario, the data delivery model is actually sink multicast and the evaluation expression is equation 9.

$$ICR_{manycast-2} = \Pr_2(\text{sink to } CH_1) \times \Pr_2(CH_1 \text{ to } CH_2) \times \Pr[E_2(CH_2 \text{ to } n_1) \cap E_2(CH_2 \text{ to } n_2)] \quad (14)$$

Note that broadcast is a special case of multicast where the group includes all 11 nodes of the WSN in Figure 1. The comparison results for broadcast, multicast, and manycast are shown in Figure 4.

From Figure 4, we can see that for a given number of sensor nodes of each subset, reliability increases as the size of the qualified group increases. In general, WSN based on sink manycast data delivery model is more reliable than WSN based on sink multicast because sink manycast provides more flexibility than sink multicast. For this example system at the mission time of 200,000 hours, the reliability of manycast under the case Q2 is 34.97% better than that of multicast under the case Q1, which is 862.02% better than that of the broadcast case.

Given Q = {n1, n2, n3}, the reliability results for WSN with sink anycast, manycast (with m=2) and multicast are compared in Figure 5. For unicast, n1 is the destination sensor node. Because sink manycast requires more than one node connected with the sink node, WSN with manycast data delivery model is less reliable than WSN with anycast data delivery model for a given qualified group.

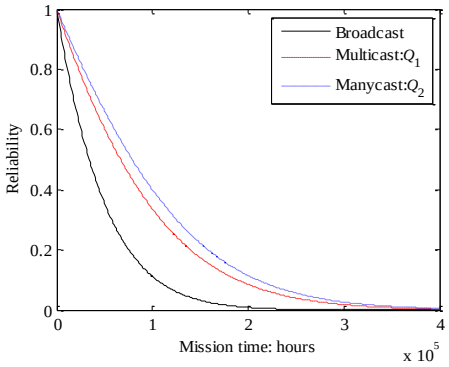

Figure 4. Comparison results for broadcast, multicast, and manycast.

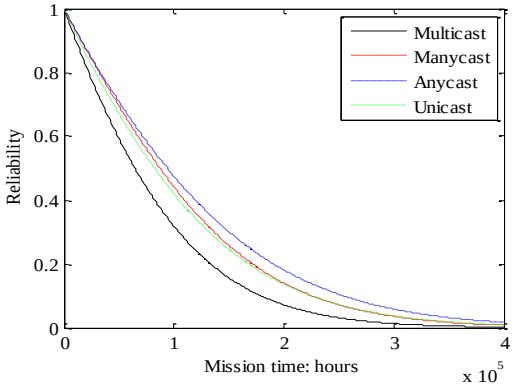

Figure 5. Comparison results for different data delivery models.

B. Tree Topology Case

In the section, two cases are studied to illustrate the applications of the proposed metrics.

Case 1: In this case, we study the ICR for different data delivery models and compare the ICR results for these models.

Figure 6 is an example WSN with two clusters, where PN1 and PN2 are PN(0) of cluster 1 and cluster 2, respectively, and PN1 is also the PN(1) of the two clusters. In this example, links and nodes are assumed to fail s-independently. The fixed failure rates of 2e-6 hr-1, 5e-7 hr-1, and 1e-6 hr-1 are assigned to the links, sink node, and sensor nodes, respectively. Note that our analysis methodology has no limitation on the type of failure distributions.

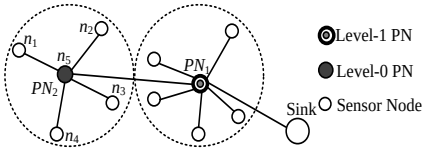

Figure 6. Example WSN with Tree Topology

For simplification of illustration, we assume all qualified sensor nodes for unicast, anycast, multicast,

and manycast are in the same cluster 2. Three cases are studied and the reliability results are presented:

ICR results for anycast-based WSN with four different qualified group (Figure 7). 1) Q1 = {n1} (unicast); 2) Q2 = {n1, n2}; 3) Q3 = {n1, n2, n3}; 4) Q4 = {n1, n2, n3, n4}.

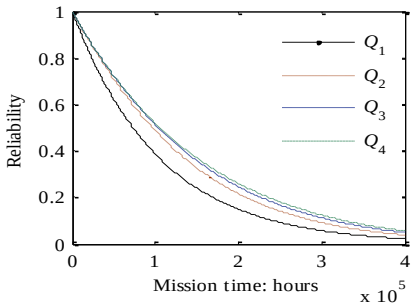

Figure 7. Anycast-based WSN

ICR results for manycast-based WSN with three different qualified groups where m = 2 (Figure 8). 1) Q1 = {n1, n2} (multicast); 2) Q2 = {n1, n2, n3}; 3) Q3 = {n1, n2, n3, n4}.

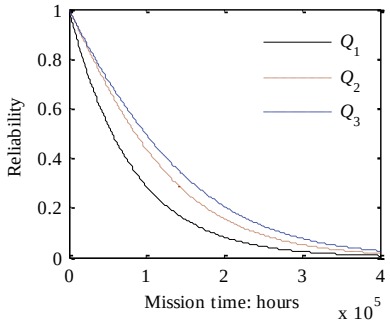

Figure 8. Manycast-based WSN

From Figure 7, we can see that the reliability of WSN increases as the number of sensor nodes in the qualified group increases for anycast. The same conclusion can be drawn for the manycast case from Figure 8. In general, anycast is the most reliable data delivery model for a given qualified group (because anycast provides the most flexibility).

Case 2: In this case, we study ICR for different WSN architectures for tree topology.

Three WSN examples with tree topology are studied. The sensor nodes are distributed the same way for all three cases but organized into different architectures by different links. Figure 9(a) is the case with the most hierarchical levels: all nodes except n10 are served as parent nodes (central nodes). Figure 9(b) is another extreme case with the least hierarchical levels (only one level): all nodes, except the root node n1, are only the basic sensor nodes which are connected to the root node. Figure 9(c) is WSN with two levels architecture: n1 and n6 are the level-0 parent nodes and n1 is the level-1 parent node (root node). The fixed failure rates of 2e-6 hr-1, 5e-7 hr-1, and 1e-6 hr-1 are assigned to the links, sink node, and sensor nodes, respectively.

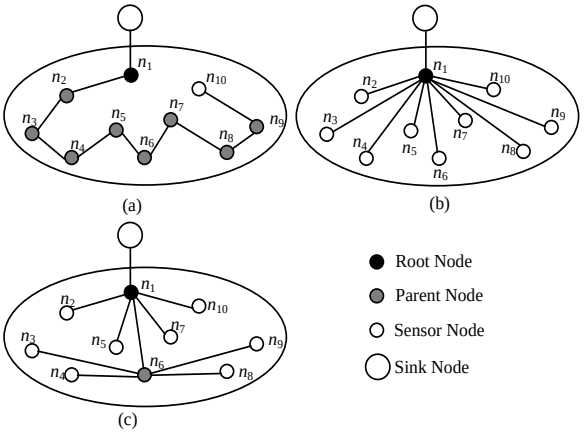

Figure 9. WSN examples with tree topology

Unicast-based WSN under the three cases are studied and reliability results at mission time 200000 hours are shown in Figure 10.

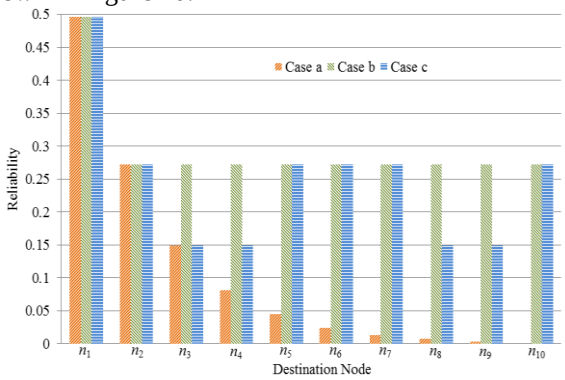

Figure 10. Unicast-based WSN

From Figure 10, the conclusions are listed as follow:

1) Case b is the most reliable architecture for unicast based WSN since all sensor nodes can be achieved in two hops. Any sensor node except the root node as the destination node can obtain the same reliability.

2) Root node is the most reliable choice for destination node, because root node is achievable when the link between the sink node and the root node is operational.

3) The reliability decreases dramatically as the destination node away from the sink node for case a, because more nodes and links are involved.

4) In most cases, case c is more reliable than case b which is not always the case. For example, n2 can be achieved by two links and one node for case a, but if n2 is connected to parent node n6 instead of the root node n1, then more links and more nodes have to be reliable.

5) In case c, any sensor node under the same parent node served as the destination node leads to the same reliability.

Broadcast-based WSN under the three cases are studied and results are shown in Figure 11.

Broadcast-based WSN is reliable when all the nodes and links are reliable. Thus, the ICR results are the same no matter which architecture is used as shown in Figure 11.

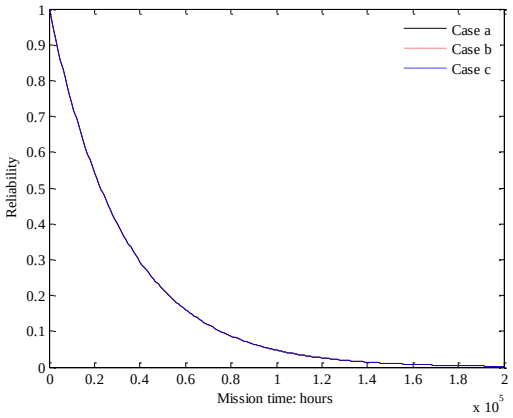

Figure 11. Broadcast-based WSN

Multicast-based WSN under the three cases are studied and results at mission time 200000 hours are shown in Figure 12. Four qualified groups are studied: (1) Q1={n2, n5, n7, n10};(2) Q2={n3, n4, n8, n9}; (3) Q3={n2, n3, n4, n5}; (4) Q4={n7, n8, n9, n10}.

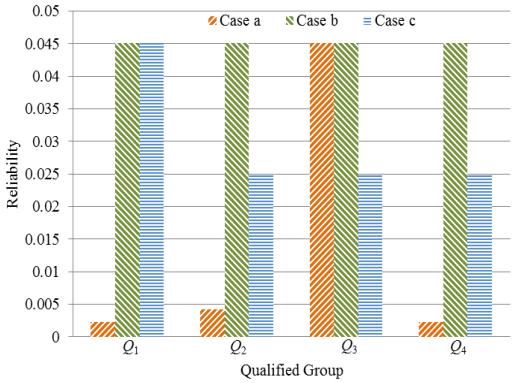

Figure 12. Multicast-based WSN

From Figure 12, the conclusions are listed:

1) Case b is the most reliable architecture for multicast-based WSN since all sensor nodes can be achieved in two hops.

2) For case a, the ICR of WSN is decided by the farthest sensor node in qualified group, because all nodes can be achieved if the farthest sensor node can be achieved.

3) If all sensor nodes in the qualified group are connected directly to the root node, the ICR under case c is the same as case b.

4) The qualified group is critical for the choice of WSN architecture between case a and case c.

Anycast-based WSN under the three cases are studied and results at mission time 200000 hours are shown in Figure 13. Four qualified groups are studied: (1) Q1={n2, n5, n7, n10};(2) Q2={n3, n4, n8, n9}; (3) Q3={n2, n3, n4, n5}; (4) Q4={n7, n8, n9, n10}.

From Figure 13, the conclusions are listed as follow:

1) Case b is the most reliable architecture for anycast-based WSN since all sensor nodes can be achieved in two hops.

2) For case a, the ICR of WSN is decided by the nearest sensor node in qualified group, because the communication is successful when any sensor node is communicated.

3) If all sensor nodes in the qualified group are connected directly to the root node, the ICR under case c is the same as case b.

4) The qualified group is critical for the choice of WSN architecture between case a and case c.

Manycast-based WSN under the three cases are studied and results at mission time 200000 hours are shown in Figure 14. Four qualified groups are studied: (1) Q1={n2, n5, n7, n10};(2) Q2={n3, n4, n8, n9}; (3) Q3={n2, n3, n4, n5}; (4) Q4={n7, n8, n9, n10}.

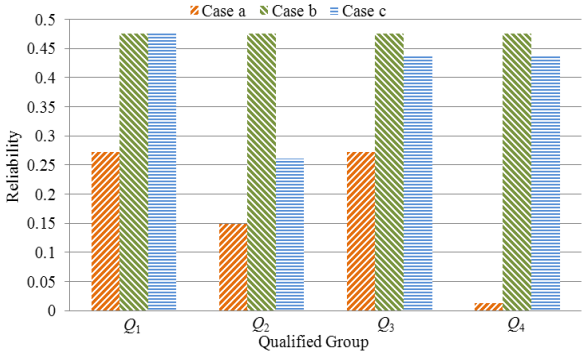

Figure 13. Anycast-based WSN

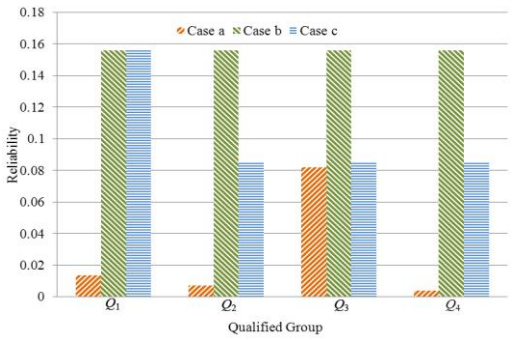

Figure 14. Manycast-based WSN

From Figure 14 the conclusions are listed:

1) Case b is the most reliable architecture for manycast-based WSN since all sensor nodes can be achieved in two hops.

2) If all sensor nodes in the qualified group are connected directly to the root node, the ICR under case c is the same as case b.

3) The qualified group is critical for the choice of WSN architecture between case a and case c.

V. CONCLUTIONS AND FUTURE WORK

Reliability models were proposed for the infrastructure communication reliability analysis of WSN with hierarchical clustered topology and tree topology. Different data delivery models are compared through illustrative examples: WSN with anycast is the most reliable and WSN with broadcast is the least reliable. The proposed models have no limitation on the type of

component failure distributions. The models can be adapted to other topologies. Relationships between reliability and network properties are investigated. In general, higher connectivity, shorter average path length, and larger average degree lead to higher reliability.

Metrics for the analysis of infrastructure communication reliability (ICR) for WSN with different topologies are proposed in this work. In particular, WSN with hierarchical clustered topology and tree topology have been studied. Five data delivery models - unicast, anycast, manycast, multicast, and broadcast - have also been studied and compared for the ICR analysis of WSN. Furthermore, WSN with different hierarchical levels with the same distribution of sensor nodes for the tree topology have been studied and compared. In the future, we will study and compare the ICR for different biconnected graphs for the mesh topology with different node degrees and average path lengths. Based on the reliability metrics, we will optimize the structure of WSN to achieve the optimal network reliability and propose an efficient broadcasting method considering topology[15]. Based on the ICR analysis, sensitivity measures will be studied and analyzed. Built on the DNA tool for traditional two-terminal network reliability evaluation, a prototype software tool is being developed to evaluate the ICR and component sensitivity for WSN with different topologies and data delivery models.

ACKNOWLEDGEMENT

This work is supported by research project of Zhejiang Normal University Xingzhi College (No. 23) And Opening Fund of Top Key Discipline of Computer Software and Theory in Zhejiang Provincial Colleges at Zhejiang Normal University (No. ZSDZZZZXK21).

REFERENCES

[1] Yongxian Song, Ting Chen, Juanli Ma, Design and Analysis for Reliability of Wireless Sensor Network, *Journal of Networks*, Vol. 7, NO. 12, pp2003-2010., December 2012.

[2] S. Tilak, N. B. A. Ghazaleh, and W. Heinzelman, "A taxonomy of wireless micro-sensor network models," *Mobile Computing and Communications Review*, Vol. 1, pp. 28-36, June 2002.

[3] Chunyu Miao, Lina Chen, Infrastructure Communication Reliability for WSN on sink-manycast and sink-anycast model, *2013 International Conference on Advanced Computer Science and Electronics Information, in press*.

[4] Rongbiao Zhang, Yongxian Song, Fuhuan Chu, Study of Wireless Sensor Networks Routing Metric for High Reliable Transmission, *Journal of Networks*, Vol. 7, NO. 12, pp2044-2050., December 2012.

[5] X. Zang, D. Wang, H. Sun, and K. S. Trivedi, "A BDD-based algorithm for analysis of multistate systems with multistate components," *IEEE Transactions on Computers*, vol. 52, no. 12, pp. 1608–1618, December 2003.

[6] A. Shrestha and L. Xing, "Quantifying application communication reliability of wireless sensor networks", *International Journal of Performability Engineering, Special Issue on Reliailty and Quality in Design*, Vol. 4, pp. 43-46, 2008. (no)

[7] X. Zhu and H. Gupta, "Fault-tolerant manycast to mobile destinations in sensor networks," *Proceedings of IEEE International Conference on Communications, Glasgow Scotland*, pp. 3596-3603, June 2007.

[8] Akhilesh Shrestha, Liudong Xing, Yan Sun, and Vinod M., Infrastructure Communication Reliability of Wireless Sensor Networks Considering Common-Cause Failures, *International Journal of Performability Engineering*, Volume 8, Number 2, pp. 141-150, March 2012.

[9] M. Wu, T. Yang, and H. Zhang, "A data-centre fast rerouting base on anycast routing in wireless self-organized sensor networks," *Proceeding of the 2006 IEEE, International Conference on Mechaatronics and Automation, Luoyang, China, June* 2006.

[10] L. Xing and A. Shrestha, "QoS reliability of hierarchical clustered wireless sensor networks," *Proceedings of The 25th IEEE International Performance Computing and Computing and Communications Conference (eSCo-Wi'06), Phoenix, Arizona*, pp. 641-646, April 2006.

[11] M. Rausand and A. Hoyland, System Reliability Theory: Models, Statistical Methods, and Applications (2nd Edition), *John Wiley & Sons, Inc, New Jersey*, 2004.

[12] Chaonan Wang, Reliability analysis of wireless sensor networks using different network topology characteristics, Quality, Reliability, Risk, 2012 *International Conference on Maintenance, and Safety Engineering*, pp. 12-16, June 2012.

[13] C. Carter, S. Yi, P. Ratanchandani, and R. Kravets. "Manycast: exploring the space between anycast and multicast in ad hoc networks," *Proceeding of the International Conference on Mobile Computing and Networking*, pp. 273-285, 2003.

[14] L. Xing, A. Shrestha, "DNA: a tool for network reliability and sensitivity analysis," *The Fourth International Conference on Quality and Reliability (ICQR4), Beijing, China, August* 2005.

[15] Keiichi Endo, Kentaro Watanabe, Dai Okano, An Efficient Position-based Broadcasting Method Considering Node Density in MANETs, *Journal of Networks*, Vol. 8, No 4 (2013), Apr 2013

Computing Model of Airspace Utilization Rate Based on Airspace Load

Zhaoning Zhang and Ping Wang*
Civil Aviation University of China, Tianjin, China
*Corresponding author, Email: zzhaoning@263.net, wangpinggl@gmail.com

***Abstract*—A model for the computation of the airspace utilization rate is put forward to help the airspace manager assess the airspace usage effectively. Through proposing the concept of "airspace load", the airspace resource is quantified and a new definition of the airspace utilization rate is introduced. Based on the new definition and the research about airspace capacity and air traffic flow management, a model is established by analyzing the flying process of an en-route to compute the utilization rate of the en-route. To know the computation feasibility and ability of the model, it is applied to a given en-route in the computational example, the results of which show that the model can simulate the operation process of the en-route and can reflect its usage situation.**

***Index Terms*—Airspace Utilization Rate; En-Route Utilization Rate; Airspace Load; Airspace Capacity; Flight Time**

I. INTRODUCTION

As the development of civil aviation transportation, a growing number of airspace is demanded by an increasing air traffic flow. Many flights are often delayed as the air traffic flow demanding exceeds the airspace capacity. It is possible to increase the air traffic flow and to reduce the number of delays by making the best use of airspace. The utilization rate of airspace is an important criterion to evaluate the airspace usage. It can help the managers improve the management of airspace by accurately calculating the utilization rate of airspace, so that the value of airspace will be used in maximum.

The research on airspace utilization rate is still underway. Min Xue analyzed the airspace tube utilization rate by "time-space" diagram, which is usually used to analyze the road traffic condition [1]. However, the author has just introduced this idea, while the detailed computing method has not been given.

Kapil S.Sheth analyzed the airspace tube utilization rate by computing instantaneous occupancy rate and volume occupancy rate [2]. The instantaneous occupancy presents how many aircraft are flying in the tube compared to the total number of aircraft at the same instant in time. This metric represents the temporal utilization of tubes. The volume utilization is defined in terms of the total number of aircraft that can possibly occupy each tube. This metric represents the spatial or volumetric utilization of tubes. However, these two definitions just take one dimension into consideration and they can't reflect the real airspace usage accurately.

Shi Heping introduced the definition of basic airspace utilization rate and actual airspace utilization rate while the computing method was not given [3]. The basic airspace utilization rate can be defined as the ratio of the airspace that can be used to the space that can be flying in. The actual airspace utilization rate can be defined as the ratio of the airspace that has been used to the airspace that can be used.

Zhang Huili introduced the effective airspace utilization rate of flexible use of airspace based on the indexes of EUROCONTROL, including the time that the airspace can be used, the number of the aircrafts in the airspace and so on [4].

Zhang Bo put forward another definition of the airspace utilization rate, built evaluation indexes, considering the management and use of airspace, and computed the airspace utilization rate in gray correlation degree method. In addition, airspace utilization rate can be defined from the dimension of the flight time, the space or capacity of airspace [5].

Wang Ping put forward a new computing method of airspace utilization rate in principal component analysis and gray correlation degree method, considering the correlation among evaluation indexes [6].

Reference [5] and reference [6] have presented good evaluating methods of a whole airspace, while when it comes to compute the utilization rate of a detailed airspace during a period from a microcosmic aspect these two methods become invalid.

Because principal component analysis [7-10] and gray correlation degree [11] method are two methods that are adaptable to evaluate objects from the macroscopic aspect. There are also some other papers which are about optimizing of airspace capacity to ensure the best use of airspace [12-14].

However, all the studies mentioned above do not make full use of the data resulted from the actual use of airspace and the data resource is wasted. If we can find a simple method and use these data properly to compute the airspace utilization rate, it will be a practical mean to assess the airspace usage and will benefit for the airspace management.

In order to token the airspace utilization rate, firstly, the concept of "airspace load" is proposed according to the characters of the airspace. Then a new definition and

doi:10.4304/jnw.9.1.71-77

a common computing formula of airspace utilization rate is introduced in this paper, considering the three dimensions synthetically, which are flight time, the space and the capacity of airspace. Finally, this method is applied to the flight level (FL) and then the detailed computing formula of the en-route utilization rate is deduced.

II. Definition of Airspace Utilization Rate

The airspace is a special kind of national resource, which is the space where the aircrafts is flying. Generally, the quantity of resources of the airspace can be measured from three dimensions: time, space and capacity. The flying of aircrafts in airspace, such as the taking off of the aircraft, the climbing of the aircraft, the cruising of the aircraft and the landing of the aircraft, is just using the resource of time, space and capacity of the airspace. In turn, it also means that the airspace provides services for the flying of aircrafts in order to ensure the safety of the aircrafts, using its resource of time, space and capacity.

Thus, the airspace undertakes and completes some work in this process. Once the aircraft enters a given airspace, the airspace begins to work to ensure aircrafts' completing of a variety of actions in this area. In the process, the airspace resource can be used repeatedly, which means the airspace is released after a aircraft departs and it can also provide services for other aircrafts later. During the available time of the airspace, it must be used instantly. If the airspace has not been used at some time, the airspace has not created any value and the value of the airspace during that time can't be used anymore. However, the total quantity of the airspace is hard to be determined.

The airspace utilization rate referred to in this paper is the actual airspace utilization rate, which is the ratio of the airspace that has been used actually by the air transports to the airspace which can be used by air transports. Therefore, the time period, the airspace that have been used actually and the airspace which can be used by air transports should be quantified in order to compute the actual airspace utilization rate. However, the quantity of the airspace that has been used actually and the airspace which can be used by air transports is so hard to determine that the definition of the airspace utilization rate is limited. Thus, when we compute the airspace utilization rate, we can't use this definition directly in practice.

In this paper, the process of using airspace is regarded as the occupying and releasing of the airspace. Based on the researches of "work load" and some results of airspace utilization, the definition of "airspace load" is proposed to measure the airspace and compute the airspace utilization rate.

The airspace load both can be used to reflect the ability to provide services of the airspace within a certain period of time, and can also be used to reflect the used parts of this ability. From this perspective, the airspace load can be divided into the available airspace load and the actual airspace load.

The available airspace load refers to the maximum ability of the airspace and it can't be exceeded in practice, otherwise it will bring serious consequences including flight delays. The actual airspace load refers to the service ability that has been provided for aircrafts in practice. A well-run airspace system should show that the actual airspace load is infinitely closed to the available airspace load, but the actual airspace load should not exceed the available airspace load. In this range, the airspace load should be as great as possible, which is different from the work load of the person. The greater the available airspace load, the more services the airspace can provide and the more available flight flow. The greater the actual airspace load is, the more actual flight flow.

Therefore, the two indicators are used to measure the degree of efficiency of the airspace in this paper. The closer the space between the actual airspace load and the available airspace load is, the greater the airspace utilization rate.

There are so many factors that influence the operation of the airspace, such as the behavior of the aircrafts, the climate, the ability of the pilot and the air traffic manager, so we need a scientific and fast method to compute the airspace utilization in practice in order to reflect the usage situation of the airspace. We can also measure the airspace load from the three dimensions, including the time, the space and the capacity of the airspace. In the process of the operation of the airspace, it is using the time, the space and the capacity of the airspace to provide the flying service for the aircrafts.

Thus, the airspace load isn't one dimension, while it is multi-dimensions. For different airspace systems, we should determine its airspace load from multi-dimensions according to its special structure and operation features in order to compute its utilization rate more accurately. If we measure the airspace load just from one dimension, there will be some deviation on the computing results, or even the computing results may be not conform to the actual situation.

Based on the analysis above, the airspace utilization rate can be redefined as follows:

In the given time period, the ratio of the actual airspace load to the available airspace load is called the airspace utilization rate. The computing formula is shown as follows:

$$U = \frac{A_a}{A_t} \times 100\% \tag{1}$$

where:

U : The utilization rate of the given airspace;

A_t : The available airspace load. It reflects the available work ability of the airspace in the given time period and it is usually decided by the maximum capacity of the airspace. It refers to the work ability of the airspace when the airspace is operated and the maximum capacity is reached. It includes both the ability that have been offered to flights and the potential capability that the airspace possesses but has not offered to flights;

A_a: The actual airspace load. It means the real ability that the airspace has provided for the actual flight and reflects the quantity of the airspace that has been used by the aircrafts.

Thus, the airspace utilization rate can be computed quantification ally. In order to ensure the practical meaning of the definition, the airspace utilization rate U should meet with the mathematical qualification shown as follows:

$0 \le U \le 1, U \in R$.

III. Computing Model of the En-route Utilization Rate

The new definition of airspace load and airspace utilization rate and formula (1) will be applied to the en-route and calculation model of en-route utilization rate will be established in this chapter.

For a given en-route, the available airspace load is decided by route capacity, which includes the fixed capacity and the passing point capacity. The fixed capacity is decided by the length of the route, which means the space of airspace. Therefore, the available airspace load of the en-route can be confirmed by considering its space and capacity simultaneously. This available airspace load, decided by all three dimensions effectively, is the maximum ability that the en-route can afford.

Thus, the airspace load of an en-route is measured form the time dimension, considering the limits of the space and the capacity of the en-route. The definition of the en-route utilization rate is the ratio of the sum of the flying time of all aircrafts in the given time period to the sum of the flying time of all aircrafts that can be served in the given time determined by the en-route capacity and the length of the en-route.

A. Assumptions and Symbol Description of the Model

For conveniences of describing problems, the basic assumptions of the model are shown as follows:

In the given time period, the route capacity is not influenced by inclement weather and other stochastic factors, so the capacity in this paper is the static capacity of the airspace.

The air traffic is controlled by radar and the factors, such as the orientation precision of the navigation equipments, the delay of the communication and the control ability of the controllers, are not considered in the paper. Therefore, the margin of the flight separation is not needed.

Each type of aircrafts fly on the primary flight level at a constant speed.

The length of the fuselage is negligible.

Symbols of the model are described as follows:

L —The length of the en-route;

m —The total number of flight levels of the en-route;

n —The number of the aircraft types;

n_i —In the given time period, the actual air traffic flow of flight level i;

S_j —The minimum safety separation between the aircrafts of type j;

V_j —The flying speed on the primary flight level of aircraft type j;

C_i —The passing point capacity of the entry of flight level i;

C_{0i} —The fixed capacity of flight level *i*;

where, $i = 1,2,\cdots m,\ j = 1,2,\cdots n$.

B. Utilization Rate of the Flight Level

Aircrafts should fly according to the assigned flight levels during the stage of cruising. Therefore, the utilization rate of the flight level should be computed first in order to get the en-route utilization rate.

Based on the assumptions and symbol descriptions mentioned above, the flight level utilization rate is computed.

1) The Capacity of the Flight Level

Supposes that flight level i is the primary flight level of aircraft type j, which flies at the speed of V_j.

According to the en-route capacity model based on the average flying speed [15-18], the passing point capacity of flight level *i* can be obtained as follows:

$$C_i = \frac{1}{S_j / V_j} = \frac{V_j}{S_j} \tag{2}$$

where, C_i is the passing point capacity. It represents the number of flights that can be cleared into the flight level *i* in an hour.

In fact, before the hour, which is the time period that is given to compute the passing point capacity, there are some flights which have already been flying on the level. In this time period, these flights can also be served. The number of these flights is called the fixed capacity of the flight level [19, 20], denoted as C_{0i}. Because the aircrafts of type *j* on the flight level *i* fly at a constant speed, so the fixed capacity is decided by the length of the en-route and the minimum safety separation between aircrafts of type *j* and it can be computed as follows:

$$C_{0i} = \frac{L}{S_j} \tag{3}$$

In addition, due to the constant speed of aircrafts, the minimum safety separation can be translated to the corresponding minimum safety time separation, the formula is shown as follows:

$$\mathrm{T}_j = \frac{S_j}{V_j} \tag{4}$$

2) The Available Airspace Load

The available airspace load, which is decided by the capacity of the flight level, is the maximum ability that can be offered by the flight level. It includes both the ability that has been offered to aircrafts and the potential ability that the airspace possesses but has not offered.

This maximum ability can be achieved only on condition that the flights are cleared and kept the minimum safety separation. Therefore, the available airspace load is computed on the same condition.

Supposes that the given time period is also an hour. In this period, the flights served by flight level i include both the newly coming flights in this period and the flights that have already been flying on flight level i at the beginning of this period. The available airspace load will be discussed and computed according to different relationships between the length L of the en-route and the speed V_j of the aircrafts flying on flight level i.

a) If $L \geq V_j$, the flying situation of flight level *i* is shown in Fig. 1.

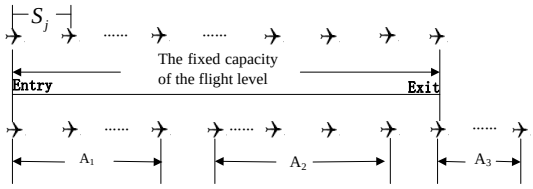

Figure 1. The flying situation of flight level when $L \geq V_j$

If $L \geq V_j$, then C_{0i} will be no smaller than C_i, i.e. $C_{0i} \geq C_i$.

Therefore, at the end of the given period, the flights on flight level *i* include the newly coming flights in this hour and the flights that have already flying on flight level *i* at the beginning of this period while not having flying out at the end of the period. The flights that can be served by flight level *i* in this period can be divided into three parts: the newly coming flights, the flights that have already been flying on flight level *i* at the beginning of this period while not having flown out at the end of the period and the flights that have already been flying on flight level *i* at the beginning of this period and have already flown out.

Therefore, in this case the available airspace load is computed as follows:

$$\begin{aligned} A_{ti} &= A_1 + A_2 + A_3 \\ &= [T_j + 2T_j + \cdots + \text{◆} C_i - 1)T_j] + (C_{0i} - C_i + 1)C_i T_j \\ &\quad + [T_j + 2T_j + \cdots + \text{◆} C_i - 1)T_j] \\ &= C_{0i} C_i T_j \end{aligned} \tag{5}$$

where:

A_1: The sum of the time that the flight level *i* can serve in an hour for the newly coming flights;

A_2: The sum of the time that the flight level *i* can serve in an hour for the flights that have already been flying on flight level *i* at the beginning of this period while not having flown out at the end of the period;

A_3: The sum of the time that the flight level *i* can serve in an hour for the flights that have already been flying on flight level *i* at the beginning of this period and have already flown out.

b) If $L < V_j$, the flying situation of flight level *i* is shown in Fig. 2.

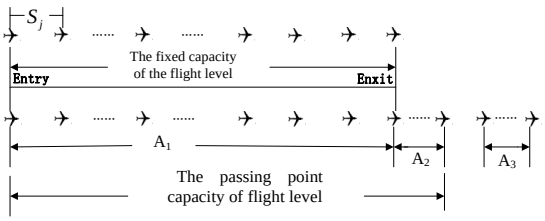

Figure 2. The flying situation of flight level when $L < V_j$

If $L < V_j$, then C_{0i} will be smaller than C_i, i.e. $C_{0i} < C_i$.

Therefore, after the given period, the flights on flight level *i* include only the newly coming flights, while the flights that have already been flying on flight level *i* at the beginning of this period have already flown out. The flights that can be served by flight level *i* in this period can also be divided into three parts: the flights that newly come into the flight level and have not flown out, the flights that newly come into the flight level but have already flown out and the flights that have already been flying on flight level *i* at the beginning of this period and have already flown out.

When computing the sum of flight time that can be used, we can unite the first kind and the third kind of flights and the sum of flight time that can be used for these flights can be obtained directly by formula (4). The flights that the passing point capacity exceeds the fixed capacity fly through the entire flight level in the period and spend the same time, which is the time an aircraft takes to fly through the entire en-route.

Therefore, in this case the available airspace load is computed as follows:

$$\begin{aligned} A_{ti} &= A_1 + A_2 \\ &= C_{0i} C_{0i} T_j + (C_i \text{-} C_{0i}) C_{0i} T_j \\ &= C_i C_{0i} T_j \end{aligned} \tag{6}$$

where:

A_1: The sum of the time that the flight level *i* can serve in an hour for the flights that newly come into the flight level and have not flown out.

A_2: The sum of the time that the flight level *i* served in an hour for the flights that the passing point capacity exceeds the fixed capacity.

A_3: The sum of the time that the flight level *i* can serve in an hour for the flights that have already been flying on flight level *i* at the beginning of this period and have already flown out.

According to the analysis above, the formulas of the available airspace load on the two conditions are the same. Both of them are decided by the length of the en-route

and the minimum safety separation of aircraft type *j* on flight level *i*. The available airspace load is proportional to the length of the en-route and inversely proportional to the minimum safety separation of aircraft type *j*, which is accordant to the practical situation.

Because the aircrafts are assumed to fly on their principle flight level, the flight level i and the aircraft type j is corresponding. Thus, according to the formula (5) and (6), the airspace load can be denoted as follows:

$$A_{ti} = C_i C_{0i} T_i \tag{7}$$

3) The Actual Airspace Load

In practice, the air traffic controllers will not control the flying of the aircrafts according to the minimum safety separation strictly, but they will increase the separation technically. The reason for this is that the speed of the aircraft is actually a random variables, it would be influenced by a lot of random factors. This may result in that the available airspace load will not be fully used.

In order to compute the actual airspace load of the flight level in the given time period, the flight flow and the flying time of each aircraft should be computed. The computing of the air traffic flow is an important part of the air traffic management.

If the entering time of an aircraft is in the given time period, the aircraft should be counted as one flight served in this period. Based on the new definition of the airspace utilization rate, a new method of computing the air traffic flow is proposed in this paper. As long as the aircraft has appeared in the airspace in the given time period, the aircraft is one of the flights which is served by the airspace in this time period.

Supposed that $T = [T_1, T_2]$ is the given time period, and $[T_1', T_2']$ is the time period that the aircraft flying in the airspace, which can be obtained according to position information of the flight in the flight data recorder. So there are five relationships between $T = [T_1, T_2]$ and $[T_1', T_2']$, which are shown in Fig. 3.

In these five situation, the time of the aircraft flying out of the airspace is earlier than the starting time of the given time period in Fig. 3(a), and the time of the aircraft entering into the airspace is later than the ending time of the given time period in Fig. 3(e). Thus, these aircrafts in these two situations should not be included in the air traffic flow during this time period.

In Fig. 3(b), Fig. 3(c) and Fig. 3(d), some time period is overlapped during the two time period, so these aircrafts should be included in the air traffic flow.

"The aircraft has appeared in the airspace in the given time period" has three instances, which is shown in Fig. 3(b), Fig. 3(c) and Fig. 3(d). According to the relationships, the actual flying time in the airspace of each aircraft can be computed.

In Fig. 3(b), the aircraft is flying in the en-route at the beginning of the given time period and has already flew out the en-route at the end of the given time. In this situation, the time that the aircraft enters into the en-route is equal to the beginning of the given time period. Thus, the actual time that the aircraft flies in the en-route can be described as $t = T_2' - T_1$.

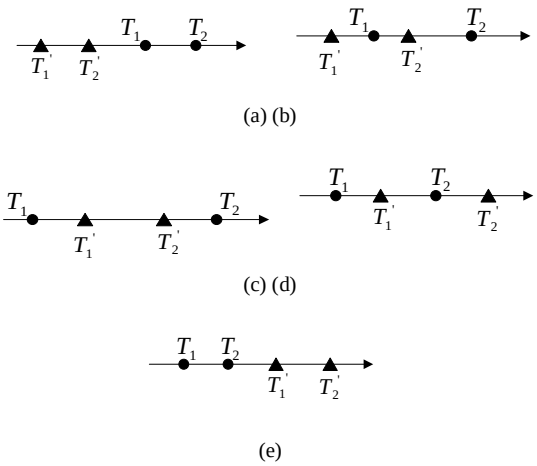

Figure 3. The relationships of the given time period and the flying time of the aircraft

In Fig. 3(c), the aircraft flies into the en-route after the beginning of the given time period and has already flew out the en-route at the end of the given time. In this situation, the actual time that the aircraft flies in the en-route can be described as $t = T_2' - T_1'$.

In Fig. 3(d), the aircraft flies into the en-route after the beginning of the given time period and has not flew out the en-route at the end of the given time. In this situation, the time that the aircraft flies out the en-route is equal to the end of the given time period. Thus, the actual time that the aircraft flies in the en-route can be described as $t = T_2 - T_1'$.

The flying time of the aircraft in the airspace is the airspace load that the airspace has taken in order to serve the flying of the aircraft. In the given time period, the sum of the flying time of all aircrafts is the actual airspace load. Suppose that in one hour, the air traffic flow is n_i, the flying time of each flight is t_{ik} ($k = 1,2,\cdots n_i$), which can be obtained with the method analyzed above. Finally, the actual airspace load can be computed as follows:

$$A_{ai} = \sum_{k=1}^{n_i} t_{ik} \tag{8}$$

4) Utilization Rate of Flight Level

After the available airspace load and the sum of the actual available airspace load is determined, according to formula (1), the utilization rate of flight level *i* can be computed as follows:

$$U_i = \frac{A_{ai}}{A_{ti}} \times 100\% = \frac{\sum_{k=1}^{n_i} t_{ik}}{C_i C_{0i} T_i} \times 100\% \tag{9}$$

TABLE I. THE RELATED DATA INFORMATION OF EACH FLIGHT LEVEL

FL	P_i	Minimum safety separation	Actual Number of Flights	Sum of the Actual Flight time	Utilization Rate
1	0.18	10 km	20	30 hours	76.92%
2	0.25	12 km	27	24 hours	73.85%
3	0.21	15 km	23	17 hours	65.38%
4	0.17	17 km	18	20 hours	87.18%
5	0.19	20 km	20	18 hours	92.30%

C. Utilization Rate of the En-route

The flying situation of all flight levels in the en-route is shown in Fig. 4.

Because all aircrafts fly on its primary flight level and the minimum safety separation of different aircraft types are different, so the air traffic flow is distributed unevenly among the flight levels. Therefore, in order to get the precise results, the probability of each aircraft type in the en-route should be got from the history data. Based on the total number of the flights in the en-route and the total number of the flights on each flight level, the probability $P_i(i=1,2,\cdots,m)$ of each aircraft type can be obtained.

Sum up the utilization rate of all flight levels weighted by the probability of each aircraft type in the en-route, the utilization rate of the en-route in a given hour can be computed as follows:

$$\mathrm{U}=\sum_{i=1}^{m}P_iU_i=\sum_{i=1}^{m}P_i\frac{\sum_{k=1}^{n_i}t_{ik}}{C_iC_{0i}T_i}\times 100\% \qquad (10)$$

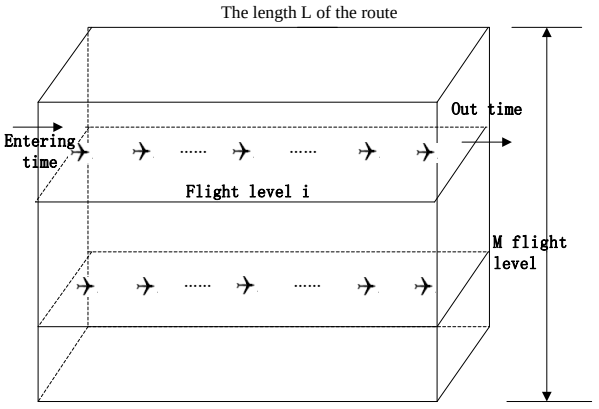

Figure 4. The Flying situation of all flight levels in the en-route

According to formula (10), the utilization rate of the en-route computed by this model has something to do with the length of the en-route and the sum of the actual flight time. When it comes to different en-routes or different time periods, the computing results will be different. This is consistent to the practical situation.

IV. COMPUTATIONAL EXAMPLE

This paper introduces a computing method of airspace utilization rate and it is suitable to different en-routes. When it comes to different en-routes, we can change the value of each parameter according to the computing object.

Thus, this paper will just take an en-route, 390 kilometers in length, as an example to verify this method. There are three flight levels in this en-route and the goal is to obtain the airspace utilization rate during a given time period 8:00-9:00. All three flight levels in the en-route are usable during this time period. There are mainly three aircraft types in the en-route and they fly on their primary flight level. Based on the history flight data, the probability of each aircraft type in the en-route can be obtained. During the time period, for each flight level, the time that each flight enters into the flight level and the time that each flight flies out of the flight level can be got according to the position information of the flight in the flight data recorder. The probability of each aircraft type in the en-route, Minimum safety separation, and other related data information is shown in Table I.

According to the time that each flight enters into the flight level and the time that each flight flies out of the flight level and based on formula (8), the actual airspace load of each flight level is obtained. The utilization rate of each flight level can be obtained according to formula (9) and finally according to formula (10) we can compute the utilization rate of the en-route at 78.40%.

This computing method can be applied to other en-routes. The parameters in this model are easy to be collected and computed. According to formula (9) and the utilization rate of each flight level, it shows that the computing result is mainly related to the speed and the flight flow and this can reflect the differences of different speed and different time period.

V. CONCLUSION

This paper introduces a new definition of airspace load and a common computing formula of the airspace utilization rate, and applies them to build the calculation model of the en-route utilization rate.

On condition that the en-route capacity is not influenced by the inclement weather and other stochastic factors, the calculation model of the en-route utilization rate is obtained, which considers the flight time, the space and capacity at the same time. The data of each parameter in this model are all easy to collect and compute. And the computing results can reflect the differences of different en-routes and time periods.

In sum, this model can benefit to the airspace management and can be the theory basis of the future research on airspace utilization rate.

ACKNOWLEDGMENT

This work was supported by the National Natural Science Foundation Project of China under grant 71171190.

REFERENCES

[1] Xue Min, "Design Analysis of Corridors-in-the-sky", *In Proceeding of AIAA Guidance, Navigation, and Control Conference*, pp. 1-11, 2009.

[2] Sheth Kapil S, Islam Tanim S, Kopardekar Parimal H, "Analysis of airspace tube structures", *In Proceeding of Digital Avionics Systems Conference*, pp. 1-10, 2008.

[3] Shi Heping, Safety Management of Air Traffic System. *Xiamen University Press, China*, 2003.

[4] Zhang Huili, "The Research on Flexible Use of Airspace Policy System". *Nanjing: Nanjing University of Aeronautics and Astronautics*, 2008.

[5] Zhang Bo, Chen Jinliang, Wang Sanqiang, "Studies on the Concept Model and Algorism of Airspace Utilization Rate", *Journal of Air Traffic Management*, No. 2, pp. 4-7, 2011.

[6] WANG Ping, YU Wenju, ZHANG Zhaoning, "Airspace Utilization Rate Based on PrincipalComponent Analysis Method and Gray Correlation Degree", *Journal of Aeronautical Computing Technique*, Vol. 42, No. 3, pp. 63-67, 2012.

[7] Shaobo Zhong, Dongsheng Zou. "Web Page Classification using an Ensemble of Support Vector Machine Classifiers", J*ournal of Networks*, Vol. 6, No. 11, PP. 1625-1630, 2011.

[8] Shafin Rahman, Sheikh Motahar Naim, Abdullah Al Farooq. "Performance of PCA Based Semi-supervised Learning in Face Recognition Using MPEG-7 Edge Histogram Descriptor", *Journal of Multimedia*, Vol. 6, No. 5, 404-415, 2011.

[9] Lei Yunqi, Lai Haibin, Li Qingmin. "Geometric Features of 3D Face and Recognition of It by PCA", *Journal of Multimedia*, Vol. 6, No. 2, 207-216, 2011.

[10] Gao Huixuan, "Multivariate Statistical Analysis", *Beijing University Press, Beijing*, 2003.

[11] Chengli Zhao, Yanheng Liu, Zhiheng Yu. "Evaluation for Survivable Networked System Based on Grey Correlation and Improved TOPSIS", *Journal of Networks*, Vol. 6, No. 10, 1514-1520, 2011.

[12] Gilbo Eugene P, "Optimizing Airport Capacity Utilization in Air Traffic Flow Management Subject to Constraints at Arrival and Departure Fixes", *Journal of IEEE Transactions on Control Systems Technology*, Vol. 5. No. 5, pp. 490-503, 1997.

[13] Kontoyiannakis K, Serrano E, Tse K, "A simulation framework to evaluate airport gate allocation policies under extreme delay conditions", *In Proceeding of the 2009 Winter Simulation Conference*, pp. 2332-2342, 2009.

[14] Gluchshenko Olga, "Dynamic usage of capacity for arrivals and departures in queue minimization", *In Proceeding of 2011 IEEE International Conference on Control Applications*, pp. 139-146, 2011.

[15] Zhaoning Zhang, Lili Wang, The Theory and Method of Air Traffic Flow Management, Science press, China, 2008.

[16] Zhang Zhaoning, Wang Lili, "The Theory and Method of Air Traffic Flow Management", *Science Press, Beijing*, 2009.

[17] Jiang Bing, "The Research of Evaluation Model and Method of Airspace", *Nanjing: Nanjing University of Aeronautics and Astronautics*, 2002.

[18] Zhou Rui, "Research on Several Issues of Terminal Airspace Design", *Nanjing: Nanjing University of Aeronautics and Astronautics*, 2009.

[19] Yu Jing, Liu Hong, Xiong Yunyu, "An improved evaluation model of En route dynamic capacity", *Journal of Sichuan University (Natural Science Edition)*, Vol. 44, No. 5, pp. 1005-1008, 2007.

[20] Zhao Dan, Dai Fuqiing, "An Improved Model of En Capacity", *Aircraft airworthiness and air traffic management academic annual meeting proceedings*, 2010.

Zhaoning Zhang was born in the city of Luannan, Hebei Province, China, in 1964. He completed his postdoctor research in Shanghai Jiaotong University. He is currently a professor and a master tutor of College of Air Traffic Management, Civil Aviation University of China, Tianjin, China. He has directed many projects and published published over 50 papers on refereed journals, patents and conference proceedings. His current research interests are about air traffic management, including transportation planning and management, airspace utilization rate, the dynamic capacity of airspace and the safety evaluation of the airspace.

Ping Wang was born in the city of Jinzhong, Shanxi Province, China, in 1985. She received her B.S degree in Statistics from Civil Aviation University of China, Tianjin, China, in 2008. Currently, she is studying in Transportation Planning and Management at Civil Aviation University of China, Tianjin, China, and will graduate in April, 2013. Her current research area is mainly about computing model and method of the airspace utilization rate.

Parameters Tracking Differentiator based on the Fuzzy Control and Varied Sliding Mode

Cai Ligang, Xu Bo, Yang Jianwu, and Zhangsen
Beijing University of Technology, Beijing 100083, China

***Abstract*—Directing at the problem of torsional vibration occurred in the start-up procedures of long shaft drive transmission existed in printing equipment, we raised a variable structure control method based on Variable parameters fuzzy. The method not only displays feature of traditional non-linear variable structure control like non-deference derivation, planning the dynamic process and good capacity of resisting disturbance, but also able to effectively suppress the vibration generated when switching sliding mode surface. By means of simulation test and platform test, we prove that, compared with traditional PID controller, the PID controller with tracking differentiator in the staring process. The maximum overshoot of the system output is reduced to 4.8% from 72.2% and its adjustment time has been shortened 210ms, which help realize the improvement of start-up speed and vibration suppression.**

***Index Terms*—Fuzzy Control; Variable Structure; Tracking Differentiator; Vibration Suppression; Torsional Vibration Suppression**

I. INTRODUCTION

With the development of the printing industry, higher and higher requirements have been raised for stability and accuracy of printing equipment. The coaxial transmission equipments are connected by shaft in the startup process, many factors, including long transmission between the shafts, system's low stiffness and overload weight, result in torsional vibration [1] in startup process. Torsional vibration not only affects the steady time in startup process, but also brings a great impact on the transmission shaft, thus affecting the life-span of printing machine. As for the vibration suppression in the start, three methods are adopted, including S curve method, Input Shaping method and filter.

According to curve of S, Nguyen KD, Ng TC and Chen IM [2], several commonly used trajectory generation methods are given. Rew KH and Kim KS [3] propose asymmetric S curve method, for fast jitter-free startup, replace the traditional S curve method. Zhou Li, Yang Shihong and Gao Xiaodong [4] propose a fast 4-order trajectory planning and feed-forward control algorithm whose core idea turns to "bang bang" control algorithm similar to the optimal control, and the jerk planning makes the system's velocity curve works only in accelerating and decelerating state, and it carries out feed forward on acceleration and jerk to improve the system's rapid response performance. Meckl and Arestides [5] optimized the parameter of the S-curve to minimize the residual vibration. Erkokmaz and Altintas [6] developed a trajectory generation algorithm to satisfy the additional jerk limitation of the quintic spline interpolation for the faster CNC system, Hong and Chang [7] proposed buffered digital differential analyzer and applied their method to an EDM for parametric curve machining. Kim [8] has surveyed and introduced the practical solutions of the problems in motion generation of linear motors.

Input Shaping is a control technique for reducing vibrations in computer controlled machines. The method works by creating a command signal that cancels its own vibration. That is, vibration caused by the first part of the command signal is canceled by vibration caused by the second part of the command. Input shaping is implemented by convolving a sequence of impulses, an input shaper, with any desired command. The shaped command that results from the convolution is then used to drive the system. If the impulses in the shaper are chosen correctly, then the system will respond without vibration to any unshaped command. The amplitudes and time locations of the impulses are obtained from the system's natural frequencies and damping ratios. Shaping can be made very robust to errors in the system parameters. Input Shaping thought, put forward by Singer [9], with convolution pulse command and planning curve, means to design Notch Filter from the angle of time domain and filter frequency components of resonant frequency point. Mohamed and Tokhi showed that input shapers were preferable to filters in suppressing vibration of a single link, flexible arm [10], [11]. Even some researchers that advocate traditional filtering methods have presented results that demonstrate that input shapers are superior to low-pass filters at reducing residual vibration [12].

The most commonly used method is linear filtering. With Notch Filter, M. Anibal [13] et al inhibit the interruption in initiation process and obtain good effect. Zanasi et al. [14] developed a nonlinear filter for the smooth motion satisfying the constraints of velocity and acceleration, and applied the filter to the motion generation of a tile printing machine. In China, ADRC in heavy load starting process have been applied and achieved good results in recent years. Tracking differentiator, proposed by Professor Han Jingqing, as a part of ADRC, uses low pass characteristics of tracking differentiator to limit coupled high frequency signal and mechanical system resonance frequency, thereby

doi:10.4304/jnw.9.1.78-84

inhibiting the system oscillation. [15] Of all the foreign studies, Levant [16] proposes to use high-order variable structure to construct nonlinear tracking differentiator, and does simulation experiments. This is nonlinear tracking differentiator which is currently widely used.

Aiming at the vibration arising in startup of printing machine, this paper presents A control algorithm method for tracking differentiator based on fuzzy sliding mode. Based on high-order variable structure, this method, adopting fuzzy control fitting sliding surface and traditional PID control, helps to construct PID controller embracing fuzzy-variable-structure tracking differentiator. Through simulation and experimental verification, it is proved that this method has better inhibition effect on start-up torsional vibration, while eliminates the chattering existing in the traditional high-order variable structure control, thus it can be applied to packaging machinery, printing equipment and other equipment to suppress vibration in start-up.

II. TORSIONAL VIBRATION PROBLEMS IN START-UP

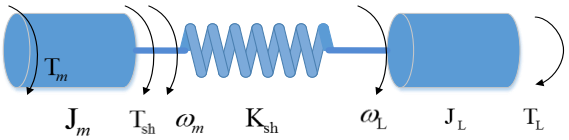

The model of two-mass system of rolling millThe problem on torsional vibration in flexible system originates in printing machine system, where the load is coupled to the driving motor by a long shaft. The small elasticity of the shaft is magnified and has a vibration effect no the load speed. The vibration is an impediment to enhance the performance of the system. The simplest model of such resonant mechanical system is two-mass system(as shown in Figure 1). Various controllers for two-mass system are proposed. As a result of some considerations.

ω_m : motor speed, ω_L : load speed

T_m : motor torque, T_L : load torque, T_{sh} : shaft torque

J_m : motor inertia, J_L : load inertia

K_{sh} : spring coefficient (stiffness) of drive shaft

The traditional PID controller, in printing machine start-up process, often arouses oscillations of the system, due to step signal as start signal. Step signal is broad-spectrum signal in attenuation, rich in frequency at a lot of spectrum. When the electrical starting signal frequency couples with the mechanical natural frequency phase, torsional vibration will arises. Secondly, the traditional PID controller will lead to derivative for error between given signal and feedback signal. In the derivation process, when the sampling takes short time, the calculation noise will be introduced in order to raise system oscillation.

In view of the above problems, low-pass filter is added in the signal input end to achieve suppression of high frequency signal in real production; however, low-order low-pass filter cannot make high frequency signal decay quickly, but the main shortcoming of high-order filter is the complex algorithm raised, and the improper selection of parameters will bring the non-convergence of filter itself and cause signal's oscillation even divergence. In view of the above problems, Levant proposes nonlinear tracking differentiator which, through the method of planning and start-up curve and non - derivative, achieves torsional vibration suppression.

III. CONSTRUCTION OF TRADITIONAL TRACKING DIFFERENTIATOR AND ANALYSIS OF BUFFETING

A. Construction of Traditional Tracking Differentiator

Levant puts forward controller based on sliding mode variable structure, and it also calculate the derivatives of signal error with non direct derivation in planning and starting process, thus it can draw robustness on measurement error and system noise. The traditional tracking differentiator and a PID controller realize hybrid control, and the system frame is as shown in Figure 2:

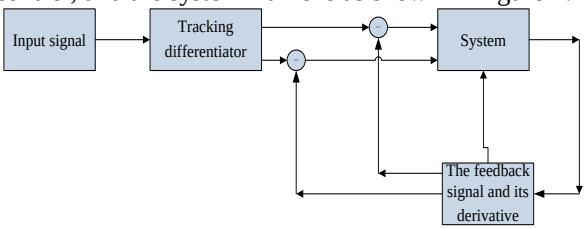

Figure 1. Diagram of PID controller with tracking differentiator

The core of the whole control system is tracking differentiator, the method of tracking differentiator (1) is shown below: [17-21]:

$$\begin{cases} \dot{x} = u \\ u = u_1 - \lambda \mid x - v(t) \mid^{1/2} sign(x - v(t)) \\ \dot{u}_1 = -\alpha * sign(x - v(t)) \end{cases} \quad (1)$$

where $\alpha > C, \lambda^2 \geq 4C\dfrac{\alpha + c}{\alpha - c}$

$C(C > 0)$ - the upper limit of input signal Lipschitz

The two-order sliding mode tracking differentiator can realize derivatives of x tracking's $v(t)$, u_1 is tracking $v(t)$. With Levant's tracking differentiator, not only for the given signal is filtered, avoiding the oscillation caused by the coupling of signal and mechanical system, but also raises a method without differentiation, thus enhancing the anti-jamming ability of the system. However, the main problem existing in the traditional tracking differentiator is the chattering of output signal.

B. Analysis of the Causes of Chattering

Chattering is mainly caused by inertia in control system, which fails the sign function sign(s) to be switched at s=0, resulting in continuous adjustment of system near the sliding mode surface, followed by jitter [10-13]. Secondly, due to excessive noise, high-order systems with noise are expressed as follows [22]:

$$\begin{cases} x^n = f(x,t) + g(x,t)u(t) + d(t) \\ y = x \end{cases} \quad (2).$$

where, $f(x,t)$ and $g(x,t)$ are known nonlinear functions, $x \in R$, $y \in R$, $d(t)$ are unknown disturbance, $|d(t)| \leq D$ (D | is bounded real), $g(x,t) > 0$.

The switching function is defined as follows:

$$S = k_1 e + k_2 \dot{e} + ... k_{n-1} e^{n-1} = ke \quad (3).$$

where, $e = x - x_d = (e, \dot{e} ... , e^{n-1})^T , k_1 ... k_{n-1}$, which meets the Hurwitz polynomial conditions. The sliding mode controller is set as:

$$u(t) = \frac{1}{g(x,t)} [-f(x,t) - \sum_{i=1}^{n-1} k_i e^{(i)} + x_d^{(n)} - u_{sw}] \quad (4).$$

where $u_{sw} = \eta sign(s), \eta > 0$. according to formula (2) and (3):

$$\dot{s} = \sum_{i=1}^{n-1} k_i e^{(i)} + x^{(n)} - x_d^{(n)} \quad (5)$$

$$\dot{s} = k_i e^{(i)} + f(x,t) + g(x,t) u(t) + d(t) - x_d^{(n)} \quad (6).$$

We integrated formula (4), then,

$$\dot{s} = d(t) - \eta sign(s) \quad (7)$$

$$s\dot{s} = d(t)s - \eta |s| \leq 0 \quad (8)$$

When the interfering $d(t)$ is relatively large, the switching control gain η will also increase, thus causing buffeting.

C. Construction of Fuzzy Tracking Differentiator

In view of the chattering problem of traditional tracking differentiator, this article proposes fuzzy variable parameter which rebuilds the tracking differentiator. Its main idea is to use fuzzy logic control to adjust the adjustable parameter of tracking differentiator. In ensuring the stability of lyapunov function, the more it tends to be switching plane, the less the output amplitude, thus achieving the purpose of reducing the chattering.

(1) The determination of fuzzy rules:

As shown in (1), let $e = x - v(t)$, then

$$\begin{aligned} \dot{e} &= u - \dot{v}(t) \\ &= u_1 - \lambda |x - v(t)|^{1/2} \ sign(x - v(t)) - \dot{v}(t) \end{aligned} \quad (9)$$

As:

$$\dot{u}_1 = -\alpha * sign(x - \dot{v}(t)) \quad (10)$$

Then

$$u_1 = -\alpha t * sign(x - \dot{v}(t)) \quad (11)$$

From (11) and (9), we get

$$\begin{aligned} \dot{e} &= -\alpha t * sign(x - \dot{v}(t)) \\ &\quad - \lambda |x - v(t)| sign(x - v(t)) - \dot{v}(t) \\ \dot{e} &= -\alpha t * \frac{e}{|e|} - \lambda \frac{e}{|e|^{1/2}} - \dot{v}(t) \end{aligned} \quad (12)$$

According to the lyapunov stability criterion we construct the fuzzy rules table. According to the stability criterion, for example, if e is PB, ($\dot{e}$) is NB, to ensure ($\dot{e}$) is NB, as shown in (12), then α , λ must be PB.

TABLE I. FUZZY RULE

Fuzzy rules	1	2	3	4	5	6	7
(IF)e	NB	NM	NS	ZO	PM	PS	PB
(THEN) α , λ	PB	PM	PS	ZO	PM	PS	PB

(2) Determination of fuzzy intervals

According to the experiment deviation, e is divided into seven fuzzy sets. Respectively they are: the negative big (NB), negative middle (NM), and negative small (NS), zero (ZO), positive small (PS), positive middle (PM), positive big (PB). Distribution of e fuzzy sets is between [-30, 30] pulse. The output of the control variable u distribution is [1, 1]. In which the output of the u is divided into seven fuzzy sets, respectively they are zero (ZO), positive small (PS), positive middle (PM), positive big (PB). The membership function distribution curve is shown in figure 3:

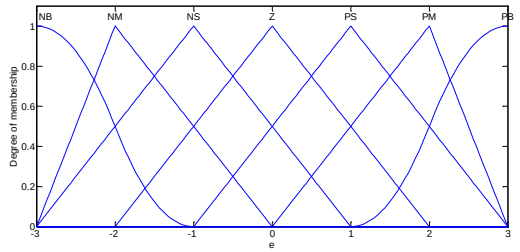

(a) Function of error membership

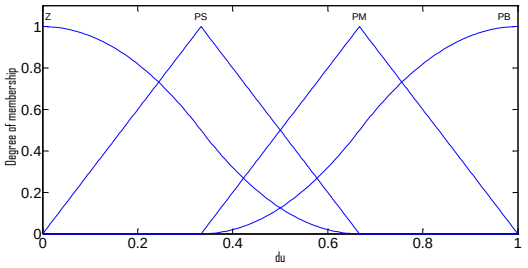

(b) Function of output value membership

Figure 2. Fuzzy rules

In the process of defuzzification, as α , λ have the same universe space, we introduce intermediate variables M, let $\alpha_1 = \alpha * M$, $\lambda_1 = \lambda * M$. According to the fuzzy rules we design fuzzy controller. In the process of the defuzzification, in order to obtain accurate amount of control and improve the precision of controller, we use the weighted average method as solution. Its defuzzification function is:

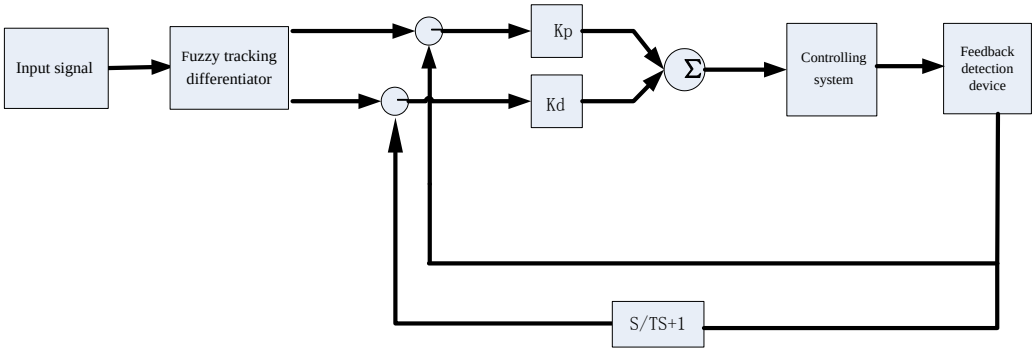

Figure 3. PID controller based on fuzzy variable parameters

$$M = \frac{\int_v v u_v(v) dv}{\int_v u_v(v) dv} \tag{9}$$

Construction of new fuzzy tracking differentiator as shown in (10)

$$\begin{cases} \dot{x} = u \\ u = u_1 - \lambda_1 \mid x - v(t) \mid^{1/2} sign(x - v(t)) \\ \dot{u}_1 = -\alpha_1 * sign(x - v(t)) \end{cases} \tag{10}$$

$$\alpha_1 = \alpha * M \qquad \lambda_1 = \lambda * M$$

D. Construction of Fuzzy Tracking Differentiator

Mixed control construction of fuzzy tracking differentiator and PID controller, as shown in Figure 4.

Respectively adding fuzzy tracking differentiator to system of the forward channel and feedback channel, we get control system which is based on fuzzy tracking differentiator. Unlike traditional PID controller, PID controller is based on fuzzy variable parameters and doesn't need the signal error derivation. It directly makes the difference between the planning derivative of the tracking differentiator and feedback channel derivative. Because encoder feedback is position signal, in the actual system we need to know the derivative of position signal and converting it into the derivative of speed signal. Then make the difference between derivative of speed signal and tracking differentiator.

IV. EXPERIMENTAL VERIFICATION

A. Tracking Differentiator Performance Verification

Comparison between fuzzy tracking differentiator and traditional tracking performance:

When we choose the same parameter for traditional tracking differentiator and fuzzy tracking differentiator ($\alpha = 10$, $\lambda = 50$), fuzzy interval of fuzzy functions is [-30, 30]. We adopt step signal 1 amplitude at 100ms to stimulate two kinds of differentiators. Simulation comparison showed that in the same parameter, convergence speed of fuzzy tracking differentiator which adopts fuzzy variable parameters is slightly slower than the conventional tracking differentiator (as shown in Figure 5 a. Its chattering amplitude is also significantly attenuated (as shown Figure 5 b). The steady chattering decreases from 0. 2 to 0. 043, and the amplitude decreased by 78%, At the same time, it can effectively eliminate the static error.

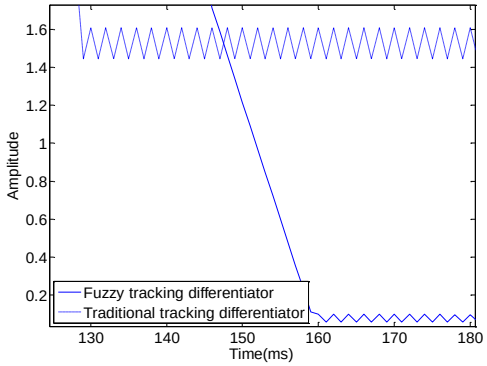

a) Magnification of the signal

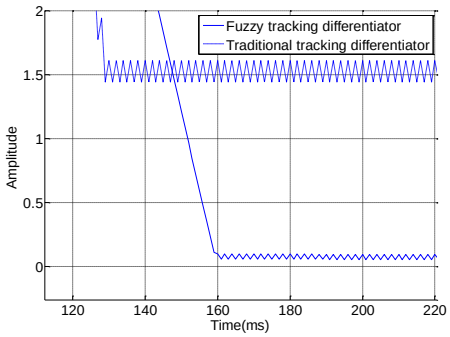

b) Magnification of the signal

Figure 4. Partial enlarged detail

(1) The signal tracking test:

Sinusoidal signal, with amplitude = 1, frequency =1rad/s, is adopted, traditional tracking differentiator and fuzzy tracking differentiator experience comparison test, in the premise of ensuring the tracking effect similar to sine signal, $\alpha = 10$ and $\lambda = 50$ for traditional tracking differentiator, and $\alpha = 600$, $\lambda = 200$ for fuzzy tracking differentiator, (with fuzzy interval selection [-30, 30]). Experiments show that, in tracking the sinusoidal signal, although the fuzzy tracking differentiator falls slightly behind the traditional tracking differentiator in signal-follow planning performance (Figure. 6 a), the derivative planning performance will be smoother, completely eliminating the chattering (as is shown in 6b and 6 c).

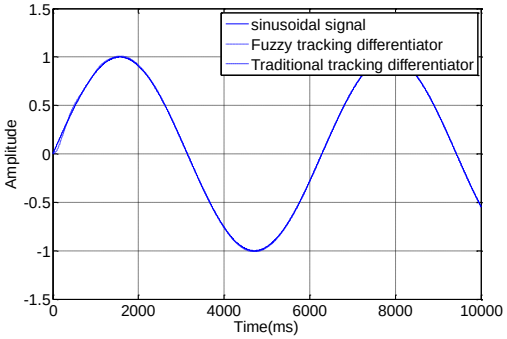

(a)Sinusoidal signal follow-up

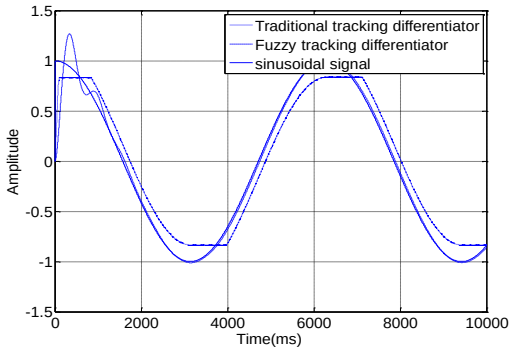

(b)Sinusoidal signal derivative follow-up

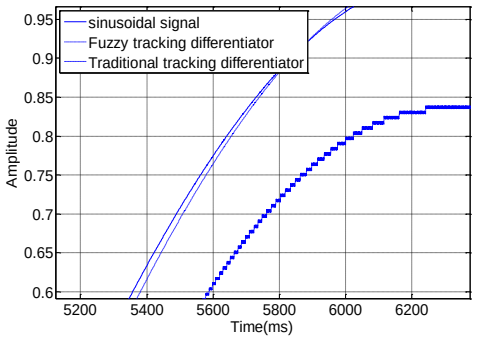

(c)Magnification of signal follow-up function

Figure 5. The traditional tracking differentiator and fuzzy differential signal follow

(2) The interference test:

For white noise pollution of 0.01%, amplitude =1, frequency=1rad/s, and tracking differentiator parameters are the same as test (2), as is shown in Figure 7. The results show that, compared with the traditional tracking differentiator, fuzzy tracking differentiator has stronger ability to resist interference signal. It, in the production line and complex electromagnetic environment, can well eliminate outside interference on signal in transmission process.

B. Validations

In order to simulate start-up of printing machine equipment, rotating platforms with different qualities are established. The platform is composed of control system, execution mechanism and a detecting device. The main control system uses X20 series PLC from B & R Company, and its sampling period can reach 400us. The mechanical structure is composed of motor, reducer, mass and spring. The specific parameters are shown in Table 2.

TABLE II. MULTITRAIT TORSION TEST PLATFORM PARAMETERS

No.	Device name	Parameters
1	Motor	20W
2	Reducer	gear ratio 14:1
3	Mass block 1	Moment of inertia 1. 5865*10(-5)
4	Mass block 2	Moment of inertia 4. 6630*10(-5)
5	Spring stiffness	2. 42×10-3~2. 58×10-3Nm/rad
6	Encoder's resolution	1000 pluse/rad
7	Main control PLC	B & R Company'S X20-PLC
10	Sampling period	1ms

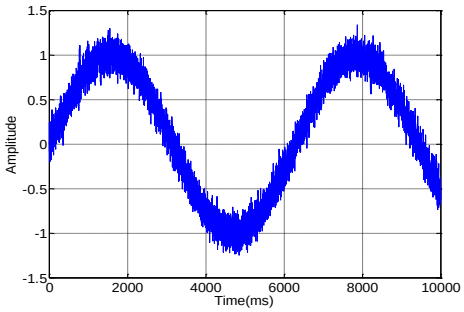

(a) The given value with noise

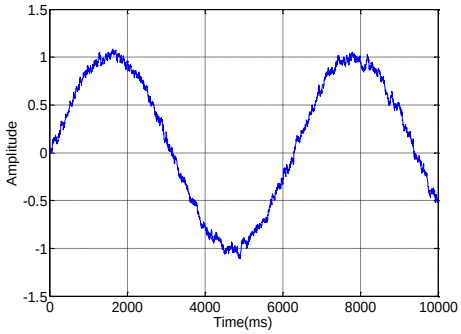

(b) Influence of fuzzy tracking differentiator on signal

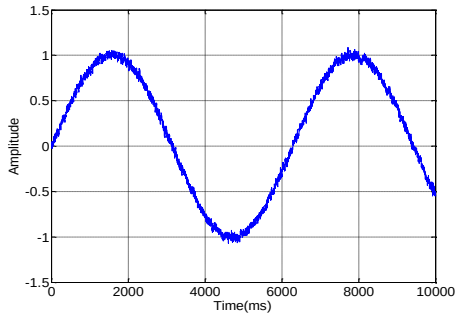

(c) Influence of traditional tracking differentiator on signal

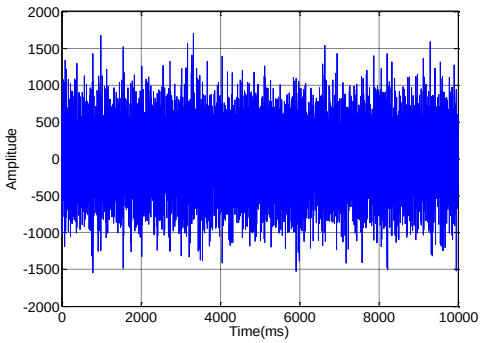

d) Differentiation

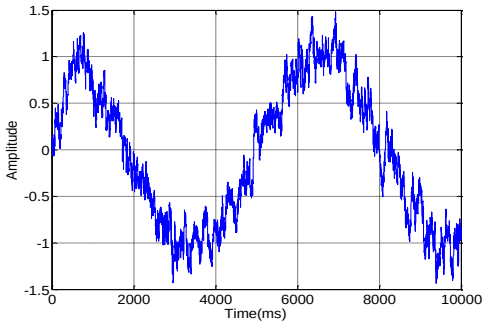

e) Influence of fuzzy tracking differentiator on signal

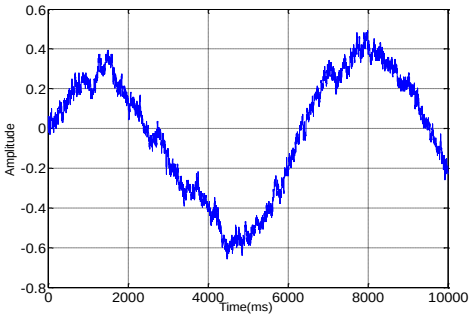

f) Influence of traditional tracking differentiator on signal

Figure 6. Anti-interference performance of traditional tracking differentiator and fuzzy tracking differentiator

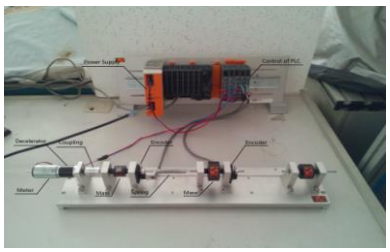

Figure 7. Quality rotation system

Position signal is feed backed to the main control PLC through the encoder, thus forming a closed loop system. Carved gate precision of encoder is 1000 line / round, and PLC sampling module divides it into 4 subdivisions, with subdivision precision of 4000 lines /round.

As is shown in Figure 8 in the actual production, the encoder is installed on the motor tail, so in the simulation of the actual working environment, the first stage of encoder is taken as feedback signal, and the second encoder as the evaluation signal. Step signal whose pulse value is 14000 excites the system, then we record the open-loop response, PID closed-loop response and fuzzy closed-loop tracking differentiator response curve; and through the monitoring software of PLC, the data are recorded as matlab to be identifiable. [23-29] When step signal excites the open-loop system, the mutual coupling of high frequency components in system and resonance frequency of signal arouses system vibration. As is shown in Figure 9 (open-loop response curve), the open-loop system shows obvious oscillation.

Fussy variable-structure tracking differentiator enables the coupling of high-frequency components of input signal and mechanical system to decay, in order to suppress the vibration. The data show that, the peak of common PID controller is 24120 pulses, and overshoot is 72.2%, while the system peak of tracking differentiator is 14677 pulses, and the overshoot is only 4.8%. The time when output curve all enter given 5% is determined as the time for steady system, the ordinary PID takes 700ms, while PID with fuzzy tracking differentiator takes only 490ms, meaning greatly speed-up response time. In order to better evaluate the vibration suppression effect, evaluation function is introduced:

$$V = \int_{t1}^{t2} |e| \, dt \tag{11}$$

where t1 is the first time to enter 5%, t2 is the time when the entire system become stable. e is the difference between measured output and planned input. Traditional PID embracing the same parameters and the PID with fuzzy tracking differentiator are compared. The traditional differentiator's v=3.0805×105. Since the range of fuzzy tracking differentiator enters 5% for the first time has been stable, so v=0. Test data show that the vibration suppression effect is obvious.

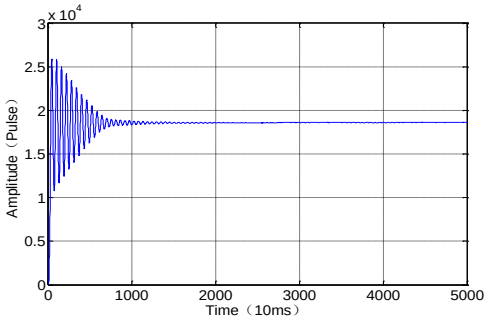

(a) The open loop response curve

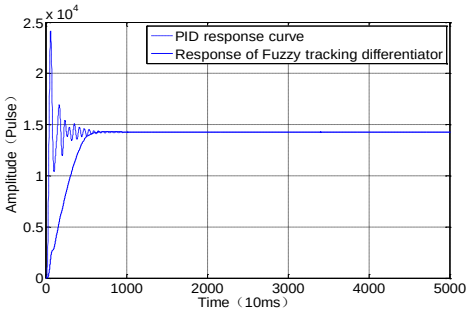

(b) Step response of General PID and the PID embracing fuzzy tracking differentiator

Figure 8. Planning of fuzzy tracking differentiator on startup curve

V. CONCLUSIONS

(1) Vibration of the traditional tracking differentiator is caused by delayed sliding mode surface switching and signal interference, and a method to construct sliding surface based on fuzzy control is put forward. This method retains the advantages of traditional tracking differentiator and eliminates system chattering.

(2) Tracking differentiator based on fuzzy sliding surface is proposed, and the method to adjust parameters is offered.

(3) Through simulation experiments and model platform experiments, it is shown that the new method preserves low-pass characteristics, non-difference derivation and dynamic planning process of traditional tracking differentiator, while it also eliminates the chattering. In the platform test, PID system and that with tracking differentiator are compared, and when the same parameters are set up, good control effect is obtained.

ACKNOWLEDGMENT

National Scientific and Technological Supporting Projects Innovation Application Demonstration Project of the First Generation CNC Mechanical Products (2012BAF13B00)

REFERENCES

[1] Rew K H, Kim K S. U sing asymmetric S curve profile for fast and vibrationless motion. *International Conference on Contronl Automation and Systems, COEX, Seoul Korea*, 2007 pp. 500-504

[2] NguyenKD, NgTC, ChenIM. On algorithms forplanning Scurve motion profiles. *International Journal of Advanced Robotic Systems*, 2008, 5 (1) pp. 99-106.

[3] Rew K H, Kim K S. U sing asymmetric S curve profile for fast and vibrationless motion. *International Conference on Contronl Automation and Systems, COEX, Seoul Korea*, 2007 pp. 500-504.

[4] Fast 4-order trajectory planning and feedforward control algorithm. *Journal of Sichuan University*, 2011, 43 (3) pp. 244-250.

[5] P. H. Meckl and P. B. Arestides. Optimized S-Curve Motion Profiles for Minimum Residual Vibration, *Proc. of the American Control Conference, Philadelphia, Pennsylvania*, pp. 2627-2631, June 1998.

[6] K. Erkokmaz and Y. Altintas, High Speed CNC System Design. Part I: Jerk Limited Trajectory Generation and Quintic Spline Interpolation, *International Journal of Machine Tools and Manufacture*, Vol. 41, pp. 1323-1345. 2001.

[7] R. C. Hong and Y. F. Chang, Parametric Curve Machining of a CNC Milling EDM *International Journal of Machine Tools & Manufacture*, Vol. 45, pp. 941-948, 2005.

[8] J. H. Kim, Control of Linear Motor using DSP, *Tong-Il Pub*., 2003.

[9] Singer N C, Sing hose W E, Seering W P. Comparison of filtering methods for reducing residual vibration. *European Journal of Contronl* 1999, 5 pp. 208-218.

[10] Z. Mohamed and M. O. Tokhi, Vibration control of a single-link flexible manipulator using command shaping techniques, *Proc. Inst. Mech. Eng. I: J. Syst. ControlEng.* vol. 216, no. 2, pp. 191–210, 2002.

[11] Z. Mohamed and M. O. Tokhi Command shaping techniques for vibration control of a flexible robot manipulator, *Mechatronics*, vol. 14, no. 1, pp. 69–90, 2004.

[12] M. Ahmad, R. R. Ismail, M. Ramli, A. Nasir, andN. Hambali, Feedforward techniques for sway suppression in a double-pendulum-type overhead crane, *in Proc. Int. Conf. Comput. Technol. Develop., Kota Kinabalu, Malaysia*, Nov. 13–15, 2009, pp. 173–178.

[13] M. Anibal Valenzuela Dynamic Compensation of Torsional Oscillationin Paper Machine Sections *IEEE Transactions On Industry Applications* 200541 (6) pp. 1458-1466.

[14] R. Zanasi, A. Tonielli, and C. Guarino Lo Bianco, Nonlinear filter for smooth trajectory generation, *Proc. 4th Nonlinear Control Systems Design Symp. NOLCOS'98* Vol. 1, *Enschede, the Netherlands*, pp. 245-250, July 1998.

[15] Han Ziqing. ADRC technology. *Beijing: National Defense Industry Press*, 2009.

[16] Levant A. High-order sliding modes, differentiation and output-feedback control. *Int of Control*, 2003, 76 (9/10) pp. 924-941.

[17] Liu Jinkun. Advanced PID control 7 MATLAB simulation, *Beijing: Publishing House of Electronics Industry*, 2011 pp. 143.

[18] Gao Wei-bing. Introduction of Variable structure control. *Beijing: Science Press*, 1989.

[19] Chen Yuhong. New method for sliding model control and buffeting suppression. *Journal of University of Electronic Science and Technology*, 1997, 26 (5) 1

[20] Li Zhongjuan & Zhang Xinzheng. Research on chattering in the theory of variable structure control systems. *Journal of Wuyi University (Natural Science Edition)*, 2003, 17 (3) 1.

[21] Wang Fengrao. Sliding model variable structure control. *Beijing: Science Press*, 1998.

[22] Liu Jinkun. The sliding mode variable structure control & Matlab simulation. *Beijing: Tsinghua University press*, 2012.

[23] Qi Rong & Xiao Weirong. Programmable computer control technology. *Beijing: Publishing House of electronics industry*, 2005.

[24] Tao Gao, Ping Wang, Chengshan Wang, Zhenjing Yao, Feature Particles Tracking for Moving Objects, *Journal of Multimedia*, Vol. 7, No. 6, pp. 408-414, 2012

[25] Li Yi, Huachun Zhou, Fei Ren, Hongke Zhang, "Analysis of Route Optimization Mechanism for Distributed Mobility Management", *Journal of Networks*, Vol. 7, No. 10, pp. 1662-1669, 2012

[26] Huan Zhao, Xiujuan Peng, Lian Hu, Gangjin Wang, Fei Yu, Cheng Xu, An Improved Speech Enhancement Method based on Teager Energy Operator and Perceptual. *Wavelet Packet Decomposition*, Vol. 6, No. 3, pp. 308-315, 2011

[27] Qian Zhang, Reconstruction of Intermediate View based on Depth Map Enhancement, *Journal of Multimedia*, Vol. 7, No. 6, pp. 415-419, 2012

[28] Qiang Deng, Yupin Luo, Saliency Detection by Selective Strategy for Salient Object Segmentation, *Journal of Multimedia*, Vol. 7, No. 6, pp. 420-428, 2012

[29] Shoujia Wang, Wenhui Li, Ying Wang, Yuanyuan Jiang, Shan Jiang, Ruilin Zhao, An Improved Difference of Gaussian Filter in Face Recognition, *Journal of Multimedia*, Vol. 7, No. 6, pp. 429-433, 2012

Cai Ligang. Beijing ad hoc engaged professor, PhD advisor, leader of mechanical manufacturing and automation discipline—the main discipline of Beijing, leader of Beijing academic innovation group, director of National Engineering Research Center (BJUT) of Precision and Ultra-precision Machining, director of the key lab of Beijing Advanced Manufacturing Technology, commissary of Milling Machine Branch of China Machine Tool & Tool Builder's Association, Senior experts for major projects about advanced manufacturing technology in Beijing Municipal Science and Technology Commission.

A Curvature-based Manifold Learning Algorithm

Yan LI and Zhiyong ZHANG
College of Information Science and Technology, Agricultural University of Hebei, Baoding, China

Xiaohua SUN
Department of Digital Media, Hebei Software Institute, Baoding, China

Fushun WANG
College of Information Science and Technology, Agricultural University of Hebei, Baoding, China
Corresponding author, Email: fswang_map@163.com

***Abstract*—Manifold learning aims to find a low dimensional parameterization for data sets which lie on nonlinear manifolds in a high-dimensional space. Applications of manifold learning include face recognition, image retrieval, machine learning, classification, visualization, and so on. By studying the existing manifold learning algorithms and geometric properties of local tangent space of a manifold, we propose an adaptive curvature-based manifold learning algorithm (CBML). With the algorithm, noises and the samples that do not belong to the neighborhood can be detected by computing the deflection between centralized samples and its local tangent space. It can not only be used to select adaptive neighborhood, but also take full advantage of information of neighbors. The algorithm can also be applied to manifold learning with local high curvature. Experiments show that the proposed algorithm in this paper is effective.**

***Index Terms*—Manifold Learning; High-Dimensional; Multivariate Data; Dimension Reduction**

I. INTRODUCTION

Modern imitated and practical data collection technology, we make it possible for engineers and scientists to produce large number of data. As a result, increasingly developed application fields is production increases gradually, is more complex in nature data. These data sets, including a variety of different samples of measured variables observed (or analog) set the whole collection. Visual assessment is a comprehensive research data, analyze the data of the first step in the goal is to make more goal-directed specific data processing and analysis model, the purpose of a meaningful part of it. Due to the watchful eye of people, and output devices are limited in three dimensional space, great threat coefficient according to the visualization of data into low dimension space, user despicable and understanding, at the same time to save most message as it can do. Dimensionality of this process was seen as a visual multivariate data is its traditional applications and methods.

Projection technology onto a low dimensional space, so that by putting a lot of points shows the multi-dimensional data reflect the specific and complex multidimensional space in the distance of the relations within the data information of the relationship between each point in the space. When the relationship is likely to be so complicated, it can not completely express the low dimension space; protrusions (considering all of the mappings) are often fuzzy. And, of course, we define the projection geometry one of degree of application - (linear) on the basis of forecast data of internal production convert. The evaluated figure behind this approach is by a group of variables "enrichment" almost model (unknown) potential factors, reducing red tape length to illustrate the data. Two main methods of projection variance or product, on the basis of internal relations, knotting have is not in a Euclidean Settings, alternative [1].

Manifold learning has goal to recover and restore all lower level dimensional composite form of sample points embedded in high-dimensional space. In recent years many effective dimensionality reduction algorithms are proposed [2-8]. Principal component analysis [2,3] is effective for linear manifold learning because of its algorithm is simple, and with fast execution speed. But it is difficult to learn non-linear manifold. LTSA [2] is an effective method for learning non-linear manifold. It starts with finding the k nearest neighbors of each sample point, then computing the projection space of each sample point, using principal component analysis to get native coherence of its tangential area. Those kinds of local coherences will be pointed to the worldwide lower level dimensional area by affixing transformation. However, LTSA is sensitive to noise; it relies on geometric properties of local tangent space. It's also not effective for high curvature manifold. Isomap [3] is an algorithm modified from Multidimensional Scaling (MDS); it uses geodesic distances to replace Euclidean distance in MDS [4]. Isomap can select neighborhood much better, but its computation complexity is large.

Adaptive LTSA recommends curvature to local tangent space, which is much effective to high curvature manifold learning than LTSA. It can be used to select adaptive neighborhood, but does not take full advantage of information of neighbors. As local tangent space reflects the global information of neighborhood, when estimating on neighbor's geodesic curvature, it can

doi:10.4304/jnw.9.1.85-91

increase the error because of other neighbors' deviation. And each computation of curvature will use singular value decomposition one time, which needs a large calculated amount. In this paper, we present the main contributions as follows:

- We suppose a fitful neighboring choices algorithm based on deflection angle of native tangent area (the algorithm is named as CBML);
- The algorithm uses Euclidean distance but take full advantage of geometric properties of local tangent space and information of neighbors.
- It can not only be used to select adaptive neighborhood, but also take full advantage of information of neighbors.
- Experiments show that the proposed algorithm can get good results for both neighborhood selection and elimination of noises.

The surplus of the paper is concluded in the following part. And section II represents the review on the manifold learning algorithms. Section III presents our proposed algorithm. Section IV gives the results of experiments. At length, the concluded remarks are provided in the following Section V.

II. MANIFOLD LAERNING ALGORITHMS

Measures for reducing dimension evaluate a map ranging from high-dimensional to low-dimensional space [5]. The most formal issue sets can be referred as following parts. We make $X \in R^{(n\times m)}$ a set of n sites in the m-dimensional characteristic area, δ_m: $R^m \times R^m \to R$ and $\delta_t : R^t \times R^t \to R$, over statistics area R^m and target area R^t severally, with $m,t \in N^*, t\langle\langle m$, being offered. A map feature φ that maps the m-dimensional statistic site ($x_i \in X$) to t-dimensional object sites ($y_i \in Y$), i.e.,

φ: $R^m \to R^t$

$$x_i \mapsto y_i, \text{ for } 1 \le i \le n, \tag{1}$$

is regarded as s.t. φ "faithfully" proximate in pairs, distant relations of X by these of $Y \in R^{(n\times t)}$ therefore map the closest (similar) sites in statistic area to equal close sites in object area, i.e., $\delta_m(x_i, x_j) \approx \delta_t(y_i, y_j)$, for $1 \le i, j \le n$, particularly speaking, an abundant map is referred to make sure that faraway statistics sites are map to remote sites.

Object space, generally has the following capabilities of degrees of freedom than to the multidimensional space modeling of distant relations, the map φ has an inherent mistakes which is supposed to be estimated by the restriction. As a result, φ is particularly supposed to make the least squares mistakes ε_φ:

$$\varepsilon_\varphi = \sum_{1\le i,j\le n} W_{i,j}(\delta_m(x_i, x_j) - \delta_t(y_i, y_j))^2 \text{ , for } W \in R^{(n\times n)} \tag{2}$$

where W is a matrix that could be applied to express the significance of some data relation or dimension. For instance, this could be applied to overlook outliers by regarding $W_{i,j} = 1/\delta_m(x_i, x_j)$ (for $\delta_m(x_i, x_j) \ne 0$). Officially, the above definition needed data and function of target distance, is a measurement standard. This means that all functions must be in conformity with positive definite and symmetric to the characteristics of the triangle a disproportionate share of the show. Based on the insight of human, the image Euclidean distance the distance metric, $L_2(p, p') = \sum 1 \le i \le q\sqrt{(p_i - p_i')^2}$ for $p, p' \in R^q$. As a result of its intuitiveness, the Euclidean remote is always regarded as the metric for the object area, $\delta_t = L_2$. Nevertheless, the remote (or dissimilarity) method of the utilization domain, δ_m, is not Euclid in most cases, might even don't point to measure some cases in A situation, psychological similarities and differences, can not metric tons. In practice, the official prerequisites may be extended appropriately, because even if is the first level mapping is, however, close to the multiple relationship. In the following section, we will review and talk about a few algorithm mentioned above an intermittent maps phi. We put them into two basic measures of the following potential main geometric Angle. If the data is located inside the fibrous lower dimensional subspace, so they can be described by again not waste by a longitudinal fundamental transformation of news [6].

These bases could be ranged in relation to their proportion of the mapping mistakes δ_ϕ and the basis is applied to minimize these mistakes. If the data is not, however, fibrous and sitting not remove various low dimensional, then solve this manifold distance relationship, can be in the absence of supervision way, and applied to the data mapping.

Measures referred to in this system is composed of the following sections carefully, show in figure 1. Method is totally dependent on internal product of linear transformation, but skill is defined as a projection is defined as a data structure that can fit in the distance relationship is not linear in composit researching skills [7]. Those skills could be divided into two kinds of basic methods. Measurement data space, the first measure is based on the graph. These data and application optimization method model diagram as graph theory study in multi-dimensional data space distance. Then it is the second measure is based on the embedding of stress concentration, which specifically identifying mappings, you can make mapping to least mistake in object space. Map errors of these measures are based on iterative optimization (stress) and can distance learning embedded non decimal.

A. Principal Components Analysis (PCA)

As the first dimension reducing process skills mentioned in this article, one of the principal component analysis (PCA) [9] of the data transmission distance relationship through orthogonal, pointing to a linear target dimension subspace of data. Specific and clear in this subspace in orthogonal prominent data has a great variety. Therefore, PCA is given a clear definition of a

"loyal" approach, as one has a perfect way to variance in the data. It has been proved that [10], through the maximum of varieties, PCA also makes data to the least amount and objects in space Euclidean distance (2) at least square error, $\delta_m = \delta_t = L_2$, under the restriction of orthogonally pointing the statistics:

$$\varepsilon_{PCA} = \sum_{1 \le i,j \le n} (L_2(x_i, x_j) - L_2(y_i, y_j))^2 \qquad (3)$$

It is worth noting that the PCA to achieve this goal, through calculating the fiber quality transformation of the effective. The resulting projection is a real and clear don't get me wrong data. Principal component analysis is the main defect is the only, because of its linear properties, it won't get nonlinear data. Based on the following consideration, we suggest a general that $X \in R^{(n \times m)}$ is focused, i.e., the ways of all statistics points which are given has been subdued from all statistic sites.

The PCA point is regarded as

$R^m \to R^t$

$$x_i \mapsto x_i \hat{\Gamma}, 1 \le i \le n, \qquad (4)$$

with $\hat{\Gamma} = \gamma^{(1)}, \ldots\ldots, \gamma^{(t)} \in R^{(m \times t)}$ being the matrix maintaining amount wise the factors of the relevant t hugest Eigen worth's of the statistics' covariance matrix $S = n^{-1} X^T X$. The hugest Eigen value lambda 1, S, hold the direction of the orthogonal projection of the data variance $\gamma_1, \hat{\Gamma}$, maintaining the t mutually orthogonal points in which orientation the statistic own the most varieties, confine a space orthonormal base in statistic space R^m. The orthogonal point to the relevant rank-t subspace in R^m is recognized by $\hat{X} = X \hat{\Gamma} \hat{\Gamma}^T$. Consequently, $\hat{X} \in R^{(n \times m)}$ is the superior rank-t-approximations of X (under L2), Using the basis $\hat{\Gamma}$, data sites xi are pointed to this sub-space which is that $\hat{x}_i = \sum_{1 \le k \le t} \gamma^{(k)} PCA(x_i)_k$, $1 \le i \le n$.

In addition to its broad applicability, image PCA can be applied to many more missions. For instance, a famous clearance values in the spectrum offers an up limit for the dimensions of the coherence of data. Gaussian noise, therefore, it is often applied for filtering or reduce the amount of data, evaluation time. PCA is a carefully crafted a skills with a long history. As a result, there are many variations and more messages, can be fited, for instance, in [11] or [12].

B. Metric Multi-dimensional Scaling (MDS)

Metric system of multidimensional scaling (MDS) [13], also regarded as the classical MDS, is an effective method, using projection to high-dimensional mapping to the lower dimensional linear space. Skills are often based on in this map, the distance from the intended target. MDS as a result, the measurement limit approximation faithfully a distance relationship to get a pair one of the best method, more accurate, the product internal relations.

Metric MDS to find an suitable linear suitable distance in pairs (least squares), assume that the distance is a metric used. If the Euclidean distance to us, the delta = L2, measure the MDS as PCA scaling and circulation. Measurement of MDS, however, finds the best linear fitting any indicators of the similarities and differences. Making special technology, we use of more flexible, than PCA. Its performance does not depend on the dimensions of the data; however, this method is very poor scalability of the number of data points [14].

Mapping error method point of view, and keep the product internal relations:

$$\varepsilon_m MDS = \sum_{1 \le i,j \le n} (x_i, x_j^T) - (y_i, y_j^T))^2 \qquad (5)$$

Let (Δ)i,j=δi,j be offered. From those metric distances, the statistic's Gram matrix of inner production is offered by G=HAHT, in which $A = -1/2\delta_{i,j}^2$, and H is a focusing matrix. The entire inherent component of G demands $O(n^3)$ time which is, in most general cases, too high for actual issues. But varieties of the measures succeed an approximation in O(nlogn) time based on a encountered method of the inherent assessment [15]. What's more, rapidly faster solutions are being put forward [16]. Metric MDS is regarded as:

$R^m \to R^t$

$$x_i \mapsto \hat{\Gamma}_i \hat{\Lambda}, \text{ for } 1 \le i \le n, \qquad (6)$$

with $\hat{\Gamma} = (\gamma^{(1)}, \ldots\ldots, \gamma^{(t)}) \in R^{(n \times t)}$ being the matrix maintain amount wise the factors of the relative t largest factors of the Gram matrix of internal products, $G = XX^T, G_{i,j} = x_i x_j^T$, Λ is the diagonal matrix maintaining the roots of the t hugest factors of G, $\Lambda = diag(\sqrt{\lambda_1} \ldots, \sqrt{\lambda_t})$.

Although measures of multidimensional scaling inner product space, the influence of the geometric method behind the instinct is same to PCA. As a result, the points are projected to the greatest variance of the linear space. Nevertheless, the sub-space is regarded as n * n of the inner product of matrix eigenvalue decomposition on the basis of measurement of MDS. Dualism among PCA and MDS becomes clear when take G with the same range of the factors of the covariance matrix (a constant factor) $S = n^{-1} X^t X = Cov(X)$ and $G = n^{-1} Cov(X^T)$. Rn gram matrix of covariance matrix, therefore, reflects the same data covariance matrix in the room is the relationship with the clients, however, reflects the linear union data points (rather than size) based system. Measurement of MDS for more information, readers can reference [17] or [18]. Although effective and elasticity, metric MDS leave without two questions, answer: (1) if the sample data from the nonlinear manifold, found close to relationship? (2) if these differences are not indicators? In the following, we will discuss the basic definition of dealing

with these two. In particular, has put forward the measure of MDS variants of kernel PCA, ISOMAP and nonmetric MDS.

C. Kernel PCA

Kernel PCA [19] is regarded as PCA and measure MDS (because of their dual) is to describe a variant of non-linear data. Although along a nonlinear symbolic distance relationship is unknown, kernel principal component analysis is based on two assumptions, nonlinear data failed to make use of PCA (linear). The first concept is, in the empty data of potential features, data is linear. The next hyphosis is that there is a function, the boundary of internal production, the data sites in the characteristic area. This feature is named the "nuclear skills" are the core of [20] and a nonlinear kernel to gain not thready data framework in the linear utilization. Officially, this setting is described as the following sections. If nuclear k is close to the inner product of the relationship of nonlinear characteristics in spatial data [21], makes

$$R^m \times R^m \to R$$

$$(x_i, x_j) \mapsto \Phi(x_i)\Phi(x_j)^T, \text{ for } 1 \le i \le n, \qquad (7)$$

where Φ is the map to characteristic area. Kernel PCA is regardedd as

K-PCA: $R^m \to R^t$

$$x_i \mapsto \hat{\Gamma}_i \hat{\Lambda}, \text{ for } 1 \le i \le n \qquad (8)$$

with $\hat{\Gamma} = (\gamma^{(1)}, \ldots\ldots, \gamma^{(t)}) \in R^{(n \times t)}$ to be the matrix containing amount wise the factors of the relative t largest factors of the Gram matrix of internal production in feature space, $G^k_{i,j} = k(x_i, x_j)$, Λ is the pitched matrix maintaining the roots of the t hugest factors of G(k), $\hat{\Lambda} = diag(\sqrt{\lambda_1}, ..., \sqrt{\lambda_t})$. Kernel principal component analysis and calculation, therefore, the data in the feature space covariance matrix of the feature vector. Although this space, and the data is almost lies in its characteristics, is unknown, the kernel mapping of data to the gram matrix inner product in the feature space. According to the validity of the license on nuclear k, we eigen nonlinear relationship analysis of captured data through the maximization of varities in characteristics area [22]. Therefore, kernel principal component method can be regarded as a generalization of (classical) was measured by MDS generation of Euclid application of communize some point products.

It is not amazing that the abstracts of kernel principal component analysis to find the "perfect" kernel. Because of the distance along the probable nonlinear data substructure of the relationship, in the general case, a previously unknown, define an intermittent kernel requires precise knowledge about the data. If we don't get this knowledge, the method will be decided more suitable for nonlinear data structure along the stood a distance relationship, without supervision and data driven [23] or [24].

Methods according to the projection work for suitable data about a linear space. It is not possible the situation. Hope after data dimension reduction, will at least one of the nonlinear model, that is to say, they sat on the manifold. This section to consider ways to learning (describe) of data points on the close relationship (nonlinear) manifold in unsupervised way. However the mapping method based on projection conversion can be expressed as the linear gain known close relationship, is this manifold learning skills [25]. In particular, we have the technology to extract the Euclidean distance relationship, and keep the distance with manifold. Figure 2 shows the projection and manifold learning is based on the difference between mappings.

III. CURVATURE-BASED MANIFOLD LEARNING ALGORITHM

In this section, we assume that a method of adaptive selection algorithm based on local tangent space deflection Angle (the algorithm named CBML); the arithmetic applies the Euclidean distance, has yet to make full use of local tangent space and geometric properties of neighbor information.

There are more than distinguished ways, to know the unclear close relationship. These methods are metric or non metric no similar data. To simulate on the manifold distance measurement, based on the graphic technology is often used to retrieve data drive local distance relationship, and the data of the project, based on the measured distance. However, there are a variety of applications, need not decimal similarity relationship certificate. Measures to deal with this problem cannot be based on the graphic, but only through direct mapping error minimization of coherent. This will lead to the no convex optimization function stress. As a result, based on the stress of the measures is the local minimum, is often slow concentration [27].

The method based on graph can be summarized as two different types: the global modeling and local modeling. Global approach, absorbed the local low dimensional submanifolds of close relationship, and then describes these relationships, for example, the method based on projection, such as measurement of MDS [28]. Local based on graphical models a parted and successful measure after it. Design is aimed at the data is divided into few classifications and solve the built-in local degree. The local system, then together", according to the overlap or anchor point. Though the projection step to find the global best choose built-in, the reconstruction of the original distance relationship laid a solid foundation, such as the shortest path problem of the optimization problem, the least squares fitting, or positive semi-definite programming [29]. In this respect, the method based on graph may also be local minimum number or more computational cost.

Nearest neighbors' selection is a key step in nonlinear manifold learning. An improper selection will result in short circuit, and then affect the final embedding results. In this section we suppose an fitful neighboring selection

arithmatic which is suitable to the region with high curvature, and can resist to noise effectively.

From the discussion, we know that $\cos\alpha = f(t_j)$ is a monotone function of $t_j = \|x_{i_j} - x_i\|$ with a small fluctuation (Fig 3.1). For two neighbor points x_{i_j} and $x_{i_{j+1}}$ which are in ordered k nearest neighbors with $t_1 \le t_2 \le \cdots \le t_k$, the straight line slope k_α of $\cos\alpha_{i,j+1}$ and $\cos\alpha_{ij}$ according to Euclidean distance is (for convenient, k_α only takes positive values):

$$k_\alpha = \frac{|\cos\alpha_{i,j+1} - \cos\alpha_{ij}|}{|t_{j+1} - t_j|} \tag{9}$$

Let $|\cos\alpha_{i,j+1} - \cos\alpha_{ij}| = \varepsilon$, from (1) it can be seen that when the value of t_j is small enough, α_{ij} has a remarkable error. To reduce the error we introduce a discrete function $g(k) \in (1, 1+\delta]$, the value of which can be decreasing as data points are increasing. Where $\delta \le 0.05$ is a positive real number to satisfy: $t_j = g(k)t_j$, then

$$\cos\alpha' = \frac{\sqrt{\hat{x}' QQ' \hat{x}}}{g(k)\|\hat{x}\|_2} \tag{10}$$

The value of k_α used in the process of neighborhood selection is as small as possible.

Algorithm 1: Curvature-based Manifold Learning (CBML)

Step 1: Use k-NN to determine the k nearest neighbors of x_i and order them by the rule of $t_1 \le t_2 \le \cdots \le t_k$, then get neighborhood set $X_i = \{x_i, x_{i_1}, \cdots, x_{i_k}\}$ and mean distance $\bar{t} = [t_1, \cdots, t_k]'e_k/k$. Compute Q_i which is a basis of $\mathcal{T}_{x_i}\mathcal{M}$. Compute $\cos\alpha'_{ij}$ by, initialize count points (statistic noise) $m = 0$, and Let D be an empty set.

Step 2: Compute $\eta_{ij} = \cos\alpha'_{i,j+1} - \cos\alpha'_{ij}$, where $j = 1, 2, \cdots, k-1$.

Step 3: Set threshold value η_i and discrete function $h(\eta_i, k)$ to delete noises. $h(\eta_i, k)$ is in reverse proportion to η_i and k. If $\eta_{ij} > \eta_i$, let $D = D + \{x_{i,j+1}\}$, $m = m+1$, compute $\eta_{ij} = \cos\alpha'_{i,j+2} - \cos\alpha'_{ij}$; If $\eta_{ij} \le \eta_i$, go to step 2. If $j = k-1$, and $m < h(\eta_i, k)$, delete the points consisted in D from whole samples, go to step 4, else delete the last $h(\eta_i, k)$ samples, go to step 4.

Step 4: Updating. Use deleted samples to set new k_i -neighborhood, go to step 5.

Step 5: Define a counter $l = 0$, compute t_j ($j = 1, 2, \cdots, k$) of $h(\eta_i, k)$ deleted samples $\{x_{h_r}\}$ ($r = 1, \cdots, h(\eta_i, k)$). If $t_j > \bar{t}$, let $l = l+1$; If $l > [k/2]+1$, delete x_{h_r}.

If noises have a large deviation from the center of local tangent space but have a small neighborhood selection, the error of tangent space will increase, which will lead to the deflection angle α increasing, then noises will not be separated from samples. However, such noises can only belong to a certain neighborhood, so we can properly choose a discrete function $h(\eta_i, k)$ which is in reverse proportion to η_i and k to determine the positions of noises in the local neighborhood approximately. According to this characteristic, the k nearest neighbors of this noise satisfy $\min_j\{t_j\} = \|\bar{x}_i - x_{h_r}\|$, so the noise which has a large deviation with tangent space can be reduced by step 5.

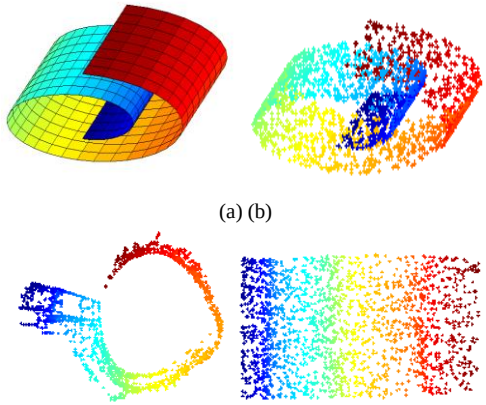

(a) (b)

(c) (d)

Figure 1. (A). The canny 'Swiss roll' manifold flexed to the ratio of 0.5. It is different from the most common cycle Swiss roll; curvature varies due to the manifold. (B). A uniform density model which is drawn according to the manifold, when N=3500. (C). The best built-in calculated by Isomap. An install of k=4 is applied to. We can draw a conclusion that higher values will lead to more cuts made according to data points in the various parts of the manifold and more complicated built-in, when k<=4 the results in these components, without connection and without unifying worldwide framework. (D). The projection which is obtained by Isomap applying our fitful neighboring methods successfully spreads the Swiss roll into a smooth surface.

IV. EXPERIMENTAL RESULTS

In experiments, we apply to Swiss-roll statistic set with n=1000. The general parameters of 3D Swiss-roll are: $t = \frac{3\pi}{2}(1 + 2rand(1, n))$, s=10rand(1,n), X=[t.ost,s,t.sint]. By adding different noises in Swiss-roll, and we do experiments with LTSA and CBML respectively. Let $\eta_i = 0.5$, $h(\eta_i, k) = k - j + 1$. With $|\alpha_{noise} - \alpha_{noise-1}| = \beta_j$, the results of experiments are as follows (In the following table, one column represents one sample with three dimensions, the samples written in boldface are indicated being deleted as running the algorithm, and only related samples are listed in the tables.):

TABLE I. NEIGHBORHOOD WITH NOISE

Noise (1,5,6), $k=10$ $\beta_8 = 0.7726$			
Samples and Noises in Neighborhood	0.789	0.253	1.90
	6.005	4.742	5.70
	7.733	7.830	4.80

TABLE II. NEIGHBORHOOD WITH NOISE

Noise (1,6,4), $k=10$ $\beta_8 = 0.7726$			
Samples and Noises in Neighborhood	3.405	0.789	1.10
	4.398	4.714	5.20
	6.081	7.734	4.30

We have valued our methods with the Isomap arithmetic on few data installs. Our evaluation methods' behavior on composites which is with greatly constant

curvature and average sampling goes according to that of Isomap which is manually-choose most suitable worth of *k*. Figure 2 describes the associations between true and approximated metrical distances on the protracted Swill roll and a 3-D space for various worth of k via our fitful measures. For these kinds of frameworks, Isomap could not evaluate content built-in with all the different installs of the arithmetic's factors. What's more, our methods fitfully chooses neighborhood at every level causing superior insertion in relatively smooth appearances however avoiding error cuts among various parts of the composite. Now we discuss relationship to real distances and a goal qualitative method. Qualitatively although it is small disagreement in relationship values, we interpret it into significant influences when referring to the resulting built-in. For instance, the built-in by k-Isomap for the protracted Swiss roll in Figure 3(a) (k=4, correlation=0.78) can be concluded in Figure 1(C). As a wisdom review, we also made our algorithm on the Isomap face database (698 images of synthetic faces under varying illumination and pose). Our fitful methods are likely to produce a content built-in, but since the true manifold is not sure, quantitative assessment is not available.

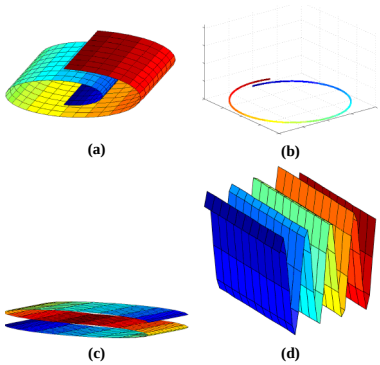

Figure 2. (a)-(d). Synthetic 2-D and 1-D manifolds embedded in 3-D.

V. CONCLUSIONS

In this section, we suppose an fitful neighboring choice algorithm which is based on deflection angle of local tangent area (the algorithm is named as CBML); The algorithm uses Euclidean distance but take full advantage of geometric properties of local tangent space and information of neighbors.

Research on dimension reduction continues at a rapid pace. This survey provides an introduction to the main concepts of dimension reduction for visualization: from linear data projection to graph- and stress-based manifold learning. Although being non-exhaustive, the comparison of state-of-the-art methods that follow the graph- or stress-based approach shows that no single method can be preferred over another. On the contrary, the effectiveness of state-of-the-art methods mainly depends on the data and application. However, the comparison also shows that there are similar research directions. At present, especially multi-level approaches show great potential and form one of the dominant research directions in both graph-and stress-based manifold learning.

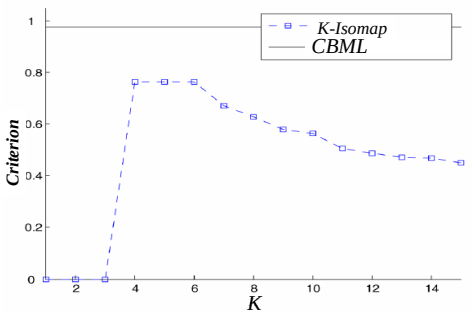

(a)

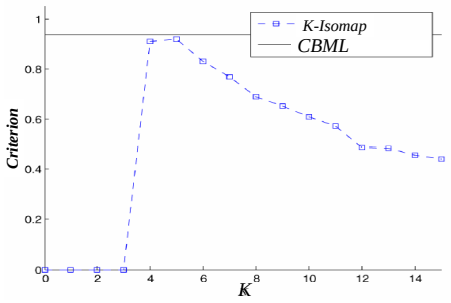

(b)

Figure 3. (a)-(b). According to the plots among real geodesic distances and Isomap evaluates using k-Isomap open with the least values of k that yields a worldwide mapping and methods.

REFERENCES

[1] L. K. Saul, K. Q. Weinberger, J. H. Ham, F. Sha, and D. D. Lee. Spectral methods for dimensionality reduction. Semi-supervised Learning. *MIT Press: Cambridge*, MA, 2012.

[2] V. D. Silva and B. J. Tenenbaum. Global versus local methods in nonlinear dimensionality reduction. *In Advances in Neural Information Processing Systems* 15, pp. 705-712, MIT Press, 2011.

[3] C. J. C. Burges. Dimension reduction: a guided tour. *Foundations and Trends in Machine Learning*, vol. 2, no. 4, pp. 135-141, 2010.

[4] A. L. John and V. Michel. Unsupervised dimensionality reduction: overview and recent advances. *In IEEE IJCNN*, pp. 1-8, 2010.

[5] U. M. Ascher and L. R. Petzhold. Computer methods for ordinary differential equations and differential-algebraic equations. *SIAM*, pp. 314-319, 1998.

[6] I. Borg and P. J. F. Groenen. Modern multi-dimensional Scaling: theory and applications. *Springer*, pp. 201-208, 2010.

[7] M. M. Bronstein, A. M. Bronstein, R. Kimmel, and I. Yavneh. Multi-grid multi-dimensional scaling. *Numerical Linear Algebra with Applications (NLAA)*, vol. 13, no. 3, pp. 149-171, 2006.

[8] J. Demmel, J. Dongarra, A. Ruhe, and H. V. Vorst. Templates for the solution of algebraic eigen value problems: a practical guide. *Society for Industrial and Applied Mathematics, Philadelphia, PA, USA*, pp. 149-155, 2000.

[9] K. Pearson. On lines and planes of closest fit to systems of points in space. *Philosophical Magazine*, vol. 2, no. 6, pp. 559-572, 1991.

[10] Y. Koren and L. Carmel. Robust linear dimensionality reduction. *IEEE Transactions on Visualization and Computer Graphics*, vol. 10, no. 4, pp. 459-470, 2004.

[11] I. T. Jolliffe. Principal Component Analysis. *Springer, second edition*, 2012.

[12] B. F. Manly. Multivariate statistical methods: a primer. *Chapman & Hall, Ltd., London, UK*, 1986.
[13] W. S. Torgerson. Theory and methods of scaling. *Wiley*, 1958.
[14] E. W. Dijkstra. A note on two problems in connation with graphs. *Numerische Mathematik*, vol. 1, no. 5, pp. 269-271, 1959.
[15] T. Yang, J. Liu, L. Mcmillan, and W. Wang. A fast approximation to multi-dimensional scaling, by. *In Proceedings of the ECCV Workshop on Computation Intensive Methods for Computer Vision (CIMCV)*, pp. 354-359, 2006.
[16] I. Koutis, G. L. Miller, and R. Peng. Approaching optimality for solving sdd linear systems. *In Proceedings of the 2010 IEEE 51st Annual Symposium on Foundations of Computer Science, FOCS '10*, pp. 235-244, *Washington, DC, USA*, 2010.
[17] W. Härdle and L. Simar. Applied multivariate statistical analysis. *Springer, 2nd edition edition*, 2007.
[18] T. Cox and M. Cox. Multi-dimensional Scaling. *Chapman & Hall, London*, 1994.
[19] B. Schölkopf, A. J. Smola, and K. R. Müller. Nonlinear component analysis as a kernel eigen value problem. *Neural Computation*, vol. 10, no. 5, pp. 1299-1319, 1998.
[20] J. H. Friedman, J. L. Bentley, and R. A. Finkel. An algorithm for finding best matches in logarithmic expected time. *ACM Transactions on Mathematical Software*, vol. 3, no. 3, pp. 290-226, 1977.
[21] S. Ingram, T. Munzner, and M. Olano. Glimmer: multilevel mds on the gpu. *IEEE Transactions on Visualization and Computer Graphics*, vol. 15, no. 2, pp. 249-261, 2009.
[22] A. Kearsley, R. Tapia, and M. Trosset. The solution of the metric stress and stress problems in multidimensional scaling using newton's method. *Computational Statistics*, vol. 13, no. 3, pp. 369-396, 1998.
[23] J. Kruskal. Multi-dimensional scaling by optimizing goodness of fit to a non-metric hypothesis. *Psychometrical*, 1964.
[24] N. R. Pal and J. C. Bezdek. On cluster validity for the fuzzy c-means model. *IEEE TFS*, vol. 3, no. 3, pp. 370-379, 1995.
[25] S. T. Roweis and L. K. Saul. Nonlinear dimensionality reduction by locally linear embedding. *SCIENCE*, vol. 290, no. 5500, pp. 2323-2326, 2008.
[26] F. V. Paulovich, D. M. Eler, J. Poco, C. P. Botha, R. Minghim, and L.G. Nonato. Piece wise laplacian-based projection for interactive data exploration and organization. *Computer Graphics Forum*, vol. 30, no. 3, pp. 1091-1100, 2011.
[27] J. W. Sammon. A nonlinear mapping for data structure analysis. *IEEE Transactions on Computer*, vol. 18, no. 5, pp. 401-409, 1969.
[28] E. Tejada, R. Minghim and L.G. Nonato. On improved projection techniques to support visual exploration of multidimensional data sets. *Information Visualization*, vol. 2, no. 4, pp. 218-231, 2008.
[29] J. B. Tenenbaum, V. Silva, and J.C. Langford. A global geometric framework for nonlinear dimensionality reduction. *Science*, vol. 290, no. 5500, pp. 2319-2323, 2006.

Blow-up in the Parablic Problems under Nonlinear Boundary Conditions

Jin Li
School of Mathematics and Statistic, Hexi University, Zhangye, Gansu 734000, PR China
Email: lijingfl1956@163.com.

***Abstract*—The paper deals with a degenerate and singular parabolic equation with nonlinear boundary condition. We first get the behavior of the solution at infinity, and establish the critical global existence exponent and critical Fujita exponent for the fast diffusive equation, furthermore give the blow-up set and upper bound of the blow-up rate for the nonglobal solutions.**

***Index Terms*—Global Existence Curve; Critical Fujita Curve; Nonlinear Boundary Condition; Blow-Up**

I. INTRODUCTION

In this paper, we consider the following the degenerate and singular parabolic equation

$$\frac{\partial u}{\partial t}=\frac{\partial}{\partial x}\left(\left|\frac{\partial u}{\partial x}\right|^{p}\frac{\partial u^{m}}{\partial x}\right),\ x>0,0<t<T, \tag{1}$$

coupled via nonlinear boundary flux

$$-\left|\frac{\partial u}{\partial x}\right|^{p}\frac{\partial u^{m}}{\partial x}(0,t)=u^{q}(0,t),\quad 0<t<T, \tag{2}$$

and initial data

$$u(x,0)=u_0(x),\quad x>0, \tag{3}$$

where parameters $0<m\le 1, -1<p<1-m, q>0,$ and u_0, is nonnegative continuous function with compact support in R_+

Nonlinear parabolic equation (1) comes from the theory of turbulent di_usion (see [2, 7] and references therein) and appears in population dynamics, chemical reactions, heat transfer, and so on. The equation (1) includes both the porous medium operator (with $p=0$) and the gradient-di_usivity the p-Laplacian operator ($m=1$) as special cases, which have been the subject of intensive study (see [2, 4, 6, 7, 8, 10, 13, 21, 25, 30, 33] and references therein). In particular, many paper have been devoted to study critical exponents of the slow di_usion case (see [2, 4, 6, 8, 10, 13, 22, 23, 26, 29, 31, 33, 34, 35] and references therein). Recently, many authors transfer their attention to the fast diffusion case (see [4, 8, 9, 14, 15, 17, 28, 32]) and many important results about critical exponents have been obtained. The concept of critical Fujita exponents was proposed by Fujita in the 1960s during discussion of the heat conduction equation with a nonlinear source (see [5]). In [7], Galaktionov and Levine studied the following single equation

$$u_t=\nabla(|\nabla u|^{\sigma}\nabla u^{m})+u^{p}, x\in R^{N}, t>0 \tag{4}$$

$$u(x,0)=u_0(x),\qquad x\in R^{N} \tag{5}$$

where $\sigma>0,\ m>1,\ p>1$ and $u_0(x)$ is a bounded positive continuous function. They shown that the critical exponent is $p_c=m+\sigma+\frac{\sigma+2}{N}$.

Recently, Jiang [10] studied the following single equation

$$\begin{cases} u_t=(|u_x|^{p}(u^{m})_x)_x, & x>0,0<t<T,\\ -|u_x|^{p}(u^{m})_x(0,t)=u^{q}(0,t), & 0<t<T,\\ u(x,0)=u_0(x), & x>0, \end{cases} \tag{6}$$

where $m\ge 1, p>0, q>0$. They obtained the critical global existence exponent $q_0=\frac{2q+m+1}{q+2}$ and the critical Fujita exponent $p_c=2q+m+1$. These results are the extensions of those of Galaktionov and Levine [8].

Motivated by the above mentioned works, in this paper, we investigate the critical global existence exponent q_0 and the critical Fujita exponent q_c of a nonlinear boundary value problem (1)-(3). We obtain the decay behavior of the solution at infinity and establish the same critical exponents. In addition, we show that the critical Fujita exponent q_c belongs to blow-up case. Furthermore, we give the blow-up set and upper bound of the blow-up rate of nonglobal solutions.

We remark the main difference between $p\ge 0, m>1$ and our current settings $-1<p<1-m,\ 0<m<1$, we take $p=0$ for example. For the former, equations (1) having $m>1$ are the well-known porous medium equations, while for the latter, Eqs. (1) having $0<m<1$ are the so-called fast diffusion equations. The porous medium equations have finite speed of propagation property, that is, solutions with compactly supported initial data stay compactly supported, which makes comparison with global supersolutions easier when one is

doi:10.4304/jnw.9.1.92-99

restricted to compactly supported initial data. However, the solutions of the fast diffusion equations shall become instantaneously positive everywhere for any nontrivial nonnegative initial data, and hence we have to take care of the decay of the solutions.

Owing to the degeneration (singularity) of problem (1)-(3), a precise definition of a weak solution is needed.

Definition let $T>0$, and denote $Q_T=\Omega\times(0,T]$ with $Q_T=\Omega\times(0,T]$. A positive function $u(x,t)\in C(\bar{Q}_T)$ is called an upper (lower) solution of (1) in Q_T with nonlinear flux u^q if:

1° $u\in L^\infty(0,T;W^{1,\infty}(\Omega))\cap W^{1,2}(0,T;L^2(Q_T)), u(x,0)\geq(\leq)u_0$; and, 2° for any positive function $\omega\in L^1(0,T;W^{1,2}(\Omega))\cap L^2(Q_T)$, we have

$$\iint_{Q_T}\left(u\frac{\partial\omega}{\partial t}-|\frac{\partial u}{\partial x}|^p\frac{\partial u^m}{\partial x}\frac{\partial\omega}{\partial x}\right)dxdt\geq(\leq)\int_0^T\int_{\partial Q_T}\omega u^q ds_x dt;$$

$u(x,t)$ is called a weak solution of (1)-(3) if it is both a weak upper and a lower solution.

The local existence of the weak solution to the problem (1)-(3) and the comparison principle can be easily established (see the survey [12] and books [3, 18, 30]). In order to investigate the blow-up properties of solutions to (1)-(3), we need to study the behavior of $u(x,t)$ for large x and obtain the following result.

In order to investigate the blow-up properties of solutions to (1)-(3), we need to study the behavior of $u(x,t)$ for large x and obtain the following result.

Theorem 1.1. The positive solution of the problem (1)-(3) has, for each $t\in(0,T)$,

$$\liminf_{x\to+\infty} x^{\frac{p+2}{1-m-p}}u(x.t)\geq\left(C_{m,p}^{-(p+1)}\right)^{\frac{1}{1-m-p}} \tag{7}$$

where T is the maximal existence time for the solution, which may be finite or infinite, and

$$C_{m,p}=\frac{1-m-p}{p+2}\left(\frac{1}{m(2p+m+1)}\right) \tag{8}$$

Now we establish the critical exponents of the problem (1)-(3) as follows.

Theorem 1.2. The critical global existence exponent and critical Fujita exponent for the problem (1)-(3) are given by $q_0=\frac{2p+m+1}{p+2}$ and $q_c=2p+m+1$, respectively. More precisely, we have

(1) if $0<q\leq q_0=\frac{2p+m+1}{p+2}$, every nontrivial and nonnegative solution of the problem (1)-(3) exists globally in time;

(2) If $q>q_0=\frac{2p+m+1}{p+2}$, then the solution of the problem (1)-(3) with appropriately large initial data blows up in a finite time;

(3) if $q_0=\frac{2p+m+1}{p+2}<q<q_c=2p+m+1$, every nontrivial and nonnegative solution of the problem (1)-(3) blows up in finite time;

(4) if $q>2p+m+1$, then the problem (1)-(3) admits nontrivial global solutions with small initial data.

Theorem 1.3. When $q=q_c$, each positive solution blows up in finite time.

Remark 1.1. Theorem 1.3 shows that the critical Fujita exponent q_c belongs to the blow-up case.

Theorem 1.4. Let $B(u)$ be the blow-up set of the solution u to (1)-(3), then $B(u)=0$.

To get the upper bound of the blow-up rate of blow-up solutions to (1)-(3), we need an extra assumption on initial data u_0 as follows

(H) $(|u_{0x}|^p(u_0^m)_x)_x\geq 0$.

Remark 1.2. We can easily obtain from the assumption that $u_t\geq 0$ for $t\in(0,T)$ (see [8, 33, 34]).

Theorem 1.5. Suppose that the initial value u_{0} satisfies (H). If the solution $u(x,t)$ of (1)-(3) blows up in finite time T, then there exists a positive constant C such that

$$u(.,t)\leq C(T-t)^{-\frac{p+1}{(p+2)q-(2p+m+1)}}.$$

The rest of this paper is organized as follows. In Section 2, we study the decay behavior of the solution and establish critical exponents of the problem (1)-(3). In Section 3 we consider the critical case $q=q_c$ and prove Theorem 1.3. The blow-up set and the estimate of the blow-up rate are considered in Section 4.

II. Decay Behavior and Critical Exponents

In this section, we begin with the decay behavior of the solution to (1)-(3), which plays an important role in the proofs of Theorems 1.2-1.3.

Proof of Theorem 1.1. Our idea is to show that any positive solution of the problem (1)-(3) is, for x large, bigger than the following similarity solution

$$U_\lambda(t,x)=\lambda^{\frac{p+2}{1-m-p}}U_1(t,\lambda x),$$

where

$$U_1(t,x)=t^{-\frac{1}{2p+m+1}}(1+C_{m,p}x^{\frac{p+2}{p+1}}t^{-\frac{(p+2)}{(2p+m+1)(p+1)}})^{\frac{p+1}{1-p-m}},$$

Let $0<\tau<T_*<T$ and $S=[\tau,T_*]\times(1,+\infty)$, Since the positive solution $u(x,t)$ is continuous in $(0,T_*]\times[0,+\infty)$, there exists $\delta=\delta(\tau,T_*)>0$ such that

$$\delta=min\, u(x,t),\ \tau\leq t\leq T_*,\ 0\leq x\leq 1. \tag{9}$$

We now select $\gamma>0$ such that

$$U_\lambda(t-\tau,x)\leq\delta,\ \tau\leq t\leq T_*,\ x\geq\frac{1}{2}. \tag{10}$$

To this aim, according to the definition of $U_\lambda(t,x)$ we need

$$\lambda^{\frac{p+2}{1-m-p}}(t-\tau)^{-\frac{1}{2p+m+1}}\left(1+C_{m,p}\lambda^{\frac{p+2}{p+1}}x^{\frac{p+2}{p+1}}(t-\tau)^{-\frac{p+2}{(2p+m+1)(p+1)}}\right)^{-\frac{p+1}{1-p-m}}\le\delta,$$

or $\delta^{\frac{m+p-1}{p+1}}\le\lambda^{-\frac{p+2}{p+1}}(t-\tau)^{\frac{1-p-m}{(2p+m+1)(p+1)}}+C_{m,p}x^{\frac{p+2}{p+1}}(t-\tau)^{-\frac{1}{p+1}}$,

for $\tau\le t\le T_*$ and $x\ge\frac{1}{2}$, which is implied by

$$\delta^{\frac{m+p-1}{p+1}}\le\lambda^{-\frac{p+2}{p+1}}(t-\tau)^{\frac{1-m-p}{(1p+m+1)(p+1)}}+C_{m,p}\left(\frac{1}{2}\right)^{\frac{p+2}{p+1}}(t-\tau)^{-\frac{1}{p+1}}. \quad (11)$$

Since the right-hand side of (11) is bounded below by $\lambda^{-\frac{2p+m+1}{p+1}}c$, where $c=c(m,p)>0$, the inequality (11) is satisfied if we choose λ such that $\lambda\le c\delta^{\frac{1-m-p}{2p+m+1}}$. Since $\frac{\partial U_\lambda}{\partial t}=\frac{\partial}{\partial x}\left(\left|\frac{\partial U_\lambda}{\partial x}\right|^p\frac{\partial U_\lambda^m}{\partial x}\right)$ in S and $U_\lambda(t-\tau)=0$ for $t=\tau, x\ge1$, by (9), (10) and the comparison principle we have $U_\lambda(t-\tau,x)\le u(x,t),\quad \tau<t<T_*,\quad x\ge1.$

Hence

$$\begin{aligned}\liminf_{x\to+\infty}x^{\frac{p+2}{1-m-p}}u(x,t)&\ge\liminf_{x\to+\infty}x^{\frac{p+2}{1-m-p}}U_\lambda(t-\tau,x)\\&=[C_{m,p}^{-(p+1)}(t-\tau)]^{\frac{1}{1-p-m}},\end{aligned} \quad (12)$$

since the right-hand side of (12) does not depend on λ, the estimate (9) holds by letting τ tend to 0 and T tend to T. The proof of Theorem 1.1 is completed.

The rest part of this section is devoted to discussion of the critical exponents and prove Theorem 1.2. First, we show critical global existence exponent, and characterize when all solutions to the problem (1)-(3) are global in time or they blow up.

Lemma 2.1. if $0<q\le q_0=\frac{2p+m+1}{p+2}$, every nontrivial and nonnegative solution exists globally in time.

Proof. In order to prove that the solution u of (1)-(3) is global, we look for a globally defined in time supersolution of the self-similar form

$$\bar u(x,t)=e^{\kappa_1 t}(M+e^{-Lxe^{\kappa_2 t}})^{\frac{1}{m}},\ x\ge0,t\ge0,$$

where

$$M\ge max\left\{\|u_0\|_\infty^m+1,\frac{1-p-m}{(p+2)me}\right\},\quad L=m^{\frac{p}{p+1}}(M+1)^{\frac{q-p+mp}{m(p+1)}},$$

$$\kappa_1=\frac{(p+1)L^{p+2}M^{p(\frac{1}{m}-1)}}{m^pM^{\frac{1}{m}}\left(1-\frac{1-p-m}{emM(p+2)}\right)}\qquad \kappa_2=\frac{1-p-m}{p+2}\kappa_1.$$

Obviously, we have $\bar u(x,0)\ge u_0(x),\bar v(x,0)\ge v_0(x),\ x\ge0$. Since $-ye^{-y}\ge-e^{-1}$ for $y>0$, after a direct computation, we obtain

$$\begin{aligned}\bar u_t&=\kappa_1e^{\kappa_1t}\left(M+e^{-Lxe^{\kappa_2t}}\right)^{\frac{1}{m}}-\frac{\kappa_2}{m}Lxe^{\kappa_2t}e^{-Lxe^{\kappa_2t}}\left(M+e^{-Lxe^{\kappa_2t}}\right)^{\frac{1}{m}-1}e^{\kappa_1t}\\&\ge\kappa_1e^{\kappa_1t}\left(M+e^{-Lxe^{\kappa_2t}}\right)^{\frac{1}{m}}-\frac{\kappa_2}{m}e^{-1}\left(M+e^{-Lxe^{\kappa_2t}}\right)^{\frac{1}{m}-1}e^{\kappa_1t}\\&\ge\left(\kappa_1-\frac{\kappa_2}{mMe}\right)M^{\frac{1}{m}}e^{\kappa_1t}=\kappa_1\left(1-\frac{1-p-m}{(p+2)mMe}\right)M^{\frac{1}{m}}e^{\kappa_1t},\end{aligned}$$

$$(|\bar u_x|^p(\bar u^m)_x=-\frac{L^{p+1}}{m^p}e^{p(\kappa_1+\kappa_2)t+(m\kappa_1+\kappa_2)t}e^{-(Lx+pLx)e^{\kappa_2t}}\left(M+e^{-Lxe^{\kappa_2t}}\right)^{p(\frac{1}{m}-1)},$$

$$(|\bar u_x|^p(\bar u^m)_x)_x\le(p+1)\frac{L^{p+2}}{m^p}e^{p(\kappa_1+\kappa_2)t+(m\kappa_1+2\kappa_2)t}M^{p(\frac{1}{m}-1)}$$

In $R_+\times R_+$. On the other hand, on the boundary we have

$$-|\bar u_x|^p(\bar u^m)_x(0,t)=\frac{L^{p+1}}{m^p}e^{p(\kappa_1+\kappa_2)t+(m\kappa_1+\kappa_2)t}(M+1)^{p(\frac{1}{m}-1)},$$

$$\bar u^q(0,t)=e^{q\kappa_1t}(M+1)^{\frac{q}{m}}.$$

By the definition of κ_1,κ_2,L,M and the assumption $0<q\le\frac{2p+m+1}{p+2}$, we can check that $\frac{\partial\bar u}{\partial t}\ge\frac{\partial}{\partial x}\left(\left|\frac{\partial\bar u}{\partial x}\right|^p\frac{\partial\bar u^m}{\partial x}\right)$ in $R^+\times R^+$ and $-\left|\frac{\partial\bar u}{\partial x}\right|^p\frac{\partial\bar u^m}{\partial x}(0,t)\ge\bar u^q(0,t)$ for $t>0$. We have shown that $\bar u$ is a supersolution of the problem (1)-(3), which implies that every solution of the problem (1)-(3) is global provided $0<q\le\frac{2p+m+1}{p+2}$ by the comparison principle.

Lemma 2.2. If $q>q_0=\frac{2p+m+1}{p+2}$, then the solution of the problem (1)-(3) with appropriately large initial data blows up in finite time.

Proof. To prove the non-existence of global solutions, we construct a blow-up self-similar subsolution of the system. Construct

$$\underline u(x,t)=(T-t)^{-k}f(\xi),\ \xi=x(T-t)^{-l} \quad (13)$$

where T is a positive constant, f is to be determined later and

$$k=\frac{p+1}{(p+2)q-(2p+m+1)},\quad l=\frac{q-m-p}{q(p+2)-(2p+m+1)}. \quad (14)$$

After some computations, we have

$$\underline u_t=(T-t)^{-(k+1)}(kf(\xi)+l\xi f'(\xi)),$$

$$|\underline u_x|^p(\underline u^m)_x=(T-t)^{-pk-pl-mk-l}|f'|^p(f^m)'(\xi),$$

$$(|\underline u_x|^p(\underline u^m)_x)_x=(T-t)^{-pk-pl-mk-2l}(|f'|^p(f^m)'(\xi))',$$

and

$$|\underline u_x|^p(\underline u^m)_x(0,t)=(T-t)^{-pk-pl-mk-l}|f'|^p(f^m)'(0),$$

$$\underline u^q(0,t)=(T-t)^{-kq}f^q(0).$$

Thus, $(\underline u,\underline v)$ is weak subsolution of (1)-(3) provided that

$$(|f'|^p (f^m)'(\xi))' \geq kf(\xi) + lf'(\xi)\xi, \quad (15)$$

$$-|f'|^p (f^m)'(0) \leq f^q(0). \quad (16)$$

Set

$$f(\xi) = (A + B\xi)^{-\frac{p+2}{1-p-m}}, \quad (17)$$

where A, B are positive constants to be determined. It is easy to see that

$$f'(\xi) = -B\frac{p+2}{1-p-m}(A + B\xi)^{-\frac{p+2}{1-p-m}-1}, \quad (18)$$

$$|f'|^p (f^m)' = -mB^{p+1}\left(\frac{p+2}{1-p-m}\right)^{p+1}(A + B\xi)^{-\frac{2p+m+1}{1-p-m}}, \quad (19)$$

$$(|f'|^p (f^m)')' = mB^{p+2}\left(\frac{2p+m+1}{1-p-m}\right)\left(\frac{p+2}{1-p-m}\right)^{p+1}(A + B\xi)^{-\frac{p+2}{1-p-m}}. \quad (20)$$

Substituting (17)-(20) into (15), then inequality (15) is valid provided that

$$k(A + B\xi)^{-\frac{p+2}{1-p-m}} - l\xi B\frac{p+2}{1-p-m}(A + B\xi)^{-\frac{p+2}{1-p-m}-1}$$

$$-mB^{p+2}\left(\frac{2p+m+1}{1-p-m}\right)\left(\frac{p+2}{1-p-m}\right)^{p+1}(A + B\xi)^{-\frac{p+2}{1-p-m}} \leq 0.$$

By taking

$$B \geq \left(\frac{k(2p+m+1)}{m(1-p-m)}\left(\frac{1-p-m}{p+2}\right)^{p+1}\right)^{\frac{1}{p+2}},$$

and $A^{\frac{q(p+2)-(2p+m+1)}{1-p-m}} \leq \left(mB^{p+1}\left(\frac{p+2}{1-p-m}\right)^{p+1}\right)^{-1}$, it is easy to check that (15) and (16) are valid. Noticing that $q > q_0 = \frac{2p+m+1}{p+2}$ implies that $k > 0$, $\underline{u}$ given by (15) and (17) is a blowup subsolution of the problem (1)-(3) with appropriately large u_0. It follows from the comparison principle that the problem (1)-(3) exists a solution blowing up in a finite time.

Now we turn our attention to the critical exponent of Fujita type. That is, we shall show when all solutions of (1)-(3) blow up in a finite time or both global and nonglobal solutions exist.

Lemma 2.3. If $\frac{2p+m+1}{p+2} = q_0 < q < q_c = 2p+m+1$, then each positive solution of the problem (1)-(3) blows up in finite time.

Proof. Without loss of generality, we first assume that u is nonincreasing in x, for if not we consider the (nonincreasing in x) solution ω corresponding to the initial value $\omega_0(x) = \inf\{u_0(y), 0 \leq y \leq x\}$, which are nonincreasing in x. If \$\omega\$ blows up in finite time, so does u. On the other hand, for every $\epsilon > 0$ and $t_0 > 0$ fixed, by Theorem 1.1, there exists a constant $M > 0$ large enough that

$$u(x,t_0) \geq \left(\frac{(C_{m,p} + \epsilon)x^{\frac{p+2}{p+1}}}{t_0^{\frac{1}{p+1}}}\right)^{-\frac{p+1}{1-m-p}} \quad for \ \ x \geq M,$$

and

$$u(x,t_0) \geq u(M,t_0), \quad for \ \ 0 \leq x \leq M.$$

Now we construct the following well-known self-similar solution (the so-called Zel'dovich-Kompaneetz-Barenblatt profile [8, 12, 24]) to (1)-(3) in the form

$$u_B(x,t) = (\tau + t)^{-\frac{1}{m+2p+1}}h(\xi), \ \xi = x(\tau + t)^{-\frac{1}{m+2p+1}}, \quad (21)$$

$$h(\xi) = \left(b^{\frac{p+2}{p+1}} + C_{m,p}\xi^{\frac{p+2}{p+1}}\right)^{-\frac{p+1}{1-p-m}} \quad (22)$$

with $\tau > 0, b > 0$ and $C_{m,p}$ is given in (10). It is not difficult to check that

$$(|h'|^p (h^m)')'(\xi) + \frac{1}{m+2p+1}\xi h'(\xi)$$

$$+\frac{1}{m+2p+1}h(\xi) = 0, \ h'(0) = 0.$$

Since $u(x,t)$ is nontrivial and nonnegative, we see that $u(0,t_0) > 0$ for some $t_0 > 0$ (compare with a Barenblatt solution of the corresponding equations). Noticing that $u(x,t_0) > 0$ is continuous (see [6, 30]), there exists $\tau > 0$ large enough and \$b\$ small enough such that $u(x,t_0) > u_B(x,t_0), \ for \ x > 0$. A direct calculation shows that $u_B(x,t)$ is a weak subsolution of (1)-(3) in $(0,+\infty)\times(t_0,+\infty)$. By the comparison principle, we obtain that $u(x,t) > u_B(x,t), \ for \ x > 0, t > t_0$.

We declare that there exist $t_* \geq t_0$ and T large enough that

$$u_B(x,t_*) \geq \underline{u}(x,0), \quad x \in (0,+\infty), \quad (23)$$

where $\underline{u}(x,t)$ is given by (13) and (17). A simple calculation shows that (23) is valid provided

$$(\tau + t_*)^{-\frac{1}{2p+m+1}} \gg T^{-k}, \quad (24)$$

$$(\tau + t_*)^{-\frac{1}{2p+m+1}} \ll T^{-l}. \quad (25)$$

Since $q_0 < q < q_c$, we have $k > 1$. Thus there exist $t_* > t_0$ and T large enough that (24) and (25) are both valid. Thus $u(x,t_*) \geq u_B(x,t_*) \geq \underline{u}(x,0), \ x \in (0,+\infty)$, which with the comparison principle implies that u blows up in a finite time.

Lemma 2.4. If $q > q_c$, then the problem (1)-(1) admits positive global solutions with small initial data.

Proof. We investigate the auxiliary function

$$\bar{u}(x,t) = (\tau + t)^{-k} F(\xi),\ \ \xi = x(\tau + t)^{-l}, \qquad (26)$$

where τ is a positive constant, $F(\xi)$ is to be determined later and

$$k = \frac{p+1}{(p+2)q - (2p+m+1)},\ \ l = \frac{q-m-p}{q(p+2) - (2p+m+1)}. \qquad (27)$$

By a direct computation, we obtain

$$\bar{u}_t = (\tau + t)^{-(k+1)}(-kF(\xi) - l\xi F'(\xi)),$$

$$|\bar{u}_x|^p (\bar{u}^m)_x = (\tau + t)^{-pk-pl-mk-l} |F'|^p (F^m)'(\xi),$$

$$(|\bar{u}_x|^p (\bar{u}^m)_x)_x = (\tau + t)^{-pk-pl-mk-2l} (|F'|^p (F^m)'(\xi))',$$

and

$$|\bar{u}_x|^p (\bar{u}^m)_x(0,t) = (\tau + t)^{-pk-pl-mk-l} |F'|^p (F^m)'(0),$$

$$\bar{u}^q(0,t) = (\tau + t)^{-kq} F^q(0).$$

Thus, $\bar{u}$ is weak supsolution of (1)-(3) provided that

$$(|F'|^p (F^m)'(\xi))' + kF(\xi) + lF'(\xi)\xi \le 0, \qquad (28)$$

$$-|F'|^p (F^m)'(0) \ge F^q(0). \qquad (29)$$

We choose

$$F(\xi) = H\left((ab)^{\frac{p+2}{p+1}} + (\xi + a)^{\frac{p+2}{p+1}} \right)^{-\frac{p+1}{1-p-m}} \qquad (30)$$

with $b > 0, H > 0, a > 0$ to be determined. After a series computations, we obtain

$$F'(\xi) = -H\frac{p+2}{1-p-m}\left((ab)^{\frac{p+2}{p+1}} + (\xi + a)^{\frac{p+2}{p+1}} \right)^{-\frac{p+1}{1-p-m}-1} (\xi + a)^{\frac{1}{p+1}},$$

$$|F'|^p (F^m)' = -mH^{p+m}\left(\frac{p+2}{1-p-m} \right)^{p+1} \left((ab)^{\frac{p+2}{p+1}} + (\xi + a)^{\frac{p+2}{p+1}} \right)^{-\frac{p+1}{1-p-m}} (\xi + a),$$

$$(|F'|^p (F^m)')' = -mH^{p+m}\left(\frac{p+2}{1-p-m} \right)^{p+1} \left((ab)^{\frac{p+2}{p+1}} + (\xi + a)^{\frac{p+2}{p+1}} \right)^{-\frac{p+1}{1-p-m}}$$

$$+mH^{p+m}\left(\frac{p+2}{1-p-m} \right)^{p+2} \left((ab)^{\frac{p+2}{p+1}} + (\xi + a)^{\frac{p+2}{p+1}} \right)^{-\frac{p+1}{1-p-m}-1} (\xi + a)^{\frac{p+2}{p+1}},$$

substituting above equalities into (28), let $y = \xi + a$, then (28) can be transformed into the following inequality with respect y

$$G(y) = -e_1 y^{\frac{p+2}{p+1}} + e_2 a y^{\frac{1}{p+1}} - e_3 (ab)^{\frac{p+2}{p+1}} \le 0, \qquad (31)$$

where

$$e_1 = mH^{p+m-1}\left(\frac{p+2}{1-p-m} \right)^{p+1} - Hk + lH\frac{p+2}{1-p-m} - mH^{p+m-1}\left(\frac{p+2}{1-p-m} \right)^{p+2},$$

$$e_2 = lH\frac{p+2}{1-p-m},$$

$$e_3 = mH^{p+m-1}\left(\frac{p+2}{1-p-m} \right)^{p+1} - Hk.$$

Since the assumptions $q > q_c = 2p + m + 1$ imply $l > k > 0$ we can choose a suitable constant $H > 0$ such that $l > mH^{p+m-1}\left(\frac{p+2}{1-p-m} \right)^{p+1} > k > 0$, for such H, it is easy to verify that $e_i > 0 (i = 1,2,3)$ and $G(y)$ is a concave function with respectto $y^{\frac{1}{p+1}}$, then $G(y)$ attains its maximum at $y_* = \frac{e_2 a}{(p+2)e_1}$. Therefore, (31) is valid provided that

$$G(y_*) = a^{\frac{p+2}{p+1}}\left(\frac{p+1}{p+2}\left(\frac{1}{e_1(p+2)} \right)^{\frac{1}{p+1}} e_2^{\frac{p+2}{p+1}} - e_3 b^{\frac{p+2}{p+1}} \right) \le 0. \qquad (32)$$

So, we only need to choose \$b\$ sufficiently large such that

$$b \ge \left(\frac{(p+1)e_2}{(p+2)e_3} \right)^{\frac{p+1}{p+2}} \left(\frac{e_2}{(p+2)e_1} \right)^{\frac{1}{p+2}}.$$ Consequently, we have proved that inequalities (28) is true.

Now we consider the boundary condition (29), for above fixed H, d, we only need to show that

$$a^{\frac{q(p+2)-(2p+m+1)}{1-p-m}} \ge m^{-1} H^{1-m-p}\left(\frac{1-p-m}{p+2} \right)^{p+1} \left(b^{\frac{p+2}{p+1}} + 1 \right)^{\frac{(p+1)(1-q)}{1-p-m}} \qquad (33)$$

The assumption $q > 2p + m + 1$ ensures that there exist a large enough such that the inequality (33) holds, which implies that the inequality (29) holds.

Thus, for the case $q > q_c = 2p + m + 1$, we have constructed a class of global selfsimilar supersolutions defined by (26) and (30). Owing to the comparison principle, the solution of the problem (1)-(3) is global if the initial data u_0 is small enough.

III. The Critical Case E $q = q_c$

In this section, by the stationary state technique used in [8, 11], we study the critical case $q = q_c$.

Proof of Theorem 1.3. Assume by contradiction that there exists a global nontrivial solution $u(x,t)$. Let $v(x,t) = u(x,1+t)$. Then $v(x,t)$ is the solution of the problem (1)-(1) with initial data $v_0(x) = u(x,1)$. Using the spatial decay given in (9), we can choose $a > 0$ and $b > 0$ such that $v_0(x) \ge g(x+b)$, where g is the Barenblatt profile given in (22). Now we make the following change of variables

$$h(\xi,\tau) = (1+t)^{\frac{1}{2p+m+1}} v\left(\xi(1+t)^{\frac{1}{2p+m+1}}, t \right),$$ where $\tau = \log(1+t)$ denotes the new time. Then it is easily checked that $h(\xi,\tau)$ is the solution of the following problem

$$
\begin{aligned}
&h_\tau = (|h'|^p\ (h^m)')'(\xi) + \frac{1}{m+2p+1}\xi h'(\xi) \\
&+ \frac{1}{m+2p+1}h(\xi),\ \ (\xi,\tau)\in R_+\times(0,+\infty), \\
&-|h'|^p\ (h^m)'(0,\tau) = h^{2p+m+1}(0,\tau), \tau\in(0,+\infty), \\
&h(\xi,0) = v_0(\xi),\quad \xi\in R_+.
\end{aligned}
\tag{34}
$$

Let $\underline{h}(\xi,\tau)$ be the corresponding solution with initial data $g(\xi+b)$. It follows that $h\ge\underline{h}$, therefore $\underline{h}$ is also global.

It can be easily verified that

$$(|g_{\xi'}|^p\ (g^m)_{\xi'})_{\xi'}(\xi+b) + \frac{1}{m+2p+1}\xi g_{\xi'}(\xi+b) + \frac{1}{m+2p+1}g(\xi+b) > 0.$$

Hence we can show that $\underline{h}$ is nondecreasing in τ (see [8]), moreover, we know that $\underline{h}$ is nondecreasing in ξ.

Next we will prove that for any $\tau>0$ we have

$$+\infty > \lim_{\tau\to\infty}\underline{h}(\xi,\tau) = H(\xi)\neq 0.$$

Otherwise,

$$\lim_{\tau\to\infty}\underline{h}(\xi,\tau) = +\infty \tag{35}$$

uniformly on $[0,\xi_0]$, since $\underline{h}$ is nonincreasing in ξ. Therefore we claim that $v(x,t)$ blows up in finite time (the claim is to be proved later). However, v was assumed to be global. This contradiction shows that the function $H(\xi)$ is well defined. In view of the regularity of the bounded solution of the problem (3.1), by using the standard arguments [8], we can pass to the limit in the first equation of (34) to get.

$$
\begin{aligned}
&(|H'|^p\ (H^m)')'(\xi) + \frac{1}{m+2p+1}\xi H'(\xi) \\
&+ \frac{1}{m+2p+1}H(\xi) = 0.
\end{aligned}
\tag{36}
$$

Because of the regularity of $\underline{h}$ in the region where $H>0$ [8], we can pass to the limit in the boundary condition in (34) for $-|h'|^p\ (h^m)'(0,\tau) = h^{2p+m+1}(0,\tau)$, and obtain $-|H'|^p\ (H^m)'(0) = H^{2p+m+1}(0)\neq 0$. However, the every solution of (36) is a Barenblatt profile and this profile does not satisfy the boundary condition, leading to contradiction. The proof of Theorem 1.3 is completed.

Now we prove the claim. By (35) there is positive τ_0 such that $\underline{h}(\xi,\tau_0) > N$ on $[0,\xi_0]$ for any $N>0$. In other words, at time $t_0 = e^{\tau_0}-1$, the profile $\underline{h}(\xi,\tau)$ in the original variables satisfies $v(x,t_0)\ge(1+t_0)^{-\frac{1}{2p+m+1}}N$ for $x\in[0,\xi_0(1+t_0)^{\frac{1}{2p+m+1}}]$. Let \$u\$ be defined in (13) and (17). Observing $q=q_c=2p+m+1$, by Theorem 1.1, there exists a constant t_0 large enough that

$$
\begin{aligned}
v(x,t_0) = u(x,1+t_0) &\ge \left(C_{m,p}^{-(p+1)}(1+t_0)\right)\frac{1}{1-m-p}x^{-\frac{p+2}{1-p-m}} \\
&\ge B^{-\frac{p+2}{1-p-m}}T^{\frac{1}{1-p-m}}x^{-\frac{p+2}{1-p-m}} \\
&= B^{-\frac{p+2}{1-p-m}}T^{\frac{(2p+m+1)(p+1)}{(q(p+2)-(2p+m+1))(1-p-m)}}x^{-\frac{p+2}{1-p-m}} \\
&> T^{-\frac{p+1}{q(p+2)-(2p+m+1)}}\left(A+BxT^{-\frac{p+1}{q(p+2)-(2p+m+1)}}\right)^{-\frac{p+2}{1-m-p}} \\
&= \underline{u}(x,0)
\end{aligned}
\tag{37}
$$

for $x>\xi_0(1+t_0)^{\frac{1}{2p+m+1}}$, and

$$
\begin{aligned}
v(x,t_0) &= (1+t_0)^{-\frac{1}{2p+m+1}}N \\
&\ge T^{-\frac{1}{2p+m+1}}A^{-\frac{p+2}{1-p-m}} \\
&= T^{-\frac{p+1}{q(p+2)-(2p+m+1)}}A^{-\frac{p+2}{1-p-m}} \\
&\ge \underline{u}(x,0)
\end{aligned}
\tag{38}
$$

for $x\in\left[0,\xi_0(1+t_0)^{\frac{1}{2p+m+1}}\right]$ provided $T=1+t_0$ and B,N are large enough. It follows from (37), (38) and the comparison principle that $v(x,t)$ blows up in finite time.

IV. The Blow-Up Set and the Blow-Up Rate

In this section, we will study the blow-up set and the blow-up rate. We assume that $q>q_0$ and consider the solution $u(x,t)$ of the problem (1)-(3) that blows up at finite time T.

Proof of Theorem 1.4. $\forall T^*<T$, let $s(T^*) = \max_{(x,t)\in[0,+\infty)\times[0,T^*]}u(x.t) < +\infty$ If u_0 has appropriate decay at infinity, we consider the following problem

$$
\begin{aligned}
&\omega_t = (|\omega_x|^p\ (\omega^m)_x)_x, \quad x\ge 0, 0<t<T, \\
&\omega(0,t) = s(T^*), \qquad t\in(0,T^*), \\
&\omega(x,0) = u_0(x), \qquad x\ge 0.
\end{aligned}
$$

We define the supersolution

$$U_1(x,t) = (x,\tau)^{\frac{1}{1-p-m}}\left(\rho_{m,p}x^{\frac{p+2}{p+1}}\right)^{-\frac{p+1}{1-p-m}},$$

where $\rho_{m,p} = \frac{1-p-m}{p+2}\left(\frac{1}{m(p+2)}\right)^{\frac{1}{p+1}}$ and $\tau>0$ large enough such that $U_1(x,0)\ge u_0(x)$. By using the comparison principle, we have that

$U_1(x,t)\ge\omega(x,t)\ge u(x,t),\ x>0,\ 0<t\le T^*$. For the arbitrariness of T^*, we have $U_1(x,t)\ge u(x,t),\ x>0\quad 0<t<T$, therefore, $B(u)=\{0\}$.

If u_0 has not appropriate decay at infinity, we also claim that Theorem 1.3 holds. Otherwise, there exists $0<x_0\in B(u)$. We consider the following problem

$$\omega_t = (|\omega_x|^p(\omega^m)_x)_x, \quad 0<x<R, 0<t<T^*,$$
$$\omega(0,t) = s(T^*), \qquad t\in(0,T^*),$$
$$\omega(x,0) = u_0(x), \qquad 0<x<R.$$

Construct the supersolution

$U_2(x,t) = (t+\tau)^{\frac{1}{1-p-m}}\eta(x)$, where η is a solution of the elliptic problem (see [1, 20])

$$(|\eta'|^p(\eta^m)')' - \frac{1}{1-p-m}\eta = 0.$$
$$\eta(0) = \eta(R) = \infty,$$

where R and τ are large enough that $R > x_0, U_2(x,0) \ge u_0(x)$ for $0<x<R$. By using the comparison principle, we have that

$U_2(x,t) \ge \omega(x,t) \ge u(x,t), \ (x,t)\in(0,R)\times(0,T^*)$. For the arbitrariness of T^*, we have

$U_2(x,t) \ge u(x,t), \ (x,t)\in(0,R)\times(0,T),$

which leads to a contradiction. The proof of Theorem 1.4 is completed.

For the rest of the section we need to assume that initial data satisfies (H). As a consequence we have that $(|u_{0x}|^p(u_0^m)_x)_x \ge 0$. Clearly, $u(0,t) = \max_{x\in[0,\infty)} u(x,t)$. Let

$M(t) = u(0,t), \ a = M^{\frac{m+p-q}{p+1}}, \ b = M^{\frac{2p+m+1-q(p+2)}{p+1}}$, and define the function $\psi_M(y,s) = \frac{1}{M(t)}u(ay, bs+t)$ in $R_+\times(-\frac{t}{b}, 0)$ for $t<T$. Then ψ_M satisfies $o\le\psi_M\le 1, \ \psi_M = 1, \ (\psi_M)_s \ge 0$. Moreover, ψ_M is a solution of the following problem

$$(\psi_M)_s = (|(\psi_M)_y|^p((\psi_M)^m)_y)_y, \ x\ge 0, \ -\frac{t}{b} < s < 0,$$
$$-|(\psi_M)_y|^p((\psi_M)^m)_y(0,s) = (\psi_M)^q(0,s), -\frac{t}{b} < s < 0.$$

The following lemma is basic for the blow-up estimate.

Lemma 4.1. Under the assumptions of Theorem 1.5, there exists constant c for M large enough such that

$$(\psi)_s(0,0) \ge c. \tag{39}$$

Proof. We will prove $(\psi)_s(0,0)\ge c$. Otherwise, e.g., there exists a sequence $M_j\to\infty$ such that $\frac{\partial\psi_{M_j}}{\partial s}(0.0)\to 0$. Since ψ_{M_j} is uniformly bounded in $C^{2+\frac{\alpha}{2}}$, passing to a subsequence we have $\psi_{M_j}\to\tilde{\psi}$ for some positive function $\tilde{\psi}$ in $C^{2+\frac{\beta}{2}}(\beta<\alpha)$ satisfying $0\le\tilde{\psi}\le 1, \tilde{\psi}(0.0) = 1, \frac{\partial\tilde{\psi}}{\partial s}\ge 0$, which is a weak solution of

$$(\tilde{\psi})_s = (|(\tilde{\psi})_y|^p((\tilde{\psi})^m)_y)_y, \ x\ge 0, \ \ s_* < s < 0,$$
$$-|(\tilde{\psi})_y|^p((\tilde{\psi})^m)_y(0,s) = (\tilde{\psi})^q(0,s), \ s_* < s < 0,$$

where s_* is some constant satisfying $-\frac{t}{b} < s_* < 0$

Set $w = \tilde{\psi}_s$. Then w satisfies

$$w_s = (p+m)(|(\tilde{\psi})_y|^p\tilde{\psi}^{m-1}w_y)_y, x\ge 0, \ \ s_* < s < 0,$$
$$-|(\tilde{\psi})_y|^p\tilde{\psi}^{m-1}w_y(0,s) = qw\tilde{\psi}^q(0,s), \ s_* < s < 0.$$

Thus w has minimum at (0,0) with $w(0,0) = 0$. By using Hopf's lemma we know that $w \equiv 0$, which means that $\tilde{\psi}$ does not depend on s. Thus

$$0 = (\tilde{\psi})_s = (|(\tilde{\psi})_y|^p((\tilde{\psi})^m)_y)_y,$$
$$-|(\tilde{\psi})_y|^p((\tilde{\psi})^m)_y(y,0) = constant$$
$$= -|(\tilde{\psi})_y|^p((\tilde{\psi})^m)_y(0,0) = (\tilde{\psi})^q(0,0) = 1,$$

and hence $\tilde{\psi}$ is unbounded. This contradiction proves the lemma

Now we give the proof for Theorem 1.5 as follows.

Proof of Theorem 1.5. If we rewrite the inequality (39) in terms of $M(t)$, we obtain

$$M^{\frac{p+m-q(p+2)}{p+1}}(t)M'(t) \ge c.$$

Integrating and taking into account that $\mathrm{M}(\mathrm{t}) = \mathrm{u}(0,\mathrm{t})$, we get

$$u(.,t) \le C(T-t)^{-\frac{p+1}{(p+2)q-(2p+m+1)}}.$$

The proof of Theorem 1.5 is completed.

REFERENCES

[1] E. Chasseigne, J. L. Vazquez, Theory of extended solutions of fast diffusion equations in optimal classes of data. *Radiation from singularities, Arch. Ration. Mech. Anal.*, 164 (2002) pp. 133-187.

[2] K. Deng and H. A. Levine, The role of critical exponents in blow-up theorems: *The sequel, J. Math. Anal. Appl.*, 243(2000) pp. 85-126.

[3] E. Dibenedetto, Degenerate Parabolic Equations, Springer-Verlag, Berlin, New York, 1993.

[4] R. Ferreira, A. de Pablo, F. Quiros and J. D. Rossi, The blow-up profile for a fast diffusion equation with a nonlinear boundary condition, *Rocky Mountain J. Math.*, 33(2003), 123-146.

[5] H. Fujita, On the blowing up of solutions of the Cauchy problem for $u_t = \Delta u + u^{1+\alpha}$, *J. Fac. Sci. Univ. Tokyo Sect.*, I 13(1966) pp. 109-124.

[6] V. A. Galaktionov, Blow-up for quasilinear heat equations with critical Fujita's exponents, *Proc. Roy. Soc. Edinburgh Sect., A* 124 (1994) pp. 517-525.

[7] V. A. Galaktionov and H.A. Levine, A general approach to critical Fujita exponents and systems, *Nonlinear Anal.*, 34(1998) pp. 1005-1027

[8] V. A. Galaktionov and H. A. Levine, On critical Fujita exponents for heat equations with nonlinear flux conditions on the boundary, *Israel J. Math.*, 94(1996) pp. 125-146.

[9] M. A. Herrero and M. Pierre, The Cauchy problem for $u_t = \Delta u^m$ when 0 < m < 1, Trans. *Amer. Math. Soc.*, 291 (1985) pp. 145-158.

[10] Z. X. Jiang, Doubly degenerate paralolic equation with nonlinear inner sources or boundary flux, Doctor Thesis, *Dalian University of Tcchnology, In China, 2009*
[11] A. S. Kalashnikov, On a nonlinear equation appearing in the theory of non-stationary filtration, *Trudy Seminara I. G. Petrovski, 1978 (in Russian).*
[12] A. S. Kalashnikov, Some problems of the qualitative theory of nonlinear degenerate parabolic equa-tions of second order, Uspekhi Mat. *Nauk.*, 42(1987) pp. 135-176; *English transl: Russian Math. Surveys 42*(1987) pp. 169-222.
[13] H. A. Levine, The role of critical exponents in blow up theorems, SIAM Rev., 32(1990) pp. 262-288.
[14] Z. P. Li and C. L. Mu, Critical curves for fast diffusive polytropic filtration equation coupled via nonlinear boundary flux, *J. Math. Anal. Appl.*, 346(2008) pp. 55-64.
[15] Z. P. Li and C. L. Mu, Critical curves for fast diffusive on-Newtonian equation coupled via nonlinear boundary flux, *J. Math. Anal. Appl.*, 340(2008) pp. 876-883.
[16] Z.P. Li, C.L. Mu, Critical exponents for a fast diffusive non-Newtonian equation with nonlinear boundary flux, submitted for publication.
[17] Z. P. Li, C. L. Mu and Z. J. Cui, Critical curves for a fast diffusive polytropic filtration system coupled via nonlinear boundary flux, *Z. angew. Math. Phys.*, 60(2009) pp. 284-296.
[18] G. M. Lieberman, Second Order Parabolic Differential Equations, World Scientific, River Edge, 1996.
[19] Z. G. Lin, Blow-up behaviors for diffusion system coupled through nonlinear boundary conditions in a half space, *Sci. China Ser., A 47*(2004) pp. 72-82.
[20] A. Mohammed, Boundary asymptotic and uniqueness of solutions to the p-Laplacian with infinite boundary values, *J. Math. Anal. Appl.*, 325 (2007) pp. 480-489.
[21] Y. S. Mi, C. L. Mu and B. T. Chen, Critical exponents for a nonlinear degenerate parabolic system coupled via nonlinear boundary flux, *J. Korean Math. Soc. Accepted*.
[22] M. Pedersen and Z. G. Lin, Blow-up analysis for a system of heat equations coupled through a nonlinear boundary condition, *Appl. Math. Lett.*, 14(2001) pp. 171-176.
[23] F. Quiros and J. D. Rossi, Blow-up set and Fujita-type curves for a degenerate parabolic system with nonlinear conditions, *Indiana Univ. Math.* J., 50(2001) pp. 629-654.
[24] A. A. Samarskii, V. A. Galaktionov, S. P. Kurdyumov and A. P. Mikhailov, Blow-up in Quasilinear Parabolic Equations, *Walter de Gruyter, Berlin*, 1995.
[25] J. L. Vazquez, The Porous Medium Equations: Mathematical Theory, *Oxford University Press, Oxford, 2007.*
[26] M. X. Wang, The blow-up rates for systems of heat equations with nonlinear boundary conditions, *Sci. China Ser.*, A 46(2003) pp. 169-175.
[27] S. Wang, C. H. Xie and M. X. Wang, Note on critical exponents for a system of heat equations coupled in the boundary conditions, *J. Math. Analysis Applic.*, 218(1998) pp. 313-324.
[28] Z. J. Wang, Q. Zhou, W. Q Lou, Critical exponents for porous medium systems coupled via nonlinear boundary flux, *Nonlinear Anal.*, 71(2009) pp. 2134-2140.
[29] Z. J. Wang, J. X. Yin, C. P. Wang, Critical exponents of the non-Newtonian polytropic filtration equation with nonlinear boundary condition, *Appl. Math. Lett.*, 20(2007) pp. 142-147.
[30] Z. Q. Wu, J. N. Zhao, J. X. Yin and H. L. Li, Nonlinear Diffusion Equations, World Scientific Publishing Co. *Inc. River Edge, NJ, 2001.*
[31] Z. Y. Xiang, Q. Chen and C. L. Mu, Critical curves for degenerate parabolic equations coupled via non-linear boundary flux, *Appl. Math. Comput.*, 189 (2007) pp. 549-559.
[32] Z. Y. Xiang, Global existence and nonexistence for diffusive polytropic filtration equations with nonlinear boundary conditions, Z. angew. Math. Phys., DOI 10.1007/s00033-009-0028-9.
[33] S. N. Zheng, X. F. Song and Z. X. Jiang, Critical Fujita exponents for degenerate parabolic equations coupled via nonlinear boundary flux, *J. Math. Anal. Appl.*, 298(2004) pp. 308-324.
[34] J. Zhou and C. L Mu, Critical curve for a non-Newtonian polytropic filtration system coupled via nonlinear boundary flux, *Nonlinear Anal.*, 68(2008) pp. 1-11.
[35] J. Zhou and C. L. Mu, On critical fujita exponents for degenerate parabolic system coupled via nonlinear boundary flux, *Pro. Edinb. Math. Soc.*, 51(2008) pp. 785-805.
[36] Jin Li was born in Gansu on January, 1957. Associate professor. The main research direction is Nonlinear partial differential equations and Applied analysis.

A Data-aggregation Scheme for WSN based on Optimal Weight Allocation

Pinghui Zou and Yun Liu*
School of Electronic and Information Engineering, Beijing Jiaotong University, Beijing, China
*Corresponding author, Email: 08111002@bjtu.edu.cn, liuyun@bjtu.edu.cn

***Abstract*—Since the measuring accuracy and environment of each sensor are different, there must exist difference in the correctness of measurement. If the testing data is not processed and utilized with distinction, it will cause impreciseness to the testing results and lead to errors of the system. It is necessary to selectively distinguish the importance among the sensors, contraposing the situation of each sensor in the testing system and the accuracy of tests. So the related concepts of data aggregation technology in wireless sensor networks and the aggregation algorithm performance evaluation criteria are introduced. The core problem in WSN, aggregation operation for sensing data, is studied deeply. The problems in node data group when the distributed clustering technology is implemented to WSN are also analyzed. Then a distributed K-mean clustering algorithm based on WSN is proposed. On the basis of this improved algorithm, we realize a network data aggregation processing mechanism based on adaptive weighted allocation of WSN. DKC algorithm is mainly used to process the testing data of bottom nodes. When reducing the data redundancy it can provide more accurate field testing information and system status information. It can make rapid packet for the network nodes. The packed data will be used to provide correct judgement, according to the size of its corresponding weight, to acquire more reasonable results. The experiments have demonstrated that our method can greatly decrease the data redundancy of WSN and save large amount of storage resources. The network bandwidth consumption is also reduced. So this scheme has high efficiency and good scalability.**

***Index Terms*—Data Aggregation; Self-Adaptive Weighted; K-Means Clustering; DKC; WSN**

I. INTRODUCTION

Wireless Sensor Networks (WSN) is made up of lots of small-scaled sensor equipments and it is a self-organized network [1] which is deployed to a designated area, to supervise and perceive the task through limited wireless communication mode.

As the ability of node communication is limited, WSN can only work in a relatively smaller scope. To increase the accuracy and authenticity of target monitoring, the sensory area of these nodes must be mutually overlapped. Data aggregation technology [2] uses this feature to transmit collected data of each node to other nodes or base station, which will reduce the count of data and delete redundancy. At present, data aggregation algorithms of wireless sensor network are mainly based on traditional Client/Server(C/S) model [3, 4], but this model has many problems:

(1) Network delay and energy consumption is large. Each sensor node can simultaneously transmit data to processing node and processing node can only receive data in a given order. When sensor node number is increasing and the total quantity of sensor data is enlarged, network delay and energy consumption are also increasing.

(2) The scalability is inefficient. When WSN supplements new sensor nodes, the network structure often needs to adjust to keep load balance.

(3) The energy consumption of nodes in unbalanced. Since nodes processing need connection of each sensor node to deal with its data, the sensor nodes will consume more energy. That needs to present super powerful energy nodes to be taken as processing data or adopt an algorithm to process the nodes in rotation, which brings additional network overhead.

Towards above problems, reference [5] provides Local Closest First (LCF) heuristic Mobile Agent (MA) data aggregation routing algorithm. When selecting the distance, the most approximate node of current sensor node is taken as the next node. It performs data aggregation on each accessing sensor node. However, it is only suitable for small-scaled sensor network in simple environment. When the network scale is constantly expanding and the distribution of sensor node is more complicated, heuristic algorithm can obtain the local optimum MA routing intelligently. Reference [6] uses Genetic Algorithm (GA) [7] to solve the local optimum MA routing of the minimized network energy. However, its aggregation energy is the function of time, instead of data size. Therefore, we cannot explain that data transmission quantity is reduced because of data aggregation, which also reduces transmission energy to approach the purpose of saving energy. Reference [8] proposes a WSN data aggregation algorithm named AGA based on adaptive genetic algorithm. The algorithm summarizes MA routing as an optimized problem. By means of grid method, AGA is applied to solve the optimal routing node sequence for mobile agents [9, 10]. Currently, wireless sensor network data aggregation technology based on Client/Server (C/S） model and MA is gradually developing in universities and research institutions. However, their basis for research is mainly established on current foreign algorithms. As one of key

doi:10.4304/jnw.9.1.100-107

technologies on wireless sensor network, data aggregation still has many problems for us to study.

Contraposing the defects in existing technology, we propose a fast packet method for the sensing data in WSN based on K-mean clustering algorithm. By analysis on current distributed clustering problems and research on clustering processing in WSN, a Distributed K-mean Clustering (DKC) method for WSN is proposed. On the basis of DKC, an in-network data aggregation algorithm based on the optimal weight distribution is also put forward. DKC algorithm can realize fast and rational packet for nodes transmission in WSN. However, the data aggregation method based on adaptive weight allocation can make effective and correct judgment with the weighted value of sensor data. The experiments results have shown that our scheme is simple and practical. It greatly reduces the data redundancy of the whole network, which also has higher efficiency and better scalability.

II. DISTRIBUTED K-MEAN CLUSTERING IN WSN

A. Process of K-mean Clustering Method

When a dataset contains n data objects and the number of clusters is k, the object of clustering algorithm is finding an algorithm for division to divide the data object into k ($k \le n$) partitions [11]. Each division represents a cluster. Generally, a guideline will be adopted, such as distance. The best known and most commonly used methods are K-means or K-center and their variants [12-16]. The K-means clustering algorithm based on centroid take k as parameter to divide n objects into k clusters. It makes relatively higher similarity inside the cluster, while the similarity among the cluster is lower. The calculation of similarity is based on the mean of object in one cluster.

K-means clustering method is an unsupervised learning algorithm. First it randomly selects k objects and each object represents a mean value or centroid of a cluster initially. For the other objects, they will be assigned to the nearest cluster according to the distance with the center of cluster. Then the mean value of each cluster is recalculated. This process is repeated continuously until the criterion function is converged. Commonly the formula $E = \sum_{i=1}^{k} \sum_{p \in C_i} | p - m_i |^2$ is used for judgement. E is the sum of squared errors of all the objects.; p is time point which denotes the given data object; m_i is the mean value of cluster C_i. This criterion tries to make the generated cluster compact and independent. The whole procedures can be summarized as the follows:

(1) Select k objects by computer randomly or artificially as the initial clustering center: $Z_1(1)$, $Z_2(1)$,…, $Z_k(1)$.;

(2) Compute the squares of distance for any two points;

(3) According to the result of above procedure find new cluster center $Z_1(j+1)$, $Z_2(j+1)$, …, $Z_k(j+1)$. Compute the mean value of object in the cluster and assign the most similar cluster to each object.

(4) If the new cluster center is the same as the previous then it stops; else return to step 2.

B. Process of Distributed Data

(a) Distributed clustering problem

We assume there are p nodes N_1, N_2 ,…, N_p in a WSN system. $X = X^{(1)} \wedge X^{(2)} \wedge ... \wedge X^{(p)}$ is the whole data set. $X^{(i)}$ is the subset of X ($i = 1, 2, ..., p$) and it denotes the subset of data in node N_i. Set $X^{(i)} = \{x_1^i, x_2^i, ..., x_n^i\}$ as the set of n_i data nodes which are perceived by the sensor in node i. The target is dividing each dataset $X^{(i)}$ into K cluster with k-means clustering algorithm and keeping it consistent with the global clustering of set X. That means that if $X_j^{(i)}$ is the subset of $X^{(i)}$ ($i = 1, 2, ..., p, j = 1, 2..., K$), then $X_j^{(i)}$ contains the part of data nodes belonging to cluster j in X, after k-means clustering algorithm is implemented. Therefore we have $X_i = X_1^{(1)} \cup X_1^{(2)} \cup ... \cup X_1^{(p)}$.

(b) Treatment in WSN

The nodes in WSN are connected with Ad Hoc and each node can only communicate with neighbour nodes in its range [17]. In addition, sending data will consume more energy than its own consumption. So the data transmission should be avoided as few as possible. We need to make full use of the computation resource of the node itself, cooperating each other to complete the aggregation of the whole network. We assume there are m nodes in WSN which are used to inspect the data and each node creates data flow S_i. There is a node $\sin k$ which is responsible for each node in the network to send and receive messages. It has stronger processing ability, which can communicate with outside users by wired or wireless means.

The process of algorithm is described in detail: First node $\sin k$ randomly extract k records from the data in WSN as initial centroid of the data cluster to be divided. Tree communication structure is adopted to issue the information of k centroids to each node. Each node will divide local data into k clusters according to these centroids and send them to the parent nodes. When the parent nodes receive the information of all the sub-nodes, they will combine the local information with the cluster information and continue to transmit it to upper node, until node $\sin k$ received all the information of sub-nodes. Then $\sin k$ combines the information of k clusters and recalculates the mean value of each cluster. If it is not convergent then new k centroids will be calculated and be issued to the network for iteration. If it is convergent then the centroids of global k clusters will be created.

In the latter simulation of our system, all the messages are spread by broadcasting, which can be received by the nodes belonging to the effective transmission radius of sending nodes. The system designs a simple MAC protocol which satisfies random delay, carrier sense and

timing delay. The length of packet is not beyond the maximum data length that can be transmitted in one time. During the process of sensing data group a relative simply message format is used, without adopting the general packet heads. If the system need to be expanded in future, then more complicated network transmission control strategy will be used. That needs to add corresponding packet heads to the protocol. When the node data is grouped the exchanged message are mainly consist of two parts: message type and data. The message processing layer explains the message segment according to the different types of message data. The length of message segment is different due to the different length of message types. The network constructing request uses initial message InitNetwork. During clustering $\sin k$ sends message Clustering and each node sends using message of k clusters LocalCluster. When the clustering results are stable $\sin k$ will send message EndMining to terminate the process. The following program provides the data structure of main message:

```
typedef struct Clustering{
int k; // number of clustering to be divided
int centroid [k,p]; //k centroids
};
typedef struct Cluster{
// data structure of message LocalCluster
int clustered; // cluster ID
int num; // number of data nodes in cluster
int sum[p]; //cumulative sum of each node in the cluster
int sumd[p];// squares of distance of each node to the centroid
}
typedef struct LocalCluster {
int nodeid; // id of node sending messages
int k; // number of clusters
Cluster C[k] ; // information of k cluster
}
```

C. Distributed K-means Clustering Algorithm for WSN

We provide the distributed K-means clustering algorithm for WSN as the follows. We adopt the Euclidean distance as dissimilarity function. Assume $i=(x_{i1},x_{i2},...,x_{ip})$ and $j=(x_{j1},x_{j2},...,x_{jp})$ is two objects in dataset and each object has p attributes. Then the distance between them is

$$d(i,j)=\sqrt{|x_{i1}-x_{j1}|^2+|x_{i1}-x_{j1}|^2+...+|x_{ip}-x_{jp}|^2}\ .$$

Input: Initial centroids of k cluster and the number of clustering

Output: Centroid of k cluster

Methods:

Step 1: Node $\sin k$ randomly select k as the initial centroid of k cluster to be divided, which are sent to each node. The initial sum of square error is set as a bigger number;

Step 2: Each node calculates the distance to k centroids of every data node in the local dataset, which are divided into k clusters;

Step 3: Beginning from the leaf node, each node in the same layer will send the information of local cluster to its parent node, including the number of data nodes, cumulative sum of each data node and the squares of distance from node to centroid;

Step 4: When the information of all sub-nodes is received, it will be combined with the information of k clusters by each parent node, to create new information. After the nodes at the same layer are processed, that will be sent to upper layer;

Step 5: When the information of all the sub-nodes is received by $\sin k$, the information of k clusters are combined to compute the sum of squared error. If the result is bigger than old value, then it will be replaced by old value. The mean value of object in each cluster will be recalculated to create new k centroids, which are sent to each node.

Step 6: Repeat step 2-5, if the sum of squared error is smaller than old value, then the clustering results are stable. $\sin k$ will send EndMining message and compute the mean value, so as to create the final centroid of k clusters and output.

III. DATA AGGREGATION ALGORITHM FOR WSN BASED ON OPTIMAL WEIGHT ALLOCATION

A. Principle Idea

After the process of DKC, the nodes in WSN will acquire relative correct packet groups. However, there are always noises in the data measured by sensors. So the estimated value acquired by testing data has estimation error. Because the estimation error is a random quantity, Mean Squared Error is usually taken as the evaluation indicators to evaluate a estimated algorithm. For the testing data with multiple nodes, since the measuring accuracy and environment of each sensor are not the same, there must exist difference in the correctness of measurement. If multiple sensors are equally treated and the testing data are processed without discrimination, it will bring big errors to the testing results and system operating results. So the importance of the sensors should be differentiated, which is the basis of optimal weight allocation algorithm for data aggregation.

To balance different accuracy of each data, we introduce the feature number weight W which signs the measuring accuracy to represent the relative importance of each measuring data, in ranging accuracy measurement. The weight should be proportional with the size of data error. According to accuracy the testing data are multiplied by the weight and averaged to raise the accuracy of testing results. In our study, the self-adaptive weighted data-aggregation method is mainly used to process the testing data of bottom nodes. When decreasing the data redundancy it can provide more accurate information for test and system. As is shown in figure 1, the sensors of each node correspond to different weight value. Under the optimal condition that the total MSE is the minimum, according to the measuring value of each sensor the optimal weight value can be found in a self-adaptive way. The aggregated value of X can get the optimum [18].

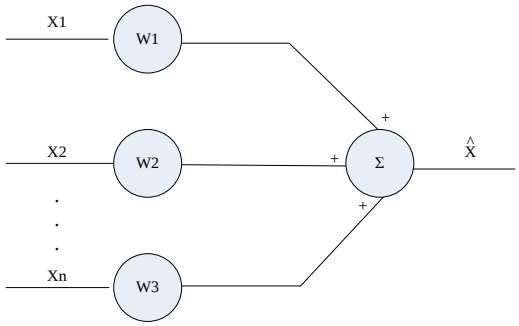

Figure 1. Estimated model of adaptive weighted data aggregation

We assume the variance of n sensors is individually σ_1^2, σ_2^2,…, σ_n^2. The true value for estimation is X. The measuring value of each sensor is X_1, X_2,…, X_n. They are independent each other and they are the unbiased estimation of X. The weighted factor of each sensor is W_1, W_2,…, W_n. Then the aggregated value of $\hat{X}$ and the weighted factor should satisfy the following formulas:

$$\hat{X} = \sum_{p=1}^{n} W_p X_p \tag{1}$$

$$\sum_{p=1}^{n} W_p = 1 \tag{2}$$

The total MSE is:

$$\begin{aligned} \sigma^2 &= E[(X-\hat{X})^2] \\ &= E[\sum_{p=1}^{n} W_p^2 (X - X_p)^2 + \\ &\quad 2 \sum_{\substack{p=1,q=1 \\ p\neq q}}^{n} W_p W_q (X - X_p)(X - X_q)] \end{aligned} \tag{3}$$

Because X_1, X_2,…, X_n are independent each other and they are the unbiased estimation of X. So $E(X - X_p)(X - X_q) = 0$ ($p, q = 1, 2, ..., n$) and σ^2 is changed as

$$\sigma^2 = E[\sum_{p=1}^{n} W_p^2 (X - X_p)^2] = \sum_{p=1}^{n} W_p^2 \sigma_p^2 \tag{4}$$

From formula 4 it can be seen that the total MSE σ^2 is a multivariate quadratic function for the weighted factor, which must has a minimum value. The problem to obtain this minimum value is a extremum problem for the weighted factors W_1, W_2,…, W_n, with the constraints which satisfies formula 2.

Base on the relative theories for extreme value of multivariate function, we can obtain corresponding weighted factor when the total MSE has minimum value:

$$W_p = 1/(\sigma_p^2 \sum_{i=1}^{n} \frac{1}{\sigma_i^2}) \tag{5}$$

The corresponding minimum MSE is:

$$\sigma_{\min}^2 = 1/\sum_{p=1}^{n} \sigma_p^2 \tag{6}$$

Above estimations are based on the measuring value at some hour of each sensor. When X is a constant, we can provide estimation according to the average value of historical data. If

$$\bar{X}_p(k) = \frac{1}{k} \sum_{i=1}^{k} X_p(i), p = 1, 2, ..., n \tag{7}$$

Then the estimation value is

$$\hat{X} = \sum_{p=1}^{n} W_p \bar{X}_p(k) \tag{8}$$

The total MSN is

$$\begin{aligned} \sigma^2 &= E[(X-\hat{X})^2] \\ &= E[\sum_{p=1}^{n} W_p^2 (X - X_p(k))^2] \\ &\quad + 2 \sum_{\substack{p=1,q=1 \\ p\neq q}}^{n} W_p W_q (X - X_p(k))(X - X_q)(k)] \end{aligned} \tag{9}$$

Similarly, $X_1(k)$,..,…, $X_n(k)$ must also be the unbiased estimation value of X, so

$$\begin{aligned} \sigma^2 &= E[\sum_{p=1}^{n} W_p^2 (X - X_p(k))^2] \\ &= \frac{1}{k} \sum_{p=1}^{n} W_p^2 \sigma_p^2 \end{aligned} \tag{10}$$

Obviously, when σ^2 obtaining the minimum value its corresponding optimal weighted factor W_p still satisfies formula 5, the minimum MSE is

$$\bar{\sigma}_{\min}^2 = 1/k \sum_{p=1}^{n} \frac{1}{\sigma_p^2} = \sigma_{\min}^2 / k \tag{11}$$

From formula 11 we can see, because $k > 1$, $\bar{\sigma}_{\min}^2$ must be smaller than $\sigma_{\min}^2$ and the value of $\sigma_{\min}^2$ will decrease with the increasing of k.

B. Computation of Variance σ_p^2

As is known from above analysis, the optimal factor W_p is determined by the variance σ_p^2 of each sensor, which is unknown generally. We can obtain it according to provided measuring value of each sensor and corresponding algorithms.

We assume any two different sensor p and q, whose measuring value is X_p and X_q. Their corresponding observing error is V_p and V_q.

$$X_p = X + V_p, \; X_q = X + V_q \tag{12}$$

In formula 12, V_p and V_q represent zero mean stationary noise, so the variance of sensor p is

$$\sigma_p^2 = E[V_p^2] \tag{13}$$

Since V_p and V_q are not correlated each other and their mean is 0. So the cross-correlation coefficient R_{pq} of X_p and X_q satisfy the follows.

$$R_{pq} = E(X_p X_q) = E[X^2] \tag{14}$$

The autocorrelation coefficient R_{pp} satisfies

$$R_{pp} = E(X_p X_p) = E[X^2] + E[V^2] \tag{15}$$

Formula 15 pluses 14 we get

$$\sigma_p^2 = E[V_p^2] = R_{pp} - R_{pq} \tag{16}$$

The value of R_{pp} and R_{pq} can be acquired by its estimation of time domain. Set the number of sensor measuring data is k. The estimation of R_{pp} and R_{pq} is $R_{pp}(k)$ and $R_{pq}(k)$ respectively. Then

$$\begin{aligned} R_{pq} &= \frac{1}{k}\sum_{i=1}^{k} X_p(i) \\ &= \frac{1}{k}[\sum_{i=1}^{k} X_p(i)X_p(i) + X_p(k)X_p(k)] \\ &= \frac{k-1}{k} R_{pq}(k-1) + \frac{1}{k} X_p(k)X_p(k) \end{aligned} \tag{17}$$

Similarly,

$$R_{pq} = \frac{k-1}{k} R_{pq}(k-1) + \frac{1}{k} X_p(k)X_q(k) \tag{18}$$

If sensor q ($q \neq p, q-1, 2, ..., n$) can provide correlated calculation with p, we can get the value of $R_{pq}(k)$. Then the mean value $\bar{R}_p(k)$ of $R_{pq}(k)$ can be taken as the estimation of R_{pq}.

$$R_{pq} = \bar{R}_p(k) = \frac{1}{n-1}\sum_{q=1, q\neq p}^{n} R_{pq}(k) \tag{19}$$

Thus, we obtain the estimation value of R_{pp} and R_{pq} in the time domain, based on the measuring value of each sensor. Accordingly the variance σ_p^2 of each sensor can be estimated.

C. Application Procedures

In actual application, the computation procedures for adaptive weighted data aggregation are:

(1) Compute and $R_{pq}(k)$ at sampling hour k with formula 17 and 18

(2) Compute $\bar{R}_p(k)$ at hour k with formula 19

(3) Compute σ_p^2 at hour k with formula 16;

(4) Compute the mean value $\bar{X}_p(k)$ of sensor p measured at hour k with formula 7;

(5) Acquire the optimal weighted factor W_p according to formula 5;

(6) Acquire the aggregation estimation value $\hat{X}$ with formula 8.

In the experiments of adaptive weighted data aggregation, we adopt 10 groups uncorrelated zero mean white noise data to simulate the observing error of each sensor. The variance of white noise is 0.05, 0.07, 0.1, 0.2, 0.3, 0.25, 0.1, 0.1, 0.2, 0.3 and true value $X = 0.1$. If X is added to the white noise, the measuring data of 10 groups of sensors can be simulated. We perform adaptive weighted data aggregation to these measuring data. Each sensor only performs one measurement to the environment in this system. Then we get the results as table 1.

TABLE I. MEASURING VARIANCE CORRESPONDING TO EACH SENSOR

x_i	x_1	x_2	x_3	x_4	x_5
σ_i^2	0.05	0.07	0.1	0.2	0.3
x_i	x_6	x_7	x_8	x_9	x_{10}
σ_i^2	0.25	0.1	0.1	0.2	0.3

TABLE II. OPTIMAL WEIGHTED FACTOR CORRESPONDING TO EACH MEASURING VALUE

W_1	W_2	W_3	W_4	W_5
0.235	0.168	0.118	0.059	0.039
W_6	W_7	W_8	W_9	W_{10}
0.047	0.118	0.118	0.059	0.039

From formula 5 we know the optimal weight factor of the first measuring data is

$$\begin{aligned} W_1 &= 1/(\sigma_i^2 \sum_{i=1}^{10} \frac{1}{\sigma_i^2}) \\ &= 1/(0.05 \times 84.952) \\ &= 0.235 \end{aligned} \tag{20}$$

Similarly we can obtain the weighted factors of other measuring data. The value of each weighted factor in table 2 satisfies formula 2. So we can conclude the weighted factor will be smaller for the data which has bigger error. While the weighted factor will be larger for the measuring data which has smaller error and it has more important status in the testing results.

IV. SIMULATION AND IMPLENMENTATION

A. Performance Analysis based on K-mean Clustering Algorithm

The first experiment is realized on PC configured with VC++6.0 and the OS is Windows XP professional. Other setting is 1G memory, 500G hard disk space and CPU frequency is 2.0 GHz. The multithreading work mode is adopted to simulate the environment of WSN. During the process, DKC method is compared with the centralized method [19] which will compute the $\sin k$ nodes returned

by all data. The following figures describe the changing of error rate and time with the increase of the number of network nodes.

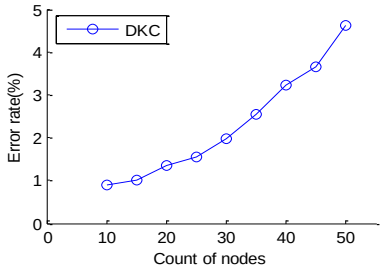

Figure 2. Error rate of DKC.

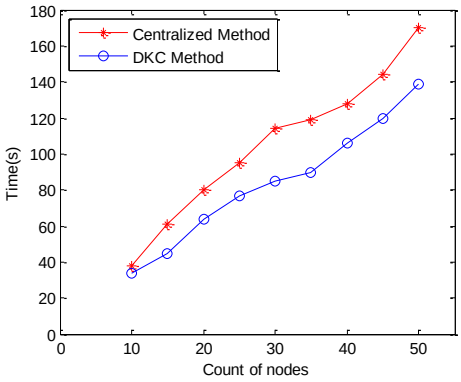

Figure 3. Execution time of DKC and centralized method.

Due to the feature of WSN, DKC algorithm may generate data loss in the process of iteration. Therefore, the accuracy of global clustering results may be decreased. To measure the accuracy of the improved method, when the initial conditions of algorithms are equivalent, the same k centroids are given to two algorithms. Then after the algorithms are terminated each particular point will lie in the same cluster of clustering results. We assume there are 100 data points of each node in WSN, which has 5 attributes each, $k = 4$. Figure 3 reflects the changing relation of the percentage that is occupied by error data points in the whole dataset, with the increase of nodes in network. It can be seen that the computation time of our scheme is obviously less than that of centralized method. Moreover, the data transmitted in centralized method is too large to be adaptable for WSN.

B. Effect on Algorithms Caused by Aggregation Cost

The aggregation cost will cause some effect on the algorithms, as is referred in the influence by data correlation. In this experiment we set the communication radius of node as 30m, the range for data correlation is 50m. The range of aggregation cost is 10 nJ / bit to 200 nJ /bit. The total energy costs of algorithm are shown as figure 4(a). With the increase of aggregation cost, the energy consumption of MST [20] and centralized method increase rapidly. While DKC method has less energy consumption when the aggregation cost is less than 80 nJ /bit. When the aggregation cost is beyond 80 nJ /bit, the total energy consumption of DKC is obviously optimal.

Figure 4 （b）and (c) describe the aggregation costs and communication costs of three algorithms. It is not hard to see that when the aggregation costs are low, MST and DKC have better effect on data aggregation and they can eliminate redundant data with lower aggregation costs. But if the aggregation costs are beyond 80 nJ /bit, since MST and centralized method need aggregation operation for each node, so their transmission energy approached a constant and the aggregation energy increase rapidly. When the aggregation costs of DKC are higher, DKC will forbid the aggregation process of many nodes, so its aggregation energy is decreasing with the increase of aggregation costs.

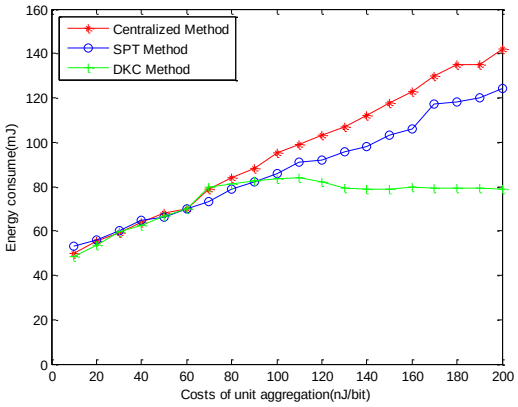

(a) Total energy costs

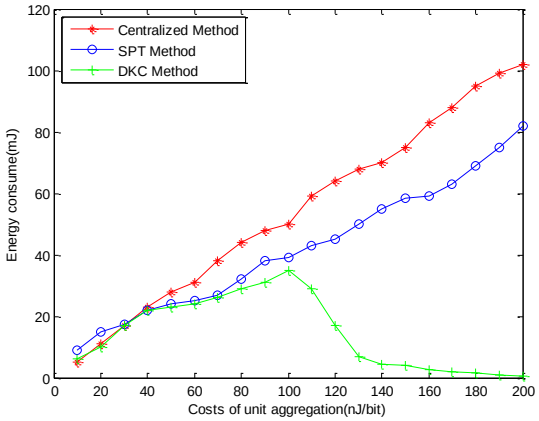

(b) Aggregation costs

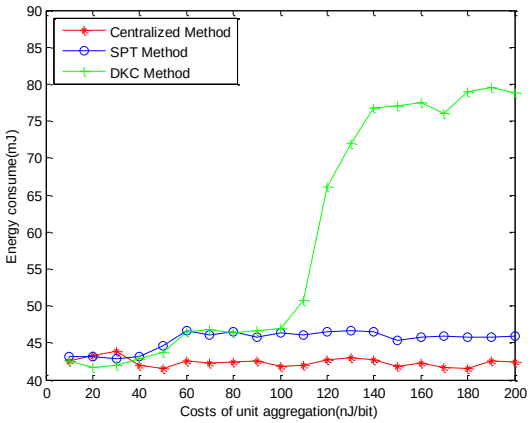

(c) Communication costs

Figure 4. The effect on algorithms caused by aggregation cost.

C. Case for Implementation

We take the application of data aggregation in ambient temperature detection as an example, to explain the working process of self-adaptive weighted algorithm. Eight WSN nodes equipped with temperature sensors are sporadically deployed in a room. Its detecting data is 35.56, 35.72, 35.82, 35.64, 35.77, 35.69, 35.93, 35.65 (℃). The variance of each sensor (σ_i^2 , i=1,2,…,8) is 0.44, 0.47, 0.52, 0.53, 0.49, 0.68, 0.81, 0.55. As is known from the above, the adaptive weight factors (W_p , p=1,2,…,8) is 0.184, 0.161, 0.131, 0.126, 0.148, 0.077, 0.056, 0.117. So the aggregation value calculated by formula 8 is:

$$\begin{aligned}\bar{X} &= \sum_{p=1}^{n} W_p \bar{X}_p(k) \\ &= \sum_{p=1}^{n} W_p X_p(k) \\ &= 35.704\end{aligned} \tag{21}$$

Then the ambient temperature measured is 35.704℃. According to the variance of each sensor the weighted factors can be acquired. The sensor owing higher measuring accuracy has bigger weighted factor. Furthermore, with the increase of times for detection, the weighted factor can be calculated based on the measuring data in each measurement. The importance in data detecting will be reflected by weighted factor. So it can fully take into account the advantage of sensors and the factor of environment, which reduces the influence of larger data deviation and improve the accuracy of measuring system.

V. CONCLUSION

Wireless sensor network has a lot of advantages like lower cost in wiring reduction, high monitoring accuracy, excellent fault tolerance, remote monitoring, easy diagnosis and maintenance etc. It has broad application prospect on network manufacturing and intelligence manufacturing. Its basic task is to correctly acquire valuable information in physical world. WSN depends on time and position information of nodes to realize the control between sensor nodes. We can also get high velocity of sensor data and low delay exchange to guarantee the correctness and real-time of the whole detection in system. However, WSN has some limitations in calculation, storage and network resource. So it is very significant to study the systematic structure of WSN, clock synchronization of nodes, node location and data aggregation.

This paper has discussed deeply the fundamental principles of node localization algorithm in WSN. It also proposes the node data packet method based on K-mean clustering algorithm. In the same packet, the adaptive weighted data aggregation is used to process the network node data. DKC algorithm can realize fast and rational packet of node sensor data in WSN. After nodes sensor data are packet, simple and effective adaptive weighted data aggregation methods can be applied to complete in-network data aggregation, which has been tested in a prototype system. The experiment results show that this method is simple and feasible. It largely reduces the data redundancy in the whole network and saves amounts of storage resource and the network bandwidth.

There are still a lot of aspects to improve our research and the next job mainly includes:

The environmental factor of WSN is a big problem to the effectiveness of algorithm. It is necessary to analyze and study real-time and reliability of the algorithm.

Since this paper do not explain many relevant routing methods in WSN, it is necessary to be studied in the future job.

As the energy effectiveness, calculation resource, storage resource of WSN nodes have large limitations, it needs related research in detail to obtain better performance in energy saving. Related specifications and performance standards also need further research.

ACKNOWLEDGEMENTS

The study was supported by the Natural Science Foundation of China (61071076).

REFERENCES

[1] Akyildiz I F, Su W, “Wireless sensor networks: a survey”, *Computer Networks*, vol. 38, no. 4, pp. 393-422, 2002.

[2] HUANG Man-guo, FAN Shang-chun, ZHENG De-zhi, “Research progress of multi sensor data fusion technology”, *Transducer and Micro system Technologies*, vol. 29, no. 3, pp. 5-12, 2010.

[3] William W. Guo, Mark Looi, A Framework of Trust-Energy Balanced Procedure for Cluster Head Selection in Wireless Sensor Networks”, *Journal of Networks*, vol. 7, no. 10, pp. 1592-1600, 2012.

[4] Yuan Ling-Yun, Zhu Yun-Long, Xu Tian-Wei, “Multi-layered energy-efficient and delay-reducing chain-based data gathering protocol for wireless sensor network”, *Journal of PLA University of Science and Technology*, vol. 9, no. 5, pp. 422-426, 2008.

[5] Chung-Min C, Agrawal H, Cochinwala M, et al, “Stream query processing for healthcare bio-sensor applications”, *Proceeding of IEEE Comput. Soc*, pp. 791-794, 2004.

[6] HyunSoon A, SeungHan L, SangKyung L, “Development of a ubiquitous healthcare system implementing real-time connectivity between cardiac patients and medical doctors”, *Proceedings of IEEE, in. Busan, South Korea*, pp. 51-54, 2005.

[7] Filippo Stanco, Davide Tanasi, Giovanni Gallo, “Augmented Perception of the Past - The Case of Hellenistic Syracuse”, *Journal of Multimedia*, vol. 7, no. 2, pp. 211-217, 2012.

[8] Hung K, Zhang Y T, Tai B, “Wearable medical devices for telehome healthcare”, *Proceedings of institute of Electrical and Electronics Engineers Inc*, pp. 5384-5387, 2004.

[9] Zhang Yangjun, Qin Chaokui, Xiao Litao, “Applicability of AGA and Weaver indices for natural gas interchangeability in China”, *Chemical Engineering of Oil & Gas*, vol. 42, no. 1, pp. 30-35, 2013.

[10] Cionca Victor, Newe Thomas, Dadârlat Vasile Teodor, “Configuration tool for a wireless sensor network integrated security framework”, J*ournal of Network and Systems Management*, vol. 20, no. 3, pp. 417-452, 2012.

[11] Mirco Nanni, Dino Pedreschi, "Time-focused clustering of trajectories of moving objects", *Journal of Intelligent Information Systems*, vol. 10, no. 3, pp. 267-289, 2006.
[12] Ming-Hua Liao, Hua Zhang, Guang Sun, "Energy aware routing algorithm for wireless sensor network based on ant colony principle", *Journal of Convergence Information Technology*, vol. 7, no. 4, pp. 215-221, 2012.
[13] Li You, Zhao Kaiyong, Chu Xiaowen, Speeding up k-Means algorithm by GPUs", *Journal of Computer and System Sciences*, vol. 79, no. 2, pp. 216-229, 2010.
[14] Xie Juanying, Jiang Shuai, Xie Weixin, "An efficient global K-means clustering algorithm", *Journal of Computers*, vol. 6, no. 2, pp. 271-279, 2011.
[15] Chen Xiaojun, Xu Xiaofei, Huang Joshua, "TW-(k)-means: Automated two-level variable weighting clustering algorithm for MultiView data", *IEEE Transactions on Knowledge and Data Engineering*, vol. 25, no. 4, pp. 932-944, 2013.
[16] Vidya T., Shama, "GA based dimension reduction for enhancing performance of k-means and fuzzy k-means: A case study for categorization of medical dataset", *Advances in Intelligent Systems and Computing*, vol. 201, no. 1, pp. 169-180, 2013.
[17] Rongbo Zhu, Intelligent Collaborative Event Query Algorithm in Wireless Sensor Networks. International Journal of Distributed Sensor Networks, Volume 2012, Article ID 728521, 11 pages.
[18] Qiufen Ni, Rongbo Zhu, Zhenguo Wu, Yongli Sun, Lingyun Zhou, Bin Zhou, "Spectrum Allocation Based on Game Theory in Cognitive Radio Networks", Journal of Networks, Vol. 8, No. 3, 712-722, Mar 2013.
[19] Liang Dai, Hongke Xu, Ting Chen, "A Task Scheduling Strategy in Heterogeneous Multi-sinks Wireless Sensor Networks", *Journal of Networks*, vol. 6, no. 11, pp. 1586-1894, 2011.
[20] LIN Jiaxiang, CHEN Chongcheng, FAN Minghui, "Algorithm of spatial out liermining based on MST clustering", *Geo-Information Science*, vol. 10, no. 5, pp. 586-592, 2008.

Fast Multipole Boundary Element Method of Potential Problems

Yuhuan Cui and Jingguo Qu
Qinggong College, Heibei United University, Tangshan, China
Email: qujingguo@163.com

Aimin Yang and Yamian Peng
College of Science, Heibei United University, Tangshan, China

***Abstract*—In order to overcome the difficulties of low computational efficiency and high memory requirement in the conventional boundary element method for solving large-scale potential problems, a fast multipole boundary element method for the problems of Laplace equation is presented. through the multipole expansion and local expansion for the basic solution of the kernel function of the Laplace equation, we get the boundary integral equation of Laplace equation with the fast multipole boundary element method; and gives the calculating program of the fast multipole boundary element method and processing technology; finally, a numerical example is given to verify the accuracy and high efficiency of the fast multipole boundary element method.**

***Index Terms*—Boundary Element Method; Fast Multipole Methods; Fast Multipole Boundary Element Method; Potential Problems; Laplace Equation**

I. INTRODUCTION

The boundary element method (BEM) [1] is a numerical method for solving the field problem based on the boundary integral equation, but there is very limited in the solving large scale. The conventional boundary element is difficult to deal with large-scale computing problems in engineering. This is because the coefficient matrix of the linear algebraic equations is a full matrix formatted by the boundary element method, but also shows the properties of asymmetric in the treatment of some special problems. The matrix operation requires a large amount of computer resources, such as direct Gauss elimination method requires $O(N_2)$ storage and $O(N_3)$CPU time, N is the degree of freedom. Therefore, computing power has become a bottleneck restricting the development and the application of the boundary element method.

From the late 1970s to now, the boundary element method has been applied to the fluid mechanics, wave theory, electromagnetism, and heat conduction problems and unsteady issues problem of composite materials axisymmetric and so on. In recent years, the boundary element method began to be used during material processing, in order to obtain numerical solutions. There are more and more engineering examples, in the engineering examples we use boundary element method to solve nonlinear problems and dynamic problems. For potential non-linear problems, such as proliferation issues we can do some transformation, so that control differential equations is linear, and solving the problem of heterogeneity.

In 1985, ROKHLIN [2] first put forward the fast multipole algorithm (Fast Multipole Methods) (FMM), Amount of the potential problem calculation for N particles interact with each other is reduced to $O(N)$. The essence of fast multipole algorithm is that multipole expansion of node clusters to approximate shows boundary integral of kernel function and boundary variable product, the amount of calculation and storage is reduced from the original $O(N_2)$ to $O(N)$. This algorithm is little demand for computer memory, and with the expansion of problems, the increased memory demand is also slow. it create a sufficient condition for the computer to large-scale operations. Computing efficiency, reduced memory usage and high accuracy will greatly strengthen the advantages of boundary element method and expand the application range of the boundary element method. this is a breakthrough. Therefore, the fast multipole algorithm is suitable for large-scale computing problems.

Using FMM to accelerate the process of solving algebraic equations in boundary element, based on iterative algorithm, using fast algorithm of FMM and recursive operations of product tree structure to replace the matrix and the unknown vector algebra equations, it is no need to form the dominant. it effectively overcomes the disadvantages of traditional boundary element calculation, so it is suitable for solving large-scale problems.

In recent years, research of FMM is used to solve the acceleration of the traditional boundary element method [3-6], namely the establishment of the fast multipole boundary element method (Fast multipole boundary element method, FM-BEM), it is successful implementation of large-scale complex engineering problems on a personal computer for million degrees of freedom, such as electromagnetism problem [4], mechanics [5-6]. For example, Nishimura N and Yoshida K of University of Tokyo in Japan used to solve three-dimensional fracture problems [7-8]; research group of Yanshan University professor Shen Guangxian apply

doi:10.4304/jnw.9.1.108-114

multipole boundary element to mechanical engineering elasto-plastic contact problems [9]. In mechanical engineering, computational mechanics, computational mathematics and other fields, FM-BEM has high efficiency for numerical calculation, and it has very broad application prospects. This new concept of "Fast multipole BEM" has generated, it is bound with the "finite difference method," "finite element method", "boundary element method", as an important numerical analysis in 21st century, and will be further development and promotion.

Based on the fundamental solution of Laplace equation, the multipole boundary element should be used for 2D, 3D potential problems, the boundary integral equations of potential problems and the basic solution is presented, then gives the basic solution of FM-BEM; then gives the calculation program of FM-BEM and processing technology; finally, numerical calculation example verify the accuracy of FM-BEM, indicating that the FM-BEM computational efficiency compared with the traditional BEM has the order of magnitude improvement, it can effectively solve large-scale complex problems. This paper belongs to computational mathematics, boundary element method, potential problems, elasticity problems, and rolling theoretical research. the research is interdisciplinary with significant academic and practical significance, and it has broad application prospects in engineering.

II. Boundary Integral Equations of Potential Problems

In the 3D domain Ω, control equations and boundary conditions for the potential u and potential gradient q:

$$\nabla^2 u = 0 \ (\text{in } \Omega) \tag{1}$$

Boundary conditions:

The basic boundary conditions: $u = \bar{u}$ (in Γ_u)

The natural boundary conditions:

$$q = \frac{\partial u}{\partial n} = \bar{q} \ (\text{in } \Gamma_q) \tag{2}$$

∇^2 is the Laplace operator; u is called the potential, and it is usually said temperature, concentration, pressure, potential in specific issues. Along the boundary q is the normal derivative of u, a source body; $\Gamma = \partial\Omega = \Gamma_u + \Gamma_q$, Γ_u is the given boundary of potential (known as the essential boundary conditions), Γ_q is the gradient of potential for the given boundary (known as natural boundary condition), n is outside the normal of boundaries Γ, as shown in figure 1.

For complex boundary conditions, use the combination of the above two parameters to be marked as

$$\alpha u + \beta q = \gamma \tag{3}$$

In the formula, α and β are the correlation coefficients. The boundary integral equation form of formula (2. 1)

$$\begin{aligned} &c^i u^i(x) + \int_\Gamma q^*(x,y) u(y)\, d\Gamma \\ &= \int_\Gamma u^*(x,y) q(y)\ d\Gamma \end{aligned} \tag{4}$$

Among them, x is source point, y is the arbitrary boundary point on the boundary Γ, c^i shape coefficient, $u^*(x,y)$ and $q^*(x,y)$ are the basic solutions of three-dimensional potential problems, usually expressed as

$$u^*(x,y) = \frac{1}{4\pi R} \tag{5}$$

$$q^*(x,y) = \frac{\partial u^*(x,y)}{\partial n} \tag{6}$$

Among them, R is distance between the source point and observation point, n is the outside normal vector of boundary Γ.

The solution domain boundary is divided into boundary element, discrete boundary integral equations form linear algebraic equations, Introducing boundary conditions, rearrange the equations to format the final equation:

$$AX = B \tag{7}$$

A is a symmetric matrix; X is an unknown vector, B is a known variable. Solving the equation (7), we can obtain the boundary unknown variable.

When using the fast multipole algorithm, all the elements of the coefficient matrix A do not need to be calculated. For a fixed source, the contribution of the unit far away from the source to the source point, we can use fast multipole algorithm through the steps of polymerization, transfer, configuration to achieve. Only a small number of units adjacent to the source point, we should use the conventional boundary element to calculate.

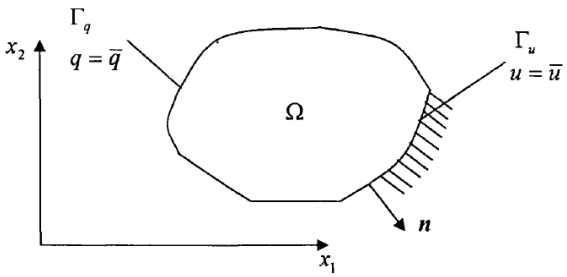

Figure 1. Schematic diagram of two-dimensional ordinary potential problems

III. The Basic Solution of FM-BEM

Multipole boundary element method can be set up, and the fundamental reason is that FMM can be applied to rapid calculating of BEM remote effects coefficient. Cross point lies in the basic solution decomposition. Through the research, we can discover that the formula of FMM to calculate the interaction potential in the set of a large number of particles can be abstracted as

mathematical formula $\sum_{i\neq j}\frac{c_i}{R_{ij}}$ (R_{ij} is distance between any two different particle charge, c_i is constant of particle charge electric), and the use of BEM to solve the potential problems of the boundary integral equation of discrete occasions, can be abstracted as mathematical formula $\sum_{i\neq j}\frac{c_i}{R_{ij}}$ (R_{ij} is distance between source and integral point, constant c_i is the influence coefficient between the source and the integral point) and its derivatives form. In BEM the core part of the boundary integral equation and its discrete form is the basic solution and related function, therefore, FMM will be applied to BEM and the key for the establishment of FM-BEM is that derive for BEM solutions and related form of kernel function for FMM, get formula related to FM-BEM.

Here, the corresponding FM-BEM solutions and related kernel function formula is derived for the potential problem, also derive first-order derivatives formula of $\sum_{i\neq j}\frac{c_i}{R_{ij}}$ and the corresponding Cartesian coordinate calculation formula in spherical coordinates

A. The Basic Solution of Cartesian Coordinates

At the point x^q , formula (2. 4) numerical integrals

$$\begin{aligned} &c^i u^i(x^q)+\sum_{k,l,s} q^*\left[x^q, y(\xi^s)\right]u^{kl}\varphi^l(\xi^s)J\left[y(\xi^s)\right]\omega^s \\ &-\sum_{k,l,s} u^*\left[x^q, y(\xi^s)\right]u^{kl}\varphi^l(\xi^s)J\left[y(\xi^s)\right]\omega^s=0 \end{aligned} \tag{8}$$

Among them, s is the integral point of unit, ω^s is integral weight function at ξ^s , $J\left[y(\xi)\right]$ is the Jacobi determinant.

By formula (8), the operation $\sum_{l,s}\varphi^l(\xi^s)J\left[y(\xi^s)\right]\omega^s$ for every unit area, the integral at all boundary points is invariant. If solving the equation by iteration method, u^{kl} and q^{kl} are assignment before the iteration, then in each iteration step, the product term $\sum_{k,l,s}u^{kl}\varphi^l(\xi^s)J\left[y(\xi^s)\right]\omega^s$ of each unit is a fixed value, similarly, the product $\sum_{k,l,s}q^{kl}\varphi^l(\xi^s)J\left[y(\xi^s)\right]\omega^s$ also has the same properties. The first sum term of the formula (8), Let

$$C_k^s=\sum_{k,l,s}u^{kl}\varphi^l(\xi^s)J\left[y(\xi^s)\right]\omega^s$$

For $q^*\left[x^q, y(\xi^s)\right]$, If it can be written as the function $1/R$, i. e.

$$q^*\left[x^q, y(\xi^s)\right]=f(x^q)(1/R)$$

Among them, x^q is the source point, $R=\left|x^q-y_c\right|$ is the distance between source point and the multipole center. Then first sum term of the formula (3.1) can be written as the follows,

$$\begin{aligned} &\sum_{k,l,s}q^*\left[x^q, y(\xi^s)\right]u^{kl}\varphi^l(\xi^s)J\left[y(\xi^s)\right]\omega^s \\ &=\sum_{k,s}f(x^q)(1/R)C_k^s \\ &=\sum_{k,s}f(x^q)(C_k^s/R) \\ &=f(x^q)\sum_{k,s}C_k^s/R \end{aligned} \tag{9}$$

Obviously, the sum term in formula (9) can be computed quickly by FMM. The second sum term in formula (8) the function $1/R$, without the need for decomposition, it can fast calculation by FMM. So, FMM can be used to solve the boundary integral equation with potential problems.

In order to make the fundamental solution $q^*(x,y)$ adapt to the the multipole expansion method, $q^*(x,y)$ will be decomposed into

$$\begin{aligned} q^*(x,y)&=\frac{\partial u^*(x,y)}{\partial n}=\frac{\partial}{\partial n}\left(\frac{1}{4\pi R}\right) \\ &=-\frac{1}{4\pi}\left[\partial_1\left(\frac{1}{R}\right)n_1+\partial_2\left(\frac{1}{R}\right)n_2+\partial_3\left(\frac{1}{R}\right)n_3\right] \end{aligned} \tag{10}$$

So, formula (8) can be rewritten as

$$\begin{aligned} &c^i u^i(x^q)-\frac{1}{4\pi}\partial_m \\ &\sum_{k,l,s}\frac{1}{\left|x^q-y_c\right|}\left\{u^{kl}\varphi^l(\xi^s)n_m\left[y(\xi^s)\right]J\left[y(\xi^s)\right]\omega^s\right\} \\ &-\frac{1}{4\pi}\sum_{k,l,s}\frac{1}{\left|x^q-y_c\right|}\left\{q^{kl}\varphi^l(\xi^s)J\left[y(\xi^s)\right]\omega^s\right\}=0 \end{aligned} \tag{11}$$

Because $m=1,2,3$, so the first sum term of the formula (8) call for multipole expansion 3 times, the second sum term of the formula (8) call for multipole expansion 1 times, for a total of 4 times.

x is column vector construct by the unknown potential and its derivatives.

B. The Basic Solution of Spherical Coordinate System.

FM-BEM theory is based on spherical coordinate system, therefore, we discuss basic solution form in the spherical coordinates. The core problem for the FMM applied to BEM is $\sum\frac{1}{r_{ij}}$ and its derivatives. In the specific implementation process, mainly manifests the form of partial derivatives for first order, two order in the local expansion

$$\Phi(X)=\sum_{j=0}^{\infty}\sum_{k=-j}^{j}L_j^k Y_{jk}(\theta,\varphi)r^j \tag{12}$$

In the formula (12), L_j^k is the expansion coefficients for the local, which is equivalent to the constant, so the problem is derivative for $Y_{jk}(\theta,\varphi)r^j$. Let

$$V = Y_{nm}(\theta,\varphi)r^n$$

$$= \sqrt{\frac{2n+1}{4\pi}\frac{(n-m)!}{(n+m)!}}P_n^m(\cos\theta)e^{im\varphi}r^n$$

$$C_n^m = \sqrt{\frac{2n+1}{4\pi}\frac{(n-m)!}{(n+m)!}} \tag{13}$$

After the strict derivation, and obtained the following results.

A fundamental solution for the potential problem relates to first order partial derivative of function 1/ R, in the first order partial derivatives, we first solve the gradient, and converts it into a rectangular coordinate form.

Firstly, solve the gradient for V

$$grda(V) = (v_r, v_\theta, v_\varphi) = \left(\frac{\partial V}{\partial r}, \frac{\partial V}{r\partial\theta}, \frac{\partial V}{r\sin\theta\partial\varphi}\right)$$

$$v_r = nr^{n-1}Y_{nm}(\theta,\varphi)$$

$$v_\theta = r^{n-1}C_n^m e^{im\varphi}\sin\theta\cdot$$

$$\left[|m|\cos\theta(\sin^2\theta)^{-1}P_n^{|m|}(\cos\theta) + |\sin\theta|^{-1}P_n^{|m|+1}(\cos\theta)\right]$$

$$v_\varphi = r^{n-1}C_n^m(\sin\theta)^{-1}P_n^{|m|}(\cos\theta)m\left[-\sin(m\varphi),\cos(m\varphi)\right]$$

The rectangular coordinate form of the first order partial derivatives: $\partial_i(V) = v_i\ (i = 1,2,3)$, in the Cartesian coordinate system, the first order partial derivative for V respectively as follows.

$$\partial_1(V) = v_1 = v_r\sin\theta\cos\varphi + v_\theta\cos\theta\cos\varphi - v_\varphi\sin\varphi$$

$$\partial_2(V) = v_2 = v_r\sin\theta\sin\varphi + v_\theta\cos\theta\sin\varphi + v_\varphi\cos\varphi$$

$$\partial_3(V) = v_3 = v_r\cos\theta - v_\theta\sin\theta$$

IV. The Basic Principle and Process of FM-BEM

Using the traditional boundary element method to solve, such as direct method and iterative method, the coefficient matrix of formula (7) needs to be stored and arithmetic formula. The basic principle of the fast multipole boundary element method is:

1) Using adaptive tree structure instead of the traditional matrix, ***A*** does not need to be explicitly stored, the information is hidden in a tree structure;

2) Based on the iterative method, the multiplication between coefficient matrix *A* and iteration vector *X* is instead by multipole expansion of basic solution approximation and tree structure in iterative process;

3) Computing and storage capacity of tree structure is *O (N).* Therefore if the iteration can converge rapidly, the amount of computation and storage of fast multipole boundary element method are approaching *O(N).*

The multipole expansion method and adaptive tree structure for basic solution of fast multipole boundary element method potential problems are explained below.

The fast multipole algorithm involves 4 steps key operation (Fig. 2) the multipole expansion, conversion between multipole moments (M2M), multipole moments to local moments (M2L) and the conversion between local moment (L2L).

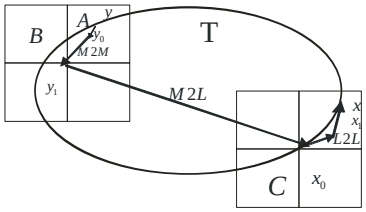

Figure 2. Key operation for fast multipole algorithm

A. Creating Adaptive Tree Structure

The operation mode of adaptive tree structure for fast multipole boundary element method includes the following steps:

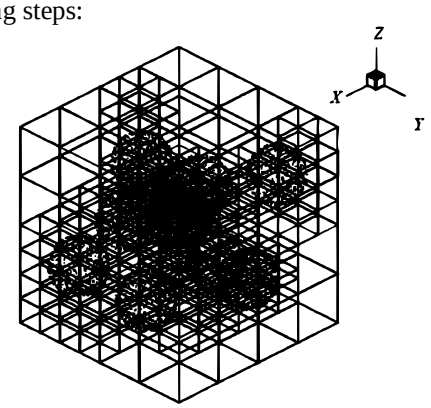

Figure 3. Three-dimensional tree structure

1) generating tree structure. Based on the 3D tree structure as an example, the solution domain is contained in a cube, on behalf of the root node of the tree structure; a large cube is decomposed into 8 sub - cube; cube further decomposition into smaller cubes, if the number of boundary element contained in cube less than a predetermined value, then stop decomposition.

2) upward traversal tree structure. The steps is used to calculate the multipole expansion coefficient of boundary element method for each leaf node.

3) downward traversal tree structure. The multipole expansion using the steps to calculate the coefficient of local expansion coefficient, interested readers see article [10].

4) using the tree structure to calculate the integral.

5) the iterative calculation. In each iteration step, by the tree structure to complete the operational equivalence matrix - vector product. Figure 3 is an example of 3D tree structure.

The fast multipole boundary element method use the storage structure of tree, each tree node includes adjacent boundary element. Generally speaking, the tree structure is the data structure of nonlinear and unbalanced, the task division of the tree structure and communication operations between the division tasks is complex than conventional matrix [11], this is the the main difficulties that fast multipole boundary element parallel format is different from the conventional boundary element.

The whole area is divided into NP task, where NP is usually a number of required processors for parallel calculation, division of the unit is a node of tree structure, division of the goal is to ensure each task contains a roughly the same number of units, but the classification method is that firstly sort boundary nodes on the tree structure and the unit in the boundary element method in accordance with the same spatial order, Then divided according to node, figure 4 shows the automatic generation diagram that of 3D problem into 4 task.

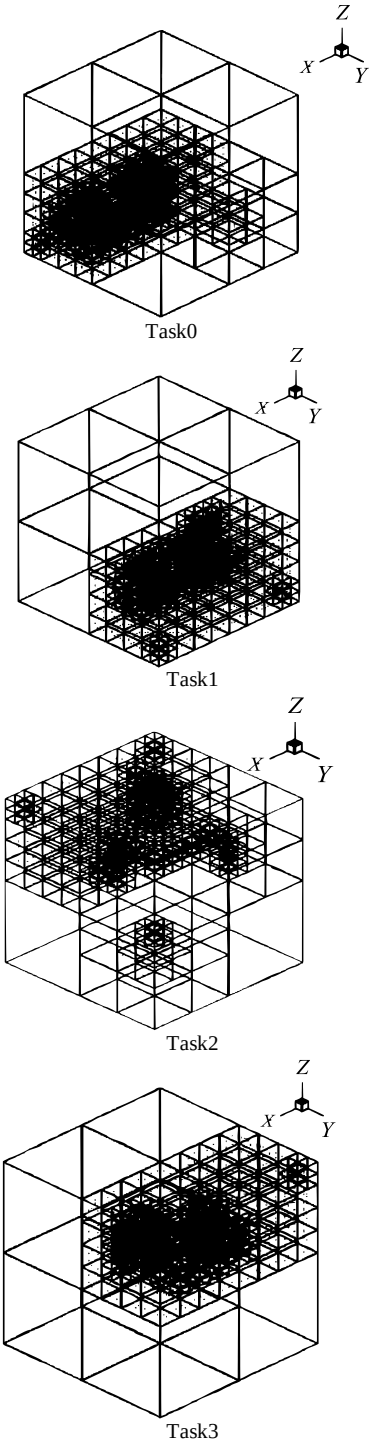

Figure 4. Task partition scheme of the tree structure

B. Calculation Procedures for Fast Multipole Boundary Element Method

The literature [11, 12] detailed description of the fast multipole boundary element method algorithm procedures, basic calculation process of this algorithm are as follows.

(1) the model boundary discrete unit by the traditional boundary element method.

(2) spanning tree structure. Contains all the boundary element model with a cube, on behalf of the root node of the tree structure; a large cube is decomposed into eight sub - cube; cube further decomposition into smaller cubes, if the number of boundary element contained in cube less than a predetermined value, then stop decomposition. This set contains the hierarchical tree structure of all boundary element, and it is used to store the multipole expansion coefficients and local expansion coefficient.

(3) Calculate multipole expansion coefficient with upward traversal. The steps is used to calculate the multipole expansion coefficient of boundary element method for each leaf node, start from the leaf nodes of the tree structure, recursive computation form a layer to a layer, until the root node.

(4) Calculate the local expansion coefficient with downward traversal. The multipole expansion using the steps to calculate the coefficient of local expansion coefficient, start from the root node of the tree structure, down recursive computation form a layer to a layer, until a leaf node.

(5) Calculate the integral using the tree structure.

(6) Iterative solution. In each iteration step, product of equation coefficient matrix and the unknown vector equivalence complete by the tree structure. The iterative process is repeated until the solution of the unknown variable converges to the reasonable accuracy, then the process ends, and we get the solution of the problem.

C. The Pretreatment Technology of Fast Multipole Boundary Element Method

Sometimes state of the coefficient matrix A formed by boundary element methods is not good, the coefficient matrix that the state is not good will lead to iterative convergence inefficient, even fail to converge, so the pretreatment of the coefficient matrix is crucial. The fast multipole boundary element algorithm uses the GMRES solver after pretreatment proposed by CHEN [13] in this paper, and combined with block diagonalization pretreatment technology for iterative solution of linear systems equations. this pretreatment technology has advantages, namely the generalized minimum residual method solver after pretreatment can store the used coefficients, and can be directly reused in the calculation of the near field contributions, so we do not have to repeat the computation of these coefficients in each iteration step, and it can accelerate the speed of iteration algorithm and improve the convergence efficiency. For large scale problems of N degrees of freedom, if the truncated term number p of multipole expansion boundary element method and number of units in each leaf node keep the set for a constant, the computational

complexity of the whole process of solving the fast multipole boundary element method is *O (N).*

V. NUMERICAL RESULTS

Examples 1: Laplace equation

$$\nabla^2 u = \frac{\partial^2 u}{\partial x^2} + \frac{\partial^2 u}{\partial y^2} = 0\,,\ (x,y) \in \Omega\,.$$

Set Ω is a square area:

$$\Omega = \{(x,y) | 0 < x < 6, 0 < y < 6\}$$

The following four straight line segments consists of the boundary Γ

$$\Gamma = \{(x,y) | x = 0,6, 0 \le y \le 6; y = 0,6, 0 \le x \le 6\}$$

The known boundary conditions:

$$u(x,y)\big|_\Gamma = \begin{cases} 300 & \Gamma = \{(x,y) | x = 0, 0 \le y \le 6\} \\ 0 & \Gamma = \{(x,y) | x = 6, 0 \le y \le 6\} \end{cases}$$

$$\frac{\partial u}{\partial n}(x,y)\big|_\Gamma = 0,\ \Gamma = \{(x,y) | y = 0,6, 0 \le x \le 6\}$$

Solve the potential on the boundary point and domain point value.

Results solved by the traditional BEM and FM-BEM by two methods are given below (see table 1).

TABLE I. POTENTIAL VALUE OF POINT (x, y)

coordinates (x, y) BEM FM-BEM Exact solutions
(1, 0) 252. 25 250. 02 250. 00
(2, 4) 200. 28 199. 98 200. 00
(3, 6) 150. 02 150. 01 150. 00
(4, 2) 99. 74 100. 01 100. 00
(5, 0) 47. 75 49. 99 50. 00
(5, 6) 47. 75 50. 02 50. 00

Seen from table 4.1, using FM-BEM to solve the potential problems, solutions are more accurate. Below we through examples show FM-BEM efficient.

Example 2: cube regional heat conduction. Cube side length is 2m, as shown in figure 4.1. the lower bottom surface temperature is 100 ℃, the upper bottom surface temperature is 0 ℃, the normal heat flux of other 4 sides is 0. Divided into 24 by 8 node quadrilateral quadratic unit, every square surface is divided into 4 units. Calculate interior point potential of angular point A (temperature).

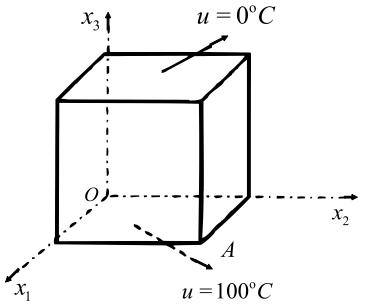

Figure 5. Heat conduction in a cub

As you can see from Figure 3, when the number of degrees of freedom $N > 2000$, the calculation results of FM-BEM and BEM compared with the analytical solution, the relative error is $\varepsilon < 0.2\%$, with the number of degrees of freedom increases, ε further reduced, thus, the truncation error introduced by multipole expansion and local expansion is very small. Figure 3clearly show that the accuracy of FM-BEM and BEM, are equivalent, demonstrated that the fast multipole boundary element method in this paper has high accuracy, meet the requirements of engineering calculations.

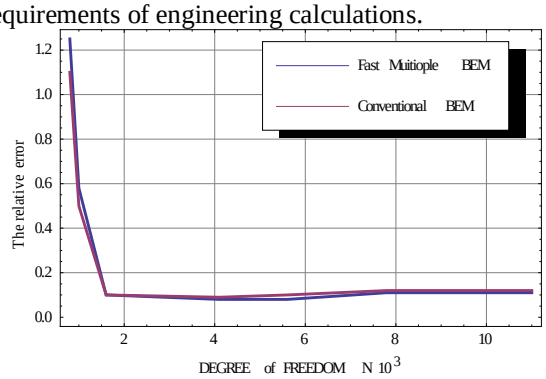

Figure 6. Calculation accuracy of FM - BEM and BEM

As you can see from figure 4, when the free degree reached 1000, computing speed of FM-BEM is faster than BEM; as the number of degrees of freedom increases, computational advantage of FM-BEM fully reflected, the calculation speed is much higher than that of BEM, effectiveness demonstrated that the computational efficiency of the FM-BEM is efficient.

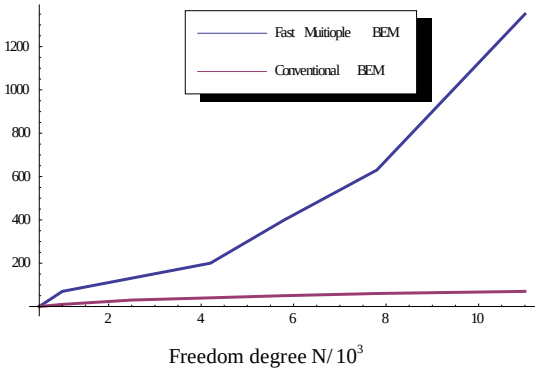

Figure 7. Calculation efficiency of FM - BEM and BEM

VI. CONCLUSIONS

In this paper, the fast multipole boundary element method is applied to solve the 3D potential problems, and do the numerical calculation. In the premise of ensuring high calculation accuracy, compared computation time and memory requirement with the conventional boundary element method. Numerical examples show that, the fast multipole boundary element method has the advantages of accuracy and efficiency, it is suitable to large scale numerical computing in the engineering.

ACKNOWLEDGMENT

This research was supported by the National Nature Foundation of China (Grant No. 61170317), the National Science Foundation for Hebei Province (Grant No. A2012209043) and Natural science foundation of

Qinggong College Hebei United University (Grant No. qz201205), all support is gratefully acknowledged.

REFERENCES

[1] Shen Guangxian, Xiao Hong, Chen Yiming. Boundary element method. Beijing: *Mechanical industry press*, 1998 pp. 26-129.
[2] Rokhlin V. Rapid solution of integral equations of classical potential theory. *Journal of Computational Physics*, 1985, 60(2) pp. 187-207.
[3] Yoshida K. Application s of fast multipole method to boundary integral equation method. *Kyoto: Kyoto University*, 2001.
[4] Chew W C, Chao H Y, Cui T J, et al. Fast integral equation solvers in computational electromagnetics of complex structures. *Engineering Analysis with Boundary Element*, 2003, 27(8) pp. 803-823.
[5] Liu Y J. A new fast multipole boundary element method for solving large-scale two-dimensional elastostatic problems. *International Journal for Numerical Methods in Engineering*, 2006, 65(6) pp. 863-881.
[6] Li Huijian, Shen Guangxian, Liu Deyi. Fretting damage mechanism occurred sleeve of oil-film bearing in rolling mill and multipole boundary element method. *Chinese Journal of Mechanical Engineering*, 2007, 43(1) pp. 95-99.
[7] Nishimura N, Yoshida K, Kobayashi S. A fast multipole boundary integral equation method for crack problems in 3D. *Engineering Analysis with Boundary Element*, 1999, 23 pp. 97-105.
[8] Yoshida K, Nishimura K, Kobayashi S. Application of new fast multipole boundary integral equation method for crack problems in 3D. *Engineering Analysis with Boundary Element*, 2001, 25 pp. 239-247.
[9] Shen Guangxian, Liu Deyi, Yu Chunxiao. Fast multipole boundary element method and Rolling engineering. *Beijing: Science press*, 2005 pp. 81-86, 185-193.
[10] Wang Haitao, Yao Zhenhan. A new fast multipole boundary element method for large scale analysis of mechanical properties in 3D particle-reinforced composites. *Computer Modeling in Engineering & Sciences*, 2005, 7(1) pp. 85-95.
[11] Ling Nengxiang. Convergence rate of E Ѣ estimation for location parameter function of one-side truncated fami1y under NA samples. *China Quartly Journal of Mathmatics*, 2003, 18(4) pp. 400~405.
[12] WU Chengjun, CHEN Hualing, HUANG Xieqing. Theoretical prediction of sound radiation from a heavy fluid-loaded cylindrical coated shell. *Chinese Journal of Mechanical Engineering*, 2008, 21(3) pp. 26-30.
[13] LIU Y J. A new fast multipole boundary element method for solving large-scale two-dimensional elastostatic problems. *International Journal for Numerical Methods in Engineering*, 2006, 65(6) pp. 863-881.
[14] Chen K, Harris P J. Efficient preconditioners for iterative solution of the boundary element equations for the three-dimensional Helmholtz equation. *Applied Numerical Mathematics*, 2001, 36(4) pp. 475-489.
[15] Cui Yuhuan, Qu Jingguo, Chen Yiming, Yang Aimin. Boundary element method for solving a kind of biharmonic equation, *Mathematica Numerica Sinica*, 34(1), pp. 49-56(2012. 2)
[16] Yuhuan cui, Jingguo Qu, Yamian Peng and Qiuna Zhang. Wavelet boundary element method for numerical solution of Laplace equation, *International Conference on Green Communications and Networks*, 2011/1/15-2011/1/17
[17] Lei Ting, Yao Zhenhan, Wang Haitao. Parallel computation of 2D elastic solid using fast multipole boundary element method. Engineering Mechanics, 2004, 21(Supp.) pp. 305~308.
[18] Lei Ting, Yao Zhenhan, Wang Haitao. The comparision of parallel computation between fast multipole and conventional BEM on PC CLUSTER. *Engineering Mechanics*, 2006, 23(11) pp. 28-32

Yuhuan Cui Female, born in 1981, Master degree candidate. Now he acts as the Math teacher in Qinggong College, Hebei United University. She graduated from Yanshan University, majoring computational mathematics. Her research directions include mathematical modeling and computer simulation, the design and analysis of parallel computation, elastic problems numerical simulation, and etc.

Jingguo Qu Male, born in 1981, Master degree candidate. Now he acts as the Math teacher in Qinggong College, Hebei United University. He graduated from Harbin University of Scince and Technology, majoring fundamental mathematics. His research directions include mathematical modeling and computer simulation, the design and analysis of parallel computation, elastic problems numerical simulation, and etc.

Research on Potential Problem based on Singular Decomposition and Boundary FM-BEM Algorithm

Chunfeng Liu
College of Science, Heibei United University, Tangshan, China
Email: qujingguo@163.com

Jingguo Qu and Yuhuan Cui
Qinggong College, Heibei United University, Tangshan, China

Aimin Yang
College of Science, Heibei United University, Tangshan, China

***Abstract*—In order to overcome the difficulties of low computational efficiency and high memory requirement in the conventional boundary element method for solving large-scale potential problems, a fast multipole boundary element method for the problems of Poisson equation is presented. First of all, through the multipole expansion and local expansion for the basic solution of the kernel function of the Poisson equation, the boundary integral equation of the fast multipole boundary element method for Poisson equation was obtained; secondly, the Laplasse transform is used for the Singularity processing treatment of Poisson equation; then, the realize the algorithm design of fast multipole boundary element method, the calculating flow of the algorithm is given; finally, a numerical example is given to verify the accuracy and the efficiency of the fast multipole boundary element method.**

***Index Terms*—Boundary Element Method; Fast Multipole Boundary Element Method; Poisson Equation; Laplace Transform; The Singular Decomposition**

I. INTRODUCTION

As a widely used numerical method of boundary element method, it has Characteristics of the lower dimension, high accuracy. But the coefficient matrix of equations formed by the traditional boundary element method is asymmetric matrix, so it has the very big restriction to the solving speed and scale. Full matrix equations are solved by using the direct method of traditional; the magnitude of the computation and storage respectively is the number of $O(N^3)$ and $O(N^2)$, Among them, a is the number of unknown variables, i.e. the number of degrees of freedom. Therefore, the traditional boundary element method is difficult to solve large-scale complex problems in engineering. In recent 20 years, the fast multipole algorithm (Fast Multipole Methods) [1] reduced the computation and storage of matrix vector multiplication operation at the same time, and the magnitude is with in $O(N)$. Under the error scope of controllable, the problem scale has improvement by orders of magnitude.

In recent years, research of FMM is used to solve the acceleration of the traditional boundary element method [2-4], namely the establishment of the fast multipole boundary element method (Fast multipole boundary element method, FM-BEM), it is successful implementation of large-scale complex engineering problems on a personal computer for million degrees of freedom, Such as mechanical engineering, computational mechanics, computational mathematics problems. research group of Tsinghua University Professor Yao Zhenhan successfully simulated the two-dimensional composite materials containing a large amount of elastic inclusions [5], two-dimensional solid [6] containing a large number of cracks and problem of three-dimensional static thin plate structure [7], and large-scale 3D elastic solid particle composites were simulated by a new adaptive scheme of FM-BEM [8]. Yanshan University professor Shen Guangxian research group completed the simulation of large-scale roll profile [9]; developing FM-BEM of elastic-plastic contact friction of a number of objects [10]; simulation temperature field of the mill work roll and bearing [11].

Fast multipole BEM will not form coefficient matrix, so it significantly reduce the amount of memory used. And memory requirements do not increase with the size of the increase, almost maintained at a low level. Traditional BEM rule contrary, due to the coefficient matrix rapidly becomes large with increasing degrees of freedom, resulting in rapid increase in memory usage. If the desired memory is more than the computer's physical memory, the operating system will enable the virtual memory of hard disk, because the transfer speed of hard disk is slower than physical memory, it will lead to decreased efficiency. The use of the fast multipole boundary element method, the demand for computer memory is small, and with the expansion of problems, the

doi:10.4304/jnw.9.1.115-122

increased memory demand is also slow. it create a sufficient condition for the computer to do large-scale operations. Computing efficiency, reduced memory usage and high accuracy will greatly strengthen the advantages of boundary element method and expand the application range of the boundary element method.

In mechanical engineering, computational mechanics, computational mathematics and other fields, FM-BEM has high efficiency for numerical calculation, and it has very broad application prospects. This new concept of "Fast multipole BEM" has generated, it is bound with the "finite difference method," "finite element method", "boundary element method", as an important numerical analysis in 21st century, and will be further development and promotion.

Based on the fundamental solution of the Poisson equation, this paper applies MBEM in potential problems, the main work are:

(1) the paper shows the boundary integral equations of potential problems and fundamental solutions, then give its FM-BEM fundamental solutions; in the calculation process of boundary element method, the kernel function need to decomposition, in the decomposition process of kernel function, when the distance is small between x and y, kernel function will produce singular integral, so the calculation is difficulties, some of the traditional method for solving singular integral are more complicated. this paper applies Laplace transform to the Boundary Element Method and gives a the three-dimensional potential Problems singularity approach based on multipole boundary element method.

(2) the paper gives the FM-BEM algorithm; Numerical examples are given to verify the accuracy of the FM-BEM, it shows that computational efficiency of FM-BEM has more magnitude improvement than traditional BEM. it can effectively solve large scale complex problems.

This paper belongs to computational mathematics, boundary element method, potential problems, elasticity problems, and rolling theoretical research. the research is interdisciplinary with significant academic and practical significance, and it has broad application prospects in engineering.

II. The Mode Establishment of Multipole Boundary Element Method

A. Poisson Equations

Poisson equation is the control equation of active filed potential problem; it is different from the passive field potential of Laplace equation. The source function is a function $b(x)$ with independent variable coordinates; it is the known function depended on the source point. Poisson equation as following:

$$\nabla^2 u = b \ (\text{in } \Omega) \tag{1}$$

Boundary conditions:

The basic boundary conditions: $u = \bar{u}$ (on Γ_u)

The natural boundary conditions:

$$q = \frac{\partial u}{\partial n} = \bar{q} \ (\text{on } \Gamma_q) \tag{2}$$

∇^2 is the Laplace operator; u is called the potential, and it is usually said temperature, concentration, pressure, potential in specific issues. Along the boundary q is the normal derivative of u, a source body; $\Gamma = \partial\Omega = \Gamma_u + \Gamma_q$, Γ_u is the given boundary of potential (known as the essential boundary conditions), Γ_q is the gradient of potential for the given boundary (known as natural boundary condition), n is outside the normal of boundaries Γ, as shown in figure 1.

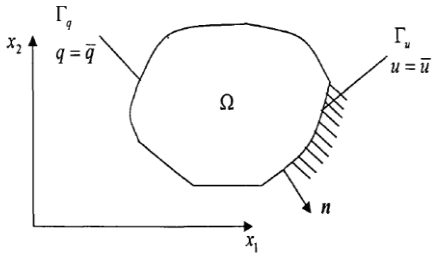

Figure 1. Schematic diagram of two-dimensional ordinary potential problems

B. The Establishment of Boundary Integral Equations

A limited region Ω, its surface boundary is Γ, the known potential surface is Γ_u, the potential gradient surface is Γ_q, and $\Gamma = \Gamma_u + \Gamma_q$, the boundary integral equation can be obtained for Poisson equation

$$\begin{aligned} &c^i u^i(x) + \int_\Gamma q^*(x,y) u(y)\, d\Gamma \\ &= \int_\Gamma u^*(x,y) q(y)\ d\Gamma - \int_\Omega u^*(x,y) b(x)\, d\Omega \end{aligned} \tag{3}$$

Among them, x is source point, y is the arbitrary boundary point on the boundary Γ, c^i shape coefficient, $u^*(x,y)$ and $q^*(x,y)$ are the basic solutions of three-dimensional potential problems, usually expressed as

$$u^*(x,y) = \frac{1}{4\pi|x-y|} = \frac{1}{4\pi R} \tag{4}$$

$$q^*(x,y) = \frac{\partial u^*(x,y)}{\partial n} \tag{5}$$

Among them, $q^*(x,y)$ is the derivative for $u^*(x,y)$ in the point x. R is distance between the source point and observation point. Formula (3) is the relationship between potential and potential gradient on the boundary, in accordance with the boundary integral conditions given, we can obtain all the unknown potential and potential gradient on the boundary. Then we can calculate the potential and potential gradient values in region interior point (for the steady temperature field, it is the temperature and temperature gradient).

C. The Discrete Form of the Boundary Integral Equations

Use the quadrilateral isoparametric discrete boundary to establish linear equations that the boundary values is unknown. Similarly, transform the problem of solving differential equations into algebraic equation about the unknown variables of nodes. Discrete form of formula (3)

$$\begin{aligned} &c^i u^i(x)+\sum_{j=1}^{N}\left(\int_\Gamma q^*(x,y)\,d\Gamma\right)u^j(y) \\ &=\sum_{j=1}^{N}\left(\int_\Gamma u^*(x,y)\,d\Gamma\right)q^j(y)-\int_\Omega u^*(x,y)b(x)\,d\Omega \end{aligned} \tag{6}$$

Isoparametric quadrilateral element, not only has a triangular element flexibility, but also keep the precision of rectangular element. With this unit, using node to establish matrix equation, the numerical solution has high precision. Especially in the practical problems encountered, often require the use of a few units to represent more complex forms of objects. In order to quadrilateral mapping to the corresponding rectangle, we must use the coordinate transformation. To establish correspondence relationship between the global and local coordinate.

By using surface coordinates (i.e. local coordinate system) describes the area increment in Cartesian coordinates for

$$\begin{aligned} d\Gamma &= \left|\frac{\partial r}{\partial \xi_1}\times\frac{\partial r}{\partial \xi_2}\right| d\xi_1 d\xi_2 \\ &= |G|\, d\xi_1 d\xi_2 \end{aligned}$$

Among them, G is the Jacobi matrix; the value of determinant $|G|$ as following

$$|G|=\sqrt{g_1^2+g_2^2+g_3^2}$$

Among them g_1, g_2, g_3 as follows

$$\begin{cases} g_1=\dfrac{\partial y}{\partial \xi_1}\cdot\dfrac{\partial z}{\partial \xi_2}-\dfrac{\partial y}{\partial \xi_2}\cdot\dfrac{\partial z}{\partial \xi_1} \\ g_2=\dfrac{\partial z}{\partial \xi_1}\cdot\dfrac{\partial x}{\partial \xi_2}-\dfrac{\partial z}{\partial \xi_2}\cdot\dfrac{\partial x}{\partial \xi_1} \\ g_3=\dfrac{\partial x}{\partial \xi_1}\cdot\dfrac{\partial y}{\partial \xi_2}-\dfrac{\partial x}{\partial \xi_2}\cdot\dfrac{\partial y}{\partial \xi_1} \end{cases}$$

Quadrilateral isoparametric element [12] can be described by a group dimensionless coordinate ξ_1, ξ_2 from -1 to 1 and the interpolation function φ_i. φ_i can be said for the bilinear function of ξ_1, ξ_2.

$$\begin{cases} \varphi_1=\dfrac{1}{4}(1-\xi_1)(1-\xi_2) \\ \varphi_2=\dfrac{1}{4}(1+\xi_1)(1-\xi_2) \\ \varphi_3=\dfrac{1}{4}(1+\xi_1)(1+\xi_2) \\ \varphi_1=\dfrac{1}{4}(1-\xi_1)(1+\xi_2) \end{cases} \tag{7}$$

Among them, ξ_1, ξ_2 is defined local coordinate in the quadrilateral unit, as shown in figure 2.

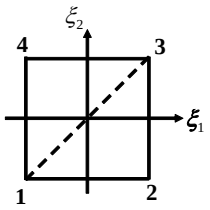

Figure 2. Quadrilateral element under local coordinate

The coordinates, potential and potential gradient of any point can be expressed by the element node,

$$x=\sum_{i=1}^{4}\varphi_i x_i\ ,\ y=\sum_{i=1}^{4}\varphi_i y_i\ \ z=\sum_{i=1}^{4}\varphi_i z_i$$

$$u=\sum_{i=1}^{4}\varphi_i u_i\ \ q=\sum_{i=1}^{4}\varphi_i q_i$$

Formula (7) is used for integral calculation on integral boundary, such as $\int_\Gamma u^* q d\Gamma$ and $\int_\Gamma q^* u d\Gamma$ become as follows

$$\int_{\Gamma_\xi} u^* q|G|\,d\xi_1 d\xi_2$$

$$\int_{\Gamma_\xi} q^* u|G|\,d\xi_1 d\xi_2$$

Let the influence coefficient of formula (6) as following

$$H_{ij}=\int_{\Gamma_j} q^*(x,y)d\Gamma$$

$$G_{ij}=\int_{\Gamma_j} u^*(x,y)d\Gamma$$

Considering the source point i is arbitrary, so

$$H_{ij}=\begin{cases} H_{ij} & j\neq i \\ H_{ij}+\dfrac{1}{2} & j=i \end{cases}$$

The domain integral item mark.

$$D^i=\int_\Omega u^*(x,y)b(x)\,d\Omega \tag{8}$$

For the boundary integral equation (6), discrete it, we can get the algebraic equations of potential and potential gradient

$$\begin{aligned} &c^i+\sum_{j=1}^{N}\hat{H}_{ij}(x,y)u_j(y) \\ &=\sum_{j=1}^{N}G_{ij}(x,y)q_j(y)-D^i \end{aligned} \tag{9}$$

The all unit nodes are as the source point, for the establishment of algebraic equations, the final matrix equation

$$HU=GQ-D \tag{10}$$

Then, using the known boundary conditions and transpose down into typical matrix equations, obtained the unknown boundary value.

As long as given the internal coordinates, the potential and potential gradient on the domain is calculated by following formula:

$$u^i(x,y)=\sum_{j=1}^{N}G_{ij}(x,y)q_j(y)-\sum_{j=1}^{N}\hat{H}_{ij}(x,y)u_j(y)-D^i \tag{11}$$

III. EXTENDED SOLUTION

The essence of fast multipole boundary element method is that multipole expansion of node clusters approximated boundary integral of kernel function and far field boundary variable product. The kernel function decomposition of Possion equation is as follows.

A. The Multipole Expansion of Basic Solutions

Theorem 1 (multipole expansion) supposed that there are N charge located in $X_1, X_2,\cdots,X_N$ and strength is $q_1, q_2,\cdots,q_N$, the spherical coordinate are respectively $(\rho_1,\alpha_1,\beta_1)$, $(\rho_2,\alpha_2,\beta_2)$, $\cdots$, $(\rho_N,\alpha_N,\beta_N)$ and $X_1, X_2,\cdots,X_N$ are located in ball which the center is at the origin and radius is a, see Fig.2. Thus, there is at any point $X=(r,\theta,\varphi)\in R^3$, when $r>a$, potential $\Phi(X)$ produced by charge $q_1, q_2,\cdots,q_N$ is as follows

$$\Phi(X)=\sum_{n=0}^{\infty}\sum_{m=-n}^{n}\frac{M_n^m}{r^{n+1}}\cdot Y_n^m(\theta,\phi)$$

$$M_n^m=\sum_{i=1}^{N}q_i\cdot\rho_i^n Y_n^{-m}(\alpha_i,\beta_i)$$

In addition, for any $p\ge 1$

$$\left|\Phi(X)-\sum_{n=0}^{\infty}\sum_{m=-n}^{n}\frac{M_n^m}{r^{n+1}}\cdot Y_n^m(\theta,\phi)\right|\le\left(\frac{\sum_{i=1}^{N}|q_i|}{r-a}\right)\left(\frac{a}{r}\right)^{p+1}$$

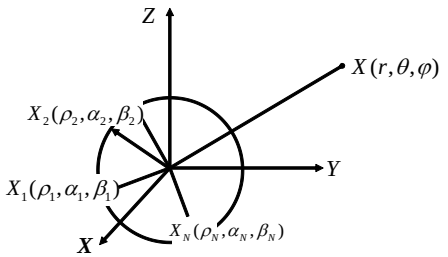

Figure 3. Multipole expansion

Proof: In Fig. 3, the origin of coordinates is O, set $X=(r,\theta,\varphi)$, $X_i=(\rho_i,\alpha_i,\beta_i)$. The distance between two points is

$$R_i=\|X-X_i\|=\sqrt{r^2+\rho_i^2+2r\rho_i\cos(\gamma)}$$

Among them, γ is the angle between the vector OX_i and OX.

Because $\rho_i\le r$, let $x=\cos(\gamma)$, $\mu=\rho_i/r$, so

$$\frac{1}{R_i}=\frac{1}{\sqrt{1-2\mu x+\mu^2}}=\frac{1}{r}\sum_{n=0}^{\infty}P_n(x)\mu^n=\sum_{n=0}^{\infty}P_n(x)\frac{\rho_i^n}{r^{n+1}}$$

And from the addition formula of Legendre function

$$P_n(x)=\sum_{m=-n}^{n}Y_n^{-m}(\alpha_i,\beta_i)Y_n^m(\theta,\phi)$$

Note

$$M_n^m=\sum_{i=1}^{N}q_i\cdot\rho_i^n Y_n^{-m}(\alpha_i,\beta_i)$$

so

$$\Phi(X)=\sum_{n=0}^{\infty}\sum_{m=-n}^{n}\frac{M_n^m}{r^{n+1}}\cdot Y_n^m(\theta,\phi)$$

Theorem 2 (local expansion) supposed that there are N charge located in $X_1, X_2,\cdots,X_N$ and strength is $q_1, q_2,\cdots,q_N$, the spherical coordinate are respectively $(\rho_1,\alpha_1,\beta_1)$, $(\rho_2,\alpha_2,\beta_2)$, $\cdots$, $(\rho_N,\alpha_N,\beta_N)$ and $X_1, X_2,\cdots,X_N$ are located in ball which the center is at the origin and radius is a, see Fig.4. Thus, there is at any point $X=(r,\theta,\varphi)\in R^3$, when $r<a$, potential $\Phi(X)$ produced by charge $q_1, q_2,\cdots,q_N$ is as follows

$$\Phi(X)=\sum_{j=0}^{\infty}\sum_{k=-j}^{j}L_j^k\cdot Y_j^k(\theta,\varphi)r^j$$

$$L_j^k=\sum_{l=1}^{N}q_l\frac{Y_j^{-k}(\alpha_l,\beta_l)}{\rho_l^{j+1}}$$

In addition, for any $p\ge 1$

$$\left|\Phi(X)-\sum_{j=0}^{p}\sum_{k=-j}^{j}L_j^k\cdot Y_j^k(\theta,\phi)r^{j+1}\right|\le\left(\frac{\sum_{i=1}^{N}|q_i|}{a-r}\right)\left(\frac{r}{a}\right)^{p+1}$$

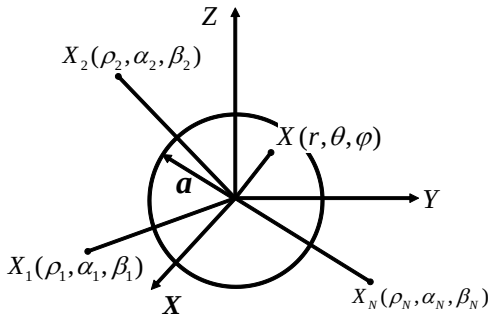

Figure 4. Local expansion

B. Translation of Multipole Expansion Coefficient of the Basic Solution.

The fast multipole method mainly includes two extension and three metastasis, the multipole expansion of th e basic solution, the multipole expansion metastasis coefficient (M2M), fast multipole expansion coefficient transfer to local expansion coefficient (M2L), transfer of local expansion coefficient (L2L). Specific transfer relationship is shown in Fig. 5.

1) Multipole Expansion

Let S_0 be a part of boundary S part away from the source point x. near the field y ,there is a point y_c and it meet $\left|\overrightarrow{y_c y}\right| < \left|\overrightarrow{y_c x}\right|$. Multipole expansion,,

$$\phi(x) = \frac{ik}{16\pi^2}\int T(k, \overrightarrow{y_c x})\, d^2 k \int_{S_0} e^{ik\overrightarrow{yy_c}}\, q(y) dS(y)$$

Then, the multipole expansion coefficient of y_c

$$M(k, y_c) = \int_{S_0} e^{ik\overrightarrow{yy_c}}\, q(y) dS(y) \tag{12}$$

2) Multipole Expansion Coefficients Metastasis (M2M).

When the multipole expansion center translate from y_c to y_c' nearby point y_c, then the multipole expansion coefficient of y_c'

$$M(k, y_c') = e^{ik\overrightarrow{y_c y_c'}}\, M(k, y_c) \tag{13}$$

This process is called M2M.

3) Local Expansion and Multipole Expansion to the Local Expansion Coefficient Metastasis

There is a point x_c near the source point x, and satisfy the condition $\left|\overrightarrow{x_c y}\right| > \left|\overrightarrow{x_c x}\right|$, so

$$\phi(x) = \frac{ik}{16\pi^2}\int e^{ik\overrightarrow{xx_c}}\, d^2 k \cdot L(k, x_c)$$

The local expansion coefficient

$$L(k, x_c) = T(k, \overrightarrow{y_c x_c})\, M(k, y_c) \tag{14}$$

formula (14) needs to meet the conditions $\left|\overrightarrow{yy_c}\right| < \left|\overrightarrow{y_c x}\right|$ and $\left|\overrightarrow{xx_c}\right| < \left|\overrightarrow{y_c x}\right|$. This process is called M2L.

4) Translation of Local Expansion Coefficient (L2L)

There is a point x_c' near the source point x ,, and satisfy the condition $\left|\overrightarrow{x_c' y}\right| > \left|\overrightarrow{x_c' x}\right|$,

Then the multipole expansion coefficient of x_c'

$$L(k, x_c') = e^{ik\overrightarrow{x_c x_c'}}\, L(k, x_c) \tag{15}$$

This process is called L2L.

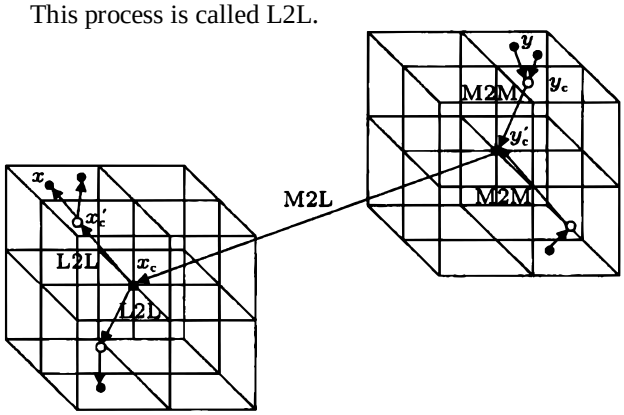

Figure 5. M2M, M2L and L2L transfer relationship of fast multipole method

IV. Singularity Resolution of Poisson Equations

Definition 1: (Laplace transform) if the function $f(t)$ is defined in real variable $t \geq 0$, the integral exits for some given s (here s is complex number)

$$\int_0^\infty e^{-st} f(t)\, dt = \lim_{T\to\infty}\int_0^T e^{-st} f(t)\, dt$$

So the following formula is called Laplace transform of the function $f(t)$

$$F(s) = \int_0^\infty e^{-st} f(t)\, dt \tag{12}$$

In the formula (12), when the original function $f(t)$=1, image function

$$F(s) = \int_0^\infty e^{-st} f(t)\, dt = \int_0^\infty e^{-st}\, dt = \frac{1}{s}$$

The domain for $F(s)$ is $\mathrm{Re}\, s > 0$. When $s = R$, $\int_0^\infty e^{-Rt}\, dt = \frac{1}{R}$, The Gauss numerical integration for $\int_0^\infty e^{-Rt}\, dt$ as follows.

$$\int_0^\infty e^{-Rt}\, dt \approx \sum_{i=1}^{n} \omega_i t_i R$$

Among them, t_i is Gauss integral point, ω_i is the weight function of different precision.

Applying Laplace transform in place multipole boundary element method (bem) of potential problems, the corresponding singularity processing method is given.

Theorem 1 The boundary integral equation of Poisson equation

$$c^i u^i(x) + \int_\Gamma q^*(x, y) u(y)\, d\Gamma$$

$$= \int_\Gamma u^*(x, y) q(y)\, d\Gamma - \int_\Omega u^*(x, y) b(x)\, d\Omega$$

When the distance between x and y is very small, it will produce singular integral, kernel function $u^*(x, y)$ and $q^*(x, y)$ at this time can be decomposed into

$$u^*(x, y) = \frac{1}{4\pi}\sum_{i=1}^{n} \omega_i t_i (x - y)$$

$$q^*(x, y) = \frac{1}{4\pi}\sum_{i=1}^{n} \omega_i t_i \left[\frac{\partial(x-y)}{\partial x_1} n_1 - \frac{\partial(x-y)}{\partial x_2} n_2\right]$$

Proof: when the distance between x and y is very small, the distance is smaller than a given threshold, the kernel function $u^*(x, y)$ and $q^*(x, y)$ at this time can be decomposed using Laplasse transform:

$$u^*(x, y) = \frac{1}{4\pi R} = \frac{1}{4\pi(x - y)}$$

$$= \frac{1}{4\pi}\sum_{i=1}^{n} \omega_i t_i (x - y)$$

$$q^*(x, y) = \frac{\partial u^*(x, y)}{\partial n} = \frac{\partial\left[\frac{1}{4\pi}\sum_{i=1}^{n} \omega_i t_i (x - y)\right]}{\partial n}$$

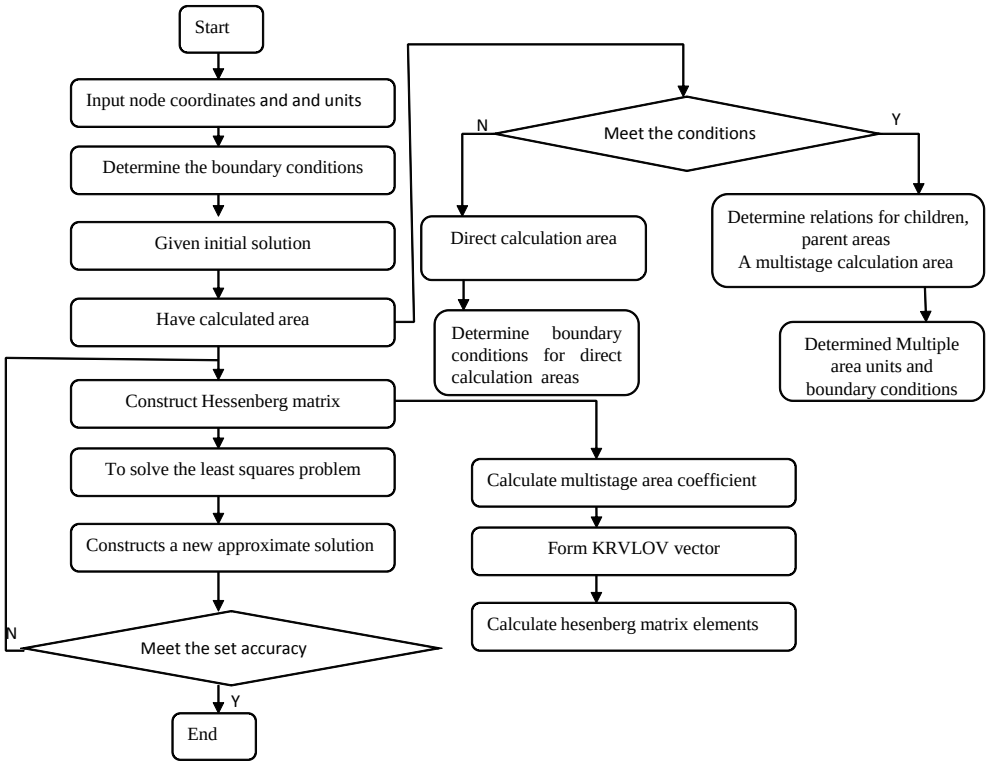

Figure 6. Computational procedure

$$= \frac{1}{4\pi}\sum_{i=1}^{n}\left[-\omega_i t_i \frac{\partial(x-y)}{\partial n}\right]$$

$$= \frac{1}{4\pi}\sum_{i=1}^{n}-\omega_i t_i\left[\frac{\partial(x-y)}{\partial x_1}n_1 - \frac{\partial(x-y)}{\partial x_2}n_2\right]$$

Through Laplace transformation and Gauss numerical integral, the items $1/R$ of kernel function can be transformed into $\sum_{i=1}^{n}-\omega_i t_i (x-y)$, thus avoiding the singularity when x is very close to y , so it improves the computational efficiency, and reduces the calculation time.

V. The Realization of the FM-BEM Algorithm

A. The Design of FM-BEM Algorithm

For simplicity, the following agreement on the multipole expansion, local expansion coefficient: $\left\{M_n^m\right\}$ is expansion coefficient for the far field, $\left\{L_n^m\right\}$ is expansion coefficient of near field; partition area calculation level of each level region can be expressed as

$$n = A^l, \left(l = 0,1,\cdots,l_{\max}; A = \begin{cases}4, surface\\ 8, space\end{cases}\right).$$

Border FM-BEM algorithm is given below.

Step 1: initialization: take $l_{\max}$, p , for example $l_{\max}=3$, $p=4$,

Step 2: on $A^{l_{\max}}$ small areas, expansion coefficient $\left\{M_n^m\right\}_{[l_{\max}],[n]}$, $n=1,2,\cdots,A^{l_{\max}}$ of the far field are formed in the center,.

Step 3: select the current level $l=l_{\max}-1$, the current calculation region i

DO $l=l_{\max}-1,\cdots,0$

DO $i=1,\cdots,A^l$

Far field expansion coefficients for its parent region are calculated by far field expansion coefficients of current region through the use of "multipole expansion translation". Method: the calculation of A sub regional center $\left\{M_n^m\right\}_{[l_{\max}],[n]}$ on current regional, use" multipole expansion translation", get the $\left\{M_n^m\right\}_{[l],[i]}$ of parent regional center on current regional.

ENDDO

ENDDO

Step 4: select the current level $l=l_{\max}-1$, the current computational domain i , calculate local regional expansion of each sub region for each level. Use $\tilde{\Psi}_{l,i}$ to express regional role from regional i .

Let $\tilde{\Psi}_{0,1}=0$, $\tilde{\Psi}_{1,i}=0, i=1,\cdots,A^l$

DO $l=2,\cdots,l_{\max}-1$

DO $i=1,\cdots,A^l$

Using the "transform of multipole expansion to local expansion ", calculate near field expansion coefficient $\left\{L_n^m\right\}_{[l],[i]}$ of region $W-S$ by far field expansion coefficient of the region i , add them to $\tilde{\Psi}_{1,i}$.

ENDDO

DO $i=1,\cdots,A^l$

Using the "local expansion translation", Near field expansion coefficients $\left\{L_n^m\right\}_{[l+1],[j]}$ of its sub regional centers are calculated by near field expansion coefficient $\left\{L_n^m\right\}_{[l],[i]}$ of the region i .

ENDDO

ENDDO

Step 5: calculate regional interaction of level $l_{\max}-1$

DO $i=1,\cdots,A^{l_{\max}}$

Using "multipole expansion translation", calculate near field expansion coefficients $\left\{L_n^m\right\}_{[l_{\max}],[j]}$ for the region $W-S$ by the far field

translation coefficient $\left\{M_n^m\right\}_{[l_{\max}],[i]}$ of current area, add them to $\tilde{\Psi}_{A^{l_{\max}},i}$, obtain local expansion $\Psi_{A^{l_{\max}},i}$ in current area i.

ENDDO

Step 6: calculate Φ_{far} of all points P_j in the area i (the points in region $W-S$ of points P_j and regional i), denoted as $\tilde{\Psi}_{l_{\max},i}\left(P_j\right)$

DO $i=1,\cdots,A^{l_{\max}}$

$\tilde{\Psi}_{l_{\max},i}\left(P_j\right)$

ENDDO

Step 7: calculate Φ_{near} of all points P_j in the area i (the role of point P_j, region i and its neighbor, the next nearest neighbor points t), denoted as $\Psi_{l_{\max},i}\left(P_j\right)$

DO $i=1,\cdots,A^{l_{\max}}$

$\tilde{\Psi}_{l_{\max},i}\left(P_j\right)$

ENDDO

Step 8: calculate $\Phi\left(P_j\right)$ for all points P_j in the current area

$$\Phi\left(P_j\right)=\Phi_{far}+\Phi_{near}=\tilde{\Psi}_{l_{\max},i}\left(P_j\right)+\Psi_{l_{\max},i}\left(P_j\right)$$

B. Calculation Process of FM-BEM

According to the above algorithm, we developed FORTRAN source program, the flow chart of calculation is shown as Fig. 6.

VI. NUMERICAL EXAMPLES

Example 1: consider the following linear boundary value problem of Possion equation in a square region $\Omega=\left\{(x,y)\middle| x\in[0,1],\ x\in[0,1]\right\}$:

$$\begin{cases}\Delta u(x,y)+\dfrac{\partial u}{\partial y}=2y+x^2\\ u(0,y)=0\\ u(1,y)=y\\ u(x,0)=0\\ u(x,1)=x^2\end{cases}$$

Use boundary element method to solve, the calculated results are compared with the exact solutions; table 1 gives the potential value of the point part of the numerical solution and the exact solution.

TABLE I. THE POTENTIAL VALUE OF THE POINT PART OF THE NUMERICAL SOLUTION AND THE EXACT SOLUTION

(x,y)	FM-BEM	exact solution
(0.0, 0.0)	0.0002	0.0000
(0.25, 0.25)	0.0157	0.0156
(0.25, 0.5)	0.3126	0.3125
(0.25, 0.75)	0.0467	0.0469
(0.5, 0.25)	0.0626	0.0625
(0.5, 0.5)	0.1250	0.1250
(0.5, 0.75)	0.1876	0.1875
(0.75, 0.25)	0.1407	0.1406
(0.75, 0.5)	0.2812	0.2813
(0.75, 0.75)	0.4219	0.4219
(1.0, 1.0)	1.0001	1.0000
(1.0, 0.25)	0.2501	0.2500

It can be seen from table 1, solution error is very small, and we got the desired result.

Example 2: the infinite prism of a rectangular section, temperature conditions on the boundary is shown as Fig.7, determine the temperature and heat flux values, the results are shown as Table 2 and Table 3.

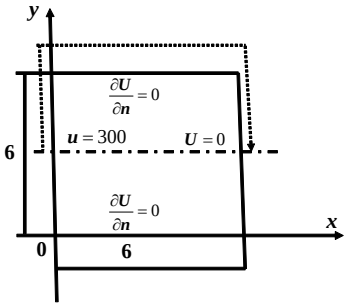

Figure 7. The problem of temperature field

TABLE II. TEMPERATURE VALUE

(x,y)	The analytical solutions	BEM	FM-BEM
(1,0)	250.00	252.20	250.04
(3,0)	150.00	150.18	149.98
(5,0)	50.00	47.85	50.02
(2,2)	200.00	200.24	199.99
(4,2)	100.00	98.80	99.98
(4,4)	100.00	98.85	100.02
(2,4)	200.00	200.11	200.03

TABLE III. HEAT FLUX

(x,y)	The analytical solutions	BEM	FM-BEM
(6,1)	-50.00	-51.96	-50.06
(6,3)	-50.00	-48.98	-49.97
(6,5)	-50.00	-51.25	-51.09

The above is comparison of BEM and FM-BEM from the calculation accuracy, the following comparison is from the computational efficiency of the two methods, see Fig.8. As you can see in Fig.8, when the freedom degree reached 3000, computing speed of FM-BEM is faster than BEM; as the number of freedom degrees increases, computational advantage of FM-BEM fully reflected, the calculation speed is much higher than that of BEM, it demonstrated that the computational efficiency is level $O(N)$ of the FM-BEM.

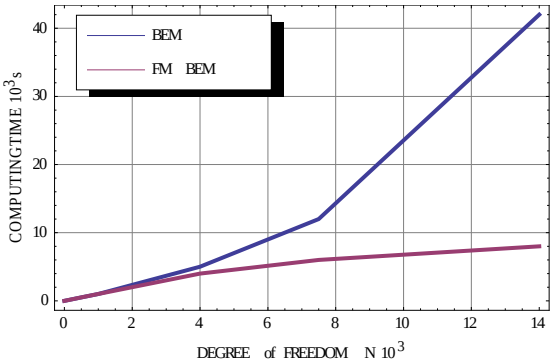

Figure 8. Calculation efficiency of FM - BEM and BEM

As you can see in figure Fig. 9, when the free degree reached 3000, with the increase of degree of freedom, the fast multipole boundary element method for the storage capacity is far lower than the conventional boundary element method. This shows that, the fast multipole

boundary element method has higher storage efficiency than the traditional boundary element method. From the curve trend in Fig.8, the relationship between storage and degrees of freedom of the fast multipole boundary element method and the traditional boundary element method are respectively $O(N)$ and $O(N^2)$ magnitude. The numerical examples demonstrated that the $O(N)$ magnitude calculation efficiency of fast multipole boundary method has higher calculation efficiency than that of the traditional boundary element method.

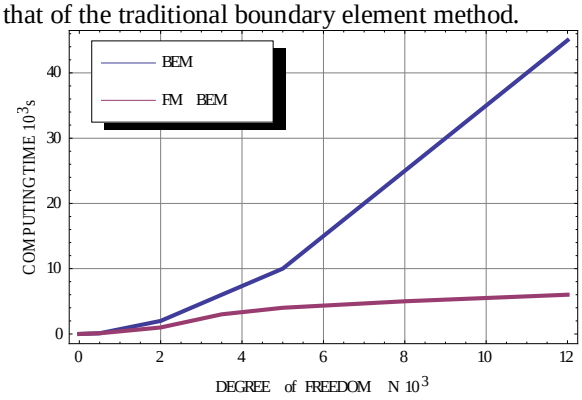

The number of degrees of freedom N/ 10^3

Figure 9. Storage comparison of FM-BEM and BEM

VII. CONCLUSIONS

This paper applies the FM-BEM to boundary integral equations of three-dimensional potential problems, discretes boundary integral equation, deals discrete singular integral term, and conduct the numerical calculation. In the premise of high accuracy, compare the computation time and memory requirements with conventional boundary element method. The example shows that fast multipole boundary element method has the advantages of accuracy and efficiency, suitable for large-scale engineering numerical calculation.

ACKNOWLEDGMENT

This research was supported by the National Nature Foundation of China (Grant No. 61170317) and the National Science Foundation for Hebei Province (Grant No.A2012209043), all support is gratefully acknowledged.

REFERENCES

[1] Greengrad L, Rokhlin V. A fast algorithm for particle simulations. *J Comput Phys*, 1987, 73 pp. 325 348.

[2] YOSHIDA K. Application s of fast multipole method to boundary integral equation method. *Kyoto: Kyoto University*, 2001.

[3] LIU Y J. A new fast multipole boundary element method for solving large-scale two-dimensional elastostatic problems. *International Journal for Numerical Methods in Engineering*, 2006, 65(6) pp. 863-881.

[4] LI Huijian, SHEN Guangxian, LIU Deyi. Fretting damage mechanism occurred sleeve of oil-film bearing in rolling mill and multipole boundary element method. *Chinese Journal of Mechanical Engineering*, 2007, 43(1) pp. 95-99.

[5] H. T. Wang, Z. H. Yao. Simulation of 2D Elastic Solid with Large Number of Inclusions Using Fast Multipole BEM. Proc. of the Second M. I. T. Conference on Computational Fluid and Solid Mechanics. *Boston, U. S. A.*, 2003

[6] WANG Pengbo, YAO Zhenhan, WANG Haitao. Fast Multipole BEM for Simulation of 2-DSolids Containing Large Numbers of Cracks. *Tsinghua Science & Technology*, 2005, 10(1) pp. 76-81

[7] ZHAO Libin, YAO Zhenhan. Fast Multipole BEM for 3-D Elastostatic Problems withApplications for Thin Structures. *Tsinghua Science & Technology*, 2005, 10(1) pp. 67-75

[8] Haitao Wang, Zhenhan Yao. Large Scale Simulation of 3D Particle-Reinforced Composites Using Fast Multipole Boundary Element Method. *COMPUTATIONAL MECHANICS, Proc. of the WCCM VI in conjunction with APCOM'04.*, 2004 pp. 709-714

[9] LIU Deyi, SHEN Guangxian. 3-d elastic fast multipole boundary element method. Journal of computational mechanics, 2004, 21(4) pp. 464-469

[10] LIU Deyi, SHEN Guangxian. Multipole BEM for 3-D Elasto-Plastic Contact with Friction. Tsinghua Science & Technology, 2005, 10(1) pp. 57-60

[11] Yan Yinling. Three-dimensional potential field fast multipole boundary element method. [*Yanshan university master degree theses of master of engineering*]. 2005 pp. 56-63

[12] Li Weite. Quadrilateral element parameters, such as its application in solving the temperature field. *Journal of engineering thermal physics*. 1995, 16(3) pp. 338-343

[13] Cui Yuhuan, Qu Jingguo, Chen Yiming, Yang Aimin. Boundary element method for solving a kind of biharmonic equation, *Mathematica Numerica Sinica*, 34(1), pp 49-56(2012. 2)

[14] Yuhuan cui, Jingguo Qu, Yamian Peng and Qiuna Zhang. Wavelet boundary element method for numerical solution of Laplace equation, *International Conference on Green Communications and Networks*, 2011/1/15-2011/1/17

[15] Jingguo Qu, Zuting Zheng, Yuhuan Cui, Linan Shi. Study of Prediction of Motor Vehicles Emission Pollutants Concentration in Urban Street. *International Journal of Digital Content Technology and its Applications*, V6, N16, 2012

Modified Hungarian Algorithm for Real-Time ALV Dispatching Problem in Huge Container Terminals

Bian Zhicheng, Mi Weijian, Yang Xiaoming, and Zhao Ning
Logistics Research Center, Shanghai Maritime University, Shanghai, China

Mi Chao*
Container Supply Chain Tech. Engineering Research Center, Shanghai Maritime University, Shanghai, China
*Corresponding Author, Email: chaomi@shmtu.edu.cn

***Abstract*—It is a fundamental decision making process in container terminals to allocate container transporting works among ALVs. Nowadays, container terminals tend to be larger in storage space and more efficient in handling. As a result, estimations of ALV travel times could be inaccurate, the scale of ALV work allocation could be quite large, and a fixed handling sequence could be hardly ensured beforehand. Hence, it is presented a real-time dispatching method, consisting of an allocation model for instantaneous ALV dispatching, and a set of events which trigger a new instantaneous dispatching. A modified Hungarian Algorithm is applied to solve the instantaneous dispatching model, and it is verified that the modified Algorithm outperforms the original one, even CPLEX, in solving these allocation problems.**

***Index Terms*—Real-Time ALV Dispatching; Huge Container Terminal; Allocation Model; Hungarian Algorithm**

I. INTRODUCTION

Nowadays, following the trend of jumbo ships, container terminals are changing gradually so that they could serve larger ships. CMA-CGM has brought into uses several ships of 16000 TEUs, and Maersk will receive even larger container ships, with capacity up to 18000 TEUs, in the coming 2 years. It could be foreseen that, ships with capacity of no less than 16000 TEUs will be the mainstream on the main shipping lines between continents and, on shipping lines all over the world, larger ships will be used. Therefore, container terminals are seeking for larger storage capacity and higher handling efficiency. For instance, the Port of Singapore Authority (PSA) is designing new container terminal to be used in the following decades, able to hold 160,000 TEUs at least, and to achieve a throughput of 20 million TEUs per annum. Besides, construction of new terminals and renovation of current ones are ongoing in several ports worldwide.

In this paper, huge container terminal refers to terminals able to deal with jumbo ships, especially those ships with a capacity of no less than 16000 TEUs. Besides the features of large storage capacity and high handling efficiency, in huge container terminals, the vehicle traffic is to enter into the storage area. As in the current automated container terminals (ACT), container blocks are arranged as strips, which are disposed in one row, all with one end closed to the berth line, and the other end away from it. In each block it is deployed an Automated Stacking Crane (ASC), which moves along the block strip, collecting a container from one end to some staking position in the block, or retrieving a container reversely (See Figures in [3-5, 7, 11, 15-16], and the left part of Fig. 1). Hence, the vehicle traffic is limited between the quayside and the storage area. However, things are different in huge container terminals. In order to cope with the high efficiency of Quay Cranes (QC), it is required that the response time of ASC is short enough, hence the length of block strips have to be limited, so that ASCs won't waste much time on travelling. Accordingly, more than one row of blocks are in need, otherwise the total storage capacity would be insufficient. As a result, vehicles have to run into the storage area to serve the blocks away from the berth line, and a mesh-like traffic topology comes into being. Fig. 1 gives a comparison on vehicle traffics between the current automated container terminals and huge ones.

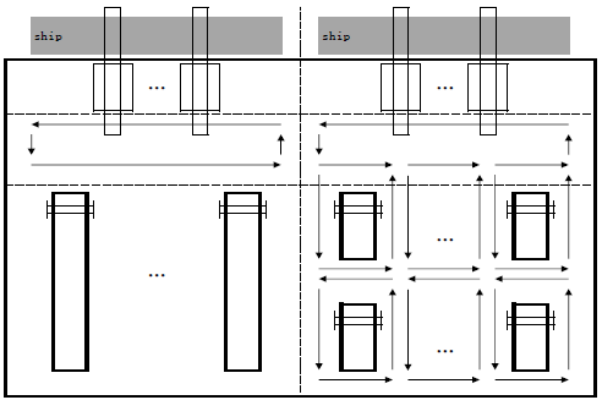

Figure 1. Comparison of vehicle traffic between current automated container terminals and huge container terminals

doi:10.4304/jnw.9.1.123-130

Automated Lifting Vehicles (ALV) is a common vehicle transporting containers between the QCs and ASCs in ACTs. This vehicle is able to pick up and put down a container by itself, without the help of cranes. Accordingly, in a container handling system using ALVs, there is almost no need for cranes to wait for a tardy vehicle, or for vehicles to wait for a tardy crane vice versa. As a result, the QCs and ASCs could concentrate on container handling process. It is widely recognized that, container handling systems using ALVs, rather than some other vehicles, is more likely to reach a higher total handling efficiency.

ALVs follow a pick-up and delivery process in transporting containers between cranes. It is defined as a work that, transporting a container from a QC to an ASC during unloading a ship, or from an ASC to a QC during loading a ship. A work comes if some crane, QC during unloading process or ASC during loading process, has decided the container to be handled next. This container is to be caught up, and released to some handling point, on the ground near the crane. As soon as the work comes, some ALV isto be dispatched to this work. This ALV moves to the handling point, pick the container up and carries it to the destination crane. The work is finished when the container is put down on the handling point of the destination crane.

There are three difficulties in allocating works among ALVs in huge container terminals, as listed below.

Estimations of ALV travel times could be inaccurate. In a mesh-like traffic topology, vehicles are likely to be slowed down or stopped temporarily at intersections, and the speed of a vehicle could be limited if there is another vehicle ahead. Considering that the travel distances in huge container terminals may be much longer than in current ones, ignorance of this inaccuracy may make a great reduction to the performance of handling system.

The scale of ALV work allocation problem could be very large. The ALVs working simultaneously in a huge container terminal could be numerous. Thanks to the high efficiency of cranes, works come frequently in huge container terminals. In view of the inaccuracy in travel time estimation, it must be permitted that; one work allocated to some ALV could be allocated again to some other ALV without load, as far as the container is actually picked up. If so, the original ALV will be dispatched for some other work. Therefore, the works to be dispatched could be also numerous. The large problem scale required a fast speed to the method used in allocation.

A fixed handling sequence could be hardly ensured beforehand. In the work plans of container terminals, containers to be handled are divided into groups. It is pre-determined the handling order among groups, but not the order of containers in the same group. Cranes always decide the next container to be handled according to the working condition. In case that a new work arrives, the allocation must be executed once again, otherwise no ALV is to take this work. Hence, it is required that the allocation method is real-time, which could be repeated if necessary.

In this paper, it is presented a real-time ALV dispatching method, which calls for no pre-determined work sequence, and is capable of dealing with the inaccuracies in travel time estimation. An allocation model is proposed for instantaneous dispatching, which allocates only works that have come and have not been picked up. A set of trigger events is also proposed so that the instantaneous dispatching could be executed whenever needed. A modified Hungarian Algorithm is used to find the solution of an instantaneous dispatching. It is verified that this modified Algorithm could find a solution very quickly, even if the problem scale reaches up to one hundred. The rest of this paper is arranged as follows. A literature review is given in Section 2. Detailed description to the instantaneous allocation model and trigger events are laid in section 3. The modified Hungarian Method is presented in section 4, as well as the results of numerical experiments. A conclusion is drawn in section 5.

II. Related Work

Dispatching and scheduling are both methods allocating container transporting works to vehicles. The difference lays in the information needed to carry out the allocation. A predictive work sequence, both with the arrival times of works, is required to carry out a scheduling. Accordingly, it is outputted by a scheduling when and which work to take for every vehicle. Yet no predicted arrival time, or even the specific order of coming works, is required for dispatching. Hence, the output of a dispatching includes only relationship between works and vehicles.

Vehicle dispatching problem and vehicle scheduling proble mare fully researched in container terminals. Dirk Briskron [3] described two formulations of the Automated Guided Vehicle (AGV) dispatching problem in container terminals, one considering due times and the other not, based on the idea that estimations on operation times may be often unreliable. Results from simulation shows that the model excluding due times leads to higher productivity. In addition, he proposed a simulation model for the seaside processes at automated container terminal [4], and compared two different AGV dispatching strategies. Martin Grunow [5] presented a simulation study of AGV dispatching strategies in a seaport container terminal, and it is compared on-line and off-line dispatching strategies. With traffic congestions neglected, the conclusion drawn from simulation results in this paper may be not convictive enough. Ebru K. Bish [6] proposed models and heuristic algorithms for vehicle dispatching problems for a single crane and multiple cranes respectively, in assumption that a set of vehicles are assigned for one ship, and the work sequence is pre-determined, which is not always the case in practice. Nguyen V D [7] proposed a mixed-integer programming model for the ALV dispatching problem in an automated container terminal. Similarly, some impractical assumptions are laid, such as the sequence of loading and unloading works is pre-determined, the cranes are always available for containers, and congestions of vehicles are

not considered. Panagiotis Angeloudis [8] proposed a dispatching model and algorithm structured on a cost/benefit concept, according to unreliable information from terminal operations. An approach as measurement to terminal uncertainties is presented as well, and it is proved that the model and algorithm works better in lower uncertainty level. Loo Hay Lee [9] makes similar assumptions as in literature [7], aside from the one that handling times of cranes are taken into consideration. It is proposed a mixed integer programming model to treat the vehicle dispatching for job sequences of multiple cranes, and a heuristic to solve the problem. Unfortunately, it could be referred from experiments that, in case the number of cranes and works are large, the computation time will be very long. Hassan Rashidi [10] defined and formulated the AGV dispatching problem as a Minimum Cost Flow model, and get it solved using a modified network simplex method. Several impractical assumptions are made such as the work sequence is pre-determined, no collisions, live-lock or dead-lock exists in transportation, and travel times between two points are provided. Binghuang Cai [11] seeks into the Straddle Carrier (SC) scheduling problem, which is treated as a Pickup and Delivery Problem with Time Windows, and a branch-and-bound based algorithm is used for solution. The traffic layout of Patrick Auto Strad container terminal is abstracted as network, and the travel times of a vehicle between two points is assumed deterministic. Riadh Moussi [12] studied the Lifting Vehicle (LV) scheduling problem at container terminal of Normandy in Le Havre port. Alike SCs, LVs are vehicles which could lift a container itself, while responsible for stacking and retrieving containers in storage yards as well. An integer programming model is built, based on assumptions including congestion-free traffic and fixed vehicle speed and travel distance. It is developed a generic algorithm, which is compared with simulating annealing algorithm in solving the problem. Hoai Minh Le [13] formulated the vehicle dispatching problem as a mixed integer programming model. It is proposed an algorithm combining DCA and branch-and-Bound method to solve the model. Wang Yuan [14] addressed an integrated vehicle dispatching problem in container terminals, and built a simulation platform to compare and evaluate different dispatching rules used in real time dispatching. Bradley Skinner [15] presents a GA-based optimization approach to solve the SC scheduling problem for container handling in the Patrick Auto Strad Terminal. The deterministic mathematical model is extended from a former one, and the proposed approach has been fully implemented in terminal operation. HamdiDkhil [16] presented a 0-1 integer programming model to resolve the planning of QC-AGV-ASC as a whole, under three different terminal layouts. It is verified that the algorithm is able to get a schedule of handling 500 containers in 1 minute.

Though great efforts has been devoted to the research of vehicle scheduling and dispatching problems in container terminals, some defects still exist, as listed below.

1. It could not always be pre-determined a definite work sequence in the near future. Even though a stowage plan is made, the actual sequence of unloading and loading is decided according to the working condition. Therefore, the assumption of predictable work sequence is impractical.

2. It is hard to make an accurate estimation of the actual travel times in huge container terminals. The velocity of vehicles may be slowed down when another vehicle is running ahead, or when it is passing some intersection. Hence, the assumption of fixed travel times between handling points is impractical, especially in huge container terminals.

3. It is worthy of discussion that, whether the time windows of works are to be considered during allocation. Thanks to the handling points in which containers could be stacked temporarily, tardiness of neither crane nor ALV have great impact on the handling efficiency of the whole handling system. However, considering the time windows, it will be rather time-consuming to solve allocation problems in large scales.

4. To the best of our knowledge, a practical real-time ALV dispatching method for huge container terminals has not been mentioned yet.

III. Problem Description

In this section, it is proposed a real-time dispatching method for ALV work allocation in huge container terminals. It is used an event-driven method [18-20], which consists of an allocation model for instantaneous dispatching, and a set of events which triggers a new instantaneous dispatching. Apart from the method, some details of ALV dispatching are also described, as is written below.

A. Some Details in ALV Dispatching

The scale of instantaneous ALV dispatching is related to the form of production organization in container terminals, that is, if an ALV could be dispatched to works from or to different QCs, or different ships. In case that the transporting works are separated by QCs, one ALV could only take works from or to one QC, and the scale of dispatching could be rather small. In case that works are separated by ships, one ALV could take works from QCs which are handling the same ship, and the scale of dispatching may be larger. In case that no separation is made, and one ALV could take works from all the QCs at the terminal, the scale of dispatching is likely to be very large. Generally, larger the dispatching scale is, the more time is needed to make a dispatching plan.

In view of the high efficiency of QCs and long travel distances in huge container terminals, pre-dispatching is an effective measure in keeping a high handling efficiency of the whole handling system. Some ALVs will be pre-dispatched to QCs unloading a ship, but with no work to take. These ALVs runs to the handling point of the QC it has been pre-dispatched, and waits there for a coming work. Once a container was put into the handling point of a QC with pre-dispatched ALVs, itcould be picked up quickly, freeing some space of the handling point. The pre-dispatching measure decreases

the possibility that the unloading process of some QC is interrupted since its handling point is full.

B. The Allocation Model for Instantaneous Dispatching

The assumptions of the model is listed below

1. The number of ALVs assigned for QCs are sufficient roughly. It occurs not very often that the number of containers waiting to be picked up far exceeds the number of ALVs which could be dispatched.

2. Only one ALV is pre-dispatched to one QC when unloading some ship.

3. An ALV transports one container at a time.

The notations used are listed below.

C A set of containers which has been caught by some spreader, and not picked up by ALV.

c The total number of elements in set ***C***.

Q A set of QCs which is unloading a ship.

q The total number of elements in set ***Q***.

d The number of works to be considered in an instantaneous dispatching, added up by the number of containers to be transported, and some QCs which is to be pre-dispatched an ALV.

A A set of ALVs which could be dispatched to containers in ***C***.

a The total number of elements in set A.

i The index of works, $i = 1, 2, ..., c + q$.

j The index of ALVs, $j = 1, 2, ..., a$.

v_j The instantaneous velocity of ALV j.

d_{ij} The travel distance between ALV j to the point of work i.

T A matrix of estimations on travel times of ALV j to the position of work i, depending on the distance and instantaneous velocity.

t_{ij} elements in matrix T.

m An extreme large number, as upper limitation to the time estimation of travel time.

x_{ij} The decision variables of the problem.

The objective of the model is to minimize the total estimated times spent on travelling to the works:

$$Min \sum_{i=1}^{d} \sum_{j=1}^{a} t_{ij} x_{ij} \tag{1}$$

i.e.

$$\sum_{i=1}^{d} x_{ij} \le 1 \tag{2}$$

$$\sum_{j=1}^{a} x_{ij} \le 1 \tag{3}$$

$$\sum_{i=1}^{d} \sum_{j=1}^{a} x_{ij} = d \tag{4}$$

$$d = \begin{cases} c, & a \le c \\ a, & c < a \le c + q \\ c + q, & a > c + q \end{cases} \tag{5}$$

$$t_{ij} = \begin{cases} Min(d_{ij} / v_j, m), & v_j > 0 \\ m, & v_j = 0 \end{cases} \tag{6}$$

$$x_{ij} = \begin{cases} 0, \text{ALV } i \text{ is dispatched to work } j \\ 1, \quad \text{otherwise} \end{cases} \tag{7}$$

Equation (2) is to ensure that every container transporting work or pre-dispatching is allocated to no more than one ALV. Equation (3) is to ensure that every ALV could be dispatched to no more than one container or QC. Equation (4) is to make as much dispatches as possible. Equation (5) gives priority to container transportation works over pre-dispatch works. Equation (6) is an estimation of the travel time if ALV j is dispatched to work i, depending on the travel distance and instant velocity of vehicle. Equation (7) formulates the decision variable of the model.

C. The Set of Trigger Events for a New Dispatching

A new instantaneous dispatching is triggered by a set of events, related to the arriving and finish of container transportation works, and the velocity fluctuation of ALVs. It is used a fixed time interval Δt, at the end of which the instant velocity of all vehicles dispatched is checked. Moreover, it is adopted a velocity scope $[v_j^-, v_j^+]$ for ALV j, depending on the instant velocity at the time of the last dispatching. In case that the instant velocity of some ALV at the end of a time interval exceeds this range, a new instantaneous dispatching is executed.

In summary, anew instantaneous dispatching is executed on either of the following events.

1. A container is caught by the spreader of some crane and is to be transported.

2. An ALV has just finished its last work.

3. At the end of some interval, the instant velocity of some ALV goes beyond the velocity scope determined in the last dispatching.

IV. PROPOSED SCHEME

Hungarian Algorithm (*HA*) is a famous algorithm for the classical assignment problem [17], and it really works on the model proposed in this paper. As for the instant dispatching problems in huge container terminals, the scope of the matrix ***T*** may be larger than one hundred, and the elements in the matrix is likely to be closed to each other. It is found that, in such matrices, the computational time using *HA* may be extremely long. Hence, it is presented a Modified Hungarian Algorithm (*MHA*) which we thought suitable especially for the instant dispatching model.

A. Hungarian Algorithm and the Defect

Before *HA* is used, the time estimation matrix T should be changed at first, into a square matrix by adding fake ALVs or transporting works. In case a container is dispatched with a fake ALV, no ALV is actually to take this container; in addition, the ALVs dispatched to fake containers are to go back to the parking area. In the algorithm, container works is listed in columns, and

ALVs is listed in rows. The notations used in the Algorithm are listed below.

N the scale of the problem, where $N = Max(d,a)$.

$\boldsymbol{X}$ the matrix consisting of x_{ij}, which is defined in section 3.2.

u_i the dual decision variable of row$i$.

v_j the dual decision variable of column$j$.

c_{ij} the cost of row$i$ if assigned to column$j$.

$\boldsymbol{C}$ the matrix consisting of c_{ij}.

q_{ij} correlation variables. Ifrow$j$ is "qualified" forcolumn$i$, then $q_{ij} = 1$; else $q_{ij} = 0$.

$\boldsymbol{Q}$ the matrix consisting of q_{ij}.

Approximately, *HA* could be divided into 5 steps in general, identified from step 1 to 5 as follows. A loop cycle lies between step 2 and 4, in which the qualified matrix $\boldsymbol{Q}$ is justified step by step, till a best solution is found.

Step 1: Initialize the dual variables u_i for each row and v_j for each column.

Step 2: Determine the matrix $\boldsymbol{Q}$. The elements q_{ij} is decided as following.

$$q_{ij} = \begin{cases} 1, c_{ij} = u_i + v_j \\ 0, \quad else \end{cases} \tag{8}$$

Step 3: Assign as many rows to those qualified columns as possible, which means the Equation (9) and (10) are kept. This process is done using an initial assigning approach, and another point-based approach to ensure that the number of rows assigned to qualified columns reaches the maximum [17]. If all the N rows are assigned to some column, then go to step 5; else, go to step 4.

$$\forall i, \prod_j (1 - q_{ij}) + \sum_j q_{ij} x_{ij} = 1 \tag{9}$$

$$\forall j, \prod_i (1 - q_{ij}) + \sum_i q_{ij} x_{ij} = 1 \tag{10}$$

Step 4: Justify the dual variables, and go to step 2.

Step 5: Record the assignment scheme and end the algorithm.

As presented in literature [17], step 3 is achieved by seeking for augmenting paths using a point-based search method. This method starts from a qualified point in a column with no row assigned to it, searching repeatedly in row for an assigned point then in column for a qualified but not assigned point. In case that the point found finally lies in a row with no column assigned, an augmenting path could be determined by backtracking the points found. The number of assignment achieved could be added by one, if the assigned points are set unassigned, and the unassigned points are set assigned along the augmenting path. The maximum number of assignments is reached, only if no more augmenting path could be found in the matrix.

Although effective, this points based search method may be time consuming owing to large number of points recorded during the searching process. Forillustration, an experiment is designed, in which 2000 random generated instances are solved using HA, in which it is collected their execution times (*time*, in seconds), the iteration times (*iter*), and the numbers of points recorded (*pn*), respectively. Following this, the averages of these four indexes are calculated, and the three instances with largest execution times are listed out. The elements in these instance matrices are generated between 0 and 100 following uniform distribution. The experiment is carried out 3 times, each with the problem scale (N) set 50, 100, and 150. The algorithm is coded using SIMPLE++, and the experiments of this paper are all run on a Dell precision 4600 laptop in Windows XP. The results are shown in Fig. 2 – 4, and Table I.

TABLE I. THREE INSTANCES WITH LONGEST EXECUTION TIMES DURING THE EXPERIMENTS USING *HA*

N	No.	time [s]	iter	pn
50	Avg	0.07	8.03	441.8
	1st	0.39	13	1476
	2nd	0.28	12	1416
	3rd	0.25	13	1901
100	Avg	0.37	5.50	1607.4
	1st	13.4	8	58048
	2nd	9.64	5	43109
	3rd	9.56	7	47608
150	Avg	5.09	4.32	15859
	1st	783.7	5	2563798
	2nd	235.9	5	716383
	3rd	200.3	5	594466

The figures and table tell that:

1. It is undoubted that the execution time is linear with the number of points recorded during solution process. The more points recorded, the longer execution time will be. Moreover, this linear relation seems stronger when the elements are closer to each other.

2. There are some hard instances, whose solution time and number of promising points recorded exceeds the average level quite a lot. This time gap, as well as the number of promising points recorded, increases while the problem scale becomes larger and larger.

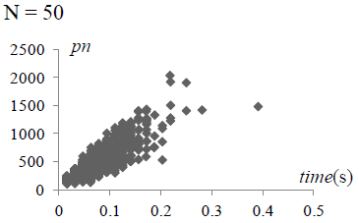

Figure 2. Experimental results using HA with random instances when

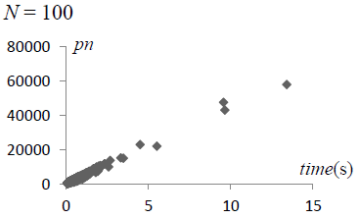

Figure 3. Experimental results using HA with random instances when

It could be concluded from the results of the experiment that, due to the massive records the point-based search may leaveduring solving process, *HA* is inadequate to ensure against extreme long execution time. For the purpose that a solution could be ensured in a

reasonable time limitation, a procedure with fewer records is recommended.

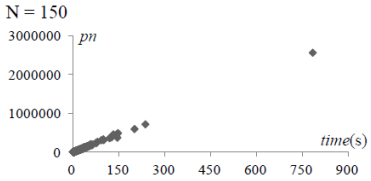

Figure 4. Experimental results using HA with random instances when

B. The Modified Hungarian Algorithm and the Performance

In order to keep the computation time in control, it is raised an edge labeling method used in searching for augmenting paths. Owing to the one-to-one assignment between rows and columns, this method records every time a promising edge, either a row or a column, rather than a promising point. Following this method, the amount of records needed when searching for augmenting paths may decline, for the reasons listed below.

1. Only the promising edges are given a character string as a record, no matter how many promising points lay in them. In the point-based searching, in case no augmenting path is found from a promising point, the search moves on to the next following promising point in the same column, and extra records will be made. However, no extra search is to be executed, if using an edge labeling method. During a search process, each edge is recorded only once.

2. In each step of iteration, the records irrelevant to any augmenting paths were kept by the edge labeling method, and could be used again in the following steps, rather than cleared and valued again. Hence, the total amount of records made during the whole solving process reduces.

A label string for some edge, row or column, consists of an edge index and several segments. The edge index indicates whether the label is derived from a row (valued "R") or from a column (valued "C"). The segments are used to trace possible routes for augmenting paths. Each segment contains an integer that is recorded as string format, and a "_" following it. A label string could be lengthened by adding extra segments behind it. In case an unassigned qualified point could be found in a labeled column, an augmenting path could be determined by tracing those correlative label strings. Otherwise, similar searching procedure is carried out from rows, after which the dual variables are justified according to the labels.

TABLE II. ILLUSTRATION OF THE EDGE LABELING METHOD

Label		C1_2_		C1_	
	1*	0	0	0	0
C1_2_	0	1*	0	1	0
	0	0	0	0	1*
	0	1	0	0	0
	0	0	1*	0	0

Table II and III gives a simple example of finding augmenting path and justifying the solution using this method. String labels are recorded in the first row and the first column in Table 2, while it is presented in the rest of the table a 5 order matrix ***Q***. An asterisk in coordinate (x,y) means row x is assigned to column y. In this example, an augmenting path could be found easily chasing the edge labels, following the elements with gray background.

TABLE III. SOLUTION JUSTIFIED ALONG AUGMENTING PATH

1*	0	0	0	0
0	1	0	1*	0
0	0	0	0	1*
0	1*	0	0	0
0	0	1*	0	0

TABLE IV. JUSTIFYING DUAL VARIABLES ACCORDING TO LABELS

Label	R1_2_			C1_2_	C1_	u_i
R1_2_	0*	4	2	7	4	0
	0	0*	1	5	5	0
	5	3	0*	2	3	0
C1_2_	3	6	9	0*	0	0
R1_	0	2	3	4	2	0
v_j	0	0	0	0	0	

TABLE V. SOLUTION FOUND AFTER JUSTIFICATION

Label	R1_2_			C1_2_	C1_	u_i
R1_2_	0*	4	2	7	4	0
	0	0*	1	5	5	0
	5	3	0*	2	3	0
C1_2_	3	6	9	0*	0	-2
R1_	0	2	3	4	2*	0
v_j	0	0	0	2	2	

Table IV and V gives a simple example of justifying dual variables according to the labels, so as to find a solution. In the 5 order matrix in the center of the Table IV, the dual variables are all 0, and at most 4 assignment could be found. The dual variables with a label started by "C" are to be justified with the minimal difference, among values in the grey grids subtracted by corresponding dual variables. After the justification, a solution could easily be found, as is shown in Table V.

In order to illustrate the effectiveness of the edge labeling method, similar experiments are conducted as described in section 3.1 is conducted. *MHA* is executed to solve 2000 randomly generated instances, in scale of 50, 100 and 150 respectively. The results are shown in Fig. 5 – 7, and in Table IV.

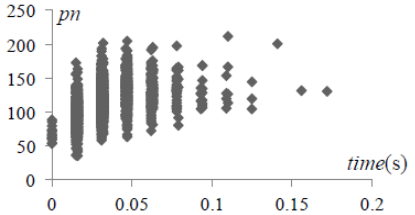

Figure 5. Experimental results using MHA with random instances when N = 50

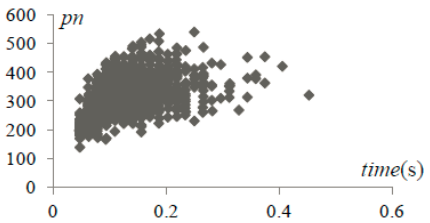

Figure 6. Experimental results using MHA with random instances when N = 100

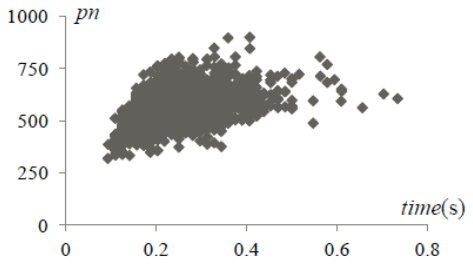

Figure 7. Experimental results using MHA with random instances when N = 150

Table VI is conclusive evidence that the edge labeling method is effective. The gap using *MHA* between average execution time and extreme long execution time is brought closer, and the average execution time is shortened in half roughly, compared to *HA*.

TABLE VI. THREE INSTANCES WITH LONGEST EXECUTION TIMES DURING THE EXPERIMENTS USING *MHA*

N	No.	time [s]	iter	pn
50	Avg	0.03	13.1	117.4
	1st	0.17	13	131
	2nd	0.16	12	132
	3rd	0.14	20	201
100	Avg	0.12	11.3	317.3
	1st	0.45	12	320
	2nd	0.41	15	420
	3rd	0.38	12	362
150	Avg	0.23	10.6	560.9
	1st	0.73	12	605
	2nd	0.70	11	627
	3rd	0.66	10	561

In order to validate that *MHA* is able to solve the hard instances met while using *HA* much faster, another experiment is designed here. First it is collected using *HA* 50 instances, in the solution process of which the number of points recorded reaches *Mpn*. Then these instances are solved again using*MHA*, and the solving times of these two algorithms (in seconds) are compared in table VII. The experiments are carried out in scale of 50, 100 and 150 respectively.

TABLE VII. COMPARISON BETWEEN *HA* AND *MHA* IN SOLVING SOME HARD INSTANCES

N	Mpn	HA		MHA	
		Avg[s]	Max[s]	Avg[s]	Max[s]
50	1000	0.174	0.312	0.064	0.125
100	8500	2.967	16.92	0.166	0.562
150	100000	139.442	2048.27	0.125	0.266

The results show that the hard instances met using *HA* could be solved with *MHA* in a reasonable time limit successfully and this limit won't increase sharply as the problem scale grows. It is proved that *MHA* outperforms *HA* due to shorter average and maximum execution time of hard instances.

C. Comparison using MHA to CPLEX

In order to test further the performance of *MHA*, it is conducted some extra comparative experiments, in which *MHA* is compared with CPLEX, by solving randomly generated instances in different scales. Suppose that the elements in the matrices are integral random numbers between 0 and *M*, and the scale of a matrix is *N*. In this experiment, *N* is first valued 50, 100, 150 and 200 sequentially, and in each case, M is valued *N*, 2*N*, 3*N*, and 4*N*, respectively. For each set of *N* and *M*, 50 random matrices are generated and solved, each using *MHA* and CPLEX, while the average solving time and the average iteration times of the former two is recorded. The results are shown in Table VIII and Fig. 8 – 11.

TABLE VIII. COMPARISON OF MHA AND CPLEX IN SOLVING MATRICES WITH RANDOM ELEMENTS

N	M	avg time[s]	
		MHA	CPLEX
50	50	0.031	0.234
50	100	0.045	0.253
50	150	0.051	0.326
50	200	0.064	0.263
100	100	0.144	0.323
100	200	0.199	0.346
100	300	0.219	0.389
100	400	0.265	0.357
150	150	0.324	0.474
150	300	0.436	0.498
150	450	0.537	0.529
150	600	0.633	0.503
200	200	0.581	0.781
200	400	0.870	0.719
200	600	1.023	0.740
200	800	1.329	0.765

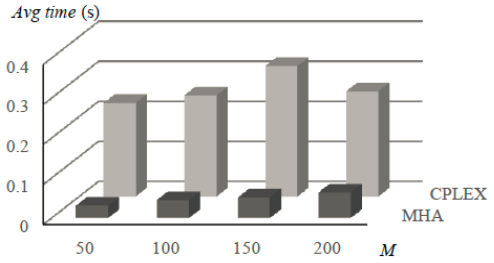

Figure 8. Average execution times when N = 50

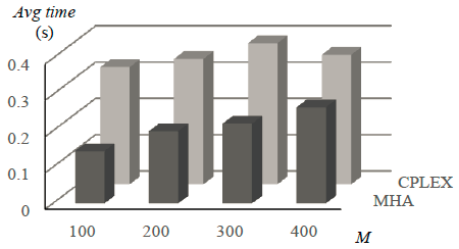

Figure 9. Average execution times when N = 100

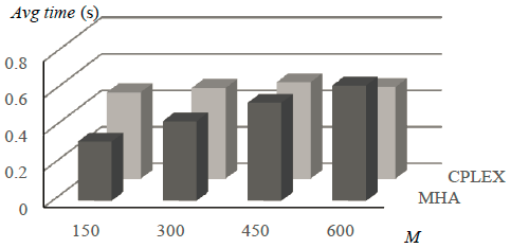

Figure 10. Average execution times when N = 150

It is obvious from the results of the experiments that, *MHA* outperforms CPLEX in solving matrices in the ALV dispatching problems at huge container terminals.

The computation times are shorter in scale of less than 200, and, the closer elements are to each other, the sharper the advantage seems.

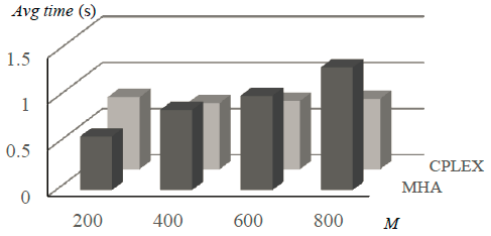

Figure 11. Average execution times when N = 200

V. CONCLUSION

According to the characteristics in huge container terminals, this paper proposed a real-time vehicle dispatching model for the ALV dispatching problem. This model consists of a simple allocation model which makes an instantaneous ALV dispatching, and a set of trigger events, on which a new instantaneous dispatching is executed. Owing to the features that the scale of the problem may be large and the elements in the problem matrix are often closed to each other, a modified Hungarian Algorithm is applied to solve the problem. Experiments are conducted to verify the effectiveness of the modified algorithm in solving this problem. Future research could be concentrated in the implementation of this real-time ALV dispatching method.

ACKNOWLEDGEMENT

This research is supported by Excellent Doctoral Dissertation Cultivation project of Shanghai Maritime University, Shanghai Maritime University Foundation (20120104) and Young University Teachers' Training project of Shanghai Education Commission.

REFERENCE

[1] Steenken D, Voß S, Stahlbock R, Container terminal operation and operations research-a classification and literature review. *OR spectrum*, Vol. 26, No. 1, pp. 3-49, 2004

[2] Stahlbock R, Voß S. Operations research at container terminals: a literature update. *OR Spectrum*, Vol. 30, No. 1, pp. 1-52, 2008

[3] Briskorn D, Drexl A, Hartmann S. Inventory-based dispatching of automated guided vehicles on container terminals. *OR Spectrum*, Vol. 28, No. 4, pp. 611-630, 2006

[4] Briskorn D, Hartmann S. Simulating dispatching strategies for automated container terminals. Operations research proceedings 2005. *Springer Berlin Heidelberg*, pp. 97-102, 2006

[5] Grunow M, Günther H O, Lehmann M. Strategies for dispatching AGVs at automated seaport container terminals. *OR spectrum*, Vol. 28, No. 4, pp. 587-610, 2006

[6] Bish E K, Chen F Y, Leong Y T, et al. Dispatching vehicles in a mega container terminal. *Springer Berlin Heidelberg*, 2007.

[7] Nguyen V D, Kim K H. A dispatching method for automated lifting vehicles in automated port container terminals. *Computers & Industrial Engineering*, Vol. 56, No. 3, pp. 1002-1020, 2009

[8] Angeloudis P, Bell M G H. An uncertainty-aware AGV assignment algorithm for automated container terminals. Transportation Research Part E, pp. *Logistics and Transportation Review*, Vol. 46, no. 3, pp. 354-366, 2010

[9] Lee L H, Chew E P, Tan K C, et al. Vehicle dispatching algorithms for container transshipment hubs. *OR spectrum*, Vol. 32, No. 3, pp. 663-685, 2010

[10] Rashidi H, Tsang E P K. A complete and an incomplete algorithm for automated guided vehicle scheduling in container terminals. *Computers & Mathematics with Applications*, Vol. 61, No. 3, pp. 630-641, 2011

[11] Cai B, Huang S, Liu D, et al. Optimisation model and exact algorithm for autonomous straddle carrier scheduling at automated container terminals. Intelligent Robots and Systems (IROS), *2011 IEEE/RSJ International Conference on. IEEE*, pp. 3686-3693, 2011

[12] Moussi R, Yassine A, Kansou A, et al. Scheduling of lifting vehicles with time windows in an automated port container terminal. Logistics (LOGISTIQUA), *2011 4th International Conference on. IEEE*, pp. 55-61, 2011

[13] Le H M, Yassine A, Moussi R. DCA for solving the scheduling of lifting vehicle in an automated port container terminal. *Computational Management Science*, Vol. 9, No. 2, pp. 273-286, 2012

[14] YUAN W. Integrated vehicle dispatching for container terminal. *National University of Singapore*, 2012.

[15] Skinner B, Yuan S, Huang S, et al. Optimisation for job scheduling at automated container terminals using genetic algorithm. *Computers & Industrial Engineering*, 2012.

[16] Dkhil H, Yassine A, Chabchoub H. Optimization of Container Handling Systems in Automated Maritime Terminal. Advanced Methods for Computational Collective Intelligence. *Springer Berlin Heidelberg*, pp. 301-312, 2013

[17] H. W. Kuhn. The Hungarian method for the assignment problem. Naval Research Logistics, Vol. 52, pp. 7-21, 2005

[18] Kieran D, Weir J, Yan W Q. A Framework for an Event Driven Video Surveillance System. *Journal of Multimedia*, Vol. 6, No. 1, pp. 3-13, 2011

[19] Gao T, Wang P, Wang C, et al. Feature particles tracking for moving objects. *Journal of Multimedia*, Vol. 7, No. 6, pp. 408-414, 2012

[20] Zheng G, Tang S. Spatial Correlation-Based MAC Protocol for Event-Driven Wireless Sensor Networks. *Journal of Networks*, Vol. 6, No. 1, pp. 121-128, 2011

Mobile Node Deployment based on Improved Probability Model and Dynamic Particle Swarm Algorithm

Xiaoxiang Han
Zilang Vocational and Technical College, Nantong, China
Email: hxxws@qq.com

***Abstract*—In order to realize node deployment in monitoring area and improve the network coverage, this paper propose a mobile node deployment method based on improved probability sensor model and dynamic multiple population particle swarm algorithm. Firstly, the improved probability sensor model was introduced by adding the energy factor to the traditional probability model, and then the node deployment mathematical model was given based on the improved probability sensor model considering the network coverage rate and energy factor. Then the SOM algorithm was used to divide the particle population to several sub populations, and the dynamic multiple population PSO method was designed to get the optimal node deployment solution in every sub-population. The simulation experiment shows the method in this paper can deploy mobile nodes evenly in monitoring area, the network coverage and energy were considered, and compared with the other methods about node deployment, it has higher coverage rate and longer network life cycle. Therefore, the proposed method is likely to have more priority and application value.**

***Index Terms*—Node Deployment; Particle Swarm Algorithm; Population; Optimal Solution**

I. INTRODUCTION

Wireless sensor network is self-organization network composed by numerous of nodes deployed in the monitoring region, its main function is to collect and process information for the perception object in the monitoring region. The goal of wireless sensor network is to realize the overall perception for a certain monitoring area, and it has been successfully applied in military, medical monitoring, traffic, environmental monitoring and other fields etc [1-3].

Node deployment is one of the basic problems in the field of wireless sensor network research field, and it can ensure effective operation of wireless sensor network.

Sensor node deployment [4-5] can be summarized as:

Numerous nodes was randomly distributed in a specified monitoring wireless sensor area, these node are periodically sense data and send the data to sink node, in order to optimize the existing network resources, and realize the goals of improving network service quality and prolong the network life cycle, some algorithm needs be proposed to compute the node position, and the position for all the nodes should satisfy the demands of covering as much area as possible and achieve the above goals.

As for some wild or abominable monitoring environments, the sensor nodes can just be deployed randomly initially, and it may lead the blind monitoring region and finally affect the monitor quality. Therefore, in order to achieve the coverage for the network area with high reliability, the sensor nodes are usually can be moved in these regions to cover more region, and the sensor node which can be move was called mobile sensor node.

Due to the limited energy of mobile sensor node, so too much times for node moving will waste much energy for nodes, so much work about mobile node deployment were concerned deploy the nodes at one time or two times after they were initially deployed. The current work about the deployment for mobile sensor node can be mainly summarized as follows:

(1) Deployment based on virtual force, namely, through the forces between nodes to realize the movement of mobile sensor nodes. Artificial potential method for sensor node deployment was firstly proposed by Howard [6] in 2002, he thought the node will move around through the repulsion forces between nodes and between nodes and obstacles in the region with big node density, after the node moving, all the nodes in the region will cover more region, and through experiment he showed his method had improved the network coverage to large extent.

Zou [7] proposed a node deployment strategy for mobile sensor node on virtual force, it used maximizing the network coverage as the sole goal, through the network clustering and the attraction and repulsion forces between coverage targets to realize the deployment for cluster member nodes.

The above two methods can adjust the location of the mobile node well, but they existed the problems such as the least minimum and uneven deployment, so they lacked of stability.

Therefore, Poduri [8] introduced the concept of node degrees on the basis of the above work, each node has the specified number of neighbor nodes for keeping the network connectivity.

doi:10.4304/jnw.9.1.131-137

Son [9] described the obstacles through the certainty degree, each working area can be divided into several small areas, each area had a certainty degree located at (0,1), through combing with the artificial potential field, the balance was achieved finally dynamically.

Nojeong [10] simulated the micro molecular equilibrium mechanism of the small world, and the equilibrium of molecules was achieved by relying on virtual repulsion between nodes.

(2) Limited node deployment. Lyamberopoulos [11] showed that the energy consumption of sensor node in the case of mobile state was much higher than that of communication and perception, therefore, limited deployment of mobile nodes refers to the node with limited energy, only can through one-time deployment node reached the location, and at the same time the hop count for implementing moving should be the least and the network coverage should be maximized.

Chellappan [12] described the initial deployment of the network as a VORONOI diagram, and transferred the problem of how to maximize the network coverage and minimize the network hop number to minimize the cost of VORONOI diagram.

Kwok [13] allocated the uneven and the changing size with time region according the energy constraint, the goal function reflected the global energy and different coverage principles, so the mobile node speed can be limited to get balance.

Greco [14] researched the omni-direction, the node had limited moving distance, and the discrete time ladder algorithm was used to get the local optimum solution for node deployment.

NAN [15] put forward a wireless sensor nodes deployment optimization method based on genetic algorithm, he regarded the deployment problem as a multi-objective optimization problem, and the objectives were saving energy and improve coverage respectively, and in order to verify the proposed methods, the Voronoi based algorithm and Boundary expansion with virtual forces based algorithm were compared with his work.

Li [16] transformed the node deployment problem into combinatorial optimization problem， the monitoring area are divided to many grids, and every network node can only be deployed in the grid of the area，in order to get the position for sensor node, the genetic algorithm was used to search the optimal solution for node deployment, and simulated annealing algorithm is used to change population for the search speed improvement.

The above works are all about node deployment, they were of great significances, but they still had some problems such as easy obtaining the local optimal solution, sometimes the coverage is too low, and energy consumption is not satisfactory, in order to solve these problems, we designed a novel method for node deployment based on improved probability sensor model and particle swarm optimization (PSO) algorithm, firstly, the mathematical model for node deployment was proposed, then the SOM algorithm was used to divide the population to sub-populations, and in order to get the optimal solution for node deployment, the particle swarm optimization (PSO) algorithm was used to get the optimal solution, and the experimental results show the effectiveness of the proposed method.

II. DEPLOYMENT OPTIMIZATION MODEL

A. Improved Probability Sensor Model

Assumptions for deployment of monitoring area can be listed as follows:

(1) The monitoring area is in two-dimension, at the initial time the nodes were distributed randomly.

(2) All the nodes have the same structure, namely, the same sensing ability and the community radius are the same.

(3) The communication radius is two times than the sensing radius of node.

(4) All the nodes can be move at one time only to reduce the energy consumption.

(5) All the nodes can adjust their transmitting distance adaptively to reduce energy consumption.

The node sensor model decides the node sensing ability and coverage area, and there were mainly two kinds of sensing model such as Boolean model and probability sensing models. The probability model is more consistent with the monitoring environment, and it can be described as follows:

Sensor nodes set in the monitoring area can be expressed as $S=\{s_1,s_2,...,s_n\}$, the position of arbitrary sensor nodes can be represented as (x_i,y_i), sensing radius can be expressed as r_i, target position can be expressed as (x_p,y_p), and the Euclidean distance between the target and the sensor node can be calculated according to the following equation:

$$d(s_i,P)=\sqrt{(x_i-x_p)^2+(y_i-y_p)^2} \tag{1}$$

The probability model of the sensor node s_i is represented as follows:

$$C(s_i,p)=\begin{cases}0 & if\ d(s_i,p)\ge r-r_e\\ e^{-\lambda\alpha^{\sigma}} & if\ d(s_i,p)\le r+r_e\\ 1 & if\ \ r-r_e\le d(s_i,p)\le r+r_e\end{cases} \tag{2}$$

In equation (2), $C(s_i,p)$ is the sensing probability, which represents the extent of sensor node s_i coverage the monitoring target position p, r_e represents the uncertainty of the error values collected by sensor node, the value of α can be expressed as $d(s_i,p)\ge r-r_e$, λ is the attenuation coefficient for sensing range $r-r_e$, where σ is the attenuation coefficient for sensing range $r+r_e$.

Due to the sensor nodes distributed in the monitoring area may be heterogeneous, the different initial energy will affect the sensing ability, therefore, the classic probability was improved by considering the sensor node remain energy, and the improved probability model in this paper can be expressed as :

$$C(s_i, p) = \begin{cases} 0 & if\ d(s_i, p) \geq r - r_e \\ \frac{E_{ir}}{E_{i0}} e^{-\lambda \alpha^{\sigma}} & if\ d(s_i, p) \leq r + r_e \\ 1 & if\ r - r_e \leq d(s_i, p) \leq r + r_e \end{cases} \quad (3)$$

In equation (3), E_{ir} and E_{i0} represent remain energy and initial energy respectively, and the other variables in equation (3) are in the same with equation (2).

B. Coverage

Maximizing network coverage for monitoring target area is the important goal for sensor network node deployment problem. Coverage can be defined as the ratio of the union area covered by all the sensor nodes to the size of the monitoring target area, and the coverage area of each sensor node is defined as a circular area with the radius r_s, according to the equation (2), assume that the sensing probability for sensor node s_i to the goal s_i can be expressed as $C(s_i, p)$, then the target covered by all sensor nodes can be expressed as follows:

$$Cov_s = 1 - \prod_{i=1}^{n} (1 - C(s_i, p)) \quad (4)$$

As we knows, if the network coverage rate is higher, the node deployment is better, therefore, the larger is the value of Cov_s, the better of the candidate solutions, which can be represented as:

$$f_1 = \max(Cov_s) \quad (5)$$

C. Network Energy Cosumption

Assume that each mobile sensor node is moving according to the linear movement. Here mainly considering energy consumption for each mobile node moving to the target position after calculating the node location, which can be represented as:

$$E_{s_i}(r) = \sum_{i=1}^{n} E_i d(s_i, e) \quad (6)$$

In equation (6), E_i represents the energy consumption of moving per unit of distance unit, $d(s_i, e)$ is the distance between the sensor node s_i and the destination is e_i, so from the equation (6), we can see the total energy consumption for all the nodes moving to the target position is proportional to the distance, therefore, the total distance should be minimized as :

$$f_x = \min(\sum_{i=1}^{n} d(s_i, e_i)) \quad (7)$$

D. Deployment Goal

Due to node is mobile, so for the nodes s_i and s_j, the connection between them should be satisfied with the connected conditions, namely:

$$c(s_i, s_j) = true \quad (8)$$

And after the mobile nodes moved, it is still in the network area, namely:

$$\forall i \in (1, n)\ e_i \in A \quad (9)$$

Therefore, considering energy consumption and network coverage for node deployment comprehensively, the overall deployment optimization model is:

$$\begin{cases} f_1 = \max(Cov_s + 1/\sum_{i=1}^{n} d(s_i, e_i)) \\ s.t.\ \ c(s_i, s_j) = true \\ \quad \forall i \in (1, n)\ e_i \in A \end{cases} \quad (10)$$

III. DEPLOYMENT BASED ON PARTICLE SWARM ALGORITHM

A. Summary of Particle Swarm Optimization (pso) Algorithm

Particle swarm optimization algorithm is proposed by Kennedy and Eberhart in 1995 on the basis of studying birds and fish swarm behavior [17-18], the feasible solution for optimization problem is responding to the Particle in the search space, each particle has a corresponding speed, location, and fitness, location decides the flying direction of particles, velocity determines the distance of per unit time of flight particles, fitness decides the quality of the corresponding current solution.

The particle swarm is initialized firstly, and then the optimal solution is obtained by iteration. In the process of iteration, the velocity and position of particle is renewed by tracking individual extreme value *lst* (individual optimal solution) and the global extreme value *gst* (all particles of the optimal solution) to update, as shown in equation (11) and (12) :

$$v_{ik}(t+1) = wv_{ik}(t) + c_1 r_1 (lst_{ik}(t) - x_{ik}(t)) + c_2 r_2 (gst_{ik}(t) - x_{ik}(t)) \quad (11)$$

$$x_{ik}(t+1) = x_{ik}(t) + v_{ik}(t+1) \quad (12)$$

In equation (11) and (12), $v_{ik}(t)$ represents the flying speed of current particle, $1 \leq k \leq N$ represents the dimensions of the current space, r_1 and r_2 are the random number in the interval between 0 and 1, where c_1 and c_2 are learning factors, c_1 is used to adjust the particle to flight to the global optimal position, c_2 is used to adjust the particle to flight to the individual optimal value, so the value for c_1 and c_2 are of neither too big nor too small, if it is too big, the particle will suddenly fly to or over the target area, and if it is too small, the particle are too far away from the target area, so in general, c_1

and c_2 were always assigned as 2, w represents the extent of particle dependent on the current speed.

B. Improved Multiple Swarm PSO Algorithm

Particle swarm algorithm can effectively optimize the deployment of wireless sensor networks, but when the standard particle swarm was flying in the search space, it is easy falling into "premature" phenomenon, which restricts the search area of the particles. Therefore, we put forward a kind of particle swarm algorithm for realizing node deployment optimization based on dynamic multiple populations (DMPSO) of wireless sensor network. In the process of optimization, through the introduction of SOM clustering algorithm, the population is divided into several sub populations, and the independent optimization is getting along among the various sub populations, at the same time, in order to enhance exchange of information between sub populations, the sub population are dynamic restructured to relieve the pursuits of particles for the local optimal point. Then the "premature" phenomenon can be effectively avoided to improve the network coverage.

The basic idea of the improved PSO algorithm can be concluded as: through the SOM algorithm to divide the population into several sub populations, the sub population is evolved independently, at the same time, after several iterations, the sub population was divided to new sub population to improve the information exchange.

Assuming the population M has m particles, and all the m particles could be divided into K populations can be expressed as:

$$P = \{P_1, P_2, P_3, ..., P_k\} \tag{13}$$

The sub-population can be represented as $P_i = \{X_{i1}, X_{i2}, X_{i3}, ...X_{is}\}$, where X_{is} represents the $s-th$ individual in population P_i , the node coordinates is mapped to the particle position, due to the node has coordinates such as x and y , so the dimensions for all the n nodes in the particle swarm is 2n, and the $j-th$ particle in the sub population P_i can be represented as:

$$X_j = \{x_{j1}, y_{j1}, x_{j2}, y_{j2}, ..., x_{jn}, y_{jn}\} \tag{14}$$

In equation (14), x_{jk} and y_{jk} are x dimension and y dimension coordinates of the $k-th$ node respectively.

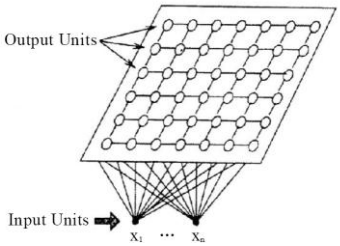

Figure 1. Structure of SOM.

C. Population division

Self-organizing neural network shorted for SOM [19] was put forward by Kohonen, and its main idea is through competition, co-operation and weight adjustment to achieve unsupervised self-organizing learning, its structure consists of input layer and output layer, as shown in figure 1:

Firstly, we use SOM algorithm to divide the whole population to several sub populations, the algorithm are defined as follows:

Algorithm 1 SOM population division algorithm

Initialization: number of input neurons n and output neurons number m;

Step 1: the current iteration number t=1, the maximum number of iterations T, learning rate factor $\psi(1)$, the neighborhood radius $N(1)$, and the initial weights $W_{ij}(1)$;

Step 2: All the initial weights and sample data are normalized;

Step 3: For every particle, the Euclidean distance between it and every output neuron is computed:

$$D_{ij}(t) = \sum_i^n (w_{ij}(t) - x_i(t))^2 \quad j = 1, 2, ..., m \tag{15}$$

Step 4: select the neuron with the minimum (j = 1, 2,..., m) value of $D_{ij}(t)$ (j=1,2,…,m) as the winning neuron;

Step 5: The neuron in the neighborhood range of the winning neuron node is adjusted as shown below:

$$w_{ij}(t+1) = w_{ij}(t) + \psi(t)(x_i - w_{ij}(t)) \tag{16}$$

Step 6: According to the equation (17) and equation (18) to win vector neural neighborhood and updates:

$$\psi(t) = \psi(1)(1 - t/T) \tag{17}$$

$$N(t) = N(1)(1 - t/T) \tag{18}$$

Step 7: If the studying rate $\psi(t)$ reduced to zero or the current number of iterations achieved maximum value T, then the algorithm ends, otherwise t=t+1, and return to step 2.

D. Node Deployment Optimization

Every particle in the monitoring area represents a scheme of how to deploy all the sensor nodes, the fitness function of the algorithm is showed in equation (10), and the node deploy optimization algorithm based on improved dynamic multiple swarm can be described as:

Algorithm 2 Node deployment based on improved PSO algorithm

Step 1: Initialization m individual particles, i.e., randomly generated location X_i and velocity V_i for each particle;

Step 2: The population is divided to K sub-populations by SOM algorithm;

Step 3: Renew the position and velocity according to the equation (11) and (12) ;

Step 4: Compute the fitness of every particle by equation (10), and compare it with the individual optimal solution lst and global optimal solution gst :

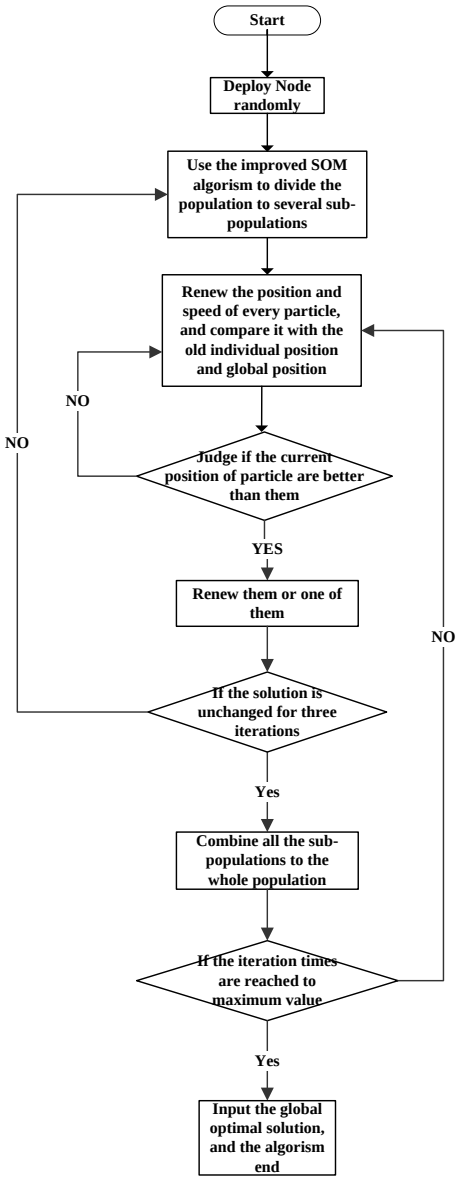

Figure 2. The proposed method flow.

If it is better than the individual optimal solution *lst* , the value of *lst* is renewed by the current particle position;

If it is better than global optimal solution *gst* , the value of *gst* is renewed by the current particle position;

Step 5: Judge whether the individual optimal solution and global optimal solution are not changing for three iterations, if it was, then go to step 2;

Step 6: Judge whether the current number of iterations reached the maximum value. If it was, the algorithm will end, otherwise t=t+1, and return to step3.

Therefore, the main flow of our proposed method can be described as figure 2:

IV. SIMULATION EXPERIMENT

A. Expeiment Environment

Using the simulation tool MatLab 7.0 to validate the proposed method, the simulation parameters are as follows: the monitor area is 20 m x 20 m, the initial value of the number for sensor nodes is 150, the sensing radius and communication radius of each sensor node are R_s =10m and $R_c = 20$ m, respectively, the numbers of the particles in the monitoring area is 40, the flying speed of particle is varied from -5m/s to 5m/s, and the maximum value of iteration time is 300, in the initial time, the nodes randomly deployed in the network area, as showed below:

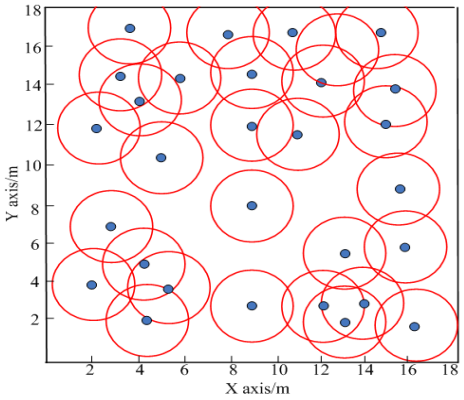

Figure 3. Initial distribution of all the sensor nodes.

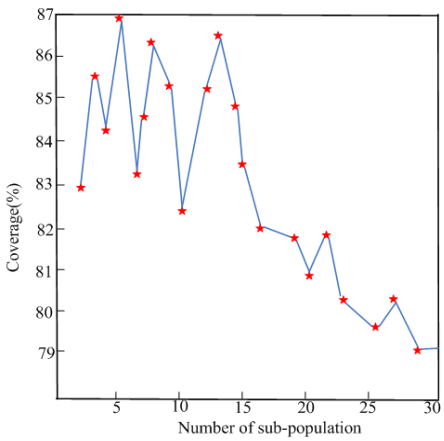

Figure 4. Coverage with different numbers of sub-population

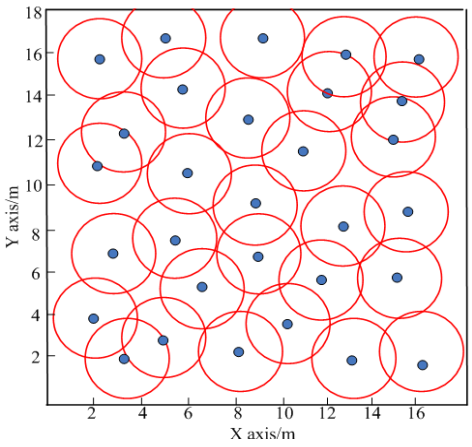

Figure 5. Results for node deployment

In figure 3, the dot represents the sensor node location, and the circle represents the sensing range of sensor node.

Firstly, the SOM algorithm was used to divide the population, the output neurons number m namely the

numbers of the sub-populations was tested varied from 3 to 30, the average value was obtained, and the network coverage changing with the numbers of sub-populations is showed as Figure 4.

Then the proposed method is used to calculate the node location, the results for node deployment is shown as figure 5.

From figure 5, we can be see that the nodes can evenly distributed in monitoring area in the randomly initially deployed, the nodes can cover as much area as possible, in order to validate the network coverage of our method with the literature [16], simulation of the coverage is carried as below:

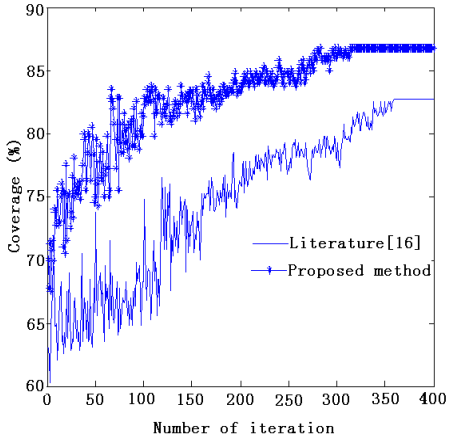

Figure 6. Comparison of coverage

From figure 6 we can see the method has the higher coverage compared with the literature [16], in the initial coverage it is 67%, and the solution is eventually converged to 88%, and the coverage rate of the method in literature [16] is only 83%, the proposed method tends to be convergent at 312 iterations, and the method in literature [16] tends to be in convergence at iteration number 364, obviously, our method has the higher efficiency and network coverage.

LEACH protocol is operated in the monitoring area to simulate the network life cycle simulation, the results are as follows:

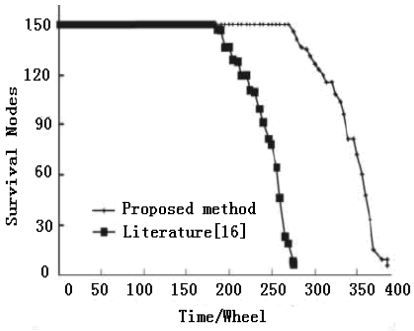

Figure 7. Survival sensor nodes with time.

From figure 7, the proposed method has the stable operation of about 300 rounds, but the method in the literature [16] can be stable running of about 200 rounds, at the mean time, the death time for the first node and the last node is 300 and 400 wheel, respectively, but the ones in the method of literature [16] are 200 and 270, respectively. It is proved that our method can improve life circle largely. It is because the probability sensor model considering the energy factors and simultaneously considering the energy consumption factor for mobile node moving in the optimization process, therefore, and the network deployed by this paper has longer network life cycle.

V. CONCLUSION

Sensor nodes are deployed in the monitoring region in order to satisfy the demands of network coverage, in order to meet the premise of data acquisition and cognitive tasks, to maximize the network life cycle and reduce energy consumption, a kind of multiple targets based on dynamic multiple population particle swarm optimization algorithm for node deployment was proposed in this paper. Firstly, the improved probability perception model was put forward by adding energy factors in traditional probability model perception, then the improved SOM algorithm was used to divide the population of particles to several sub populations, finally, the improved PSO algorithm was used to find the optimal solution. Simulation result proves the feasibility and effectiveness of the proposed method.

ACKNOWLEDGMENT

This work was supported in part by a grant from Natural science fund project of Jiangsu province (BK2010192), Science and technology plan projects of Nantong (BK2012035), Characteristic major construction project of Zilang Vocational and Technical College (201104)

REFERENCES

[1] C. Song, M. Liu, J. Cao, Yuan Zheng, Haigang Gong, Guihai Chen. “Maximizing network lifetime based on transmission range adjustment in wireless sensor networks”. *Computer Communication*, vol. 31, pp. 1316-1325, 2009.

[2] Z, Rosberg, R. P. Liu, T. L. Dinh, et al. “Statistical reliability for energy efficent data transport in wireless sensor networks”. *Wireless Netw*, vol. 16, pp. 1913-1927, 2010.

[3] Z. N. Chen, G. F. Nan. Optimization of sensor deployment formobile wireless sensor networks. I*nternational Conferenceon Computational Intelligence and Vehicular System. Washington D C: IEEE Computer Society*, pp. 218- 221, 2010.

[4] A Kwork, S Martinez. “Deployment Algorithms for a power-constrained mobile sensor network”. *International Journal of Robust and Nonlinear Control*, pp. 745-763, 20, 2010.

[5] L Greco, M Gaeta, B Piccoli. “Sensor Deployment for Network-like Environments”. IEEE Transactions on Automatic Control, pp. 2580-2585, 55, 2010.

[6] A. Howard, M. J. Mataric, G. S. Sukhatme. “Mobile Sensor Networks Deployment using Potential Fields: A Distributed, Scalable Solution to the Area Coverage Problem”. *Japan: International Symposium on Distributed Autonomous Robotics Systems*, 2002.

[7] Y. Zou, K. Chakrabarty. “Sensor Deployment and Target Localization Based on Virtual Forces”. *USA: Proc of IEEE Infocom conferenc*e. 2003, 2 pp. 1293-1303.

[8] S Poduri, G. S Sukhatme. Constrained coverage for mobile sensor netework, New Orleans, *USA: IEEE Intl Conference on Robotics and Automation*, 2004.

[9] G. M Song, W Zhuang, H. G Wei. “Self-Deployment Algorithm for Mobile Sensor Network in unknown Environment”. *Journal of South China University of Technology*(*Natural Science Edition*), pp. 26-30, 34, 2006.

[10] H Nojeong, P. K Varshney. Energy-efficiency Deployment of Intelligent Mobile Sensor Networks, I*EEE Transactions on Systems, Man and Cybernetics*: *PartA*, pp. 78-92, 35, 2005.

[11] D. Lymberopoulos, A. Savvides. “XYZ: A Motion-enables, Power Aware Sensor Node platform for Distributed Sensor Network Applications”. *Los Angeles: Proc. Of Intl Symposium of Information Process Sensor Network* (IPSN), 2005.

[12] S Chellappan, X Bai, B Ma, et al. “Mobility Limited Flip-Based Sensor Network Deployment”. IEEE Trans on Parallel and Distributed Systems, pp. 199-211, 18, 2007.

[13] Kwok A, Martinez S. “Deployment Algorithm for A power-constrained Mobile Sensor Network”. *International Journal of Robust and Nonlinear Control*, pp. 745-763, 20, 2010.

[14] Kuang L. N, Cai Z. X. “Genetic algorithm based on redeployment scheme in wireless sensor networks”, *Control and Decision*, pp. 1329-1332, 25, 2010.

[15] NAN Guo-fang, CHEN Zhong-nan. ”Deployment Algorithm of Mobile Sensing Nodes Based on Evolutionary Optimization”, *ACTA ELECTRONICA SINICA*, pp. 1017-1022, 40, 2012.

[16] Yi L, ”Wireless Sensor Network Deployment Based on Genetic Algorithm and Simulated Annealing Algorithm”, *Computer simulation*, pp. 171-174, 28, 2011.

[17] Guangming Zhang, Zhiming Cui, Pengpeng Zhao, Jian Wu, A Novel De-noising Model Based on Independent Component Analysis and Beamlet Transform, *Journal of Multimedia*, Vol. 7, No. 3, pp. 247-253, 2012

[18] Rongbo Zhu, Yingying Qin and Jiangqing Wang. Energy-aware distributed intelligent date gathering algorithm in wireless sensor networks. International Journal of Distributed Sensor Networks, 2011, Article ID 235724, pp. 1-13.

[19] Li Yi, Huachun Zhou, Fei Ren, Hongke Zhang, "Analysis of Route Optimization Mechanism for Distributed Mobility Management", *Journal of Networks*, Vol. 7, No. 10, pp. 1662-1669, 2012

DC Voltage Balance Control Strategy for Medium Voltage Cascaded STATCOM Based on Distributed Control

Xuehua Zhao and Liping Shi
Department of Electrical Engineering, China University of Mining and Technology, Xuzhou, China
Email: cumtzxh2013@126.com, shiliping98@126.com

***Abstract*—DC bus capacitors of Medium Voltage Cascaded STATCOM are independent. DC side voltage balance control method is the key influencing factor of current control. The imbalance of DC bus voltage increases harmonic current and affects the safety of device. In this paper, the unbalance mechanism of DC side capacitor voltage is analyzed. Based on the unipolar dual frequency and carrier phase-shifted SPWM (CPS-SPWM) modulation algorithms, the distributed control algorithms, which need multi- FPGA structure, are proposed. By changing the instantaneous active power input of single module, the voltage balance control strategies of DC bus capacitors are realized. The strategy can be applied in each inverter, respectively. Simulation and experiment results show the feasibility and effectiveness of the strategy.**

***Index Terms*—STATCOM; Cascaded Multilevel; Distributed Control; Vector Superposition; DC Voltage Balance Control**

I. INTRODUCTION

The Medium Voltage Cascaded STATCOM is one of flexible AC transmission devices, which are connected to distribution network. During the STATCOM operation, it consumes active power of its own, and absorbs or outputs reactive power, which affects power factor significantly. While it works in capacitive mode, the device of STATCOM will output reactive power for distribution network; on the contrary, if STATCOM needs to absorb reactive power, it works in inductive mode. Compared with the traditional reactive power compensation device, the STATCOM has advantages of regulating voltage and reactive power continuously, low harmonic current, fast response and smaller size.

As an effective method for regulating power quality for distribution system, Medium Voltage Cascaded STATCOM becomes the research focus in recent years. Relative to the traditional transformer multiple, cascaded STATCOM with H-bridge structure has obvious advantages of no multiple transformers, high efficiency, scalability, modular design.

The technology of DC bus voltage balance control is the key factor of current control in STATCOM. The voltage unbalance of capacitors will bring many adverse effects, which will result in a series of problems. The harmonic distortion of output current will be increased and the quality of output voltage will be reduced. The increasing imbalance degree of capacitor voltage will affect the safe operation of the device. Therefore, the reliable voltage unbalance control strategies and algorithms should be applied to ensure DC bus voltage balance control in capacitive mode, inductive mode or standby mode. The changes of parameters in H-bridges should also be considered in the process of balance control. Two types of DC bus voltage balancing control method are applied frequently: the first method for achieving DC bus voltage balance control is the external control circuit, which requires additional hardware circuits, such as energy exchange of the AC BUS voltage control method [1]; another control strategy is the establishment of its own balance algorithm models, such as adjusting the phase shift angle for each link to achieve the voltage balance [2]. Based on the system development background of Medium Voltage Cascaded STATCOM, the control structure of system is established. In this paper, the distributed control scheme, which consists of central control unit and single module controllers, is also proposed. In actual application, multi-FPGA control structure is used for the design of distributed control algorithm, which can be achieved in each inverter unit, respectively. So the adjacent inverter units have not couplings. As a result of the distributed control structure, the strategy can be applied in each inverter, respectively. The interaction between DC voltage balance control and upper current control will not exist. The unipolar dual frequency and carrier phase-shifted SPWM (CPS-SPWM) modulation algorithms are introduced to realize real-time put out of multiplex PWM waves. Fourier series expressions of modulation strategies are derived. By Fourier analysis, better dynamic regulation performance, better harmonic characteristics and lower switching frequency characteristics are realized. At the same time, DC bus capacitors of Medium Voltage Cascaded STATCOM are independent. DC-side voltage balance control is the key influencing factor of current control. According to the analyses of DC side capacitor voltage unbalance mechanisms, DC voltage balance control strategies for Medium Voltage Cascaded STATCOM are achieved. By changing the instantaneous active power input of single module, the voltage balance control methods of DC side capacitors are realized.

doi:10.4304/jnw.9.1.138-146

This paper archives two main conclusions: one is that the distributed control scheme, which consists of central control unit and single module controllers, is proposed. Multi-FPGA control structure is applied in the design of distributed control algorithm; the other is that the changing of instantaneous active power input is used to realize voltage balance control of DC capacitors.

Finally, based on the development background of Medium Voltage Cascaded STATCOM, simulation models and experimental devices are established. In the simulation system, the dynamic control process of DC side capacitor voltage between single modules and DC voltage value between phases are achieved. According to the analysis of simulation waves and experimental results, the quality of output current, which is influenced by DC voltage balance control method, is also analyzed. Simulations and experiment results show that the strategies are feasible and effective. This algorithm can well control the DC bus voltage, which ensures lower current distortion and the same dynamic range of each unit.

II. TOPOLOGICAL STRUCTURE

A. Topological Structure of Medium Voltage Cascaded STATCOM

As shown in figure 1, main circuit model of Medium Voltage Cascaded STATCOM, which uses Y-Connection topology structure, is established. By using LCL filters, the output current of STATCOM is optimal controlled.

$u(t)$ – Output voltage of the inverter; $i_1(t)$ –Current of the inverter; $u_s(t)$ –Output voltage of the power grid; $i_2(t)$ –Current of the power grid; $u_c(t)$ – Voltage of the capacitors; $i_c(t)$ – Current of the capacitors; $i_s(t)$ –Current of the system; L_1, L_2 –Inductance of LCL filter; R_1, R_2 – Added resistances of LCL filter; C –Filtering capacitor of LCL filter; R_d –Resistance of LCL filter;

Based on H-bridges, the cascaded structure of Medium Voltage Cascaded STATCOM is designed. Each phase consists of 12 H-Bridge cells in cascaded H-Bridges structure. The DC-side capacitors are used for energy storage. According to the DC bus voltage synthesis strategy, the desired output voltage is obtained. The three-phase cascade STATCOM, which uses Y-Connection and coupling inductances, is connected to power grid. By changing the size and phase of output voltage, the power exchange between grids and STATCOM is realized. The measured voltage and current signals are accessed in STATCOM controller to generate trigger control signals.

B. Analysis of DC Bus Voltage Unbalances Mechanism

Each DC bus capacitor of H-bridges in cascaded STATCOM is independent. At the same time, the parameters of capacitors are also different. According to series losses, parallel losses and mixing losses, the problems of the capacitor voltage imbalance control are unavoidable. Under the consideration of various losses, H-bridge unit equivalent circuit of STATCOM is shown in figure 2.

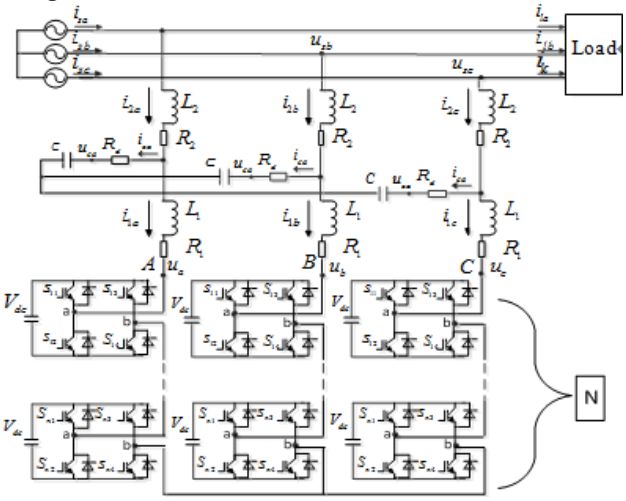

Figure 1. Main circuit model of Medium Voltage Cascade STATCOM

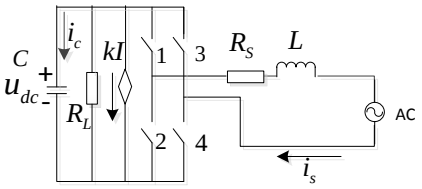

Figure 2. H-bridge unit equivalent circuit of STATCOM

R_S - Equivalent resistance of series losses: conduction losses of the switching devices and anti-parallel diodes; R_L - Equivalent resistance of parallel losses: off-state losses of the switching devices and buffer circuit losses; KI - Equivalent hybrid losses of controlled source; I - AC side RMS current, Equivalent losses of freewheeling diode reverses recovery losses and switching device switching losses.

Based on the above analysis, the equation current formula of DC side capacitor can be established in the following form,

$$C_{\mathrm{dc}}\frac{du_{dc}}{dt}=\frac{u_{dc}}{R_L}+KI+i_sS(t) \tag{1}$$

The DC component and AC component of current and voltage are expressed as follows,

$$\begin{cases} u_{dc}(t)=\overline{u_{dc}}(t)+u_{dc}(t) \\ i_s(t)=\sqrt{2}I_f\sin(\omega t-\varphi)+i_h(t) \\ S(t)=M\sin(\omega t-\triangle\theta)+S_h(t) \end{cases} \tag{2}$$

$\overline{u_{dc}}(t)$ - DC component of voltage; $u_{dc}(t)$ - AC component of voltage; I_f - Fundamental component; i_h - Harmonic component; $\triangle\theta$ - Trigger pulse delay error; $S(t)$ - The equivalent switching function.

If the voltage fluctuations of capacitors, the high frequency component of switching function and the

influence of harmonic currents are ignored in steady-state operation, the following formula will be obtained.

$$C_{dc}\frac{d\bar{u}_{dc}}{dt}=\frac{\bar{u}_{dc}}{R_L}+KI+\frac{\sqrt{2}IM}{2}\cos(\varphi-\triangle\theta) \quad (3)$$

The stable value of capacitor voltage could be expressed in the following form,

$$\bar{u}_{dc}=-R_L I\left[k+\frac{\sqrt{2}M}{2}\cos(\varphi-\triangle\theta)\right] \quad (4)$$

According to the above analyses, trigger delay, parallel losses and mixing losses of H-bridges are the main reasons of DC bus voltage imbalance.

III. PROPOSED SCHEME

A. Carrier Phase-Shifted SPWM (CPS-SPWM) Modulation Algorithm based on Unipolar Dual Frequency

The output voltage of inverter circuit using SPWM (sinusoidal pulse width modulation) is composed of a series of rectangular pulses in equal magnitude and unequal width, and it is not an ideal sinusoidal wave. The modulation strategies of cascaded STATCOM are used for controlling the switch of modules, which can make output voltage into sinus waveform. To get higher equivalent switching frequency and better output harmonic characteristics of STATCOM, unipolar dual frequency modulation algorithm is applied in carrier phase-shifted SPWM (CPS-SPWM) modulation algorithm. Its equivalent switching frequency has been increased several times.

It assumes that the number of inverter is L_x and modulation methods use lower switching frequency. The phase difference of each triangular carrier is $2\pi/L_x$ in the process of CPS-SPWM modulation. The common modulation wave signals are applied in all inverters to generate PWM signals. The voltage vector superposition method is adopted to obtain output voltage. Obviously, the only difference between the Fourier series expansion of each module is initial phase of the triangular carrier. Triangular carrier phase angle of the L_x converter is $\varphi_c+2\pi L/L_x$ and the corresponding double Fourier series expressions of output waveforms are shown in the below formula.

$$\begin{aligned}F_L(\mathrm{t})=&\frac{2E}{\pi}Q_{Km}\cos(\omega t+\varphi_{Km})\\&+\sum_{m=1}^{\infty}\frac{4E}{m\pi}J_0(mQ_{Km})\sin\left(\frac{m\pi}{2}\right)\cos\left[m\left(\omega_c t+\varphi_c+\frac{2\pi L}{L_x}\right)\right]\\&+\sum_{m=1}^{\infty}\sum_{n=\pm1}^{\pm\infty}\frac{4E}{m\pi}J_n(mQ_{Km})\sin\left[\frac{(m+n)\pi}{2}\right]\\&\cos\left[m\left(\omega_c t+\varphi_c+\frac{2\pi L}{L_x}\right)+n(\omega_m t+\varphi_{Km})\right]\end{aligned} \quad (5)$$

φ_{Km} -Phase modulation of modulating wave; φ_c - Phase modulation of carrier; Q_{Km} - Amplitude of modulating wave; J_0 -Zero-order Bessel function; J_n -N order Bessel function;

Based on the voltage vector superposition algorithm, Fourier series is shown in the following formula.

$$F_T(\mathrm{t})=\sum_{K=1}^{\infty}C_{TK}\cos(K\omega t+\varphi_{LK})=\sum_{L=0}^{L_X-1}F_L(\mathrm{t}) \quad (6)$$

Through the analysis of the above formula, the new Fourier series forms are shown in the following formula.

$$\begin{aligned}F_T(\mathrm{t})=&L_x\frac{2E}{\pi}Q_{Km}\cos(\omega_m t+\varphi_{Km})\\&+\sum_{m=1}^{\infty}\frac{4E}{m\pi}J_0(mL_xQ_{Km})\sin\left(\frac{mL_x\pi}{2}\right)\cos\left[mL_x(\omega_c t+\varphi_c)\right]\\&+\sum_{m=1}^{\infty}\sum_{n=\pm1}^{\pm\infty}\frac{4E}{m\pi}J_n(mL_xQ_{Km})\sin\left[\frac{(mL_x+n)\pi}{2}\right]\\&\cos\left[\left(mL_x(\omega_c t+\varphi_c)\right)+n(\omega_m t+\varphi_{Km})\right]\end{aligned} \quad (7)$$

According to the above analysis, the output signals of CPS-SPWM modulation algorithm consist of three parts, respectively.

a) Fundamental component of CPS-SPWM modulation algorithm using Fourier transform

If the parameter value of K is one, fundamental component formulas are shown in the following;

$$C_{T1}=L_x\frac{2E}{\pi}Q_{Km}$$

$$\varphi_{T1}=\varphi_{Km}$$

In conclusion, the amplitude of fundamental component is increased to L_x times, and Phase remains unchanged

b) Carrier harmonics of CPS-SPWM modulation algorithm using Fourier transform

If the parameter value of K is mL_xK_c, $m=1,2,3\cdots$, Carrier harmonics formulas are expressed in the following;

$$C_{TK}=\frac{4E}{m\pi}J_0(mL_xQ_{Km})\sin\left(\frac{mL_x\pi}{2}\right)$$

$$\varphi_{TK}=mL_x\varphi_c$$

When the parameter value of K is $L_x\bullet K_c$, the lowest-order harmonic of carrier harmonics will be obtained. In conclusion, the equivalent switching frequency of CPS-SPWM is increased to L_x times, and if even numbers are assigned to mL_x, the carrier harmonics does not exist.

c) Sideband harmonics of the CPS-SPWM modulation algorithm using Fourier transform

If the parameter value of K is mL_xK_c+n, $m=1,2,3\cdots;n=\pm1,\pm2,\pm3\cdots$, Sideband harmonics expressions are shown in following formulas:

$$C_{TK} = \frac{4E}{m\pi} J_n(mL_x Q_{Km}) \sin\left[(mL_x + n)\frac{\pi}{2}\right]$$

$$\varphi_{TK} = mL_x \varphi_c + n\varphi_{km}$$

If even numbers are assigned to $mL_x K_c + n$, the sideband harmonics does not exist.

By using unipolar dual frequency and carrier phase-shifted SPWM (CPS-SPWM) modulation algorithm, higher equivalent switching frequency and better output harmonic characteristics of the STATCOM are realized.

B. Control Principle of Distributed Control Structure with multi-FPGA

The distributed control strategies with multi-FPGA of cascaded STATCOM are combined with the central controller and single-link controllers. The upper control algorithms of the double-loop control with the current inner loop and capacitor voltage outer loop are achieved by central controller. To eliminate the periodic errors and get good dynamic performance, the capacitor voltage outer loop and current inner loop have been designed based on the traditional PI control and repetitive PI control algorithm. Single controller with FPGA is used for achieving DC voltage balance control and generating the PWM pulses. Distributed control system can simplify the central control software and hardwires circuits. Using independent controller in the distributed control system, each module provides hardware and software platforms for DC voltage balance control. Schematic of distributed control system is shown in Figure 3.

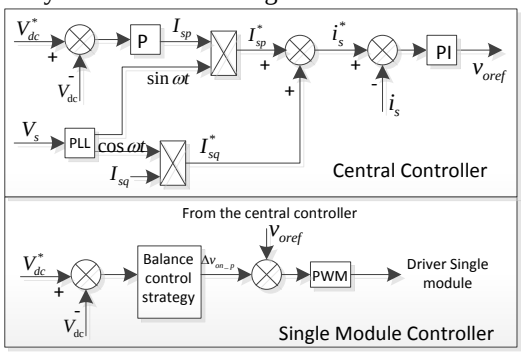

Figure 3. Schematic of distributed control system

a) The principle of current control

Using accurate tracking and detection calculated algorithm, the main function of double-loop control with the current inner loop is to realize the purpose of reactive power compensation. As shown in Figure 4, the current control block diagram of the central control is detailed expressed in the following. Further study of current inner loop control, it takes the DC capacitor voltage values as feedback signal to reflect active power demand. In the DC voltage outer loop control algorithm, the DC capacitor voltage Real-time value is compared with reference DC voltage value to generate error signals for active current command. PI control algorithms are applied in the process of active current control. The instantaneous active current command will be achieved by phase-locked loop and error signals. At the same time, phase-locked loop and amplitude detection of reactive current are also used for generating instantaneous reactive current instruction. These vector superposition algorithms of instantaneous active power and the instantaneous reactive power instructions are applied to solve the problems of instantaneous current control. Then, to form closed-loop control structure for generating current error signals, the instantaneous current control instructions are compared with AC side output current value of the device. Based on PI control and repetitive control, pulse width modulated signals will be realized. Finally, based on the unipolar dual frequency and carrier phase-shifted SPWM (CPS-SPWM) modulation algorithm, switch driving signals will be generated to drive H-Bridges.

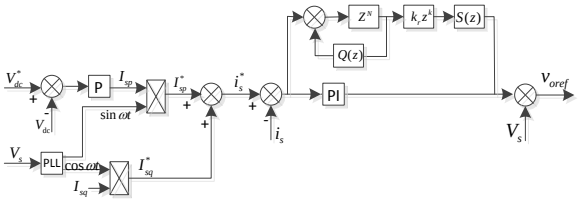

Figure 4. Schematic diagram of system current

b) DC voltage balance control strategy

By changing the active power input in H-bridge modules, DC bus voltage of capacitors can be adjusted. The changes of output voltage or current phase angles in H-bridge modules will be able to change the active power input. Therefore, by changing itself trigger pulses, the output voltage value of each module can be adjusted. Accordingly, by changing the magnitude or phase of output voltage, the H-bridge modules will be able to change its active power. By using this control strategy, the changes of DC capacitor voltage value and balance control of DC bus voltage are realized.

1) Characteristic analysis of voltage vector superposition

Firstly, v_{oL} and i_s are defined as output voltage vector and current vector of the number L module in AC side; its expression formulas are shown in the following,

$$v_{oL} = \begin{cases} v_{oL\_p} \\ v_{oL\_q} \end{cases}, i_s = \begin{cases} i_{sp} \\ i_{sq} \end{cases} \tag{8}$$

v_{oL_p} - The *p*-axis component of output voltage instantaneous value;

v_{oL_q} - The *q*-axis component of output voltage instantaneous value;

P-axis is defined in the direction of i_s; the instantaneous value of active power input in the number L module can be shown in the following formula.

$$p_{ol} = v_{oL}^T \times i_s = V_{oL\_p} \times I_s \tag{9}$$

According to the formula (9), the respective modules will absorb or release active power. The process is determined by AC voltage instantaneous value in the direction of I_S.

Therefore, by adding voltage vector to output voltage instantaneous value in the direction of i_s, the instantaneous active power of the number L module will be changed. Accordingly, the control method for DC voltage balance control will be realized. At the same time, the changes of voltage vector will not affect the output of instantaneous reactive power. The vector analysis is shown in Figure 5.

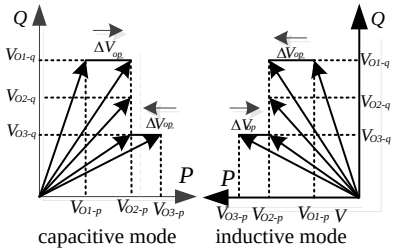

Figure 5. Vector diagram of cascaded STATCOM

In actual application, the phase detection of i_s will be difficulty. In fact, under the stable state, the phase angle between phase current and network voltage is close to 90 degrees. At the same time, the phase angle between the Phase-Locked Loop signal $\cos\omega t$ and network voltage is 90 degrees. Therefore, the phase of i_s can be replaced by the signal of $\cos\omega t$. In practical system, phase difference between $\cos\omega t$ and i_s will not affect the stability of system.

2) Algorithm of DC-side voltage balance control

DC bus voltage of capacitors can be adjusted by changing the active power input in H-bridge modules for active power loss. The real-time value of DC bus voltage is compared with reference DC voltage value to generate error signals, which will be able to determine the direction between superposition voltage vector and the signal of i_s. Therefore, the symbol analyzing function should be introduced to analysis positive and negative error signals. At the same time, the function is also applied to extract positive and negative signals of phase current instantaneous value in the reference direction. In conclusion, through the positive or negative signals of phase current instantaneous value and the signal of $\cos\omega t$, the phase signals of i_s could be determined.

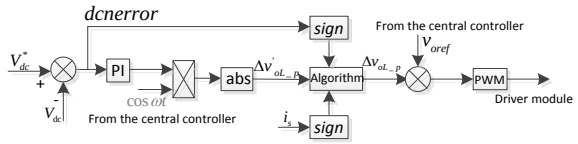

Figure 6. Schematic diagram of DC-side voltage

$\cos\omega t$ -The voltage phase information of the grid. The phase-locked loop (PLL) of the central controller is used to get accurate phase information.

sign - The symbol analyzing function. It is introduced to analysis positive and negative error signals of variables.

By adjusting the DC capacitor voltage value in the H-bridge modules, DC voltage balance control method is achieved. In the process of adjustment, control algorithm depends on the signals of i_s and DC voltage error signals of $v_{dcLerror}$.

The specific algorithm is shown in table 1:

TABLE I. CONTROL ALGORITHM OF DC VOLTAGE

control algorithm		Sign(v_{dcLerr})	
		+	-
Sign(i_s)	+	$\Delta v_{oL\_p}=\Delta v'_{oL\_p}$	$\Delta v_{oL\_p}=-\Delta v'_{oL\_p}$
	-	$\Delta v_{oL\_p}=-\Delta v'_{oL\_p}$	$\Delta v_{oL\_p}=\Delta v'_{oL\_p}$

If the signals of $v_{dcLerror}$ and i_s are positive, the component of signal v_{oref} can be expressed to signal v_{orefp}. Then, if the signal v_{orefp} is positive, the respective module absorbs active power, which will raise the value of DC capacitor voltage.

IV. SIMULATION RESULTS

A. Control Structure of System

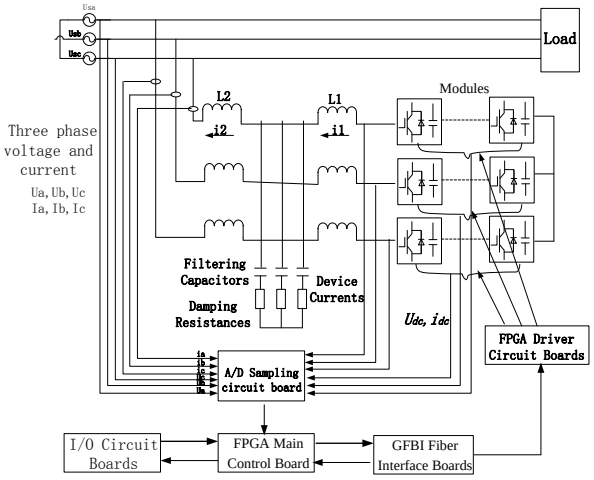

Figure 7. Structure diagram of system controller

Based on the development background of Medium Voltage Cascaded STATCOM, the specific model of control structure is shown in figure 7.The reactive power capacity of Cascaded STATCOM is ±2.8MVar .

The devices are composed of main control cabinet, power cabinets, starting control cabinet, LCL filters, etc. The design concepts of devices take the main FPGA control board, A/D sample boards, I/O boards, GFBI Fiber Interface boards and power boards as core control circuits. By using XC3SD1800A of Xilinx as core control chip, the functions of sampling, control and human-computer interaction are realized. The small-capacity FPGA (XC3S200A) is used for achieving signal sampling, filtering, producing PWM signals, and signal transmission from main FPGA. In the structure of Cascaded STATCOM, the number of system modules is thirty-Six.

B. System Simulation

a) Simulation model of the system

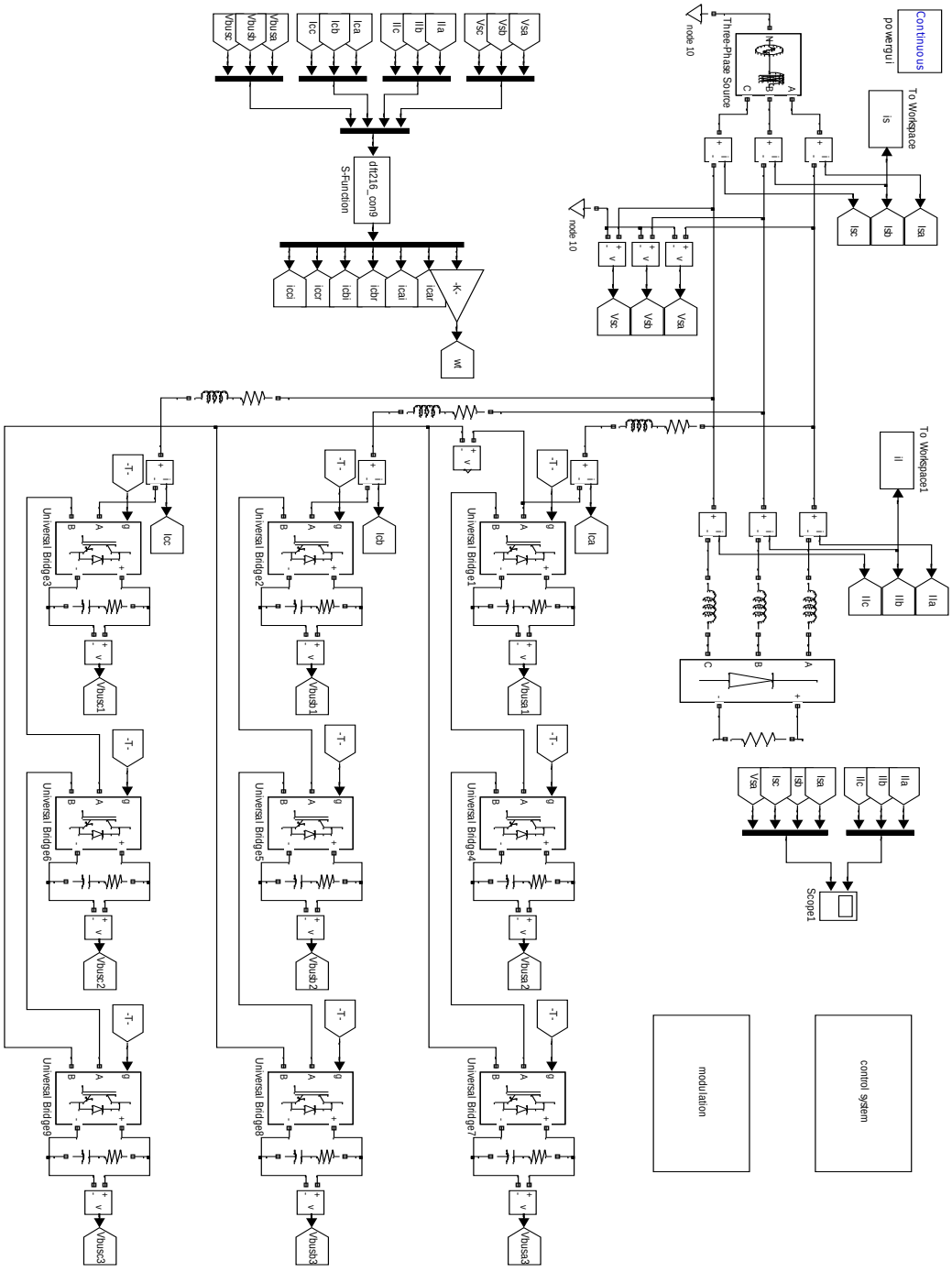

Figure 8. Simulation model of the system

As shown in figure 8, the cascaded STATCOM actual simulation circuits, in order to prove the validity of theory analysis and simulation results, are built in MATLAB. Later, the control algorithms of DC-side capacitor voltage balance control and reactive power compensation are validated in the process of simulation. The distributed control structure and double-loop control strategy with multi- FPGA are also adopted in the control system. The main simulation parameters are shown in table 2.

b) Analysis of simulation results

1) Constant control of DC-side capacitor voltage

The initial value of capacitor voltage is 800/3(V). After system booting, the DC-side capacitors will enter into charge and discharge dynamic process. At about 0.1 seconds, the system gets into relatively steady-state control process, and finally the balanced control of bus voltage is realized. The dynamic control process of single DC bus voltage is shown in figure 9 (a). At the same time, figure9 (b) shows the dynamic control process of DC-side voltage between phase and phase. Its voltage waveforms remain the same dynamic performance.

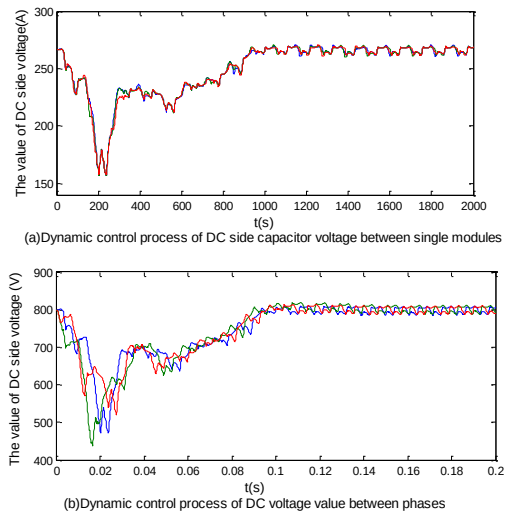

Figure 9. Constant control of DC-side capacitor voltage

TABLE II. SIMULATION PARAMETERS

Parameters Name	Setting Value
Line voltage RMS(V)	380
Peak voltage(V)	$\sqrt{2}\times 380$
DC side capacitors(uF)	3000,
Reference voltage of capacitors(V)	800
Initial voltage of capacitors(V)	800/3
Inductance of filter(mH)	4.8
Equivalent resistance of filter(Ω)	0.03

2) The analysis of current control

As shown in figure 10 (a), the capacitor voltage balance control is the key factor for output current. Stability of capacitor voltage affects current waveform. By using the fast Fourier Transform (FFT) method, the analysis of load current is shown in figure 11. Through the analysis, total harmonic distortion (THD) of load current is 23.91%. After the compensation of reactive power as well as harmonic control, total harmonic distortion (THD) of system current is3.34%.

C. Analysis of Experimental Results

When the experiment device is not running, the three-phase current waveforms are shown in figure 12 (a).On the basis of current waveforms, the harmonic content of output current has been evaluated analytically in figure12 (b). As shown in figure12 (b), total harmonic distortion (THD) is 11.55%. After the start-up of experiment devices, the three-phase output current is used for eliminating current harmonic and compensating reactive power. The analysis of three-phase current waveforms and harmonic content is shown in figure 13.The experiment results prove that the devices can reduce the total harmonic distortion from 11.55% to 1.7% and make the output waveform into sine wave. The structure of Y connection has been adopted in cascaded STATCOM system, so that, three integer multiple harmonic current does not exist in theoretical analysis. In the process of experiment, five, seven and eleven times current components exist in system current. Through the above analysis, experimental results are consistent with theoretical analysis. In the process of experiment, the reactive current value is changed from 150(A) to 50(A) alternately. As shown in figure 15, the results show that real-time dynamic tracking control of reactive current is realized perfectly. The DC-side capacitor voltage data is obtained from touch screen. As shown in figure 16, the maximum value of DC-side voltage is about 837 (V), and its minimum value is about 808 (V), so the difference of DC bus voltage is29 (V). Finally, according to the analysis results, the distributed control algorithm with multi-FPGA can be able to solve the DC voltage unbalance control problems, which are caused by parallel loss, switching loss, differences of modulation ratio and pulse delay. In conclusion, the experiment proves the validity and feasibility of the algorithm mentioned in control theory.

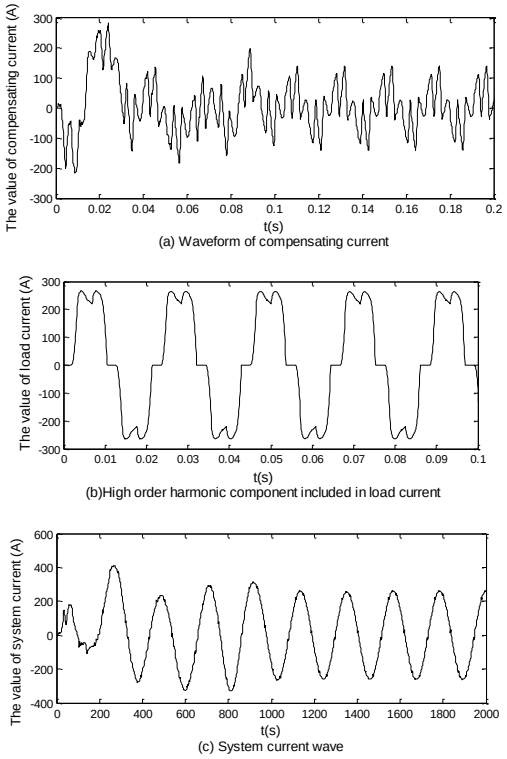

Figure 10. The analysis of current control

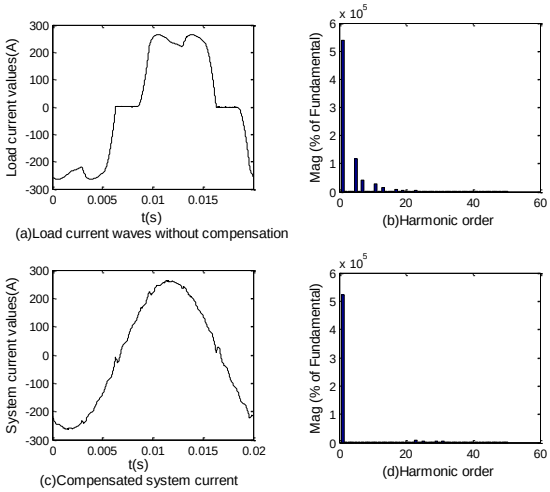

Figure 11. Harmonic analysis of current

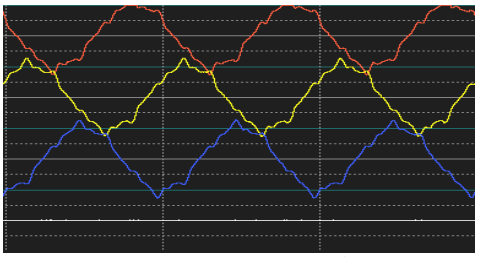

(a) Three-phase current waveforms

1:	100.00	2:	0.11	THD	11.55			
3:	0.68	19:	0.19	35:	0.16			
4:	0.32	20:	0.01	36:	0.00			
5:	9.21	21:	0.01	37:	0.19			
6:	0.15	22:	0.04	38:	0.02			
7:	3.95	23:	0.15	39:	0.07			
8:	0.25	24:	0.00	40:	0.02			
9:	0.09	25:	0.09	41:	0.00			
10:	0.43	26:	0.05	42:	0.01			
11:	5.12	27:	0.02	43:	0.08			
12:	0.07	28:	0.03	44:	0.00			
13:	0.94	29:	0.09	45:	0.00			
14:	0.14	30:	0.02	46:	0.01			
15:	0.06	31:	0.22	47:	0.05			
16:	0.09	32:	0.04	48:	0.00			
17:	2.20	33:	0.07	49:	0.06			
18:	0.03	34:	0.02	50:	0.00			

(b) Harmonic content of the load current

Figure 12. Three-phase current waveforms and harmonic analysis of load current

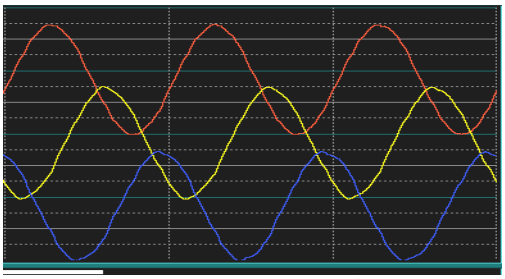

(a) Three-phase current waveforms

1:	100.00	2:	0.11	THD	2.44			
3:	0.29	19:	0.22	35:	0.20			
4:	0.18	20:	0.03	36:	0.00			
5:	1.48	21:	0.01	37:	0.14			
6:	0.04	22:	0.03	38:	0.02			
7:	1.41	23:	0.09	39:	0.03			
8:	0.22	24:	0.00	40:	0.01			
9:	0.09	25:	0.06	41:	0.05			
10:	0.13	26:	0.02	42:	0.00			
11:	0.75	27:	0.03	43:	0.04			
12:	0.04	28:	0.01	44:	0.00			
13:	0.82	29:	0.11	45:	0.00			
14:	0.08	30:	0.02	46:	0.00			
15:	0.05	31:	0.09	47:	0.00			
16:	0.03	32:	0.03	48:	0.00			
17:	0.43	33:	0.05	49:	0.01			
18:	0.02	34:	0.02	50:	0.00			

(b) Harmonic content of the system current

Figure 13. Three-phase current waveforms and harmonic analysis of system current

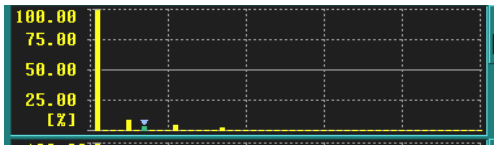

Figure 14. Bar chart of current harmonic component

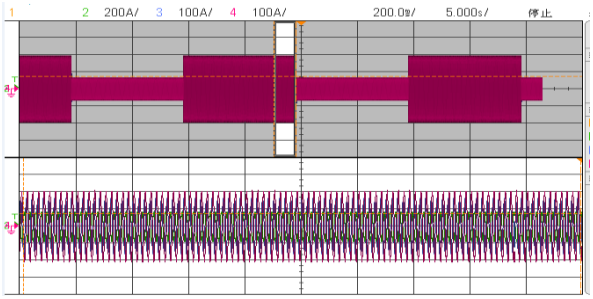

Figure 15. Alternate changes of reactive current value

Figure 16. Experiment results of capacitors voltage

V. CONCLUSIONS

Based on the distributed control algorithm with multi-FPGA, the distributed control scheme, which consists of central control unit and single module controllers, is proposed in this paper. The DC bus voltage unbalance mechanism of cascaded STATCOM is analyzed in detail. By changing the instantaneous active power input of single module, the voltage balance control strategies of DC capacitors are realized. As a result of the distributed control structure, the strategy can be applied in each inverter, respectively. The independent control of coupling relationship between DC voltage balance control and upper current control could be realized. Finally, the simulation and experimental results show that the distributed control strategies have good control effect and application value.

REFERENCES

[1] Wenhua. Liu, Qiang. Song, Letian. Teng, "Balancing control of DC voltages of 50MVA STATCOM based on cascade multilevel inverters", *J. Proceedings of the CSEE*, vol. 24, pp. 145-150, April 2004.

[2] Yidan. Li, Wen sheng. Lu, Xiuyan. Peng, "DC voltage measurement and control for cascaded STATCOM", *J. Proceedings of the CSEE*, vol. 3, pp. 14-19, March 2009.

[3] Juncheng. Geng, Wen hua. Liu, Xufeng. Yu, "Modeling of cascaded STATCOM", *J. Proceedings of the CSEE*, vol. 23, pp. 66-70, June 2003.

[4] Chunyan. Zang, Zhenjiang. Pei, "Research on DC-link capacitor voltage control strategies of the cascaded STATCOM", *J. High Voltage Apparatus*, vol. 46, pp. 17-21, Jan. 2010.

[5] Mingwei. Ren, Yukun. Sun, "Voltage balance control of DC capacitors of 11-level cascade STATCOM", *J. High Voltage Apparatus*, vol. 10, pp. 10-15, April 2010.

[6] Zhao. Liu, Bangyin. Liu, Shanxu. Duan, "DC capacitor voltage balancing control for cascade multilevel STATCOM", *J. Proceedings of the CSEE*, vol. 30, pp. 7-12, September 2010.

[7] Youjie. Ma, Jinxia. Gong, "Parameter selection and the effect on voltage stability of STATCOM", *J. Journal of Tianjin University of Technology*, vol. 5, pp. 46-48, October 2010.

[8] Wei. Sun, Xiaojie. Wu, "Overview of current control strategy for Three-Phase voltage source rectifier with LCL filters", *J. Transactions of China Electrotechnical Society*, vol. 23, pp. 90-96, January 2008.

[9] Fei. Liu, Shanxu. Duan, Xiaoming. Zha, "Design of Two Loop controller in Grid-connected Inverter with LCL filters", *J. Proceedings of the CSEE*, vol. 29, pp. 234-240, December 2009.

[10] Yinghong. Hu, Jiajia. Ren, Jianze Wang, "Balancing control method of DC voltage of cascaded H-bridge

Statcom", *J. Electric Machines And Control*, vol. 14, pp. 31-36, November 2010.
[11] Xin. Zhang, Wen chang. Shao, Shuying. Yang, "Multiloop control scheme of grid side converter with LCL-filter", *J. Journal of Hefei University of Technology*, vol. 32, pp. 972-976, July 2009.
[12] Yongjian. Ma, Zheng. Xu, "Studies of closed-loop control strategy of active power filters", *J. Transactions of China Electrotechnical Society*, vol. 21, pp. 73-78, February 2006.

Xuehua Zhao, studying in department of Electrical Engineering, China University of Mining and Technology, China, the research interests include power electronics and power transmission. Research and development of Medium Voltage Cascaded STATCOM is the main research direction.

Liping Shi Graduated from department of Electrical Engineering, China University of Mining and Technology, China, with a doctor degree in power electronics and power transmission, the main work is to accomplish teaching tasks.

Research on the Multilevel STATCOM based on the H-bridge Cascaded

Guifeng Wang
School of Electronic Information and Electrical Engineering, Shanghai Jiao Tong University Shanghai 200030 China
Email: wgfmy@163.com

Jianguo Jiang and Shutong Qiao
Key Laboratory of Control of Power Transmission and Conversion, Ministry of Education Shanghai Jiao Tong University, Shanghai 200030 China
Email: qiao_shu_tong@sjtu.edu.cn, jiang@sjtu.edu.cn

Lifeng Guo
School of Information and Electrical Engineering, China University of Mining and Technology, Xuzhou 221116 China
Email: guolifeng1228@163.com

Abstract—This paper mainly studies the main circuit topology, the working principle, modulation technique and control strategy of the STATCOM based on H-bridge. The STATCOM direct power control algorithm based on the virtual flux is used to control the AC side reactive power compensation, and in accordance with the principle of conservation of power, the DC side voltage imbalance factors are analyzed, and a distributed DC voltage control algorithm is also introduced. The DC side control algorithm is divided into upper and lower control parts, of which the upper control section is aimed at the average of DC side capacitor voltage of the sub-module unit for the STATCOM device, the lower control part is mainly for each sub-module DC side capacitor voltage. Finally, the control strategy is verified in a three level chain STATCOM system with VME control box as its core controller, and the experimental results show that the algorithm is feasible.

***Index Terms*—Cascade Multi-Level; STATCOM; Carrier Shift Phase PWM; Direct Power Control; Distributed Control System**

I. INTRODUCTION

Flexible AC Transmission System (FACTS) is an important technical means for power grid to reduce energy consumption and improve power quality. As FACTS core equipment, static synchronous compensator (STATCOM) based on H-bridge cascade, which takes the full-controlled power electronic devices constitute a voltage source inverter (IGBT) as the core, and uses the cascade multi-level and PWM technology, has many advantages, such as: small output harmonic currents, less area, short response time, a wide range of reactive power compensation, easy to maintain, easy to expand, and low cost etc. So it has become the focus of research of domestic and foreign experts, and gradually applied to the high-voltage transmission grid [1, 2, 3, 4].

Nowadays, STATCOM AC side control algorithm has been widely used in power decoupling PWM control, which has achieved the decoupling of power model by the PI regulator. It is easy to use and has small amount of calculation; however, to guarantee its normal operation, the network voltage as well as the network voltage transformer are required [5, 6]. The power system is strongly coupled and nonlinear, and the local linearization control of the control theory of nonlinear system is used [7]. This method achieves the Taylor expansion of STATCOM nonlinear state equation, and carries out local linearization at a certain point to obtain the localized linear equation. Then, the modern control theory is adopted to design the controller based on the obtained equation. Although this method has excellent properties of control, the local linearization method has limited the operation range of STATCOM to some extent.

The virtual flux-based STATCOM direct power control algorithm has introduced the concept of virtual flux to obtain the information about network voltage indirectly, thus omitting the network voltage transformer, which has optimized the control structure of the system and improved its reliability [8, 9, 10].

Firstly, the paper studies the main circuit structure and working principle of the STATCOM based on the H-bridge cascade and carrier phase shift PWM (CPS-SPWM) technology; Secondly, On the basis of the STATCOM direct power control algorithm based on virtual flux, the distributed DC side voltage control algorithm is introduced through the principle of power conservation. Finally, the control strategy is verified on three chain STATCOM system controlled by a VME chassis.

II. MAIN CIRCUIT STRUCTURE AND PRINCIPLE OF THE STATCOM BASED ON THE H-BRIDGE CASCADE

The STATCOM based on H-bridge cascaded, which is constituted by the H-bridge module unit in series, has both triangle and star connection mode. Star connection is

doi:10.4304/jnw.9.1.147-152

shown in Figure 1, equipment capacity can be improved by a simple increase in the number of link module, and it is low cost, easy to implement and small footprint. Ideally, an equivalent circuit diagram of the STATCOM is shown in Figure 2. L_c and R_c are the total inductance and resistance in the apparatus main loop (including the connecting reactance and the inverter impedance), v_s is the grid voltage, v_c is output voltage of the STATCOM, i_c is absorption current of the STATCOM equipment.

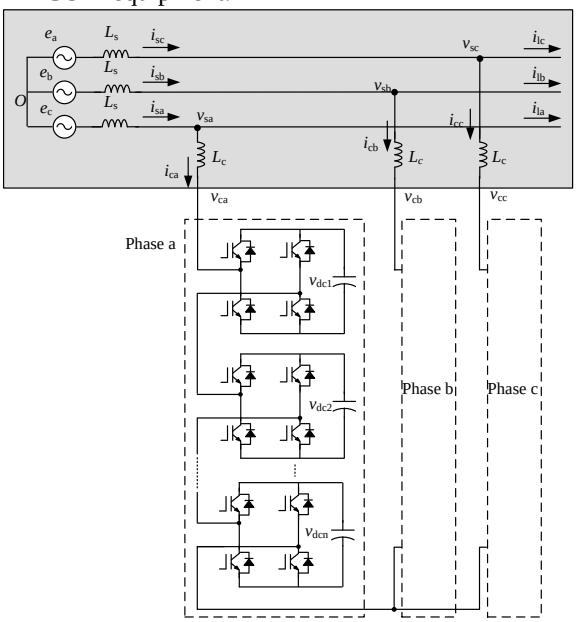

Figure 1. Cascaded STATCOM topological structure

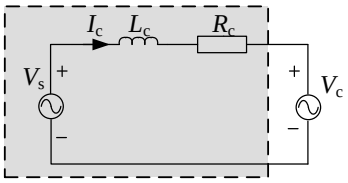

Figure 2. Equivalent circuit of STATCOM

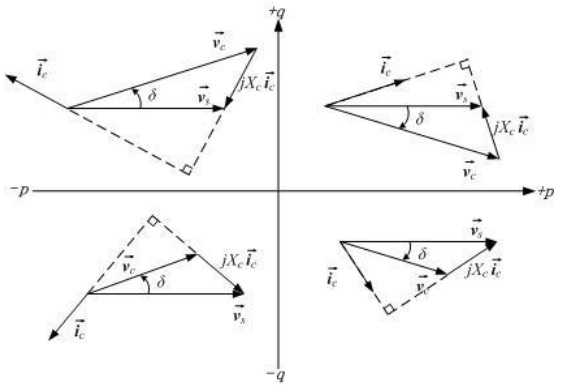

Figure 3. Voltage and current vectors diagram of STATCOM

The phase and amplitude of the current absorbed by STATCOM from the grid can be controlled by changing the STATCOM output voltage amplitude and phase with respect to v_s. And the nature and magnitude of the reactive power can be further controlled [3, 4], Figure 3 shows the voltage and current vectors diagram when the reactive power compensation system connects to the grid through an ideal inductor current, X_c is the value of loop inductance, σ is the angle of the STATCOM output voltage with the grid voltage. According to Figure 3, when the STATCOM output voltage amplitude v_c and phase changes, the size and nature of active and reactive power of which absorbed by the STATCOM also vary accordingly[5, 6, 7].

III. Modulation Algorithm of H-Bridge Cascade Multilevel Converter

Currently, the modulation algorithm H-bridge cascade multilevel converter mainly includes: the ladder wave modulation [11], space voltage vector method [12, 13] and carrier phase shift PWM method [14, 15]. Ladder wave modulation is a baseband modulation method, the switching frequency is low, and conducive to high-power implementation of STATCOM, but the harmonic content of the output voltage is great, only in the case of a large number of level is high-quality output voltage obtained; In contrast, space voltage vector method with a high DC voltage utilization is easy to facilitate the digitization method, but with the increase in the number of output level, especially after more than 5 level, it is difficult to achieve, and the amount of controller operations is increased; CPS-SPWM is a multi-carrier SPWM modulation algorithm. PWM trigger pulse is generated through a multi-channel carrier moving on the timeline $T_s/(2\cdot N)$ (T_s is carrier cycle, N is the number of modules in series).

Figure 4 is a schematic diagram of the 2 modules in series CPS-SPWM, this method is simple to be designed, and easy to be implemented, and can make the same as the number of switching cycles of the equipment unit module, and is also easy to implement the DC side of capacitor voltage equalizer control.

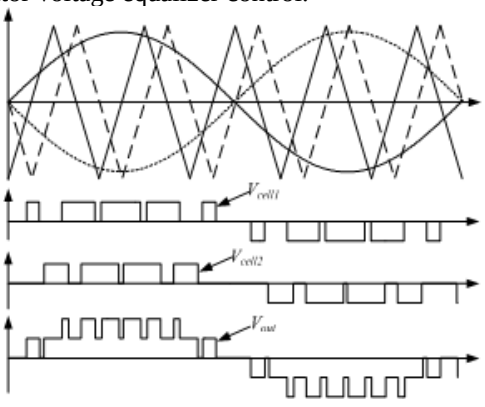

Figure 4. Multilevel phase-shifted carrier-based techniques

IV. STATCOM Control Strategy Based on H-Bridge Cascade

A. STATCOM Direct Power Control Based on Virtual Flux

1) Principle of Virtual Flux Observer

The principle of virtual flux is that overall grid side with converter access is seen as a three-phase AC motor [16], as is shown in the dark part of the box of Figure 1 and Figure 2, STATCOM converter grid voltage v_s is equivalent to induced electromotive force which is generated by the AC motor air gap magnetic field in the stator winding, the inductor L_c and the resistor R_c are equivalent to the equivalent resistance of the stator winding and the stator leakage inductance respectively, so it can be seen that three-phase grid voltage is gotten through a virtual air gap flux induction. Thus the application flux can be applied instead of the grid voltage in accordance with the relationship that flux phase lags induced electromotive force phase angle of 90°.

According to the relationship between flux and induced electromotive force, the estimated value $\psi_{s\alpha}$, $\psi_{s\alpha}$ of virtual flux in α,β coordinate system are:

$$\begin{cases}\psi_{s\alpha}=\int v_{s\alpha}dt\\ \psi_{s\beta}=\int v_{s\beta}dt\end{cases} \tag{1}$$

Among (1), $v_{s\alpha}$, $v_{s\beta}$ are the grid voltage component in the α,β coordinate system, according to STATCOM voltage equation under the coordinate system

$$\begin{cases}v_{s\alpha}=L_c\dfrac{di_{c\alpha}}{dt}+v_{c\alpha}+R_c\cdot i_{c\alpha}\\ v_{s\beta}=L_c\dfrac{di_{c\beta}}{dt}+v_{c\beta}+R_c\cdot i_{c\beta}\end{cases} \tag{2}$$

Among (2), $i_{c\alpha}$, $i_{c\beta}$ are the STATCOM current flows in the α,β coordinate system, if the equivalent resistance R_c is ignored, the estimated value of virtual flux is:

$$\begin{cases}\psi_{s\alpha}=\int[\sqrt{\dfrac{2}{3}}v_{dc}(\sum\limits_{i=1}^{n}S_{ai}-\dfrac{1}{2}(\sum\limits_{i=1}^{n}S_{bi}+\sum\limits_{i=1}^{n}S_{ci}))]dt\\ \qquad +Li_{c\alpha}\\ \psi_{s\beta}=\int[\dfrac{1}{\sqrt{2}}v_{dc}(\sum\limits_{i=1}^{n}S_{bi}-\sum\limits_{i=1}^{n}S_{ci})]dt+Li_{c\beta}\end{cases} \tag{3}$$

Among (3), v_{dc} is the H-bridge module sub-unit DC bus voltage, S_{ai}, S_{bi} and S_{ci} are respectively *i*-th unit of each bridge arm switching state.

By the formula (3), virtual flux signal can be seen as the system phase-locked loop to participate in the system control, phase lock circuit and the grid voltage sensor are omitted, at the same time, when the grid voltage distorts, the satisfied grid angular information can be obtained because of the existence of the integral part.

Since the pure integral part of the formula (3), if the integral initial value isn't selected properly, The DC bias will be introduced to the virtual flux. Usually a low pass filter is used instead of a pure integrator in order to eliminate the steady state DC offset.

According to the literature [12], the improved virtual flux observer using cascade inertia instead of the pure integral part is shown in Figure 5, the transfer function of the cascade inertia.

$$H(s)=\frac{N}{s+\omega_c}\cdot\frac{N}{s+\omega_c}=\frac{N^2s}{(s+\omega_c)^2}\cdot\frac{1}{s} \tag{4}$$

No difference in amplitude and phase shift should be ensured when the pure integrator is replaced. Under these two conditions, the relationship can be obtained as follows.

$$N=\sqrt{2\omega},\quad \omega_c=\omega \tag{5}$$

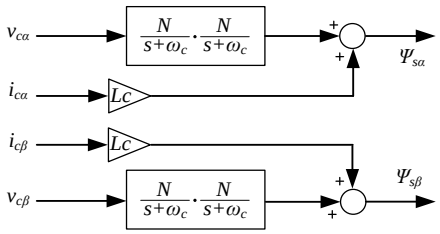

Figure 5. Improved virtual flux observer

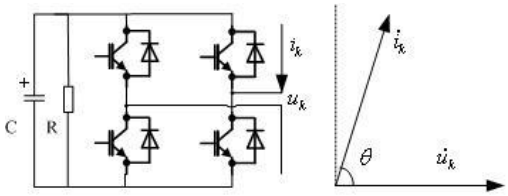

Figure 6. The circuit and vector of the cell

2) Instantaneous Power Detection Based on Virtual Flux

Improved virtual flux observer is able to achieve fast and accurate flux estimates, According to the instantaneous power theory, the instantaneous power absorbed by the STATCOM device can be expressed as:

$$\begin{cases}\mathrm{p}=\mathrm{Re}(\vec{v}_s\cdot\vec{i}_c)\\ \mathrm{q}=\mathrm{Im}(\vec{v}_s\cdot\vec{i}_c)\end{cases} \tag{6}$$

where, $\vec{v}_s$ is the grid voltage vector, $\vec{i}_c$ is the inflow of the STATCOM current vector. In accordance with the principles of the virtual flux the grid voltage is:

$$\begin{aligned}\vec{v}_s&=\frac{d}{dt}\vec{\psi}_s=\frac{d}{dt}(\psi_s e^{j\omega t})\\ &=\left.\frac{d\psi_s}{dt}\right|_{\alpha}+\left.\frac{d\psi_s}{dt}\right|_{\beta}+j\omega(\psi_{s\alpha}+j\omega\psi_{s\beta})\end{aligned} \tag{7}$$

Binding of formula (6) and (7), and when the system meets the three-phase balanced sinusoidal line voltage, the virtual flux amplitude is constant. It is possible to obtain the instantaneous power absorbed by the STATCOM:

$$\begin{cases}\mathrm{p}=\omega(\psi_{s\alpha}i_{c\beta}-\psi_{s\beta}i_{c\alpha})\\ \mathrm{q}=\omega(\psi_{s\alpha}i_{c\alpha}+\psi_{s\beta}i_{c\beta})\end{cases} \tag{8}$$

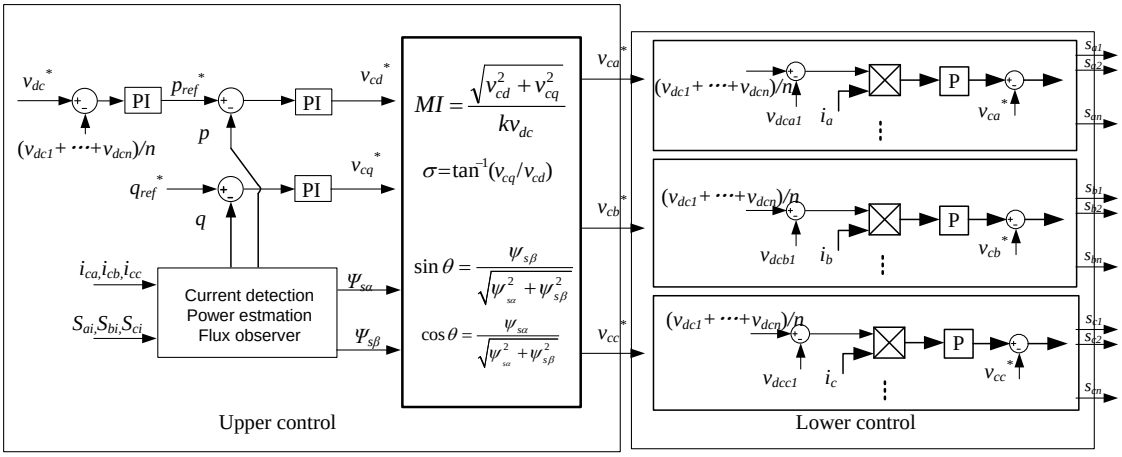

Figure 7. Hierachical controller for system

According to the formula (4) and (8), the STATCOM direct power control system block diagram based on virtual flux is shown in Figure 7 the upper control is the STATCOM direct power control based on virtual flux, θ is grid voltage orientation angle. As Figure 7 is shown, the STATCOM control strategy does not require a grid voltage transformer through introducing virtual flux theory. So it can effectively overcome the problem of the detection error due to a voltage transformer, the algorithm is simple and easy to digital implementation.

B. The Control Strategy in the Distributed DC Side

DC capacitor of each module of STATCOM based on H-bridge cascade is independent of each other, and switching losses, circuit losses, the switch allocation status and pulse delay differences, which led to the DC bus voltage imbalance exists [17,18]. In this paper, the DC side control strategy of the hierarchical distributed which is divided into the upper control and lower control is adopted. The upper control stabilizes overall DC bus voltage, that is the average of the entire device module DC bus voltage; lower control stabilizes each module DC bus voltage.

The upper control takes all module DC voltage as a whole C, according to the power balance, the mathematical models for the STATCOM DC side capacitor voltage in the $d-q$ coordinate system is

$$\frac{dv_{dc}}{dt}=\sqrt{\frac{3}{2}}\frac{K}{C}(i_{\mathrm{d}}\cos\delta+i_{\mathrm{q}}\sin\delta)+\frac{\sqrt{3}V_{\mathrm{S}}}{L_{\mathrm{c}}} \qquad (9)$$

where, v_{dc} is the average value of DC capacitor voltage, K is SPWM modulation ratio, C is the DC bus voltage, V_s is the AC grid voltage peak. δ is angle between STATCOM output voltage vector and the grid-side voltage vector, if δ is small, v_{dc} and i_{d} can be regarded as a linear relationship. So that the DC bus voltage upper control is designed for the outer ring of the active current.

Lower control is for sub-module DC bus voltage, according to the principle of power balance, as is shown in Figure 6, C is DC capacitor, R is module equivalent loss resistance, i_k is arm current, u_k is the module output voltage fundamental amount. The active amount absorbed and emitted by the sub-module unit is decided by i_k, u_k and their phase angle θ. Thus, the DC side capacitor voltage can be adjusted by adjusting the amplitude and phase of u_k. The adjustment amount, which has relationship with the bridge arm current, is designed to P regulator, the output is superimposed to the output modulated wave of the reactive power compensation in the AC side, and this does not affect the reactive power control in the AC side.

According to the AC and DC side control algorithm analysis, the cascaded STATCOM control block diagram is shown in Figure 7. Where, $s_{\mathrm{ak}}, s_{\mathrm{bk}}, s_{\mathrm{ck}}$ are the modulation waves of the carrier shift phase PWM modulation.

V. EXPERIMENTAL VERIFICATION

To verify the above control strategy, a 3 H-bridge cascade STATCOM system in a star connection is developed. As is shown in Figure 7, the main circuit parameters are shown in Table 1. The host controller for experimental platform is control cabinet based on the VME bus produced by the wing company in United States, the laboratory equipments connect with 380V power grid through the auto-transformer.

Figure 8 shows the output of the converter line voltage v_{cbc}, v_{cca} and the grid line voltage v_{sab}, v_{sbc}. The line output voltage of the converter is 13 level, it can be seen by comparing STACOM output line voltage v_{cbc} with the grid voltage v_{sbc}, according to the principle of virtual voltage, grid voltage phase directional meets the control requirements .

Figure 9 is the converter dynamic test waveform, the reactive power is measured by output of D / A board of the VME chassis. Figure 9(a) is transient waveform when STATCOM system absorbs the inductive reactive power, Figure 9(b) is transient waveform when it absorbs the capacitive reactive power, the system running the current value is 3.5 A. In the case of a capacitive mode, the output current THD of inverter is 2.8%, which is 3.2% in

the case of inductive mode. The figure shows that the control system is stable, good dynamic performance, and the stability of the DC bus voltage is good.

TABLE I. MAIN PARAMETERS OF THE LABORATORY EQUIPMENT

Parameter	Value
Grid voltage (rms) U_s /V	230
Grid frequency f /Hz	50
Grid inductance L_c /mH	4mH
Module DC capacitor C/uf	3400
DC bus voltage v_{cd} /V	63
Rated output current I_c /A	10

Figure 10 is reactive power compensation system, in the case of a capacitive load, The STATCOM system is not put into operation firstly, and opened at time t. The waveform shows that the system compensation effect is good and the current amplitude is significantly reduced.

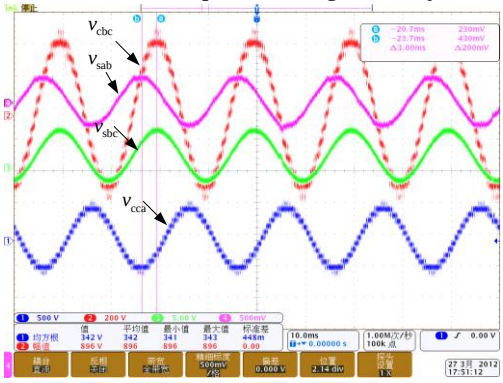

Figure 8. The line voltage of the 3-cells cascade STATCOM and grid

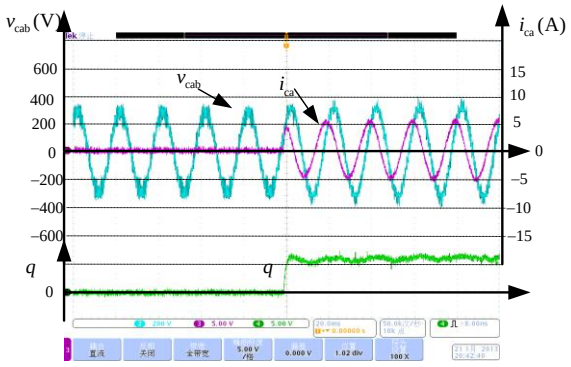

(a) STATCOM absorbs the inductive reactive power

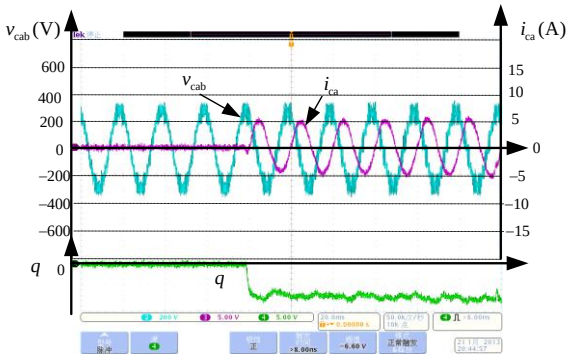

(b) STATCOM absorbs the capacitive reactive power

Figure 9. The dynamic waveforms of the 3-cells cascade STATCOM

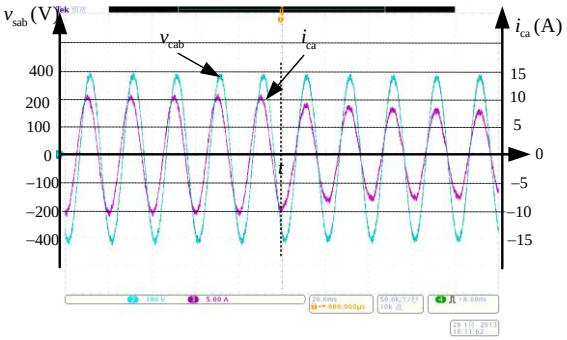

Figure 10. The voltage and current waveforms of grid voltage

VI. CONCLUSION

The main circuit structure and principle of STATCOM based on the H-bridge cascade, the carrier phase shift PWM technology, direct power control algorithms based on virtual flux and distributed DC voltage control algorithm are studied in this paper. The control strategy on 3 H-bridge cascade STATCOM system controlled by a single VME chassis is tested by the experiment, the results show that the STATCOM direct power control algorithm based on the virtual flux is simple, the amount of calculation is small, grid voltage transformer is not needed, and the dynamic performance of the STATCOM system is good; The hierarchical, distributed DC voltage control algorithm can effectively suppress the DC bus voltage fluctuations. The above algorithm can also be extended to the multi-stage high-pressure STATCOM system based on H-bridge cascaded.

ACKNOWLEDGMENT

This work was supported by the National High Technology Research and Development Program of China (863 Program) under Grant No. 2011AA050403; Doctoral Program of Higher Specialized Research Fund (new teachers class) Project (20110073120034)

REFERENCES

[1] K. Eel-Hwan, K. Jae-Hong, K. Se-Ho, et al. Impact analysis of wind farms in the Juju Island power system. *IEEE trans on Systems Journal*, 2012(6) pp. 134-139.

[2] Qing-qing Zheng, Jing Wu, Xuan Wang. The application of carrier phase shift technology chain STATCOM. *Power electronics technology*, 2010, 44(12) pp. 122-124 (Chinese)

[3] Y. Pal, A. Swarup, B. Singh. A Review of Compensating Type Custom Power Devices for Power Quality Improvement. *IEEE Power India Conference*, 2008 pp. 1-8

[4] L. Zhao, L. Bangyin, D. Shanxu, el al. A Novel DC Capacitor Voltage Balance Control Method for Cascade Multilevel STATCOM. *IEEE Trans on Power Electronics*, 2012. 27(1) pp. 14-27.

[5] Zhang Yong Gao, Kang Yong, Liu Liming, etc. Double-loop control design of STATCOM. *Electric Power Automation Equipment*, 2006, 26 (10) pp. 62-66.

[6] Sirisukprasert S, Huang AQ, and Lai J-S. Modeling analysis and control of cascaded-multilevel converter-based *STATCOM. Proc. Power Eng. Soc. General Meeting*, 2003 pp. 2561-2568

[7] Chia B H K, Morris S, Dash P K. A feedback linearization based fuzzy-neuro controller for current source inverter-basesd STATCOM. *Power Engineering Conference*, 2003 pp. 172-179.
[8] CAO Kai, Jiang Jianguo, Yangxing Wu, etc. Direct Power Control with Constant Switching Frequency for STATCOM with Compensation in Virtual Flux Estimation. *Electrical Automation*, 2010, 370 (50) pp. 31-35.
[9] Shi-chao Liu, Xing-wu Yang, Jian-guo Jiang. Direct Power Control with Constant Switching Frequency for STATCOM Based on Virtual Flux. *Electrical Automation*, 2009, 31(5) pp. 21-23. (Chinese)
[10] Hansen S, Malinowski M, Blaabjerg F, et al. Sensorless control strategies for PWM rectifier. *Fifteenth Annual IEEE Applied Power Electronics Conference and Exposition*, 2000 pp. 832-838.
[11] Ben-Sheng Chen, Yuan-Yih Hsu. A Minimal Harmonic Controller for a STATCOM. *IEEE Trans on Industrial Electronics*, 2008, 55(2) pp. 655-664.
[12] Aneesh M A S, Gopinath A, Baiju M R. A Simple Space Vector PWM Generation Scheme for Any General n-Level Inverter. *IEEE Trans on Industrial Electronics*, 2009, 56(5) pp. 1649-1656.
[13] Lin Ping, Wang Qiao, Li Jianlin, et al. Based on Cascaded wrong sampled space vector modulation multi-level converter APF study. *China Proceedings of the CSEE*, 2005, 25 (8) pp. 70-74.
[14] McGrath B P, Holmes D G. Multicarrier PWM strategies for multilevel inverters. *IEEE Trans on Industrial Electronics*, 2002, 49(4) pp. 858-867.
[15] Young-Min Park, Han-Seong Yoo, Hyun-Won Lee, el al. A Simple and Reliable PWM Synchronization & Phase-Shift Method for Cascaded H-Bridge Multilevel Inverters based on a Standard Serial Communication Protocol. *IEEE Industry Applications Conference*, 2006 pp. 988-994.
[16] Cichowlas M, Malinowski M, Kazmierkowski M P, Sobczuk D L, Rodriguez P, Pou J. Active filtering function of three-phase PWM boost rectifier under different line voltage conditions. *IEEE Trans on Industrial Electronics*, 2005, 52(2) pp. 410-419.
[17] Woodhouse M L, Donoghe M W. Type testing of the GTO values for a novel STATCOM convertor. *IEEE Trans on AC-DC Power*, 2001, 48(5) pp. 84-90.
[18] WANG Zhibing, YU Kunshan, ZHOU Xiaoxin. Control Strategy for DC Bus Voltage Balance in Cascaded H-bridge Multilevel Converters. *Proceedings of the CSEE*, 2012, 32 (6) pp. 56-63.

Guifeng Wang was born in Linyi Shandong province China in February, 1982. He received the bachelor and master degree in School of Information and Electrical Engineering at China University of Mining and Technology, China, in 2004 and 2007, respectively. He is a PH.D Candidate in School of Electronic Information and Electrical Engineering at Shanghai Jiao Tong University. His mainly recent research interests in the field of power electronic converters for power quality.

Jianguo Jiang was born in Yancheng Jiangsu province China in December, 1956. He received his B.Sc., M.Sc. and the Ph.D. degrees in Department of Electrical Engineering at China University of Mining And Technology, China, in 1982, 1985 and 1988, respectively. He is now a Professor of Shanghai Jiao Tong University and the director of the Key Laboratory of Control of Power Transmission and Conversion, Ministry of Education. His current research interests include power electronic converters for electrical drives and power quality.

Shutong Qiao was born in Hebei province China in 1978. He received the bachelor and master degree in School of Information and Electrical Engineering at China University of Mining and Technology, China, in 2001 and 2004, respectively. He isa research assistant of Shanghai Jiao Tong University. His mainly recent research interests in the field of power electronic converters for power quality.

Lifeng Guo was born in Renqiu Heibei province China in October,1986. He received the bachelor degree at China University of Mining and Technology, China, in 2006. He is now a graduate student in School of Information and Electrical Engineering at China University of Mining and Technology. His mainly recent research interests in the field of power quality.

Inter-cell Interference Mitigation in Multi-cell Cooperating System Based on SLNR Method

Wu Mingxin
Higher Education Research Institute, Beijing University of Aeronautics and Astronautics, Beijing 100191, China

***Abstract*—Coordinated Multi-Point transmission/reception (CoMP) can increase the performance of the cell edge users, the spectrum efficiency and mitigate the inter-cell interference among cells. In the CoMP scenario, several base stations which usually need satisfy the cooperating condition serve a single or several cell-edge users cooperatively. As we know, the CoMP techniques can be characterized into many classes. For the joint transmission system which is a classical CoMP system, a large number of data sharing and channel information exchange will be needed, where the system inevitably become comparatively complex. However, in this paper, the coordinated beam forming system will be considered, where several base stations cope with the inter-cell interference among cells, and all the base stations will only exchange the channel information. Further, the downlink multi-cell coordinated beam forming system is considered in this paper. In this downlink multi-cell coordinated beam forming system, it is crucial to design appropriate pre-coding schemes that are able to mitigate the inter-cell interference. In obtainable pre-coding schemes, the Signal-to-leakage-and-noise ratio (SLNR) pre-coding scheme is a promising pre-coding scheme in downlink multi-cell coordinated beam forming system, which makes closed-form solution accessible. Moreover, the problem in designing the pre-coding vectors is not a coupled problem since the cooperative base stations need not optimize the pre-coding vectors jointly, which are responsible for their own design of pre-coding vectors, that is, they will just carry out independent optimization. In this paper, we proposed a novel pre-coding scheme based on the SLNR scheme, which will determine the pre-coding vectors via iteration. The simulation results show that, the proposed method outperforms the conventional SLNR pre-coding scheme in bit error rate performance..**

***Index Terms*—CoMP; Pre-Coding Scheme; SLNR; Interference; Iteration; BER Performance**

I. INTRODUCTION

According to the relevant protocol and standard of the next generation mobile communication system, the LTE-Advanced systems utilize orthogonal frequency division multiplexing (OFDM) on the downlink and single-carrier frequency division multiplexing (SC-FDM) on the uplink [1]. Therefore, in the next generation mobile communication system which will use the LTE-Advanced technology, the intra-cell interference can be eliminated since the data intended to different users is transmitted at orthogonal subcarriers via SC-FDMA or OFDMA technique [2]. However, the inter-cell interference especially for the users at the cell boundary is the main reason for decreasing the system performance. In order that the system has certain immunity to inter-cell interference, Coordinated Multi-Point transmission /reception (CoMP) was put forward by 3rd Generation Partnership Project as one of the promising inter-cell interference mitigation techniques in March, 2008. To meet the performance requirement, 3rd Generation Partnership Project brought forward the future advancement of long term evolution techniques (LTE-Advanced), which ITU proposed for IMT-Advance system [3]. Since the users at the cell boundary are known to undergo a severe inter-cell interference in the next generation mobile communication systems with universal frequency reuse. Worse, the inter-cell interference will cause sharp degradation of system performance and can't be mitigated by enhancing the transmit power of desired signals. Luckily, the CoMP techniques which can cope with this problem is introduced in LTE-Advanced. CoMP shall also benefit the whole system capacity and increase the spectrum efficiency of users at the cell boundary [4].

In this context, 3GPP started Long Term Evolution (LTE) project. Project based on OFDM/FDMA technology as the core, some improvement and Optimization Based on wireless network architecture and wireless interface, used to reduce the delay spread to increase data rate! to increase coverage and system capacity and reduce the operation cost of communication network. Although CoMP presents an evident significant advantage in terms of system capacity, throughput, spectrum efficiency and bit error rate, the system complexity is an aspect which we have to confront. Based on the previous research on CoMP, the CoMP technologies contain several kinds of schemes [5].

In the joint processing system which is a classical CoMP system, the base station which generates the inter-cell interference to the target user also transmits the desired signal to the target user [6]. For this, the inter-cell interference is transmitted into useful signal, and all the transmitting base stations can process the transmitting data intended to the particular user jointly. Naturally, the received signal quality will be increased [7, 8]. A simple joint transmission system is depicted in Fig. 1. It is a pity that the joint processing scheme will require a large number of data sharing and channel information by utilizing a high-speed optical fiber backbone. Therefore the system complexity is large inevitably. To avoid the burdensome data sharing and channel information, we

doi:10.4304/jnw.9.1.153-160

can choose some other CoMP technologies which only need to exchange the channel information. An alternative scheme of CoMP termed coordinated beam forming needs only exchange the channel information [9, 10]. In this paper, we consider the downlink multi-cell coordinated beam forming system. In the downlink multi-cell coordinated beam forming system, it is indispensable to design appropriate pre-coding schemes that are able to mitigate the inter-cell interference [11].

LTE many new performance requirements makes the 3G air interface technology of the traditional hard to meet their requirements, so we need to use a new air interface technology in the technical proposal, according to the duplex mode can be divided into two orthogonal ways for orthogonal frequency division multiple access mode and; according to the wireless link and modulation can be divided into OFDM and CDMA two ways. Uplink physical layer of LTE mainly focus on the research of SC FDMA, so as to achieve the peak to average power ratio (Peak terminal transmits to Average can be reduced, to reduce the volume and cost of the terminal. Downlink physical layer is mainly division multiple access, thus effectively improving the spectrum efficiency of uplink and downlink respectively by the two techniques, can be very good to get rid of restriction of CDMA core technology patent.

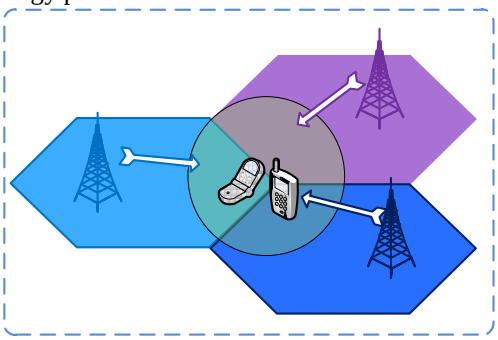

Figure 1. The joint transmission system

Some works about pre-coding vectors designing have proposed schemes for eliminating the inter-cell interference for each user in multi-cell cooperative system [12]. The pre-coding vectors designing by maximizing the output signal-to-interference-plus-noise (SINR) for each user is known to be not available because of its coupled personality and no closed-form solution [13]. One more tractable but suboptimal pre-coding scheme is Block Diagonalizatiom (BD), which enforces the inter-cell interference of each user to zero [3, 9, 10]. The BD scheme requires global Channel State Information (CSI) and imposes a restriction on system configuration in terms of the number of antennas at base stations, that is to say, it call for the number of the transmitting antennas at base stations to be larger than the receive antennas. This requirement is indispensable in order that enough degrees of freedom are met for the zero-forcing solution to force the inter-cell interference to zero at each user.

In [14], an alternative scheme of designing the pre-coding vectors was proposed, which will maximize the Signal-to-leakage-and-noise ratio (SLNR). The scheme transforms a coupled optimization problem in SINR scheme into a completely decoupled one and carries out an analytical closed-form solution for pre-coding vectors [15, 16]. Moreover, in contrast to the BD scheme, the SLNR solution does not require any dimension limitation on the number of transmit/receive antennas. It further takes the influence of noise into account and outperforms BD solution even when the dimension condition for BD solution is satisfied [17].

In this paper, a novel SLNR method for the inter-cell interference mitigation in the downlink multi-cell coordinated beam forming system is proposed, which takes into account the effect of interference as well as the leakage-plus-noise based on the conventional SLNR pre-coding scheme, and optimizes the pre-coding vectors via iteration. Simulation results confirm that, the proposed method outperforms the original SLNR pre-coding scheme in bit error rate performance.

Both codebook-based pre-coding for FDD systems and non-codebook based pre-coding for TDD systems schemes can be considered in the next generation mobile communication system [18]. For FDD systems, the instantaneous channel in uplink and downlink are characteristically uncorrelated and only long term statistical properties such as a time average covariance matrix can be used. For TDD systems, however, since we can assume that uplink and downlink are at the same frequency, short-term pre-coding based on momentary channel knowledge can be considered. In this paper we discuss the downlink multi-cell coordinated beam forming system under TDD mode, which is the so-called TD-LTE system [19].

The reminder of this paper is organized as follows. In Section II, we outline the system model of the downlink multi-cell coordinated beam forming system. In Section III we describe the pre-coding algorithm based on the conventional SLNR scheme [20]. In Section IV, we present a novel SLNR-based method and provide the detailed procedure of the proposed algorithm. In section V, we provide the simulation results and performance analysis, and Section VI concludes the paper.

Notations: $(\cdot)^H$, $(\cdot)^{-1}$, and $E(\cdot)$ denote, conjugate transpose, inverse, and expectation, respectively. $\|\cdot\|_F$ represents the Frobenius norm. Besides, $C^{M\times 1}$ represents the set of $M\times 1$ matrices in complex field [21-23].

II. System Model

We consider a downlink multi-cell coordinated beam forming system under TDD mode in this paper, which contains 3 Base Stations (BS's) and 3 paired users for description convenience with a frequency reuse factor equal to 1 as depicted in Fig.1. In this paper, we especially consider the cell-edge users. Fig. 2 is a conceptual illustration of downlink multi-cell coordinated beam forming system, each base station only serves its own user utilizing pre-coding. We assume that each BS transmits the signal using M transmit antennas with pre-coding and each user receives the signal using a single

antenna. The objective that all the base stations operate cooperatively is that the service quality of all the users can be guaranteed. In the TDD system, since the uplink and downlink work at the same frequency, that is to say, the reciprocity principle can be exploited between the uplink and downlink transmissions. Therefore the estimated channel in uplink can guide the downlink transmission, such as the design coefficient of pre-coding vectors in downlink can be obtained from estimated uplink channel. Then in our downlink multi-cell coordinated beam forming system user TDD mode, with the orthogonal pilot signal, we can assume that the user can estimate the channel information [6] and at the same time the BS can get the downlink channel information for pre-coding vectors designing via the reciprocity principle between the downlink and uplink. In the downlink multi-cell coordinated beam forming system, we could suppose that the maximum time delay of signals from all the cooperative cells is not longer than the CP length in order that the inter-symbol interference is not introduced in our downlink multi-cell coordinated beam forming system.

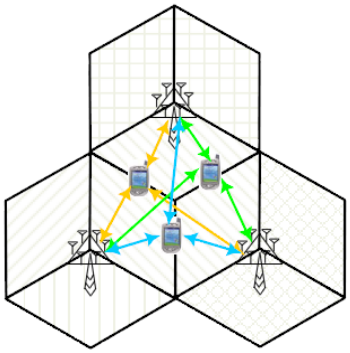

Figure 2. The downlink multi-cell coordinated beam forming system

Let $s_i(n)$ denotes the data transmitted by the base station i at the subcarrier n of OFDM symbol. Before transmitting over the channel, the data symbol $s_i(n)$ is multiplied by an $M \times 1$ pre-coding vector w_i. In this way, the $M \times 1$ transmitted vector at subcarrier n at base station i is given by

$$x_i(n) = w_i(n)s_i(n) \tag{1}$$

The normalization of $s_i(n)$ and the pre-coding vector $w_i(n)$ can be implemented as follows:

$E|s_k(n)|^2$, $\|w_k(n)\|^2 = 1$

And in our system k = {1, 2, 3}.

The $M \times 1$ vector $x_i(n)$ denotes the transmitting vector from base station i over the channel. Let $H_{i,k}(n) \in C^{M \times 1}$ denotes the channel from the i th base station to the k th user. We can assume the channel is a narrow-band channel, and then the received signal at the k th user at subcarrier n can be written by

$$y_k(n) = H_{k,k}(n)w_k(n)s_k(n) + \sum_{i=1,i\neq k}^{3} H_{i,k}(n)w_i(n)s_i(n) + n_k \tag{2}$$

where the second term is the inter-cell interference from other cells caused by the multi-cell nature of the system and the third term is the additive white Gaussion noise with $E\left[n_k n_k^H\right] = \sigma_k^2$. For notational convenience, the index of n can be omitted in following fomulas. In the downlink multi-cell coordinated beam forming system in TD-LTE scenario, each base station can estimate the downlink channel from uplink transmissions to adjust the downlink transmission coefficients of pre-coding vectors by utilizing the channel reciprocity between uplink and downlink. At the input of the user, the SINR can be given by

$$SINR_k = \frac{\left\|H_{k,k}w_k\right\|^2}{\sigma_k^2 + \sum_{i=1,i\neq k}^{3}\left\|H_{i,k}w_i\right\|^2} \tag{3}$$

In fact, the SINR at the receiver is usually considered as the measurement of performance evaluation. Therefore, we could also take the SINR expressed in (3) for $k = \{1,2,3\}$ as an optimization criterion to choose the pre-coding vectors $\{w_i\}_{i=1}^3$, which would be determined so as to maximize the SINR for each user k. However, the design of the pre-coding vectors pursuing the SINR optimization is challenging since all the pre-coding vectors $\{w_i\}$ are coupled [7] from the expression (3) and the optimization criterion.

In order to avoid the coupled problem, some previous works have tried to enforce the co-channel interference (CCI) to zero, therefore the pre-coding vectors $\{w_i\}$ can be determined according to

$$H_{i,k}w_k = 0, \ for \ all \ i,k = \{1,\cdots,K\}, i \neq k \tag{4}$$

From the expression (4), the zero-forcing schmes will certainly result in good performance since the schemes cancel the interference completely. However, the schemes are considerably sensitive to some distortion or the interference which are not modeled and the system configuration in terms of the number of antennas must be met for determining the pre-coding vectors $\{w_i\}$ according to the expression (4). That is, the number of transmit antennas must be larger or equal to the number of all the receive antennas. Meanwhile, the signal-to-noise-ratio can not be satisfied in this solution because of having ignored the noise power in choosing the pre-coding vectors $\{w_i\}$.

For above reasons, an alternative approach for designing the pre-coding vectors become considerably promising, which will maximize SLNR at each user. The scheme need not the limitation on the number of transmit/receive antennas and need not solve the coupled problem like SINR scheme and most important of all, the performance of the system using the approach is better than that of the system utilizing zero-forcing solution. The method is so-called SLNR scheme as advanced in [5] and used in [8].

Composition of 3G network is composed of base station, radio network controller, Serving GPRS support node and gateway GPRS support node 4 network nodes. The main function of RNC for wireless resource management network function, maintenance and operation of radio resource control are network management system interface. The major drawback of RNC for many of the features associated with the air interface in RNC, resulting in resource allocation and business can't be adapted to the channel, protocol structure is too complex, not conducive to system optimization. The main function of eNB is: In the attached AGW; send paging information and broadcasting information; dynamic radio resource allocation, radio resource management includes a plurality of cells; the measurement setup and provide eNB; control radio bearer; radio admission control: in connection mobility control "associated with the air interface functions are concentrated in the eNB activation state, wireless link control and media access control are in the same network node, which can be combined with optimization and design. EUTRAN architecture is shown in Figure 3.

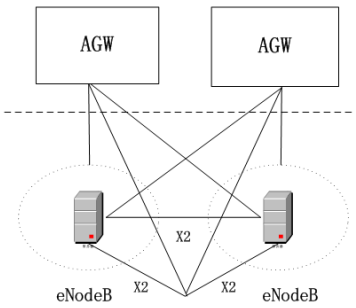

Figure 3. EUTRAN architecture.

In UTRAN, a radio network controller (RNC) between connected through Iur, Iur can be connected or connected through the transmission network through direct physical between RNC. RNC is used to allocate and control connected with or related to NodeB wireless resources. NedeB is complete conversion between Iub interface and Uu interface data flow, but also take part in radio resource management. This structure makes the load of RNC is very large, leading to many disadvantages: many of the features associated with the air interface in RNC, resulting in resource allocation and business can't be adapted to the channel, protocol structure is too complex, not conducive to system optimization.

Can be seen in the new LTE system, RNC and NodeB WCDMA system has been com., called E NodeB, in which eNB and AGW IbJ interface for connecting 51. The Iu PS interface, a 51 interface similar to the UTRAN, between eNB and eNB interface to XZ interface. Associated with the air interface functions are concentrated in the eNB, the radio link control (RLC) and media access control (MAC) are in the same network node, which can be combined with optimization and design. Thus the cross-layer resource allocation scheme provides a framework and a good platform for the operability of the implementation is greatly enhanced. The wireless access network such as LTE will greatly simplify. The first base station will join wireless management and routing functions, this will reduce the level of the network, data transmission delay and call setup delay will be reduced, in order to meet the requirements of real-time data service. The radio resource management are implemented in eNB. The base station will become an access point, and the core network will not only support mobile access, and supports the fixed access. The core network in the future will be divided into mobile network and fixed network no longer, but only a full IP network, its structure is not vertical, but the plane.

III. The Conventional SLNR-based Pre-coding Algorithm

From (2), $\left\|H_{k,k}w_k\right\|^2$ denotes the power of the desired signal for the user k. At the same time, $\left\|H_{k,k}w_k\right\|^2$ is the power of the interference caused by the base station k on the UE i in the i th cell. We thus define a quantity which denotes the leakage of the base station k to express the total power leaked from this base station k to all other UEs in other cells :

$$\sum_{i=1,i\neq k}^{3}\left\|H_{k,i}w_k\right\|^2$$

For each user k, we would like its desired signal power $\left\|H_{k,i}w_k\right\|^2$ to be large, and the power leaked from the user k to other USERs in other cells and the noise power at the receiver are small correspondingly. Base on the clue, we will introduce the quantity termed SLNR which can be defined as

$$SLNR_k=\frac{\left\|H_{k,k}w_k\right\|^2}{\sigma_k^2+\sum_{i=1,i\neq k}^{3}\left\|H_{k,i}w_k\right\|^2} \tag{5}$$

where, $SLNR_k$ denotes the SLNR of the user k and σ_k^2 is the noise at the receiver.

According to the concept of SLNR, we can design an optimization criterion on pre-coding which will maximize the SLNR. In detail, we could select the pre-coding vectors $\{w_i\}_{i=1}^3$ so as to maximize the SLNR expressed in (5) subject to $\left\|w_i\right\|^2=1$. We define a quantity $\tilde{H}_k$:

$$\tilde{H}_k=[H_1\cdots H_{k-1}H_{k+1}\cdots H_K]^T$$

which is an extended channel matrix that excludes $H_{k,k}$ only, and then the SLNR expressed in (5) also can be written as

$$SLNR_k=\frac{\left\|H_{k,k}w_k\right\|^2}{\sigma_k^2+\left\|\tilde{H}_k w_k\right\|^2} \tag{6}$$

According to the SLNR criterion, the pre-coding vector w_k^o is designed based on the following metric

$$w_k^o = \arg\max_{w_k} SLNR \quad (7)$$

This is a general Rayleigh entropy problem, and then the solution of expression (7) can be obtained from the solution of the general Rayleigh entropy problem. From [13], we know that the solution of the expression (7) which will optimize the SLNR can be given by

$$w_k^o = \max .eigenvector((\sigma_k^2 + \tilde{H}_k^H \tilde{H}_k)^{-1} H_k^H H_k) \quad (8)$$

That is, the pre-coding vector w_k^o is the eigenvector corresponding to the largest egienvalue of the matrix $(\sigma_k^2 + \tilde{H}_k^H \tilde{H}_k)^{-1} H_k^H H_k$. And the optimal pre-coding vector w_k^o could be normalized according to $\left\| w_k^o \right\|^2 = 1$.

Compared to the solution of the pre-coding vectors according to the SINR criterion, the pre-coding vector w_k^o obtained from the SLNR criterion is evidently not optimal. Under normal circumastances, the system which has maximal SLNR does not always has maximal SINR. After all, the SINR criterion is usually considered as the measurement of the system performance evaluation. However, as mentioned before, optimizing SINR over the pre-coding vector w_k is challenging and therefore we are now using the alternative SLNR criterion.

From the solution of the SLNR criterion, we know that the problem is not a coupled problem and the solution for pre-coding vector is an analytical closed-form solution. Moreover, in contrast to the BD scheme, the SLNR solution need not satisfy any dimension condition. It further takes the influence of noise into account and outperforms BD solution even when the dimension requirement for BD solution is satisfied. Therefore, the SLNR criterion is considered as the pre-coding scheme in our downlink multi-cell coordinated beam forming system reasonably.

IV. Proposed Novel SLNR-based Pre-coding Scheme

According to the conventional SLNR criterion, the pre-coding vectors are designed separately and need only exchange the channel information. Therefore the SLNR scheme has low complexity. In this section, we propose a novel SLNR method for the inter-cell interference mitigation in the downlink multi-cell coordinated beam forming system, which will maintain the structure of (5) and reserve the nature of low complexity. The novel scheme based on the conventional SLNR not only take into account the leakaged power to the USERs in other cells but also take the interference from other cells into consideration. To implement the novel scheme, we revise (5) as

$$SLINR_k = \frac{\left\| H_{k,k} w_k \right\|^2}{\sigma_k^2 + \sum_{i=1,i\neq k}^{3} \left\| H_{k,i} w_k \right\|^2 + \sum_{i=1,i\neq k}^{3} \left\| H_{i,k} w_i \right\|^2} = \frac{w_k^H A w_k}{w_k^H B w_k} \quad (9)$$

where $A = H_{k,k}^H H_{k,k}$,

$$B = \sum_{i=1,i\neq k}^{3} H_{k,i}^H H_{k,i} + (\sigma_k^2 + \sum_{i=1,i\neq k}^{3} \left\| H_{i,k} w_i \right\|^2) I$$

The solution of the novel SLNR problem can be expressed the independent optimization problem as

$$w_k^* = \arg\max_{w_k} SLINR \quad (10)$$

The novel scheme chooses the pre-coding vectors iteratively at the same time considering the interference from other cells and the leakged power and noise. There are 4 steps for implementing this scheme being described.

Obtain the channel coefficients from all the base stations to all the USERs. In our TDD system, the uplink and downlink transmissions are at the same frequency so that the reciprocity principle makes the estimated uplink channel guide the downlink transmission. So we can assume that the user can estimate the channel information using a pilot signal and the BS can get the channel information via the reciprocity principle between the downlink and uplink.

Solving the classical SLNR problem expressed in the (7), we can obtain the initial pre-coding vectors w_1^0, w_2^0, w_2^0 .

Substitute the initial pre-coding vectors w_1^0, w_2^0, w_2^0 into (11), then solve the novel SLNR problem, we obtain the new pre-coding vectors w_1, w_2, w_3 .

Repeat the 3 step, update the pre-coding vectors iteratively.

Wireless communication system is a limited resource, how to use the limited system resources to meet the growing demand, has become the mobile communications equipment manufacturer and operation business problems to be solved. If there is no effective radio resource management strategies, transmission technology more advanced, more wide bandwidth will also can give full play to its advantages because of scheduling process is not appropriate. Packet scheduling is aimed at the characteristics of different packet data service, management and scheduling of packet data services. The basic problem to be solved for packet scheduling: when more than one packet traffic waiting to receive service, must determine reasonable service rules, arrange business flow sequence of service, business hours and the transmission packet bit rate, to meet the different QoS requirements of business flows.

The scheduler is a function entity for packet scheduling. The basic model of the scheduler in wireless communications was shown in figure 4. Scheduler for scheduling is the first operations of the N queue, and then the packet processing, the last packet scheduling. A good scheduling algorithms guarantee user QoS requirements while maximizing the system capacity, to both throughput and user of the system's QoS requirements. In order to meet this requirement, the need to provide some information for the external scheduler, such as user channel conditions, data queue length. A comprehensive consideration of various factors, in the full use of channel state information and user service queue information at

the same time, to reduce the signaling and other aspects of the cost, maximize the performance of the system.

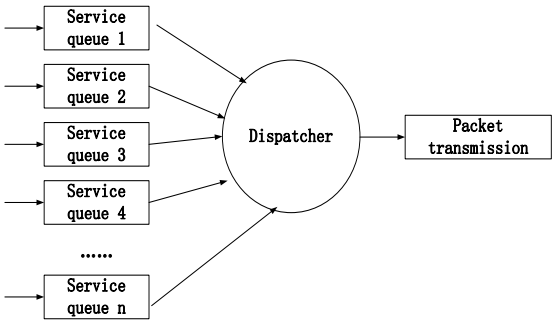

Figure 4. The scheduler model in wireless communication.

Since the mobile data business growth, many scholars believe that the high speed packet access will be the only way which must be passed the evolution of mobile communications. Considering the future mobile communication system is based on data traffic, in order to meet this demand, ensure real-time, non real-time, high speed, different service quality service at low speed, and at the same time on the radio resources to optimize use, need to use flow control technology, combined with the characteristics of wireless links, improve data throughput by grouping scheduling algorithm is advanced, guarantee user fairness and meet the industry QoS.

Wireless packet scheduling algorithm is a key technology of improving the system capacity, it is to maximize the system throughput as the goal, to guarantee the fairness among users as the premise, in order to ensure the quality of service requirements of different service flow based. Wireless packet scheduling algorithm is mainly assigned to which users of wireless resource decision what to communicate at any time, the wireless resources including time, frequency, code, or even subcarrier. The main function of wireless packet scheduling can be summarized as: sharing the air interface resources available in the packet transmission channel between users; determined for each user packet data transmission; load monitoring group distribution and system.

V. Simulation Results

In this section, we will provide the simulation results to demonstrate the effectiveness of our proposals for the novel pre-coding scheme based on the conventional SLNR pre-coding scheme. We assume the channel is a quasi-static flat fading channel in our system. Without loss of generality, we consider the BER as the performance measurement to verify the advantage of our scheme in this paper.

In order to verify the system performance, the downlink multi-cell coordinated beam forming system in TD-LTE scenario needs a multi-cell interference model. As shown in Fig. 5, this is a cellular system with 19 cells. The round dot denotes the base station in a hexagonal grid. We will select the cooperative base stations from the second tier and the rest are interference cells. The cooperative base stations will exchange the channel information but not signal information. On the one hand, to achieve better performance, the number of cooperative cells should be large enough. On the other hand, some factors limit the number of cooperative cells. For simplicity, in our downlink multi-cell coordinated beam forming system, we have simulated 3 cooperative cells where each base station is equipped with 2 transmit antennas, and each cell-edge user is equipped a single antenna.

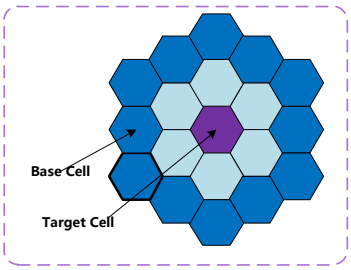

Figure 5. Multi-cell model

The simulation parameters of the downlink multi-cell coordinated beam forming system under TDD mode are presented in Table I. Spatial Channel Model Extended (SCME) is considered as the channel model used in the simulations and the modulation is Quadrature Phase-Shift Keying (QPSK). Fig. 5 presents the BER performance comparison for various SNR. In the factual system and the simulation system, the FFT size is larger than the available subcarriers. From the simulation results, we know that the performance of the proposed pre-coding scheme termed the novel SLNR method for the inter-cell interference mitigation in downlink multi-cell coordinated beam forming system is better than the conventional SLNR pre-coding scheme.

TABLE I. Simulation Parameters

Parameters	Assumption
Cellular layout	Hexagonal grid, 19 cell sites
Inter-site distance	1000 m
Carrier frequency	2.6 GHz
Channel model	SCME
System bandwidth	5 MHz
UE speed	3 km/h, 30 km/h
Modulation	QPSK
Antenna configuration	1 Tx/1 Rx
FFT size	512
Number of sub-carrier	256
Cyclic prefix	160 (pilot symbol),140 (data symbol)
SNR in uplink	10 dB

Fig. 6 compares the BER performance of BER performance in conventional SLNR pre-coding scheme with the novel SLNR method for the inter-cell interference mitigation in downlink multi-cell coordinated beam forming system. The ordinate axis represents BER and the abscissa axis represents Signal to Noise Ratio (SNR).

As Fig. 6 shows, for the inter-cell interference mitigation in multi-cell cooperating system, the BER performance of the novel SLNR method proposed in this paper outperforms about 1dB at the BER of 10^{-1} from the conventional SLNR pre-coding scheme. The simulation results show that, the proposed method

outperforms the conventional SLNR pre-coding scheme in BER performance.

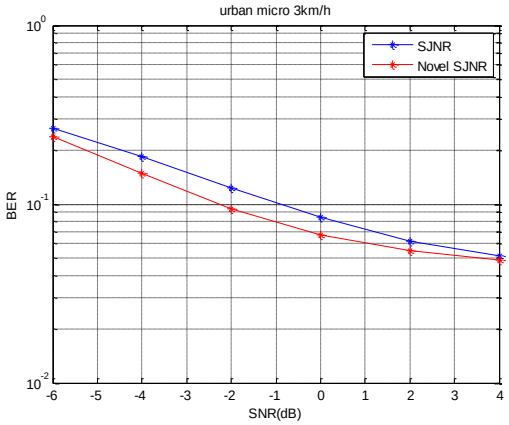

Figure 6. BER performance in the original SLNR pre-coding scheme and the novel SLNR method for the inter-cell interference mitigation in multi-cell cooperating system, with UE speed=3 km/h

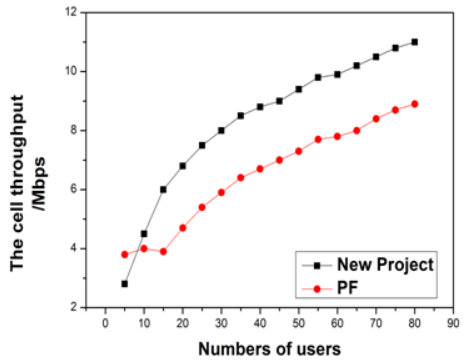

Figure 7. The relationship between the cell throughput and the number of users.

Figure 7 is the comparison between different schemes can obtain the cell throughput in different user number case. As shown in Figure 7, the cell throughput for the suggested to use square markers of the curve of the scheme can be obtained, as the traditional PF algorithm can be obtained by circle markers curve cell throughput. This graph shows, when the user is small (the users within the cell number is less than 10), high throughput can be obtained by the traditional PF algorithm. Such as when the user number is 5, the traditional PF algorithm can achieve throughput for 3.7MbPs, the new scheme can improve the throughput of 2.gMbPs. This is mainly because the area of less number of users, the uplink interference between users is not too serious.

The new scheme considering the interference to the adjacent cell transmitting user uplink signal, resulting in a part of the adjacent cell interference users cannot obtain the service, thereby reducing the cell throughput of new scheme. But when more users (users within the cell number is greater than 10), the new scheme can obtain the cell throughput will be far greater than the traditional PF algorithm can achieve throughput, compared to the traditional PF algorithm, the new scheme can make the cell throughput increase about 20%. Such as when the user number is 100, the traditional PF algorithm can achieve throughput for 9.2MbPs, the new scheme can achieve throughput for llMbPs, the new scheme makes the cell throughput up to 20%. This is mainly because when more users within a cell, the uplink interference between users is more serious. The new scheme takes into account the interference user uplink signal to adjacent cells, as far as possible for users to choose the interference between adjacent cells and smaller PRB use, reduces the interference between adjacent cells, so as to enhance the cell throughput.

This chapter firstly introduces the classification of simulation technology, important meaning and function of the system level simulation in order to make the reader understand this. Then, this chapter introduces the system level simulation modeling method of the key modules in the system level simulation and the process design and parameter setting etc. On the basis of the proposed uplink interference coordination scheme for multi-cell cooperative scheduling based on simulated, and compared with the traditional PF algorithm, the simulation results show that the proposed scheme can effectively reduce interference between adjacent cells, thereby obtaining the cell throughput is high and cell edge throughput, and can better adapt to the users within the cell, the business of the.

VI. CONCLUSION

In this contribution, we consider downlink multi-cell coordinated beam forming system which can achieve the better system performance gain by carrying out preceding at the base station based on channel information. We have developed and evaluated a method of the novel SLNR method for the inter-cell interference mitigation in multi-cell cooperating system in the guidance of the view that the proposed method not only take into account the leak aged power to the UEs in other cells but also take the interference from other cells into consideration. The method includes the merits of the conventional SLNR pre-coding scheme. It has been observed that the scheme provides an improvement performance in comparison with the conventional SLNR pre-coding scheme in BER performance. In addition, the scheme also is available to improve the BER performance in the multi-user multiple input multiple output system where one base station equipped with multiple antennas will serve multiple users equipped with multiple antennas or a single antenna.

To further investigate the potential advantage of the SLNR pre-coding scheme in the multiple cooperating cells, some factual factors should be considered, such as the impacts of the uplink channel estimation process, the influence of the uplink channel sounding imperfection, etc. Also the applicable occasions of the SLNR pre-coding scheme need to be considered. Further, we need to simulate some system level evaluations to see the impact on system performance.

REFERENCES

[1] 3GPP TR 36. 913, “Requirements for Further Advancements for E-UTRA (LTE-Advanced) (Release 8)”, www. 3gpp. org, 2008.

[2] M. Schubert, H. Boche, "Solution of Multiuser Downlink Beam forming Problem with Individual SINR Constraints", *IEEE Transactions on Vehicular Technology*, vol. 53, no. 1, pp. 18-28, 2004.
[3] Q. H. Spencer, A. L. Swindlehurst, M. Haardt. "Zero-Forcing Methods for Downlink Spatial Multiplexing in Multiuser MIMO Channel", *IEEE Transactions on Signal Processing*, vol. 52, no. 2, pp. 461-471, 2004.
[4] M. Sadek, A. Tarighat, A. H. Sayed, "A Leakage-based Pre-coding Scheme for Downlink multi-user MIMO Channels", *IEEE Transactions on Wireless Communications*, vol. 26, no. 8, pp. 1505-1515, 2008.
[5] A. Tarighat, M. Sadek, A. H. Sayed, "A multi User Beam forming Scheme for Downlink MIMO Channels based on Maximizing Signal-to-Leakage Ratios", *IEEE International Conference on Acoustics, Speech, and Signal Processing*, pp. 1129-1132, 2005.
[6] J. van de Beek, O. Edfors, M. Sandell, S. Wilson, P. Borjesson, "On Channel Estimation in OFDM System", *in Proceedings of the IEEE Vehicular Technology Conference*, pp. 815-819, 1995.
[7] K. Wong, R. Cheng, K. B. Letaeif, R. D. Murch, "Adaptive antennas at the mobile and base stations in an OFDM/TDMA system", *IEEE Transactions on Communications*, vol. 49, no. 1, pp. 195-206, 2001.
[8] M. Sadek, A. Tarighat, A. H. Sayed, "Active Antenna Selection in multi-user MIMO Communications, " *IEEE Transactions on Signal Processing*, vol. 55, no. 4, pp. 1498-1510, 2007.
[9] 3GPP TS 36. 300, "Evolved Universal Terrestrial Radio Access (E-UTRA) and Evolved UTRA (E-UTRA)", Dec. 2008. V8. 0. 0.
[10] L Tong, G Xu, B Hassibi, and T Kailath, "Blind channel estimation based on second-order statistics: a frequency-domain approach", *IEEE Trans. Inform. Theory*, vol. 41, pp. 329-334, 1995.
[11] Y Zhao, A Huang, "A novel channel estimation methods for OFDM mobile communication systems based on pilot signals and transform domain processing", *inPro. IEEE 47th Vehicular Technology Conference, Phoenix, USA*, pp. 2089-2093, 1997.
[12] Qiufen Ni, Rongbo Zhu, Zhenguo Wu, Yongli Sun, Lingyun Zhou, Bin Zhou, "Spectrum Allocation Based on Game Theory in Cognitive Radio Networks", Journal of Networks, Vol. 8, No. 3, 712-722, Mar 2013.
[13] Sinern Estimation Coleri, Mustafa Ergen, Anuj Puri, Ahmad Bahai. A Study of Channel in OFDM Systems. IEEE VTC, Vancouver, Canada. September, 2002.
[14] D. B. Van, O. Edfors, and M. Sandle, "On channel estimation in OFDM systems", *Proc. IEEE Vehic. Tech. Conf*, pp. 815-819, 1999.
[15] H. Landau, H. O.. Prolate, "spheriodal wave functions, Fourier analysis and uncertainty-III: The dimension of the space of essentially time and band-limited signal", *Bell Syst. Tech.* pp. 1295-1336, 2002.
[16] Bingyang Wu; Shixin Cheng; Ming Chen; Haifeng Wang, "Analysis of decision aided channel estimation in clipped OFDM", *Vehicular Technology Conference*, vol. 2, pp. 25-28, 2005.
[17] Effrided Dustin, Keff Rasjka, John Paul, "Automated Software Testing Introduction, Management, and Performance", *Addison-Wesley*, 2002.
[18] G. Patel, S. Dennett. "The 3GPP and 3GPP2 Movements Toward an All-IP Mobile Network", *IEEE Pet. Commun*, vol. 7, pp. 62 - 64, 2002.
[19] Chernak Y, "Validating and improving test-case effectiveness", *Software. IEEE*, vol. 18, no. 1, pp. 81-86, 2001.
[20] Qinqun Feng, Zhang Wuguang, Peng Yan, "Research on software testing tool based on Internet", *Computer applications and software*, vol. 23, pp. 133-135, 2006.
[21] Pool Baoyong, Yu Zhiping stone, "a review of. CMOS RF integrated circuit analysis and design", vol. 32, pp. 31-35, 2007.
[22] Li Genqiang, Kuang Wang, Wen Zhi-cheng, "RF and wireless technology", *Beijing: Electronic Industry Press*, vol. 12, pp. 13-15. 2009.
[23] Cao Peng, Qi Wei, "Broadband wireless communication transceiver technology", *Beijing: mechanical industry*, vol. 80, pp. 33-35, 2012.

An Improved K-means Clustering Algorithm

Huang Xiuchang
Yiwu Industrial and Commercial College, Yiwu Zhejiang, 322000, China
Email: tty4589000@163.com

SU Wei
College of Art, Hebei University of Science and Technology, Shijiazhuang 050018, China

***Abstract*—An improved k-means clustering algorithm based on K-MEANS algorithm is proposed. This paper gives an improved traditional algorithm by analyzing the statistical data. After a comparison between the actual data and the simulation data, this paper safely shows that the improved algorithm significantly reduce classification error on the simulation data set and the quality of the improved algorithm is much better than K-MEANS algorithm. Such comparative results confirm that the improved algorithm is a powerful for this problem.**

***Index Terms*—Trajectories Pattern Analysis; Clustering; K-MEANS**

I. INTRODUCTION

Faced with so much information in information society, analyzing and extracting knowledge from massive data cannot be finished only by manpower, which led to the repaid development of data mining areas. In pattern classification, there is a phenomenon that massive periodical statistical data in different objects show many broken line trajectories, for example, monthly blog postings of each Blogger. It is of significance to try to find out the same pattern in different objects, in order to help people analysis relevant problem, which has some rule to follow when confront with some same or similar problems. Generally, concrete quantification values attract little attention, but pay more attention to the variation trend of statistical data according to certain reference system in this kind of problems. For example, the studying on the behavior of customer visiting web site, often only focuses the attention on the change of browse capacity with time, while the concrete browse capacity is often ignored. By comparing data of the different user and finding out the same or similar changing tendency, user's behavior patter can be analyzed.

There are many methods to solve this kind of problems, such as machine learning, clustering analysis and so on. However, traditional clustering algorithms also exist some deficiency in this problem. This paper attempts to improve clustering algorithm represented by K-MEANS, in order to be more suitable for this problem. The paper is not care about the numerical value, but only consider if their shape is conform. Even though the numerical value is considered, the same or similar shape should also be strictly guaranteed. Otherwise, comparative analysis cannot be utilized. Therefore, it is possible for us to define a parameter such as mean value to measure the difference between parameters value. So we may safely say that shape difference is much more important than numerical difference. There are several following respects mainly in this kind of problem:

The insensitivity of numerical value of statistical data; A wide variation range, a big unpredictable characteristic, and more and complex noise; The same pattern class with different distribution. Because of the three characteristics, this lead to the result that the classic K-MEANS algorithm cannot obtain expected results. Specific explanations are done as following.

The analysis of the behavior pattern is not sensitive to numerical value, which the traditional K-MEANS clustering algorithms relatively sensitive to numerical value.

A simple example is given. Let us assume there are two horizontal lines, the value of which one is a and the other is b ($a \gg b$). From the view of the conception and mathematical significance, they both on its own part represent two different trajectories. But from the view of the analysis of the behavior pattern, they are very similar in many cases.

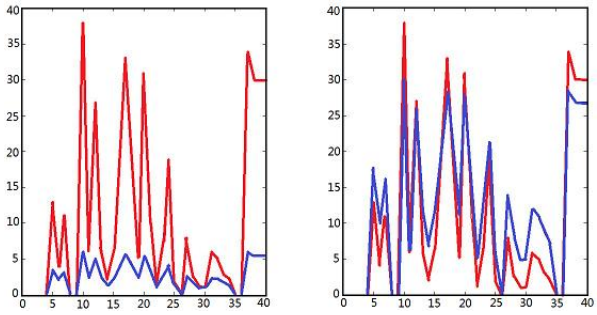

Figure 1. The two trajectory curves with similar shape and different value.

Owning to the more noise and the big unpredictable characteristic, while the traditional K-MEANS clustering algorithms relatively sensitive to noise. The most of algorithms have to consider the noise, but the influence of the noise is much more notable for the large scale data. If the high-dimensional feature is selected as measure scale, this may be useful for solving this problem. The measurement of time dimensional is shown as an example, but this will miss the hidden periodic or characteristic behavior pattern, which cause behavior to

doi:10.4304/jnw.9.1.161-167

become more and more blurry. For example, study on the trajectory of sleeping time with a month as unit. This might hide the feature that there is more sleep time in weekend, while make the trajectory curve is featureless. High-dimensional data can reduce the effects of the noise, but cause severe distortion. So in some situations, we have to use low-dimension data to measure, which will bring up another issue how to process the noise in the data.

The different distribution may be possible in the same pattern class, causing the data usually cannot be recognized by K-means Clustering Algorithm.

For example, when analyzing web click streams on the portal websites, the access amount of two users is shown in figure 2. Significant difference existed in time, but it is easy to understand that the curves are same or similar behavior pattern in essence. The web site is not known or understood at the beginning, so the click amount is less. After a while, recommended or unexpected discovery cause the web site is used persistently, which the amount increases quickly. Finally, lost gradually interest, which the amount starts to descend. From this example we can see that the kind of behavior pattern has apparent feature, namely: the behavior pattern is not sensitive to measurement dimension (time), allow deviation to some extent.

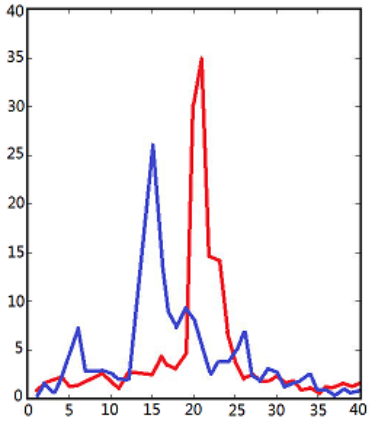

Figure 2. The two trajectory curves with similar shape on the time.

But it is undeniable that study on certain behavior pattern focuses relatively on the independence of time. For example, studying on the trajectory of electricity usage, we can know that it is very common that the peak value of the electricity usage is appeared in winter and summer. It is an abnormal performance if the peak value is only located in the spring or autumn. Even their trajectory curves are similar, cannot be almost divided into one group.

II. ALGORITHM DESCRIPTION

A. The Algorithm Flow

Based on three features mentioned above in paper, we apply dimensionless method to the data for solving the properties of non-sensitive and data smoothing for removing noise. According to the cutting track of key peak, only peak is matched to solve similar behavior pattern with different distribution. An algorithm flowchart is given out as following:

(1) Nondimensional parameters were used to treat original data.

(2) Choose a bigger number of cluster, then the data processed by a method mentioned in *A* section, is clustered to gain the cluster result.

(3) Obtain the clustering centers (average), then normalization processing is carried out (further minimizing error).

(4) The trajectory curves of the clustering centers are smoothed.

(5) Employing the key peak processing technology to find out similar trajectory curves divided into one group.

(6) After classification, the new trajectories of clustering centers are calculated via weighted mean method as the representation of new clusters according to the raw value. The following sections will describe those in detail.

B. The Definition of Similar Trajectory

How to define the similarity of the trajectory is a difficult problem, which the difficulties of the problem are how to define the "similarity". Its similarity condition is different for different type problems. The following information will introduce the area similarity method proposed by author for solving this problem.

Firstly, define a trajectory $y=(y(1),y(2),...,y(n))$, where $\forall k\in[1,n], y(k)\geq 0$. So the area $Area(y)$ of trajectory y is defined as the area surrounded by the curve y and x axis, namely

$$Area(y)=\sum_{k=1}^{n-1}\frac{y(k+1)+y(k)}{2}=\frac{y(1)}{2}+\sum_{k=2}^{n-1}y(k)+\frac{y(n)}{2} \quad (1)$$

The intersection between trajectory y_i and y_j is defined as following:

$$y_{\cap ij}=(\min\{y_i(1),y_j(1)\},\min\{y_i(2),y_j(2)\},...,\min\{y_i(n),y_j(n)\})$$

Similarly, union operations between trajectory y_i and y_j is defined as following:

$$y_{\cup ij}=(\max\{y_i(1),y_j(1)\},\max\{y_i(2),y_j(2)\},...,\max\{y_i(n),y_j(n)\})$$

Subsequently, their similarity measure $Sim(y_i,y_j)$ is defined as following:

$$Sim(y_i,y_j)=\frac{Area(y_{\cap ij})}{Area(y_{\cup ij})} \quad (2)$$

C. The Dimensionless Method

Aimed at the numerical sensitivity problems proposed in 2.2 section, let us take Figure 2.1 as example, where the below numerical of trajectory is square root of above trajectory. The two curves represent respectively union and intersection of trajectories. If untreated, they cannot be almost divided into one group. Therefore, it is necessary to use the dimensionless method.

The normalization of the dimensionless method is adopted in the improved algorithm. The essential meaning of normalization originated from computational

geometry, is to transform a vector to unit vector in elongation and shortening method. The trajectory after the normalization is defined as following.

$$y'_i = (\frac{y_i(1)}{l}, \frac{y_i(2)}{l}, ..., \frac{y_i(n)}{l}) \quad (3)$$

Contrast the definition with the euclidean distance of K-MEANS algorithm. If the trajectory y_i is treated as a point p_i in n dimensions space, the euclidean distance between trajectory y_i and y_j is equal to the euclidean distance between point p_i and point p_j. If the trajectory y_i is further treated as a n-dimensional vectorial $\bar{y}_i$, so the l in above formula is the norm $|\bar{y}_i|$ of the vector, namely, the normalization in the above definition is the unit length of the vector normalization. The euclidean distance between trajectories is the distance between vectors, which is a norm of the error between vectors, namely,

$$Dist(y_i, y_j) = |\bar{y}_i - \bar{y}_j| \quad (4)$$

K-MEANS algorithm is a clustering algorithm based on partition and can realize the optimum effect at convex spherical spaces. After using normalization in all samples, all the vectors are on the unit sphere in Euclidean space. The norm of differential vector between vectors is used as the weight criterion of clustering. So it is also shown vectors normalization might bring more accurate result of clustering based on partition. There is no obvious difference between the standardization and the normalization in the actual effect of the proposed question, therefore we adopt normalization in the paper.

III. THE SMOOTHING METHOD

To solve the noise corruption problem in the clustering algorithm, the small zigzag edge and meaningless patterns are smoothed in the trajectory. The specific methods are introduced in the following: let us assume the measure dimension of the trajectory y is time and define $Y_{\max} = \max_{k=1}^{n}\{y(k)\}$, $Y_{\min} = \min_{k=1}^{n}\{y(k)\}$. An extremely long continuous track is obtained between certain time s and time t, and satisfy the following conditions:

$$\frac{|y(k)-y(s)|}{Y_{\max}-Y_{\min}} < \delta_{smooth}, \quad \forall k \in [s,t] \quad (5)$$

So we can modify the trajectory into

$$y_{smooth}(k) = y(s) + \frac{y(t)-y(s)}{t-s}(k-s) \quad (6)$$

From the beginning of time t, the above calculation steps are repeated until all the data are treated in the trajectory.

So far, we have solved first two mentioned problems above. The traditional mathematical method can get excellent effect for the first two problems. The conventional method can not better solve the third question. The method considered naturally is curve shift. Enumerating the translation, we can calculate the similarity between curves.

This thought is seemingly simple and intuitionistic, but in general it is relatively small to match a similar curve. Examples are given in figure 3. It is shown that the double peaks in one curve correspond to the double peaks in other curve. Due to the different distribution patterns, only one peak can overlap, no matter how to shift. So it is difficult to match similar trajectory for the two curves.

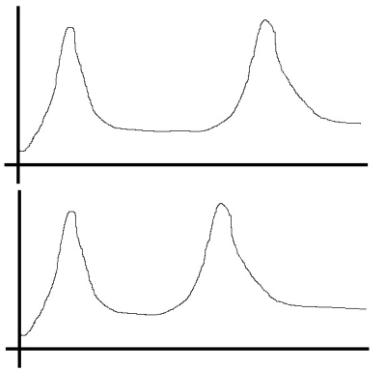

Figure 3. The two trajectory curves with similar peak and different position

In this improved algorithm, the division between peak and valley was used to solve above question. Since the position of peak and valley must be alternative, namely, the peak situate in between two valleys. So it is feasible only to consider one of them. In the paper, we only consider to recognize the peak of the trajectory.

As shown in figure 3, let us assume to consider only two peaks. According to our thoughts of the shift, the two trajectories can get very good match result, and thus lead to the extraction of "feature peak".

Suppose a trajectory is expressed as $y = (y(1), y(2), ..., y(n))$ and the threshold between peak and valley of the trajectory is δ_M, so define the peak point set P_M as following:

$$P_M = \{\forall k \in [1,n] \mid \frac{y(k)-Y_{\min}}{Y_{\max}-Y_{\min}} \geq \delta_M\} \quad (7)$$

Similarly, the valley point set V is defined as following:

$$P_V = \{\forall k \in [1,n] \mid \frac{y(k)-Y_{\min}}{Y_{\max}-Y_{\min}} < \delta_M\} \quad (8)$$

The definition of peak is $M = (y(i), y(i+1), ..., y(j))$, then is denoted a $(M(1), M(2), ..., M(j-i+1))$. A peak group is defined as $Pe = (M_1, M_2, ...M_r)$, where r is the number of peaks in the peak group.

Then, an algorithm flowchart is given out as following.

(1). Achieve the maximum value $Y_{\min}$ and minimum value $Y_{\max}$.

(2). Define a closed flag F_{close}, if its value is *true*, this show the present continuous trajectory do not contain the peak. Otherwise, that means have peak. Its initial value is *true*, and the peak group and the peak set are all empty.

(3). The cycling scanning is used to scan a complete trajectory, for present point i:

If $i \in P_M$, i will be fed into P, and F_{close} is modified as *false*.

If $i \in P_V$ and $F_{close} = true$, skip the present point i without any treatment.

If $i \in P_V$ and $F_{close} = false$, the point in P is put into Pe as a new peak. Then, P is cleared and F_{close} is modified as *true*.

Finally, the peak in peak group Pe is the extracted "feature peak".

The closed flag F_{close} plays a state transition flag role in above algorithm. There are two states in the state machine. The state 1 expresses the peak constituted by several points and it can put continuously the point into the peak. The state 2 expresses there is currently no peak. The definition between the peaks is the valley between them. If the valley has only one point, according to the algorithm we can regard them as the two peaks. But in fact it can only be a continuous fluctuation peak. So we can increase the number of the source state based on need. For example, a added state 3 expresses the present point has reached the valley, but it is still going on (If finding a valley again at the moment, delete the peak point, then move on to state 2; If finding a peak, put continuously the point into the peak, then move on to state 1). So we add a buffer state and our code is written based on the three states.

A. The Similarity of the Peak

The length of the peak M_1 and the peak M_2 are l_1 and l_2 respectively, so construct the trajectory $A = (A(1), A(2), ..., A(l_1 + 2l_2))$, where

$A(1, 2, ..., l2) = (0, 0, ..., 0)$

$A(l_2 + 1, l_2 + 2, ..., l_1 + l_2) = (M_1(1), M_1(2), ..., M_1(l_1))$

$A(l_1 + l_2 + 1, l_1 + l_2 + 2, ..., l_1 + 2l_2) = (0, 0, ..., 0)$

Enumerating i in range of $[1, l_1 + l_2 + 1]$, we can define $B_i = (B_i(1), B_i(2), ..., B_i(l_1 + 2l_2))$, where

$B_i(1, 2, ..., i-1) = (0, 0, ..., 0)$

$B_i(i, i+1, ..., i + l_2 - 1) = (M_2(1), M_2(2), ..., M_2(l_2))$

$B_i(i + l_2, i + l_2 + 1, ..., l_1 + 2l_2) = (0, 0, ..., 0)$

So we can get $Sim_i = Sim(A, B_i) = \frac{X_i}{Y_i}$.

Actually using the idea of translation for reference, compare the two peaks fixed one of the two peaks and shifted another peak from left to right. B_1 corresponds to B peak, and locates at left side. The right margin of B peak coincides with the left margin of A peak; $B_{l_1+l_2+1}$ corresponds to B peak, and locates at right side. The left margin of B peak coincides with the right margin of A peak;

So define the maximum similarity $Sim_{\max}$ as following

$$Sim_{\max} = \max_{i=1}^{l_1+l_2+1}\{sim_i\} = \frac{X_{\max}}{Y_{\max}} \quad (9)$$

Similarly, the minimum similarity $Sim_{\min}$ is defined as following:

$$Sim_{\min} = \min_{i=1}^{l_1+l_2+1}\{sim_i\} = \frac{X_{\min}}{Y_{\min}} \quad (10)$$

According to the similarity threshold $\delta_{sim(M)}$ between peaks, if $Sim_{\max} > \delta_{sim(M)}$, the similarity of the two peaks $Sim(M_1, M_2) = \frac{X}{Y}$ is $Sim_{\max}$. Conversely, the similarity is $Sim_{\min}$.

B. The Similarity of the Peak Groups

Define the similarity between peak A and peak B is $Sim(A, B) = \frac{X}{Y}$ and guarantee the size of X and Y is proportional to the size of peak A and B. For example, due to the same ratio s, $\frac{X_1}{Y_1} = s = \frac{X_2}{Y_2}$, if the former peak shape is bigger than the latter, so $X_1 > X_2$, $Y_1 > Y_2$, and vice versa.

The assumed simplest situation is there is the same number of peaks in peak groups Pe_1 and Pe_2, and denote the number is s. Then the similarity of the corresponding peak in two peak groups is calculated in order, and is denoted by $(\frac{X_1}{Y_1}, \frac{X_2}{Y_2}, ..., \frac{X_s}{Y_s})$. So the similarity of two peak groups can be calculated by following equation:

$$Sim(Pe_1, Pe_2) = \frac{X_1 + X_2 + ... + X_s}{Y_1 + Y_2 + ... + Y_s} \quad (11)$$

According to the similarity threshold δ_{Pe} between peak groups, if $Sim(Pe_1, Pe_2) > \delta_{Pe}$, the two trajectories is similar, otherwise they are dissimilarity.

The reasons using the additive method rather than the multiplicative method to define similarity are as following.

Let us assume three peak groups *A, B, C* contained two peaks with a larger one and smaller one, which the peaks is a significant difference in size. The small peak of *A* and The small peak of *B* have higher similarity, while the big peak of *A* and the big peak of *C* have higher similarity. We conclude, in generally, *C* is more similar with *A*. Assume the similarity between the peak groups C and A is calculated: the similarity between the bigger peaks is 100/200 = 0.5, while the similarity between the smaller

peaks is 8/10 = 0.8; In the peak groups *A* and *B*, the similarity between the bigger peaks is 140/200 = 0.7, while the similarity between the smaller peaks is 5/10 = 0.5; According to the multiplicative method, the similarity between the peak groups can be obtained by multiplying all the similarity between the peaks. So the similarity between the peak groups *C* and *A* is 0.7×0.5 = 0.35, while the similarity between the peak groups ***B*** and *A* is 0.5×0.8 = 0.40, which obviously the former is bigger than the latter. The result is not in accordance with the fact that C and A are more similar. However, according to the additive method, the similarity between the peak groups *B* and *A* is (100+8)/(200+10)≈0.514, while the similarity between the peak groups *C* and *A* is (140+5)/(200+10)≈0.690, which is more accordant with the actual situation. This is the reason why the size of *X* and *Y* need to be proportional to the size of peak *A* and *B* proposed in the beginning of the section.

IV. PERFORMANCE EVALUATION

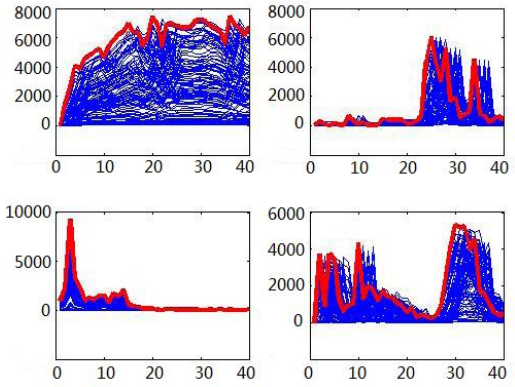

Figure 4. The test dataset

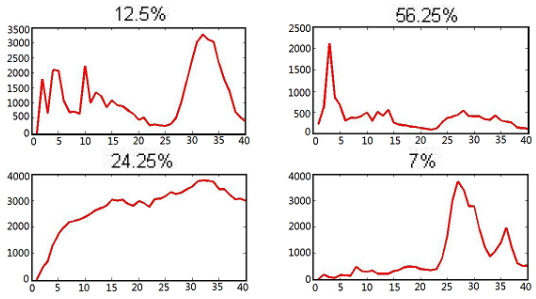

(a) the results of the K-MEANS algorithm

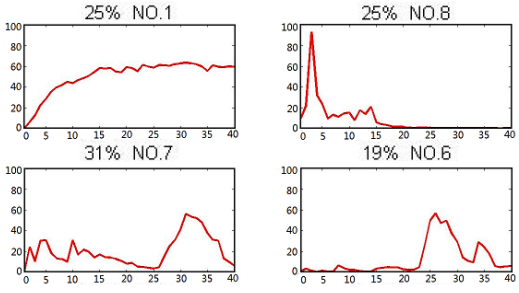

(b) The results of the improved algorithm

Figure 5. The comparison between the K-MEANS algorithm and the improved algorithm

In order to compare the advantages and disadvantages of the proposed algorithm and traditional K-MEANS clustering algorithm, we choose four trajectories with magnification and added noise in different degree. Then micro-translation is used in a part of the curves. The designed data is shown as following in figure 4, where the red thick lines denote the 100 times magnification effect of original trajectory, and the blue thin line denote the original trajectory, and there are 100 trajectories in each cluster.

TABLE I. THE COMPARISON OF ERROR RATE BETWEEN THE K-MEANS ALGORITHM AND THE IMPROVED ALGORITHM

Serial number	Our method	K-MEANS algorithm	Serial number	Our method	K-MEANS algorithm
1	10	28.5	11	2.25	24.25
2	0.5	31.25	12	3	28.75
3	12.5	30.25	13	19.25	28.75
4	3.25	35.75	14	16.75	36.5
5	3	33.75	15	15	32
6	27.5	28	16	16.5	32.5
7	2.5	36.75	17	11.25	18
8	18.25	35	18	6	41.25
9	26	35.5	19	0	39.5
10	25	18.75	20	14	30

TABLE II. THE DATA STATISTICS

The error rate data statistics(number)	Our method	The K-MEANS algorithm
<10%	8	0
[10%, 20%)	9	2
[20%, 30%)	3	5
[30%, 40%)	0	12
>40%	0	1
best	0%	18%
worst	27.5%	41.25%
average	11.625%	31.2%

The running result of the K-MEANS algorithm in one time is shown in figure 5(a), while the running result of the improved algorithm in one time is shown in figure 5(b). In order to decrease the errors as much as possible and make the results more accurate and credible, two algorithms are run for 20 times on the same running environment and the number of iterations, which the experiments are shown in tables 1 and 2. It is obvious that the improved algorithm has a more advantage over the traditional K-MEANS algorithm. The improved algorithm can not only reach a better effect (the result of the improved algorithm is 11.625%, while another is 31.2%), but also the expected result is also relatively good. The error rate of clustering data in the improved algorithm is lower than the traditional K-MEANS algorithm. So based on simulation dataset, we can see that the improved algorithm is more suitable for solving the user's behavior pattern clustering problem.

The paper selects the number of posts in internet company as actual test data. The data is measured by per month, lasted for 40 months. There are 10000 valid user data collected in this study.

The clustering results of 100 trajectories from 10000 users are shown in figure 6, where the clustering result without the normalization is shown in figure 6(a), the clustering result with the normalization is shown in figure 6(b). It can be seen that the most clusters can get an ideal result, but there is 47% data in the last cluster. So the distribution of the number of trajectory is uneven in each

cluster and the result of the last cluster cannot reach satisfied effect. Contrasted figure6(b), the clustering results with the normalization not only lead to a more uniform sample number, but also the result is more accurate.

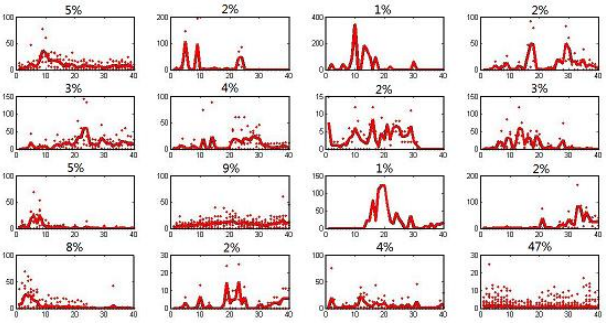

(a) the clustering results without the normalization

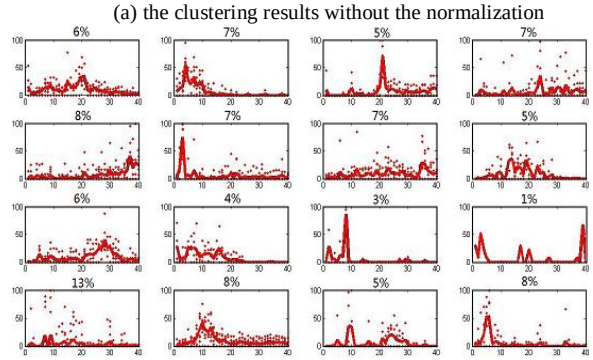

(b) the clustering results with the normalization

Figure 6. The clustering results of 100 trajectories

The figure 7(a) shows all the 10000 user data are classified into 30 clusters. Especially if the data is large, the result is too cluttered when all the results are showed in figure, so only demonstrate the trajectory of the clustering centers. Because the trajectory of the clustering centers use the arithmetic average of all the trajectories in cluster, this will lose the unit feature of the original data, thus once again the normalization processing make the calculation results are accurate and reliable, as shown in figure 7(b). The figure 7(b) shows most of the data has a small zigzag fluctuation, due to the effect of noise which is allocated into all the original data. At the moment, the noise is very small and controllable. Based on the model analysis, the small perturbation of the data would influence the extraction of "feature peak" and the calculation of similarity. And in general, it is not helpful to analyse model. The Figure 7(c) is the clustering result with the smoothing method based on Figure 7(b), while the Figure 7(d) shows the peak after spatial smoothing process. We can see that many small peaks are abstracted. Raising the threshold δ_M may help to reduce the small peak, but also affect the quality of the extractive peak. On the one hand, due to the definition of similarity using the additive method, the blank peak is adopted to match the small peak, which it is not influential in final result. So it is important to select a proper threshold. In this paper, the threshold is $\delta_M = 20\%$. The figure 7(e) shows the trajectories with the same clustering centers. For the sake of brevity, some dissimilar trajectories are omitted. Finally, merge the similar trajectories of the clustering centers, which the result is shown in figure 7(f). Contrasted figure 7(a), we can see that the classification results of the improved method are more uniform and there is no the extreme case, at the same time the shape of the trajectories is more clear. Thus, our improved algorithm has better performance than the traditional K-MEANS method in the actual data.

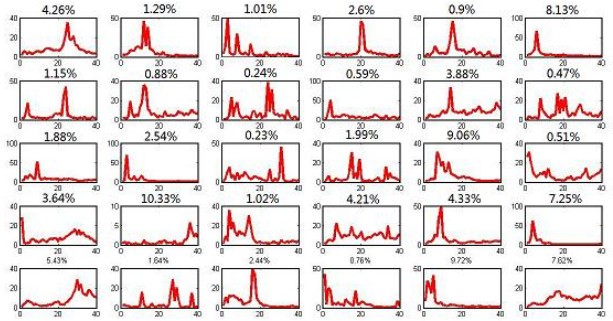

(a) the clustering result of the whole data

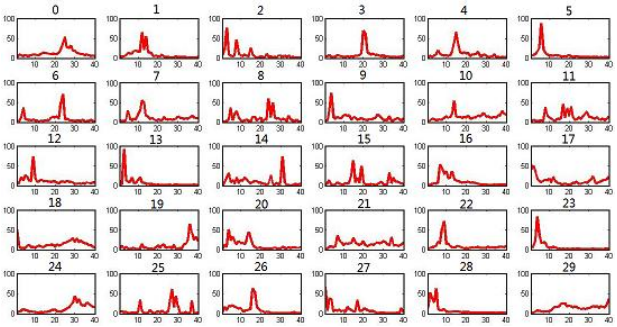

(b) the clustering result with the normalized clustering centers

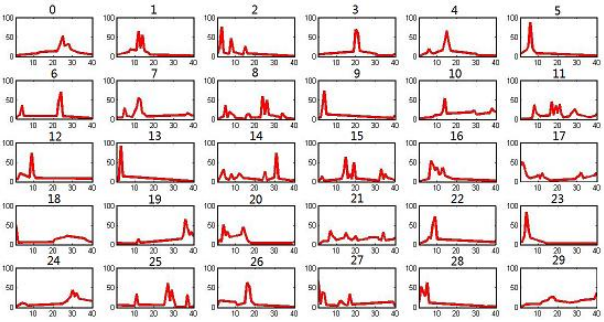

(c) the clustering result with the smoothing method

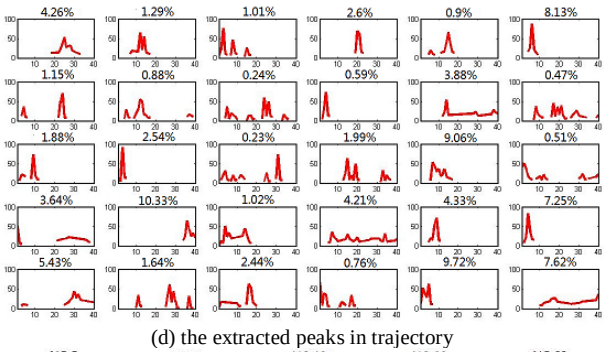

(d) the extracted peaks in trajectory

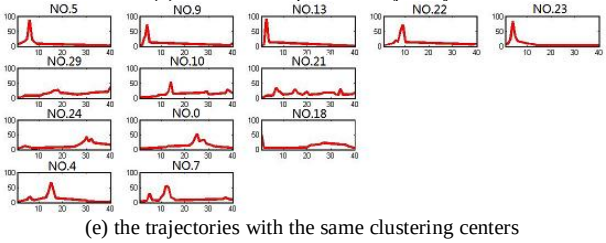

(e) the trajectories with the same clustering centers

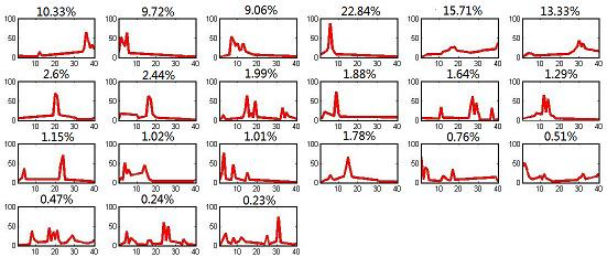

(f) the clustering result based on merging the similar clusters

Figure 7. The clustering results of actual data

V. CONCLUSION

A kind of problem based on user behavior pattern analysis is proposed, which has the insensitivity of numerical value, strong noise, uneven spatial and temporal distribution characteristics. Owing to these characteristics, the traditional clustering algorithm has not played its proper role. This paper comprehensively analyses the existing clustering methods, trajectory analysis methods, and behavior pattern analysis methods, and combines clustering algorithm into the trajectory analysis. Due to the main characters that our problem has, the paper brings forward a series solution measures. By modifying the traditional K-MEANS clustering algorithm, we propose an improved algorithm which is suitable to solve the problem of user behavior pattern analysis. Compared with traditional clustering methods on the basis of the test of the simulation data and actual data, the results demonstrate that the improved algorithm is more suitable for solving the trajectory pattern of user behavior problems.

REFERENCES

[1] Roundy, Shad, et al. "Power sources for wireless sensor networks." *Wireless sensor networks. Springer Berlin Heidelberg*, 2004 pp. 1-17.

[2] Jamieson, Kyle, Hari Balakrishnan, and Y. C. Tay. "Sift: A MAC protocol for event-driven wireless sensor networks." *Wireless Sensor Networks. Springer Berlin Heidelberg*, 2006 pp. 260-275.

[3] Ye, Wei, John Heidemann, and Deborah Estrin. "An energy-efficient MAC protocol for wireless sensor networks." *INFOCOM 2002. Twenty-First Annual Joint Conference of the IEEE Computer and Communications Societies. Proceedings. IEEE*. Vol. 3. IEEE, 2002.

[4] Heinzelman, Wendi Rabiner, Joanna Kulik, and Hari Balakrishnan. "Adaptive protocols for information dissemination in wireless sensor networks." *Proceedings of the 5th annual ACM/IEEE international conference on Mobile computing and networking. ACM*, 1999.

[5] Polastre, Joseph, Jason Hill, and David Culler. "Versatile low power media access for wireless sensor networks." *Proceedings of the 2nd international conference on Embedded networked sensor systems. ACM*, 2004.

[6] Krishnamachari, L., Deborah Estrin, and Stephen Wicker. "The impact of data aggregation in wireless sensor networks." *Distributed Computing Systems Workshops, 2002. Proceedings. 22nd International Conference on. IEEE*, 2002.

[7] Karlof, Chris, and David Wagner. "Secure routing in wireless sensor networks: Attacks and countermeasures." *Ad hoc networks* 1.2 (2003) pp. 293-315.

[8] Doherty, Lance, and Laurent El Ghaoui. "Convex position estimation in wireless sensor networks." *INFOCOM 2001. Twentieth Annual Joint Conference of the IEEE Computer and Communications Societies. Proceedings. IEEE*. Vol. 3. IEEE, 2001.

[9] Polastre, Joseph, et al. "Analysis of wireless sensor networks for habitat monitoring." *Wireless sensor networks (*2004) pp. 399-423.

[10] Estrin, Deborah, et al. "Instrumenting the world with wireless sensor networks." *Acoustics, Speech, and Signal Processing, 2001. Proceedings. (ICASSP'01). 2001 IEEE International Conference on*. Vol. 4. IEEE, 2001.

[11] Romer, Kay, and Friedemann Mattern. "The design space of wireless sensor networks." *Wireless Communications, IEEE* 11.6 (2004) pp. 54-61.

[12] Patwari, Neal, et al. "Locating the nodes: cooperative localization in wireless sensor networks." *Signal Processing Magazine, IEEE* 22.4 (2005) pp. 54-69.

[13] Rajendran, Venkatesh, Katia Obraczka, and Jose Joaquin Garcia-Luna-Aceves. "Energy-efficient, collision-free medium access control for wireless sensor networks." *Wireless Networks* 12.1 (2006) pp. 63-78.

[14] Karlof, Chris, Naveen Sastry, and David Wagner. "TinySec: a link layer security architecture for wireless sensor networks." *Proceedings of the 2nd international conference on Embedded networked sensor systems. ACM*, 2004.

[15] Patwari, Neal, et al. "Relative location estimation in wireless sensor networks." *Signal Processing, IEEE Transactions on* 51.8 (2003) pp. 2137-2148.

[16] Halkes, Gertjan P., and K. G. Langendoen. "Crankshaft: An energy-efficient MAC-protocol for dense wireless sensor networks." *Wireless Sensor Networks. Springer Berlin Heidelberg*, 2007 pp. 228-244.

[17] Wang, Xiaorui, et al. "Integrated coverage and connectivity configuration in wireless sensor networks." *Proceedings of the 1st international conference on Embedded networked sensor systems. ACM*, 2003.

[18] Chang, Jae-Hwan, and Leandros Tassiulas. "Maximum lifetime routing in wireless sensor networks." IEEE/ACM Transactions on Networking (TON).*ACM* 12.4 (2004) pp. 609-619.

[19] Wang, Yun, Weihuang Fu, and D. Agrawal. "Gaussian versus uniform distribution for intrusion detection in wireless sensor networks." (2013) pp. 1-1.

[20] Voigt, Thiemo, Luca Mottola, and Kasun Hewage. "Understanding link dynamics in wireless sensor networks with dynamically steerable directional antennas." *Wireless Sensor Networks. Springer Berlin Heidelberg*, 2013 pp. 115-130.

[21] Branch, Joel W., et al. "In-network outlier detection in wireless sensor networks." *Knowledge and information systems* 34.1 (2013) pp. 23-54.

Target Localization Based on Improved DV-Hop Algorithm in Wireless Sensor Networks

Huang Xiaolong
Department of Mathematics & Computer Information Engineering, Baise University, Baise, Guangxi 533000, China

***Abstract*—The node localization technology of wireless sensor networks is essential and prerequisite to many applications, which it is one of the important support technologies for wireless sensor networks. The node localization is to get the position information of blind node by using location information of few known nodes and some special mechanisms. This paper primarily investigates a kind of target localization technology based on the improved DV-Hop algorithm in wireless sensor networks. We firstly compute the distances measured by RSSI and the mean value of one-hop distance. Then we can use the differences between the mean and the actual distance to get the error correction between the total distance and average one-hop distance. Replace trilateration with hybrid localization of MIN-MAX and weighted least square method. Finally, simulation experiment results show the improved algorithm can effectively carry out the network localization, thus has a certain of practical value.**

***Index Terms*—Wireless Sensor Network; DV-Hop Algorithm; Least Square Method; Localization**

I. INTRODUCTION

With the development of microelectronics technology, computer technology and wireless communication technology, a low power consumption and all-purpose sensor has been widely applied in various fields. Wireless Sensor Network (WSN) is composed of numerous small size and low cost sensor nodes. They are mainly distributed in the monitored area, and can be self-organized to form a system with multi-hop by wireless communication. The data can be perceived and obtained by WSN in the monitored area, and then the interesting data information is transmitted to monitoring staff. The task of sense technology contains information acquisition, the task of communication technology is to spread them, while the task of computer technology is to process them. Several difficult problems will emerge when obtaining data in real using environment, such as cabling difficulty and acquisition data with big size. the location information is crucial for the monitoring activities of sensor network in WSN. Since the positions of events or nodes locations of acquisition information are the most important part of monitoring information from sensor nodes, monitoring information will be meaningless without the location message. The position information of sensor nodes must be pre-determined, which is the foundation to take further measures and make decision.

In addition to offer the positions of events, the location information has the following values: monitor and track the movement route of object in real time, and predict the trajectory of object; help routing to provide the namespace for network, for example, using the location information of nodes to transfer geographical routing protocol, avid effectively the information being spread in a whole network, and achieve orientable information query; conduct network management, using the location information returned by sensor node to built network topology and count the network coverage rate in real time, which in low density area the effective measures will be taken to achieve load balancing and self-configuration of network topology, and so on. So the rapid and accurate location of sensor node plays an important role in practical applications in WSN. The wireless sensor network (WSN) is used more and more widely, such as military defense, environment monitor, disaster prediction, etc. If some deliberate attacked nodes cannot be used ordinarily, it is impossible to cause crash of the whole network in wireless sensor network. If the world network building virtual world makes people's lifestyle is changing, the WSN is a combination of virtual world and real world, which it obviously changes communication way between human and nature. With the development of WSN, It can be said that our lives has undergone enormous changes.

The most representative and influential research and application of wireless sensor network has Remote Battlefield Sensor System (shortened form: REMBASS), Network Center War (NCW), Skillful Sensor Network (SSN), Smart Dust, Intel ®Mote, Smart-Its, Habitat Monitoring, and so on. Especially the successful development of the “wolves” with low cost based on WSN of ground platform, marks major breakthrough in electronic warfare. “A Line in the Sand” is a wireless sensor network system, which is still under development in Ohio. The system can scatter tripwires to everywhere. In civilian application, the developed countries such as the United States and japan have developed many applications in the different areas based on constant development of the technology.

Wireless sensor network is new high-technology which achieved great development in recent year, and the application and development of the technology has provided enormous convenience for human's daily life. Wireless self-organizing network is without the need of infrastructure based support devices, its characters is as

doi:10.4304/jnw.9.1.168-175

following: multi-hop, self-organized and reconfiguration. This kind of networks topology structure and channel environment will be dynamic change due to the mobility of the node. And it can construct rapidly the communication environment in the military and civilian fields. Acquiring the position information is one of the most primary task of monitoring object in WSN. It is important link in the whole monitoring activities to accurately master the place that the event happened. Generally, the sensor nodes are randomly deployed into the monitoring range, for example, the network can be deployed for monitoring the ecological environment, the fire scene etc. Though these sensor nodes do not know their own position, once the sensor nodes are deployed, they can have automatic localization rapidly. Besides these descriptions, the location technique has other function, such as network management, improvement routing and target tracking and so on.

With regard to network management, the acquired sensor node data can be used to build the topological structure, in order to know the range of coverage, which make the place with few node can adopt rapidly corresponding correcting measures. The node coordinate data has a special function, which assist to achieve routing. A arbitrary node and the coordinate in surrounding areas are known, thus the network can reach to improve its performance and route. The advantage of the optimal routing method is to improve the efficiency of the system, security, and saving power.

Consequently, in every application of WSN, it plays an irreplaceable role to locate accurately the sensor nodes. The accurate location is the foundation of WSN application, even is a main supporting technology. We can see that the node location technologies in wireless sensor networks have a pretty good practical prospect.

DV-Hop Algorithm, is firstly proposed by D. Niculescu and B. Nath, etc, whose principle is similar to that of the classic distance vector routing algorithm. In DV-Hop algorithm, beacon node broadcasts a beacon to the network and the beacon contains the location information of this beacon node and a hop parameter whose initial value is 1. The beacon is delivered in the net work by flooding way and the hop count increases 1 every time when the beacon is delivered. The receiver node saves the beacon with the minimum-hop count among all the beacons about a certain beacon node which the receiver node has received and discards the beacons in the same beacon node with relative large hop counts. Through this mechanism, all nodes in network, including other beacon nodes obtain the minimum hop account of each beacon node, which indicates the hop count from node in network to the beacon node A.

To transfer the hop count into the physical distance, the system needs to assess the average single hop distance in network. For the beacon node has the hop counts of other beacon nodes into internal network and the location information of these beacon nodes, the beacon node can compute the real distance away from other beacon nodes. After computing, a beacon node gets the average single hop distance in network and broadcasts the accessing value into network, which is called correction. Each node which once receives the correction can estimate the distance from itself to the beacon node. If a node can obtain the accessing distances from at least 3 beacon nodes, it can estimate the location itself with the least square method.

DV-Hop algorithm has similarities with the range-based algorithm, which are that both algorithms need to obtain the distance from the unknown node to beacon node. However, the way in which DV-Hop gets the distance is through computing the topological structure information of network but not through measuring the radio wave signal. In the range location algorithm, the unknown node can only get the distance of beacon node in its coverage of radiofrequency, while DV-Hop algorithm can obtain the distance of beacon nodes outside of the unknown node's wireless range, which can obtain more useful data and improve the location accuracy.

One disadvantage of Sum-dist is the node's range errors will cause cumulative effect in multi-hop broadcasting. The range errors will present especially obviously when the network scale is very large, or the quantity of beacon nodes is relatively little and hardware errors of the node ranging is relatively large. A method with a better robustness is to calculate hop count by the topology information of network but not the accumulated distances. In Ad-Hoc positioning, it is called Ad-Hoc positioning and Hop-TERRAIN in Robust positioning. Actually, DV-Hop is composed of two wave flooding, the first of which is similar to Sum-dist whose node obtains the location information and the minimum hop count of beacon node; and in the second wave flooding, the hop information is transferred into distance information. Each beacon node estimates the actual average single hop distance with Equation (1), according to the hop count information and distance information recorded in the first wave.

$$Hopsize = \frac{\sum_{j \neq i} \sqrt{(x_i - x_j)^2 + (y_i - y_j)^2}}{\sum_{j \neq i} Hops_i} \quad (1)$$

In the formula above, (x_i, y_i) and (x_j, y_j) are the coordinate of beacon nodes; Hop_j is the hop count between beacon nodes i and j ($i \neq j$). After calculating the average single hop distance, the beacon node broadcasts the information with survival duration field in groups into network and the unknown node only records the first average single hop distance and transmits it to neighbor node. This strategy can make sure that most nodes can receive the average single hop distance from the nearest beacon node and the unknown node can calculate its distance away from every beacon node after receiving the average single hop distance, according to the recorded hop count.

DV-Hop algorithm consists of 3 periods. Firstly, all node of network can obtain the distance in hopscotch from beacon node by making use of the representative

distance vector exchange protocol. In the second stage, after getting other beacon nodes, location and apart hop-distance, beacon node calculate each average single hop distance which then will be broadcast into network as a correction. The correction is broadcast in network with controllable flooding method, which means one node only receives the first obtained correction and discards all subsequent correction. This strategy makes sure that most nodes can receive the correction from the nearest beacon node. In large-scale network, to set up a TTL for the data packet can decrease the communication traffic. Receiving the correction, the node calculates its distance from beacon node according to hop count. When the unknown node gets at least 3 distances from beacon node, it can execute trilateration localization in the 3rd stage.

II. IMPROVED DV-HOP ALGORITHM

A. Rang Error Correction of DV-Hop Algorithm

In the original algorithm, the *average* single *hop distance* HopDis_{ef} of the known node is thought as the distance from testing node to the known node, which equals to the average single hop distance x hop count. But in real environment, the path from testing node to the known node is usually curvilinear, which will lead to a relatively large error in the original algorithm.

All the contents, for example, the coordinate and hop count of the known node, will be delivered to other known nodes in broadcasting. When any a node obtains the other known nodes, data, it can calculate the real distance between them according to the coordinates of 2 known nodes. One can compute the average value of the sum of the distance measured by RSSI and every single hop distance, then compute the difference between the last value and the real distance, and finally get the total error correction len_{ef} of node e and f.

It is supposed that the known node e,s average single hop distance is HopDis_{ef}; The total hop counts from the known node e to f (e≠f)is m; Dis_{ef} presents the sum of single hop distance from the known node *e* to other known nodes; Dis_{ef} is the real distance from the known node *e* to other known nodes; and the total error correction is as the following:

$$len_{ef} = \left(\sum RSSI + dis_{ef}\right) \div 2\text{-}Dis_{ef} \tag{2}$$

Path loss distribution model:

$$PL(k) = PL(k_0) + 10q\log(k/k_0) + \mathrm{Y}_0 \tag{3}$$

$$RSSI = PL(k_0) - 10\log(k) \tag{4}$$

In Equation (2), the following formula is to hold.

$$Dis_{ef} = HopDis_{ef} \times m \tag{5}$$

$$Dis_{ef} = \sqrt{\left(x_e - x_f\right)^2 + \left(y_e - y_f\right)^2} \tag{6}$$

In Equations (3) and (4), K_0: the receiver node's reference length(k_0=1); k:the length between the receiver and transmitter; PL(k_0):the received power of k_0 node. q: path loss ratio whose value is in the range of (2,4); Y_0:the random variable of a generalized Gaussian distribution with zero-mean.

For the distances from any a testing node to a known node are different, their distance error value is not the same, too. We should use different corrections to calculate. It is supposed that the total hop counts from a known node e to a known node 1, and then the average single hop error correction of e is avge_{ef}:

$$avge_{ef} = \left[\left(\sum RSSI + \mathrm{Dis}_{ef}\right)/2\text{-}\mathrm{Dis}_{ef}\right]/m \tag{7}$$

In network, all known nodes broadcast the m, len_{ef}, and avge_{ef} out from itself to other known nodes, which can make any a known node can get other known nodes, value of m, len_{ef}, and avge_{ef} that are once obtained by a known node, the node will keep these contents in a routine table, that is $\{\mathrm{ID}_k,x_k,y_k,\mathrm{hop}_k\}$. Then the known node will transfer these information to its neighbor nodes and increase 1 to the hop count.

Each node gets a hop count and then always compares with the past value of hop_k in $\{\mathrm{ID}_k,x_k,y_k,\mathrm{hop}_k,\mathrm{mm},\mathrm{len}_{ef},\mathrm{avge}_{ef}\}$. If the new value of hop_k is less than the past one, the new value will replace the past one in $\{\mathrm{ID}_k,x_k,y_k,\mathrm{hop}_k,\mathrm{mm},\mathrm{len}_{ef},\mathrm{avge}_{ef}\}$, otherwise discard this information. During the process, it carries on the total length error correction and average single hop error correction at the same time. After all the steps above, we can get the minimum length between testing node and the known node.

Through information transmission of the first two steps, the testing node owns the information of 3 or more than 3 known nodes nearest to itself and the information includes the total length error correction len_{ef} and the average single hop error correction $\mathrm{avge}_{ef.}$, by which, the testing node can get the length between itself and all the known nodes.

Suppose that there is a testing node w near the known node e. M means the total hop counts between the testing node w and the known node e. The sum of single hop distances of the testing node w and the known node e is HopDis_e*M. avge_{ef} presents the average single hop distance error correction of node e. We can get the distance D_{we} between the testing node w and the known node e.

$$D_{we} = HopDis_{ef} \times M\text{-}avge_{ef} \times M = \left(HopDis_{ef}\text{-}avfe_{ef}\right) \times M \tag{8}$$

B. The Combination of Min-Max Method and Weighted Least Square Method

To calculate the node's coordinate with trilateration will introduce some errors and a relatively much quantity of floating-point operations at the same time. MIN-MAX algorithm decreases the quantity of floating-point operations and reduces the computing cost. The location accuracy depends on the known nodes, quantity. The increased known nodes, quantity will certainly improve cost and enlarge power consumption. As a result, the combination of MIN-MAX method and weighted least square method will replace trilateration.

There are two stages in this method, in the first of which, the MIN-MAX algorithm is used to get the rough

location of the testing node, according to the little known coordinate; and in the second stage, the weighted least square algorithm is used to further accurate estimate the coordinate of the testing node.

(l) MIN-MAX algorithm

MIN-MAX algorithm takes the known node as center of a circle and the estimated length between testing node and this known node as radius, and builds a circumscribed square outside a circle. We can build some squares with the estimated value and coordinate and find the intersection of these squares, whose geometrical center is the estimated location of the testing node.

In the plane coordinate system, when the node's communication model is a circle and the radius is ks. When the node's coordinate is estimated, the circumscribed square outside of the cycle is considered as its communication range, and its maximum comm. Length of one hop is $t=\sqrt{2}k_s$ (each side of the square is 2ks). If the quantity of the unknown node's neighbor known nodes is v, its coordinate must be in the intersection of the communication ranges of these known nodes, as is shown in figure 1.

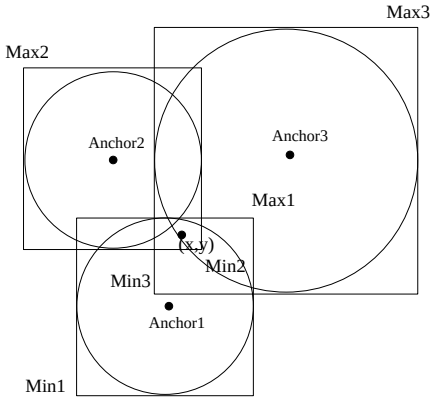

Figure 1. The Schematic Diagram of MIN-MAX Algorithm

We can get the range of the known node (x_s, y_s) from [(x_s-k_s), (y_s-k_s)]*[(x_s+k_s), (y_s+k_s)]. Among them, k_s means the estimated length between the testing node and the known node. The intersection range can be obtained by formula (9):

$$\left[\max\left(x_s-k_s\right),\max\left(y_s-k_s\right)\right]\times\left[\max\left(x_s+k_s\right),\max\left(y_s+k_s\right)\right],s=1,2,...v \quad (9)$$

The estimated location $\left(\hat{x}_{s0},\hat{y}_{s0}\right)$ of the testing node is the geometrical center of the intersection, and we can get it in Equation (10):

$$\left(\hat{x}_{s0},\hat{y}_{s0}\right)=\frac{1}{2}\begin{bmatrix}\min\left(x_s+k_s\right)-\max\left(x_s-k_s\right),\\ \min\left(y_s+k_s\right)-\max\left(y_s-k_s\right)\end{bmatrix} \quad (10)$$

(2) Weighted least square algorithm

There are G estimated length values between testing node and the known node, and these values build the residual equation, that is, ts(x). Under the prerequisite of having not the estimated distance value, we can get the estimated coordinate value of the testing node with Equation (11):

$$\hat{x}=\arg\min\sum_{s=1}^{G}t_s^2\left(x\right) \quad (11)$$

Suppose that all the estimated distance value is known, and we can build weighted coefficient ws with these values. Finally, the estimated value of weighted least square algorithm is:

$$\hat{x}=\arg\min\sum_{s=1}^{G}w_s t_s^2\left(x\right) \quad (12)$$

If the testing node's location is (x,y), and the known node's location is (x_s,y_s), and the estimated length is k_s

$$t_s\left(x,y\right)=k_s-\sqrt{\left(x_s-x\right)^2+\left(y_s-y\right)^2} \quad (13)$$

where, t_s(x,y) is a nonlinear function, whose value can be processed by the nonlinear optimization. The formula of the linearization solution of t_s(x,y) is in the following:

$$k_s^2=\left(x_s-x\right)^2+\left(y_s-y\right)^2 \quad (14)$$

$$k_1^2=\left(x_1-x\right)^2+\left(y_1-y\right)^2 \quad (15)$$

We can get the following equation group after subtracting Equation (15) from Equation (14)

$$k_s^2-d_1^2=x_s^2-x_1^2+2x_1x-2x_sx+y_s^2-y_1^2+2y_1y-2y_sy \quad (16)$$

The final equation is:

$$k_s^2-k_1^2=x_s^2-x_1^2+y_s^2-y_1^2-2\left(x_s-x_1\right)x-2\left(y_s-y_1\right)y \quad (17)$$

Suppose the following equation group is set up:

$$\begin{cases}p=2\left(x-x\right)\\ q_{s1}=2\left(y-y\right)\\ r_{s1}=x_s^2-x_1^2+y_s^2-y_1^2-d_s^2+d_1^2\end{cases} \quad (18)$$

After linear processing, the result of the least square algorithm is as the following:

$$\begin{cases}\hat{x}=\dfrac{\sum_{s=1}^{G}p_{s1}r_{s1}\sum_{s=1}^{G}q_{s1}^2-\sum_{s=1}^{G}q_{s1}r_{s1}\sum_{s=1}^{G}p_{s1}q_{s1}}{\sum_{s=1}^{G}p_{s1}^2\sum_{s=1}^{G}q_{s1}^2-\left(\sum_{s=1}^{G}p_{s1}q_{s1}\right)^2}\\ \hat{y}=\dfrac{\sum_{s=1}^{G}q_{s1}r_{s1}\sum_{s=1}^{G}p_{s1}^2-\sum_{s=1}^{G}p_{s1}r_{s1}\sum_{s=1}^{G}p_{s1}q_{s1}}{\sum_{s=1}^{G}p_{s1}^2\sum_{s=1}^{G}q_{s1}^2-\left(\sum_{s=1}^{G}p_{s1}q_{s1}\right)^2}\end{cases} \quad (19)$$

It can be represented in matrix:

$$\hat{x}=\left(A^TA\right)^{-1}A^Tb \quad (20)$$

The estimated coordinate of weighted least square algorithm (WLS) is:

$$\hat{X}=\left(A^TWA\right)^{-1}A^TWb \quad (21)$$

In Equation (21):

$$\hat{x}=\begin{bmatrix} x \\ y \end{bmatrix}, A=\begin{bmatrix} 2(x_G-x_1) & 2(y_G-y_1) \\ \vdots & \vdots \\ 2(x_G-x_{G-1}) & 2(y_G-y_{G-1}) \end{bmatrix} \quad (22)$$

$$b=\begin{bmatrix} x_1^2-x_G^2+y_1^2-y_G^2+k_G^2-k_1^2 \\ \vdots \\ x_{G-1}^2-x_G^2+y_{G-1}^2-y_G^2+k_G^2-k_{G-1}^2 \end{bmatrix} \quad (23)$$

$$W=\begin{bmatrix} w_1 & 0 \\ \vdots & \vdots \\ 0 & w_G \end{bmatrix} \quad (24)$$

Only when W is a symmetric positive definite matrix, $\hat{x}$ can be fixed as the minimum variance unbiased estimation. If $W=M^{-1}$, the estimated value $\hat{x}$ reaches the minimum mean square error, and M means the variance matrix with length error.

In this period, weight value of the known node is 1, and the weight value of the testing node increases gradually on the base of 0.1, whose value range is [0,l]. The step length is 0.05. When in circular refinement, the weight value of the testing value increases gradually 0.05.

(3) The locating process

Process 1. We can roughly estimate the location in this process. With MIN-MAX algorithm, the unknown algorithm can get the solution of its range according to the neighbor nodes, location and comm. model by Equation (11). Using Equation (12) further, we can estimate the rough coordinate of the unknown node and introduce the weight coefficient at the same time. The smaller the range calculated with Equation (11), the more accurate is the coordinate of the unknown node estimated with Equation (12), and the weight value is increasing in the meantime.

Process 2. In this process, we can get the location and refinement. The node changes its data, for example the coordinate by the weighted least square algorithm. After process 1, other unknown nodes all have their initial coordinates and carry on the cyclic refinement with weighted least square algorithm. Each time the unknown node's coordinate is changed, the weight coefficient of the surrounding node increases once, whose weight value increases 0.05 in each cycle on the base of 0.1.

As the cycle times and the unknown node's weight value constantly increase, the value grows gradually towards the weight value 1 of the known node. Once the weight value of unknown node is larger than 1, or the coordinates obtained in 2 times are quite close, the cycle step will stop. After all unknown nodes carry out this process, that is to say, all unknown nodes have been located, and this algorithm will expire.

III. Numerical Results

In accordance with the key point of wireless sensor network, we should suppose on the wireless sensor network of node location as the following: (1) Wireless sensor network is deployed in the two dimension, and the unknown node only needs three beacon nodes, locations and distances when in location; but if the location is performed in the three dimension area, the node needs four beacon nodes, locations and distances. (2) The sensor node adopts free space wave propagation model, that is, the node's communication range is a cycle. (3) The sensor node can search its neighbor node and it can real free communication among the neighbor nodes. (4) The sensor nodes have the symmetrical communication power, the communication radius is the same, and all information can be received correctly. (5) Only several sensor nodes become the beacon nodes by outfitting GPS receiver or manual localization and the rest nodes all own the same processing capability. (6) The nodes have two different markers: beacon and single. These two markers separately mean beacon node and the known node.

Suppose there are N sensor node in a two dimension wireless sensor network and they are evenly and randomly distributed in a $L \times L$ square domain, without obstacle and interference. A small part of nodes, coordinate is known (GPS location or manual deployment), which is called Beacon Node.

Communication Model: suppose the communication model of node is a cycle with itself being the center. R represents the communication radius. The beacon node has the same communication capability with unknown nodes and the communication radius all is R. There are symmetrical communication capability among nodes and the same sending and receiving power.

The distance value between practical estimated location of unknown nodes and the real value of the node's location means location error of each node. The definition of the average error of the algorithm is:

$$error=\frac{\sum_{i=1}^{n}((x_{cal}-x_{real})^2+(y_{cal}-y_{real})^2)}{n} \quad (25)$$

The basic scheme (Scheme 1) in the following :
Border Length=100;
Node Amount=200;
Beacon Amount=20;
UN Amount=Node Amount –Beacon Amount;
R=60;

Then we can get the values: error =38.9140, Accuracy=0.6486. The simulation result is in the figure 5.

TABLE I. The Location Scheme

Scheme	Border Length	Node Amount	Beacon Amount	R	Error	Accuracy
1	100	200	20	60	34.9382	0.5823
2	200	200	20	60	57.6661	0.9611
3	100	100	20	60	34.3157	0.5719
4	100	200	10	60	33.3250	0.5554
5	100	200	20	40	30.9272	0.7732
6	50	100	10	40	16.8312	0.4208

The simulation experiment result is shown in figure 3. By changing the coefficients of the basic scheme 1 and changing one coefficient once, we can get schemes from 2 to 5 with a quite strong comparison.

Compared with the result above, we can get the following relationships by research: error is proportional to Border Length, in inverse proportion to Node Amount and Beacon Amount, proportional to R; Accuracy is proportional to Border Length, in inverse proportion to Node Amount, Beacon Amount, and R. In the view of the compared result, we enact an optimal scheme, that is scheme 6, whose coefficient is in the following:

Border Length=50;
Node Amount=100;
Beacon Amount=10;
UN Amount=Node Amount-Beacon Amount;
R=40;

Then we get the values: error =16.8312, Accuracy =0.4208. The simulation result is in the figure 13 and 14. Compared with scheme 1, the error and accuracy decrease obviously.

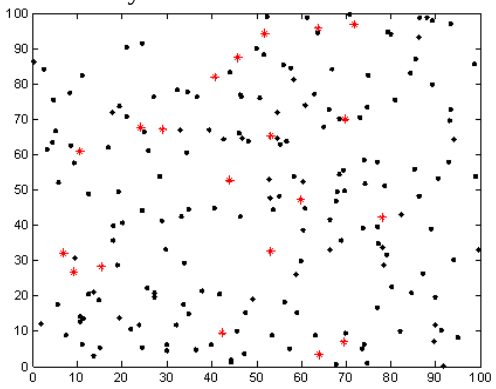

Figure 2. The distribution map of network nodes in Scheme 1

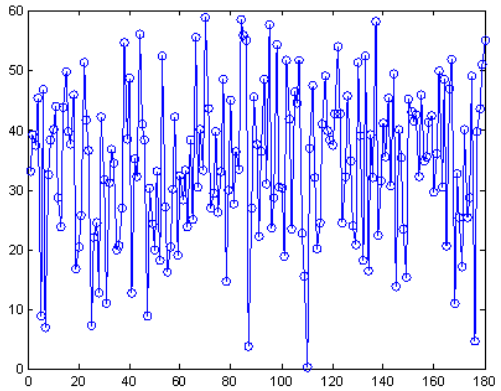

Figure 3. Each unknown node's error in Scheme 1

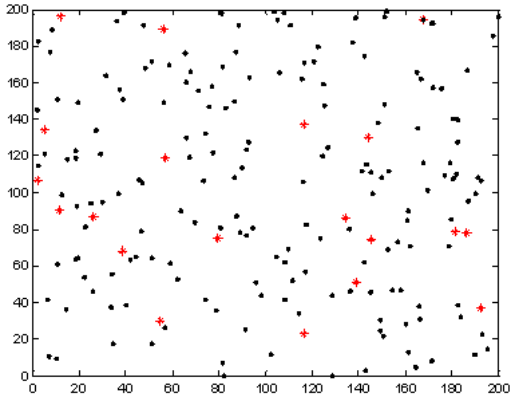

Figure 4. Distribution map of network nodes in Scheme 2

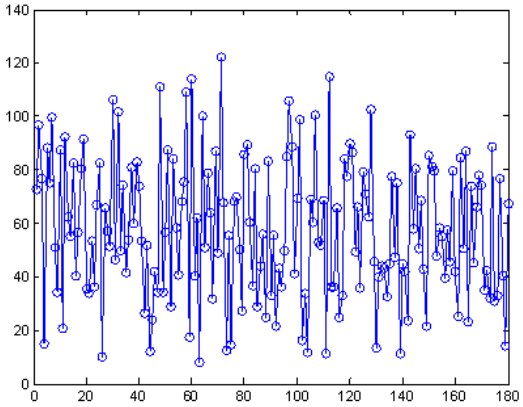

Figure 5. Every unknown node's error in Scheme 2

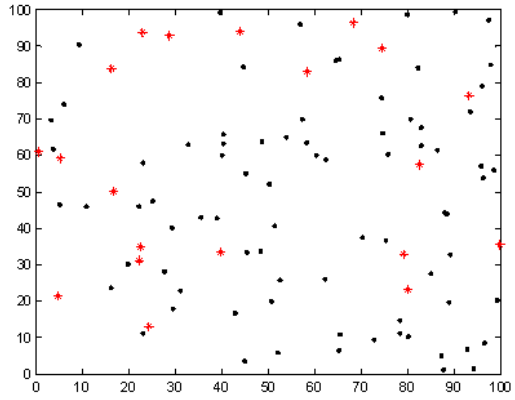

Figure 6. The Distribution Map of the Network Nodes in Scheme 3

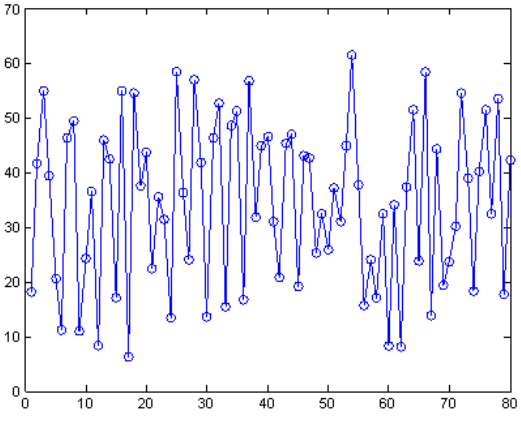

Figure 7. Every unknown node's error in Scheme 3

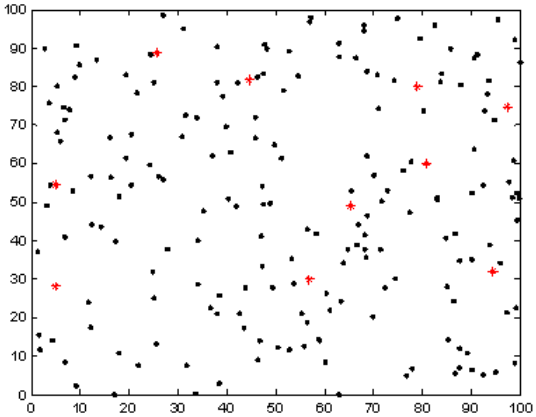

Figure 8. The Distribution Map of Network Map in Scheme4

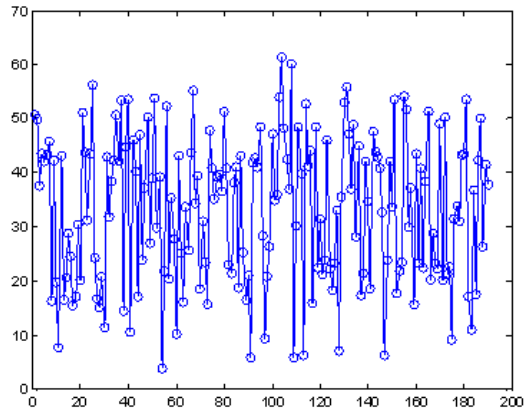

Figure 9. Every unknown node's error in Scheme 4

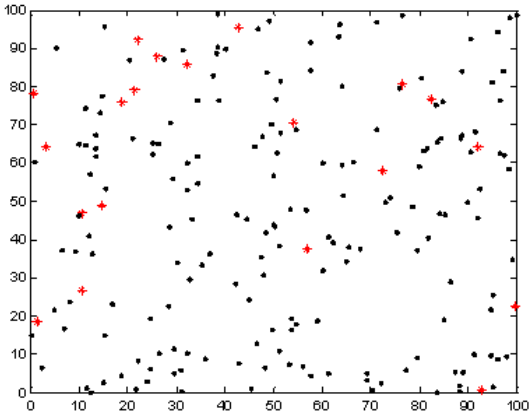

Figure 10. The distribution map of network nodes in Scheme 5

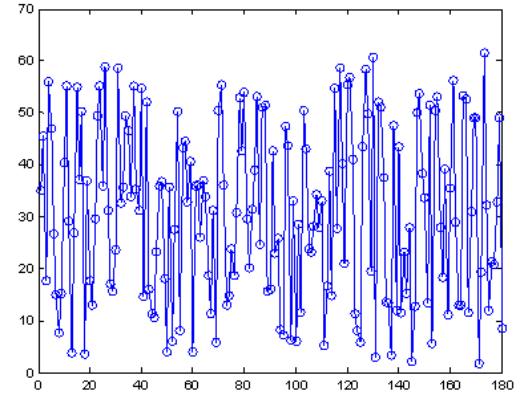

Figure 11. Every unknown node,s error in Scheme 5

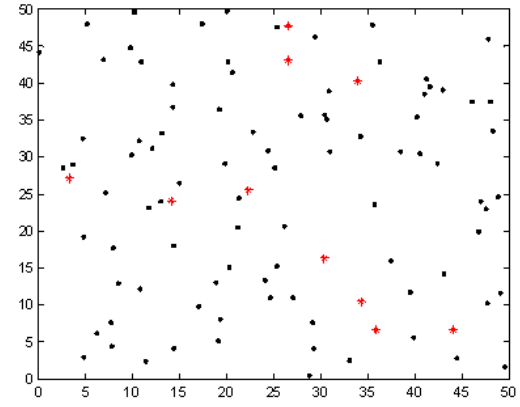

Figure 12. The Distribution Map of Network Node in Scheme 6

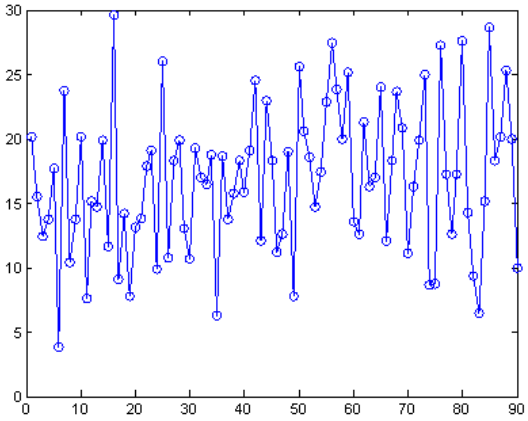

Figure 13. Every unknown node's error in Scheme 6

IV. CONCLUSION

According to some disadvantages in this algorithm, this article proposes the following improved schemes: we can calculate the average value of the sum of distance value measured by RSSI and every single distance, and make use of the difference between the last value and real length in order to finish the distance error correction; and we can adopt the combination of MIN-MAX algorithm and weighted least square algorithm to replace the least square algorithm of trilateration. In this paper, we make MATLAB stimulation analysis on DV-Hop algorithm, and draw a conclusion: error is proportional to Border Length, in inverse proportion to Node Amount and Beacon Amount, proportional to R; Accuracy is proportional to Border Length, in inverse proportion to Node Amount, Beacon Amount, and R. As a result, we enact an optimal location scheme.

REFERENCES

[1] He, Tian, et al. "Range-free localization schemes for large scale sensor networks." *Proceedings of the 9th annual international conference on Mobile computing and networking. ACM, 2003.*

[2] Langendoen, Koen, and Niels Reijers. "Distributed localization in wireless sensor networks: a quantitative comparison." *Computer Networks* 43.4 (2003) pp. 499-518.

[3] Dil, Bram, Stefan Dulman, and Paul Havinga. "Range-based localization in mobile sensor networks." *Wireless Sensor Networks. Springer Berlin Heidelberg*, 2006. 164-179.

[4] Shang, Yi, and Wheeler Ruml. "Improved MDS-based localization." *INFOCOM 2004. Twenty-third AnnualJoint Conference of the IEEE Computer and Communications Societies. Vol. 4. IEEE, 2004.*

[5] Boukerche, Azzedine, et al. "Localization systems for wireless sensor networks." *wireless Communications, IEEE 14.6* (2007) pp. 6-12.

[6] Mao, Guoqiang, Barış Fidan, and Brian Anderson. "Wireless sensor network localization techniques." *Computer networks* 51.10 (2007) pp. 2529-2553.

[7] Li, Zang, et al. "Robust statistical methods for securing wireless localization in sensor networks." *Information Processing in Sensor Networks, 2005. IPSN 2005. Fourth International Symposium on. IEEE, 2005.*

[8] Ssu, Kuo-Feng, Chia-Ho Ou, and Hewijin Christine Jiau. "Localization with mobile anchor points in wireless sensor

networks." *Vehicular Technology, IEEE Transactions on* 54. 3 (2005) pp. 1187-1197.

[9] Chandrasekhar, Vijay, et al. "Localization in underwater sensor networks: survey and challenges." *Proceedings of the 1st ACM international workshop on Underwater networks. ACM, 2006.*

[10] Wang, Yun, et al. "Range-free localization using expected hop progress in wireless sensor networks." *Parallel and Distributed Systems, IEEE Transactions on 20.10* (2009) pp. 1540-1552.

[11] Huang, Qiqian, and S. Selvakennedy. "A range-free localization algorithm for wireless sensor networks." *Vehicular Technology Conference, 2006. VTC 2006-Spring. IEEE 63rd. Vol. 1. IEEE, 2006.*

[12] He, Tian, et al. "Range-free localization and its impact on large scale sensor networks." *ACM Transactions on Embedded Computing Systems (TECS) 4.4* (2005) pp. 877-906.

[13] Shang, Yi, Jing Meng, and Hongchi Shi. "A new algorithm for relative localization in wireless sensor networks." *Parallel and Distributed Processing Symposium, 2004. Proceedings. 18th International. IEEE, 2004.*

[14] Wong, Sau Yee, et al. "Multihop localization with density and path length awareness in non-uniform wireless sensor networks." *Vehicular Technology Conference, 2005. VTC 2005-Spring. 2005 IEEE 61st. Vol. 4. IEEE, 2005.*

[15] Hongyang, Chen, et al. "A robust location algorithm with biased extended Kalman filtering of TDOA data for wireless sensor networks." *Wireless Communications, Networking and Mobile Computing, 2005. Proceedings. 2005 International Conference on.* Vol. 2. IEEE, 2005.

[16] Lazos, Loukas, and Radha Poovendran. "SeRLoc: Robust localization for wireless sensor networks." *ACM Transactions on Sensor Networks (TOSN)* 1.1 (2005) pp. 73-100.

[17] Sit, Terence Chung Hsin, et al. "Multi-robot mobility enhanced hop-count based localization in ad hoc networks." *Robotics and Autonomous Systems* 55.3 (2007) pp. 244-252.

Wireless Sensor Networks Target Localization Based on Least Square Method and DV-Hop Algorithm

JIANG Kun and YAO Li
The Digital Center of Xiking Hospital, The Fourth Military Medical University, Xi'an, Shanxi, 710032, China
Email: hoof4577@126.com

FENG Juan
Pharmacy Department of Xiking Hospital, The Fourth Military Medical University, Xi'an, Shanxi, 710032, China

***Abstract*—Wireless sensor node localization is one of the most crucial techniques on wireless sensor network. For reducing localization cost and improving localization accuracy, we propose an improved wireless sensor network DV-Hop localization algorithm. The mobile beacon node is introduced into DV-Hop and allows a moving beacon node to move on the pre-arranged way, continuously broadcast its position information to form multiple virtual beacons. The simulation experiment result shows our method can reduce the localization cost and the complexity of network while improving the node localization accuracy and efficiency.**

***Index Terms*—Wireless Sensor Node Network; The Mobile Beacon; The Optimized Path; DV-Hop Localization Algorithm**

I. INTRODUCTION

In Wireless Sensor Networks, WSN are composed by lots of cheap micro sensor nodes deployed in monitoring area [1]. They form a multi-hop self-organizing network system through wireless communication in order to collaboratively sense, collect and process information of sensory target in covering area, and transmit them to observers. Sensor network nodes are uncontrollable while deploying. In a large wireless sensor network application, nodes are usually spread into a wide area, and most of their positions are unknown. But a large amount of wireless sensor network's applications require those nodes' position information for obtaining those network events' happening location and source location. Thus, localization is one of the main applications of wireless sensor network [2]. For most applications, it is meaningless to sense data without nodes' positions. Only when sensor nodes are located rightly, the happening events and its specific location information detected by sensor nodes can be determined [3]. Nodes must clarify their position for indeed explaining "where the specific event happens". Then the localization and tracking for outside target can be achieved. Otherwise, to utilize nodes' position information when designing routing protocol can improve routing efficiency while offering namespace for network, reporting the coverage quality of network for establishers, and achieving network's load balancing and self-organizing of network topology [4]. Thus, the nodes localization problem has become a crucial research direction for wireless sensor network.

Wireless sensor nodes self-localization is a system determining its own position through estimating the distance between it to neighbor nodes and the number of neighbor nodes and utilizing the information exchange between nodes [5]. On sensor network, the ability that nodes can self-determine their locations is considered as their basic ability and one of the basic services of this system. For WSN, manpower deployment or the allocation of GPS devices for every network node will be limited by cost, power consumption, expansibility and other problems. Thus, searching WSN self-localization system has become the problem discussed by many research institutes and scholars [6].

On wireless sensor network, according to the fact that whether the distance between nodes is measured, the localization system can be divided into: range-based localization and range-free localization [5]. The former one needs the measurement of the absolute distance between nodes, and utilizes the real distance to determine unknown target's node location; the second one only uses the associated relationship of the distance between nodes to calculate nodes' locations. Range-based algorithm can locate through measuring the real distance or direction between neighbor nodes. The specific methods include: Time of Arrival [6], Time Difference of Arrival, Radio Signal Strength (RSSI) and Angle of Arrival [7] and so on.

Although the mobility of nodes makes the localization process more complicated, using this feature can improve localization accuracy and reduce localization cost. In Bergamo and some' researches, there are 2 fixed beacons on network to send the coordinate information to whole network. The others in activity can locate themselves based on the strength of received signals [8]. Scholars home and abroad have made lots of researches on localization problems, and they proposed several

doi:10.4304/jnw.9.1.176-182

relatively typical localization algorithm [9]. But there are these listing limitations [10]: 1.dependence on the support of special hardware; 2.the need for special network topology. But to introduce mobile nodes onto wireless sensor network can help enhancing its functions. As reference [11], through moving several unknown nodes into those areas with relatively sparse network nodes to compensate the insufficiency of inhomogeneous density distribution of nodes. Reference [12] mentions to use moving reference nodes and RSSI (instruction of the strength of received signal) to locate unknown nodes. But in real environment, temperature, obstacles, broadcasting ways and other elements are dynamic, which made the practice of RSSI in real application is difficult. Especially when the requirement of energy consumption and volume is stricter for nodes, so this range-based localization technique cannot be applied in most of the time. Range-free localization algorithm does not need the measurement of the distance between nodes, but the use of distance vector routing [13]. The condition of network connection or GPS localization and other ideas suggest a distributed localization method without distance measuring [14]. Undoubtedly this method reduced network cost. However there is no support of suitable hardware. Some errors still exist on localization. When some obstacles appear, the Euclidean distance between nodes will cause larger errors because of the bending routine, and the accuracy will be lowered [15]. So how to improve this range-free localization algorithm's accuracy also became a hot field of research.

The localization algorithm based on beacon nodes studies the choosing of mobile beacons, the routine of moving, the calculating method of localization and mobile nodes [16]. Because beacon nodes need to be moved, it is extremely important on network to design the mobile beacon nodes and study wireless sensor network's application system according to sensor network's features. For reducing localization cost and improving localization accuracy, we proposed an advanced wireless sensor network DV-Hop localization algorithm. This method introduces mobile beacon nodes into DV-Hop localization algorithm and allows moving beacon nodes to move and broadcast its position information on the pre-arranged path in order to form multiple virtual beacons [17] [18]. The result of simulation experiment shows our method can make the localization cost and network's complexity lower while developing nodes localization's accuracy and efficiency.

II. PROPOSED ALGORITHM

The accuracy of the node localization algorithm relies on the intensity of beacon nodes in wireless sensor network. But the cost of beacon nodes is high as 100 times the cost of normal nodes. For reducing localization cost, we propose a wireless sensor network nodes localization algorithm based on mobile beacon and DV-Hop. From the foundation of DV-Hop localization algorithm [19] [20], allow a moving beacon node to move and broadcast its position information on the pre-arranged path in order to form multiple virtual beacons. Those unknown nodes record the hop count of every virtual beacon, and use the weighted processing to calculate the average hop distance and the distance between every virtual beacon. Finally it utilizes three border measurements to calculate the location information of unknown nodes in order to achieve accurate localization for nodes. Because only one mobile beacon is adopted, the cost and the complexity of network are both reduced which prove the practicability of this method [21].

Wireless sensor network is composed by huge amount of sensor nodes deployed in monitoring area. Every node form a multi-hop self-organizing network through wireless communication, then collaboratively sense, collect and treat every relative monitoring information in nature world. Under many circumstances, the nodes on wireless sensor network need to know their physical location when tracking target and in emergencies. Basically wireless sensor nodes are randomly deployed into different areas. Because of the limitation of cost, energy and volume, those nodes randomly deployed cannot determine their locations but only to estimate them according to other nodes' known locations with some kind of localization system. For the localization of wireless sensor network nodes, many scholars have made deep researches. They proposed many localization systems and algorithms. According to the result of whether the distance measurement is needed, localization algorithm can be separated into range-based and range-free. Range-based algorithm has the dependence on hardware condition and in nature environment, there are various unpredictable elements can bother it. Range-free localization algorithm majorly include centroid algorithm, DV-Hop, Amorphous algorithm, APIT algorithm and so on. Range-free localization algorithm has larger errors comparing with range-based algorithm yet can meet most needs of engineering applications [22] [23]. That is why this algorithm is popular now. At the same time, many scholars did lots of researches to improve the accuracy of range-free algorithm, but finally increased the algorithm complexity and energy cost. For this situation, we proposed a localization algorithm based on advanced sensor network DV-Hop to reduce the cost and complexity while improving the localization accuracy [24] [25] [26].

On the basis of DV-Hop, this algorithm allows a moving beacon node to move and broadcast its position information on the pre-arranged path in order to form multiple virtual beacons. Those unknown nodes record the hop count of every virtual beacon, and use the weighted processing to calculate the average hop distance and the distance fits its location's grid. Then it is multiplied with hop count to get the distances with each virtual beacon. Finally it uses advanced three-border measurement to calculate location information for achieving accurate localization. Because only one mobile beacon is used, and there is no need to deploy other beacon nodes, the cost and network's complexity are reduced.

A. DV-hop Localization Algorithm

Dragos Niculescu and some from Lutegesi University U.S use distance vector routing and GPS localization's idea to propose DV-Hop localization algorithm [27] [28] [29]. It is composed by three stages: firstly, make every node on network obtain the hop count of beacons; then, after getting other beacon locations and hop distances, beacons calculate the average single hop distance and give it a survival period; after that broadcast its correction value. The unknown nodes will record the first received correction value, and forward it to neighbor nodes. This strategy can ensure that most nodes can receive the average single hop distance from latest beacons. Afterward, the unknown nodes can calculate the total distance to beacons according to the recorded hop count [30].

DV-Hop algorithm can calculate the unknown node's location which is far away from beacons. And it does not need extra information. However, the level of errors can vary based on the difference of bending degree. Because one unknown node can only get hop count through one path, it needs the average single hop distance to calculate its own location, which leads to the large error. Let's suppose a DV-Hop model as Figure 1:

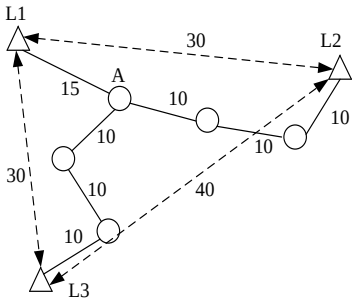

Figure 1. The DV-hop localization algorithm model

where, L1, L2, L3 are beacons. A is an unknown node. The distances among L1, L2, and L3 are known as 30, 30, and 40 respectively. It is 15 from A to L1, the number of frame skip is 1. The number of frame skip from A to L2, L3 is 3, and the average single hop is 10.

Firstly, beacon broadcast include location information and the package whose started label is 1. When signal is transmitted to another node, the number of frame skip adds 1 automatically. So the distance between every node and beacons can be calculated. When beacons receive another beacons' signal, we can start to calculate the average single hop distance, the average single hop distances of L1, L2, and L3 are as following [31].

$$\text{L1: } (30+30) / (4+4) = 7.5 \quad (1)$$

$$\text{L2: } (30+40) / (4+6) = 7 \quad (2)$$

$$\text{L3: } (30+40) / (4+6) = 7 \quad (3)$$

After calculating the average distance, beacons will broadcast it to other nodes. When unknown nodes get the average single hop distances, they can get the distance to beacons, which means L1,L2,L3 will broadcast the three distance values: 7.5, 7, 7. Nevertheless, because there is only one hop between A to L1, the average single hop distance received by A is 7.5. And it calculates the distance with L1, L2, L3, namely, AL1=7.5, AL2=AL3=7*3=21. Next, the trilateration is used to locate node A. Actually the distance is AL1=15. But the estimated result by DV-Hop is 7.5, so a large error existing. Thus there is a big difference between calculated location and real location after using trilateration. DV-Hop localization mechanism is very similar to distance vector routing mechanism in traditional networks [32] [33]. The distance vector localization mechanism is divided into three stages as following:

In the first stage, the minimum hop is calculated firstly between the unknown node and the beacon node. The beacon node announces its packet of location information to all its neighbor nodes, which include the hop count field and the initial value, is one. Receiver node records the minimum hop of each beacon node, ignoring the packet of larger hop from the same beacon node [34] [35] [36]. Then the hop count is increased 1 and forward to the neighbor nodes. Through the method, all nodes in the network can get the minimum hop of each beacon node [37] [38].

In the second stage, the actual hop distance is calculated between the unknown node and the beacon node. According to the location information and the minimum hop in the first stage, the average hop's actual distance in each beacon nodes can be estimated by adopting the following equation (4).

$$HopSize_i = \frac{\sum_{j \neq 1} \sqrt{(x_i - x_j)^2 + (y_i - y_j)^2}}{\sum_{j \neq i} h_j} \quad (4)$$

In the equation above, (x_i, y_i) and (x_j, y_j) are the coordinate of beacon nodes. The h_j is the hop count between beacon nodes i and j ($i \neq j$). Then the beacon node broadcasts the information with survival duration field in groups into network, and the unknown node only records the first average single hop distance and transmits it to neighbor node. The unknown node can calculate its distance away from every beacon node after receiving the average single hop distance, according to the recorded hop count [39] [40].

In the third stage, according to the recorded hop distance away from every beacon node in the second stage, trilateration localization and maximum likelihood method are adopted to calculate the coordinate of unknown node.

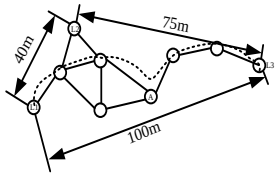

Figure 2. DV-Hop algorithm

B. The Error Analysis in the Localization Algorithm

In DV-Hop localization algorithm, the obtained beacon nodes are small number in communication range, but the

unknown node can get the estimate distance of the multiple beacon nodes out of the communication range via multi-hop transmission, which make full use of the much information to obtain the node localization. When network average connectivity is 8 and beacon proportion is 10%, the localization error is about 1/3 of sensors' RF communication distance. The following suppositions are made:

(1) Each sensor node in the network communicate with corresponding neighbor nodes when their fixed distance is the same;

(2) The sensor node's communication distance *r* affect positioning accuracy, which only moderate size can achieve a better positioning accuracy;

(3) The positioning accuracy in the monitoring region depends on the network connectivity and beacon node ratio.

For some sensor network in real environment, it is unpractical for us to deploy a large number of beacon nodes with known position, while deploying a certain proportion of beacon nodes with GPS will increase the cost of the network.

In sensor network, let us assume the coordinate of unknown node is (X_n, Y_n), while the real coordinate is (X_n, Y_n), so their distance is as following:

$$D = \sqrt{\left(X_n - x_n\right)^2 - \left(Y_n - y_n\right)^2} \tag{5}$$

The definition of the average location error is related to the node's wireless transmission region, namely,

$$\Delta = \frac{1}{NR}\sum_{n=1}^{N}\Delta d_n \times 100\% \tag{6}$$

The performance of the localization algorithm is analyzed by establishing experimental simulation environment, we mainly analyze the location accuracy influence under different beacon proportion. In the MATLAB simulation platform, we simulate 100 unknown nodes are distributed widely in a square shape with a 50cm side and RF communication distance is 10m. The error is only analyzed when the beacon nodes are from 3 to 10, as shown in figure 3.

According to the figure 3, we can see that the beacon node proportion is proportional to localization error. The more beacon node is, the smaller the average localization error and the mean square error are. So in order to improve the positioning accuracy, the beacon nodes should be increased.

In order to more accurately calculate the estimated average hop distance, the concept of the weight is introduced in this paper. Due to the uneven distribution of the network node, the weighted average is used to rectify the hop distance, and each node receives a plurality of average hop distance values from the virtual nodes. The closer the average hop distance of unknown node, the better the unknown node case is reflected in the network area, even the greater impact the average hop distance has.

It should has a larger weights that make the calculated position of the unknown node more accurate, which is closer to actual result than the average value. To express accurately and conveniently, we assume the unknown node N_j in the network can receive many average hop distance values from virtual nodes. The average hop distance calculated by the virtual beacon A_i is denoted as D_i, and the hop is denoted as H_i from the node Nj to beacon.

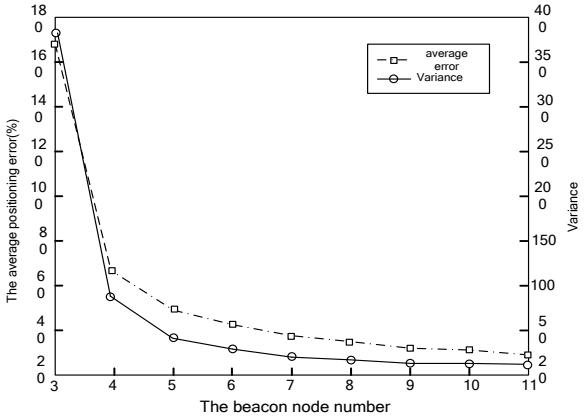

Figure 3. The effect of the location error on beacon node number

Weighting factor is reflected the influence of the average hop distance calculated by the unknown node on that of virtual beacon node. Assume the unknown node receive three average hop distances (D1,D2,D3) respectively from virtual nodes (A1,A2,A3), while the recorded hops in the look up table of the unknown node is respectively H1, H2, H3 away from three virtual beacon nodes. Thus, the node's average distance is as following:

$$\begin{aligned}\overline{D}_1 = &\frac{1/H_1 \times D_1}{1/H_1 + 1/H_2 + 1/H_3} + \\ &\frac{1/H_2 \times D_2}{1/H_1 + 1/H_2 + 1/H_3} + \frac{1/H_3 \times D_3}{1/H_1 + 1/H_2 + 1/H_3}\end{aligned} \tag{7}$$

The sum of average hop's weights is 1, which reflects the influence degree of the average hop distance that is finally obtained on each average hop distance. So the average hop distance of the calculated node is denoted as following:

$$\overline{D}_i = \sum_{i=1}^{n}\frac{1}{H_j\sum_{j=1}^{n}\left(1/H_j\right)}D_i \tag{8}$$

So far, the hop between the virtual beacon node and the unknown node has been calculated, and we have got the average hop distance suited for our network area, so the coordinate of the unknown node N_j can be computed by using the three-border measurement.

III. SIMULATION ANALYSIS

Simulation experiment is provided to validate the model and algorithm under the OMNeT++ development environment, and use MATLAB software to auxiliarily

analyze experiment data. In the OMNeT++ development environment, 100 sensor nodes are randomly deployed in 50 m × 50 m area with 30 m communication range. And a mobile beacon getting its position can move according to Gauss-Markov model, where the average velocity is 5 and the initial direction angle is 90°. The coefficient is changed on the edge region, namely, α=0.75 in Eq. (4-5). The broadcast calculator is set to 2s, that is to say the mobile node will broadcast localization information after every 2s-movemen. The simulation result is the average value of 20 independent measurements, so that the result of simulation is close to the reality.

A. Coverage Rate and Localization Precision

Mobile beacon move with a predetermined motion model and periodically broadcast the location information packet. Namely, the more virtual beacon, the higher the positioning accuracy is which leads too much positioning time. Their relationship is shown as Figure 4. It is obvious that the moving distance of mobile beacon becomes more and more large with the passage of time and its broadcast information is more, so the more the virtual beacon is, the less the localization error. Similarly, the more coverage the trajectory of the mobile beacon is, the more unknown nodes the beacon can obtain to calculate its own position, which the positioning coverage is also continuously increasing.

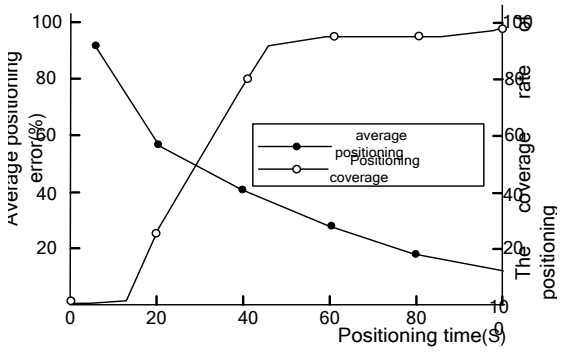

Figure 4. The localization error and coverage rate

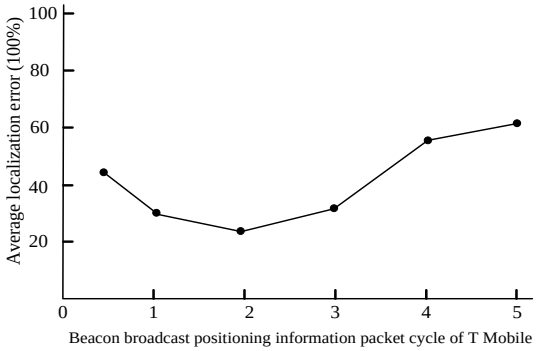

Figure 5. The relationship between the broadcast period and the mean localization error

B. The Influence of the Localization Information Period T Broadcast By Beacon Node

When the mobile beacon node is moved with Gauss-Markov model of a fixed parameter, the less the period is, the denser the virtual beacons are. That is to say the more virtual beacons in unit area, the more consumption the node information produce and the greater the error becomes. When the period *T* enlarges to certain extent, the broadcast localization information is less if continuously increased. If the used virtual beacon is too few, this will lead to an increasing positioning error. Optimal positioning period in size is determined by the communication radius. When the communication radius grows, the broadcast period should also be increased accordingly. When the broadcast period T is changed, the relationship between the localization error and its period is shown in Figure 5.

C. Comparison of the Localization Error

The algorithm is evaluated by the localization error, the mobile node will broadcast localization information packet after every movement 2s. Namely, a virtual beacon is constructed in network. The comparison of the simulation result is shown in Figure 6.

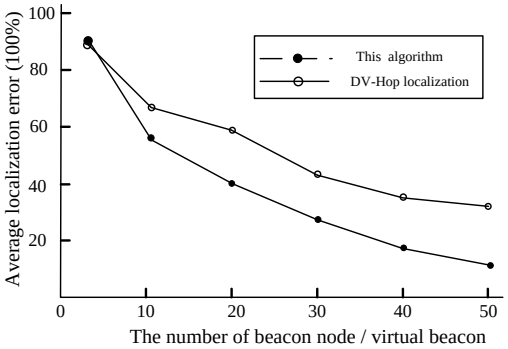

Figure 6. The comparison of the localization error between DV-hop and the proposed method

As shown in Figure 6, the two positioning algorithm error decrease with the increase of the beacon node. When there are more beacon nodes, the error of the proposed method is decreased significantly. When the more virtual beacon got by a node, the closer realistic network conditions the average hop distance is after weighted.

IV. CONCLUSION

This paper mainly introduces the localization algorithm based dynamic selection of mobile beacon in wireless sensor network, The mobile beacon node is introduced into DV-Hop, and allow a moving beacon node to move on the pre-arranged way, continuously broadcast its position information to form multiple virtual beacons. The simulation experiment result shows our method can reduce the localization cost and the complexity of network while improving the node localization accuracy and efficiency.

REFERENCES

[1] Zou, Yi, and Krishnendu Chakrabarty. "Sensor deployment and target localization based on virtual forces." *INFOCOM 2003. Twenty-Second Annual Joint Conference of the IEEE Computer and Communications. IEEE Societies*. Vol. 2. IEEE, 2003.

[2] Zou, Yi, and Krishnendu Chakrabarty. "Sensor deployment and target localization in distributed sensor networks." *ACM Transactions on Embedded Computing Systems (TECS)* 3.1 (2004) pp. 61-91.
[3] Willoughby, Twyla R., et al. "Target localization and real-time tracking using the Calypso 4D localization system in patients with localized prostate cancer." *International Journal of Radiation Oncology* Biology* Physics* 65.2 (2006) pp. 528-534.
[4] Liu, Juan, et al. "Distributed group management for track initiation and maintenance in target localization applications." *Information Processing in Sensor Networks. Springer Berlin Heidelberg*, 2003.
[5] Kaplan, Lance M., Qiang Le, and N. Molnar. "Maximum likelihood methods for bearings-only target localization." *Acoustics, Speech, and Signal Processing, 2001. Proceedings. (ICASSP'01). 2001 IEEE International Conference on*. Vol. 5. IEEE, 2001.
[6] Verellen, Dirk, et al. "Quality assurance of a system for improved target localization and patient set-up that combines real-time infrared tracking and stereoscopic X-ray imaging." *Radiotherapy and oncology* 67.1 (2003) pp. 129-141.
[7] Yeung, Daniel, et al. "Systematic analysis of errors in target localization and treatment delivery in stereotactic radiosurgery (SRS)." *International Journal of Radiation Oncology* Biology* Physics* 28.2 (1994): 493-498.
[8] Gielen, Frans LH, Victor PJ Duysens, and Johan FM Gijsberg. "Dual electrode lead and method for brain target localization in functional stereotactic brain surgery." *U.S. Patent* No. 6,011,996. 4 Jan. 2000.
[9] Vayssiere, Nathalie, et al. "Magnetic resonance imaging stereotactic target localization for deep brain stimulation in dystonic children." *Journal of neurosurgery* 93.5 (2000) pp. 784-790.
[10] Cevher, Volkan, Marco Duarte, and Richard G. Baraniuk. "Distributed target localization via spatial sparsity." *European Signal Processing Conference (EUSIPCO*). 2008.
[11] Holtzheimer III, Paul E., David W. Roberts, and Terrance M. Darcey. "Magnetic resonance imaging versus computed tomography for target localization in functional stereotactic neurosurgery." *Neurosurgery* 45.2 (1999) pp. 290.
[12] Godrich, Hana, Alexander M. Haimovich, and Rick S. Blum. "Target localization accuracy gain in MIMO radar-based systems." *Information Theory, IEEE Transactions on* 56.6 (2010) pp. 2783-2803.
[13] Bednarz, Greg, et al. "Evaluation of the spatial accuracy of magnetic resonance imaging-based stereotactic target localization for gamma knife radiosurgery of functional disorders." *Neurosurgery* 45.5 (1999) pp. 1156.
[14] Sumanaweera, Thilaka, et al. "Mr geometric distortion correction for improved frame-based stereotaxic target localization accuracy." *Magnetic resonance in medicine* 34.1 (1995) pp. 106-113.
[15] He, Tian, et al. "Range-free localization schemes for large scale sensor networks." *Proceedings of the 9th annual international conference on Mobile computing and networking. ACM*, 2003.
[16] Hu, Lingxuan, and David Evans. "Localization for mobile sensor networks." *Proceedings of the 10th annual international conference on Mobile computing and networking. ACM*, 2004.
[17] Shang, Yi, and Wheeler Ruml. "Improved MDS-based localization." *INFOCOM 2004. Twenty-third AnnualJoint Conference of the IEEE Computer and Communications Societies. Vol. 4. IEEE*, 2004.
[18] Dil, Bram, Stefan Dulman, and Paul Havinga. "Range-based localization in mobile sensor networks." *Wireless Sensor Networks. Springer Berlin Heidelberg*, 2006. 164-179.
[19] Lazos, Loukas, and Radha Poovendran. "SeRLoc: Secure range-independent localization for wireless sensor networks." *Proceedings of the 3rd ACM workshop on Wireless security. ACM*, 2004.
[20] Sheu, Jang-Ping, Pei-Chun Chen, and Chih-Shun Hsu. "A distributed localization scheme for wireless sensor networks with improved grid-scan and vector-based refinement." *Mobile Computing, IEEE Transactions on* 7.9 (2008) pp. 1110-1123.
[21] Shen, Xingfa, et al. "Connectivity and RSSI based localization scheme for wireless sensor networks." *Advances in intelligent computing. Springer Berlin Heidelberg*, 2005 pp. 578-587.
[22] Sun, Guolin, et al. "Signal processing techniques in network-aided positioning: a survey of state-of-the-art positioning designs." *Signal Processing Magazine, IEEE* 22.4 (2005) pp. 12-23.
[23] Chandrasekhar, Vijay, et al. "Localization in underwater sensor networks: survey and challenges." *Proceedings of the 1st ACM international workshop on Underwater networks. ACM*, 2006.
[24] Tian, Shuang, et al. "A selective anchor node localization algorithm for wireless sensor networks." Convergence Information Technology, 2007. *International Conference on. IEEE*, 2007.
[25] Wang, Yun, et al. "Range-free localization using expected hop progress in wireless sensor networks." *Parallel and Distributed Systems, IEEE Transactions on* 20.10 (2009) pp. 1540-1552.
[26] Wong, Sau Yee, et al. "Multihop localization with density and path length awareness in non-uniform wireless sensor networks." *Vehicular Technology Conference*, 2005. VTC 2005-Spring. 2005 IEEE 61st. Vol. 4. IEEE, 2005.
[27] Wang, Sheng-Shih, Kuei-Ping Shih, and Chih-Yung Chang. "Distributed direction-based localization in wireless sensor networks." *Computer Communications* 30.6 (2007) pp. 1424-1439.
[28] Yao, Qi, et al. "An area localization scheme for large wireless sensor networks." *Vehicular Technology Conference, 2005. VTC 2005-Spring*. 2005 IEEE 61st. Vol. 5. IEEE, 2005.
[29] Shang, Yi, Jing Meng, and Hongchi Shi. "A new algorithm for relative localization in wireless sensor networks." *Parallel and Distributed Processing Symposium*, 2004. *Proceedings. 18th International. IEEE*, 2004.
[30] Koutsonikolas, Dimitrios, Saumitra M. Das, and Y. Charlie Hu. "Path planning of mobile landmarks for localization in wireless sensor networks." *Computer Communications* 30.13 (2007) pp. 2577-2592.
[31] Liao, Wen-Hwa, Kuei-Ping Shih, and Yu-Chee Lee. "A localization protocol with adaptive power control in wireless sensor networks." *Computer Communications* 31.10 (2008) pp. 2496-2504.
[32] Tay, Jeffrey HS, Vijay R. Chandrasekhar, and Winston Khoon Guan Seah. "Selective Iterative Multilateration for Hop Count-Based Localization in Wireless Sensor Networks." *Mobile Data Management, 2006. MDM 2006. 7th International Conference on. IEEE*, 2006.
[33] Kim, Kyunghwi, and Wonjun Lee. "MBAL: A mobile beacon-assisted localization scheme for wireless sensor networks." Computer Communications and Networks, 2007. ICCCN 2007. *Proceedings of 16th International Conference on. IEEE*, 2007.

[34] Wang, Yun, et al. "Localization algorithm using expected hop progress in wireless sensor networks." *Mobile Adhoc and Sensor Systems (MASS)*, 2006 IEEE International Conference on. IEEE, 2006.

[35] Wang, Jiangang, Fubao Wang, and Weijun Duan. "Application of Weighted Least Square Estimates on Wireless Sensor Network Node Localization." *Application research of computers* 9 (2006) pp. 011.

[36] Biaz, Saad, and Yiming Ji. "A survey and comparison on localisation algorithms for wireless ad hoc networks." *International Journal of Mobile Communications* 3.4 (2005) pp. 374-410.

[37] Stoleru, Radu, et al. "StarDust: a flexible architecture for passive localization in wireless sensor networks." *Proceedings of the 4th international conference on Embedded networked sensor systems. ACM*, 2006.

[38] Qian, Qingji, Xuanjing Shen, and Haipeng Chen. "An improved node localization algorithm based on DV-Hop for wireless sensor networks." *Computer Science and Information Systems* 8.4 (2011) pp. 953-972.

[39] Chang, Tzu-Chien, Kuochen Wang, and Yi-Ling Hsieh. "Enhanced color-theory-based dynamic localization in mobile wireless sensor networks." *Wireless Communications and Networking Conference*, 2007. WCNC 2007. IEEE. IEEE, 2007.

[40] Suo, Hui, et al. "Issues and challenges of wireless sensor networks localization in emerging applications." *Computer Science and Electronics Engineering (ICCSEE), 2012 International Conference on.* Vol. 3. IEEE, 2012.

Localization Algorithm based on Improved Weighted Centroid in Wireless Sensor Networks

Shyi-Ching Liang, LunHao Liao, and Yen-Chun Lee
Chaoyang University of Technology, Taiwan, 41349
Email: jerry.scliang@gmail.com

***Abstract*—Location technology is becoming more and more important in wireless sensor networks. The weighted centroid localization offers a fast and simple algorithm for the location equipment in wireless sensor networks. The algorithm derives from the centroid measurement and calculation device of the adjacent anchor in the average coordinate. After the analysis of the radio propagation loss model, the most appropriate log-distance distribution model is selected to simulate the signal propagation. Based on the centroid algorithm and the weighted centroid algorithm, this paper proposes an ellipse centroid localization algorithm. This algorithm makes use of ellipse's characteristic to estimate the unknown node's coordinate. The main idea of ellipse centroid localization algorithm is the precision control factor that can control the algorithm's location precision. In ellipse centroid localization algorithm, node is extended as anchor in order to strengthen anchor density's dynamic characteristic. The simulation result shows the ellipse centroid localization algorithm is more effective than the centroid algorithm and the weighted centroid precision algorithm.**

***Index Terms*—Wireless Sensor Networks; Centroid Localization; Weighted Centroid Localization; Ellipse Centroid; Node Localization**

I. INTRODUCTION

The development of Micro-electro-mechanical system has aroused people's great interest in the wireless sensor networks. The network consist of a large quantity of densely deployed nodes with sensor and driving function, which are finite energy resources and assumed to be produced in large scale by people. Recently, the network has been widely used in various fields, for example, military affairs, agriculture, and transport industry, etc, which includes target detection, the tracking of the syncphase axis, environment monitoring, and traffic management, etc [1] [2]. These applications mainly depend on the sensor node's geo-information to ensure the tracking object's location that can provide assistance in the fields in which people have interest and also supply sensor scheduling so as to reduce overlapping. Lately, lots of localization algorithms in wireless sensor networks have been put forward in order to offer each node's location information.

In a large wireless sensor network application, nodes are usually spread into a wide area, and most of their positions are unknown. But a large amount of wireless sensor network's applications require those nodes' position information for obtaining those network events' happening location and source location. Thus, localization is one of the main applications of wireless sensor network. For most applications, it is meaningless to sense data without nodes' positions. Only when sensor nodes are located rightly, the happening events and its specific location information detected by sensor nodes can be determined [3]. Nodes must clarify their position for indeed explaining "where the specific event happens". Then the localization and tracking for outside target can be achieved. Otherwise, to utilize nodes' position information when designing routing protocol can improve routing efficiency while offering namespace for network, reporting the coverage quality of network for establishers, and achieving network's load balancing and self-organizing of network topology [4]. Thus, the nodes localization problem has become a crucial research direction for wireless sensor network.

Wireless sensor nodes self-localization is a system determining its own position through estimating the distance between it to neighbor nodes and the number of neighbor nodes and utilizing the information exchange between nodes. On sensor network, the ability that nodes can self-determine their locations is considered as their basic ability and one of the basic services of this system. For WSN, manpower deployment or the allocation of GPS devices for every network node will be limited by cost, power consumption, expansibility and other problems [4]. Thus, searching WSN self-localization system has become the problem discussed by many research institutes and scholars.

On wireless sensor network, according to the fact that whether the distance between nodes is measured, the localization system can be divided into: range-based localization and range-free localization [5] [6]. The former one needs the measurement of the absolute distance between nodes, and utilizes the real distance to determine unknown target's node location; the second one only uses the associated relationship of the distance between nodes to calculate nodes' locations. Range-based algorithm can locate through measuring the real distance or direction between neighbor nodes. The specific methods include: Time of Arrival (TOA) [7] [8], Time Difference of Arrival (TDOA) [9] [10] [11], Radio Signal Strength (RSSI) and Angle of Arrival (AOA) [12] [13] and so on.

doi:10.4304/jnw.9.1.183-189

Although the mobility of nodes makes the localization process more complicated, using this feature can improve localization accuracy and reduce localization cost. In Bergamo and some' researches, there are 2 fixed beacons on network to send the coordinate information to whole network. The others in activity can locate themselves based on the strength of received signals [14] [15] [16]. Scholars home and abroad have made lots of researches on localization problems, and they proposed several relatively typical localization algorithms [17] [18] [19]. But there are these listing limitations [20] [21]: 1.dependence on the support of special hardware; 2.the need for special network topology. But to introduce mobile nodes onto wireless sensor network can help enhancing its functions. As reference [22], through moving several unknown nodes into those areas with relatively sparse network nodes to compensate the insufficiency of inhomogeneous density distribution of nodes. Reference [23] [24] mentions to use moving reference nodes and RSSI (instruction of the strength of received signal) [25] [26] [27] to locate unknown nodes. But in real environment, temperature, obstacles, broadcasting ways and other elements are dynamic, which made the practice of RSSI in real application is difficult. Especially when the requirement of energy consumption and volume is stricter for nodes, so this range-based localization technique cannot be applied in most of the time. Range-free localization algorithm does not need the measurement of the distance between nodes, but the use of distance vector routing. The condition of network connection or GPS localization [28] [29] [30] and other ideas suggest a distributed localization method without distance measuring. Undoubtedly this method reduced network cost. However there is no support of suitable hardware. Some errors still exist on localization. When some obstacles appear, the Euclidean distance between nodes will cause larger errors because of the bending routine, and the accuracy will be lowered [31] [32] [33]. So how to improve this range-free localization algorithm's accuracy also became a hot field of research.

Considering the location estimation mechanism, we divide these protocols into two categories: range-based and range-free localization algorithm. The former, according to the protocol, uses point-to-point absolute value estimation or angle estimation to calculate location, including TOA, TDOA, AOA and RSSI; and the latter doesn't assume the information's availability or validity, which includes centroid algorithm, MDS [34] [35], APIT [36], AHLos [37] and Euclidean Dv-Hop algorithm [38] [39]. In addition, the localization algorithm in wireless sensor networks still need these characteristics, for example, robustness, high efficiency, distributed computing and ad hoc network [40] [41].

In the paper, we propose an ellipse centroid localization algorithm based on weighted centroid. In ellipse centroid localization algorithm, PCF is firstly built to control precision factor, then several unknown nodes are located by the ellipse localization algorithm, and the rest of the unknown nodes are located in the weighted centroid localization measurement based on RSSI. In order to estimate the new algorithm's efficiency, we make several simulation experiments and the simulation result shows that, the ellipse centroid localization algorithm is more accurate and effective than traditional centroid localization algorithm and the weighted centroid algorithm.

II. Proposed Algorithm

A. Analysis of Radio Propagation Loss Model

The radio propagation loss has a great influence on measurement precision of RSSI. There are several common propagation loss models, including free space propagation model, Log-distance path loss model, Hata model and Log-distance path distribution model, etc [42]. The node of wireless sensor is always scattered in open space, so the free space propagation model and Log-distance path distribution model select to simulate the process of radio propagation. The free space propagation loss model is as follow:

$$Loss = 32.44 + 10 \times k \times \log_{10}(d) + 10 \times k \times \log_{10}(f) \quad (1)$$

In equation (1), "d" is the distance between object and source; 'f' is the signal RSSI's frequency; and 'k' is path loss factor.

Due to the surrounding environment, the radio propagation loss model still has errors of certain degree that will be influenced by environmental factors, for example, height, factory building, transmission power and packaging, etc. As a result, the Log-distance path distribution model is more effective than free space distribution model [43] [44]. The Log-distance distribution model is listed as follow:

$$PL(d)[dB] = PL(d_0) + 10 \times k \times \log(\frac{d}{d_0}) + X_0 \quad (2)$$

In equation (2), PL(d) denotes the propagation loss after spreading d meters' distance; X_0 is a gaussion random variable whose mean value is 0. In the above equation, the signal intensity received by the unknown node is:

$$RSSI = P_{SEND} + G_{ANT} - PL(d) \quad (3)$$

In equation (3), P_{SEND} is transmission power; G_{ANT} is antenna gain; and PL(d) is path loss ;

B. Centroid Localization

The classic centroid localization algorithm was proposed by N. Bulusu and J. Heidemann. The unknown node is located by the adjacent anchors that transmit the signal of their own coordinate (Xi, Yi) and the centroid calculation equation is as the following:

$$(X_{est}, Y_{est}) = \left(\frac{x_1 + x_2 + ...x_N}{N}, \frac{y_1 + y_2 + ...y_N}{N} \right) \quad (4)$$

In order to improve the algorithm, an advanced algorithm, that is, the weighted centroid localization algorithm is put forward to improve location precision.

C. Weighted Centroid Localization.

When the distance between two nodes gets increased, the measurement error of RSSI will become larger correspondingly. In order to reduce the location error, a new concept, "weight", will be introduced here. The weighted centroid localization algorithm is described as follow:

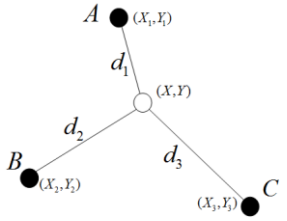

Figure 1. The weighted centroid localization

In Figure1, A, B and C are three anchors; D is an unknown node; and the signal RRSI from node A, B, or C can be received by node D; the respective distance d_1, d_2, d_3 from node D to the three anchors A, B and C can be calculated. Suppose D' is the barycenter of the triangle ABC, then D' coordinate can be calculated and the distance between D' and A, B and C can also be calculated. In the end, the coordinate of unknown node D' deduced by the weighted centroid localization algorithm is as the following:

$$(X,Y)=\left(\begin{array}{l}\dfrac{d_1^{'}X_1/d_1+d_2^{'}X_2/d_2+d_3^{'}X_3/d_3}{d_1^{'}/d_1+d_2^{'}/d_2+d_3^{'}/d_3},\\ \dfrac{d_1^{'}Y_1/d_1+d_2^{'}Y_2/d_2+d_3^{'}Y_3/d_3}{d_1^{'}/d_1+d_2^{'}/d_2+d_3^{'}/d_3}\end{array}\right) \quad (5)$$

where, d_1'/d_1, d_2'/d_2, d_3'/d_3 denote the "weight "of three anchors A, B and C.

D. Ellipse Localization Algorithm

In Figure 2, P_1 and P_2 denote two anchors in wireless sensor networks. Node P is an unknown node. The length of PP_1 and PP_2 are denoted as a and b. Therefore, Node P is located in the ellipse with P_1 and P_2 as its focus and the length of node P is a+b. We draw a plumb line through node P to the line P_1P_2 and get the intersection point P' with P_1P_2. The ellipse localization algorithm takes the coordinate of P as the coordinate of unknown node P'. The location error is PP'.

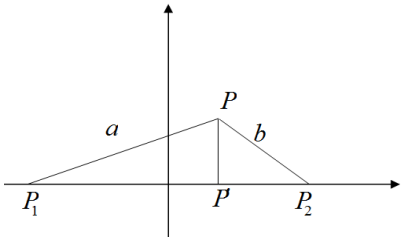

Figure 2. The ellipse localization principle

From figure 2, we can see, the closer is $\angle P_1PP_2$ to 180°, the higher is the localization precision obtained from ellipse localization algorithm [45] [46]. To improve the ellipse localization precision, a maximum error should be set up. In figure 3, the maximum error can not exceed the length of the minor axis.

In Figure 3, the maximum error of ellipse localization is OA's length.

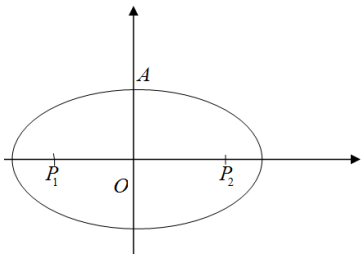

Figure 3. The maximum error

The ellipse's minor axis is the maximum error of ellipse localization algorithm and different ellipses get different precisions [47] [48]. Therefore, a precision control factor, PCF [49] [50], should be proposed to control the precision of ellipse localization algorithm, which is defined as follow:

$$PCF=\frac{a+b}{P_1P_2} \quad (6)$$

From equation, we can get, the PCF's value must be equal to or larger than 1. The closer is the PCF's value to 1, the higher is the algorithm's localization precision.

Suppose the maximum effective length of RSSI is L, then the maximum value of P_1P_2 in wireless sensor networks is 2L. If the maximum error is E, we can know the OA's length is E. From figure 4, the PCF's value can be calculated.

In figure 4, the length of P_1P_2 is 2L, and the length of OA is E. Because angle of AOP_1 is 90°, the length of AP_1 is:

$$AP_1=\sqrt{E^2+L^2} \quad (7)$$

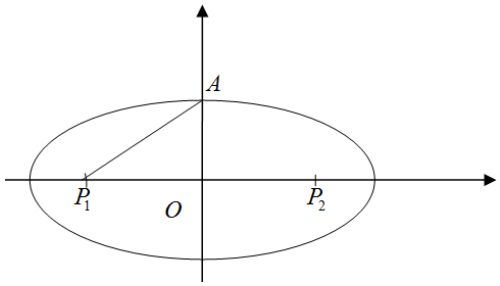

Figure 4. The computing result of PCF

Obviously, the length of AP_1 is half of the length of a+b, so PCF can be get from Equation (8).

$$PCF=\frac{AP_1}{L} \quad (8)$$

E. The Ellipse Centroid Localization Algorithm

The ellipse centroid localization algorithm is the combination of ellipse localization and weighted centroid localization. In the ellipse centroid localization algorithm, several unknown nodes are located by ellipse localization algorithm and then the located nodes are extended as the anchors that increase the anchor density in wireless sensor networks. Finally, other unknown nodes are located by weighted centroid localization algorithm.

III. Simulation Experiment

In order to examine and verify the efficiency of ellipse centroid algorithm, a series of experiments are carried out. We also make multiple comparative experiments among the ellipse centroid algorithm, centroid algorithm and the weighted centroid algorithm. The location error is defined as the following:

$$Position\ \ error = \frac{|L_e - L_a|}{R} \times 100\% \qquad (9)$$

The notation Le is the node's estimating distance; the notation La is the node's actual distance; and the notation R denotes the node's communication radius.

The abbreviations of these three algorithms; certain algorithm, weighted centroid algorithm and ellipse centroid algorithm are C, WC, and EC respectively. Suppose all nodes are scattered in wireless sensor networks, and PCF is set up as 1.1. Figure 5 shows the comparative simulation result when the anchor density is 5% and the similar simulation result is shown in figure 6 when the anchor density increases to 10%.

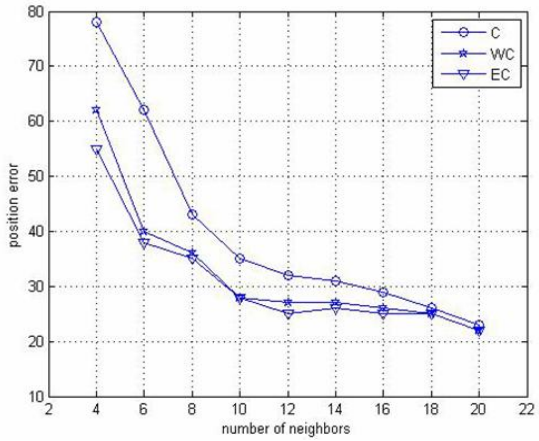

Figure 5. Comparative of simulation result when the anchor density is 5%

Figure 5 and figure 6 show that, the ellipse centroid algorithm is more accurate and effective than centroid algorithm and weighted centroid algorithm. The localization precisions of these three algorithms are connected closely with the anchor densities in networks. When the anchor density increases, the location errors of three algorithms all decrease and the location error of ellipse centroid algorithm is the small. Therefore, obviously, ellipse centroid algorithm is the best algorithm among these three algorithms.

In the above chapters, we talk about the importance of PCF in ellipse centroid algorithm. To verify PCF's importance, several simulation experiments are performed and the simulation results are shown in figure 7 and figure 8. Figure 7 shows the comparison of simulation results with different PCF when the anchor density is 5%. When the anchor density increases to 10%, the similar simulation result is shown in figure 8.

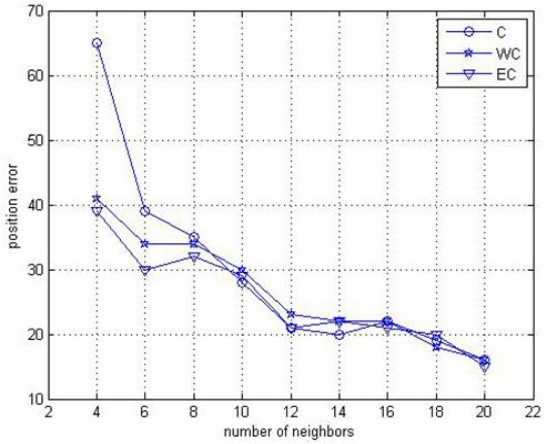

Figure 6. Comparative of simulation result when the anchor density increases to 10%.

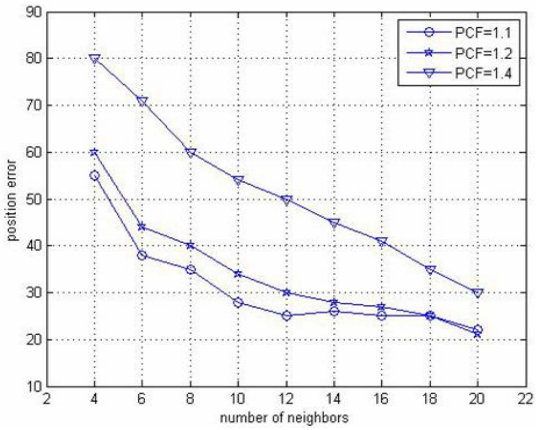

Figure 7. Comparison of simulation results with different PCF when the anchor density is 5%.

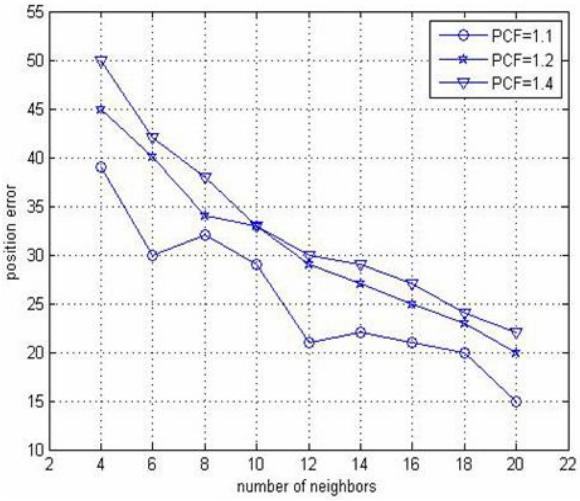

Figure 8. Comparison of simulation results with different PCF when the anchor density is 10%

Compared with figure 7 and figure 8, we can see that the location error is still influenced by the anchor density in networks. The ellipse centroid algorithm will get higher precision than other algorithms when the anchor density in networks increases.

IV. CONCLUSION

This paper proposes a new distributed ellipse centroid localization algorithm based on the centroid algorithm and weighted centroid algorithm. After the analysis of the radio propagation loss model, the log-distance distribution model selects to simulate the propagation of signal RSSI. The ellipse centroid algorithm sets up the precision control factor, PCF, which divides two anchors into a group, combines all anchors and finds the unknown nodes that suit the precision control condition. The localization node is extended as anchor. Therefore, all anchors use weighted centroid algorithm to find the rest of unknown nodes. In the end, all unknown nodes in wireless sensor networks are found. In the meantime, there are still some disadvantages in ellipse centroid algorithm that are the ellipse centroid algorithm consumes more power than centroid algorithm and weighted centroid algorithm. The ellipse centroid algorithm is based on the ellipse localization algorithm. The smaller is the anchor density in networks, the larger is the location error obtained from the ellipse centroid algorithm. The main idea of the ellipse centroid algorithm is PCF, so the setting method of PCF needs to be improved in the future work. Additionally, to perform the ellipse centroid algorithm in the heterogeneous environment is also our work to be done in the future.

REFERENCES

[1] Zou, Yi, and Krishnendu Chakrabarty. "Sensor deployment and target localization based on virtual forces." *INFOCOM 2003. Twenty-Second Annual Joint Conference of the IEEE Computer and Communications. IEEE Societies. Vol. 2. IEEE, 2003.*

[2] Zou, Yi, and Krishnendu Chakrabarty. "Sensor deployment and target localization in distributed sensor networks." *ACM Transactions on Embedded Computing Systems (TECS) 3.1* (2004) pp. 61-91.

[3] Willoughby, Twyla R., et al. "Target localization and real-time tracking using the Calypso 4D localization system in patients with localized prostate cancer." *International Journal of Radiation Oncology* Biology* Physics 65.2* (2006) pp. 528-534.

[4] Liu, Juan, et al. "Distributed group management for track initiation and maintenance in target localization applications." *Information Processing in Sensor Networks. Springer Berlin Heidelberg*, 2003.

[5] Kaplan, Lance M., Qiang Le, and N. Molnar. "Maximum likelihood methods for bearings-only target localization." *Acoustics, Speech, and Signal Processing, 2001. Proceedings. (ICASSP'01). 2001 IEEE International Conference on.* Vol. 5. IEEE, 2001.

[6] Verellen, Dirk, et al. "Quality assurance of a system for improved target localization and patient set-up that combines real-time infrared tracking and stereoscopic X-ray imaging." *Radiotherapy and oncology 67.1* (2003) pp. 129-141.

[7] Yeung, Daniel, et al. "Systematic analysis of errors in target localization and treatment delivery in stereotactic radiosurgery (SRS)." *International Journal of Radiation Oncology* Biology* Physics 28.2* (1994) pp. 493-498.

[8] Gielen, Frans LH, Victor PJ Duysens, and Johan FM Gijsberg. "Dual electrode lead and method for brain target localization in functional stereotactic brain surgery." *U.S. Patent* No. 6,011,996. 4 Jan. 2000.

[9] Vayssiere, Nathalie, et al. "Magnetic resonance imaging stereotactic target localization for deep brain stimulation in dystonic children." *Journal of neurosurgery* 93.5 (2000) pp. 784-790.

[10] Cevher, Volkan, Marco Duarte, and Richard G. Baraniuk. "Distributed target localization via spatial sparsity." *European Signal Processing Conference (EUSIPCO)*. 2008.

[11] Holtzheimer III, Paul E., David W. Roberts, and Terrance M. Darcey. "Magnetic resonance imaging versus computed tomography for target localization in functional stereotactic neurosurgery." *Neurosurgery* 45.2 (1999) pp. 290.

[12] Godrich, Hana, Alexander M. Haimovich, and Rick S. Blum. "Target localization accuracy gain in MIMO radar-based systems." *Information Theory, IEEE Transactions on* 56.6 (2010) pp. 2783-2803.

[13] Bednarz, Greg, et al. "Evaluation of the spatial accuracy of magnetic resonance imaging-based stereotactic target localization for gamma knife radiosurgery of functional disorders." *Neurosurgery* 45.5 (1999) pp. 1156.

[14] Sumanaweera, Thilaka, et al. "Mr geometric distortion correction for improved frame-based stereotaxic target localization accuracy." *Magnetic resonance in medicine* 34.1 (1995) pp. 106-113.

[15] He, Tian, et al. "Range-free localization schemes for large scale sensor networks." *Proceedings of the 9th annual international conference on Mobile computing and networking.* ACM, 2003.

[16] Hu, Lingxuan, and David Evans. "Localization for mobile sensor networks." *Proceedings of the 10th annual international conference on Mobile computing and networking.* ACM, 2004.

[17] Shang, Yi, and Wheeler Ruml. "Improved MDS-based localization." *INFOCOM 2004. Twenty-third AnnualJoint Conference of the IEEE Computer and Communications Societies*. Vol. 4. IEEE, 2004.

[18] Dil, Bram, Stefan Dulman, and Paul Havinga. "Range-based localization in mobile sensor networks." *Wireless Sensor Networks. Springer Berlin Heidelberg*, 2006. 164-179.

[19] Lazos, Loukas, and Radha Poovendran. "SeRLoc: Secure range-independent localization for wireless sensor networks." *Proceedings of the 3rd ACM workshop on Wireless security*. ACM, 2004.

[20] Sheu, Jang-Ping, Pei-Chun Chen, and Chih-Shun Hsu. "A distributed localization scheme for wireless sensor networks with improved grid-scan and vector-based refinement." *Mobile Computing, IEEE Transactions on* 7.9 (2008) pp. 1110-1123.

[21] Shen, Xingfa, et al. "Connectivity and RSSI based localization scheme for wireless sensor networks." *Advances in intelligent computing. Springer Berlin Heidelberg*, 2005. 578-587.

[22] Sun, Guolin, et al. "Signal processing techniques in network-aided positioning: a survey of state-of-the-art positioning designs." *Signal Processing Magazine, IEEE* 22.4 (2005) pp. 12-23.

[23] Chandrasekhar, Vijay, et al. "Localization in underwater sensor networks: survey and challenges." *Proceedings of*

the 1st ACM international workshop on Underwater networks. ACM, 2006.

[24] Tian, Shuang, et al. "A selective anchor node localization algorithm for wireless sensor networks." Convergence Information Technology, 2007. *International Conference on. IEEE, 2007*.

[25] Wang, Yun, et al. "Range-free localization using expected hop progress in wireless sensor networks." *Parallel and Distributed Systems, IEEE Transactions on 20.10* (2009) pp. 1540-1552.

[26] Wong, Sau Yee, et al. "Multihop localization with density and path length awareness in non-uniform wireless sensor networks." *Vehicular Technology Conference, 2005. VTC 2005-Spring. 2005 IEEE 61st.* Vol. 4. IEEE, 2005.

[27] Wang, Sheng-Shih, Kuei-Ping Shih, and Chih-Yung Chang. "Distributed direction-based localization in wireless sensor networks." *Computer Communications 30.6* (2007) pp. 1424-1439.

[28] Yao, Qi, et al. "An area localization scheme for large wireless sensor networks." *Vehicular Technology Conference, 2005. VTC 2005-Spring. 2005 IEEE 61st.* Vol. 5. IEEE, 2005.

[29] Shang, Yi, Jing Meng, and Hongchi Shi. "A new algorithm for relative localization in wireless sensor networks." *Parallel and Distributed Processing Symposium, 2004. Proceedings. 18th International.* IEEE, 2004.

[30] Koutsonikolas, Dimitrios, Saumitra M. Das, and Y. Charlie Hu. "Path planning of mobile landmarks for localization in wireless sensor networks." *Computer Communications* 30.13 (2007) pp. 2577-2592.

[31] Liao, Wen-Hwa, Kuei-Ping Shih, and Yu-Chee Lee. "A localization protocol with adaptive power control in wireless sensor networks." *Computer Communications* 31.10 (2008) pp. 2496-2504.

[32] Tay, Jeffrey HS, Vijay R. Chandrasekhar, and Winston Khoon Guan Seah. "Selective Iterative Multilateration for Hop Count-Based Localization in Wireless Sensor Networks." *Mobile Data Management, 2006. MDM 2006. 7th International Conference on. IEEE, 2006.*

[33] Kim, Kyunghwi, and Wonjun Lee. "MBAL: A mobile beacon-assisted localization scheme for wireless sensor networks." *Computer Communications and Networks, 2007. ICCCN 2007. Proceedings of 16th International Conference on. IEEE, 2007*.

[34] Wang, Yun, et al. "Localization algorithm using expected hop progress in wireless sensor networks." *Mobile Adhoc and Sensor Systems (MASS), 2006 IEEE International Conference on. IEEE, 2006*.

[35] Wang, Jiangang, Fubao Wang, and Weijun Duan. "Application of Weighted Least Square Estimates on Wireless Sensor Network Node Localization" *Application research of computers 9* (2006) pp. 011.

[36] Biaz, Saad, and Yiming Ji. "A survey and comparison on localisation algorithms for wireless ad hoc networks." *International Journal of Mobile Communications 3.4* (2005) pp. 374-410.

[37] Stoleru, Radu, et al. "StarDust: a flexible architecture for passive localization in wireless sensor networks." *Proceedings of the 4th international conference on Embedded networked sensor systems.* ACM, 2006.

[38] Qian, Qingji, Xuanjing Shen, and Haipeng Chen. "An improved node localization algorithm based on DV-Hop for wireless sensor networks." *Computer Science and Information Systems 8.4* (2011) pp. 953-972.

[39] Chang, Tzu-Chien, Kuochen Wang, and Yi-Ling Hsieh. "Enhanced color-theory-based dynamic localization in mobile wireless sensor networks." *Wireless Communications and Networking Conference, 2007. WCNC 2007. IEEE. IEEE, 2007*.

[40] Suo, Hui, et al. "Issues and challenges of wireless sensor networks localization in emerging applications." *Computer Science and Electronics Engineering (ICCSEE), 2012 International Conference on.* Vol. 3. IEEE, 2012.

[41] Gou, Haosong, Younghwan Yoo, and Hongqing Zeng. "A partition-based LEACH algorithm for wireless sensor networks." *Computer and Information Technology, 2009. CIT'09. Ninth IEEE International Conference on. Vol. 2. IEEE, 2009.*

[42] Rueckert, Daniel, et al. "Nonrigid registration using free-form deformations: application to breast MR images." *Medical Imaging, IEEE Transactions on* 18.8 (1999) pp. 712-721.

[43] Gou, Haosong, Younghwan Yoo, and Hongqing Zeng. "A partition-based LEACH algorithm for wireless sensor networks." *Computer and Information Technology, 2009. CIT'09. Ninth IEEE International Conference on.* Vol. 2. IEEE, 2009.

[44] Chen, Jian-Ming, Jian-Jun Lu, and Qing-Hai Wang. "Research and improvement of adaptive topology algorithm leach for wireless sensor network." *Wireless Communications, Networking and Mobile Computing, 2008. WiCOM'08. 4th International Conference on. IEEE, 2008.*

[45] Sinclair, Gavin, et al. "Interactive application in holographic optical tweezers of a multi-plane Gerchberg-Saxton algorithm for three-dimensional light shaping." *Optics Express 12.8* (2004) pp. 1665-1670.

[46] Abdulsalam, Hanady M., and Layla K. Kamel. "W-LEACH: Weighted Low Energy Adaptive Clustering Hierarchy aggregation algorithm for data streams in wireless sensor networks." *Data Mining Workshops (ICDMW), 2010 IEEE International Conference on. IEEE, 2010.*

[47] Katiyar, Vivek, et al. "Improvement in LEACH protocol for large-scale wireless sensor networks." *Emerging Trends in Electrical and Computer Technology (ICETECT), 2011 International Conference on. IEEE, 2011.*

[48] Nam, Do-hyun. "An energy-efficient clustering using a round-robin method in a wireless sensor network." *Software Engineering Research, Management & Applications, 2007. SERA 2007. 5th ACIS International Conference on. IEEE, 2007.*

[49] Leach, Andrew R., and Keith Prout. "Automated conformational analysis: directed conformational search using the A* algorithm." *Journal of Computational Chemistry 11.10* (1990) pp. 1193-1205.

[50] Jones, Gareth, et al. "Further development of a genetic algorithm for ligand docking and its application to screening combinatorial libraries." *ACS Symposium Series. Vol. 719. Washington, DC: American Chemical Society,* [1974]-, 1999.

Shyi-Ching Liang, He is working at Department of Information Management at Chaoyang University of Technology, Taiwan. In the university he is an associate professor. His research interests include e-learning, system integration, and optimization.

LunHao Liao, He is a lecturer at Department of Information Management at Chaoyang University of Technology, Taiwan.

In the university he is also a PhD candidate. His research interests include signal processing and wireless communication.

Yen-Chun Lee, He is a lecturer at Department of Information Management at Chaoyang University of Technology, Taiwan. In the university he is also a PhD candidate. His research interests include IT Governance and Evaluating Operational Efficiency.

Road Geometric Features Extraction based on Self-Organizing Map (SOM) Neural Network

Zhenyu Shu
Institute of Geophysics and Geomatics, China University of Geosciences, Wuhan, China
College of Electronic Information Engineering, South-Center University for Nationalities, Wuhan, China
Email: szyscuec@gmail.com

Dianhong Wang*
Faculty of Mechanical & Electronic Information, China University of Geosciences, Wuhan, China
*Corresponding author, Email: wangdh@cug.edu.cn

Cheng Zhou
Hubei Key Laboratory of Intelligent Wireless Communications, South-Center University for Nationalities, Wuhan, China
Email: zcresearch@gmail.com

***Abstract*—Geometry is the key parameter when extracting road from high-resolution remote sensing imagery. We propose a method for road geometry parameters extraction from high spatial resolution remote sensing imagery automatically based on self-organizing map (SOM) neural network algorithm. SOM is a no-tutor clustering segmentation method and the algorithm is the foundation of later road automatic extraction. Our approach may adjust cluster number and cluster center of the image through analyzing the point density distribution of self-organizing feature map neural network competition layer, which is good for flexible processing on the image excessive segmentation problem and succeed in accurate segmentation object. Then we can extract geometric features of the terrain target. The results are demonstrated that the algorithm proposed is both accurate and effective.**

***Index Terms*—Organizing Map (SOM) Neural Network; High-Resolution Remote Sensing Imagery; Geometric Features; Road; Geometric Moments**

I. INTRODUCTION

Automatic road extraction from the high-resolution remote sensing imagery is the trend of the automated information processing which provided favorable information for the extraction of the road, but at the same time the adverse information (such as shadows, occlusion, defects, cars on roads, and sidewalk lines, etc.), also affects the precision of the extraction of road information through computer [1-3]. To achieve the desired effects of road information extraction, traditional road extraction methods such as using spectral or geometric features to extract road information can no longer meet the requirements, rather the method that using comprehensive information of spectral features, geometric features, texture features and context features of the terrain target to extract road has become mainstream means of road extraction [4, 5].

The parameters of geometric features that can be used in extracting road information from many terrain targets are length, width, length-width ratio, size, geometric center of the target and target's long axis direction. In order to extract the geometric features, a segmentation of remote sensing imagery is needed first to obtain meaningful and separated information of terrain targets, based on which an extraction of geometric features can be done. It can be concluded from all previous researches that the imagery segmentation algorithm is divided into four categories, including the color histogram method, the physical segmentation method, regional and boundary method, and clustering segmentation method [6]. A comparison of the four methods shows that, the simple color histogram method operates easily [7, 8], but it is vulnerable to outside interference, and has low accuracy of results; the physical segmentation method uses two-color reflection model for color image segmentation [9, 10], but the materials, the shape of the objects and lighting conditions and etc. are difficult to meet the segmentation conditions in actual scenes; region and boundary method uses a regional growth method [11, 12], the number of regions depends on the initial seed numbers, and the result will produce irregular borders and apertures. Clustering segmentation algorithm reach the clustering in the color space by the statistical results of color characteristic quantity which extracting from each pixel of a image [13, 14], so that each class corresponds to a divided region. this method is greatly improved in accuracy and validity compared with other methods.

Due to the high effective image segregation by clustering method, scholars use different methods to do clustering research of image especially through neural network method which separating and clustering image by simulating the working principles of human brain cells. Commonly used neural network algorithms including BP neural network, Hopfield network [15], radial basis

doi:10.4304/jnw.9.1.190-197

function neural network and wavelet neural network [16], all the results show that these algorithms can truly enhance the accuracy of image segmentation [17], but relying on the samples of the network training, and distribution of the sample data directly affect the accuracy of the results, moreover, other defects such as BP algorithms which bears a slower speed of network training and the convergence is always difficult. Self-organizing neural network which clusters automatically according to the information of imagery points and can adjust the levels of classes and numbers according to the actual need is an autonomous and unsupervised learning model with no teaches signals. This approach is greatly improved in validity and accuracy of the results compared to the other neural network algorithms [18, 19].

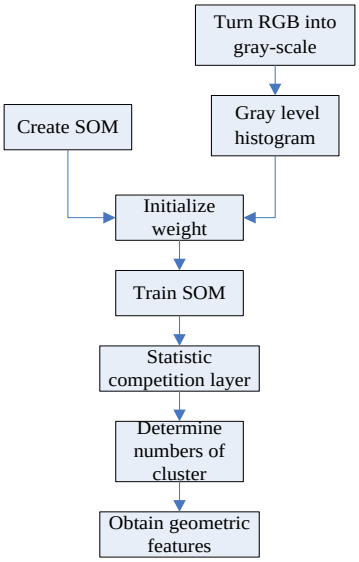

Figure 1. Workflow of road parameter

This paper is focused on how to extract road information from high-resolution remote sensing imagery based on SOM method. And the main contribution of this thesis is to calculate the geometrical parameters to improve the accuracy and validity of the extraction results. The algorithm flow to extract the geometric features is shown in figure 1. In order to speed up the convergence rate of the neural network, the first step is to convert RGB color image into the gray one and count the statistical results of the gray histogram which were used to initialize the incipient weights of the neurons of the competitive level. Secondly, we begin to train this neural network by inputting random selected RGB values of image pixel. The third step was to import all the RGB values of the image to the trained neural network and then all the picture elements would mapping to the corresponding neurons of the competitive layer. Next, we can obtain the outline information of the objects and realize clustering segmentation of the high spatial resolution remote sense images by following tracks of the edge of the targets. At last, the features of the geometrical parameters are able to get by adopting geometric moments invariant theory.

II. Related Work

A. Network Structure and Size

As an unsupervised learning classifier, self-organizing feature map neural network (SOFM) was raised by the Finnish scholars in 1987. In the biological nervous system, there is a "lateral inhibition" phenomenon that a nerve cell generates inhibition to other nerve cells around through its branches after its excitability. This lateral inhibition makes the phenomenon of competition between nerve cells. Every cell has different degree of excitement at the beginning stage and once a cell is excited to a specific target, it will suppress the excitability of the cells ambient to the same stimulation. This phenomenon exacerbated the competition between the nerve cells, as a result that the most excited nerve cells overcome other cells around, that is to say the surrounding cells were all losers. So the lateral inhibitions which lead to the result of a specific area of different degree of cell response to specific stimulation are the mechanism self-organizing neural network clustering.

In this method, self-organizing neural network algorithm uses a two-level structure which includes input layer and competition layer. Because the nodes of input layer equals to the dimensions of the samples, in addition, RGB images which are composed by three parameters of R, G and B are objects of our study, there are 3 nodes in the input layer. The RGB image has features that the composed three colors are high correlation which are not fit to segment and analyze the image directly [20]. In order to get accurate result, the values of R, G and B needs to normalize through formula (1).

$$\begin{cases} r = R/(R+G+B) \\ g = G/(R+G+B) \\ b = B/(R+G+B) \end{cases} \quad (1)$$

Input information can be transferred to the competition layer through input layer, weighted with competitive layer neurons vector to determine Euclidean distance, and the minimum distance nerve elements win the competition. Competitive layer neurons are arranged in a variety of forms, such as dimensional linear array, two-dimensional planar array and three-dimensional grid array.

The two-dimensional planar array is the most typical one. Figure 2a and 2b show two arrangements of neurons in the form of a two-dimensional plane and figure 2a is a rectangular architecture with the distance between a neuron node and its neighbor nodes is not exactly equal while Figure 2b is composed by hexagon which has same distance from the node to all the adjacent ones.

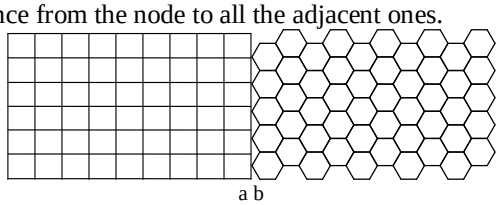

a b

Figure 2. a. Rectangular architecture, b. Hexagon architecture

B. Network Initialization

Before iterating the neural network, we must first initialize the weighted value $W_j = [w_{j1}\ w_{j2},\ w_{j3}]^T$ of neurons node of competitive layer and $w_{j1}\ w_{j2},\ w_{j3}$ corresponding to the normalized results of tri-color values of RGB respectively. There are several ways to initialize the weighted values and the first one is setting uniform weights for all neurons whose convergence of speed is slow and easy to make the results into a global minimum [21]. The second one is the improved method which set different values for the initialization of neurons through generating random numbers.

Figure 3. Remote image

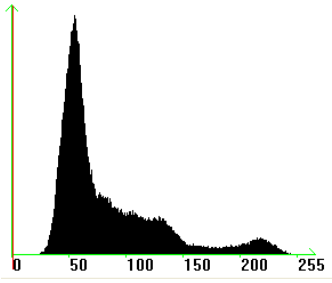

Figure 4. Gray histogram

In order to speed up the convergence, we can also set different initial values based on the results of the image statistical histogram. According to the numbers of neuron nodes in competition layer and the density relationship of pixel by statistical result of histogram, the initial weights of competitive layer can be determined by choosing attribution of target pixel uniformly to normalize. This initialized method includes the probability density of the samples in essence that can accelerate the speed of the convergence of the neuron network. The figure 3 shows the original remote sense image and its corresponding statistical result of grayscale histogram is shown in figure 4.

C. Iterative Process

The number of iterations in network settings T. in an iterative process, randomly selected sample Xi to obtain the vector distance of neurons weights between competition layer and input layer:

$$\left\|X_i - W_j\right\| = \left(\sum_{k=1}^{3}(x_{ik} - w_{jk})^2\right)^{\frac{1}{2}} \cdots k = 1,2,3 \qquad (2)$$

We use Euclidean distance as a standard in this paper, X_i represents the sample vector i and W_j means the neuron j in the competitive layer. If the distance between the X_i and the neuron j* is minimum, the Wj* win. The formula (3) shows the above.

$$\left\|X_i - W_{j^*}(t)\right\| = \min\left(\left\|X_i - W_j\right\|\right) \qquad (3)$$

Then we adjust the neuron weights of a certain neighborhood of j *which as a center. Depending on the different degrees of neuronal excitability, the adjusted weights of surrounding neurons varies from their distances to the winning neuron. Meanwhile, with the increasing in the number of iterations, the numbers of neurons which needs to weight adjustment become fewer which mean the neighborhood range narrows. The formula (4) determines the radius of the neighborhoods.

$$R(t) = INT[R(0) * (1 - t/T)] \qquad (4)$$

INT [ ] indicates rounding and R (0) is the initial radius. Usually the initial radius includes all the neurons. T means the total number of iterations. With the increasing of the numbers of iterations, the iterative radius gradually turns smaller. At the same time, the degree of weight adjustment also varies from different radius, which determined by neighborhood function. The neighborhood function is as follows formula (5).

$$\begin{cases} F_{j^*}(j,t) = 1 - d_{j^*j}/R(t) & d_{j^*j} \le R(t) \\ F_{j^*}(j,t) = 0 & d_{j^*j} > R(t) \end{cases} \qquad (5)$$

d_{j^*j} means the distance between the neuron j and the winning neuron j*.

Not only the function of the neighborhood impacts the changes of weight, but also a learning rate of the network, which is a function η (t) that controls the change speed of weight, and the function is defined as formula (6).

$$\eta(t) = \eta(0) * (1 - t/T) \qquad (6)$$

η (0) is the initial value, with the increasing of time (frequency), η (t) is reducing and its learning rate slowing down too.

According to neighborhood function and learning rate function, weight adjustment function of neuron j* and its neighborhood neurons can be determined as formula (7).

$$W_{jk}(t+1) = W_{jk}(t) + \eta(t) * F_{j^*}(j,t) * \left\|X_i - W_{j^*}(t)\right\| \qquad (7)$$

In the formula (7), k = 1, 2, 3, are labels of weight vector.

When the iteration number t = T, the work of clustering iteration of remote sensing imagery which based on the standard of spectral features complete. Various of terrain targets will be mapped to the plane of the two-dimensional layer of competition and form a probability distribution map with "appropriate density ". If making a terrain target of a certain neuron as the center, and its terrain target which corresponding to the neurons around will be similar to it, this similarity will be gradually reduce with the increase of the distance of the neurons. The specific classification of the terrain target

can be determined when a certain probability density is selected, based on which to determine the edge contour of the terrain target through edge tracking method.

III. PROPOSED ALGORITHM

A. Automatic Clustering Based on Statistics

The weight of the neurons which were trained above 100, 000 times in the output layer would be confirmed that means the successful of the training of the neural networks. Next, we can obtain the graph of the result about the classification of the sample set after inputting all the specimens into the front neural networks. However, problems would be occurred that are how many kinds of classification objects and the number of the neurons in the output layer during the specific implementation process.

There are some methods can solve such problems based on existing research. And the first one is determining the numbers of the nerve cell of the competitive level are equal to which in the output layer, namely, one neuron is corresponding to the result of one classification. Applying this method, the neural network has features of simple structure, rapid speed of the training and seldom numbers of the neurons but which needs to be determined the amount of the class. Especially, misclassification would be appeared because one neuron means one class which would easy to trap in local minima. And the second approach is called heuristic method that means since it is difficult to confirm the exact amount of the objects we can analyze the clustering effect in different class number and choose the result with better effectiveness through providing different numbers of cluster and running the self-organizing neural network separately. Although we can gain a superior result by using this kind of cluster way, the operation process spends too much time and not suits to the demand of automatic clustering. The last method means offering enough nerve cells in the competitive layer and mapping many neurons to the one kind of clustering by means of certainly mapping relation under condition of indefinite of cluster number. This way suits for uncertain class number and is able to control the phenomenon of rough segmentation and over segmentation through adjusting clustering boundary.

In consideration of each object class there are the features of highest similarity, long inter-class distance and relatively gather together of the samples in the space, the paper adopts the third method to obtain the number and the center of the cluster. We apply formula 7 to count the number of the specimens of each neuron in the competition layer.

$$u_j = \frac{\sum_{i=1}^{M} k_{ij}}{\sum_{j=1}^{N}\sum_{i=1}^{M} k_{ij}} \qquad k_{ij} = \begin{cases} 1 \cdots X_i \in N_j \\ 0 \cdots X_i \notin N_j \end{cases} \qquad (8)$$

X_i is the sample i and N_j is the neuron j. When Nj becomes the winner to the neurons of the sample Xi, the kij equals 1 and if not it is 0. The formula 7 adds up all the samples which corresponding to the winner neurons and deals them with normalization. Owing to the competitive layer is the two-dimensional structure, the statistical result is the three dimensional structure.

TABLE I. THE STATISTICS RESULT OF WINNER NEURONS

0.001797	0.00259	0.002828	0.001718	0	0.000264	0.0034093	0.002828	0.00333	0.000766	0	0.001824	0.00296	0.006819	0.002696
0.001903	0.022623	0.005524	0.000211	0.000555	0.001982	0.0022728	0.011761	0.004202	0.000185	0.000608	0.002299	0.004176	0.011179	0.011946
0.002537	0.008536	0.002722	0.003356	0.003013	0.000317	0.00259	0.003013	0.005999	0.00296	0.002564	0.000733	0.007004	0.017575	0.014953
0.001189	0.002777	0.01036	0.005788	0.003753	0.001982	0.0017443	0.002009	0.002194	0.00444	0.006766	0.000819	0.003119	0.010862	0.008589
0.000291	0.005312	0.007955	0.012844	0.008642	0.002643	0.002405	0.003489	0.002035	0.004995	0.008669	0.000211	0.00259	0.008616	0.005709
0.002114	0.002405	0.00333	0.008563	0.005471	0.001744	0.0041757	0.003251	0.002167	0.005867	0.010016	0.003251	0.002801	0.005999	0.006052
0.002009	0.003409	0.001559	0.005312	0.002643	0.002009	0.0135049	0.002854	0.001401	0.003145	0.017363	0.009937	0.001533	0.003066	0.00518
0.003119	0.005497	0.001824	0.001586	0.002854	0.007823	0.0156192	0.00148	0.002537	0.007585	0.016016	0.010281	0.005629	0.004202	0.005471
0.00259	0.002801	0.001374	0.001454	0.005999	0.009699	0.0270099	0.003145	0.002379	0.008061	0.015804	0.009409	0.004096	0.001533	0.003013
0.002669	0.001586	0.000581	0.001771	0.004149	0.004731	0.0227549	0.001982	0.002167	0.005312	0.014694	0.012184	0.002881	0.00111	0.002405
0.001718	0	0.000819	0.001216	0.000872	0.001559	0.0034093	0.004625	0.003092	0.005999	0.012051	0.006264	0.002616	0.002088	0.004916
0.000264	0.000529	0.001665	0.00259	0.000793	0	0.001665	0.003092	0.002722	0.00259	0.005788	0.004704	0.002009	0.003832	0.005867
0.002035	0.002854	0.002564	0.002881	0.002061	0.000714	0.002035	0.003317	0.001374	0.002141	0.003119	0.002273	0.005259	0.00962	0.006792
0.003198	0.004255	0.003885	0.005418	0.002749	0.002114	0.0017707	0.002616	0.002251	0.004916	0.007981	0.00629	0.002986	0.004466	0.005312
0.002379	0.003806	0.004149	0.003964	0.0037	0.002564	0.0015329	0.001533	0.002616	0.004995	0.006713	0.005312	0.002669	0.003911	0.004176

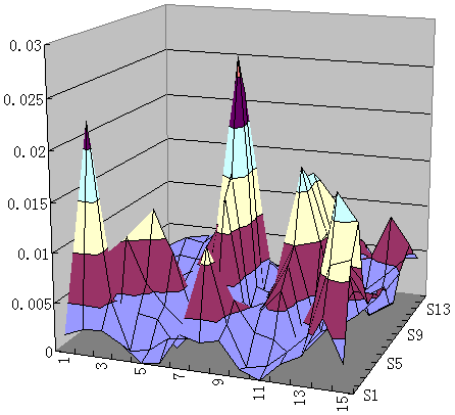

Figure 5. The distribution map of clustering in competition layer

The structure of the input layer of the self-organizing neural network consists of three neurons of one one-dimensional linear structure and the competition layer's configuration are 15*15 hexagons. By means of training and statistics, the normalization results of each winner neurons are shown in the table 1 and its three dimensional results are shown in graph 3. In the process of the clustering some nerve cells become dead centers because they are not winners to any samples which turn into the demarcation points of the two classifications. the curves which compose of the curved surface's minimum value are boundary lines of each classification, meanwhile, the neurons which corresponding to the points of local maximum value becomes the centers of every class that can be certified by the method of curve fitting.

B. Extraction of Geometrical Feature

Interference information (such as the shade of a tree, building shadow and occlusion, etc.) in the high-resolution remote sensing imagery changes the original spectral characteristic of the road target. we will get the wrong results if relying solely on the spectral characteristics to extract road information. Also there is the phenomenon of "same spectrum but different objects "in terrain target, such as cement concrete pavement and part of the roof, as well as square and the road surface. These different terrain targets have the same (similar) spectral characteristics because their surface material are the same, so that relying solely on the spectral

characteristics of the clustering method can not extract road information properly. In addition, the roads in different regions reflect different spectral characteristics due to different materials of the road surface and thus can not be clustered as a class properly which result in incomplete extraction of road information.

Therefore, in order to identify the road target accurately and completely, we need to combine variety of feature information of road targets, and make a comprehensive identification. During extraction of road targets, the geometric characteristics which were more used including: size, perimeter, the geometric center, aspect ratio, extending direction etc becomes very crucial in the extraction of the roads. The important geometric features include area, circumference, geometric center, aspect radio, and extension direction and so on. Some of the features play the important role in discrimination of the road objects directly and others are synthesized to obtain the values of parameters of the road through counting.

C. Extraction Aspect Ratio

As to scattered targets, the area of the road is very large. So we can get the aspect ratio information indirectly by calculating the area and perimeter. The area is defined as formula (9).

$$S = n * div^2 \tag{9}$$

The Div represents remote sensing imagery resolution and n is the number of pixels of the target area.

The perimeter is the product of the edge contour pixels number and resolution of the target. L means the perimeter which can be counted by formula (10).

$$L = n' * div^2 \tag{10}$$

Aspect ratio I of terrain targets can be reflected by the formula (11).

$$I = \frac{\sqrt{S}}{L} \tag{11}$$

When the target external characteristic tends to be circular, the value of I is about 0. 28 and if the external characteristic is a square I equals 0. 25. if the value of I is less than 0. 25, the target external characteristics tends to be rectangular. When the value of S and L is same, the target is a linear objective with very small width. Size parameters can also identify whether the target is sidewalk lines or road defects with other parameters.

D. Geometric Center

Geometric moment theory is used to obtain the coordinates of geometric center of the terrain targets in the paper. According to the geometric moment theory proposed in 1962 by Hu (Visual pattern recognition by moment invariants), we defines f (x, y) the pixel density of coordinates (x, y) in the image and the moments of p, q of the terrain target in the image can be defined as formula (12).

$$M_{pq} = \sum_{i=1}^{m}\sum_{j=1}^{n} x_i^p * y_j^q * f(x_i, y_j) \text{ (p,q=0,1,…)} \tag{12}$$

In the formula x_i, y_j is the pixel coordinate of the terrain target and the sum of all the coordinates is the total number of all the pixels belonging to the terrain target. By the centroid formula, the centroid coordinates of the terrain target is (M_{10}, M_{01}).

When focus solely on the geometric shapes rather than material density of the terrain target, f (x_i, y_j) is defined as the constant value 1. The geometric moment of the terrain target would be formula (13).

$$M'_{pq} = \sum_{i=1}^{m}\sum_{j=1}^{n} x_i^p * y_j^q \text{ (p,q=0,1,2⋯)} \tag{13}$$

Then coordinates of geometric center of terrain target is (X_c, Y_c) :

$$\begin{aligned} X_c &= M'10 \\ Y_c &= M'01 \end{aligned} \tag{14}$$

Because the consistency of the material of local targets, we can use the distance between the centroid and the geometric center of the target as the regularity of the objects which has turned into the evidence of the roads.

E. Extending Direction of Target

In the road extraction process, an important geometric characteristic parameter is the extending direction of the road that is means the direction of a straight line which the road is regarded as. As to the geometric moment of the terrain target, when the origin of coordinates is moved to the geometric center of the terrain target, its geometric moment values of p, q order can be obtained by formula (15). (For the image in an arbitrary coordinate, define f (xi, yj) = 1)

$$U_{pq} = \sum_{i=1}^{m}\sum_{j=1}^{n} (x_i - x_c)^p * (y_j - y_c)^q \text{ (p,q=0,1,2…)} \tag{15}$$

U_{pq} is called invariant geometric moments of a terrain target, which have invariant feature in rotation, translation, scaling, and other characteristics. The angle θ of the long axial direction (that is the extending direction) of the terrain target define as formula (16).

$$\theta = \frac{1}{2}\arctan^{-1}\left(\frac{2U_{11}}{U_{20} - U_{02}}\right) + \frac{k}{2}\pi \text{ ,k=1,2,3…} \tag{16}$$

The centerline of the target can be obtained through the extending direction and the geometric center of the terrain target, and thus to determine a linear terrain target whether as part of the road or just rectangular building objectives.

Accurate target information of road can be extracted through the combination of individual or multiple geometric features of the road above. And can also be extracted through combination of spectra, texture, and context of the road.

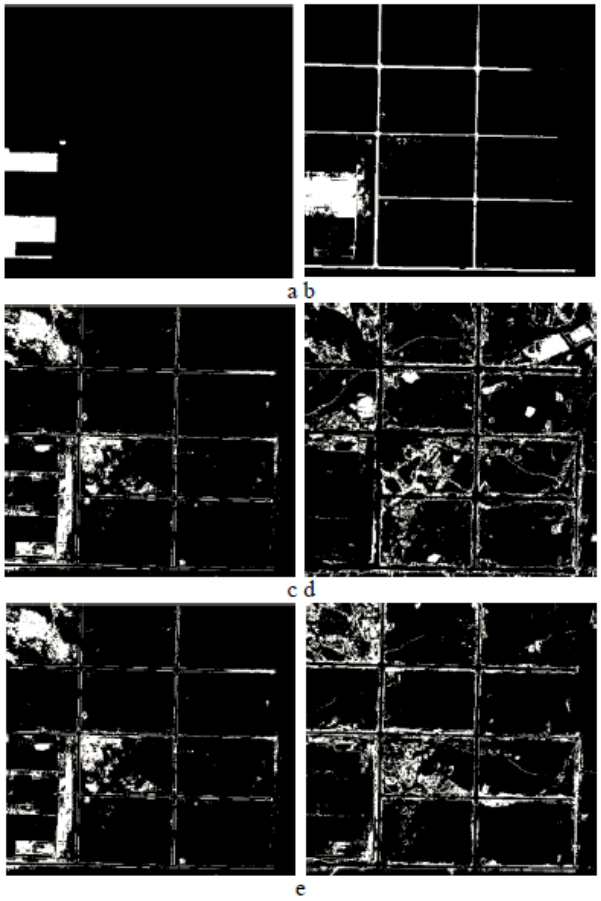

Figure 6. Each landmark could be divided into independent object

IV. EXPERIMENTS

In the process of extracting road information from the high spatial resolution remote sensing imagery, we clustered the segmentations of self-organizing neural network image, as can be seen in Figure 3 which is the original image firstly. Figure 6a to 6e showed each target of segmentation respectively that white signified the segmented targets and black was the background. Each landmark could be divided into independent object as shown in the figure 6. Nevertheless the only input attribute of the SOM was spectral characteristic so that an apparent segmentation mistake could be found as the phenomenon of same spectral with different material. As a result, in the figure 6c the road of cement pavement and the factory building with concrete rooftop were segmented as one kind. In order to correct this mistake, we could calculate geometrical parameters, such as because the shape of factory building closes square the aspect radio equals probably to 0. 25 and the length-with radio is far less than 0. 25 of the road so we could simply classify them by the value of length-with radio.

Anther mistake in the SOM segmentation is dividing the same object with different spectral feature into various classifications. Part of road on the top right corner in the figure 6d was the extension of the road as shown in the figure 6c. Although they both had beautiful length-with radio to be determined as roads, them were be shown as various objects with different material (cement and clay) in the pavement which lead to diverse spectral feature. At this time, it could be determined to parts of road or not by calculating centroid position and extension direction.

Some objects have regular shape such as rectangle, quadrate and circle and so on and then the geometrical parameters of them are easy to obtain. For example, the blue factory building in the figure 6b were easy to get its length-width radio, center position and extension direction. Therefore it was very simple to distinguish it from the roads because their geometrical parameters were quite different.

We could also adjust the numbers of clusters of competitive layer in self-organizing neural network, integrate the two types of targets with few differences in the spectral features into one or divided different objects with similar spectral character into various objects. So adjusted the numbers of clusters of the output layer according to the mapping density distribution of competitive layer of self-organizing neural network, the final segmentation result could be controlled flexibly. Thus to achieved the purpose of separating both side roads and green belt from the roads, even achieved defects and shadows in the roads. For instance, the dashed line as the segmented result was the auxiliary road actually so that it could be combined into the trunk road as the one object by adjusting the numbers of classification which could be shown in the figure 6d and 6e.

Figure 7b was the segmentation result of the landmark targets about road through SOM methods of 7a. As shown in the figure, parts of road objects were segmented roughly, at the same time some non-roads were determined as roads because of similar spectral features such as green space and bare land and so on. In order to separate the non-road objects we could use two methods, and the first one was to add the numbers of the classification of the SOM which was very easy to estimate some parts of roads as non-roads because of similar spectral features; and the second one was to calculate the geometric characters of the segmentation results and excluded road objects by using them. The square objects and irregular arc ones and so on could be determined non-roads by calculating length-width radio, geometric center and extension direction in the figure 7b.

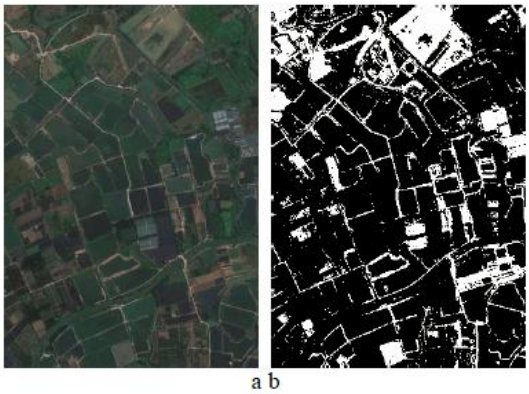

Figure 7. a. Remote image, b. Segmentation result of a

V. CONCLUSION

This paper focused on automatic extraction of roads information from the high spatial resolution remote sensing image and raised an automatic extraction method to extract road geometric features based on self-organizing map (SOM) neural network. This method can deal with the segmentation size flexibly, solve the problem of over-segmentation, and lay the foundation for the extraction of geometric features correctly. In order to get accurate and multiple information from the images, future researches will explore the extraction of feature information of other geometric features, or other multi-feature information such as texture and context of the road targets and so on.

ACKNOWLEDGMENT

This work is partly supported by National Natural Science Foundation of China under Grant # 61201268 to Cheng Zhou and Fundamental research funds for the Central Universities project special fund of the South-Central University For Nationalities under Grant # CZY12003 to Zhenyu Shu.

REFERENCES

[1] Xiaoying Jin, Curt H. Davis. "An integrated system for automatic road mapping from high-resolution multi-spectral satellite imagery by information fusion," *Information Fusion* pp. 257–273, 2005

[2] Li Gang, An Jinliang, Chen Chunhua. "Automatic road extraction from high-resolution remote sensing image based on bat model and mutual information matching," *Journal of Computers*, vol. 6, no. 11, pp. 2417-2426, 2011.

[3] Jianghua Cheng, Yongfeng Guan, Xishu Ku, Jixiang Sun. "Semi-automatic road centerline extraction in high-resolution SAR images based on circular template matching," *Electric Information and Control Engineering (ICEICE), 2011 International Conference on*, pp. 1688 – 1691, 2011.

[4] T. T. Mirnalinee & Sukhendu Das & Koshy Varghese. "An Integrated Multistage Framework for Automatic Road Extraction from High Resolution Satellite Imagery," *Journal of the Indian Society of Remote Sensing*, Vol. 39, No. 3, pp. 1–25, 2011.

[5] Dal Poz, A. P. , Gallis, R. A. B. , da Silva, J. F. C. , Martins, E. F. O. "Object-Space Road Extraction in Rural Areas Using Stereoscopic Aerial Images," *Geoscience and Remote Sensing Letters, IEEE*, Vol. 9, no. 4, pp. 654 – 658, 2012.

[6] Nuzillard, Danielle, Lazar, Cosmin. "Partitional clustering techniques for multi-spectral image segmentation", *Journal of Computers*, vol. 2, no. 10, pp. 1-8, 2007.

[7] J. C. Terrillon, M. David, S. Akamatsu. "Detection of human faces in complex scene images by use of a skin color system and of invariant Fourier-Mellin moments," *IEEE International Conference on Pattern Recognition*. pp. 1350-1355, 1998.

[8] M. Chapron. "A new chromatic edge detector used for color image segmentation," *IEEE International Conference on Pattern Recognition*, 1992, pp. 311-314.

[9] Mohammadzadeh, A. Tavakoli, A. Valadan Zoej, M. J. "Automatic linear feature extraction of Iranian roads from high resolution multi-spectral satellite imagery," *In: XXth ISPRS Congress, Istanbul, Turkey*, pp. 764–768, 2004.

[10] Maxwell B A, Shafer S A. "Physics-based Segmentation of Complex Objects Using Multiple Hypotheses of Image Formation," *Color Research and Application*, Vol. 65, No. 2, pp. 269-295, 1997

[11] Lalit Gupta, Utthara Gosa Mangai, Sukhendu Das. "Integrating region and edge information for texture segmentation using a modified constraint satisfaction neural network," *Image and Vision Computing*, Vol. 26, 1106–1117, 2008.

[12] X. Munoz, J. Freixenet, X. Cufi, J. Marti. "Strategies for image segmentation combining region and boundary information," *Pattern Recognition Letters*, Vol. 24, pp. 375–392, 2003.

[13] Cheng H D, Sun Y. "A Hierarchical Approach to Color Image Segmentation Using Homogeneity, " *IEEE Trans on Image Processing*, Vol. 9, No. 12, pp. 2071-2082, 2000.

[14] Pieter M J Van Der Zwet, Boudewijn P F Lelieveldt, Rob J Van Der Geest. "A Multi-resolution Image Segmentation Technique Based on Pyramidal Segmentation and Fuzzy Clustering," *IEEE Trans on Image Processing*, Vol. 9, No. 7, pp. 1238-1248, 2000.

[15] O. Ecabert, J. -P. Thiran, "Variational image segmentation by unifying region and edge information," in: *16th IEEE International Conference on Pattern Recognition*, pp. 885–888, 2002.

[16] Liu Yuan, "Wavelet fuzzy neural network based on modified QPSO for network anomaly detection", *Journal of Networks*, vol. 6, no. 9, pp. 1344-1350, 2011.

[17] José Luis García Balboa & Francisco Javier Ariza López. "Generalization-oriented Road Line Classification by Means of an Artificial Neural Network," *Geoinformatica. No*. 12, pp. 289–312, 2008.

[18] Kohonen, T. "Self-Organizing Maps," 2nd edn. Springer-Verlag, Boston, 1997.

[19] Patrick Yuri Shinzato, Denis Fernando Wolf. "A Road Following Approach Using Artificial Neural Networks Combinations", *Journal of Intelligent & Robotic Systems*, Vol. 62, no. June, pp. 527-546, 2011

[20] Deng Jiabin, Hu Juanli, Wu Juebo. "A study of color space transformation method using nonuniform segmentation of color space source," *Journal of Computers*, vol. 6, no. 2, pp. 288-296, 2011.

[21] Cui Xue-rong, Zhang Hao, Aaron Gulliver, T. "Threshold selection for Ultra-Wideband TOA estimation based on neural networks," *Journal of Networks*, vol. 7, no. 9, pp. 1311-1318, 2012.

Zhenyu Shu was born in xiantao, October 29th, 1978. He received the B. S. and M. S. from the China University of Geosciences degree in physics from the China University of Geosciences, Wuhan, China, in 2001 and 2005. He is now a doctoral student in the University of Geosciences.

He is currently a Instructor with the department of electronics and information engineering, South-Central University for Nationalities(SCUEC), Wuhan, china, and he has been engaged in the research of image processing.

Dianhong wang received the B. S. degree in electronics engineering from from the China University of Geosciences, the M. S. degree and Ph. D in pattern recognition and intelligent systems at Institute of Pattern Recognition and Artificial Intelligence, Huazhong University of Science and Technology, Wuhan.

He is currently a Professor of the China university of Geosciences. His research interests mainly include digital signal and image processing, image/video compression.

Cheng Zhou was born in wuhan, April 2nd, 1979. He received the B. S. degree in electronics and information engineering from Hubei University, Wuhan, China, in 2001, and the M. S. and the Ph. D. degrees in pattern recognition and intelligent systems and in control science and control engineering from Huazhong University of Science and Technology, Wuhan, China, in 2007 and 2010, respectively.

He is currently a Instructor with the department of electronics and information engineering, South-Central University for Nationalities(SCUEC), Wuhan, china, and he has been engaged in the research of multimedia signal processing, particularly, video coding for MPEG-4, H. 264, AVS(China) and HEVC standards since 2004.

Security Analysis and Improvement of User Authentication Framework for Cloud Computing

Nan Chen and Rui Jiang
School of Information Science and Engineering, Southeast University, Nanjing, China
Email: chennseu@126.com, R.Jiang@seu.edu.cn

***Abstract*—Cloud Computing, as an emerging, virtual, large-scale distributed computing model, has gained increasing attention these years. Meanwhile it also faces many secure challenges, one of which is authentication. In this paper, we firstly analyze a user authentication framework for cloud computing proposed by Amlan Jyoti Choudhury et al and point out the security attacks existing in the protocol. Then we propose an improved user authentication scheme. Our improved protocol ensures user legitimacy before entering into the cloud. The confidentiality and the mutual authentication of our protocol are formally proved by the strand space model theory and the authentication test method. The simulation illustrates that the communication performance of our scheme is efficient.**

***Index Terms*—Cloud Computing; Remote User Authentication; Smartcard; Security Protocols; Formal Analysis**

I. INTRODUCTION

Recently, cloud computing has been greatly interested by both academic and industry communities. It is like a "resource pool", which can provide the cost-effective and on-demand services to meet the needs by outsourcing data. In [1], cloud computing is defined as follows: "Cloud computing refers to both the applications delivered as services over the Internet and the hardware and systems software in the data centers that provide those services."

The emerging of cloud computing allows companies to focus more on their core business and brings perceived economic and operational benefits [2]. Thus the security issues of the cloud platform become critical important As mentioned in [3], cloud security issues can be classified into four categories: authentication, data integrity, data confidentiality and access control. User authentication is the paramount requirement for cloud computing that restricts illegal access to cloud server. So far many schemes have been proposed. Generally, the cloud computing system contains three parts: a data owner, a user and a cloud service provider. The data owner outsources the encrypted data to cloud and the authorized users request for the corresponding data. When the data owner requests for checking the stored data or the user requests for the data, the authentication of the legality of the user identity is quite important. In this paper, we mainly discuss the identity authentication between the user and cloud server.

In many circumstances, there only needs a single password to access a web-based application, and it is weak to be broken. To help combat these attacks, users may couple a password with a second authentication mechanism. With two factor authentication even if someone has stolen your password, they'll need physical access to your secondary authentication mechanism in order to access your cloud-based data.

In 2000, M. S. Hwang et al [4] proposed a new remote user authentication scheme using smart cards. The scheme is based on the ElGamal's public cryptosystem and does not require a system to maintain a password table for verifying the legitimacy of the login user. But this scheme does not resist impersonate attack. A legitimate user can impersonate other valid user to use his ID and PW without knowing the secret key. In 2002, Chien et al [5] proposed an efficient password based remote user authentication scheme, and claimed that their scheme has the merits of providing mutual authentication, no verification table, freely choosing password, and involving only few hashing operations. In 2004, Ku–Chen [6] showed that Chien et al.'s scheme is vulnerable to a reflection attack [7], insider attack [8] and is not reparable. In 2010, Chen and Huang [9] proposed a user participation-based authentication combining CAPTCHA and visual secret sharing. Later Chun-Ta Li et al [10] pointed out that Chen et al's scheme existed masquerading attack when the smartcard had been stolen. Recently the user login security is more and more concerned in the case of smartcard lost [10] [11].

In 2011, Amlan Jyoti Choudhury et al [12] presented a user authentication frame for cloud computing. They applies identity authentication with smartcard to cloud computing and it is a new idea. The scheme verifies user authenticity using two-step verification, which is based on password, smartcard and out of band authentication. However, through our security analysis, the scheme exist extremely serious attacks.

In this paper, we focus on secure user authentication in cloud computing. We analyze the vulnerability and attacks existing in Choudhury et al's protocol. To overcome these issues, we propose an advanced authentication protocol. In our scheme, we realize the basic requirements for evaluating a password authentication scheme [13].

doi:10.4304/jnw.9.1.198-203

The rest of the paper is organized as follows. Section 2 gives a brief introduction of the related authentication frame proposed by Amlan Jyoti Choudhury et al and points out the vulnerabilities and attacks to the protocol. The new remote user authentication scheme against smartcard security breach is proposed in Section3 and formal proof and security analysis of our protocol are explained in Section4. Finally, we conduct a performance simulation in Section5 and make a conclusion in Section6.

II. Review of Related Works

Recent years, a few password-based remote authentication schemes using smartcard have been proposed in cloud computing. In this section, we review one recent password-based remote authentication scheme. For convenience of description, we will list the common notations used throughout this paper first.

A. Notations

A : A login user
S : The cloud server
ID : Identity of the user
PW : The password of the user
K : Onetime key
x : A user's secret number
y : A servers secret number stored at the server
p : A large prime number
G : Primitive element in the Galois field GF(p)
$h(\bullet)$: One way hash function
$E_K(\cdot)/D_K(\cdot)$: The symmetric encryption/decryption function with key K
$||$: Concatenation operation
$X \rightarrow Y$: Message M is sent X to Y through public channel
$X \Rightarrow Y$: Message M is sent X to Y through secure channel
$\oplus$: The XOR operation

B. Brief review of Choudhury et al's Frame

There are four phases in Choudhury et al's scheme [12]: registration, login, authentication and password change. Different phases work as follows.

Registration phase

Step 1: $A => S : ID$, $h(PW \oplus x)$, $h(x)$

User A sends $\{ID, h(PW \oplus x), h(x)\}$ to the cloud server through a secure channel, where x is a random number generated by A.

Step 2: The cloud server sends the smartcard to the user A.

Upon receiving the message, cloud server checks the ID firstly. If ID is available, the cloud server computes $J = h(ID \oplus h(PW \oplus x))$, $I = h(ID \| y)$ and $B = g^{h(y)+h(I\|J)+h(x)} \bmod p$. y is a random number generated by server. Then S stores $\{I, J, B, p, g, h(.)\}$ in the smartcard and sends smartcard to the user.

Having received the smartcard, the user enters x into the smartcard. S stores ID in the ID table maintained in the server.

Login phase

Step 1: A inserts the smartcard and enters ID and PW.

Local system computes $J_1 = h(ID \oplus h(PW \oplus X))$, and check whether $J_1 = J$ or not. If true, proceed to the next step, otherwise abort.

Step 2: $A \rightarrow S : B, C$

A computes $C = h(I \| J)$ and sends $M_1 =< B, C >$ to the server.

Step 3: $S \rightarrow A$: $h(B^{"})$, $h(L)$

The server generates K and then computes $B^{"} = g^{C+h(y)} \bmod p$, $h(B^{"})$, $L = h(B^{"} \| K)$ and $h(L)$. S sends $M_2 =< h(B^{"}), h(L) >$ to the user using public channel. At the same time, S sends onetime key K to user's mobile phone using OOB channel.

Step 4: A checks $h(B^{"})$, $h(L)$

Upon receiving M_2, A computes $B^{'} = Bg^{-h(x)} \bmod p$, $h(B^{'})$, $L^{*} = h(B^{'} \| K)$ and $h(L^{*})$. Then A checks whether $h(B^{'}) = h(B^{"})$ and $h(L^{*}) = h(L)$. If both equations are true, then proceed to the next step. Otherwise terminate the login session.

Authentication phase

Step 1: $A \rightarrow S : I, h(R), T$

A computes $R = h(T \| B^{'})$ and sends $M_3 =< I, h(R), T >$ to the server, where T is the timestamp of the current time.

Step 2: $S \rightarrow A$: $h(S_k)$

Firstly, the server checks if T' - $T \leq \Delta T$, where ΔT is the maximum legal time difference for an authentication session defined for a networking system and T' is the current time stamp of the server. If it is false, then rejects the session. Otherwise, S computes $I^{'} = h(ID \| y)$ and $R^{*} = h(T \| B^{"})$, and checks whether $h(R^{*}) = h(R)$ and $I^{'} = I$. If both equations are true, S will generate $S_k = (R \oplus L)$ and send the hash value of S_k to the user. If they are not true, the server terminates the communication.

At last, the user checks $h(S_k)$ by computing $h(S_k^{*}) = h(R \oplus L)$.

Password change phase

The user A chooses a change of password in the self system. Then A enters ID and PW, and computes $J^{*} = h(ID \oplus h(PW \oplus x))$. Local system will check $J^{*} = J$, if $J^{*} \neq J$, then rejects the request, otherwise A enters a new password $PW^{'}$ and generates $x^{'}$. The smartcard computes $J^{'} = h(ID \oplus h(PW^{'} \oplus x^{'}))$ and replaces J by $J^{'}$ and x by $x^{'}$ in the smartcard.

C. The Attacks

Masquerading attack

If a user's smartcard is lost or stolen and it is got by an attacker, the attacker can extract the secret information stored in the smartcard. As the messages sent from A to S are only related with secret data stored in the smartcard, the attacker can masquerade as a legal user. The attacker can compute $C = h(I \| J)$, $B^{'} = Bg^{-h(x)} \bmod p$, $h(R) = h(h(T \| B^{'}))$. Therefore, the messages in login phase step 2 and authentication phase step1 can be generated by the attacker so that the attacker can successful makes a valid login request as a legal user.

Besides, at the end of the authentication phase, S sends $h(S_K)$ to A. A computes S_K^{*} and checks whether $h(S_K^{*}) = h(S_K)$ or not. If the attacker modifies $h(S_K)$, A will not be able to authenticate server. Therefore, it will cause that the server completes the authentication while the client doesn't think so. The communication between user and server cannot be established. Mutual authentication is imperfect.

OOB attack

In this scheme, the authors think the major advantage of the scheme is the OOB (out of band) factor. To improve the security, the cloud server generates the onetime key for the mobile network through HTTP/SMS gateway. The mobile network delivers the onetime key to the user's mobile phone via SMS. However, some facts show that this method is not as good as the authors think.

Lots of attacks for out-of band have been proposed such as SMS interception, phone flooding or SMS phishing. The details are described in [13]. In the cybercrime trend of future, these attacks will become a great threat for the out-of-band authentication.

Password change phase flaw

In the phase of password changing, the user only makes the change of J and x in the smartcard. But the user does not change B, which is used in the authentication. This may lead to login failures once the user change the password. For example, the original parameters were PW, J and x. After the user altered the password, these parameters change to $PW^{'}$, $J^{'}$ and $x^{'}$. Then when the user logins into the cloud server, in the step3 of the login phase, the server computes $B^{"} = g^{C+h(y)} \bmod p = g^{h(I\|J^{'})+h(y)} \bmod p$. Then the server sends $h(B^{"})$ to the user for verification. The user computes $B^{'} = Bg^{-h(x^{'})} \bmod p = g^{h(I\|J)+h(y)+h(x)+h(x^{'})} \bmod p$ in step4. Obviously, $h(B^{'}) \neq h(B^{"})$. The authentication fails and the login fails.

III. Our Proposed Scheme

In this section, we improve the Choudhury et al's scheme. Our proposed scheme resolves their security flaws and enhances the security. This scheme has four phases: registration phase, login phase, authentication phase and password change phase. The details are described as follow.

A. Registration Phase

In the registration phase, user provides appropriate identification details to the cloud server. Then the cloud server issues a smartcard to the user according user's data.

1. A selects a random number x and computes $h(PW \oplus x)$.
2. $A => S$: ID, $h(PW)$, $h(PW \oplus x)$.
3. S checks whether the ID has existed in server. If ID has existed in server, S rejects registration request. Otherwise, S generates y and computes: $I = h(ID \| y)$, $B = g^{ID+h(PW)+h(y)} \bmod p$.
4. S => A : a smartcard which contains $\{I, B, p, g, h(\cdot)\}$.
5. A enters x into his smartcard. Now smartcard contains $\{I, B, p, g, h(\cdot), x\}$.
6. S stores ID and $h(PW \oplus x)$ in the server.

B. Login Phase

This phase is invoked when user wants to login into the cloud.

1. A inserts his smartcard and enters ID and PW.
2. The smartcard computes $C = h(I \| h(PW \oplus x) \| T_u)$, where T_u denotes A 's current timestamp.
3. $A \rightarrow S$: ID, C, T_u.

C. Authentication Phase

After receiving the login request message $\{ID, C, T_u\}$, the server verifies the identity of the user. The procedure is as follows.

1. If $T_u^{'} - T_u > \Delta T$, S rejects A 's login request. Otherwise, S performs the following computations: $I^{*} = h(ID \| y)$, $C^{*} = h(I^{*} \| h(PW \oplus x) \| T_u)$, where $T_u^{'}$ is the current timestamp of server and ΔT is the maximum time interval for transmission delay. If C^{*} equals C, S accepts the user A 's login request and computes $K^{'} = g^{ID+h(y)} \bmod p$, $h(K^{'})$ and $R = h(K^{'} \| T_s)$. T_s is S 's current timestamp. S generates a random number a.
2. $S \rightarrow A$: $E_{h(K^{'})}\{R, T_s, a\}$.
3. A computes $K^{"} = Bg^{-h(PW)} \bmod p$ and $h(K^{"})$. Then A decrypts $E_{h(K^{'})}\{R, T_s, a\}$ with $h(K^{"})$, and gets $\{R, T_s, a\}$. A checks the timestamp. If T_s is invalid, A terminates this session. Otherwise, A computes $R^{'} = h(K^{"} \| T_s)$ and compares $R^{'}$ to the received R. If equal, A successfully authenticates S.
4. $A \rightarrow S$: $h(a)$

5. S checks $h(a)$. If $h(a)$ is correct, mutual authentication successes. Now both user A and server S can compute the session key $S_K = h(K^{'} || a) = h(K^{''} || a)$.

D. Password Change Phase

This phase is invoked when the user wants to change his password.

1. A inserts his smartcard into smartcard reader and enters ID and PW.

2. $A \to S$: $E_{S_K}\{h(PW \oplus x) || h(PW^{'} \oplus x) || b\}$.

A and S execute the login and authentication phase mentioned above. If A passes the verification, A will send a password change request to S, and then submit $h(PW \oplus x)$ and $h(PW^{'} \oplus x)$, where $PW^{'}$ is A 's new password, b is a random number.

3. S checks $h(PW \oplus x)$ and replaces it by $h(PW^{'} \oplus x)$.

4. $S \to A$: $h(b)$

5. A checks $h(b)$. If it is correct, the smartcard performs the following computations: $Z = Bg^{-ID-h(PW)} \bmod p$, $B^{'} = Zg^{ID+h(PW^{'})} \bmod p$.

6. A replaces B by $B^{'}$ in the smartcard.

IV. SECURITY ANALYSIS

In this section, we show the formal analysis of our improved scheme based on strand space model and authentication testing methods, and prove its correct mutual authentication.

According to strand space model theory, our improved identity authentication protocol can be formalized as the following two types of regular strands (figure 1).

Initiator U strands with trace $\langle +ID\{I\{PW\}_{K_x} T_u\}_{K'_{pub}} T_u, -\{\{\{ID\}_{K_{pub}}\}_{K_{T_s}} T_s a\}_{K_{h(K')}}, +\{a\}_{K'_{pub}} \rangle$, where $ID, I, PW, T_u, T_s, a \in \mathbf{T}$, $K_x, K_{pub}, K_{T_s}, K_{h(K')}, K'_{pub} \in \mathbf{K}$. $Init[ID, C, T_u, T_s, a]$ will denote the set of all strands with the trace shown.

Responder CS strand with trace $\langle -ID\{I\{PW\}_{K_x} T_u\}_{K'_{pub}} T_u, +\{\{\{ID\}_{K_{pub}}\}_{K_{T_s}} T_s a\}_{K_{h(K')}}, -\{a\}_{K'_{pub}} \rangle$, where $ID, I, PW, T_u, T_s, a \in \mathbf{T}$, $K_x, K_{pub}, K_{T_s}, K_{h(K')}, K'_{pub} \in \mathbf{K}$. $\mathrm{Re}\,sp[ID, C, T_u, T_s, a]$ will denote the set of all strands with the trace shown.

Proposition 1 Let C be a bundle in $\sum$, and s be an initiator's strand in $Init[ID, I, PW, T_u, T_s, a]$ with C-height 2. Assume $K_{T_s} \notin K_p$, and suppose that ID is uniquely originating. Then there must be a responder strand $s' \in \mathrm{Re}\,sp[ID, C, T_u, T_s, a]$ with C-height 2.

Proof. We show first that the first and second nodes no s form an incoming test for ID. $\{\{ID\}_{K_{pub}}\}_{K_{T_s}}$ is a test component for ID in $\langle s, 2 \rangle$, because it contains ID, and no regular node has any term of this form as a proper subterm. Checking the assumptions, it follows that $\langle s, 1 \rangle \Rightarrow^{+} \langle s, 2 \rangle$ is an incoming test for ID in $\{\{ID\}_{K_{pub}}\}_{K_{T_s}}$.

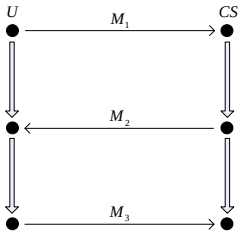

Where: $M_1 = ID\{I\{PW\}_{K_x} T_u\}_{K'_{pub}} T_u$

$M_2 = \{\{\{ID\}_{K_{pub}}\}_{K_{T_s}} T_s a\}_{K_{h(K')}}$

$M_3 = \{a\}_{K'_{pub}}$

Figure 1. Normal bundle of our authentication protocol

By Incoming Test, there exist regular nodes $n_0, n_1 \in C$ such that $\{\{ID\}_{K_{pub}}\}_{K_{T_s}}$ is a component of n_1 and $n_0 \Rightarrow^{+} n_1$ is a transforming edge for ID.

Because n_1 is a positive regular node and $\{\{ID\}_{K_{pub}}\}_{K_{T_s}} = term(n_1)$, ID is uniquely originating in $\langle s, 1 \rangle$, then there must exist a negative regular node n_0 to receive ID. Since n_0 is a negative node, n_0 is $\langle s', 1 \rangle$ for some responder strand $s' \in \mathrm{Re}\,sp[ID, C, T_u, T_s, a]$. Since $\langle s', 1 \rangle \Rightarrow^{+} \langle s', 2 \rangle$ and $term(\langle s', 2 \rangle) = \{\{ID\}_{K_{pub}}\}_{K_{T_s}}$, we see that $T_u^{'} = T_u$ and $T_s^{'} = T_s$. Therefore the C-height of s' is 2.

Proposition 1 realizes the security certificate of CS depending on the assumption that $K_{T_s} \notin K_p$. Thus our improved protocol can prevents any malicious active and passive attack in the first two steps.

Proposition 2 Let C be a bundle in $\sum$, and s be a responder's strand in $\mathrm{Re}\,sp[ID, C, T_u, T_s, a]$ with C-height 3. Assume $K_{h(K')} \notin K_p$, and suppose that a is uniquely originating. Then there must be an initiator strand $s' \in Init[ID, C, T_u, T_s, a]$ with C-height 3.

Proof. We show first that the second and third nodes no s form an outgoing test for a. $\{\{\{ID\}_{K_{pub}}\}_{K_{T_s}} T_s a\}_{K_{h(K')}}$ is a test component for a in $\langle s, 2 \rangle$, because it contains a, and no regular node has any term of this form as a proper subterm. Checking the assumptions, it follows that $\langle s, 2 \rangle \Rightarrow^{+} \langle s, 3 \rangle$ is an outgoing test for a in $\{\{\{ID\}_{K_{pub}}\}_{K_{T_s}} T_s a\}_{K_{h(K')}}$.

By Outgoing Test, there exist regular nodes $n_0, n_1 \in C$ such that $\{\{\{ID\}_{K_{pub}}\}_{K_{T_s}} T_s a\}_{K_{h(K')}}$ is a component of n_0 and $n_0 \Rightarrow^{+} n_1$ is a transforming edge for a.

Because n_1 is a positive regular node and $\{\{\{ID\}_{K_{pub}}\}_{K_{T_s}} T_s a\}_{K_{h(K')}} = term(n_1)$, a is uniquely originating in $\langle s,2\rangle$, then there must exist a negative regular node n_0 to receive a. Since n_0 is a negative node, n_0 is $\langle s',2\rangle$ for some initiators strand $s' \in Init[ID, C, T_u, T_s, a]$. Since $\langle s',2\rangle \Rightarrow^{+} \langle s',3\rangle$ and $term(\langle s',3\rangle) = \{\{\{ID\}_{K_{pub}}\}_{K_{T_s}} T_s a\}_{K_{h(K')}}$, we see that $T_s' = T_s$. Therefore the C-height of s' is 3.

Proposition 2 realizes the security certificate of U depending on the assumption that $K_{h(K')} \notin K_p$. Thus our improved protocol can prevents any malicious active and passive attack in the last two steps.

Combining the proof of proposition 1 and 2, we achieve the secure mutual authentication between users and cloud server. Our scheme can resist relay attack, man in the middle attack and so on. For example, the transmitted messages $C = h(I \| h(PW \oplus x) \| T_u)$, $R = h(K^{'} \| T_s)$ contain timestamp, hence our scheme is strong against replay attack; If ID is modified into ID^* in login phase, $I^* = h(ID^* \| y)$, $C^* = h(I^* \| h(PW \oplus x) \| T_u)$. Then $C^* \neq C$, terminate the communication. No matter which message is modified by adversary, the communication will terminate. Hence man in the middle attack is resisted.

Compared to Choudhury et al's scheme, our protocol has greatly enhanced the security in the following aspects.

Withstanding masquerade attack: our proposed scheme can withstand masquerade attack with smartcard revealing. When A 's smartcard has been stolen, the attacker can breach the data $I, B, p, g, h(\bullet)$ stored in the smartcard. The attacker cannot compute $h(I \| h(PW \oplus x) \| T_u)$ according these parameters. And neither $K^{'}$ nor $K^{''}$ can be got by the attacker without knowing PW or y. So even if the smartcard is stolen, our protocol can protect users' login security.

Besides, our proposed scheme can provide mutual authentication. At the step2 of authentication phase, S sends $E_{h(K^{'})}\{R, T_s, a\}$ to A. A checks R to verify S. Meanwhile A sends a response $h(a)$ to S for verification. Thus the mutual authentication is performed.

Avoiding OOB attack: our proposed scheme does not use onetime key K. Instead, we use $h(K^{'})$ to encrypt the message to ensure protocol secure. Thus we avoid transmitting K through OOB channel and avoid OOB attack.

Password change: our proposed scheme facilitates users to change password. As described in password change flaw, Choudhury et al's scheme cannot achieve the function of changing password. In our scheme, when we change the password, we change $h(PW \oplus x)$ in the server and B in the smartcard at the same time for the later authentication. It is inherently stronger compared static password based scheme

V. PERFORMANCE SIMULATION

We make the performance simulation of the user authentication protocol with NS2 and compare with some other related protocols. We assume the bandwidth of the wireless network is 2Mbps. In the simulation, we adopt AES as our encryption algorithm. Finally we plot the simulation result.

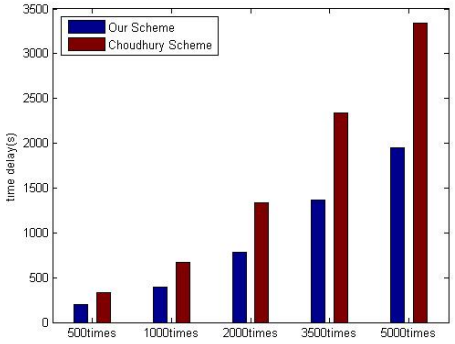

Figure 2. Time delay

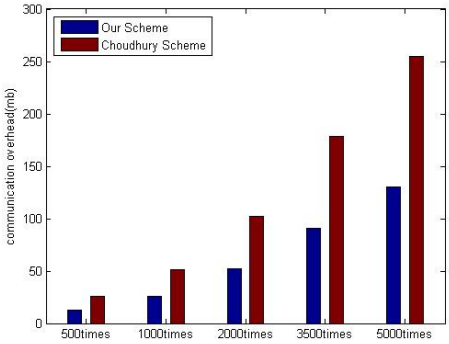

Figure 3. Communication overhead

The time delay and the communication overhead of our protocol and Choudhury's protocol are shown in fig2 and fig. 3. Blue represents our improved scheme, red represents Choudhury's scheme. The simulation result shows that our total time delay is respectively 191.148s, 388.237s, 780.594s, 1367.039s and 1954.485s when our protocol runs 500 times, 1000times, 2000times, 3500times and 5000 times. Choudhury's total time delay is 334.495s, 671.992s, 1347.332s, 2351.465s and 3371.955s. Obviously, we can see that our delay time is shorter than the original scheme's. And with the increasing of the login times, the advantage is more and more obvious. Figure3 shows the total communication overhead during the authentication process when the protocols run 500 times, 1000 times, 2000times, 3500times and 5000 times. Our protocol's communication overhead is respectively 12.56mb, 26.71mb, 54.13mb, 90.77mb and 130.49mb. Choudhury's is respectively 25.48mb, 50.89mb, 103.21mb, 180.33mb and 256.27mb. From the simulation results, we can see that our scheme's time delay and communication overhead is smaller than Choudhury's. In our protocol, there are only three interactive messages while there are four interactive messages in Choudhury's

protocol. And the computation of these two protocols is almost the same. Therefore our scheme's performance is better than Choudhury's scheme'. Overall, our protocol can not only improve the security performance but also make the communication performance better.

VI. CONCLUSION

In this paper, we make a security analysis on the user authentication framework proposed by Amlan Jyoti Chouhury et al and point out some security attacks to it. Then we proposed an improved scheme for cloud computing. Our scheme inherits the merits of Choudhury's protocol and enhances the security for user communicating with cloud server. Formal proof and security analysis are presented in section 4 and performance simulation runs in Section 5. The results show that our scheme can not only improve the security performance but also make the good communication performance.

REFERENCES

[1] Michael Armbrust, Armando Fox, Rean Griffith, Anthony D. Joseph, Randy Katz, Andy Konwinski, Gunho Lee, David Patterson, Ariel Rabkin, Ion Stoica, Matei Zaharia. A view of cloud computing. *Communications of the ACM*, 2010, 53 (4) pp. 50-58.

[2] H. Takabi, J. B. D. Joshi, G. J. Ahn. Secure cloud: towards a comprehensive security framework for cloud computing environments [C]//2010 *IEEE* 34*th Annual Computer Software and Applications Conference Workshops*. Seoul, 2010 pp. 393-398.

[3] Chun-Ting Huang, Zhongyuan Qin, C.-C. J. Kuo. Multimedia Storage Security in Cloud computing: An Overview [C]// 2011 *IEEE* 13*th International Workshop on Multimedia Signal Processing*. Hangzhou, China, 2011 pp. 1-6.

[4] M. S. Hwang, L. H. Li. A new remote user authentication scheme using smart cards. *IEEE Transactions on Consumer Electronics*, 2000, 46 (1) pp. 28-30.

[5] H. Y. Chien, J. K. Jan, Y. M. Tseng. An efficient and practical solution to remote authentication smart card. *Computers & Security*, 2002, 21(4) pp. 372–375.

[6] W. C. Ku, S. M. Chen. Weaknesses and improvements of an efficient password based remote user authentication scheme using smart cards. *IEEE Transactions on Consumer Electronics*, 2004, 50(1) pp. 204–207.

[7] C. Mitchell. Limitations of challenge-response entity authentication. *Electronic Letters*, 1989, 25(17) pp. 1195–1196.

[8] W. C. Ku, C. M. Chen, H. L. Lee. Cryptanalysis of a variant of Peyravian–Zunic's password authentication scheme. *IEICE Transactions on Communication*, 2003, E86-B(5) pp. 1682–1684.

[9] T. H. Chen, J. C. Huang. A novel user-participating authentication scheme. *The Journal of Systems and Software*, 2010, 83(5) pp. 861–867.

[10] Chun-Ta Li, Cheng-Chi Lee. A robust remote user authentication scheme using smart card. *Information Technology and Control*, 2011, 40(3) pp. 236-240.

[11] H. C. Hsiang, W. K. Shih. Weaknesses and improvements of the Yoon-Ryu-Yoo remote user authentication scheme using smart cards. *Computer Communications*, 2009, 32(4) pp. 649–652.

[12] Amlan Jyoti Choudhury, Pardeep Kumar, et al. A strong user authentication framework for cloud computing. [C]// 2011 *IEEE Asia-Pacific Services Computing Conference*. Jeju Island, 2011 pp. 110-115.

[13] Szu yu Lin. Enhancing the security of out-of-band one-time password two factor authentication in cloud computing. Taiwan: National Taiwan University of Science and Technology, 2010.

Improvement Priority Handoff Scheme for Multi-Service Wireless Mobile Networks

ChengGang Liu, ZhenHong Jia*, and Xi-Zhong Qin
School of Information Science and Engineering, Xinjiang University, Urumqi 830046, China
*Corresponding Author, Email: jzhh@xju.edu.cn

Lei Sheng and Li Chen
Subsidiary Company of China mobile in Xinjiang, Urumqi 830063, China

***Abstract*—In this study, a new handoff strategy to improve the performance of wireless mobile networks is presented. It has been found form this study that the dropping probability of handoff calls is drastically reduced compared to the existing method of channel reservation strategy of handoff calls and the performance of new calls can be improved. The strategy is that the new call should be delayed then it can use the last idle channel. The time that all the channels are holding has been shortened. Opportunities of the new call and handoff call occupancy channel are increased; the scheme also takes into account the priority of different data types, and only when the high-priority data packets queue is empty, the data packets in low-priority data queue can be transmitted. Simulation results show that, to let the new voice call delay in the allowable range, can effectively reduce the dropping probability of handoff call and the blocking probability of high-priority data while improving the probability of new call to enter into the systems.**

***Index Terms*—Queuing Theory; Handoff; Multi-Service; Priority; Markova Process**

I. INTRODUCTION

With the rapid development of mobile communication technology, the distribution of the cell becomes close under the limited spectrum capacity in order to meet the rapidly increasing demand of users. Meanwhile, due to accelerate the moving speed of the users, the numbers of the users that need to handoff and the handoff during an ongoing call are increased continuously. The possibility of call interruption caused by the handoff will increase during a call. Besides, the growth of the transmission bandwidth expanded the types of mobile communications service. In addition to voice services, data services such as Internet, image also appeared. In order to effectively use wireless resources, and improve the system capacity and service QoS. To design handoff strategy that is suitable for voice, data and multi-service has been a hot research [1-3].

The blocking probability of new call and the dropping probability of handoff call represent the grade of service of a wireless mobile network. In handoff strategy, in order to improve the two indicators, two priorities are considered in many handoff strategies. Some handoff strategy taking into account different priorities between different service types have been proposed [4-6], the different priorities between handoff calls and new calls other handoff are considered in other strategies. A new call being blocked is not as disastrous as a handoff call being dropped, so these strategies [7-9] consist of giving higher priority to handoff call than new call. At the same time, according to the different type of data service, consideration should also be given priority of different data types.

Movable boundary strategy; real time service has a higher priority than the non-real-time service [4]. In order to increase the bandwidth utilization, non-real-time service is allowed to borrow unused channels from the real time service. Since handoff calls and new calls use the same set of channels, the dropping probability of handoff call is high when there are too many new calls. The guard channel strategy that gives the handoff call a higher priority than a new call [7]. This strategy consists of having a fixed number of channels in each cell, reserved exclusively for handoff call. It effectively reduces the dropping probability of handoff call. However, the drawback for using guard channel for handoff call is that the channels that are reserved may be unoccupied for a long duration and new calls are blocked because they have no channels can be used. The guard channel strategy [10] that consists of having a fixed number of channels in each cell, reserved exclusively for data call. When the arrival rate of voice services is high, voice services can not occupy the guard channel of data services. This will result in a high blocking probability of voice service. Some people have recently proposed a strategy to dynamically reserve guard channel for handoff calls [11]. Although the dropping probability of handoff call is reduced, the blocking probability of new call is increased because it can not occupy the idle channel reserved for handoff call. Some people proposed a movable boundary and guard channel strategy [12], they consider two priorities that real time service has a higher priority than the non-real-time service and the handoff call has a higher priority than a new call. The dropping probability of handoff call is significantly lower. However, the performance of new calls has been reduced

doi:10.4304/jnw.9.1.204-209

and this strategy did not consider the different priorities between the various data services.

In the present study, a new handoff strategy based on multi-service is proposed. When services are busy in wireless mobile networks, handoff calls have a higher priority than new calls when call request. Idle channel can be assigned to handoff call immediately. If there is only one idle channel in the cell, new call would be delayed before it occupy the idle channel. Although the delay time of new calls are increased in new strategy, the probability of new call and handoff call to obtain a free channel are increased, the quality of voice service are improved.

In a data packet communication environment, data packets have different requirements. Some non real-time data packets can tolerate delays whereas real-time data packets are sensitive to delays. At the same time the strategy to provide differentiated services for data service can create more value for the communication operators. Combined with these characteristics of current data service in wireless mobile networks, new strategy takes different queue policies. According to the different importance of data services, data services are divided into high and low priority packet. For the smooth presentation of the idea of the new handoff strategy for performance improvement, the 4D Erlang theory with new handoff strategy is described. The reserved channel strategy and movable boundary channel strategy are compared with the new handoff strategy.

II. System Model

The system model is shown in Figure 1. In the following, the new strategy assume that the total number of channels in the channel pool shared by voice service and data service in each cell is fixed and denoted by *C*. *N* channels can be allocated to voice services, and *C-N* channels are allocated to data services. The voice calls are divided into handoff calls and new calls. Voice calls only can occupy the previous N channels. Handoff calls and new calls are endowed with the same priority in the previous *(N-1)* channels. Handoff calls are assigned priority over new calls when the N-idle channel is allocated to voice call. When the N-th channel is idle in the cell, if the handoff call arrives, the N-th channel can be directly occupied by the handoff call; if the new call arrives, the N-th channel can not be directly occupied by the new call, the new call would be delayed. During the delay time, if the users in the previous *(N-1)* channels complete the call, then the idle channel in the previous *(N-1)* channels can be occupied by the new call. If there is still no idle channel when the delay time is over, the N-th idle channel can be occupied by new call.

According to the different importance of data services, data services are divided into high and low priority packet. When a data call arrives, if it is high-priority packet. It is stored in the queue Q_2. If it is a low-priority packet. It is stored in the queue Q_1. When the data packet is transmitted, the packet is removed from the queue. When the queue Q_2 is empty, the low priority packets can be transmitted in the queue Q_1. When the channel *(C-N)* of the data service is busy, the channel assigned to the voice service in the idle time can be occupied by data services.

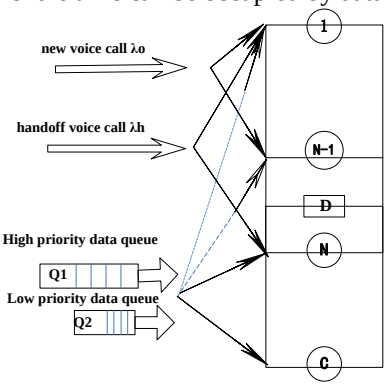

Figure 1. Voice call and data call channel allocation model, the new voice call, handoff voice call, data call number of channel is N-1, N, C-1.

When a voice call arrives, an idle channel from *N* channels can be assigned to the call. If there is no free channel can be occupied by voice call, while channels of the voice service are occupied by data services, the channel must be released immediately by the data call, the data call is placed in the queue Q_2 until there are the idle channels can be occupied. If the previous *(N-1)* channels are occupied by all the voice calls, the voice call is treated differently according to the type of the call. As shown in Figure 1, The N-th channel can be occupied by handoff call immediately. The new call would be delayed. During the delay time, the system has been in a state D. In the D state, there is at least one idle channel in the cell. The time that all channels are occupied is reduced. The time that the cell stays in the *(N-1)* state has been extended. Thereby the dropping probability of handoff call and the blocking probability of new call are reduced.

When the delay time *d (t)* is over, if the users in the previous *(N-1)* channels leave the cell, then the idle channel in the previous *(N-1)* channels can be occupied by the new call. If there is not idle channel to be occupied in the previous *(N-1)* channels, the N-th channel can be occupied by the new call.

III. Traffic Model

This queuing system with C servers and an infinite number of users consisting of both voice and data service accords to Poisson process. The arrival rate of new calls is λ_o; the arrival rate of handoff calls is λ_h. Their service times are negative exponential distribution [13]. Their service rate are μ_o and μ_h. The maximum length of the data packets waiting queue is Q_1 and Q_2 ($Q_1 > Q_2$), the arrangement rule is FIFO. The arrival rate of low priority packets and the arrival rate of high priority packets were λ_{d1} and λ_{d2}. The length of data packet is negative exponential distribution, the mean length of data packet is L_d *bits*. Assuming that the transmission of data packet uses the same encoding, the transmission rate of data packet is V_d *kbit /s* in the coding mode. The average transmission time of the low priority data packet and the high priority data packet is $1/\mu_d = L_d / V_d$.

Let states (i, j, l, g) be a vector representing the state of the cell with a four-dimensional Markov chain, where *i* number of channels used by new calls in N; *j* number of channels used by handoff calls in N; *l* number of high priority data calls in Q_2; *g* number of data calls in cell. The value ranges of discrete parameters are $i \in [0, N]$, $j \in [0, N]$, $l \in [0, Q_2]$, $g \in [0, C+ Q_1+ Q_2]$.

Since the steady-state distribution of the multi-dimensional continuous time Markov process is not solved easily, and the actual system meets $\mu_d / (\mu_o + \mu_h) >> 1$, the four-dimensional continuous time Markov process is decomposed into two consecutive two-dimensional continuous time Markov process. The two parts are voice calls and data calls [14].

A. Voice Calls Section

The state transition diagram of voice call is shown in Figure 2. For *i* and *j* of State (*i, j*), *i* is the number of new calls in the cell and *j* is the number of handoff calls in the cell. $\delta^{-1}=d$, *d* is the delay time of new call. State D represents the state that the new call is delayed; the arrival rate to reach the state D is δ. The stationary probability states of call are given by the following equations:

$$\lambda_0 \pi_{(0,y)} = \mu_0 \pi_{(1,y)} \tag{1}$$

$$(\lambda_0 + \mu_0)\pi_{(1,y)} = \lambda_0 \pi_{(0,y)} + 2\mu_0 \pi_{(2,y)} \tag{2}$$

$$(\lambda_0 + x\mu_0)\pi_{(x,y)} = \lambda_0 \pi_{(x-1,y)} + (x+1)\mu_0 \pi_{(x+1,y)} \tag{3}$$

where, $\pi\ (x, y)$ indicates the stationary probability of the state *(x, y)*.

Let $\rho_o=\lambda_o/\mu_o$, ρ_o is the call intensity of new call. The arrival of a new call is Poisson distribution parameters for ρ_o. The service time is negative exponential distribution parameters for 1. Steady-state probability for each row of *N* states (x, y) is:

$$\pi_{(x,y)} = \frac{\rho_0^x}{x!}\pi_{(0,y)} \quad 0 \le x \le n-y, 0 \le y \le n-1 \tag{4}$$

Let $\rho_h=\lambda_h/\mu_h$, ρ_h is the callintensity of hand off call. The a rrival of ahand off call is Poissondistri bution parameters for ρ_h. The service time is negative exponential distri bu tion parameters for 1. Steady-stateprob ability for each column of (N+1) states (x, y) is:

$$\pi_{(x,y)} = \frac{\rho_h^y}{y!}\pi_{(x,0)} \quad 0 \le x \le n-y, 0 \le y \le n-1 \tag{5}$$

By substituting x=0 in (5) and the resulting $\pi\ (0, y)$ so obtained, if substituted in (4), results in the following expression for the stationary probability states $\pi\ (x, y)$:

$$\pi_{(x,y)} = \frac{\rho_0^x}{x!}\frac{\rho_h^y}{y!}\pi_{(0,0)} \quad 0 \le x \le n-y, 0 \le y \le n-1 \tag{6}$$

In addition to (6), the following equations are derived for finding the remaining states $\pi\ (D, y)$ and $\pi\ (n\text{-}y, y)$:

$$\begin{aligned}(\lambda_0 / \mu_0 + (n-y-1)\mu_0)\pi_{(n-y-1,y)} &= \lambda_0 \pi_{(n-y-2,y)} \\ +(n-y-1)\mu_0 \pi_{(D,y)} &+ (n-y)\mu_0 \pi_{(n-y,y)}\end{aligned} \tag{7}$$

$$(\delta + (n-y-1)\mu_0)\mu_0 \pi_{(D,y)} = \lambda_0 \pi_{(n-y-1,y)} \tag{8}$$

$$(n-y)\mu_0 \pi_{(n-y,y)} = \delta\, \pi_{(D,y)} \tag{9}$$

After solving the above equations, the following relations, thee xpressions for $\pi(D, y)$and $\pi\ (n\text{-}y, y)$are obtained:

$$\pi_{(D,y)} = \frac{\lambda_0}{\delta + (n-y-1)\mu_0}\frac{\rho_h^y}{y!}\frac{\rho_0^{n-y-1}}{(n-y-1)!}\pi_{(0,0)} \tag{10}$$

$$\pi_{(n-y,y)} = \frac{\delta}{\delta + (n-y-1)\mu_0}\frac{\rho_h^y}{y!}\frac{\rho_0^{n-y}}{(n-y)!}\pi_{(0,0)} \tag{11}$$

where:

$$\pi_{(0,0)} = \left(\sum_{y=0}^{n-1}\sum_{x=0}^{n-y}\frac{\rho_h^y}{y!}\frac{\rho_h^x}{x!} + Y\right)^{-1} \tag{12}$$

$$Y = \sum_{y=0}^{n-1}\rho_0 g_y \frac{\rho_h^y}{y!}\frac{\rho_0^{n-y-1}}{(n-y-1)!} + \sum_{y=0}^{n-1}\frac{\delta}{\mu_0}g_y\frac{\rho_h^y}{y!}\frac{\rho_0^{n-y}}{(n-y)!} \tag{13}$$

$$g_y = \frac{\mu_0}{\delta + (n-y-1)\mu_0} \tag{14}$$

The dropping probability of handoff call in this case is:

$$P_d = \sum_{y=0}^{n}\pi_{(n-y,y)} = \sum_{y=0}^{n}\frac{\delta}{\mu_0}g_y\frac{\rho_h^y}{y!}\frac{\rho_0^{n-y}}{(n-y)!}\pi_{(0,0)} \tag{15}$$

And the blocking probability of new call is obtained as:

$$\begin{aligned}P_b &= \sum_{y=0}^{n-1}\pi_{(D,y)} + \sum_{y=0}^{n}\pi_{(n-y,y)} \\ &= \sum_{y=0}^{n-1}\rho_0 g_y \frac{\rho_h^y}{y!}\frac{\rho_0^{n-y-1}}{(n-y-1)!}\pi_{(0,0)} \\ &+ \sum_{y=0}^{n}\frac{\delta}{\mu_0}\frac{\rho_h^y}{y!}\frac{\rho_0^{n-y}}{(n-y)!}\pi_{(0,0)}\end{aligned} \tag{16}$$

B. Data Calls Section

When there are *w (w = i + j)* channels occupied by voice call in the system, the maximum of data calls simultaneously serviced is *k* (*k = C-w*) in the system. For *l* and *g* of state (*l, g*), *l* is the number of the high priority packets in the queue Q_2, *g* is the total number of packets in the system. The state transition diagram of data call is shown in Figure 3.

Each state transition diagram of data call is described in Figure 3, the principle of which is the flow conservation. Let inflow speed is equal to the outflow

rate for each state. The steady state balance equation can be expressed as:

$$(\lambda_{d1}+\lambda_{d2})\pi_{(l,g)} = (k+1)u_d\pi_{(l,g+1)} \qquad 0 \le g \le k-l, l = 0 \quad (17)$$

$$\begin{aligned}
&([1-u(g-k-Q_1)]\lambda_{d1} + [1-u(l-Q_2)]\lambda_{d2} \\
&+u(l-1)ku_d + \delta(l)\delta(g-k-1)ku_d)\pi_{(l,g)} \\
&= \lambda_{d1}\pi_{(g-1,l)} + u(l-1)\lambda_{d2}\pi_{(l-1,g-1)} \\
&+\delta(l)\delta(g-k)\lambda_{d2}\pi_{(l,g-1)} \\
&+u(Q_2-l-1)ku_d\pi_{(l+1,g+1)} \\
&+\delta(l)u(k+Q_1-g-1)ku_d\pi_{(l,g+1)} \\
&k \le g \le k+Q_1+Q_2, 0 \le l \le Q_2
\end{aligned} \quad (18)$$

where $\pi(l, g)$ is the state transition probability of the system that is in state (l, g). Let $u(x)$ denote the step function, which is defined as follows: $u(x)=1$ when $x \ge 0$ and $u(x)=0$ when $x<0$; $\delta(x)=1$ when $x=0$ and $\delta(x)=0$ when $x \ne 0$.

For state equation of (15) and (16), there are $(k + (Q_1 + 1) \times (Q_2 + 1))$ equations. We coupled on the state probability normalized condition as (19); we can obtain the steady-state solution of state by solving linear equation.

$$\sum_{g=0}^{k-1}\pi_{(0,g)} + \sum_{l=0}^{Q_2}\sum_{g=k+l}^{k+Q_1+Q_2}\pi_{(l,g)} = 1 \quad (19)$$

The dropping probability of low priority data call in this case is:

$$P_{d1} = \sum_{l=0}^{Q_2}\pi_{(l,g+Q_1+l)} \quad (20)$$

And the dropping probability of high priority data call is obtained as:

$$P_{d2} = \sum_{g=k+Q_2}^{k+Q_1+Q_2}\pi_{(Q_2,g)} \quad (21)$$

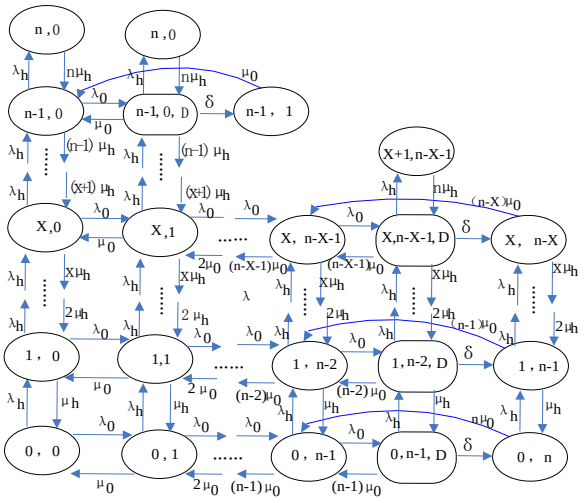

Figure 2. State transition diagram of voice call

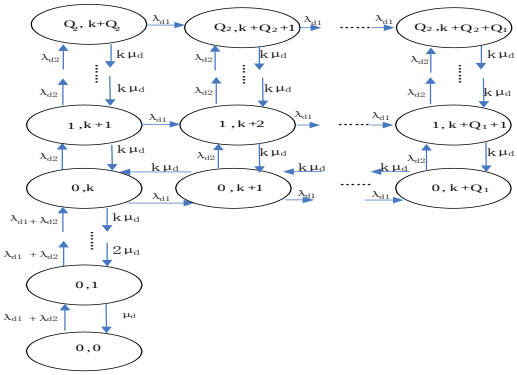

Figure 3. State transition diagram of data call

IV. Result and Discussion

A. Theoretical Calculation and Simulation Scenario

For the numerical appreciation of the obtained results, the following parameters are assumed for a cell of a mobile cellular system: number of channels in the cell, C=14, number of channels for voice services N=10, high priority queue length Q_1=200, low priority queue length Q_2=10, average length of data packets L_d =12000bit. Assuming that the transmission of data packet uses the same encoding, the transmission rate of data packet is V_d =9.05*kbit /s* in the coding mode. The arrival rate of new calls λo= (1.34-8.04)min^{-1}, the arrival rate of handoff calls λ_h=(1.66-5.0)min^{-1}. Their service rate are μ_o= 0.67$min^{-1}$and μ_h=0.83min^{-1}. The arrival rate of low priority packets was λ_{d1}, the arrival rate of high priority packets was λ_{d2}. $\lambda_{d1}=2\lambda_{d2}$, λ_{d1}=0.45 packets per second. When change the value of λ_0, λ_h, the blocking probability of new call is P_b, the dropping probability of handoff call is P_d, the dropping probability of low priority data call is P_{d1}, the dropping probability of high priority data call is P_{d2}.

In the reserved channel strategy, reserved channels for handoff calls r=3, number of channels for data calls in the cell m=4. In the movable boundary channel strategy, the channel is not reserved for the handoff calls. When the voice dedicated channel is idle, the data call can occupy the voice channel, but when a voice user arrives, the data call must be released immediately channel.

B. Analysis and Evaluation of the Traffic Model Performances

Since the new call would be delayed before it occupy the idle channel. The time of all channels were occupied is shorten, the time of the system in the state $(N-1)$ has been extended. The probability of new call and handoff call to obtain a free channel are increased. As is shown in figure 4 and figure 6, the dropping probability of handoff calls P_d has been greatly improved in the new handoff strategy, compared with reserved channel strategy and movable boundary strategy.

Since there are not reserved channels in the new handoff strategy and movable boundary strategy, the new calls are less affected by handoff calls, there are smaller blocking rate in these two strategies than reserved strategy. As is shown in figure 5 and figure7, the probability of an idle channel after a delay of a new call

in the new handoff strategy is greater than the movable boundary strategy, so the blocking probability of new call in the new handoff strategy is small than the movable boundary strategy.

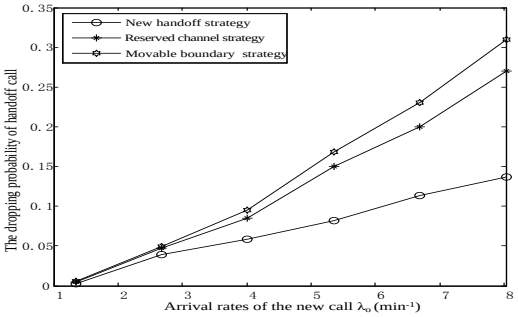

Figure 4. The dropping probability of handoff call by arrival rates of the new call

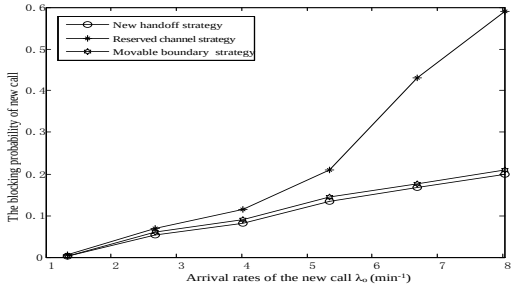

Figure 5. The blocking probability of new call by arrival rates of the new call

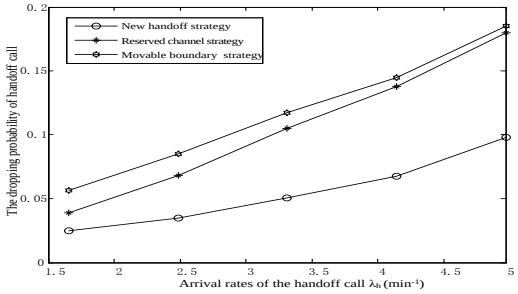

Figure 6. The dropping probability of handoff call by arrival rates of the handoff call

The arrival rate of new calls λ_o= 5.358min-1, the arrival rate of handoff calls λ_h=4.14min^{-1}. Their service rate are μ_o= 0.67$min^{-1}$and μ_h=0.83min^{-1}. With the growth of the delay time of a new call, the probability of the idle channel will increase when the call arrives. As is shown in figure 8 and figure9, since the handoff calls are given higher priority, an idle channel can be occupied by the handoff call immediately, the dropping probability of handoff calls decreased more significantly. Since the N-th idle channel is not allowed by the new calls, the blocking probability of new call is not changed significantly as the delay time increases.

The new handoff strategy is proposed that only when the high-priority data packets queue is empty, the data packets in low-priority data queue can be transmitted. As is shown in figure10 and figure11, compared with the dropping probability of low priority data call P_{d1}, the dropping probability of high priority data call P_{d2} has been greatly improved.

Meanwhile, since the new call is not able to occupy the channel reserved for the handoff calls and data calls can borrow reserved channels in the reserved channels strategy, the dropping probability of data calls in the reserved channels strategy should be less than the new handoff strategy. However, the dropping probability of data calls will rapidly increase when the handoff call arrival rate is high.

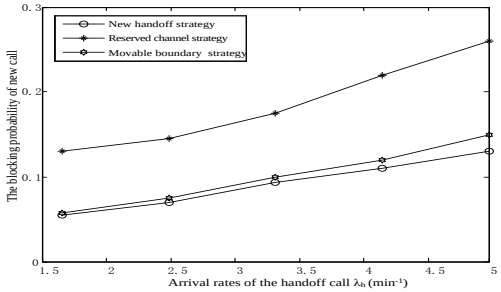

Figure 7. The blocking probability of new call by arrival rates of the handoff call

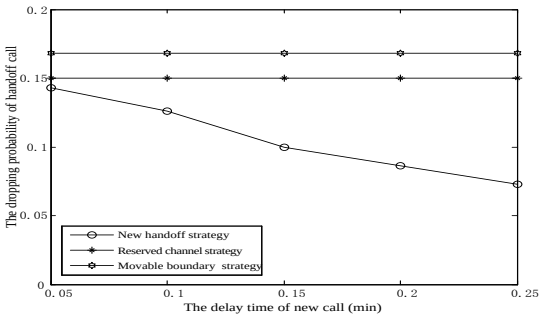

Figure 8. The dropping probability of handoff call by the delay time of new call

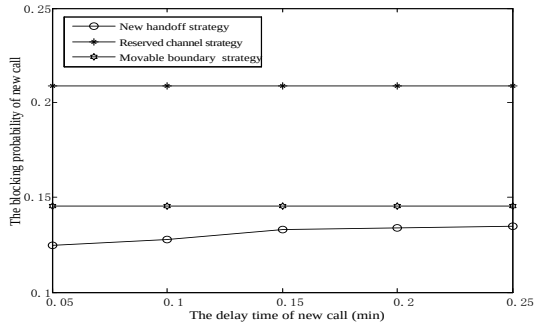

Figure 9. The blocking probability of new call by the delay time of new call

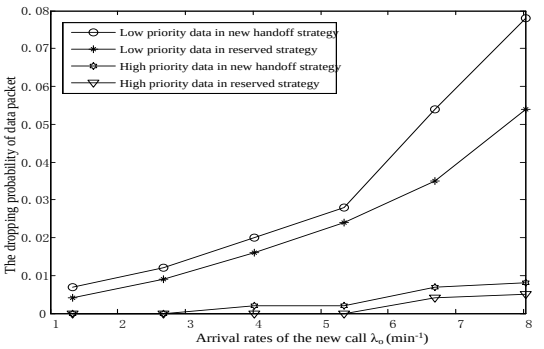

Figure 10. The dropping probability of data packet by arrival rates of the new call

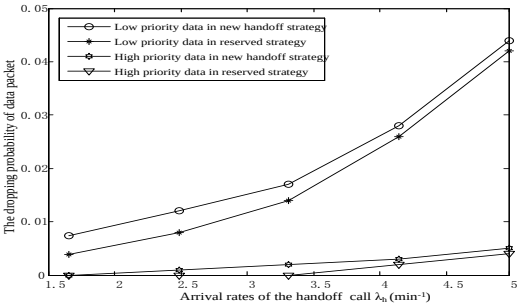

Figure 11. The dropping probability of data packet by arrival rates of the handoff call

V. CONCLUSION

A new handoff strategy based on business was presented in this article. In the actual communication process, users are more willing to accept occupies channel after the appropriate delay not directly blocked. A new call was allowed occupying idle channel after delay within the scope in this policy. The probability of the voice call into the system was increased. And the dropping probability of handoff call was reduced. The quality of service of a new call was improved at the same time. The dropping probability of high-priority data was reduced because it gives the data call a different priority. In order to reflect actual problems, we consider that the service time of handoff calls and new calls are different. New handoff strategy for improving network performance has certain significance.

ACKNOWLEDGMENT

The Fundamental Research Funds for China Mobile Communications Group Co., Ltd. Xinjiang (Grant No. XJM2012-01)

REFERENCES

[1] Hamad, Ahmed Morsy, Ehab Adel, Performance analysis of a handoff scheme for two-tier cellular CDMA networks, *Egyptian Informatics Journal* Vol. 8, No. 6, June 2011, pp. 456-462.

[2] Sharna, S. A., Amin, et al, Call admission control policy for multi-class traffic in heterogeneous wireless networks, *Communications and Information Technologies (ISCIT), 11th International Symposium on*, 2011, pp. 433-438.

[3] Yuan-yuan Su, Ren-yong Wu, Ren-fa Li, et al, A novel measurement-based call admission control algorithm for wireless mobility networks under practical mobility model, *Communications and Mobile Computing (CMC), International Conference on*, 2010, pp. 364-368.

[4] P. Venkata Krishna, Sudip Misra, An efficient approach for distributed dynamic channel allocation with queues for real-time and non-real-time traffic in cellular networks, *Journal of Systems and Software* Vol. 7, No. 82, June 2009, pp. 1112-1124.

[5] Al Khanjari, S., Arafeh, et al, An adaptive bandwidth borrowing-based Call Admission Control scheme for multi-class service wireless cellular networks, *Innovations in Information Technology (IIT), 2011 International Conference on*, pp. 556-564.

[6] Suleiman, K. H., Chan, et al, Analysis of serving discipline algorithms for cellular networks. *Wireless Communication, Vehicular Technology, Information Theory and Aerospace & Electronic Systems Technology (Wireless VITAE)*, 2nd *International Conference* on, 2011.

[7] Idil Candan, Muhammed Salamah, Analytical modeling of a time-threshold based bandwidth allocation scheme for cellular networks, *Computer Communications* Vol. 5, No. 30, December 2009, pp. 1036-1043.

[8] Sheu, TSang-Ling Wu, Yang-Jing Li, et al, A generalized channel preemption model for multi-class traffic in mobile wireless networks, *IEEE Transactions on Vehicular Technology* Vol. 5, No. 56, May 2007, pp. 2723-2732.

[9] Nasr, A. A., El-Badawy, et al, Connection Admission Control Reward Optimization for Different Priority Classes in Homogeneous Wireless Network. Wireless and Mobile Communications (ICWMC), 2010 6th *International Conference on*, pp. 549-555.

[10] Haw-Yun Shin, Jean-Lien C. Wu, The study of dynamic multi-channel scheme with channel de-allocation in wireless networks. *Computer Networks* Vol. 5, No. 45, July 2004, pp. 463-482.

[11] Zhihua Zheng, Performance analysis of A QoS guaranteed dynamic channel reservation for handoff prioritization in cellular mobile networks. *//Proc. of WICOM'08. 4th International Conference on Wireless Communications*, 2008.

[12] Huang Q and Chan S, An enhanced handoff control scheme for multimedia traffic in cellular networks, *IEEE, Communications Letters* Vol. 3, No. 8, March 2004, pp. 195-197.

[13] RiveroAngeles, M. E., LaraRodriguez, Differentiated backoff strategies for prioritized random access delay in multi-service cellular networks. *IEEE Transactions on Vehicular Technology* Vol. 1, No. 58, January 2009, pp. 381-397.

[14] Ghani S, Schwartz M, A decomposition approximation for the analysis of voice/data integration. *IEEE Transactions on Communications* Vol. 7, No. 42, May1994, pp. 2441-2452.

Chenggang Liu received his Bachelor's degree in Xinjiang University 2011. Now he is a master's degree candidate of Xinjiang University. His research interests include mobile communication network, digital signal processing.

Zhenhong Jia received his PhD in electronic information engineering from Shanghai JiaoTong University, Shanghai, China, in 1995. He is a professor in the College of information science and engineering, Xinjiang University. His research interests include mobile communication network, digital signal processing.

APA with Evolving Order and Variable Regularization for Echo Cancellation

JI Chang-Peng
School of Electronic and Information Engineering, Liaoning Technical University, Huludao, China
Email: ccp@lntu.edu.cn

JI Hong-Hong, GUO Wei-Ping, and Wang Jun
Institute of Graduate, Liaoning Technical University, Huludao, China
Email: hongji19880610@163.com

***Abstract*—Recently APA has become one of most popular algorithms in application of Acoustic Echo Cancellation. Because of the contradictory factors of convergence rate and steady-state misalignment, a new algorithm by the behavior of associating variable regularization and evolving order has been proposed in this paper. Despite of the conventional assumption that the a posteriori error is zero, we take the statistical characteristic of the noise into consideration during the adaptation process. Exact and approximate formulations for the optimal regularization factor are derived. Numerical simulation results show that the proposed algorithm improves the performance of the APA in terms of its faster convergence rate and lower steady-state misalignment compared to existing variable regularization APA and evolving order APA, respectively. Meanwhile it can be seen that near-end speech signal has been restored more effectively.**

***Index Terms*—Variable Regularization; Evolving Order; APA; Acoustic Echo Cancellation**

I. INTRODUCTION

The acoustic echo is mainly generated by transferring far-end speech signal to the local to amplify and put out through the speaker, then the signal is picked up by microphone and transmitted to the far-end together with the local voice signal. With the development of communication technology, the communication quality is constantly improved to satisfy the requirement of people's living standard. Whereas, echo which not only affects our call quality but also makes a normal call impossibly is engendered inevitably through the communication [1]. The basic principle of the echo canceller is that an adaptive filter is utilized to imitate the echo path. Then the impulse response will approach to the actual echo path through adjusting the adaptive filtering algorithm so that we can gain predicted echo signal. In final, echo cancellation will be realized in the way of subtracting the predicted echo signal from voice signal received from the microphone. Adaptive echo cancellation technology is internationally recognized as the most promising technologies, but also the practical application of the most used technologies. At present, there are already a variety of adaptive echo cancellation algorithms and solutions based on high-speed digital signal processing chips in reference [2].

Affine projection algorithm (APA) has many applications in our real life such as wireless channel equalizer, echo cancellation, noise cancellation and speech enhancement and so on in reference [3]. Particularly in echo cancellation, APA has presented a perfect performance. The APA has been advanced optimized and its high performance has been required due to the diversity and complexity of the communications environment, as well as taking into account the characteristics of the adaptive filter.

APA adopts the method of repeating use of the signal sample values. The higher the correlation of input data is, the faster the convergence speed will be. However, there is larger amount of calculation and worse steady-state misalignment than the NLMS algorithm in APA iterative process in the reference [4]. It was shown in reference [5] that a variable regularization factor APA could greatly reduce the steady-state error. An evolving order APA namely E-APA proposed in reference [6] had adjusted the current order based on steady-state mean square error, which could improve the contradiction between the fast convergence rate and the low steady-state misalignment and reduce the calculation greatly. In reference [7], a data selective segment proportionate affine projection algorithm for echo cancellation has been proposed by combining proportionate adaption with the framework of set-membership filtering in order to decrease the computational complexity of the algorithm. The frequency of updates of the filter coefficients has been reduced, where the filter coefficients are updated so that the output estimation error is upper bounded by a predetermined threshold. In reference [8], an improved set-membership affine-projection adaptive-filtering algorithm has been proposed. The proposed paper utilized two error bounds one of which is used to realize faster convergence and the other is used to suppress impulsive-noise interference. Through this way, the misalignment is reduced.

This article derives a new affine projection algorithm in the way of coordinating variable regularization in reference [5] and evolving order in reference [6], because

doi:10.4304/jnw.9.1.210-215

we have found that variable regularization can reduce the misalignment and the evolving order can speed up the convergence. We also incorporate the statistical characteristic of the noise into the adaptation process.

Moreover we will test and confirm the performance of the algorithm proposed in this paper from three aspects of convergence rate, steady-state misalignment and computational complexity [10]. Convergence rate refers to iteration time or number of iteration of the algorithm from the beginning to the stable stage. Convergence speed has a high relationship with the step size that we have chosen in the affine projection algorithm. Practically, convergence rate can be controlled by the selected step size [11]. The judgment for the iteration time should be based on the hardware environment. The steady-state misalignment provides the degree of deviation between the final mean square error adaptive algorithm and minimum mean square error generated by Wiener filter for an interesting algorithm [12]. We can conclude that step size and the order of the algorithm have a great effect on steady-state misalignment. Computation of an algorithm is the memory size used or occupied by the cost of a full iteration and storage of data and program. The greater the amount of calculation is, the higher the requirement of algorithm hardware environment will be, so the construction costs will be even great [13].

The paper is organized as follows. Section II give a brief introduction of the conventional APA model where will introduce its basic conception. In Section III, the optimization APA is provided including variable regularization, evolving order and its combination. The simulation results will be depicted in Section IV and conclusions are presented in Section V.

II. CONVENTIONAL APA MODEL

Many algorithms will appear to the problem of slow convergence rate when the input signal is colored in the adaptive filter. Data reuse algorithms are considered to be one of methods to improve the convergence rate of the adaptive filter algorithm in case of the relevance for input data [14]. Affine projection algorithm (APA) is one of data reuse algorithms; APA which evolves from the minimum mean square algorithm is also a normalized least mean square algorithm. Actually, APA is derived from least mean square algorithm (LMS) [15]. LMS is a searching algorithm where the calculation of the gradient vector is simplified by adjusting the objective functions appropriately. It is because of simple calculation that LMS algorithm and its associated algorithms have been widely used in reference [16].

We first define the adaptive filter coefficients $\boldsymbol{w}(n)= [w_0(n),w_1(n),\ldots,w_{L-1}(n)]^{\mathrm{T}}$ and the input signal vector $\boldsymbol{X}(n)= [x(n),x(n\text{-}1),\ldots,x(n\text{-}L\text{+}1)]^{\mathrm{T}}$ where the superscript T donates the transposition, $d(n)$ is the desired signal, K is the order of the APA, L is the length of unknown FIR system, $\boldsymbol{A}(n)= [\boldsymbol{X}(n),\boldsymbol{X}(n\text{-}1),\ldots,\boldsymbol{X}(n\text{-}K\text{+}1)]^{\mathrm{T}}$ is $L\times K$ affine projection matrix. $\boldsymbol{w}_{opt}$ is the unknown matrix for the filter to be estimated, Suppose $\boldsymbol{w}(n)$ is an estimation of $\boldsymbol{w}_{opt}$ at iteration n, n is the time index, $\boldsymbol{v}(n)$ is the noise signal. The basic formulas of the affine projection algorithm [17], [18] are as follows:

$$d(n) = y(n) + v(n) = X^T(n)w_{opt} + v(n) \qquad (1)$$

The updating formula of classic filter coefficient is:

$$w(n) = w(n-1) + \mu A(n)(A^T(n)A(n) + \delta I)^{-1}e(n) \quad (2)$$

The error formula is:

$$\mathbf{e}(n) = \mathbf{d}(n) - \mathbf{A}^T(n)\mathbf{w}(n-1) \qquad (3)$$

$\boldsymbol{I}$ is a $K\times K$ identity matrix. μ is the step size. Step size acts to be an important part in iteration. When the step size is big, the algorithm will converge very fast, but steady-state misalignment will increase. When step size is small, the convergence is slow, but the final misalignment is small. Let its value be 1 here. δ is the regularization factor which is employed to avoid the inversion of possibly rank-deficient matrix $\boldsymbol{A}^T(n)\boldsymbol{A}(n)$. What's more, it plays a significant role between the convergence rate and the steady-state misalignment of the conventional APA. On the one hand, a big value of step size will be obtained, responding to a small value of regularization factor, at the same time, the speed of the convergence will increase. However, this will lead to high steady-state misalignment. On the other hand, a large value of the regularization factor will result in a small step size, slow convergence rate and of course a low misalignment. In order to solve the contradiction of convergence speed, steady-state misalignment and computation of affine projection algorithm, this paper tries to figure out this problem from the aspect of variable parameters. Consequently, we expect to improve the performance of the APA by using a variable regularization factor.

III. OPTIMIZATION OF APA

In the traditional algorithm, the posteriori error was generally set as zero. It meant that noise was ignored. However, the statistical properties of the noise will be taken into account during the adaptive process in this paper. On the one hand, we want to minimize the steady-state error in order to increase the stability of convergence by adjusting the regularization factor [19]. On the other hand, it is expected to speed up the convergence rate of the algorithm and reduce the computational complexity by the way of regulating projection order. Although the larger projection order is the faster the convergence rate will be, the steady-state error also increases. The proposed algorithm has better performance through the synergistic effect of the variable regularization factor and evolving order [20], [21].

In order to increase the stability and decrease the steady-state error of the algorithm, it uses the variable $\delta(n)$ to modify the δ, so formula (2) can be rewritten as

$$\mathbf{w}(n) = \mathbf{w}(n-1) + \mu\mathbf{A}(n)(\mathbf{A}^T(n)\mathbf{A}(n) + \delta(n)\mathbf{I})^{-1}\mathbf{e}(n) \qquad (4)$$

By defining $\boldsymbol{S}(n)=(\boldsymbol{A}^{\mathrm{T}}(n)\boldsymbol{A}(n)+\delta(n)\boldsymbol{I})^{-1}$, then $\boldsymbol{w}(n)=\boldsymbol{w}(n\text{-}1)+\boldsymbol{A}(n)\boldsymbol{S}(n)\boldsymbol{e}(n)$. We can name $\boldsymbol{e}(n)$ the a priori error and $\boldsymbol{\varepsilon}(n)=\boldsymbol{d}(n)-\boldsymbol{A}^{\mathrm{T}}(n)\boldsymbol{w}(n)$ the a posteriori error. So the

relationship of $\boldsymbol{\varepsilon}(n)$ can be expressed as follow: $\boldsymbol{\varepsilon}(n)=\boldsymbol{A}^{\mathrm{T}}(n)(\boldsymbol{w}_{opt}-\boldsymbol{w}(n))+\boldsymbol{v}(n)$.

Ideally supposing that posteriori error $\boldsymbol{\varepsilon}(n)=0$, a priori error $\boldsymbol{e}(n)\neq 0$, and the assumption reveals that the reduction of the expectation of the l_2 norm of systematic error should be minimum. We can have the formula of $\boldsymbol{\varepsilon}(n)$ through simplification. Actually the noise signal is always present. It is obvious that $\boldsymbol{\varepsilon}(n)$ will be minimum only when $\boldsymbol{w}_{opt}-\boldsymbol{w}(n)=0$, and $\boldsymbol{w}_{opt}=\boldsymbol{w}(n)$.

So we get $\boldsymbol{\varepsilon}(n)=\boldsymbol{v}(n)$. Therefore, the solution for $\delta(n)$ is obtained such that $E\{\|\boldsymbol{\varepsilon}(n)\|^2\}=E\{\|\boldsymbol{v}(\mathrm{n})\|^2\}$. And we can reach to the following equation:

$$E\{\|\mathbf{v}(n)\|^2\}=E\{\mathbf{e}^T(n)(\mathbf{I}-\mathbf{A}^T(n)\mathbf{A}(n)\mathbf{S}(n))^T,\ (\mathbf{I}-\mathbf{A}^T(n)\mathbf{A}(n)\mathbf{S}(n))\mathbf{e}(n)\} \tag{5}$$

The equation will be simplified by means of eigenvalue decomposition. The eigenvalue decomposition of the Gram matrix $\boldsymbol{A}^{\mathrm{T}}(n)\boldsymbol{A}(n)$ is given by

$$\mathbf{A}^T(n)\mathbf{A}(n)=\mathbf{U}(n)\boldsymbol{\Lambda}(n)\mathbf{U}^T(n) \tag{6}$$

where $\boldsymbol{\Lambda}(n)$ is the diagonal matrix formed with the Eigenvalues of $\boldsymbol{A}^{\mathrm{T}}(n)\boldsymbol{A}(n)$, and $\boldsymbol{U}(n)$ are the eigenvectors of $\boldsymbol{A}^{\mathrm{T}}(n)\boldsymbol{A}(n)$. So the matrix $\boldsymbol{S}(n)$ can be given as

$$\mathbf{S}(n)=\mathbf{U}(n)(\boldsymbol{\Lambda}(n)+\delta(n)\mathbf{I})^{-1}\mathbf{U}^T(n) \tag{7}$$

The diagonal matrix whose kth diagonal element is $(\delta(n)/(\lambda k(n)+\delta(k)))^2$ is expressed as

$$\mathbf{Q}(n)=(\mathbf{I}-\boldsymbol{\Lambda}(n)(\boldsymbol{\Lambda}(n)+\delta(n)\mathbf{I})^{-1})^2 \tag{8}$$

The relationship of noise signal and posteriori error is obtained by putting (6), (7) and (8) into (5)

$$E\{\|\boldsymbol{v}(n)\|^2\}=E\{\boldsymbol{e}^T(n)\boldsymbol{U}(n)\boldsymbol{Q}(n)\boldsymbol{U}^T(n)\boldsymbol{e}(n)\} \tag{9}$$

Which mostly relies on the decomposition of Eigenvalues of the matrix $\boldsymbol{A}^{\mathrm{T}}(n)\boldsymbol{A}(n)$ from the formula derivation process. So it is apparently impossible to obtain the variable regularization factor through this method. However, it can be approximated in other ways. It also can be seen that the kth diagonal element of $\boldsymbol{A}^{\mathrm{T}}(n)\boldsymbol{A}(n)$ is the l_2 norm of the input signal vector, so a exploratory approximation has been given as

$$\lambda_k(n)\approx L\sigma_x^2(n)\ \ 1\le k\le K \tag{10}$$

$\sigma 2x(n)$ is the variance of input signal. Substituting this formula into (9) results in

$$\delta(n)=\frac{L\sigma_x^2(n)\sqrt{E\{\|v(n)\|^2\}}}{\sqrt{E\{\|e(n)\|^2\}}-\sqrt{E\{\|v(n)\|^2\}}} \tag{11}$$

From (11), it can be perceived that the value of a priori error $\boldsymbol{e}(n)$ is very large at the beginning stage of the adaption, and the value of the $E\{\|\boldsymbol{e}(n)\|^2\}$ is large, so the value of $\delta(n)$ is small corresponding to the fast convergence rate. While during the adaptive process $E\{\|\boldsymbol{v}(\mathrm{n})\|^2\}$ is gradually play an important role, the value of $\delta(n)$ increases, of course the coefficients of the adaptive filter start to adjust slowly and convergence rate is steady.

In general, $\delta(n)\ge 0$ because of $||\boldsymbol{e}(n)||>||\boldsymbol{v}(n)||$. When the algorithm begins to converge, the distance between $\|v(n)\|$ and $\|e(n)\|$ will be small and $\delta(n)$ may turn to be negative in reference [11]. So we set $\delta(n)=\delta(n\text{-}1)$ to avoid $\delta(n)<0$. In this paper it will also use the formulas as follows:

$$\begin{cases} E\{\|\mathbf{e}(n)\|^2\}=K\hat{\sigma}_{\mathbf{e}}^2(n) \\ \sigma_x^2(n)\approx\frac{1}{LK}Tr\left\{\mathbf{A}^T(n)\mathbf{A}(n)\right\} \\ \hat{\sigma}_{\mathbf{e}}^2(n)=\alpha\hat{\sigma}_{\mathbf{e}}^2(n-1)+(1-\alpha)\mathbf{e}^2(n) \end{cases} \tag{12}$$

$E\{\|v(n)\|^2\}=K\sigma 2v$, where $Tr\{\cdot\}$ denotes the trace of a matrix, α is a forgetting factor and its value is 0.998.

The steady-state error will be anabatic with the guarantee of variable regularization factor. What's more, there is a fact that fast convergence is our perpetual and unchanging pursuit. The algorithm in this paper will continue to explore the problem of the convergence rate. The larger the projection order is, the faster the convergence will be, but the greater the steady-state error is, the higher the computational complexity will be in APA in reference [22]. Variable order APA adjusts the current order according to the steady-state mean square error, which not only solves the contradiction between convergence rate and steady-state misalignment effectively, but also can reduce the amount of computation greatly in reference [23].

At the beginning of iteration of the algorithm, the order of the input matrix is large to ensure the convergence rate is high. At the Stable stage, the order decreases which can result in less steady-state misalignment and computational cost [24], [25].

If the order is available in APA, we can set the evolving order as K_i at the time i, so the formula should be rewritten as:

$$\delta_{K_n}(n)=\frac{L\sigma_{xK_n}^2(n)\sqrt{E\{\|\mathbf{v}_{K_n}(n)\|^2\}}}{\sqrt{E\{\|\mathbf{e}_{K_n}(n)\|^2\}}-\sqrt{E\{\|\mathbf{v}_{K_n}(n)\|^2\}}} \tag{13}$$

of course the formula has to do a corresponding change when it relates to the order. We will adopt the formula of K_i in [6]:

$$K_n=\begin{cases}\min(K_{n-1}+1,K_{\max}),\eta_n<\mathbf{e}^2(n)\\ K_{n-1},\theta_n<\mathbf{e}^2(n)\le\eta_n\\ \max(K_{n-1}-1,1),\mathbf{e}^2(n)\le\theta_n\end{cases} \tag{14}$$

where η_i is the error limit in the ith iteration process and θ_i is the error floor. The range of K_i presents $1\le K_i\le K_{max}$, K_{max} is the maximum projection order, and $K_{max}\le L$. During the calculation process of the algorithm, the formula of η_i and θ_i also employs the expression in [6], showing as:

$$\begin{cases} \eta_i = \delta_v^2 \dfrac{\mu(i-1)K_{i-1}+2}{2-\mu(i-1)} \\ \theta_i = \delta_v^2 \dfrac{\mu(i-1)(K_{i-1}-1)+2}{2-\mu(i-1)} \end{cases} \quad (15)$$

$\delta 2v$ is the measured noise variance. Actually we call it as "Evolving order with variable step-size affine projection algorithm (EVSAPA)". Considering that the step-size in the proposed algorithm is always 1, so η_i and θ_i can be rewritten as:

$$\begin{cases} \eta_i = \delta_v^2 (K_{i-1}+2) \\ \theta_i = \delta_v^2 (K_{i-1}+1) \end{cases} \quad (16)$$

From the analysis of the algorithm of evolving order, it will be found that there is an important relationship between η_i, θ_i and steady-state misalignment which is relied on the projection order in the meantime. The order of iteration will decrease one to obtain small steady-state misalignment when the output error is less than θ_i. Moreover the order of iteration will plus one to gain fast convergence rate when the output error is more than η_i [26].

As can be seen from the final formula (13), when the state stay in the initial stage of iteration, error is relatively large and regularization factor is high with large order of the algorithm, which results in fast convergence. When the algorithm has converged, the order decreases so that the steady-state misalignment reduces too. Compared to the traditional APA, the order of this algorithm has greater flexibility. At the beginning of the adaption, there is a considerable computational cost in the proposed algorithm just like traditional APA [27], [28], [29]. The computational complexity is $O(K^2L)$ for the traditional affine projection algorithm in one of iterations. The complexity of this algorithm is $O(K^2L)$. But in the adaptation proceeds, the computational cost will be reduced greatly accompanied with the adaption of the order. So the algorithm proposed in the paper shows superiority.

IV. Simulation Results

The voice speech from IEEE-AP database acts as an object of simulation. The effect of echo cancellation and the convergence performance will be compared and analysis with the proposed algorithm and the algorithm in [5], [6]. *SNR*=25dB, α=0.998, μ=1, L=64, the beginning order is 30, and the misalignment will be evaluated by using:

$$MIS = E\left\{\frac{\| \mathbf{w}_{opt} - \mathbf{w}(n) \|^2}{\| \mathbf{w}_{opt} \|^2}\right\}.$$

In order to make the algorithm more persuasive, we consider some simulations. Before using the real speech we consider the AR and ARMA signals which are obtained by filtering a white zero-mean Gaussian random sequence through a first order system the AR(0.8) and ARMA(2, 2) signals whose formulas are $G_1(z)=1/(1-\rho_1 z^{-1})$ and $G_2(z)=(1+0.5z^{-1}+0.81z^{-2})/(1-0.59z^{-1}+0.4z^{-0.2})$ respectively, and ρ_1=0.80. The noise $v(n)$ is white Gaussian.

Fig. 1 shows the speech signal and the near-end speech signal superimposed the analog echo signal. The simulation in Fig. 2 reveals the channel impulse responses whose input signal is far-end speech signal. And the impulse response order is 64.

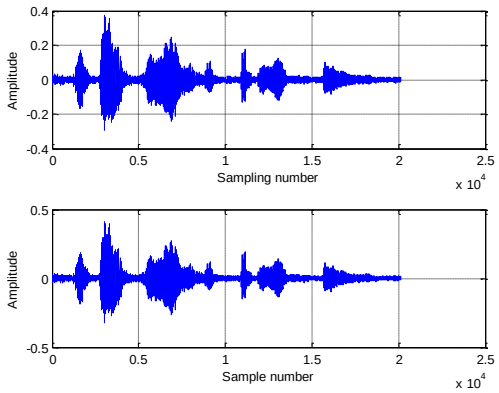

Figure 1. Speech signal and Speech signal coupled with echo signal

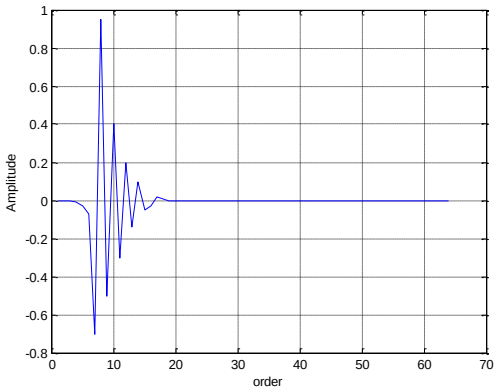

Figure 2. Simulated echo path by using speech signal

Fig. 3 shows the convergence curve of AR (0.8) for three algorithms. It can be seen that variable regularization APA converges quickly compared to evolving order APA, but the magnitude of convergence of variable regularization APA is large. Moreover the convergence rate of the proposed algorithm is faster than algorithms both in [5] and [6]. The steady-state error of the proposed algorithm are both less than the others apparently. In comparison, Fig. 4 shows the algorithm has a faster convergence speed; the steady-state error of the proposed algorithm is slightly worse than the performance in [6] but significantly better than its behavior in [5]. The two simulations of Fig. 3 and Fig. 4 show the superiority of the proposed algorithm.

As is depicted in Fig. 5, there are three convergence curves of the algorithm in this paper and in reference [5], [6]. According to the convergence rate, in the initial stage of algorithm, relatively, the convergence rate is lower in terms of variable regularization in reference [5]. While compared to the evolving order algorithm in reference [6], the proposed algorithm has a slight advantage and a great benefit over the both. However, in the stable stage of

adaption, the magnitude of the convergence curve in reference [5] is higher than the magnitude in reference [6], but both are much lower than the magnitude of the proposed algorithm. Considering the steady-state misalignment, in the entire convergence process, the error in reference [5] tends to be maximum, the error of the proposed algorithm is minimum, and the algorithm is also comparatively stable under the same conditions, which corresponds to a better stability of the system during echo cancellation, the performance and the effect of the echo cancellation is better.

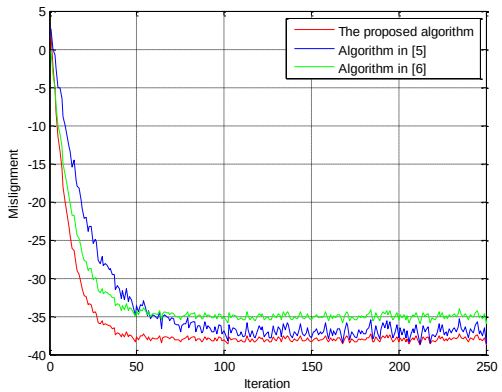

Figure 3. Misalignment for AR (0.8) of the proposed algorithm and algorithm in [5], [6]

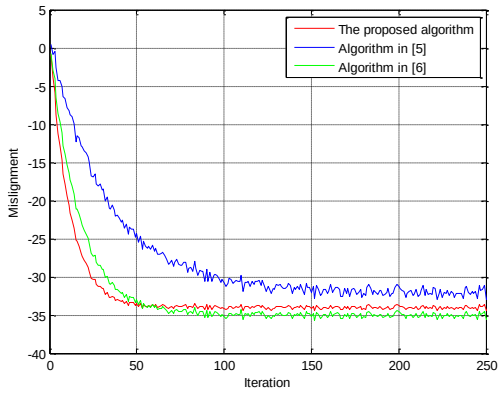

Figure 4. Misalignment for ARMA (2, 2) of the proposed algorithm and algorithm in [5], [6]

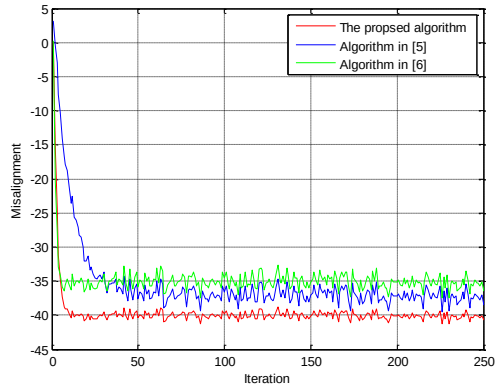

Figure 5. Misalignment for speech signal of the proposed algorithm and algorithm in [5], [6]

Fig. 6 demonstrates the near-end speech signal obtained after the echo cancellation by the way of the variable regularization factor, evolving order and the proposed algorithm, respectively. It can be concluded from the Fig. 6 compared to Fig. 1 that the variable regularization factor algorithm has poor results; the effect of the proposed algorithm is best which is able to get more realistic near-end speech signal.

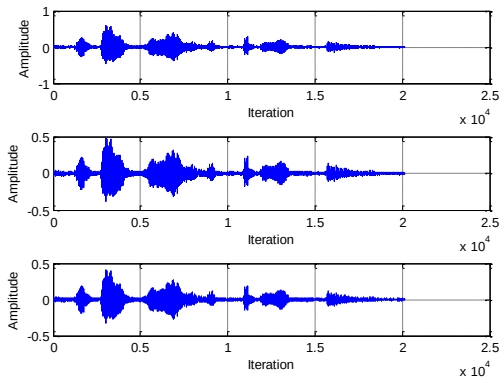

Figure 6. The speech signal after echo cancellation by using the proposed algorithm and algorithm in [5], [6]

V. CONCLUSION

Nowadays along with people's continuously improving requirements on call quality, more and more attention has been paid to the performance of the echo cancellation. Actually APA has a very important position in the echo cancellation. In connection with the status of low convergence and large amount of calculation for the existing APA algorithms, this paper proposes an algorithm combined with variable order and variable regularization factor. The convergence rate has been speeded up by changing the order of the algorithm. And the steady-state misalignment will be reduced by introducing the variable regularization factor during convergence, which makes the algorithm more stable. The method in this paper improves the performance of fast convergence rate and small steady-state error. The simulation results depicted that the algorithm has a good performance in convergence speed, steady-state misalignment and the mount of calculation in echo cancellation, which can better satisfies the needs of the people on the call quality compared with the existing algorithms.

REFERENCES

[1] J. G. Yang, E. Sobelman, "Efficient m-law improved proportionate affine projection algorithm for echo cancellation", *Electronics Letters*, vol. 47, pp. 73-74, January 2011.

[2] Yang Zengli, Y.R. Zheng, S. L. Grant, "Proportionate affine projection sign algorithms for network echo cancellation", *IEEE Trans on Audio, Speech and Language Processing*, vol. 19, pp. 2273-2284, November 2011.

[3] H.-C. Shin, A. H. Sayed, W.-J. Song, "Variable step-size NLMS and affine projection algorithms", *IEEE Signal Processing Letters*, vol. 11, pp. 132-135, February 2004.

[4] H. Rey, L. R. Vega, S. Tressens, et al, "Variable explicit regularization in affine projection algorithm: Robustness issues and optimal choice", *IEEE Trans on Signal Processing*, vol. 55, pp. 2096-2109, May 2007.
[5] Yin Wutao, A. S. Mehr, "A Variable regularization method for affine projection algorithm", *IEEE Trans on Circuits and Systems II: Express Briefs*, vol. 57, pp. 476-480, June 2010.
[6] Seong-Eun Kim, Se-jin Kong, Woo-jin Song. "An affine projection algorithm with evolving order," *IEEE Signal Processing Letters*, vol. 16, pp. 937-940, November 2009.
[7] Jun Xu, Tao Liu, Xiao-dong Gu, "A data selective segment proportionate affine projection algorithm for echo cancellation," *Wireless Communication, Networking and Mobile Computing, 2011 7th International conference on*, pp, 1-4.
[8] Md. Zulfiquar Ali Bhotto, Andreas Antoniou, "Robust set-membership affine-projection adaptive-filtering algorithm," *IEEE Transactions on Signal Processing*, vol. 60, pp. 73-81, 2012.
[9] Diniz P. S. R., Werner S., "Set-membership binormalized data-reusing LMS algorithm," *IEEE Transactions on Signal Processing*, vol. 5, pp. 124-134, 2003.
[10] Werner S., Diniz P. S. R., Moreira J. E. W., "Set-membership Affine Projection algorithm with Variable Data-reuse Factor," *Circuits and Systems, 2006. ISCAS 2006. Proceedings. 2006 IEEE International Symposium on. IEEE*, pp. 261-264, 2006.
[11] Almeida S. J. M., Bermudez J. C. M., Bershad N. J., "A statistical analysis of the affine projection algorithm for unity step size and auto-regressive Inputs," *IEEE Transaction on Circuits and Systems-I: Regular Papers*, vol. 52(7), pp. 1394 -1405, 2005.
[12] Shao T., Zheng Y. R., Benesty J., "An affine projection sign algorithm robust against impulsive interferences," *IEEE Signal Processing Letters*, vol. 17, pp. 327-330, 2010.
[13] Sung Jun Ban, Chang Woo Lee, Sang Woo Kim, "Adaptive regularization parameter for pseudo affine projection algorithm," *Signal Processing Letters, IEEE*, vol. 16, pp. 382-385, 2009.
[14] Shin H. C., Sayed A. H., "Mean-Square Performance of a Family of Affine Projection Algorithms," *IEEE Trans. On Signal Processing*, vol. 52, pp. 90-102, 2004.
[15] Pradhan S. S., Reddy V. U., "A new approach to subband adaptive filtering," *IEEE Trans. on Signal Processing*, vol. 47, pp. 655-664, 1998.
[16] C. Paleologu, J. Benesty, S. CIOCHINA, "Regularization of the affine projection algorithm," *IEEE Trans on Circuits and Systems II: Express Briefs*, vol. 58, pp. 366-370, June 2011.
[17] V. Myllyla, G. Schmidt. "Pseudo-optimal regularization for affine projection algorithms," *Acoustics, Speech, and Signal Processing (ICASSP)*, vol. 2, pp. 1917-1920, June 2002.
[18] Arablouei, R., Dogancay, K., "Affine projection algorithm with variable projection order," *Communication* (*ICC*), 2012 *IEEE international Conference on*, pp. 3681-3685, 2012.
[19] Shin Hyun-Chool, A. H. Sayed, "Mean-square performance of a family of affine projection algorithms," *IEEE Trans. on Signal Processing*, vol. 52, pp. 90-102, January 2004.
[20] Ming Dexiang, Zhong Xiaopeng, Liu Lili, Ma Xiandong, "Design of a reconfigurable platform for navigation signal simulation," *Journal of Networks (JNW)*, vol. 8, pp. 1019-1026, 2013.
[21] J. Benesty, H. Rey, L. R. Vega, et al. "A Nonparametric VSS-NLMS Algorithm," *IEEE Signal Processing Letters*, vol. 13, pp. 581-584, 2006.
[22] T. Aboulnasr, K. Mayya, "Selective coefficient update of gradient based adaptive algorithms," *IEEE Conf Acoust Speech and signal Process*, vol. 3, pp. 1929-1932, 1997.
[23] D. Almeida S. J. M., Bermudez J. C. M., Bershad N. J., "A statistical analysis of the affine projection algorithm for unity step size and auto-regressive inputs," *IEEE Transaction on Circuits and Systems-I: Regular Papers*, vol. 52, pp. 1394 -1405, 2005.
[24] I. Yamada, K. Slavakis, K. Yamada, "An efficient robust adaptive filtering algorithm based on parallel subgradient projection techniques," *IEEE Trans. On Signal Processing*, vol. 50, pp. 1091-1101, 2002.
[25] J. Benesty, H. Rey, L. Rey Vega, S. Tressens, "A non-parametric VSS-NLMS algorithm," *IEEE Signal Processing Letters*, vol. 13, pp. 581-584, 2006.
[26] S. M. Nikjoo, S. M. A. Moghadas, A. Salmanpour, and A. S. Tehrani, "Performance analysis of VS-APA, QR-RLS, and approximated APA on feedback cancellation in hearing aids," *Signal Processing and Information Technology, IEEE International Symposium on*, pp. 737-741, 2007.
[27] K. Ozeki, T. Umeda, "An adaptive filtering algorithm using an orthogonal projection to an affine subspace and its properties," *IEICE Trans*, vol. 67, pp. 19-27, 1984.
[28] Y. S. Choi, H. C. Shin, W. J. Song, "Adaptive regularization matrix for affine projection algorithm," *IEEE Trans. On Circuits Syst. II, Exp. Briefs*, vol. 54, pp. 1087-1091, 2007.
[29] S. J. M. de Almeida, J. C. M. Bermudez, N. J. Bershad, M. H. Costa, "A statistical analysis of the affine projection algorithm for unity step size and autoregressive inputs," *IEEE Trans. Circuits Syst. I, Reg. Papers*, vol. 52, pp. 1394-1405, 2005.

Changpeng Ji received the B.E. and M.S. degrees, in computer engineering from Liaoning Technical University of China, Fuxin, China, in 1993 and 2002. Professor of Liaoning Technical University, master instructor. The main research direction: computer communication & networks, signal detection and estimation, wireless communication.

Honghong Ji (1988-), Huaibei, Anhui Province , student , main research areas: signal detection and estimation. Email: hongji19880610@163.com

Weiping Guo (1987-), Shijiazhuang, Hebei Province, student , main research areas: weak signal detection and estimation. Email: weipingguo1987@sina.com

Jun Wang (1989-), Zaozhuang, Shandong Province, student, main research areas: P2P network. Email: june1016@126.com

Global Trust Value Grading Calculation Method in P2P Network

Min Liu [1, 2*] and Ying Li[3]
1. Changsha Aeronautical Vocational and Technical College, 410014 Changsha, China
2. School of Information Science and Engineering, Central South University, 410083 Changsha, China
3. School of Information Engineering, Jiaozuo University, 454000 Jiaozuo, China
*Corresponding author, Email: liuminei@163.com, 18531390@qq.com

***Abstract*—The paper has proposed that the global situation trust value doesn't depend on any set of high trust nodes in a P2P network environment of grading calculating model. It has given its distributed implementation. This model introduces subtraction clustering method to a large-scale network is logically divided into a number of small networks, and re-organized as overlay network structure of the upper and lower levels, the iterative algorithms in parallel in a small-scale network. Global situation trust value of each node is obtained, the convergence of the iteration level synthesis iterations results. Theoretical analysis and simulation results show that, compared with the existing model, the model has improved greatly reduce the amount of computation and communication overhead, and accelerate the iterative convergence.**

***Index Terms*—Global Situation Trust; Trust Value; Grading Calculation; P2P Network**

I. INTRODUCTION

Since the Peer-to-Peer (P2P) networking technology since the emergence of the concern and has made considerable progress. P2P computing architecture has been widely used in peer collaboration, resource sharing, knowledge management and other fields, such as BitTorrent, eDonkey and other applications have also been a growing number of user groups. In the P2P network, each participate entity (Peer) server role both as a client and play the role of equality between the nodes. P2P network is dynamic, anonymous, self-organization and other characteristics, has brought great convenience to the user. However, it is precisely because of these characteristics, P2P networks there are also a lot of security risks. For example, node status uncertain, nodes represent not only the nodes are free to join or leave the network, each node self-treatment based on different interests interact with other nodes, nodes only enjoy but do not provide services (free-riding), malicious nodes distribute illegal documents, etc. [1]. The root of these security risks is due to lack of appropriate P2P network management institutions, individual behavior of nodes has not been any constraints and limitations. These problems have greatly reduced the user's confidence in the system, hindering the P2P system further promotion. In view of this, the introduction of trust in the P2P network management system, these problems can be largely mitigated the impact [2-5]. Trust mechanism for research in the field of P2P technology has become a hot topic. In short, P2P trust modeling purposes is to use appropriate mathematical model will be a variety of information sources (node transactions direct experience, third-party recommendation information) come together, making the trust mechanism robust to various attacks.

Peer-to-Peer network is an emerging distributed server network model in distributed computing, file sharing, electronic market a wide range of applications [1]. However, there is still a lack of an effective mechanism to improve the global availability of the system, which is very significant ground performance for the application in the presence of a large number of fraud and unreliable service. Kazaa [2] showed that: There is more than 50% of the audio file pollution [3]. Irresponsible users freely file upload service. The quality of service can not get a better guarantee. P2P network environment, it is essential to establish a distributed trust management mechanism, this necessity is reflected not only in the effective use of the users of the P2P network, and is also reflected in the favor of the benign development of the network.

Trust value is to believe in each other, said one node to another node's credibility, honesty judgment. Global situation trust based on a combination of individual trust established generally trust the judgment of the entire network of groups of nodes. Global situation trust more meaningful than the individual trust. The individual global situation trust model can effectively curb the node deception and a small portion of nodes collaborative cheating the strong robust, and therefore more suitable for P2P network. However, when the network size is large, the existing global situation trust model computation and communication overhead are large, the impact of the application of the model and promotion. This paper aims to construct the global situation trust model does not rely on any high-confidence set of nodes in a P2P environment, and propose a global situation trust value grading calculation method based on the introduction of subtractive clustering algorithm effectively reduce global situation trust value computation and communication overhead.

Trust and credibility so far no accepted strict definition. Typically, the trust said that interactions exist between entities behavioral expectations, is relatively subjective.

doi:10.4304/jnw.9.1.216-222

Reputation is a combination of more than one entity trust information. P2P network trust model has achieved some results. The existing trust model, based on the reputation of trust researchers modeling is more than concerned about the direction of the branch. It mimics the human society, the idea of building trust. For any node i, node i's trust model based on historical transactions and other nodes of its evaluation, as i assign a reputation value, making the other nodes reputation value of i can decide whether their transactions.

As far as we known, EigenTrust [4] global situation trust model is the first P2P network environment, it is proposed by Stanford University in 2003, also known as EigenRep. It is the cornerstone of the global situation trust model. Subsequent global situation trust model mostly has based on EigenTrust model improvements, such as PeerTrust [5] and SWRTrust [6]. They are mainly to improve the model trust relationship the reasonable expression as well as the security of the model itself, very little analysis of the global iteration algorithm computation and communication overhead. Reference [7] and [8] studies have shown that P2P network traffic already accounts for the largest portion of global Internet traffic, P2P networks is an urgent need to reduce the additional communication overhead. Therefore, the global situation trust model while trying to curb the bad behavior of malicious nodes, but also to solve the key issues is how to reduce global iteration algorithm for the calculation of the amount of communication overhead.

EigenTrust assuming a fixed trusted node set P (such as early users and moderator) exists in the network, in the system the initial state, and they have a high global situation trust value, while the other nodes in global situation trust values are both zero . Recommended more reliable global model global situation trust value node principle, the recommendation of the high trust nodes in the global situation trust account for a large weighting in the synthesis, which makes distributed the iterative convergence faster [9]. However, this assumption is reasonable debatable, because this assumption essentially makes some nodes have the privilege of "innate", similar to the network in the presence of a trusted third party, P2P networks exclusion of such programs, at the same time specify which nodes set P is a difficult operation.

PowerTrust [10] on in EigenTrust foundation proposed a dynamic election m the very trusted node (PowerNodes) algorithm, these m PowerNodes replace P in EigenTrust collection. As PowerNodes election is dynamic rather than fixed specified in line with the actual situation of P2P networks. In but election of m PowerNodes is a based on the nodes in the amount of feedback into curtain law distribution of this fact, the statistics of the amount of feedback provided by each node to the network, you need to construct a trust covering network, dynamic collection of feedback for each node distributed sort, to take the very top of the m^{th} node. The algorithm itself adds additional network communication overhead and computation.

In response to these problems, the paper constructs a non-dependent on any set of high trust nodes global situation trust value grading computing model. Global iteration algorithm for the calculation of the amount of communication overhead is very sensitive to the characteristics of the network size, use subtractive clustering algorithm, based on the node physical distance proximity to large-scale P2P network is logically divided into a number of small-scale network, and then organize them into a grading hybrid unstructured overlay networks, similar to Kazaa, iterative algorithm in a small area. Global situation trust value of each node is obtained, then the convergence of the iteration level synthesis iterations results. Theoretical analysis and simulation results show that, compared to the previous model, the model in the large-scale network there is a large degree of improvement in the computation and communication overhead.

II. Global Situation Trust Value Grading Computational Model

A. The Basic Concepts

Definition 1: Indirect trust called Recommended trust between nodes indirect Recommended by others.

Definition 2: The definition of global situation trust is a trust of the entire network groups on a node, t_i global situation trust value of i node.

Definition 3: Local trust also known as direct trust is a trust node to another node derived based on the history of direct interaction behavior, judgment on the basis of their own knowledge and experience. The s_{ij} said node i the node local trust value j in, the s_{ij} normalized local trust value, with r_{ij} said.

Definition 4: The tuple of $\langle B_{ij}, G_{ij} \rangle$ node i to node j, B_{ij} and G_{ij} node i is satisfied with the evaluation of the number of nodes j accumulated historical transactions and not satisfied with the evaluation of the number, is also retained in the local history.

B. The Calculation of Local Trust Value

The previous model [4, 5, 6, 10] in the local trust value is calculated using the following formula:

$$s_{ij} = B_{ij} - G_{ij}, r_{ij} = \frac{\max(s_{ij}, 0)}{\sum_j \max(s_{ij}, 0)}$$

However, the method cannot been distinguished between satisfactory number of evaluations of B_{ij}, and dissatisfaction evaluation is equal to the number of times G_{ij} and not zero, or both to zero, and the former is smaller than the latter three cases. In other words, when the node j shared resources, and provides services for node i or node j does not share any resources, do not provide any services (called free riding, free-rider), or provide full service for leave, node i r_{ij} of the local node j trust value is zero. Principle deviates from P2P network to encourage the sharing of resources (even if some fake resources) in combating free riding [11]. P2P

network nodes are free to ride. The network does not have the resources, the loss of the meaning of existence. In this paper, the inadequacies of a new local trust value are calculated as follows:

$$s_{ij} = h\left(1-\exp\left(-B_{ij}\right)\right)\exp\left(-G_{ij}\right)+\varepsilon \tag{1}$$

$$r_{ij} = w\frac{s_{ij}}{\sum_{j=1}^{n} s_{ij}}+(1-w)\frac{1}{n} \tag{2}$$

where in exp() is the exponential function; h is the amplification factor, can be any of a larger number, located here $h=1000$; n the total number of network nodes; ε is a small number, can be set of $\varepsilon=10^{-5}$; w is the weighting factor, generally Let $w=0.9$, i.e. node i 90% of the established trust based on the interaction history Credits; while there is no interaction history, node i to each node only average trust value, model average trust value for a given value of the 10% confidence level. ε in equation (1) generally do not have influence, but when node i do not interact with any node in the network, node i give without any evaluation of such nodes is called a lazy node. At this time, by the formula (1) and formula (2), can be obtained: $s_{ij}=\varepsilon, r_{ij}=1/n$; That is, in this case the node i to each node in the network (including their own) an average trust value. After such treatment: $0<r_{ij}\le 1$; and when i is fixed for any j: $\sum r_{ij}=1$, apparently matrix $R=\left(r_{ij}\right)$ is a random matrix to ensure after the iterative convergence (See section D).

C. The Calculation of Global Situation Trust Value

Distributed implementation and security issues are discussed in Section 4, in order to make the mathematics of the model to describe more clearly, in this section assumes that all nodes are aware of the whole network computing work like a central server. The same time, the assumption has been proposed clustering algorithm clusters network nodes by physical distance proximity clustering, and to determine the center of each cluster node. Logic, the entire network to form a mixed upper and lower levels of unstructured overlay networks, an iterative algorithm in parallel network of small-scale, the entire calculation process is as follows:

(1) The calculation of the trust value of the underlying network node cluster within any cluster c_v.

$t_{c_{v_i}}$ denote any node $i\in c_v$ clusters trust value within the cluster c_v, $r_{c_{v_{ij}}}$ any node $i\in c_v$ the standardization forms of local trust value of any node $j\in c_v$.

$$r_{c_{v_{ij}}} = w\frac{s_{ij}}{\sum_{i,j\in c_v} s_{ij}}+(1-w)\frac{1}{|c_v|} \tag{3}$$

$$t_{c_{v_i}} = \sum\nolimits_{j\in c_v}\left(r_{c_{v_{ji}}} t_{c_{v_j}}\right) \tag{4}$$

(2) The upper network cluster global situation trust value relative to the whole network.

$s_{c_v c_u}$ for any cluster c_v any cluster the c_u the local trust value, standardized in $r_{c_v c_u}$, $c_v\cap c_u=\phi$; t_{c_v} said c_v global situation trust value; t_{c_u} cluster the c_u global situation trust value.

$$s_{c_v c_u} = \sum_{i\in c_v, j\in c_u} s_{ij} \tag{5}$$

$$r_{c_v c_u} = w\frac{s_{c_v c_u}}{\sum_{c_u} s_{c_v c_u}}+(1-w)\frac{1}{|c|} \tag{6}$$

$$t_{c_v} = \sum_{c_u}\left(r_{c_u c_v} t_{c_u}\right) \tag{7}$$

(3) More than two layers of the calculations were carried out in parallel until they converge, level synthesis each node based on the network-wide global situation trust value. Global example of any node $i\in c_v$ trust value:

$$t_i = t_{c_v} t_{c_{v_i}} \tag{8}$$

Be seen from the above calculations, iterative algorithm in a small-scale network, any node i's global situation trust value t_i embodies the comprehensive evaluation of the entire network groups of nodes i.

D. Convergence of Iterative Algorithm

Related by the Markov chain theory shows that: a line $n\times n$ random matrix can be used as an n-state Markov chain transition probability matrix. According to the above equation shows that certain matrix R, R_c, etc. are OK random matrix, can be used as a finite state Markov chain transition probability matrix, its own specific set of states that all nodes in the network. In EigenTrust and PowerTrust model, the presences of high-trust node set not only accelerate the iterative convergence speed, but also to ensure the finite-state Markov chains with a non-periodic, irreducible properties. In this model, these two characteristics by a local trust value constructor to be guaranteed. It is worth noting that the introduction of clustering method does not affect the convergence of Markov chain, so the following only discuss the case of the network in the absence of clustering convergence. According to the formula (1) and Equation (2) shows that: the Markov chain transition probability matrix R, there is no absorbing state, each state to any other state has a transition probability, and vice versa. At the same time it also has its own transition probability. Corresponds to the transition probability matrix R has a finite-state Markov chain is irreducible, aperiodic properties. Therefore, it is ergodic, and there must be a unique stationary distribution.

III. DISTRIBUTED IMPLEMENTATION STRATEGY

A. The Network Clustering Layered Security Access Measures

Subtractive clustering method [14] is a fast and effective method used to estimate the number of categories and cluster centers will each data point as a potential cluster centers, and is calculated based on the density of the data points around each data point the point as to the possibility of the cluster center. It requires only a relative distance between any two points, without having to know the absolute coordinates of the data points in the coordinate space. In a network environment, the relative distance between the nodes can be measured by sending a probe message. The assumption underlying network (Internet) using the shortest path routing protocol, will be able to reflect the actual distance of the physical layer network IP layer routing hops. The design of a message referred to as a detector (detector), is sent by the source node to the destination node, the statistical via path hops. The destination node hops extracted from the message, it has been the distance between two nodes, and vice versa. Thus, each node knows the distance to other nodes (hop count). Therefore, the introduction of P2P network clustering grading subtractive clustering method based on node distance proximity is entirely feasible. In particular, if the network size is large, excessive each cluster nodes can be used recursively subtraction clustering algorithm, the network is divided into multi-layered, but pay attention to adjust the parameters of each layer clustering algorithm. The calculation method is similar to grading calculation of the multi-layer network with two network classification. This paper only describes the global situation trust value of the two-tier network classification calculated. According to the reference [14], can be easily distributed subtractive clustering algorithm design suitable for a P2P network, not described in detail here.

In the P2P node high degree of autonomy under the distributed environment, you need to have the centralized data management solutions to achieve secure storage and query of the node global situation trust value. Global situation trust value storage should be such that any node i limited overhead ready access to other nodes j current global situation trust value t_j . However, t_j placed in node j itself or let node j of their choice to place the nodes are not desirable, which may lead to fraud. One possible way is through distributed hash list (DHT) [15] mechanism for node assign one or more global situation trust value management node, is responsible for the storage and computing global situation trust value of the node simultaneously submit to the other nodes in the query global situation trust value and associated data of the management node. This article is based on the Chord protocol [16] for the network each node configuration management node. Chord protocol, a node i only managed node M_i , but an arbitrary node j may serve several nodes of node management. According to the reference [16] discusses seen, Chord protocol to ensure that: 1) the management node of any node i M_i can not know the physical address of the node i ; 2) any node i can not select i own identity, so that it just is the logical address of a node in the Chord network management node j . It is worth noting that the subtractive clustering algorithm based on distance proximity Chord protocol storage global situation trust value is not contradictory, but requires that each node maintain two simultaneous overlay network protocols.

B. Global Situation Trust Value Distributed Algorithm

The network above Clustering hierarchy, each node knows the central node of the cluster. Since the introduction of security mechanisms, each node has two roles, both general user node, and the management node of the other nodes. When node i as a normal user, only calculate local trust value, the calculated results to the management node M_i ; computing cluster node cluster node i as the management node, which in conjunction with other management nodes within the cluster trust value; particular, when the node i is the cluster center node, in addition to its involvement in the above two calculation, but also participate in the calculation of the upper level network, it is representative of the present cluster, in conjunction with other cluster center node calculation of all the clusters of the global situation trust value. The specific algorithm of distributed system initial setting is described in Section C of III.

Algorithm 1: The management node within any cluster c_v collaborative computing the trust value of the cluster known as node cluster.

BottomValue( )
{ For any p-management node i do
Send s_{ij} to x_v of the cluster c_v ;
According to formula (3) calculated $r_{c_{v_{ij}}}$;
Send $r_{c_{v_{ij}}} t_{c_{v_i}}^{(k)}$ to $M_j \in c_v$;
End for
Repeat
For any p-management node i do
Wait for all $M_j \in c_v$ return $r_{c_{v_{ji}}} t_{c_{v_j}}^{(k)}$;
According to formula (4) calculated $t_{c_{v_i}}^{(k+1)}$;
Send $r_{c_{v_{ij}}} t_{c_{v_i}}^{(k+1)}$ to $M_j \in c_v$;
End for
Until $\forall i \left| t_{c_{v_i}}^{(k+1)} - t_{c_{v_i}}^{(k)} \right| < \varepsilon$ }

Algorithm 2: Any node i calculate local trust value

LocalValue( )
{ if Node i and node j trading success then
$B_{ij} = B_{ij} + 1;$
Else
$G_{ij} = G_{ij} + 1;$
Endif
According to the formula (1) calculated s_{ij} ;
Send the message (s_{ij}, i, j) to M_i ;
}

Algorithm 3: Management node p to the cluster center of each cluster within any node joint global situation trust value computing nodes

GlobalValue( )
{ if $p \in c_v$ then

Query clusters c_v 's node to t_{c_v} ;

For any p-management node i do

$t_i = t_{c_v} t_{c_{v_i}}$;

End for

Endif

}

Algorithm 4: Management node of the cluster center collaborative computing cluster global situation trust value

TopValue( )

{ Calculated $s_{c_v c_u}$ according to the formula (6);

Calculated $r_{c_v c_u}$ according to the formula (7);

Send $r_{c_v c_u} t_{c_v}^{(k)}$ to the center node for all other clusters;

Repeat

Waiting for all other cluster center node returns $r_{c_u c_v} t_{c_u}^{(k)}$;

Calculated $t_{c_v}^{(k+1)}$ according to the formula (8);

Send $r_{c_v c_u} t_{c_v}^{(k+1)}$ to the center node for all other clusters;

Until $\left| t_{c_v}^{(k+1)} - t_{c_v}^{(k)} \right| < \varepsilon$ }

IV. Simulation and Results Analysis

Query Cycle Simulator open source package [17] and PeerSim open source software packages, and then add some code to achieve a model of this paper, EigenTrust model as well as a simple model. In a simple model, the local trust value calculated using formula (1) and (2), the global situation trust value calculated using the full network of EigenTrust model iterative method, setting α=0, i.e. excluding high trust nodes collection. The simulation experiments on a 2.6GHz CPU, 2048MB RAM of computer, simulation-based Java implementation. In the simulation of the stand-alone, DHT mechanism can be simplified and each node of the management node is any node randomly assigned.

Query Cycle Simulator software is able to emulate the typical peer-to-peer file-sharing networks, and trusted computing basic functions. PeerSim a framework-simulation platform contains many popular components. Meanwhile, any software can be added to the platform, as its components. User has making a plain text configuration file to call the number of components to complete the simulation task. Structured P2P network and unstructured P2P networks can be simulated on this platform. Components which generate a scale to 10,000 nodes and curtain regular topology of the network, and then randomly select n ($n \le 1000$) from which the nodes form a P2P file sharing network. Assumes that the file-sharing network is ideal, any node can find any file their claims that all nodes of the owner of the file (the file may not be true); the node behavior than simple, that is, from all claim to have the documents they need node choose the highest value of global situation trust node download.

A. Simulation and Analysis of Successful Download Rate

Successful download rate (η) is the ratio of normal node successfully downloads all downloads total normal nodes. It directly reflects the effect of the trust model application. The experimental network size is 100 nodes and simulation of 10 cycles. After the end of every period, according to the B_{ij} and G_{ij} calculation file successfully download rate $\eta = \left(\sum B_{ij}\right) / \left(\sum \left(B_{ij} + G_{ij}\right)\right)$, simulation results are shown in figure 1. Random model is the model does not use any trust mechanism, the requesting node each randomly select response nodes as download source.

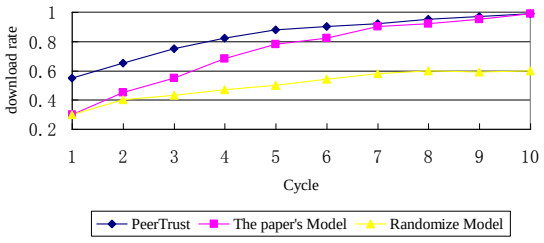

Figure 1. Download rate changes in the law with the simulation cycle

The EigenTrust model present high trust nodes, but also as a download source node always choose the highest trust value of the node, so EigenTrust model there is a higher simulation initial success download rate. Our model does not have any high-confidence set of nodes, initially equivalent stochastic model. However, only 10 simulation cycles our model will be able to achieve the same success with EigenTrust model download rate (98%). Be seen, our model even though no high trust node set, can also be identified within a very short time malicious nodes ensure that the normal node has a high success download rate.

B. The Convergent Speed Simulation and Analysis

If a node's global situation trust value converges in a desired manner, then either takes the normal node i and a malicious node j, i of global situation trust value is greater than j, the global situation trust value established with high probability. Node is always selected for the highest value of global situation trust node downloads as the simulation proceeds, the number of failure in the network to download gradually closer to 0, the successful download rates gradually close to 100%. Different network size, simulation test simulation time when the normal node successfully download rate of 99% consumed by the various models, in seconds, the simulation results shown in figure 2 below.

In EigenTrust model, the high-trust node sets accounted for 10% of the total number of normal nodes, and its credibility as high as 60%, the simulation results show that: the high trust nodes set to accelerate the iterative convergence, the simulation time than the simple model by many. Although our model does not have any high trust node set, but due to network clustering grading iteration within a small range, each iteration required fewer multiplication operation, and all clusters (comprising a central node within the cluster) iterative calculation are all parallel, thereby greatly reducing the total running time and improve the convergence speed of the model. When the network size of 1000 nodes, our model has only takes 725s, apparently iteration convergence soon.

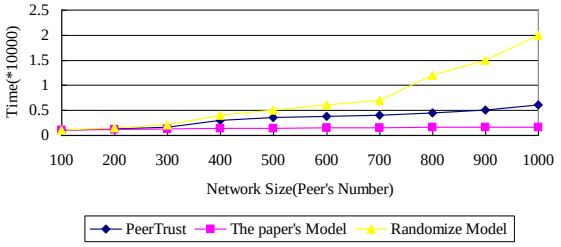

Figure 2. Various models of simulation time under different network size

C. Simulation and Analysis of Communication Overhead

On simulation PeerSim platform, the communication overhead only have to all messages through the path of the total number of hops. Under different network size, when the normal node successful download rate reached 99%, the total number of hops simulation test various trust model message experienced path, the simulation results shown in figure 3.

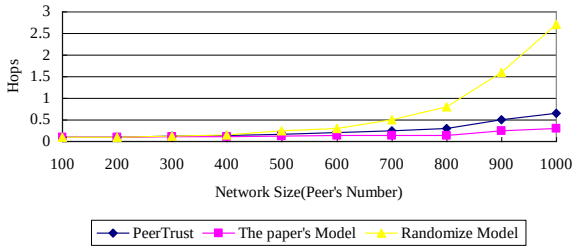

Figure 3. All kinds of different network size model of communication overhead

The total numbers of hops of the simple model with the network scale growth quickly, indicating that such models may be poor scalability. EigenTrust model in the initial network of smaller, small average path length, a small number of messages, but as the network size increases, the average path length increases, the total number of messages increased, so that the message the total number of hops faster growth. Introduction of our model clustering layered approach, distributed iteration only in a small range within the cluster, the average path length is reduced, the fewer the number of messages, the messages reduces the total number of hops. When the network size of 1000 nodes, total hops 3.81×10^7, almost half of EigenTrust traffic shows that our model is highly scalable.

D. The DownloadSpeed Simulation and Analysis

In the download Experiment, Gnutella protocol as the basis for evaluation, where the type of service nodes are file downloads, no need to consider the type of trust between nodes.

There are 20,000 files randomly distributed in 2000 nodes, each node is assigned 200 mutually different files. These nodes are both resource requester, but also the resource provider. Requesting node intervals file message request, the new node in the initial trust value $[-1,1]$ generated between high confidence assume that the network nodes in the ratio of 70%. With the operation of the system between nodes reputation value depends only on the historical transaction information.

In this experiment, only consider the resource provider behavior on the impact of the download process, ignoring other factors. Determine whether a transaction is the only criterion of success authenticity of the downloaded file, the following four aspects were simulated from realized PeerTrust Model, Randomize Model and the Paper's Model.

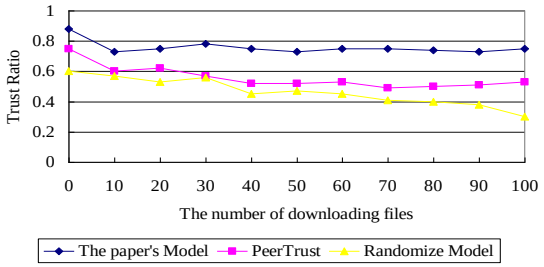

Figure 4. Trust relationship diagram node ratio

Figure 4 represents a node in response to a request to provide a ratio occupied trusted resource nodes. Experimental results show that the algorithm is based on trust perception downloaded resources to ensure more reliable by a trusted nodes.

In the experiment of figure 5, the malicious nodes are in proportion 10%, 20%, 30%, 40%, 50%. The results show that the perception of trust-based search algorithm, even when the proportion of malicious nodes is 50% of the cases, is still a relatively high percentage can be downloaded to a trusted file.

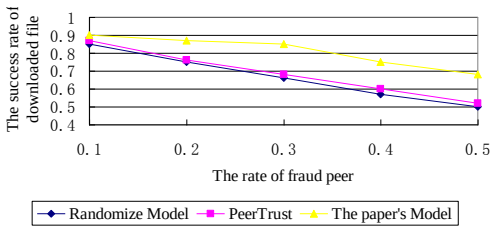

Figure 5. Fraud node and success ratio diagram download file

Figure 6 is a comparison of the success rate of resource search. Three curves undulating, relatively close, indicating that the perception of trust-based search algorithm to ensure the success rate of resource discovery, with good usability.

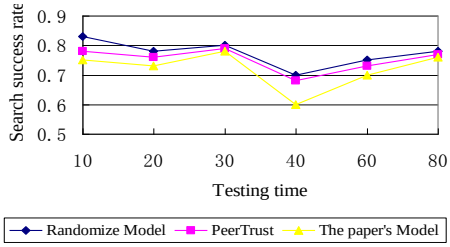

Figure 6. Resource search success rate

Figure 7 is a comparison of the load system messages. Indicates the system if there are 10, 20, 30, 40, 50, 60, 70,

80, 90, 100 nodes simultaneously send a query, then the system message payloads. The results show that the perceptions of trust-based search algorithms on multiple nodes simultaneously send the resource request in the case greatly reduces the load on system messages and enhanced system scalability.

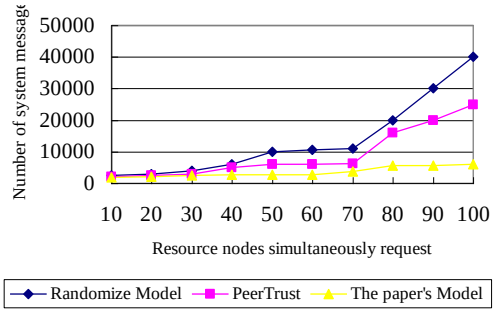

Figure 7. Load comparison system messages

V. CONCLUTIONS

This paper constructs a global situation trust model is not dependent on any set of high trust nodes introduced subtractive clustering method based on the calculation method of the classification of a global situation trust value and gives the mathematical description of the model and the distribution style. Simulation results show that, in large-scale P2P network environment, our model can not only ensure high download rate of normal nodes, but also significantly reduces the computation and communication overhead solving global situation trust value.

How to consider the sudden failure and node dynamically join and leave the iteration is the next step in the process of solving global situation trust value. In the use of the global situation trust value, we always choose the highest trust value node download easily cause load imbalance, a hot spot phenomenon, and vulnerable to a distributed denial of service (DDOS) attacks. Previous model proposed global situation trust value is proportional to the probability to choose to download the source, but we do not agree with this method, because it in a sense and allows low trust value of the node providing false documents to the trust mechanism had a negative impact. How to use the copy of the copy made structure trust-aware adaptive topology network is the next step to solve the problem of the node load imbalance trust mechanism.

REFERENCES

[1] Granville L Z, Rose D M, Panisson A, et al, "Managing computer networks using peer-to-peer technologies," *IEEE Communications Magazine*, vol. 43, no. 10, pp. 62-68, 2005.
[2] Kazaa(EB/OL). http://www.kazaa.com/, 2006.
[3] Liang J, Kumar R, Xi Y, et al, "Pollution in P2P file sharing systems," *In Proceeding of the IEEE Infocom, Taiwan*, pp. 1174-1185, 2005.
[4] Kamwar S D, Schlosser M T, Garcia-Molina H, "The EigenTrust algorithm for reputation management in P2P networks," *In Proceeding of the 18th International World Wide Web Conference, Budapest, Hungary*, pp. 640-651, 2009.
[5] Xiong L, Liu L, "PeerTrust: supporting reputation-based trust for peer-to-peer electronic communities," *IEEE Transactions on Knowledge and Data Engineering*, vol. 16, no. 10, pp. 843-857, 2004.
[6] Li J T, Jing Y N, Xiao X C, et al, "A trust model based on similarity-weighted recommendation for P2P environments," *Journal of Software*, vol. 18, no. 1, pp. 157-167, 2007.
[7] Saroiu S, Gummadi K P, Dunn R J, et al, "An analysis of Internet content delivery systems," *In Proceedings of the 5th Symposium on Operating Systems Design and Implementation, Association*, pp. 315-327, 2002.
[8] Sen S, Wang J, "Analyzing peer-to-peer traffic across large networks," *IEEE Transactions on Networking*, vol. 12, no. 2, pp. 219-232, 2004.
[9] Zhou R, Hwang K, "PowerTrust: a robust and scalable reputation system for trusted peer-to-peer computing," *IEEE Transactions on Parallel and Distributed Systems*, vol. 18, no. 5, pp. 460-473, 2007.
[10] Hughes D, Coulson G, Walkerdine J, "Free riding on Gnutella revisited: The bell tolls?," *IEEE Distributed Systems Online*, vol. 6, no. 6, pp. 1-18, 2005.
[11] Feldman M, Papadimitriou C, Chuang J, et al, "Free-riding and whitewashing in peer-to-peer systems," *IEEE Journal on Selected Areas in Communications*, vol. 24, no. 5, pp. 1010-1019, 2006.
[12] Kamvar S D, Haveliwala T H, Manning C D, et al, "Extrapolation methods for accelerating PageRank computations," *In Proceedings of the 12th International World Wide Web Conference*, New York, pp. 261-270, 2003.
[13] Chen J Q, Xi Y G, Zhang Z J, "A clustering algorithm for fuzzy model identification," *Fuzzy Sets and Systems*, vol. 98, no. 3, pp. 319-329, 1998.
[14] Ratnasamy S, Shenker S, Stoica I, "Routing algorithms for DHTs: Some open questions," *In Proceedings of the 1st International Workshop on Peer-to-Peer Systems*, Cambridge, pp. 45-52, 2001.
[15] Stoica I, Morris R, Karger D, et al, Chord: a scalable peer-to-peer lookup service for Internet applications [EB/OL]. http://www.pdos.lcs.mit.edu/chord/papers,2001.
[16] Schlosser M T, Condie T E, Kamwar S D, "Simulating a file-sharing P2P network," *In Proceedings of the 8th Workshop on Semantics in P2P and Grid Computing*, pp. 69-80, 2009.
[17] PeerSim P2P simulator [EB/OL]. http://peersim.sourceforge. net/, 2006.

Min Liu, born in 1972, received his B.S. degree in material science from Wuhan University of Technology, Wuhan, China in 1995, his M. S. degree in computer science and technology from National University of Defense Technology, Changsha, China in 2001. He is an associate professor at Changsha Aeronautical Vocational and Technical College, Changsha, China. His current research interests include Wireless Sensor Networks security and Application of Database.

Ying Li, born in 1977, received her B.S. degree in application of electronic technology from Xinyang Normal University, Xinyang, China in 2001. Her current research interests include Artificial Intelligence and Networks Security.

The PeerBehavior Model based on Continuous Behavioral Observation P2P Network Neighbors

Xianwen Wu [1*], Zhiliang Xue [1], and Jingwen Zuo [2]
1. Department of Information Engineering, Hunan Railway Professional Technology College, Zhuzhou 421001, China
2. Computer Center, College of ChengNan, Changsha University of Science & Technology, Changsha 410076, China
*Corresponding author, Email: 252167977@qq.com, 780186029@qq.com, zojw@qq.com

***Abstract*—Honor-based trust mechanism is an important means to evaluate the behavior of the P2P network node, and it is used to ensure the health of the P2P network application. Trust mechanisms need to evaluate a node to other node local trust value and local trust value because they do not consider the policy node and human evaluation error of two important factors. The calculation is difficult to accurately reflect the characteristics of the nodes of the network. Evaluation models of the behavior of a P2P network neighbor. The PeerBehavior model has used a deterministic finite state machine (DFA) depicts the continuous behavior of the neighbor state changes cause a negative evaluation of any continuous behavior by focusing neighbors almost died, both able to more accurately discover policies node in the network, but also be able to tolerate a certain degree of human evaluation error simulation experiment showed that this model was significantly improve the accuracy of the local trust value, and reducing the estimation error of the global trust value, was significantly superior to the calculation method of the current value of the other local trust.**

***Index Terms*—P2P Network; Trust Mechanism; Reputation; Strategic Peer; Human Judgment Error**

I. INTRODUCTION

Peer-to-peer (P2P) online communities can be seen as truly distributed computing applications in which peers (members) communicate directly with one another to exchange information, distribute tasks, or execute transactions. They can be implemented either on top of a P2P network [1] or using a conventional client-server platform. Gnutella is an example of P2P communities that are built on top of a P2P platform. Person-to-person online auction sites such as eBay and many business-to-business (B2B) services such as supply-chain-management network are examples of P2P communities built on top of the client-server architecture. In eCommerce settings P2P communities are often established dynamically with peers that are unrelated and unknown to each other. Peers have to manage the risk involved with the transactions without prior experience and knowledge about each other's reputation. One way to address this uncertainty problem is to develop strategies for establishing trust and develop systems that can assist peers in assessing the level of trust they should place on an E-Commerce transaction. For example, in a buyer-seller market, buyers are vulnerable to risks because of potential incomplete or distorted information provided by sellers. Trust is critical in such electronic markets as it can provide buyers with high expectations of satisfying exchange relationships.

Recognizing the importance of trust in such communities, an immediate question to ask is how to build trust. There is an extensive amount of research focused on building trust for electronic markets through trusted third parties or intermediaries [7]. However, it is not applicable to self-regulating P2P communities where peers are equal in their roles and there are no entities that can serve as trusted third parties or intermediaries. Reputation systems provide a way for building trust through social control by utilizing community-based feedback about past experiences of peers to help making recommendation and judgment on quality and reliability of the transactions. The challenge of building such a reputation based trust mechanism in a P2P system is how to effectively cope with various malicious behavior of peers such as providing fake or misleading feedback about other peers. Another challenge is how to incorporate various contexts in building trust as they vary in different communities and transactions. Further, the effectiveness of a trust system depends not only on the factors and metrics for building trust, but also on the implementation of the trust model in a P2P system. Most existing reputation mechanisms require a central server for storing and distributing the reputation information. It remains a challenge to build a decentralized P2P trust management system that is efficient, scalable and secure in both trust computation and trust data storage and dissemination. Lastly, there is also a need for experimental evaluation methods of a given trust model in terms of the effectiveness and benefits.

With the increase of P2P network, P2P applications gradually occupy the majority of network traffic [1], and because some of the characteristics of P2P networks, such as various forms of malicious nodes distributed, anonymous network affected development of many applications, especially in large-scale P2P E-Commerce applications. malicious node trying to deceive other nodes in order to achieve the purpose of profit or damage the system, so how to evaluate the node in the P2P network, in particular, to distinguish the malicious node is crucial.

doi:10.4304/jnw.9.1.223-230

Honor-based trust mechanism proved to be an effective means to solve the above problems, and recently on eBay trust mechanism. A user feedback system is one hundred and eleven studies that [2-3]. Positive feedback increases the seller's revenue, while negative feedback reduces their income. Currently the most trust mechanisms are provided by the node local trust value, the use of certain methods to calculate the global trust value, and thus the local trust value accurate or not greatly affect the accuracy of the global trust value [4].

Local trust value calculation method, such as the simple average [5], a moving average [6], Bayesian learning [7], unable to prevent the destruction of strategic node, these strategies node every certain number of transactions of honest deception remains will get a higher local trust value, and thus be able to hide the node type.

In this paper, a the neighbor behavior evaluation model PeerBehavior the model by the observation of the continuous behavior of neighbors, concerned about the neighbors, the probability of negative evaluation, taking into account node evaluation error caused in any consecutive trading, which can help a more accurate evaluation of node neighbor's behavior. The experimental results show that, compared to PeerBehavior and other methods can significantly improve the accuracy of the trust value in the local estimation error, thereby reducing the global trust value caused by inaccurate due to the value of the local trust.

Reputation-based trust research stands at the crossroads of several distinct research communities, most notably computer science, economics and sociology. We first review general related reputation research E-Commerce and agent systems and then review a number of recent works on reputation based systems in P2P networks.

Dellarocas [12] provides a working survery for research in game theory and economics on the topic of reputation. Mui et al. [2] also give a review summarizing existing works on reputation across diverse disciplines including distributed artificial intelligence, economics, and evolutionary biology. The game theory based research [14] lays the foundation for online reputation systems research and provides interesting insight into the complex behavioral dynamics. Most of the game theoretic models assume that stage game outcomes are publicly observed. Online feedback mechanisms, in contrast, rely on private (pair-wise) and subjective ratings of stage game outcomes. This introduces two important considerations, the incentive for providing feedback and the credibility or the truthfulness of the feedback [8].

A number of reputation systems and mechanisms were proposed for online environments and agent systems. Abdul-Rahman et al. [15] proposed a model for supporting trust in virtual communities, based on direct experiences and reputation. They introduced the semantic distance of the ratings. However, there are certain aspects of their model that are ad-hoc, such as the four trust degrees and fixed weightings assigned to the feedback. Pujol et al. [6] applied network flow techniques and proposed a generalized algorithm that extracts the reputation in a general class of social networks. Josang et al. [7] developed and evaluated the beta reputation system for electronic markets based on b distribution by modeling reputation as posterior probability given a sequence of experiences. Among other things, they showed that a market with limited duration rather than infinite longevity of transaction feedback provides the best condition. Sabater et al. [3] proposed regret system and showed how social network analysis can be used in the reputation system. Sen et al. [11] proposed a word-of-mouth reputation algorithm to select service providers. Their focus is on allowing querying agent to select one of the high-performance service providers with a minimum probabilistic guarantee. Yu et al. [9] developed an approach for social reputation management and their model combines agents' belief ratings using combination schemes similar to certainty factors. The reputation ratings are propagated through neighbors.

Managing Trust [8] is the first P2P network trust management based on the honor system, since the research community many honors management mechanisms, such as PeerTrust [4], EigenTrust [5], PowerTrust [9], GossipTrust [10] and the literature [11]. Most honor-based trust management systems are dependent on local trust value of each node to calculate the value of global trust. Far as we know, there are three categories of local trust value calculation. They are a simple average moving average and Bayesian learning methods.

The simple average method is the simple sum of the node individual transactions evaluation, and then averaging EigenTrust [5] that the use of this method to calculate the local trust value. EBay feedback system is to use a similar method, for all transactions Evaluation The sum of such methods has obvious flaws, such as difficult to guard against malicious nodes, every once in a while, the strategy of betrayal node, the node in the betrayal still be able to get a positive local trust value.

Moving average [6] is another method to calculate the local trust value, the method given recent transaction evaluation weight. Moving average method has high sensitivity evaluation, but still unable to prevent the policy node. If you give a new evaluation of excessive rights, misjudgment of bona fide node will reduce its local trust value, which means that the method assumes that all evaluation node neighbors are correct, this assumption is not always is established.

Trust management mechanism using Bayesian learning method to calculate local trust value [7], and PowerTrust [9], the method and the two methods differ, Bayesian learning method is based on analysis method, the node evaluation as reflect neighbor behavioral characteristics of the sample. Estimated results become more accurate when the sample is large. There will be a large error when the sample is less.

II. PEERBEHAVIOR MODEL

A. Neighbor Type of Behavior to Determine Method

(1) The DFA description of the method of the neighbor type of behavior judgment

This paper to describe the method to design a deterministic finite automaton (DFA), the DFA from the 7-state, they can be divided into four groups: an initial state, the normal-state set, the punished state and the observed state where each state represents at he node of the result of the determination of the neighbors acts, while the transfers between the different states represent nodes on neighbor views change process. DFA formally described as follows.

A. Behavioral state set QD

{Initial status (q_0), the normal state (q_1 , q_2 , q_3 , q_4), punishment state (q_5), the observed state (q_6)}.

B. $\sum$ is an input parameter set $\{C, B, m, n, \alpha\}$ C, B, M}, in which:

C represents the neighbor's behavior caused the positive evaluation of the node, the node determines cooperation;

B expresses the neighbor behavior caused negative evaluation of the node, node determines betrayal;

m represents the number of neighbor penalty condition to the normal state require continuous cooperation, i.e. penalize the cycle length;

n represents the number of neighbors from the observation state to the normal state requires a continuous cooperation, i.e., the length of the observation period.

The α parameter states q_3 to state q_3 probability, the node forgotten probability, that node tolerance once negative experience.

C. FD can be accepted set of states, $FD = QD$.

D. δ states transfer function.

E. DFA state transition diagram shown in figure 1.

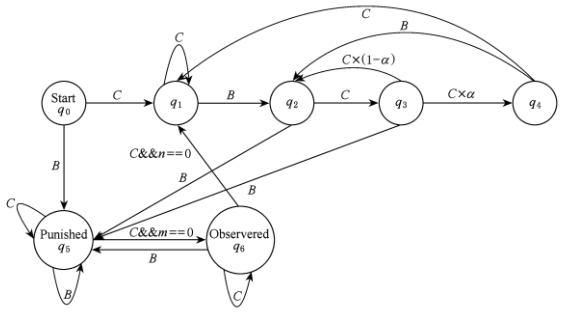

Figure 1. The DFA transition diagram of the evaluation method of neighbor's behavior

(2) Neighbor behavior judgment analysis

A. The node tolerance ranges of the parameter α

Let T to betrayal of B from state q_1 experience once to q_2 , go through several cooperation to reach the state q_4 required average number of transactions, the $1/T$ represents the biggest betrayal frequency can be tolerated in any continuous time.

Event A ={the state q_3 experienced a partnership after turning state q_4 }, and

$\Pr(A=1)=\alpha$, $\Pr(A=0)=1-\alpha$

It can be obtained the $EA=\alpha$; said a partnership from state q_3 to q_4 success, the number of can deduce, experienced an average of $1/\alpha$ cooperation, the state q_3 direct steering to q_4 ; cooperation will make the rest $1/\alpha-1$ the q_3 steering to q_2 .

Thereby the relationship between T and tolerance α are as follows:

$$T=\begin{cases}3+2\wedge(1/\alpha-1), 0\le\alpha<1\\ 3, \alpha=1\end{cases} \quad (1)$$

Assumed that the malicious nodes in the network every λ times cooperation betrayal, betrayal of a probability of $1/\lambda$ and $\lambda\ge 3$, also assumes that human evaluation error probability of occurrence for the ε and $\varepsilon\le 1/3$ in the only meet $\varepsilon\le 1/T\le 1/\lambda$ of the case, the neighbor behavior determining method to be able to distinguish between a policy node malicious behavior and human error.

a. $1/T\le 1/\lambda$, it is found that $T\ge\lambda$, by equation (1) to $3+2\wedge(1/\alpha-1)\ge\lambda$ and $\lambda\ge 3$ solution was:

$$\begin{cases}\alpha\le\dfrac{1}{(1+lb(\lambda-3))}, if\ \lambda>3\\ \alpha=1, if\ \lambda=3\end{cases} \quad (2)$$

b. $\varepsilon\le 1/T$, easily obtained, and $T<1/\varepsilon$, i.e., the $3+2\wedge(1/\alpha-1)\le 1/\varepsilon$ and $\varepsilon\le 1/3$.

$$\begin{cases}\alpha\ge\dfrac{1}{(1+1b(1/\varepsilon-3))}, if\ \varepsilon<1/3\\ \alpha=1, if\ \varepsilon=1/3\end{cases} \quad (3)$$

Formula (2) and formula (3) tolerance of the range of values of the parameter of α :

$$\begin{cases}\dfrac{1}{(1+lb(1/\varepsilon-3))}\le\alpha\le\dfrac{1}{(1+lb(1/\lambda-3))}, if\ \lambda>3, \varepsilon<1/3\\ \alpha=1, if\ \lambda=3, \varepsilon<1/3\end{cases} \quad (4)$$

Due to the strategy node malicious behavior and human evaluation error will cause a negative evaluation, so only reasonable to select the node latitude to be able to distinguish between good both cases. The formula (4) gives the reasonable range of the distinguished node between malicious behavior and evaluation of error tolerance.

B. Feature analysis

The method introduces a tolerance α, that is, negative evaluation after the neighbors a behavior caused, the next two trading forgotten, or in more rounds were forgotten with probability α, α reflects the degree of tolerance of a node, also said that the degree of tolerance of human assessment error. Node tolerance introduced, can prevent the malicious node by multiple transactions Evaluation speculated strategy, thereby ensuring the effectiveness of the strategy.

Soon enter the neighbor experienced punishment state n round observation status, behavior is judged in the observed state of the betrayal, the state re-set to punish state, experienced continuous n round behavior is judged to be cooperative transaction neighbor node state to the normal state, thereby eliminating the negative impact of the behavior of the past.

B. Local Trust Value Calculation

Local trust value is calculated based on the historical behavior of the neighbors to give an overall assessment. Which comprises two steps: first, the accumulated partial trust value calculated according to the history of cooperation of the neighbor; then combined the neighbor behavior type judgment method results to be updated on the local trust value.

A. Use the following method to calculate the historical behavior of the neighbors:

$$LR = \frac{\sum_{i=1}^{n} Evaluation(i) \times T(i)}{\sum_{i=1}^{n} T(i)} \tag{5}$$

Parameter Description:

$Evaluation(i)$ is a node on the evaluation of the behavior of the i[th] neighbors;

$T(i)$ is the i[th] transaction from the current time span.

B. Local trust value calculation

Local trust value has calculated by combining the result of the neighbor behavior type judgment method, the formula (5) in the calculation result of update. Neighbor type of behavior to determine methods of punishment strategy trigger their normal local trust value halved punishment.

$$LocalTrust = \begin{cases} LR/2, Punishment \\ LR, Other \end{cases} \tag{6}$$

From formula (5) and (6) can be seen, the negative evaluation led to the neighbor's local trust value exponentially decline, a positive assessment can only make local trust value increases linearly.

C. PeerBehavior Analysis

The PeerBehavior model had general said to have the following characteristics:

A well-intentioned, it is assumed that every stranger is a bona fide node.

After two fault tolerance, the neighbors a behavior caused a negative assessment, the node is not eager to punish, but observed it in the next $3+2\wedge((1-\alpha)/\alpha)$ round trading again is judged to be betrayed. Finalized malicious nodes and its malicious behaviors have server for penalties, which can tolerate behavior misjudgment.

Angered when the opponent's behavior is ultimately determined to be malicious, in each round of trading will no longer tolerate their betrayal in a significant reduction in the local trust values to punish every betrayal.

Tolerance in the opponent's betrayal after m round after punishing round of the observation period and n, forgotten, and ultimately forgiving neighbors last betrayal.

PeerBehavior tit-for-tat strategy [12] is not only has excellent characteristics, but also has the characteristics of fault tolerance. These features can propel the entire network toward the direction of the development of cooperation, while the introduction of fault tolerance, making it better able to adapt to the actual environment, resulting in a more accurate evaluation.

III. THE EXPERIMENTAL RESULTS AND ANALYSIS

A. Simulation Parameters Settings

We conducted in the P2P simulation software Peersim on simulation experiments driven use Peersim cycle engine to simulate P2P networks using 150 nodes, with the characteristics of the Power-law topology Simulation trust overlay network. Experiment assumes the existence of certain malicious nodes, and occupied the end of the Power-law curve malicious nodes.

The global trust value calculation method does not depend on the local trust value, the paper selects a common method of calculation of the value of global trust, different local trust value calculated on the basis of this unified global trust value. Each node before the transaction using the method of maximum likelihood estimation (MLE) [13] to calculate the global trust value of the neighbor, we use the following equation to calculate the value of global trust estimation error, where θ_i is the calculated global trust value, $\theta_i^{'}$ represents the type of node. 1 indicates that the node is well-intentioned, and 0 is malicious, k is the number of transactions in the experiment nodes.

$$MeanError = \frac{\sum_{i=1}^{k} \left| \theta_i - \theta_i^{'} \right|}{k} \tag{7}$$

In the experiment, we let each encounter node consecutive trading 4 times, and after each transaction to evaluate the behavior of the opponent, also assumes that the well-intentioned nodes with a certain probability misjudgment opponent malicious node every cycle make your betrayal. Experiment some of the parameters the set values or ranges, such as shown in Table I:

TABLE I. THE VALUE OR RANGE OF THE PARAMETERS IN THE SIMULATION

Parameter	Basic Definition	Default Value or Range
N	Number of peers in the P2P system.	150
C	The number of cycles our simulation runs.	100
m	The length of staying in punished state in ETFT.	2
n	The length of staying in observed state in ETFT.	4
C_1	The cheat interval of strategic peers.	6
Iv	Initial reputation of a stranger.	[0.5, 0.7]
γ	Percentage of strategic peers in the system.	[0.1, 0.9]
ε	The probability of human judgment error.	[0.01, 0.05]
α	Tolerance degree in the ETFT.	[0, 1]

We designed two different types of experiments: the first category is the comparison of the accuracy of the calculation of local trust value of different calculation methods; the other is to investigate different local trust value calculated in the different parameters of the impact of the global trust value. They are different local trust value calculation method comparison, the human evaluation errors on different local trust value calculated PeerBehavior performance under different scenarios. According to the equation $MeanError = f(\gamma, \varepsilon, \alpha)$ to derive the simulation results, mainly examine the policy node share probability of γ , human error ε and evaluation node tolerance α on the influence of the average error.

B. Simulation Results and Its Analysis

(1) Comparison of the accuracy of the calculation results of the different local trust value calculation method

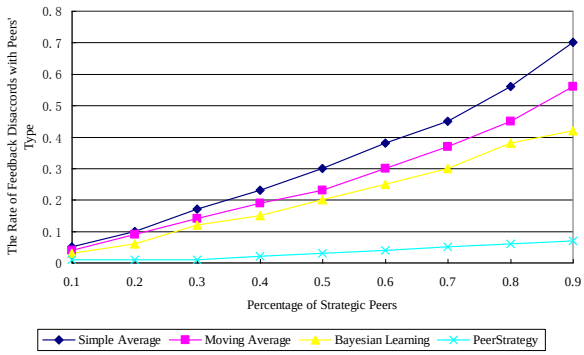

Figure 2. The trend of the mean error with the increase of the proportion of strategic peers in the network

Node neighbors local trust value calculated with the neighbor before the transaction, if local trust value is greater than 0.5, while the neighbors are good-node or local trust value is less than 0.5, and the neighbor is a malicious node, we call these two cases local trust values are correctly reflect the type of neighbor, otherwise error to reflect the value of the local trust node type. We statistical local trust value node type of error is reflected proportion in the case of the different proportions of the policy node in the network, i.e., the error ratio of the local trust value varied with the increase of the proportion of the network policy node.

We compared in the same experimental parameter settings local trust value error ratio calculated PeerBehavior and three kinds of local trust value calculation method. In the experiment, we let the policy node in the network the proportion of from 0.1 up to 0.9, and the growth rate was 0.1, while assuming human evaluation error 0.01, the node tolerance in PeerBehavior 0.5.

Figure 2 shows the value of the error ratio of the local trust with the increase in the proportion of the policy node changes, it can be seen PeerBehavior significantly better than the other three kinds of calculation methods, and always less than 0.1. The other three methods, including the simple average and Bayesian learning completely coincide with the increase in the proportion of policy node, a substantial increase in the proportion of local trust value error.

(2) Different local trust value calculation method Error of estimated global trust value

We compare the same set of experimental parameters PeerBehavior and three kinds of local trust value calculation of the global trust value estimation error. In the experiment, we let the policy node in the network the proportion of from 0.1 up to 0.9, and the growth rate was 0.1, while assuming human evaluation error 0.01, the node tolerance in PeerBehavior 0.5. That is, according to the equation $MeanError = f(\gamma, 0.01, 0.5)$ to produce the experimental results, calculate the global trust value with MLE estimation error, and then we examine the performance of the different local trust value calculation.

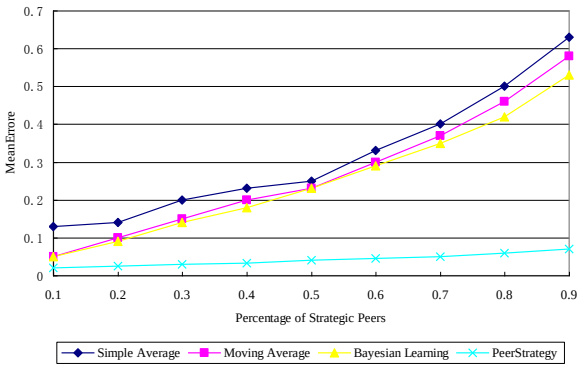

Figure 3. The trend of mean error of the global trust with the proportion of the strategic peers in the network

Four different local trust values calculating the performance of the method is easy to see from figure 3. Obviously, PeerBehavior caused by global trust value estimation error is minimized, significantly better than the value calculated for several trust. In this calculation method, the moving average method is better than a simple average calculation method, Bayesian learning methods appear in the range of 0.5 before and after a large variation. When the proportion of the policy node in the network is less than 0.5, Bayesian learning method performance worse than the other two methods, and when greater than 0.5, the performance of the Bayesian learning methods than the other two methods is good.

However, with the increase in the policy node, the current estimation error of the other three methods had greatly increased. Because they are dependent on the historical behavior of the node, strategy node strategy can easily escape punishment, which, after the betrayal still able to obtain a higher local trust value, the higher the proportion of the policy node, the greater the error.

Binding to figure 2 and figure 3 can be seen, the small local trust error ratio algorithm having a smaller error in the calculation of the global trust value remains, this is because the global trust value calculation depends on the local trust value, if the value of the local trust can not reflect the node characteristics, global trust value, however combination of local trust values are unable to find the type of node, resulting in greater estimation error.

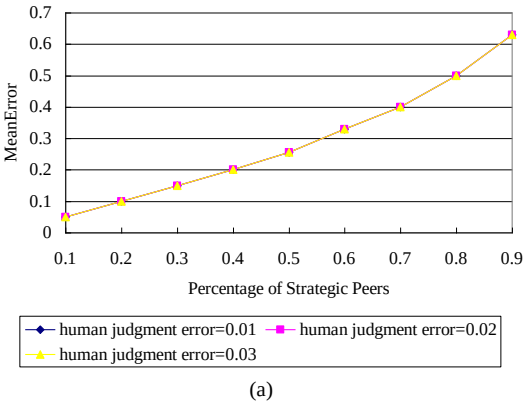

(a)

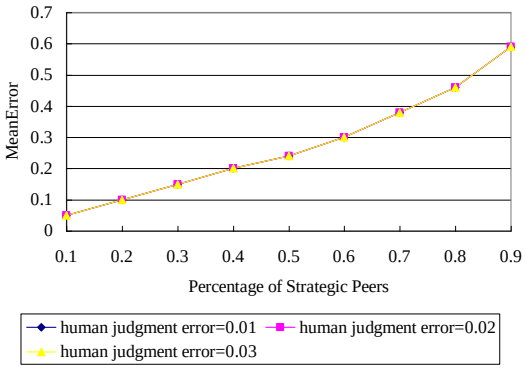

(b)

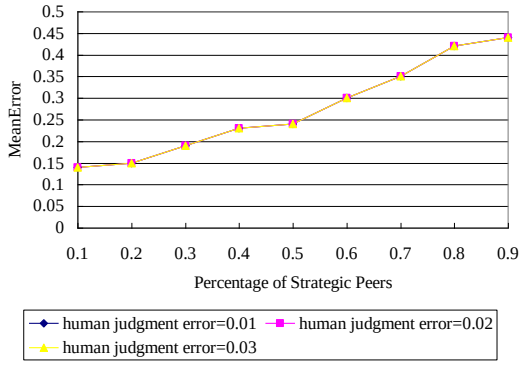

(c)

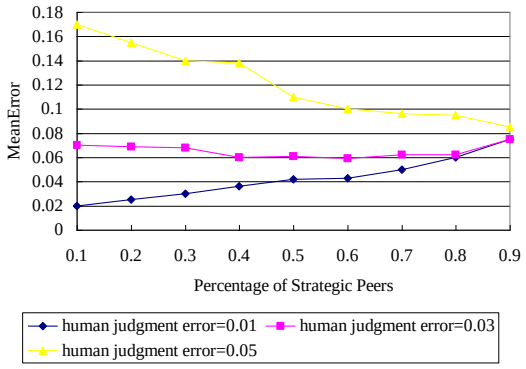

(d)

Figure 4. The trend of mean error of the global trust with the variance of strategic peers' proportion under different human judgment error. (a) Simple average; (b) Moving average; (c) Bayesian learning; (d) PeerBehavior.

(3) Human evaluation of error of different local trust value calculated

We look at the reaction the current three kinds of methods and PeerBehavior of error and strategies for human evaluation node, we let the proportion of malicious nodes in the network to increase from 0.1 to 0.9, and the growth rate was 0.1. We also examine the various methods three different human evaluation error performance. i.e. according to the equation $MeanError1 = f(\gamma, 0.01, 0.5)$, $MeanError2 = f(\gamma, 0.03, 0.5)$, $MeanError3 = f(\gamma, 0.05, 0.5)$ to produce experimental results.

As can be seen from figure 4, simple average, moving average, and Bayesian learning methods in different human evaluation error performance identical, in other words, they are not the estimated error into consideration. In addition, if the human evaluation error is large, most of the estimated error is caused by the misjudgment of bona fide node, so when the increase of the proportion of the policy node, the estimation error to show a downward trend. When the human evaluation of error is small, most of the global trust value estimation error is caused by a misjudgment strategy node, so with the increase in the proportion of the policy node, the upward trend estimation error.

(4) The punishment strategy node and tolerance tradeoff between human evaluation errors

In this experiment, we mainly investigated the performance of PeerBehavior tolerance of different human evaluation error and node. Node set tolerance growth from 0 to 1, the growth rate was 0.1, and assume that the proportion of malicious nodes in the network 0.7 and human evaluation of growth error rate of 0.01 from 0.01 to 0.05. The formula will becomes $MeanError = f(0.7, \varepsilon, \alpha)$.

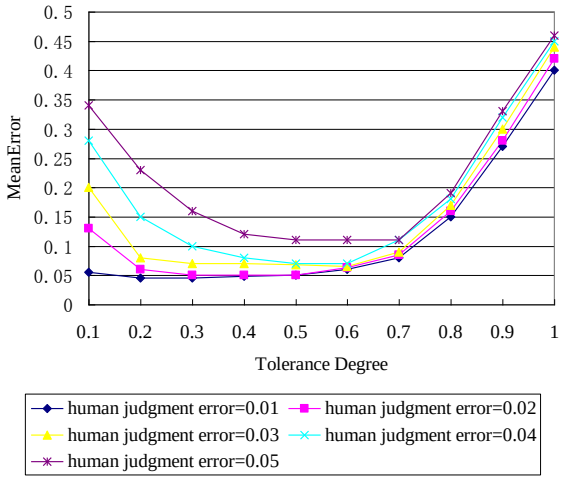

Figure 5. The influence of tolerance degree and human judgment error on the mean error of PeerBehavior

Figure 5 has been shown the performance of PeerBehavior in different nodes tolerance, easy to see, when the node tolerance certain higher, human evaluation error, global trust value the greater the estimated error. In addition, in certain human evaluation error, node

tolerance is larger or smaller, will cause the estimated error is larger. This is because, the node small tolerance, PeerBehavior some goodwill node mistakenly believe that a malicious node, and human evaluation error is larger, resulting in a system estimation error is large; while nodes tolerance is large, PeerBehavior malicious node will mistakenly believe is well-intentioned node, which led to a larger system estimation error.

Comprehensive figure 4 and figure 5 can be seen, human evaluation errors and strategies of malicious node strategy will impact global trust value estimation error, so it should be tolerated to strike a balance between human evaluation errors and punish node that is to select the appropriate node tolerance.

IV. CONCLUSTIONS

Impact due to the presence of human assessment error and Policies node local trust values reflect the characteristics of network nodes, thus increasing the value of global trust estimation error. To address this issue, we propose the neighbors behavioral evaluation model PeerBehavior based on continuous behavior observed, the simulation results show that human assessment error and the strategy of the malicious node strategy will lead to misjudgment of the local trust value calculated on the characteristics of network nodes, PeerBehavior by adjusting node tolerance applies to a different environment, to strike a balance between the tolerance of human assessment error and punishment policy node, compared with other current methods, can significantly improve the accuracy of local trust reflects the value of the network nodes characteristics, reducing the global trust estimated the impact of the error.

In short, PeerBehavior model can be able to more accurately calculate local trust evaluation value node neighbors and local trust value is the basis of most of the trust mechanism, which can reduce the estimated error in global trust value trust mechanism.

ACKNOWLEDGMENT

This work is supported by the Project Supported by Scientific Research Fund of Hunan Provincial Education Department (No. 11C0875, No. 12B005).

REFERENCES

[1] Iwasa Y, Ohtsuki H, "How should we define goodness reputation dynamics in indirect reciprocity," *Journal of Theoretical Biology*, vol. 231, no. 1, pp. 107-120, 2004.

[2] Houser D, Wooders J, "Reputation in auctions: Theory and evidence from eBay," *Journal of Economics and Management Strategy*, vol. 15, no. 2, pp. 353-369, 2006.

[3] Melnik M I, Alm J, "Does a seller's ecommerce reputation matter's evidence from eBay auctions," *Journal of Industrial Economics*, vol. 50, no. 3, pp. 337-349, 2010.

[4] Xiong L, Liu L, "PeerTrust: Supporting reputation-based trust in peer-to-peer communities," *IEEE Transactions on Knowledge and Data Engineering*, vol. 16, no. 7, pp. 843-857, 2006.

[5] Kamvar S, Schlosser M, Garcia-Molina H, "The EigenTrust algorithm for reputation management in P2P networks," *In Proceedings of the 12th International Conference on World Wide Web, New York: ACM*, pp. 640-651, 2003.

[6] Bin Yu, Singh M P, Sycara K, "Developing trust in large-scale peer-to-peer systems," *In Symposium on Multi-Agent Security and Survivability, New York: IEEE*, pp. 1-10, 2004.

[7] Buchegger S, Boudec J-Y L, "A robust reputation system for P2P and mobile ad-hoc networks," *In Proceedings of the 2nd Workshop on Economics of P2P Systems, New York: IEEE*, pp. 1-37, 2004.

[8] Aberer K, Despotovic Z, "Managing trust in a peer-2-peer information system," *In Proceedings of the 10th International Conference on Information and Knowledge Management, New York*: ACM, pp. 310-317, 2001.

[9] Zhou R, Hwang K, "PowerTrust: A robust and scalable reputation system for trusted P2P computing," *IEEE Transactions on Parallel and Distributed Systems*, vol. 18, no. 4, pp. 460-473, 2007.

[10] Zhou R, Hwang K, "Gossip-based reputation aggregation for unstructured peer-to-peer networks," *IEEE Transactions on Knowledge and Data Engineering*, vol. 20, no. 9, pp. 1282-1295, 2008.

[11] Jiang Shouxu, Li Jianzhong, "A reputation-based trust mechanism for P2P E-commerce systems," *Journal of Software*, vol. 18, no. 10, pp. 2551-2563, 2007.

[12] Axelrod R M, *The Evolution of Cooperation*. New York: Basic Books, 1984.

[13] Despotovic Z, Aberer K, "Maximum likelihood estimation of peers performances in P2P networks," *In Proceedings of the 2nd Workshop on the Economics of Peer-to-Peer Systems, New York: IEEE*, pp. 1-9, 2004.

[14] Xiaonan LIU, Zhiyi FANG, Huanhuan TANG, "A Direction-based Search Algorithm in P2P Network," *Journal of Computational Information Systems*, vol. 6, no. 1, pp. 25-31, 2010.

[15] Fuyong YUAN, Jian LIU, Chunxia YIN, Yulian ZHANG, "A Distributed Recommendation Mechanism based on Collaborative Filtering in Unstructured P2P Networks," *Journal of Computational Information Systems*, vol. 4, no. 3, pp. 1111-1118, 2008.

[16] A. Abdul-Rahman, S. Hailes, "Supporting trust in virtual communities," *In Proceedings of 33rd Annual Hawaii International Conference on System Sciences*, 2000.

[17] C. Dellarocas, "The digitization of word-of-mouth: Promise and challenges of online reputation mechanism," *Management Science*, vol. 49, no. 10, pp. 34-40, 2007.

[18] J. M. Pujol, R. Sanguesa, J. Delgado, "Extracting reputation in multi-agent systems by means of social network topology," *In Proceedings of 1st International Joint Conference on Autonomous Agents and Multiagent Systems*, 2002.

Xianwen Wu, born in 1973, received her B.S. degree in Engineering from Xiangtan University, Xiangtan, China in 1996, her M.S. degree in computer science and technology from National University of Defense Technology, Changsha, China in 2004. Also, she is an associate professor at the College of Information Technology, Hunan Railway Professional Technology College, Zhuzhou, China. Her current research interests include Wireless Sensor Networks security and High Performance Network.

Zhiliang Xue, born in 1976, received her B.S. degree in National University of Defense Technology, Changsha, China in 2001, her M.S. degree in computer science and technology

from Central South University, Changsha, China in 2010. Also, she is a lecturer at hunan railway professional technology college, Zhuzhou, China. Her current research interests include Wireless Sensor Networks Security and Vocational Theory.

Jingwen Zuo, born in 1977, received his B.S. degree in China University of Political Science and Law, Beijing, China in 1999, his M.S. degree in Industry & Business Administration from HeFei University of Technology, Hefei, China in 2002. Also, he is a engineer at Changsha University of Science and Technology, Changsha, China. His current research interests include Peer-to-Peer Network Security and Image Segmentation.

Access Authentication Scheme Based on Authorized Certificate in Wireless Mesh Networks

Liangyu Luan [1], Yingfang Fu [2 *], and Peng Xiao [3]
1. College of Applied Science, Beijing University of Technology, Beijing 100124, China
2. Fantai Lingshi Technology (Beijing) Limited, Beijing 100044, China
3. College of Computer Science and Technology, Beijing University of Technology, Beijing 100124, China
*Corresponding author, Email: luanly@bjut.edu.cn, fuyingfang@bjut.edu.cn, xp1984@emails.bjut.edu.cn

***Abstract*—The main benefits of the access authentication in IEEE 802.11s are both easy administration of the subscribers and compatibility with IEEE 802.11i. However, there still exist some shortcomings, such as worse authentication delay, suffering from intermediate attack, lower expansibility and the inequality among users. In order to overcome these shortcomings, a zone-based hierarchical topology structure, virtual certification authority (CA), off-line CA, authorized certificates and authorized keys are used in the access authentication scheme proposed in this paper. Qualitative analysis and simulation show that the access authentication scheme would improve authentication of the 802.11s in authentication latency, security, expansibility and the inequality in users.**

***Index Terms*—Wireless Mesh Network, Authentication, Certificate, Virtual CA**

I. INTRODUCTION

The use of wireless mesh network (WMN) technology to provide internet connectivity is becoming a popular choice for wireless Internet service providers because the technology provides fast, easy and inexpensive network deployment. However, without a solid security solution, WMN with open medium won't be able to succeed. Currently, the authenticate scheme in 802.11s standard for WMN has some shortages [1, 2]. So, securing network access is the first line of protection against unauthorized users from getting access to network services and authentication scheme is essential for securing access to the network. Several results related to the access authentication described in this paper have already been loosely presented in [3]. In this paper, we propose a detailed access authentication scheme for wireless mesh network, and we show that our access authentication scheme would improve the authentication method of IEEE 802.11s standard in authentication latency, security, expansibility and the inequality in users through qualitative analysis and simulation.

The rest of this paper is organized as follows. In the next section, we review some related work in authentication schemes for WMN. In Section 3, we present a new access authentication scheme. In Section 4, we present a detailed performance evaluation thorough analysis. Finally, we conclude this paper in Section 5.

II. RELATED WORK

The most straightforward way for securing access to a WMN is to adopt IEEE 802.1X so that mobile nodes can be authenticated by the mesh access router. The IEEE 802.1X standard defines a port based network access scheme to prevent access a LAN network until authentication and authorization succeeds [4]. It carries EAP (Extensible Authentication Protocol) [5] messages between a user and an access point (AP). Then, the AP relays EAP messages to the authentication server (usually an AAA server like RADIUS or Diameter). After authentication succeeds, the user is registered as a MAC address authorized to access the LAN, and the (AP) is registered as a MAC address with the user. Moreover, the AP exchanges keys with the user, and the 4-way handshake method for key establishment is defined in the IEEE 802.11i standard [6]. In the scheme, authentication is done at layer 2. The association between a user and an AP is done through MAC addresses. However, MAC addresses may be forged, as the result of the network easily suffers from intermediate attacks. Furthermore, most of EAP based authentication methods in use are quite complex and the communication and computational overheads are heavy, and the authentication delay is worse [7]. A secure architecture for WMNs based on EAP-TLS over PANA was proposed [8]. Although EAP-TLS provides excellent security, e.g. mutual authentication and robustness against malicious attacks, the use of asymmetric cryptography requires heavy computation, which is not suitable for light ad hoc networks. It also involves a great deal of complexity due to the need of establishing and managing a PKI [9].

III. AN ACCESS AUTHENTICATION SCHEME FOR WMN

A. The Network Model

We present a zone-based hierarchical network model for WMN. The whole network consists of one backbone network and one or more local area networks called zones. The backbone network consists of backbone routers, an off-line CA which only connects to the network under the condition that it is notified of the existence of an attacker, being it a terminal user, a zone router or a backbone

doi:10.4304/jnw.9.1.231-237

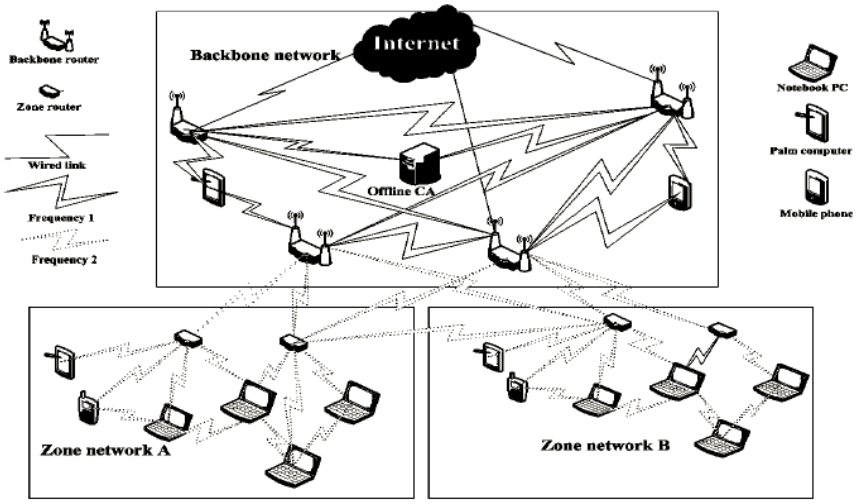

Figure 1. Network model

router, and a database of authorized certificates that are shared only among the backbone routers. Each backbone router uses three special frequencies. The first one is for the backbone routers to transmit data and the other two are for zone routers or terminal users to transmit wireless ingress traffic and egress traffic, respectively. There are also at least two backbone routers connected to the Internet. Each zone network has two zone routers connected to the backbone network and to the users. There is also a database that stores user information, such as user ID, zone ID, authorized key, etc., which is shared between the two zone routers. Users can roam from one zone to another. Users in a zone network communicate with each other within a relatively shorter range and those in a backbone network communicate with each other within a relatively longer range. Let's assume without loss of generality that users communicate with each other in frequency 1 and the backbone routers communicate with each other in frequency 2. Fig. 1 illustrates the network model in our authentication scheme. In the network model, we assume that communication between users has the following characteristics:

(1) One zone router may connect to one or more terminal users.
(2) The terminal users connect to the Internet through backbone routers and any one of the two zone routers.
(3) The terminal users in the same zone network may communicate directly.
(4) The terminal users in adjacent zone networks may communicate with each other through their zone routers.
(5) Cryptographic communication between users adopts the identity-based cryptosystem [11].
(6) Authentication between users would use authorized certificates.
(7) A terminal user gets access to a zone network service by using his/her an authorized certificate along with an authorized key.
(8) The cost of communication through the backbone network is higher than that in zone networks.

B. System Initialization

Before assigning an authorized certificate and an authorized key to a user, the system completes the following initialization steps:

The off-line CA creates two pairs of private and public keys, one for itself and the other one for the whole system using the RSA algorithm. The public key for the system is denoted as K and its corresponding private key as S.

Before accessing a zone network or the backbone network, every terminal user must register with the off-line CA. If a terminal user wants to serve as a backbone router or zone router, the terminal user must submit an application to the off-line CA besides its user information.

The off-line CA identifies and assigns to a new terminal user the zone ID, user ID, the public key K of the system, a pair of public-private keys created using the RSA algorithm as well as the corresponding certificate. If the terminal user is approved of being a backbone or zone router, the off-line CA would confirm it as a backbone or zone router. Every user broadcasts its user ID to all other users.

The off-line CA would select n terminal users with higher performance as the backbone router $Br_1 \cdots Br_n$, which serve as private key generation (PKG) nodes. These n backbone routers would then form a virtual CA and manage the keys using the (t, n)-threshold cryptographic method [10]. That is, the off-line CA publishes the public key K of the system to all the users while the private key S of the system is partitioned into n pieces $S_1 \cdots S_n$ and assigns the n pieces to the n different backbone routers. Any t out of the n backbone routers could reconstruct the private key S. The t out of the n backbone routers are marked as $Br_{i_r}(r = 1 \cdots t)$ and its sub private key is marked as s_{i_r}. Therefore, any m out of the n backbone routers cannot reconstruct private key S unless $m \geq t$. The relationship between s_{i_r} and S can be expressed in equation (1) and the value of c_{i_r} can be obtained using equation (2).

$$s = \sum_{Br_i \in A, r=1}^{t} c_{i_r} s_{i_r} \quad (1)$$

$$c_{i_r} = \prod_{1 \le j,r \le t, j \ne r} \frac{x_{i_j}}{x_{i_j} - x_{i_r}} \left(x_{i_r} = i_r \right) \quad (2)$$

C. Authorized Certificates

We present a new method to assign an authorized certificate to a user based on multi-signature scheme [12]. In the scheme, we first select and calculate the following parameters and announce them to all the users: (a) a secure hash function; (b) a large prime p and q is the large prime factor of p, which makes it difficult to solve the discrete logarithm in Z_p^*. The parameter α is the largest generator of Z_p^* with q order. In general, $2^{511} \le p \le 2^{512}$ and $2^{159} \le q \le 2^{160}$; (c) $y = \alpha^s \bmod p$; (4) $Br_i \in A, y_r = \alpha^{s_{i_r}} \bmod p$

Any t out of n backbone routes make t sub signature $sig_r(m)$ for the terminal user U using (3) and (4):

$$\delta_r = H(m) b_r + (c_{i_r} + 1) s_{i_r} \bmod q \quad (3)$$

$$sig_r(m) = (w_r, \delta_r) \quad (4)$$

In (3), b_r is a secret random integer in [0, q-1], m is the user information. In (4), $w_r = \alpha^{b_r} \bmod p$ and w_r is announced to all the users and $sig_r(m)$ is a sub signature of the terminal user U.

After receiving the sub signature $sig_r(m)$, terminal user U verifies if the sub signature is valid or not by using equation (5). If the equation holds, the sub signature is valid. Otherwise, the sub signature is invalid. The terminal user U would submit the application for an authorized certificate to another backbone router when it deduces that a sub signature is invalid.

$$\alpha^{\delta_r} = w_r^{H(m)} y_r^{(c_{i_r}+1)} \bmod p \quad (5)$$

Proof (5):

$\alpha^{\delta_r} = \alpha^{[H(m)b_r + (c_{i_r}+1)s_{i_r} + n_0 q]}$ (The parameter n_0 is an integer)

$= \alpha^{H(m)b_r} \alpha^{(c_{i_r}+1)s_{i_r}} \alpha^{n_0 q}$ ($\alpha^{n_0 q}$ equals unit element.)

$= \alpha^{H(m)b_r} \alpha^{(c_{i_r}+1)s_{i_r}} w_r^{H(m)} y_r^{(c_{i_r}+1)} \bmod p$

$= (\alpha^{b_r} + n_1 p)^{H(m)} (\alpha^{s_{i_r}} + n_2 p)^{(c_{i_r}+1)} \bmod p$ (The parameter n_1, n_2 are integers)

$= \alpha^{H(m)b_r} \alpha^{(c_{i_r}+1)s_{i_r}} \bmod p$

$= \alpha^{H(m)b_r} \alpha^{(c_{i_r}+1)s_{i_r}}$

Therefore, $\alpha^{\delta_r} = w_r^{H(m)} y_r^{(c_{i_r}+1)} \bmod p$, i.e., $sig_r(m)$ is a valid sub signature. After colleting t sub signatures, terminal user U would obtain his/her multi-signature $Br_1 \cdots Br_n$, i.e. an authorized certificate through calculating (6), (7) and (8).

$$R = \prod_{Br_i \in A} w_r \bmod p \quad (6)$$

$$I = \prod_{Br_i \in A} \delta_r \bmod q \quad (7)$$

$$sig_r(m) = (R, I) \quad (8)$$

The authorized certificates of the backbone routers $Br_1 \cdots Br_n$ are created by any t out of the n-1 backbone routers, i.e., no backbone router can assign a sub private key based on identity or a sub signature to itself. The method on how to assign a private key based on identity to a user is proposed in [13].

D. Authorized Keys

If a terminal user U wants to access a zone network services or the backbone network services, it must authenticate using its own authorized certificate and negotiate an authorized key with the two zone routers. First, the two zone routers would generate through negotiation a large prime number p and g for the terminal user U such that g is primitive mod p. These two integers don't have to be secret, though. The following steps for negotiating an authorized key is based on the Diffie-Hellman protocol [14] and are illustrated in Fig. 2.

Terminal user U chooses two random large integers *x*, N_u and calculates $X = g^x$, and then sends $(N_u \mid X)$ to zone router Zr_1.

Zone router Zr_1 chooses two random large integers *y*, N_{Zr_1} and calculates $Y = g^y$, and then sends $(N_u \mid N_{Zr_1} \mid Y)$ to zone router Zr_2.

Zone router Zr_2 chooses two random large integers *z*, N_{Zr_2} and calculates $Z = g^z$, and then sends $(N_u - 1 \mid N_{Zr_1} \mid N_{Zr_2} \mid Z)$ to terminal user U. If receiving random integer $N_u - 1$, terminal user U would send $(N_{Zr_1} - 1 \mid N_{Zr_2} \mid Z' = Z^x \bmod p)$ to zone router Zr_1.

If receiving the random integer $N_u - 1$, the terminal User U will send $(N_{Zr_1} - 1, N_{Zr_2}, Z' = Z^x \bmod p)$ to the zone router Zr_1.

If receiving the random integer $N_{Zr_1} - 1$, zone router Zr_1 would send $(N_u - 1 \mid N_{Zr_2} - 1 \mid X' = X^y \bmod p)$ to zone router Zr_2.

If receiving random integers $N_u - 1$ and $N_{Zr_2} - 1$, zone router Zr_2 would send $(N_u - 1 \mid N_{Zr_1} - 1 \mid N_{Zr_2} - 1 \mid Y' = Y^z \bmod p)$ to terminal user U. receiving random integers $N_u - 1$, $N_{Zr_1} - 1$ and $N_{Zr_2} - 1$, terminal user U would calculate the authorized key $nk = Y'^x \bmod p$;

If receiving random integer $N_{Zr_1} - 1$, zone router Zr_1 would calculate $nk = Z'^y \bmod p$;

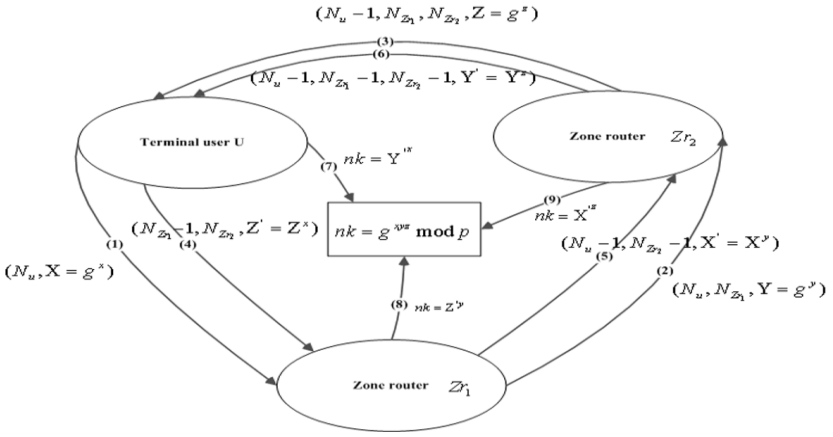

Figure 2. Authorized key negotiation

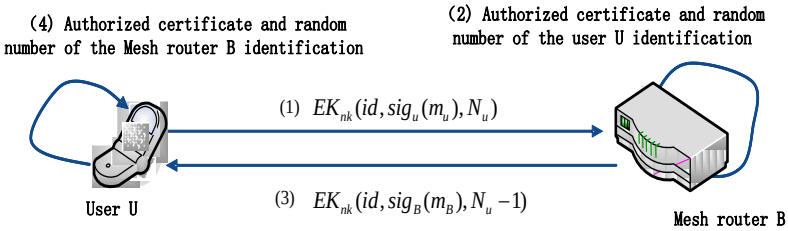

Figure 3. Access authentication flow

If receiving random integers $N_u - 1$ and $N_{Zr_2} - 1$, zone router Zr_2 would calculate $nk = X^{'z} \bmod p$. Therefore, the authorized key nk between the terminal user U and the two zone routers is $nk = g^{xyz} \bmod p$ By the way, the symbol "|"is for series connection and the process of negotiation between the terminal users and access routers, i.e., zone routers and backbone routers, adopts the identity-based cryptosystem [9], i.e., the sender encrypt data with the ID and the zone public key of the receiver and then send it to the receiver. The receiver obtains the data through decrypting the message sent to it by the sender with its own private key based on identity.

E. Access Authentication

A terminal user U wants to access a zone network, both the user and a zone router could mutually authenticate each other through identifying the authorized certificate of the other side. This is done by identifying authorized certificate through using (8) and by showing that (9) holds. If (9) holds, the authorized certificate of the other side is valid. Otherwise, the authorized certificate is invalid.

$$Y_A = \prod_{Br_i \in A} y_r \bmod p \tag{8}$$

$$\alpha^I = R^{H(m)} Y_A y \bmod p \tag{9}$$

Proof (9):

$\alpha^I = \alpha^{(\sum_{Br_i \in A} \delta_r + m_1 q)}$ (Parameter m_1 is an integer)

$= \alpha^{\sum_{Br_i \in A} \delta_r} \alpha^{m_1 q}$ ($\alpha^{m_1 q}$ equals unit element.)

$= \alpha^{\sum_{Br_i \in A} \delta_r}$

$= \prod_{Br_i \in A} \alpha^{\delta_r}$

$R^{H(m)} Y_A y \bmod p$

$= (\prod w_r \bmod p)^{H(m)} (\prod y_r \bmod p) a^s \bmod p$

$= (\prod w_r^{H(m)})(\prod a^{s_{i_r}}) a^{\sum_{Br_i \in A} c_{i_r} s_{i_r}} \bmod p$

$= (\prod w_r^{H(m)})(\prod a^{s_{i_r} + c_{i_r} s_{i_r}}) \bmod p$

$= \prod a^{b_r H(m) + (c_{i_r} + 1) s_{i_r}} \bmod p$

$= \prod_{Br_i \in A} a^{\delta_r} \bmod p$

$= \prod_{Br_i \in A} a^{\delta_r}$

Therefore, $a^I = R^{H(m)} Y_A y \bmod p$ which shows that the authorized certificate of the other side is a valid, i.e., the other side is a credible authorized user.

The following steps for access authentication are illustrated in Fig. 3.

User U asks for access to zone network through sending the message $EK_{nk}(id, sig_u(m_u), N_u)$ to mesh router B. In the message, id is the session sequence, $sig_u(m_u)$ is the authorized certificate of user U, N_u is random number, $EK_{nk}()$ is encryption function with the encryption key nk, and the encryption key nk is the authorized key between the terminal user U and the two zone routers.

Mesh router B decrypts the message with the authorized secret key nk and identify the validity of the user U's authorized certificate with equation (9).

If the authorized certificate of user U is validity, the mesh router B sends the message $EK_{nk}(id, sig_u(m_u), N_u - 1)$ to user U, the meanings of the variables or the function in the message is same to the message $EK_{nk}(id, sig_u(m_u), N_u)$.

The user U decrypts the message with the authorized secret key nk and identify the validity of the mesh router B's authorized certificate with equation (9) too.

IV. Simulation and Qualitative Analysis

We have performed some simulation using OPNET 10.5 under Windows XP to compare the performance of our access authentication scheme with that of the access authentication scheme in 802.11s.

TABLE I. Simulation scenarios

Node number	50
Zone router number	2
Square field	300m×300m
Channel transmission rate	11Mbps
Power	1W
Interval of sending packet	0.01s

In order to compare the performance of our access authentication scheme with that of the access authentication scheme in 802.11s well and truly, we set all parameters of simulation scenarios of the access authentication scheme in 802.11s be same to ours, as the table 1 shows, but one zone router is replaced with AS (Authentication Server).We initially distribute 50 nodes randomly and two zone routers (or one router and an authentication server) over a square field of constant dimensions 300m×300m. The channel transmission rate of the wireless receiver is 11Mbps, the power is 1W and the interval of sending packet is 0.01*s*. Processing time for authentication is not considered for authentication algorithms are optional due to various applications. As shown in the Fig. 4 and Fig. 5.

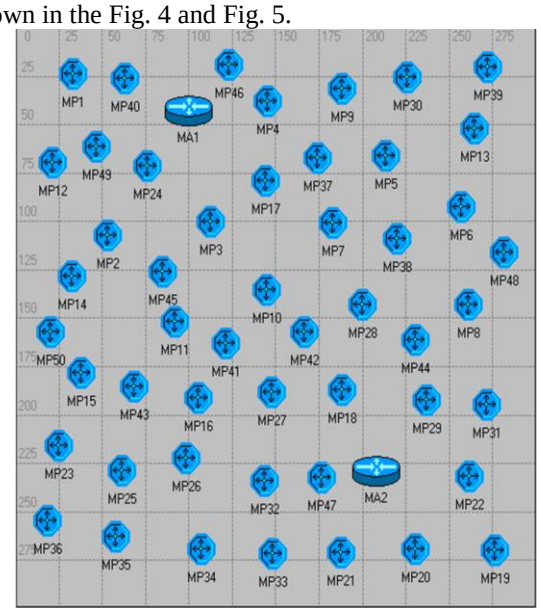

Figure 4. Simulation scenarios of our scheme

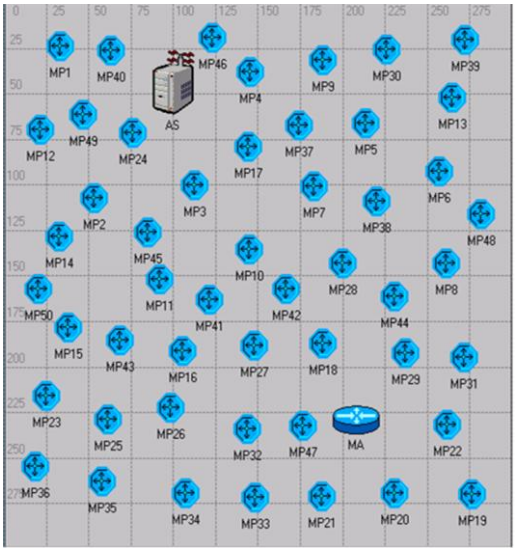

Figure 5. Simulation scenarios of 802.11s

We compare the performance of our scheme with that of 802.11s through simulating the success rate and average delay of authentication in different network scale. The authentication success rate is defined as the number of nodes successfully getting access to the network divided by the total number of nodes requesting for network service. The average authentication delay is defined as the total authentication delay of all the nodes successfully getting access to the network divided by the total nodes those authenticated successfully. The retransmission number is defined as the number that the nodes are allowed to request access to the network if authentication fails. The simulation results are shown in Fig. 6 to Fig. 10. In these figures, the axis of abscissa is the network scale, i.e., all nodes in the network. The axis of ordinate is success rate and average delay of authentication respectively. The unit of delay is second. In our simulation, all nodes in the network random launch request to a near zone router for getting access to the network in 2s. We draw the following conclusions through analysis the simulation results:

When the retransmission number is 1, the average authentication delay of our scheme is 0.0302*s*, which is lower than that of 802.11s 0.0308*s*. All the authentication success rate of our scheme is 100%, when the number of nodes requesting for accessing to the network is less than 6. But that of 802.11s is 100% only when the node number is 1.Two scheme have same authentication success rate, when the node number is from 6 to 9. When the node number is from 11 to 50, the authentication success rate of our scheme is relatively stabilizer and higher than that of 802.11s. When the retransmission number is 3, the authentication success rate and average authentication delay of our scheme are near that of 802.11s in the small network scale (node number<6). In the middle network scale (6<node number<35), the authentication success rates of our scheme are lower than that of 802.11s, but their average authentication delay are higher than ours. In the large network scale (35<node number,) our authentication success rate and average authentication delay are better than that of 802.11s.

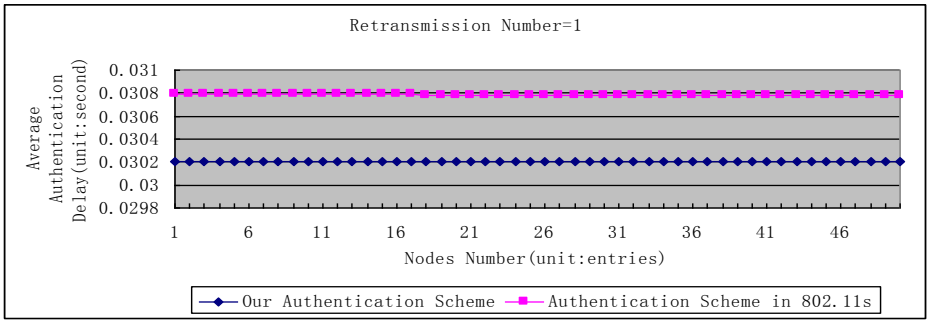

Figure 6. Comparison of average authentication delay of two schemes, retransmission number=1

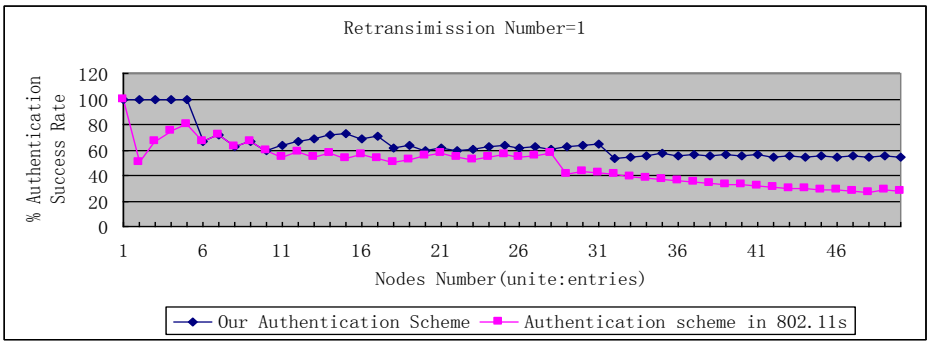

Figure 7. Comparison of authentication success rate of two schemes, retransmission number=1

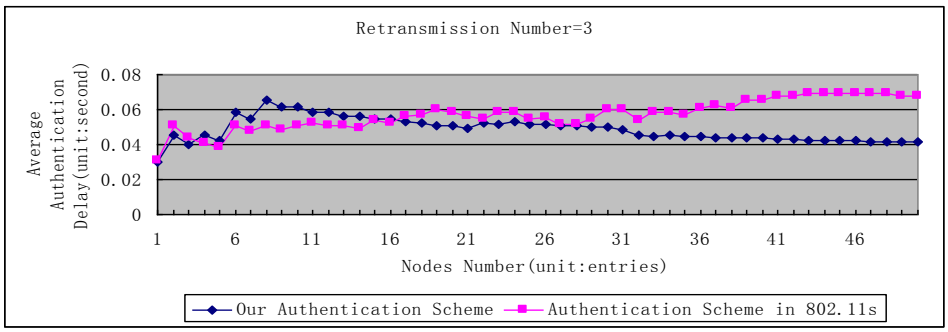

Figure 8. Comparison of average authentication delay of two schemes, retransmission number=3

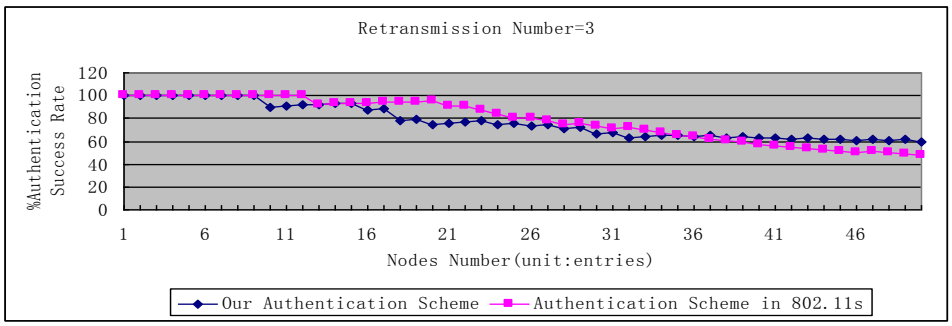

Figure 9. Comparison of authentication success rate of two schemes, retransmission number=3

V. Conclusion and Future Work

By analyzing and identifying the advantages and limitations of existing authentication schemes for such networks, we can see that our scheme has the following advantages:

We use a zone-based hierarchical network topology in a WMN, which can be extended easily to deal with a WMN of any size and integrated easily with different networks.

The sub signature and authorized certificate can not be forged. There are three reasons for it. First, only knowing the private key s_{i_r} and the random integer b_r, one can make a sub signature sig_r. However, the private key s_{i_r} and the random integer b_r are secret to all system

members except the backbone router Br_{i_r}. Second, according to the values of y, w_r and y_r, one can not obtain the master private key S, the random number b_r and the sub private key s_{i_r} because it is difficult to resolve a discrete logarithm in Z_{p^*}. Third, it is also difficult for one to obtain the value of s_{i_r} through multi sub signatures because $\delta_r = H(m) \quad b_r + (C_{i_r} + 1)s_{i_r}$ mode q includes two unknown parameters. Using identity-based cryptosystem and random number to create an authorized key can be effective to fight against intermediate attacks. These characteristics help to improve the authentication scheme in security.

In the scheme presented in [8], authentication uses asymmetric cryptography, requires a PKI and needs four-way handshake. In our scheme, we use identity-based cryptosystem and random numbers to create an authorized key and a multi-signature scheme to create an authorized certificate. Therefore, users don't need to create and broadcast their own public keys in the network. Neither does our scheme need to manage a PKI. Furthermore, mutual authentication between users would only need two-way handshake. These characteristics help to improve performance by decreasing network traffic, computational overhead and storage space in a WMN.

In contrast to the scheme presented in [5], in our scheme, a terminal user gets access to the network services through any access router with the same authorized certificate, which improves convenience and fault tolerance. Therefore, our scheme is suitable for authentication and authorization in multi-hop WMNs.

In this paper, we presented an access authentication scheme based on authorized certificate in WMN. Theoretical analysis and simulation experiments show that our access authentication scheme has a high performance, availability and security. However, our access authentication scheme only realizes the authentications for identity users, but the integrality of users' platform. Therefore, our future work is to solute this problem.

REFERENCES

[1] IEEE Std 802.11sTM-2011 Wireless LAN Medium Access Control (MAC) and Physical Layer (PHY) specifications Amendment 10: Mesh Networking, 10 September 2011.

[2] Hiertz, G., Max, S., Berlemann, L., IEEE 802.11s: The Wlan Mesh Standard. *IEEE Wireless Communications, February*, 2010, pp. 104-111.

[3] Fu, Y., He, J., Wang, R., etc. "Mutual Authentication in Wireless Mesh Networks". *The 43rd IEEE International Conference on Communications (ICC 2008), Beijing, China*, May 19-23, 2008.

[4] IEEE Standard 802.1X-2004: Standard for Local and Metropolitan Area Networks: Port-Based Network Access Control, Dec. 2004.

[5] Aboba, B., Blunk, L., Vollbrecht, J. Carlson, J. and Levkowetz, H., "Extensible Authentication Protocol (EAP)", *RFC 3748*, June 2004.

[6] IEEE Standard 802.11i-2004: Standard for Information Technology - Telecommunication and Information Exchange between Systems - Local and Metropolitan Area Networks-Specific Requirements, July 2004.

[7] He B., Agrawal D.P., "An Identity-based Authentication and Key Establishment Scheme for Multi-operator Maintained Wireless Mesh Networks", *The 7th International Conference on Mobile Ad hoc and Sensor Systems (MASS), San Francisco, Nov. 2010.*

[8] O. Cheikhrouhou, M. Laurent-Maknavicius, H. Chaouchi, "Security Architecture in a Multi-hop Mesh Network", *In Proc.5th Conference on Safety and Architectures Networks (SAR 2006), Seignosse, Landes, France, June 2006.*

[9] Khan, K. and Akbar, M., "Authentication in Multi-Hop Wireless Mesh Networks", *Transactions on Engineering, Computing and Technology*, Vol. 16, Nov. 2006, pp. 178-183.

[10] Khalili, A., Katz, J. and Arbaugh, W.A., "Toward Secure Key Distribution in Truly Ad-Hoc Networks", *In Proc. Symp, on Applications and the Internet Workshop*, 2003, pp. 342-346.

[11] Zhou, L. and Haas, Z.J., " Securing Ad Hoc Network", *IEEE Networks*, Vol. 13, No. 6, 1999, pp. 24-30.

[12] Zhang, X., "The Signature Scheme with Fault Tolerance based on Threshold", *Journal of the Graduate School of the Chinese Academy of Sciences*, Vol. 21 No. 3, July 2004, pp. 398-401.

[13] Fu, Y., He, J., Wang, R. and Li, G., "A zone-based distributed key management scheme for wireless mesh networks", *The 32nd Annual IEEE International Computer Software and Applications Conference (COMPSAC 2008), Turku, Finland*, July 28-August 1, 2008.

[14] Bishop, M., "An Application for a Fast Data Encryption Standard Implementation", *Computing Systems*, Vol. 1, No. 3, 1988, pp. 221–254.

Instructions for Authors

Manuscript Submission

We invite original, previously unpublished, research papers, review, survey and tutorial papers, application papers, plus case studies, short research notes and letters, on both applied and theoretical aspects. Manuscripts should be written in English. All the papers except survey should ideally not exceed 12,000 words (14 pages) in length. Whenever applicable, submissions must include the following elements: title, authors, affiliations, contacts, abstract, index terms, introduction, main text, conclusions, appendixes, acknowledgement, references, and biographies.

Papers should be formatted into A4-size (8.27" x 11.69") pages, with main text of 10-point Times New Roman, in single-spaced two-column format. Figures and tables must be sized as they are to appear in print. Figures should be placed exactly where they are to appear within the text. There is no strict requirement on the format of the manuscripts. However, authors are strongly recommended to follow the format of the final version.

All paper submissions will be handled electronically in EDAS via the JNW Submission Page (URL: http://edas.info/N10935). After login EDAS, you will first register the paper. Afterwards, you will be able to add authors and submit the manuscript (file). If you do not have an EDAS account, you can obtain one. If for some technical reason submission through EDAS is not possible, the author can contact jnw.editorial@gmail.com for support.

Authors may suggest 2-4 reviewers when submitting their works, by providing us with the reviewers' title, full name and contact information. The editor will decide whether the recommendations will be used or not.

Conference Version

Submissions previously published in conference proceedings are eligible for consideration provided that the author informs the Editors at the time of submission and that the submission has undergone substantial revision. In the new submission, authors are required to cite the previous publication and very clearly indicate how the new submission offers substantively novel or different contributions beyond those of the previously published work. The appropriate way to indicate that your paper has been revised substantially is for the new paper to have a new title. Author should supply a copy of the previous version to the Editor, and provide a brief description of the differences between the submitted manuscript and the previous version.

If the authors provide a previously published conference submission, Editors will check the submission to determine whether there has been sufficient new material added to warrant publication in the Journal. The Academy Publisher's guidelines are that the submission should contain a significant amount of new material, that is, material that has not been published elsewhere. New results are not required; however, the submission should contain expansions of key ideas, examples, elaborations, and so on, of the conference submission. The paper submitting to the journal should differ from the previously published material by at least 30 percent.

Review Process

Submissions are accepted for review with the understanding that the same work has been neither submitted to, nor published in, another publication. Concurrent submission to other publications will result in immediate rejection of the submission.

All manuscripts will be subject to a well established, fair, unbiased peer review and refereeing procedure, and are considered on the basis of their significance, novelty and usefulness to the Journals readership. The reviewing structure will always ensure the anonymity of the referees. The review output will be one of the following decisions: Accept, Accept with minor changes, Accept with major changes, or Reject.

The review process may take approximately three months to be completed. Should authors be requested by the editor to revise the text, the revised version should be submitted within three months for a major revision or one month for a minor revision. Authors who need more time are kindly requested to contact the Editor. The Editor reserves the right to reject a paper if it does not meet the aims and scope of the journal, it is not technically sound, it is not revised satisfactorily, or if it is inadequate in presentation.

Revised and Final Version Submission

Revised version should follow the same requirements as for the final version to format the paper, plus a short summary about the modifications authors have made and author's response to reviewer's comments.

Authors are requested to use the Academy Publisher Journal Style for preparing the final camera-ready version. A template in PDF and an MS word template can be downloaded from the web site. Authors are requested to strictly follow the guidelines specified in the templates. Only PDF format is acceptable. The PDF document should be sent as an open file, i.e. without any data protection. Authors should submit their paper electronically through email to the Journal's submission address. Please always refer to the paper ID in the submissions and any further enquiries.

Please do not use the Adobe Acrobat PDFWriter to generate the PDF file. Use the Adobe Acrobat Distiller instead, which is contained in the same package as the Acrobat PDFWriter. Make sure that you have used Type 1 or True Type Fonts (check with the Acrobat Reader or Acrobat Writer by clicking on File>Document Properties>Fonts to see the list of fonts and their type used in the PDF document).

Copyright

Submission of your paper to this journal implies that the paper is not under submission for publication elsewhere. Material which has been previously copyrighted, published, or accepted for publication will not be considered for publication in this journal. Submission of a manuscript is interpreted as a statement of certification that no part of the manuscript is copyrighted by any other publisher nor is under review by any other formal publication.

Submitted papers are assumed to contain no proprietary material unprotected by patent or patent application; responsibility for technical content and for protection of proprietary material rests solely with the author(s) and their organizations and is not the responsibility of the Academy Publisher or its editorial staff. The main author is responsible for ensuring that the article has been seen and approved by all the other authors. It is the responsibility of the author to obtain all necessary copyright release permissions for the use of any copyrighted materials in the manuscript prior to the submission. More information about permission request can be found at the web site.

Authors are asked to sign a warranty and copyright agreement upon acceptance of their manuscript, before the manuscript can be published. The Copyright Transfer Agreement can be downloaded from the web site.

Publication Charges and Re-print

The author's company or institution will be requested to pay a flat publication fee of EUR 360 for an accepted manuscript regardless of the length of the paper. The page charges are mandatory. Authors are entitled to a 30% discount on the journal, which is EUR 100 per copy. Reprints of the paper can be ordered with a price of EUR 100 per 20 copies. An allowance of 50% discount may be granted for individuals without a host institution and from less developed countries, upon application. Such application however will be handled case by case.

More information is available on the web site at http://www.academypublisher.com/jnw/authorguide.html.

(Contents Continued from Back Cover)